MATERIALS FOR ADVANCED ULTRASUPERCRITICAL STEAM TURBINES

Final Technical Report

Reporting Period: Oct.1, 2009 – Sep. 30, 2015

Principal Authors:

Robert Purgert
John Shingledecker
Deepak Saha
Mani Thangirala
George Booras
John Powers
Colin Riley
Howard Hendrix

December 2015

DOE Cooperative Agreement: DE-FE0000234
Ohio Coal Development Office Grant Agreement: D-05-02(B)

Energy Industries of Ohio
Park Center Plaza
6100 Oak Tree Boulevard, Suite 200
Independence, OH 44131

Electric Power Research Institute
3420 Hillview Ave.
Palo Alto, CA 94304

General Electric Company
Power & Water Division
1 River Road
Schenectady, NY 12345

U.S. Department of Energy Disclaimer

This report was prepared as an account of work sponsored by an agency of the United States Government. Neither the United States Government nor any agency thereof, nor any of their employees, makes any warranty, express or implied, or assumes any legal liability or responsibility for the accuracy, completeness, or usefulness of any information, apparatus, product, or process disclosed, or represents that its use would not infringe privately owned rights. Reference herein to any specific commercial product, process, or service by trade name, trademark, manufacturer, or otherwise does not necessarily constitute or imply its endorsement, recommendation, or favoring by the United States Government or any agency thereof. The views and opinions of authors expressed herein do not necessarily state or reflect those of the United States Government or any agency thereof.

Project Consortium Legal Notice/Disclaimer

This report was prepared by the Energy Industries of Ohio in conjunction with the Electric Power Research Institute, Inc. (EPRI); General Electric Company, acting through GE Energy Business; pursuant to a Grant partially funded by the U.S. Department of Energy (DOE) under Instrument Number DE-FE000234 and the Ohio Coal Development Office/Ohio Development Services Agency (OCDO/ODSA) under Grant Agreement Number CDO/D-05-02(B). NO WARRENTY OR REPRESNTATION, EXPRESS OR IMPLIED, IS MADE WITH RESEPCT TO THE ACURACY, COMPLETENESS, AND/OR USEFULNESS OF INFORMATION CONTAINED IN THIS REPORT. FURTHER, NO WARRENTY OR REPRESENTATION, EXPRESS OR IMPLIED, IS MADE THAT THE USE OF ANY INFORMATION, APPARATUS, METHOD, OR PROCESS DISCLOSED IN THIS REPORT WILL NOT INFRINGE UPON PRIVATELY OWNED RIGHTS. FINALLY, NO LIABILITY IS ASSUMED WITH RESPECT TO THE USE OF, OR FOR DAMAGES RESULTING FROM THE USE OF, ANY INFORMATION, APPARATUS, METHOD OR PROCESS DISCLOSED IN THIS REPORT.

Reference herein to any specific commercial product, process, or service by trade name, trademark, manufacturer, or otherwise, does not necessarily constitute or imply its endorsement, recommendation, or favoring by the Department of Energy and/or the State of Ohio; nor do the views and opinions of authors expressed herein necessarily state or reflect those of said governmental entities.

ABSTRACT

The U.S. Department of Energy (DOE) and the Ohio Coal Development Office (OCDO) have sponsored a project aimed at identifying, evaluating, and qualifying the materials needed for the construction of the critical components of coal-fired power plants capable of operating at much higher efficiencies than the current generation of supercritical plants. This increased efficiency is expected to be achieved principally through the use of advanced ultrasupercritical (A-USC) steam conditions. A limiting factor in this can be the materials of construction for boilers and for steam turbines. The overall project goal is to assess/develop materials technology that will enable achieving turbine throttle steam conditions of 760°C (1400°F)/35MPa (5000 psi).

This final technical report covers the research completed by the General Electric Company (GE) and Electric Power Research Institute (EPRI), with support from Oak Ridge National Laboratory (ORNL) and the National Energy Technology Laboratory (NETL) – Albany Research Center, to develop the A-USC steam turbine materials technology to meet the overall project goals. Specifically, this report summarizes the industrial scale-up and materials property database development for non-welded rotors (disc forgings), buckets (blades), bolting, castings (needed for casing and valve bodies), casting weld repair, and casting to pipe welding. Additionally, the report provides an engineering and economic assessment of an A-USC power plant without and with partial carbon capture and storage.

This research project successfully demonstrated the materials technology at a sufficient scale and with corresponding materials property data to enable the design of an A-USC steam turbine. The key accomplishments included the development of a triple-melt and forged Haynes 282 disc for bolted rotor construction, long-term property development for Nimonic 105 for blading and bolting, successful scale-up of Haynes 282 and Nimonic 263 castings using traditional sand foundry practices, and a techno-economic study of an A-USC plant including cost estimates for an A-USC turbine which showed A-USC to be economically attractive for partial carbon and capture compared to today's USC technology. Based on this successful materials research and a review with U.S. utility stakeholders, a new project to develop a component test facility (ComTest) including the world's first A-USC turbine has been proposed to continue the technology development.

TABLE OF CONTENTS

Executive Summary 5

1. Introduction and Project Background 7

2. Summary of Accomplishments 9

3. Task 3 - Materials for Non-Welded Rotors, Buckets, and Bolting 23

4. Task 4 - Cast Superalloy Development 110

5. Task 5 – Superalloy Weld Repair Technology Development 368

6. Task 6 – Process development and characterization of Casting-Pipe Welds 382

7. Engineering and Economic Analysis of an Advanced Ultra-Supercritical Pulverized Coal Power Plant with and without Post-Combustion Carbon Capture 404

Executive Summary

The overall objective of the project is the development of materials technology for use in an advanced ultrasupercritical (A-USC) steam turbine capable of operating with steam conditions up to 760°C (1400°F), 35 MPa (5000 psi). The lack of materials with the necessary fabricability and resistance to creep, oxidation, and fatigue at the higher steam temperatures and pressures currently limit the adoption of A-USC steam conditions in pulverized coal-fired plants.

A Phase 1 (three year national effort) sponsored by the U.S. Department of Energy (DOE) and the Ohio Coal Development Office (OCDO) was completed in June 2009. This initial Phase 1 addressed the need to identify and analyze candidate A-USC turbine materials from the perspective of steam side conditions and pressure ranges to be encountered in various components of an A-USC turbine. The Phase 1 effort completed a detailed review, process modeling, microstructural prediction, and short-term mechanical testing of materials for rotor forgings, buckets (blades), bolting, and lab-scale castings. Based on this comprehensive 'screening' effort, key alloys were selected for Phase 2 which this final technical report (Oct. 2009 to Sep. 2015) covers.

The Phase 2 effort specifically addressed the following industrial scale-up materials issues required to confidently design and fabricate an A-USC Turbine:

- The development of a full-scale nickel-based alloy forging for an A-USC steam turbine rotor based on a bolted disc construction
- The process development and supply chain engagement necessary to utilize the learnings from lab-scale castings to industrial relevant conditions and sizes needed for an A-USC Turbine
- The development of welding and weld repair technologies for casting and joining the turbine to the boiler (casting to forging welding)
- Long-term property development and microstructural stability of all key candidate alloys

Concurrently, the Phase 2 also assessed the techno-economics of an A-USC plant including cost estimates for an A-USC turbine and a comparison with current state-of-the-art USC technology with partial carbon and capture.

The project was highly successful and met all the target objectives to enable the next step in A-USC steam turbine development. For the turbine forgings, the project successfully developed Haynes alloy 282 from its standard double-melt commercial product form to a full-scale size steam turbine rotor disc. Notable accomplishments for this development were:

- First demonstration of triple-melt Haynes 282 ingots (2 were produced)
- The successful development of the Haynes 282 forging process culminating in the forging of a 44" diameter disc

- Detailed characterization of the forged disc which showed excellent grain size control through careful process control resulting in superior fatigue, creep-fatigue (hold-time fatigue), and tensile properties in comparison to the standard Haynes 282 product

For bolting and blading, long-term testing found that Nimonic Alloy 105 satisfies all the needs for high-temperature creep strength, relaxation resistance, tensile properties, and aging resistance. For the turbine castings, which are needed for turbine shells and large valve bodies, the project started with a multitude of ~15lb lab scale ingots and achieved a ~17,000 lb pour weight casting. This major scale-up effort on the order of 3 orders of magnitude in size and corresponding technical challenges achieved the following:

- Demonstration of the world's largest sand casting of alloy Haynes 282
  - Excellent through thickness properties achieved
  - Developed unique casting modeling tools to enable direct application to future design needs
- Engaged multiple US based suppliers in casting both Haynes 282 and Nimonic 263
- Showed that no compositional changes were required to achieve excellent cast properties
- Developed and validated unique computationally designed heat-treatments to ensure homogenization (and no cracking during post-casting heat-treatment)
- Successfully developed weld repair processes for the castings
- Successfully developed a casing to pipe weld with multiple filler metals

For the techno-economic study, it was found that an A-USC steam turbine was approximately two times the cost of a comparable (on a MW basis) state-of-the-art USC steam turbine due to the use of nickel-based alloys in the high pressure (HP) and intermediate pressure (IP) parts of the turbine. However, this increase in cost was not the major factor for the cost increase in comparing a USC to A-USC power plant. This project confirmed other studies which showed A-USC is approximately 10% higher in capital cost. For this study, the estimated capital cost was $2,933/kW, and the Levelized Cost of Electricity (LCOE) was $84.70/MWh. A significant contributor to the higher cost is the long main and reheat steam piping lines, which would be fabricated from nickel-based alloys. This has led the power industry to respond with several innovative boiler concepts which may bring the cost of an A-USC plant into parity with an equivalently sized USC plant. Furthermore, the study (which only considered a traditional boiler design and turbine arrangement) clearly showed that when partial carbon capture and storage are considered, the A-USC plant has a lower LCOE compared to USC because less CO_2 is produced so less needs to be captured.

1. Introduction and Project Background

This report is organized into seven sections due to the extensive developments on specific individual tasks which each contain detailed summaries and in some cases appendices of data and model results. The section numbers follow the original project proposal and statement of project objectives task numbering. To aid the reader, a summary section (Section 2) is presented first to provide the entire project results prior to the detailed technical sessions. The format is as follows:

- Section 1: Introduction and Project Background
- Section 2: Summary of Accomplishments
- Section 3: Materials for Non-Welded Rotors, Buckets, and Bolting
- Section 4: Cast Superalloy Development
- Section 5: Superalloy Weld Repair Technology Development
- Section 6: Process Development and Characterization of a Casing-Pipe Weld
- Section 7: Techno-economic assessment of A-USC turbine and plan technology with and without partial carbon capture and storage

The overall objective of the project is to contribute to the development of materials technology for use in advanced ultrasupercritical (A-USC) pulverized coal power plants capable of operating with steam up to 760°C (1400°F), 35 MPa (5000 psi). R&D is needed on newly developed materials to lead to a full-scale demonstration, and eventual commercialization, of A-USC power plants. The lack of materials with the necessary fabricability and resistance to creep, oxidation, and fatigue at the higher steam temperatures and pressures currently limit the adoption of A-USC steam conditions in pulverized coal-fired plants.

A Phase 1 (three year national effort) sponsored by the U.S. Department of Energy (DOE) and the Ohio Coal Development Office (OCDO) was completed in June 2009 and the final report was submitted. The Phase 1 effort was performed under a prime contract with Energy Industries of Ohio (EIO) through a consortium made up of the Electric Power Research Institute (EPRI), Oak Ridge National Laboratory (ORNL) and all of the U.S. domestic turbine manufactures: General Electric, Alstom Power and Siemens Westinghouse. This initial Phase 1 addressed the need to identify and analyze candidate A-USC turbine materials from the perspective of steam side conditions and pressure ranges to be encountered in various components of an A-USC turbine. The Phase 1 effort completed a detailed review, process modeling, microstructural prediction, and short-term mechanical testing of materials for rotor forgings, buckets (blades),

bolting, welded rotors, and lab-scale castings. Based on this comprehensive 'screening' effort, key alloys and processes were selected for Phase 2 which this final technical report (Oct. 2009 to Sep. 2015) covers.

At the completion of Phase 1, Alstom Power and Siemens Corporation withdrew participation due to business reasons. Funding for Phase 2 was provided by OCDO and DOE with cost sharing and technical participation from General Electric, Co. and EPRI. Oak Ridge National Laboratory and NETL-Albany Research Center also participated in the project through direct DOE funding support. The national laboratory efforts were reported on a quarterly basis and results of direct importance to the project are highlighted in the appropriate locations within the report. The original Phase 2 effort included the evaluation of both welded and non-welded rotor construction. However, with the Alstom Power withdrawal from the project, the welded rotor task (Task 2) was eliminated and the project only focused on non-welded rotor materials technology developments.

Thus, the Phase 2 effort specifically addressed the following industrial scale-up materials issues required to confidently design and fabricate an A-USC Turbine:

- **Task 3**: The development of a full-scale nickel-based alloy forging for an A-USC steam turbine rotor based on a bolted disc construction and long-term property development and microstructural stability of wrought alloys for rotors, buckets (blades), and bolting
- **Task 4**: The process development and supply chain engagement necessary to utilize the learnings from lab-scale castings to industrial relevant conditions and sizes needed for an A-USC Turbine including casting trials, casting model development, and material property characterization
- **Task 5**: The development of weld repair technologies for casting
- **Task 6**: The development of welding technologies for joining the turbine to the boiler (casting to forging welding)
- **Task 7:** A techno-economic assessment of an A-USC plant including cost estimates for an A-USC turbine and a comparison with current state-of-the-art USC technology with partial carbon and capture.

Topical reports were released during the project on Task 3, 4, and 7. Sections 3, 4, and 7 are based largely on these topical reports with additional data, analysis, and reporting and supersede these topical reports.

2. Summary of Accomplishments

At the completion of this project and a companion DOE project to develop the materials technology to build and operate an A-USC Steam Boiler with the same steam conditions, a final review of learnings was held with the joint consortium. The following represents the summary from this meeting related to A-USC steam turbine materials as well as the key findings from the technical details contained within this report. Overall, the project was highly successful and addressed the major goals identified for the turbine development. Based on this success, the consortium, with the engagement and support of the utility industry, has proposed a component test facility (ComTest) to take the next technological step in the development of A-USC technology which includes the world's first functional A-USC steam turbine.

Task 3: Materials for Non-Welded Rotors, Buckets, and Bolting

The goal of Task 3 was to characterize the materials suitable for mechanically coupled rotor (bolted construction), buckets and bolting operating with an inlet temperature of 760°C (1400°F). Phase 1 had identified a number of potential alloys for this application and selected Haynes®282® and Nimonic 105 for the rotor forging and buckets/bolting, respectively. The selection criteria was based on available data, processing considerations, and options for material choices/trade off during the detailed design of large components.

Commercially available Nimonic 105 and Haynes®282® were evaluated for microstructural stability by long term thermal exposure studies. Material properties requisite for design such as tensile, creep / rupture, low cycle fatigue, high cycle fatigue, fatigue crack growth rate, hold-time fatigue, fracture toughness, and stress relaxation were produced which showed both materials met the criteria for the selected components and conditions.

A key requisite for the success of the program was a need to demonstrate the successful scale up of the down-selected alloys, to large components. All property evaluations in the past were performed on commercially available bar/billet forms. Components in power plant equipment such as rotors and castings are several orders in magnitude larger and there is a real need to resolve the scalability issue. Nimonic 105 contains high volume fraction γ' [>50%], and hence the alloy is best suited for smaller forging and valve internals, bolts, smaller blades. Larger Nimonic 105 forgings, would precipitate γ' during the surface cooling during forging, leading to surface cracks. The associated costs in forging Nimonic 105 to larger sizes [hotter dies, press requirements], were beyond the scope of this task and not investigated further. Haynes®282® has 20 - 25% volume fraction γ' was a choice for large components, albeit untested.

A larger ingot diameter is pre-requisite for a larger diameter forging and achieves the “typically” accepted working ratio of 2.5-3:1. However, Haynes®282® is manufactured via a double melt process [VIM-ESR] limited by size [<18-16” diameter], which limited the maximum size of the final forging. The project successfully developed a 24” diameter triple melt ingot [VIM-ESR-VAR], surpassing the current available technology (Figure 1). A second triple melt ingot was manufactured and successfully forged into a 44” diameter disk (Figure 2). The successful developments in triple melting process and the large diameter forging of Haynes®282® resolved the scalability issues and involved the first of its kind attempt in the world for this alloy. The complete characterization of Haynes®282® forging was performed and documented. The dataset from the commercially available Haynes®282® [grain size ASTM 3-4] and the finer grain size disk forging [ASTM 8-9] offer an additional design tradeoff to balance creep and fatigue during the future design process. One result of this optimization of grain size was that the forged triple-melt disc showed superior creep-fatigue (hold-time fatigue) properties in comparison to typical nickel-based alloys such as Inconel 617 (Figure 3) with little debit observed in fatigue even using a typically damaging 6 hour hold-time.

Figure 1. 24” Diameter Triple Melt Haynes 282 Ingot

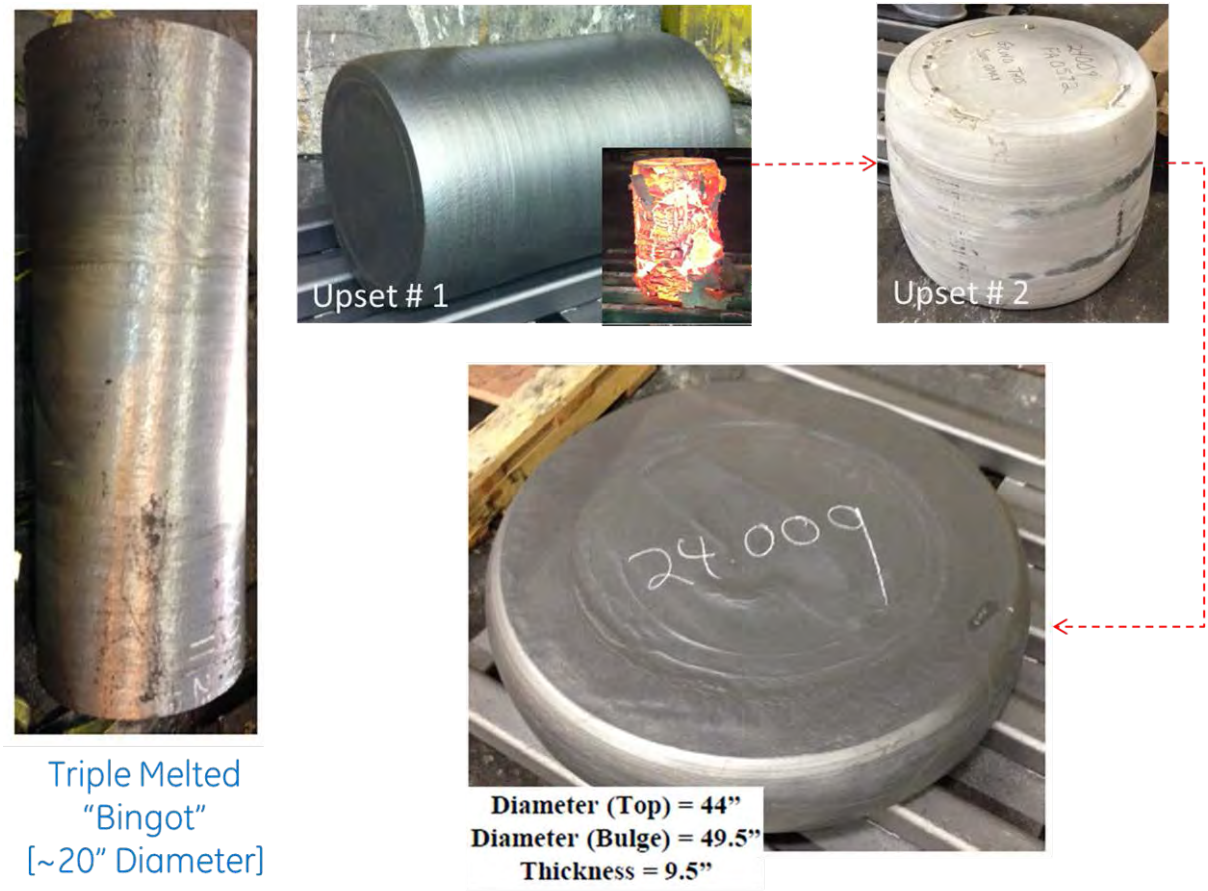

Figure 2. Forging process development of the Haynes 282 triple-melt ingot resulting in a 44" Diameter disc

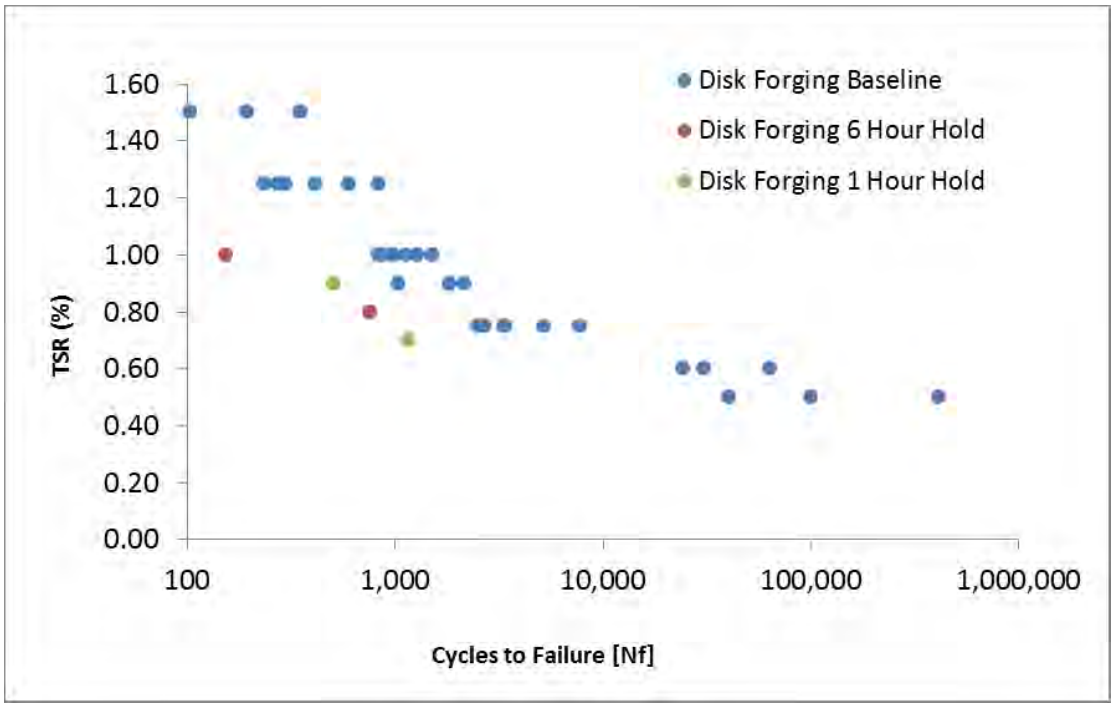

Figure 3. Fatigue and hold-time fatigue (creep-fatigue) cycle to failure data for Haynes 282 forged disk. A small debit in hold-time fatigue is observed for 1 to 6 hours hold time. Typical nickel-based alloys such as alloy 617 show a factor of 10 to 100 reduction in cycles to failure with hold times of only 0.1 to 1 hour.

Task 4: Cast Superalloy Development

The Steam Turbine critical stationary structural components are high integrity Large Shell and Valve Casing heavy section castings, containing high temperature steam under high pressures. Hence to support the development of advanced materials technology for use in an A-USC steam turbine capable of operating with steam conditions of 760°C (1400°F) and 35 MPa (5000 psia), casting alloy selection and evaluation of mechanical, metallurgical properties and castability with robust manufacturing methods are mandated.

Alloys were down selected from Phase 1 based on producability criteria and creep rupture properties tested by NETL-Albany and ORNL who directed the consortium to investigate cast properties of Haynes 282 and Haynes 263. The goals of Task 4 in Phase 2 were to understand a broader range of mechanical properties and the impact of manufacturing variables on those properties, and to scale up the size of heats to production levels to facilitate the understanding of the impact of heat and component weight, on metallurgical and mechanical behavior.

GE Power & Water Materials and Processes Engineering for the Phase 2, Task 4.0 Castings work, systematically designed and executed casting material property evaluation through multiple test programs which started with 15 lbs. cylinder castings and completed the world's first 17,000 lbs. poured weight heavy

section large steam turbine partial valve Haynes 282 super alloy casting. This has demonstrated scalability of the material for A-USC steam turbine applications.

Successful activities under Task 4.0, investigated and characterized various mechanical properties of Cast Haynes 282 and Cast Nimonic 263. The development stages involved were:

1) **Small Cast Evaluation:** 4 inch diam. Haynes 282 and Nimonic 263 Cylinders. This provided effects of liquidous super heat range and first baseline mechanical data on cast versions of conventional vacuum re-melted and forged Ni based super alloys.
2) **Step block castings of 300 lbs. and 600 lbs**: Haynes 282 from 2 foundry heats were evaluated which demonstrated the importance of proper heat treat cycles for homogenization, and solutionizing parameters selection and implementation.
3) **Step blocks casting of Nimonic 263**: Carried out casting solidification simulation analysis, NDT inspection methods evaluation, detailed test matrix for Chemical, Tensile, LCF, stress rupture, CVN impact, hardness and J1C Fracture toughness section sensitivity data and were reported. (Figure 4)

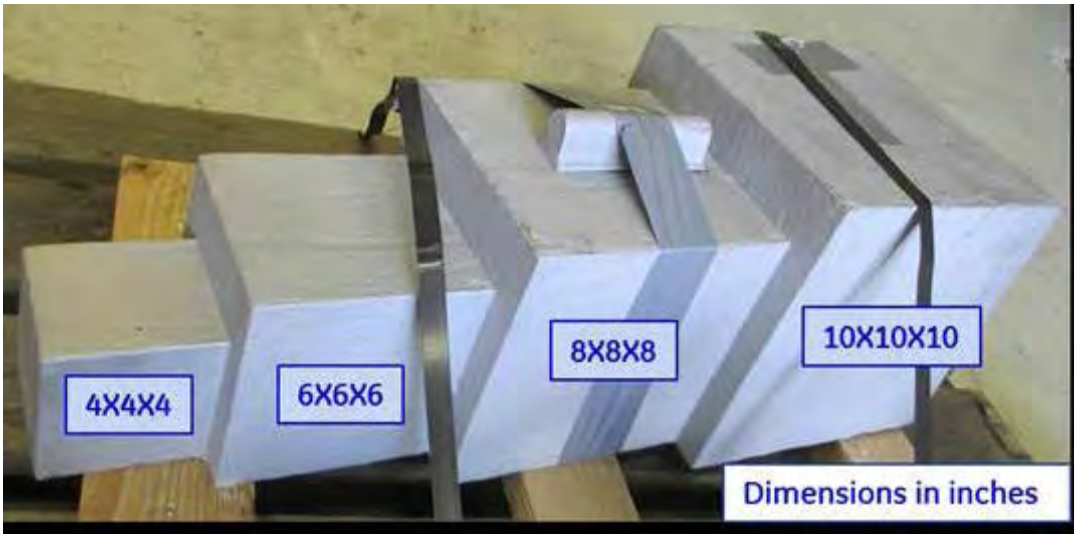

Figure 4. Nimonic 263 step block casting weighing 605lbs. The project completed a detailed assessment of section size effects after optimization of the homogenization and age hardening heat-treatments which were computationally designed based on the resultant as-cast microstructure

4) **Centrifugal Casting of Haynes 282**: Weighing 1400 lbs. with hybrid mold (half Graphite and half Chromite sand), the mold assembly was cast using compressor casing production tooling. This test provided Mold cooling

rates influence on centrifugally cast microstructure and mechanical properties. Graphite mold section out performs sand mold across all temperatures for 0.2% YS; %Elongation, %RA, UTS at 1400°F. Both Stress-LMP and conditional fracture toughness plots data were in the scatter band of the wrought alloy.

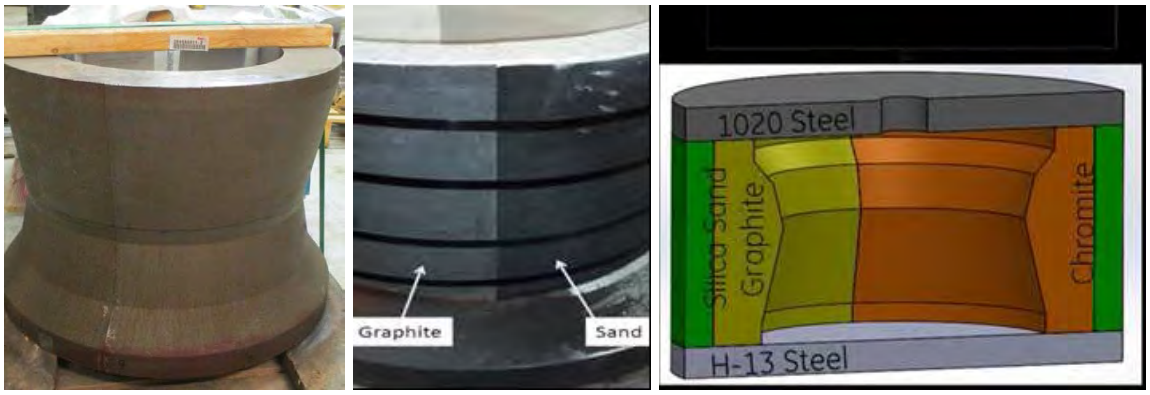

Figure 5. Haynes 282 Centrifugal casting with mold assembly comprising half Graphite and half chromite sand

5) **Fundamental studies on cooling rates and SDAS test program**: Evaluated the influence of 6 mold materials, Silica, Chromite, Alumina, Silica with Indirect Chills, Zircon and Graphite, on casting solidification cooling rates. Actual Casting cooling rates through Liquidus to Solidus phase transition were measured with 3 different locations based thermocouples placed in each mold. Compared with solidification simulation cooling rates and measurement of SDAS, microstructure features were reported. The test results provided engineered casting potential methods, applicable for heavy section Haynes 282 castings for optimal properties, with foundry process methods and tools.

6) **Large casting of Haynes 282:** Drawings and Engineering FEM models and supplemental requirements with applicable specifications were provided to suppliers for the steam turbine proto type feature valve casing casting. Molding, melting and casting pouring completed per approved Manufacturing Process Plan during 2014 Q4. The partial valve casing was successfully cast (Figure 6, 7, and 8) after casting methods were validated with solidification simulation analysis and the casting met NDT inspection and acceptance criteria. The casting was heat treated and sectioned to extract trepan samples at different locations comparing with cast on coupons test data. Material properties requisite for design, such as tensile, creep/rupture, LCF, Fracture Toughness, Charpy V-notch chemical analysis testing were carried out.

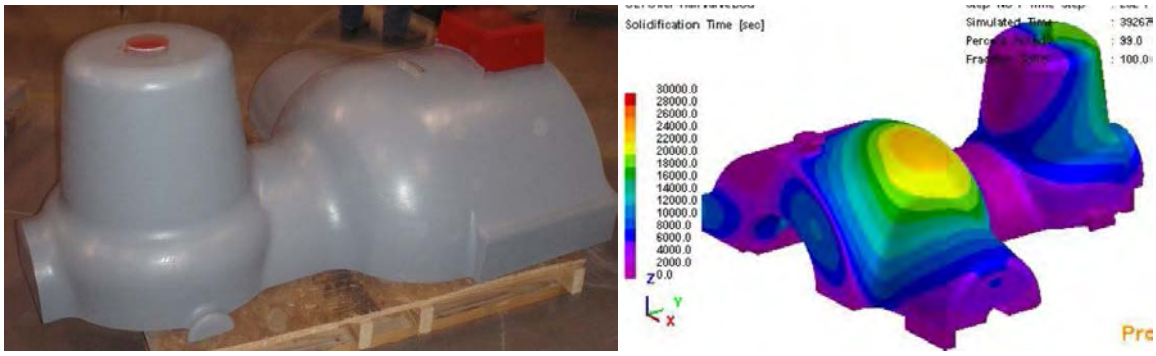

Figure 6. Foundry Casting Design (left) and Solidification Simulation (right) for Half-Valve Body

Figure 7. Pouring of the Haynes 282 half-valve body after deslagging with covered ladles ensuring targeted pouring temperatures and times (17,000 lb pour weight)

Figure 8. Final Haynes 282 casting during liquid penetrate testing (LPT)

Overall, this task had numerous major scale-up successes which overcame the technical challenges on developing the processing and data for developments on the scale of 3 orders of magnitude in size. These successes included:

- Demonstration of the world's largest sand casting of alloy Haynes 282
    - Excellent through thickness properties achieved
    - Developed unique casting modeling tools to enable direct application to future design needs
- Engaged multiple US based suppliers in casting both Haynes 282 and Nimonic 263
- Showed that no compositional changes were required to achieve excellent cast properties
- Developed and validated unique computationally designed heat-treatments to ensure homogenization (and no cracking during post-casting heat-treatment)

Task 5: Superalloy Casting Weld Repair Technology Development

The objective of this task was to produce and characterize repair welds in a casting alloy suitable for the casing using a weld filler material similar to the casing alloy. Six plates of Haynes 282 (H282) and five plates of alloy 263 (H263) each approximately 2x4x5 inches were poured by NETL-Albany. Some casting defects were identified and marked on the castings. The pieces were shipped to Arc Applications (York, PA) for machining and welding. The machining was performed to avoid the defect areas of the casting and the set-up is shown in Figure 9. Successful hot-wire TIG welds were made with matching Haynes 282 and 263 filler metals in the castings. Short-term tensile, low cycle fatigue, and short-term creep-rupture testing was conducted on both materials with acceptable behavior. Some plates were sent to ORNL for detailed microstructural characterization and long term creep testing of the specimens. The short-term welds tests from small plates behaved as expected without any detrimental results, but the welds in the Haynes 282 showed some areas along the fusion with small cracks [100-300 micrometers]. However, cross-weld creep rupture tests all failed in the base metal or weld metal and not in the heat-affected zone suggesting these small incidences of cracking are not critical to long-term performance of the overall structure.

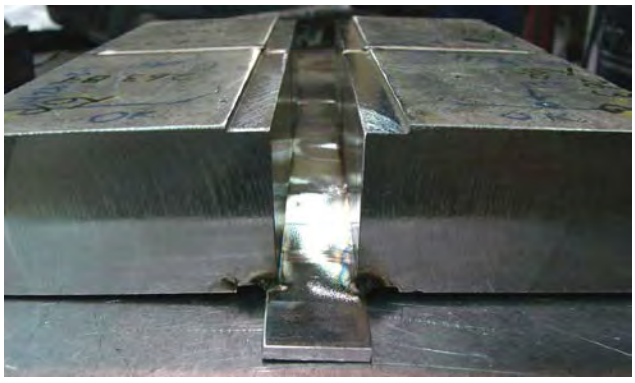

Figure 9. Cast plate welding set-up

Task 6: Process Development and Characterization of a Casing-Pipe Weld

The goal of this task was to make butt welds of a prototypical main steam line pipe to a cast casing alloy. Based on input from the A-USC Steam Boiler Consortium, an Inconel 740H pipe was selected as the likely main steam piping and a 3.5” wall thickness pipe section was obtained. A successful valve body was cast in Q4/2014 and was subsequently homogenized and heat treated to full Haynes 282 properties in Q1/Q2 2015 (Task 4). A section of the casting was cut from the main casting for a pipe-cast welding. Figure 10 show the casting pipe extracted from the large casting for the cast – pipe weld trial.

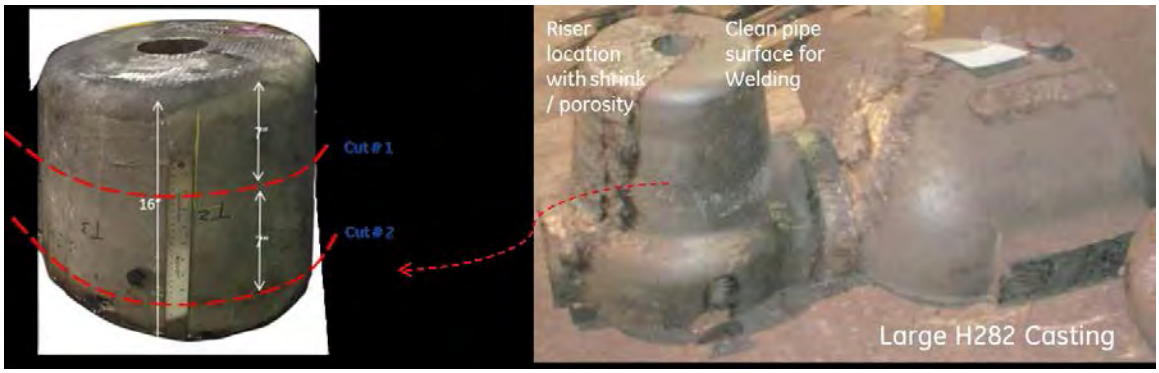

Figure 10: Extraction location from the large Haynes 282 casting for the pipe to casting trial.

Successful weld were completed between H282 cast and Inconel 740H pipe using the hot-wire TIG process with Haynes 282 filler metal. Original work on smaller welds showed Inconel 740H filler metal was also acceptable. Figure 11 shows the design of the weld joint and figure 12 shows a cross-section of the weld joint after successful welding. The casting was fully heated and machined during Q1/Q2 2015, with the project officially ending ion 9/30/15. Further property tests will be conducted by ORNL outside the scope of this project.

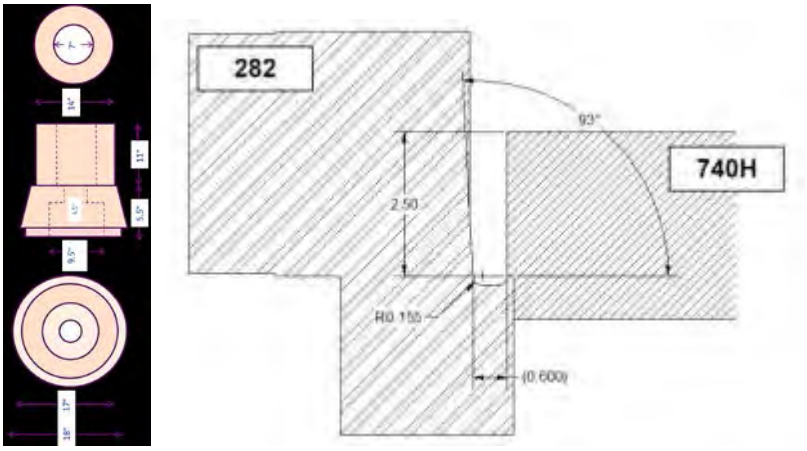

Figure 11: Dimensions and joint design for the Haynes 282 casting to Inconel 740H piping weld

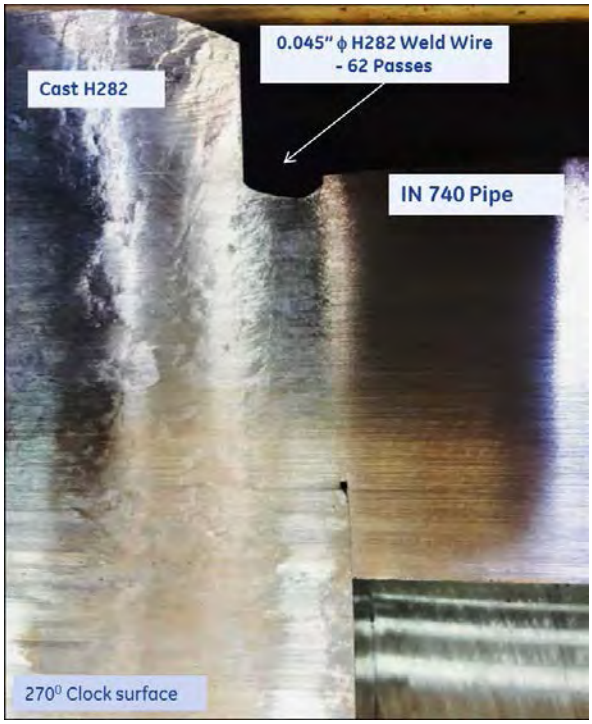

Figure 12: Close-up image of successful Inconel 740H pipe to Cast 282 weld

Task 7: Engineering and Economic Analysis of an A-USC Pulverized Coal Power Plant with and without Post-Combustion Carbon Capture

The goal of this task was to evaluate the economics and performance of two A-USC PC power plants:

- Case 1 is a conventionally configured A-USC PC power plant with state-of-the-art emission controls, but without CO_2 removal.
- Case 2 adds a post-combustion carbon capture (PCC) system to the plant of Case 1, using the design and heat integration strategies from EPRI's 2015 report, "Best Integrated Coal Plant." The capture design basis for this case is "partial," to meet EPA's proposed New Source Performance Standard, which was initially proposed as 500 kg-CO_2/MWh (gross) or 1100 lb-CO_2/MWh (gross), but modified in August 2015 to 636 kg-CO_2/MWh (gross) or 1400 lb-CO_2/MWh (gross). Both standards were examined.

This task successfully drew upon the collective experience of consortium members, with EPRI and General Electric leading the study. General Electric provided the steam cycle analysis as well as the steam turbine design and cost estimating. EPRI performed integrated plant performance analysis using EPRI's PC Cost model.

Prior to evaluating both cases, a review was conducted of previous studies by other consortium members as well as other international A-USC program. There exists no consensus as to the optimum A-USC steam conditions in terms of pressure. Using the EPRI economic tools and GE's steam cycle balances, an initial study was conducted where the capital cost increase for each operating pressure above 242 bar (3515 psia) was estimated, and compared to the efficiency improvement. The results indicate that relative to a 242 bar (3515 psia) unit, the cost increase of the 294 bar (4265 psia) unit was approximately $350,000 per Btu/kWh. The cost increase of the 346 bar (5015 psia) unit was approximately $650,000 per Btu/kWh more than the 242 bar (3515 psia) case. Previous studies and recent commercial experience have shown that a 1 Btu/kWh of heat rate improvement is valued by U.S. utilities in the range of $50,000 to $150,000. As a result, these cost increases are higher than what the U.S. utility industry would traditionally pay for improvements in heat rate. Therefore, it was decided to use the 242 bar (3515 psia) steam cycle as the basis for Case 1.

Burning Powder River Basin (PRB) coal, the Case 1 (Table 1) configuration has an estimated efficiency of 41.4% on a higher heating value (HHV) basis. The arrangement of the boiler in PC Cost for this case is based on a "traditional" boiler configuration. Using on these assumptions, the plant in Case 1 has a capital cost of $2,933/kW and a levelized cost of electricity (LCOE) of $84.70/MWh. As part of this research, it was found that an A-USC steam turbine was approximately two times the cost of a comparable (on a MW basis) state-of-the-art USC steam turbine due to the use of nickel-based alloys in the high pressure (HP) and intermediate pressure (IP) parts of the turbine. However, as will be discussed this cost increase is relatively minor compared to the cost of the main steam and hot-reheat piping systems.

Case 2 (Table 1) added a near term "advanced" solvent for CO_2 removal. The plant also included a high degree of heat integration to maximize the net power output while meeting CO_2 emissions regulations. With this design approach, for a proposed emission standard of 500 kg-CO_2/MWh (1100 lb-CO_2/MWh), plant efficiency dropped by only 2.5 percentage points to 38.9% (HHV basis). The capital cost of the A-USC plant increased by only 8%, but on a $/kW (net) basis, the cost increased to $3,370/kW (a 15% increase) due to the decrease in net power. The LCOE with CO_2 removal increased to $100.20/MWh.

Two weeks prior to the completion of the project, President Obama and the EPA released the Clean Power Plan. Under this plan, the CO_2 emission rate for a new coal fired power plant was increased from 500 kg-CO_2/MWh (1100 lb-CO_2/MWh) to 636 kg-CO_2/MWh (1400 lb-CO_2/MWh). This improved the Case 2 plant efficiency to 40.3% (HHV) or 1.1 percentage points below the "base" AUSC plant with no carbon capture. The capital cost was estimated to be $3,190/kW, and the LCOE was estimated to be $93.30/MWh – an increase of approximately 10% above the Case 1 AUSC power plant.

This project confirmed other studies which showed A-USC is approximately 10% higher in capital cost compared to a USC unit. A significant contributor to the higher cost is the long main and reheat steam piping lines, which would be fabricated from nickel-based alloys. This has led the power industry to respond with several innovative boiler concepts which may bring the cost of an A-USC plant into parity with an equivalently sized USC plant. Furthermore, the study (which only considered a traditional boiler design and turbine arrangement) clearly showed that when partial carbon capture and storage are considered, the A-USC plant has a lower LCOE compared to USC because less CO_2 is produced so less needs to be captured. This is shown in Figure 13 where the A-USC plant of equivalent CO2 emission has a lower LCOE compared to a USC unit of the same electrical output.

Table 1. Case Comparison for A-USC Techno-Economic Study (SI Units)

Description	No Carbon Capture	500 kg CO_2/MWh	635 kg CO_2/MWh
Feedwater heaters	Five LP, deaerator, three HP, topping desuperheater		
Feed pump drive	Motor		
Cooling system	Mechanical draft cooling tower		
Emission controls	SCR, ESP, Wet FGD, and $CaBr_2$ injection into the furnace for NO_x, particulate, sulfur, and mercury control		
Throttle conditions	242 bar/732°C/760°C	242 bar/732°C/760°C	242 bar/732°C/760°C
Main steam flow	1,818,000 kg/h	1,818,000 kg/h	1,818,000 kg/h
Hot reheat flow	1,563,000 kg/h	1,563,000 kg/h	1,563,000 kg/h
Condenser flow	1,412,000 kg/h	1,440,000 kg/h	1,186,000 kg/h
Condenser pressure	6.7 kPa	6.7 kPa	6.7 kPa
Final feedwater temp	304°C	304°C	304°C
Steam to PCC System	N/A	161,000 kg/h	71,700 kg/h
Gross plant output, kW	825,000	809,071	818,438
Auxiliary load, kW	70,801	100,742	84,060
Net plant output, kW	754,199	708,329	734,338
Net plant heat rate	8,698 kJ/kWh	9,261 kJ/kWh	8,933 kJ/kWh
Net plant efficiency, % (HHV)	41.4	38.9	40.3
Plant fuel consumption	338,000 kg/hr	338,000 kg/hr	338,000 kg/hr
CO_2 emission without PCC	596,000 kg/hr	393,000 kg/hr	506,200 kg/hr
CO_2 emission without PCC	722 kg/MWh, gross basis	500 kg/MWh, EPA gross basis	635 kg/MWh, EPA gross basis
Total Capital Cost, $(000)	$2,212,000	$2,379,000	$2,344,000
Total Capital Cost, $/kW	$2,933	$3,370	$3,190
Total Operating Costs, $(000)/yr	$448,410	$498,067	$480,231
LCOE, $/MWh	$84.70	$100.20	$93.30

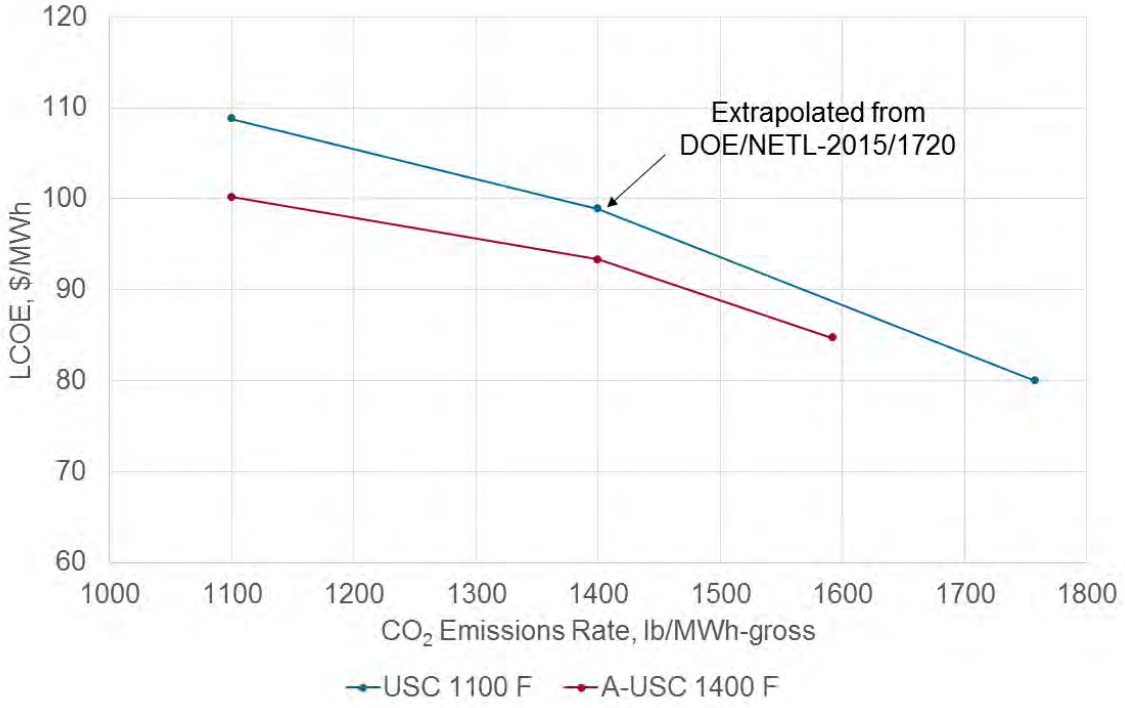

Figure 13. Comparison between the LCOE of an A-USC and USC plant as a function of CO_2 emission with and without partial carbon capture and storage (CCS). A-USC is shown to be more favorable economically for a given CO_2 emission target using partial CCS.

3. Task 3 - Materials for Non-Welded Rotors, Buckets, and Bolting

Note: this section contains its own numbering and table of contents

ABSTRACT

The primary objective of the task was to characterize the materials suitable for mechanically coupled rotor, buckets and bolting operating with an inlet temperature of 760°C (1400°F). A previous study DOE-FC26-05NT42442, identified alloys such as Haynes®282®, Nimonic 105, Inconel 740, Waspaloy, Nimonic 263, and Inconel 617 as potential alloys that met the requirements for the necessary operating conditions. Of all the identified materials, Waspaloy has been widely utilized in the aviation industry in the form of disk and other smaller forgings, and sufficient material properties and vendor experience exist, for the design and manufacture of large components. The European program characterizing materials for A-USC conditions are evaluating Nimonic 263 and Inconel 617 for large components. Inconel 740 has been studied extensively as a part of the boiler consortium and is code approved. Therefore, the consortium focused efforts in the development of material properties for Haynes®282® and Nimonic 105 to avoid replicative efforts and provide material choices/trade off during the detailed design of large components.

Commercially available Nimonic 105 and Haynes®282® were evaluated for microstructural stability by long term thermal exposure studies. Material properties requisite for design such as tensile, creep / rupture, low cycle fatigue, high cycle fatigue, fatigue crack growth rate, hold-time fatigue, fracture toughness, and stress relaxation are documented in this report.

A key requisite for the success of the program was a need to demonstrate the successful scale up of the down-selected alloys to large components. All property evaluations in the past were performed on commercially available bar/billet forms. Components in power plant equipment such as rotors and castings are several orders in magnitude larger and there is a real need to resolve the scalability issue. Nimonic 105 contains high volume fraction γ' [>50%], and hence the alloy is best suited for smaller forging and valve internals, bolts, smaller blades. Larger Nimonic 105 forgings, would precipitate γ' during the surface cooling during forging, leading to surface cracks. The associate costs in forging Nimonic 105 to larger sizes [hotter dies, press requirements], were beyond the scope of this task and not investigated further. Haynes®282® has 20 - 25% volume fraction γ' and was a choice for large components, albeit untested.

A larger ingot diameter is pre-requisite for a larger diameter forging and achieves the "typically" accepted working ratio of 2.5-3:1. However, Haynes®282® is manufactured via a double melt process [VIM-ESR] limited by size [<18-16" diameter], which limited the maximum size of the final forging. The report documents the development of a 24" diameter triple melt ingot, surpassing the current available technology. A second triple melt ingot was manufactured and successfully forged into a 44" diameter disk. The successful developments in triple melting process and the large diameter forging of Haynes®282® resolved the scalability issues and involved the first of its kind attempt in the world for this alloy.

The complete characterization of Haynes®282® forging was performed and documented in this report. The dataset from the commercially available Haynes®282® [grain size ASTM 3-4] and the finer grain size disk forging [ASTM 8-9] offer an additional design tradeoff to balance creep and fatigue during the future design process.

TABLE OF CONTENTS

ABSTRACT 24
FIGURES 27
TABLES 30
PROJECT BACKGROUND & INTRODUCTION 31
EVALUATION OF NIMONIC 105 33
EVALUATION OF COMMERCIALLY AVAILABLE HAYNES®282® 48
FORGEABILITY OF COMMERCIALLY AVAILABLE HAYNES®282® FOR SMALLER FORGINGS 53
TRIPLE MELTING OF HAYNES®282® FOR LARGER FORGING 58
LARGE FORGING OF HAYNES®282® 64
CHARACTERIZATION OF THE LARGE FORGING OF HAYNES®282® 70
CONCLUSIONS 80

FIGURES

Figure 1: Typical γ' precipitate size in Nimonic 105 33
Figure 2 Typical γ' precipitate size in Nimonic 105 from 8.75" diameter billet 34
Figure 3: TEM image identifying $Cr_{23}C_6$ as primary carbide phase in N105 34
Figure 4: Tensile strength in Nimonic 105 after a 1 & 2 year thermal exposure at 1425°F (774°C) [Longitudinal Orientation] 35
Figure 5: Tensile strength in Nimonic 105 after a 1 & 2 year thermal exposure at 1425°F (774°C) [Transverse Orientation] 36
Figure 6: 0.2% Yield Strength in Nimonic 105 after a 1 & 2 year thermal exposure at 1425°F (774°C) *[Longitudinal Orientation]* 36
Figure 7: 0.2% Yield Strength in Nimonic 105 after a 1 & 2 year thermal exposure at 1425°F (774°C) [*Transverse Orientation*] 37
Figure 8: ..... % Elongation in Nimonic 105 after a 1 & 2 year thermal exposure at 1425°F (774°C) [*Longitudinal Orientation*] 38
Figure 9: ..... % Elongation in Nimonic 105 after a 1 & 2 year thermal exposure at 1425°F (774°C) [*Transverse Orientation*] 38
Figure 10: % RA in Nimonic 105 after a 1 & 2 year thermal exposure at 1425°F (774°C) [*Longitudinal Orientation*] 39
Figure 11: % RA in Nimonic 105 after a 1 & 2 year thermal exposure at 1425°F (774°C) [*Transverse Orientation*] 39
Figure 12: Toughness in Nimonic 105 after a 1 & 2 year thermal exposure at 1425°F (774°C) 40
Figure 13: Alternating stress with cycles for Nimonic 105 at various A ratios 41
Figure 14: da/dn versus ΔK for Nimonic 105 at various temperatures & load ratio's. 42
Figure 15: Figure showing fatigue threshold as a function of load ratio and temperature for Nimonic 105 43
Figure 16: Larson-Miller Parameter (LMP) – Rupture Stress plot of Nimonic 105 43
Figure 17: Plots of creep rate as a function of time 44
Figure 18: MCR [min. creep rate] versus time to rupture for Nimonic 105 44
Figure 19: LMP plot of time to reach 0.2% Strain and Stress [Ksi] 45
Figure 20: LMP plot of time to reach 1.0% Strain and Stress [Ksi] 45
Figure 21: Dominant Creep Mechanism in N105 47
Figure 22: Typical γ' precipitate size of Haynes®282® [67 ± 15.5 nm]. (From NETL) 48
Figure 23: TEM image identifying $Cr_{23}C_6$ as a carbide phase in Haynes®282®. (From NETL) 48
Figure 24: Tensile strength in Haynes®282® after a 1 & 2 year thermal exposure at 1425°F (774°C) [*Longitudinal Orientation*] 49
Figure 25: 0.2% Yield Strength in Haynes®282® after a 1 & 2 year thermal exposure at 1425°F (774°C) [*Longitudinal Orientation*] 49
Figure 26: % Elongation in Haynes®28²® after a 1 & 2 year thermal exposure at 1425°F (774°C) [*Longitudinal Orientation*] 50

Figure 27: % RA in Haynes®28²® after a 1 & 2 year thermal exposure at 1425°F (774°C) [*Longitudinal Orientation*].....50
Figure 28: KQ or Conditional Fracture toughness of Haynes®282® after 1 & 2 year thermal exposure at 1425°F (774°C) 51
Figure 29: Figure showing alternating stress and cycles to failure at various A ratios 52
Figure 30: Debit in Hold Time Fatigue of Haynes®282® 52
Figure 31: Flow Stress curves of Haynes®282® at 1600°F (871°C) 54
Figure 32: Flow Stress curves of Haynes®282® at 1700°F (927°C) 54
Figure 33: Flow Stress curves of Haynes®282® at 1800°F (982°C) 55
Figure 34: Flow Stress curves of Haynes®282® at 1900°F (1038°C) 55
Figure 35: Flow Stress curves of Haynes®282® at 2000°F (1093°C) 56
Figure 36: Pictures showing the 18” VIM / 22” ESR and the final 24” VAR Ingot. 59
Figure 37: Variation in VAR Melt range [lbs/min] for marco evaluation 60
Figure 38: Representative microstructures of 24” ingot EX0045PW after homogenization 61
Figure 39: EX0045PW was forged into 8” diameter for macro-segregation evaluation 61
Figure 40: Representative microstructures of ingot EX0045PW after hot working to the 8” diameter bars (a) Surface (b) mid-radius and (c) center locations.61
Figure 41: Representative macro slices from EX0045PW and etched with Canada’s Etch to reveal segregation tendencies.....62
Figure 42 Second ingot EX0046PW billetized in (a) as forged condition and (b) after surface grinding to final diameter.....62
Figure 43: Second ingot EX0046PW slice revealed no indication of segregation at (a) Head and (b) Toe [2]. Slices shown for microstructures.....63
Figure 44: Representative micro-graphs showing starting microstructure from the 20” diameter EX0046PW ingot head 63
Figure 45: Coarsening studies of starting material exposed at 1800°F (982°C) at various times.....65
Figure 46: Coarsening studies of starting material exposed at 1900°F (1038°C) at various times.....66
Figure 47: Grain size map of a subscale forging forged in two operations of 2:1 reduction ratio each. 67
Figure 48: Grain size map of a subscale forging forged in a straight 4:1 reduction ratio. 68
Figure 49: Demonstration of a large diameter Haynes®282® forging 69
Figure 50: EBSD image of the grain size obtained in the Haynes®282® forging [Courtesy ORNL]. Typical grain size was ASTM 8-9, ALA ASTM 4.....70
Figure 51: UTS as a function of temperature from Haynes®282® forged disk....71
Figure 52: 0.2%YS as a function of temperature from Haynes®282® forged disk 71
Figure 53: % Elongation a function of temperature from Haynes®282® forged disk 72

Figure 54: % RA a function of temperature from Haynes®282® forged disk.....72
Figure 55: High cycle fatigue data from Haynes®282® disk forging [A=INF].....73
Figure 56: High cycle fatigue data from Haynes®282® disk forging [A=1] 73
Figure 57: High cycle fatigue data from Haynes®282® disk forging [A= 0.5] 74
Figure 58: Low cycle fatigue data from Haynes®282® disk forging compared to commercially available Haynes®282® billet/bar.....74
Figure 59: Hold Time Haynes®282® disk forging.....75
Figure 60: Fracture toughness of Haynes®282® disk forging compared to commercially available Haynes®282® billet/bar.....76
Figure 61: Fatigue crack growth rates in Haynes®282® disk forging 77
Figure 62: Fatigue threshold in Haynes®282® disk forging as a function of R ratio at various temperatures. 78
Figure 63: LMP – Rupture Stress plot of Haynes®282® disk forging 79

TABLES

Table 1: Grain size after compression tests and exposing the pieces at various temperatures for 2 hours of Hayne®282®.....57
Table 2: Chemistries obtained from the Hayne®282® ingots 60
Table 3: Creep-Rupture data obtained from Haynes®282®disk 78

LIST OF ACRONYMS AND ABBREVIATIONS

TEM……Transmission Electron Microscope
γ'……..Gamma Prime
UTS……Ultimate Tensile Strength
0.2YS……0.2% Yield Strength
% Elongation……% Elongation to failure
%RA……...% Reduction in Area
LMP……Larson-Miller Parameter; is a function of time and temperature in the form T(C + log t); where T is the temperature in degrees R, C is a constant and t is the time in hours
KQ……..Conditional Fracture Toughness
VIM……Vacuum Induction Melting
ESR……Electrode Slag Remelting
VAR……Vacuum Arc Remelting
A Ratio……Ratio of the amplitude of the stress in the cycle to the mean stress in the cycle
R Ratio…… Ratio of minimum stress in the cycle to the maximum stress in the cycle

PROJECT BACKGROUND & INTRODUCTION

The overall objective of the project is to contribute to the development of materials technology for use in advanced ultrasupercritical (A-USC) pulverized coal power plants capable of operating with steam up to 760°C (1400°F), 35 MPa (5000 psi). R&D is needed on newly developed materials to lead to a full-scale demonstration, and eventual commercialization, of A-USC power plants. The lack of materials with the necessary fabricability and resistance to creep, oxidation, corrosion and fatigue at the higher steam temperatures and pressures currently limit the adoption of A-USC steam conditions in pulverized coal-fired plants.

A Phase 1 (three year national effort) sponsored by the U.S. Department of Energy (DOE) and the Ohio Coal Development Office (OCDO) was completed in June 2009 and the final report was submitted. The Phase 1 effort was performed under a prime contract with Energy Industries of Ohio (EIO) through a consortium made up of the Electric Power Research Institute (EPRI), Oak Ridge National Laboratory (ORNL) and all of the U.S. domestic turbine manufactures: General Electric, Alstom Power and Siemens Westinghouse. This initial Phase 1 addressed the need to identify and analyze candidate USC turbine materials from the perspective of steam side conditions and pressure ranges to be encountered in A-USC turbines. The Phase 1 effort has accomplished these goals, and a more robust five year Phase 2 effort has just been initiated. This Phase 2 efforts focused on the identified candidate alloys to address specific fabrication abilities, particularly metal casting, of these alloys for use in making components such as casings, housings, valves and ingots. In particular, efforts associated with high nickel alloys will be targeted for developing the specific means of casting these alloys using electric arc AOD (argon-oxygen-decarburization), vacuum and/or pressure casting.

At the completion of Phase 1, Alstom Power and Siemens Corporation withdrew participation due to business reasons. Funding for Phase 2 is now being provided by OCDO and DOE with cost sharing and technical participation from General Electric, Co. and EPRI. Oak Ridge National Laboratory and NETL-Albany Research Center are also participating in the project and are being funded directly by DOE to provide support.

Specific objectives of the Phase 2 effort include conducting more detailed evaluations of the weldability, mechanical properties and reparability of the selected candidate alloys for rotors, casings and valves and to perform scale up studies to establish a design basis for commercial scale components. A

supplemental program funded by the OCDO will undertake supporting tasks such as testing and trials using existing atmospheric, vacuum and developmental pressure furnaces to define specific metal casting techniques needed for producing commercial scale components.

The goal of this task was to continue to develop and assess materials for non-welded rotors, buckets and bolting for the steam turbine. Two potential alloys were considered in Phase 1 of this project and documented in report DE-FC26-05NT42445. The potential alloys that met the requisite creep rupture properties were identified as Nimonic 105 and Haynes 282 (primarily based on creep rupture life of 250,000 hours at 15 Ksi) and LCF life. The primary goal of Phase 2 is twofold;

1) Develop sufficient mechanical property information on nickel-base blade/bolting candidate alloys so preliminary steam turbine design calculations for rotors, buckets and bolts and valve internals can be initiated

2) Analyze the materials under study:

- Understand the effect of environment on fatigue
- Measure long term mechanical property degradation due to high temperature exposure
- Characterize the micro-structure
- Determine strengthening precipitate coarsening behavior
- Identify any deleterious phases that might degrade long term properties

EVALUATION OF NIMONIC 105

Phase 1 of the program [DOE-FC26-05NT42442] characterized material of Nimonic 105 obtained from 2" diameter bar. In this program 8.75" diameter hot finished billet was obtained for testing. The material was heat treated to achieve peak hardness.

Solution Anneal: 2100°F (1149°C) 4 Hours

Age Treatment 1: 1950°F (1066°C) 16 Hours
Age Treatment 2: 1560°F (849°C) 16 Hours

The billet was cut into two additional pieces and placed in a furnace maintained at 1425°F (774°C). The two pieces would provide data on the embrittlement of the material during the long term exposure of this alloy. The National Energy Technology Laboratory (NETL) provided the transmission electron microscope (TEM) analysis of the 2" diameter Nimonic alloy. The primary γ' size was estimated to be in the range of 60 nm [Figure 1].

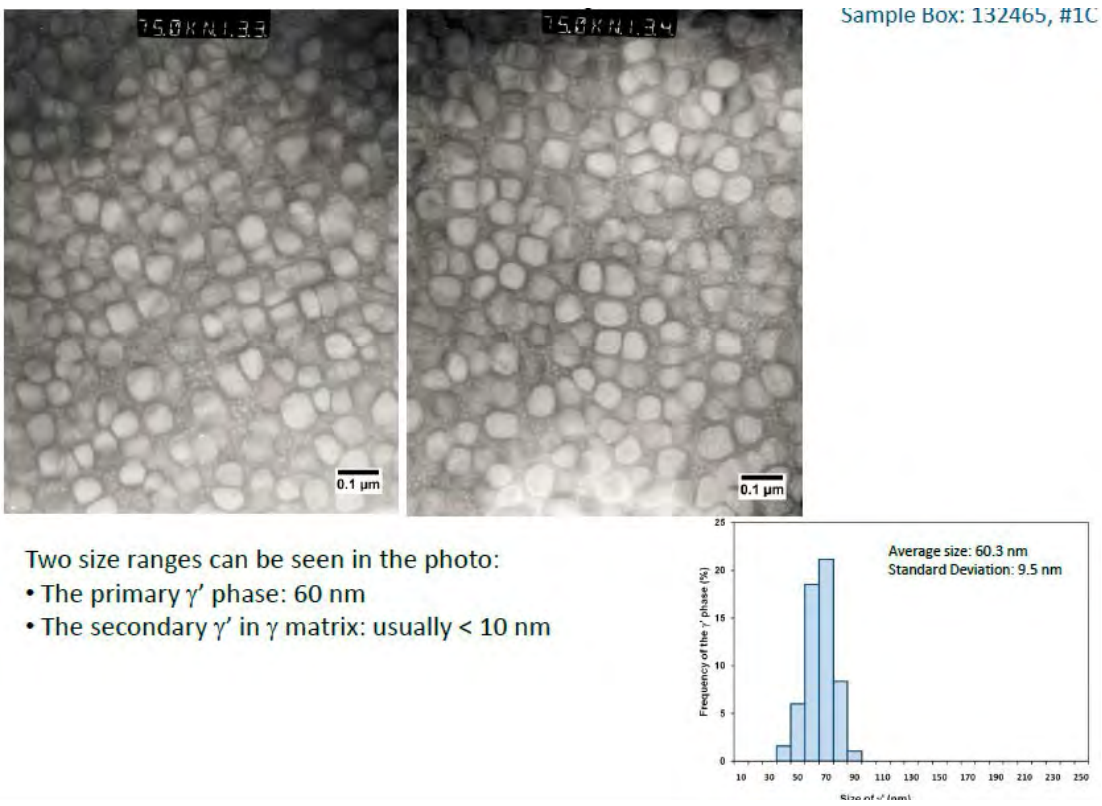

Figure 1: Typical γ' precipitate size in Nimonic 105

Similar TEM analysis was performed by GE Global Research on the starting γ' form the 8.75" diameter billet. The size was double the smaller diameter bar and in the range of 140-150 nm [Figure 2]. Figure 3 shows the presence of $Cr_{23}C_6$ as primary carbide phase in N105 at the grain boundary of Nimonic 105.

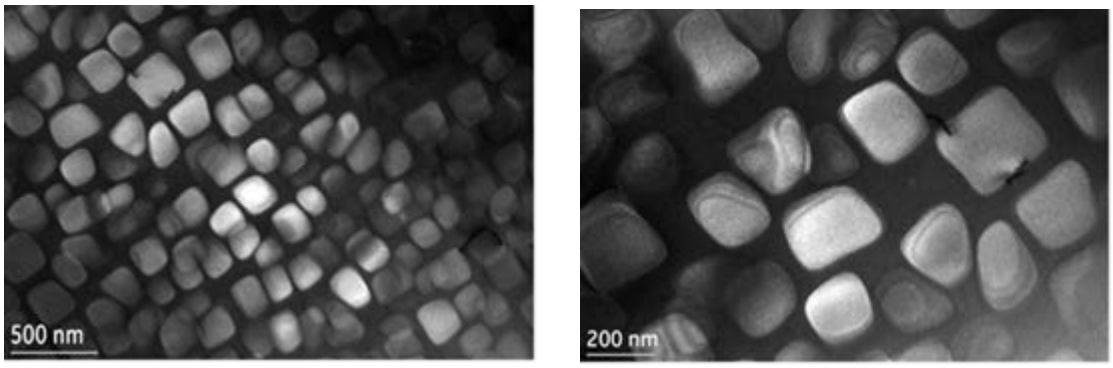

Figure 2 Typical γ' precipitate size in Nimonic 105 from 8.75" diameter billet

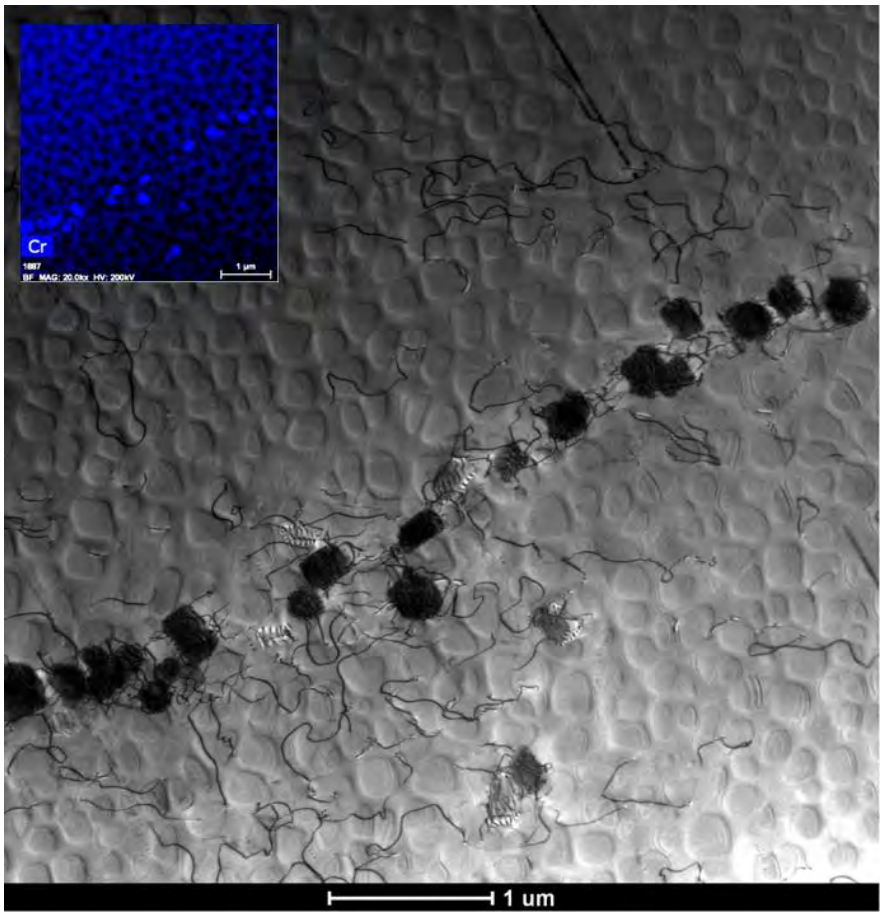

Figure 3: TEM image identifying $Cr_{23}C_6$ as primary carbide phase in N105

Figure 4 through Figure 11 show the properties obtained from Nimonic 105 after a thermal exposure of 1425°F (774°C) for 1 year / 8760 hours and 2 year / 17500 hours. The data consists of a mix of different orientations and is compared against baseline data tests obtained from the Phase 1 report. Based on the dataset Nimonic 105 shows a debit in Elongation and Reduction of Area (RA) after a year of exposure and levels after the initial drop. This is very typical of Nickel based alloys due to the coarsening of γ'. The longitudinal orientation exhibited % Elongation and % RA in excess of acceptable values of 10%.

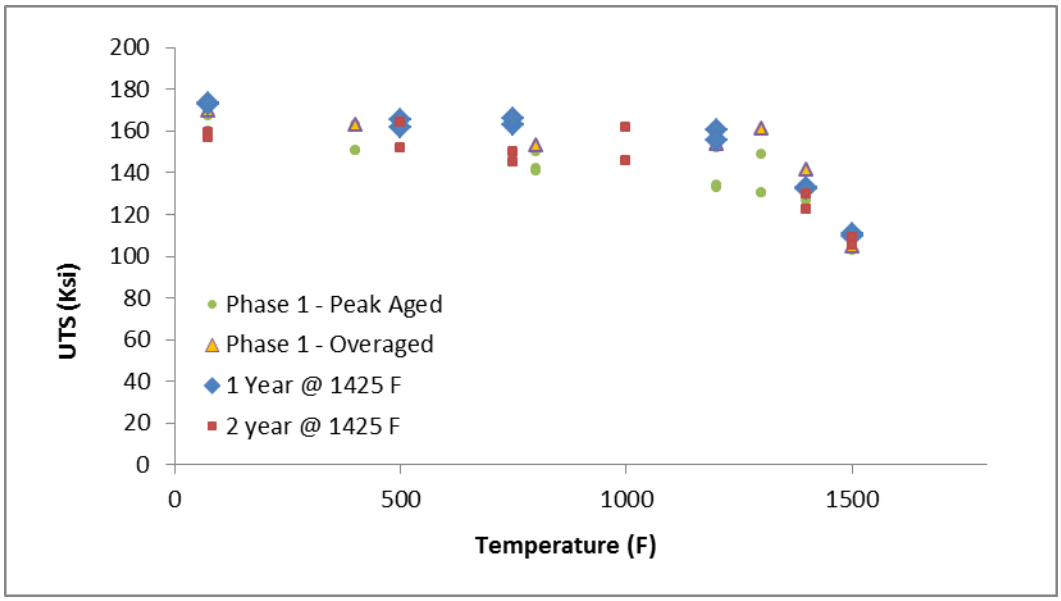

Figure 4: Tensile strength in Nimonic 105 after a 1 & 2 year thermal exposure at 1425°F (774°C) [Longitudinal Orientation]

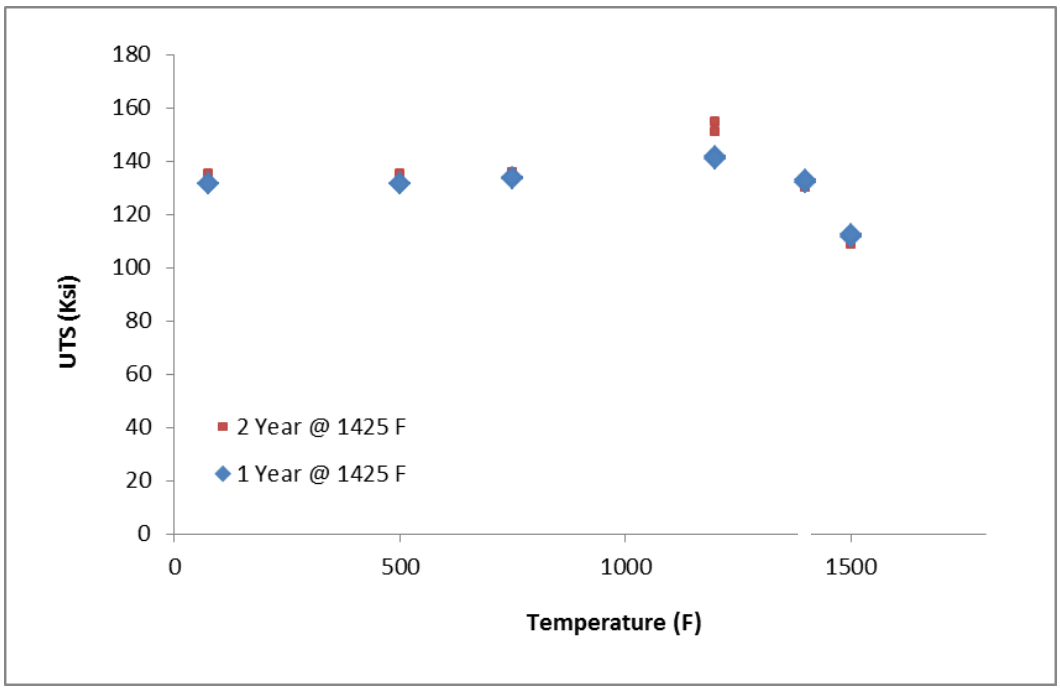

Figure 5: Tensile strength in Nimonic 105 after a 1 & 2 year thermal exposure at 1425°F (774°C) [Transverse Orientation]

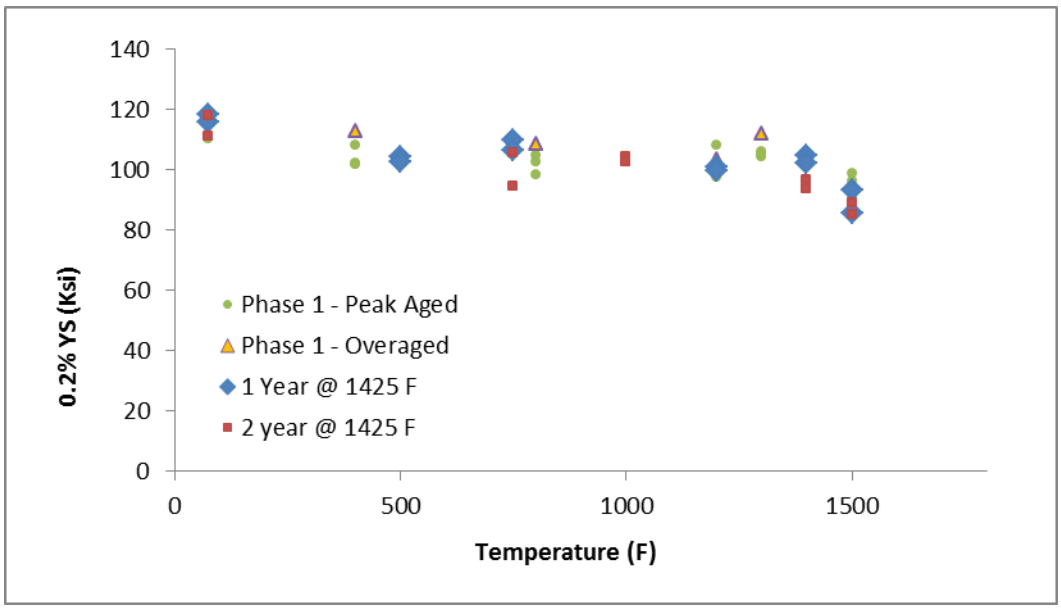

Figure 6: 0.2% Yield Strength in Nimonic 105 after a 1 & 2 year thermal exposure at 1425°F (774°C) *[Longitudinal Orientation]*

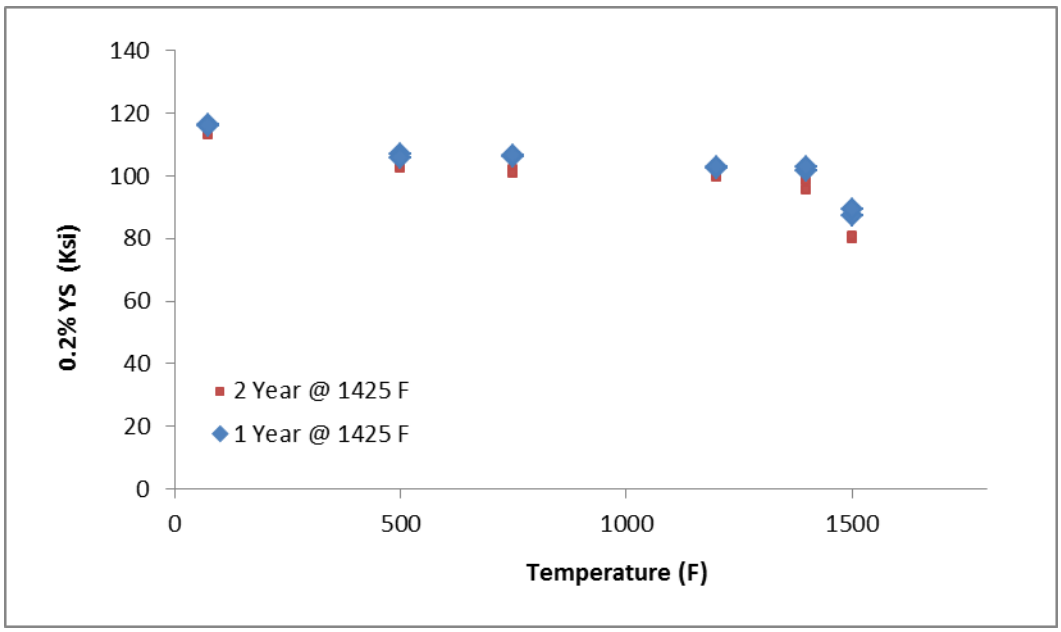

Figure 7: 0.2% Yield Strength in Nimonic 105 after a 1 & 2 year thermal exposure at 1425°F (774°C) [*Transverse Orientation*]

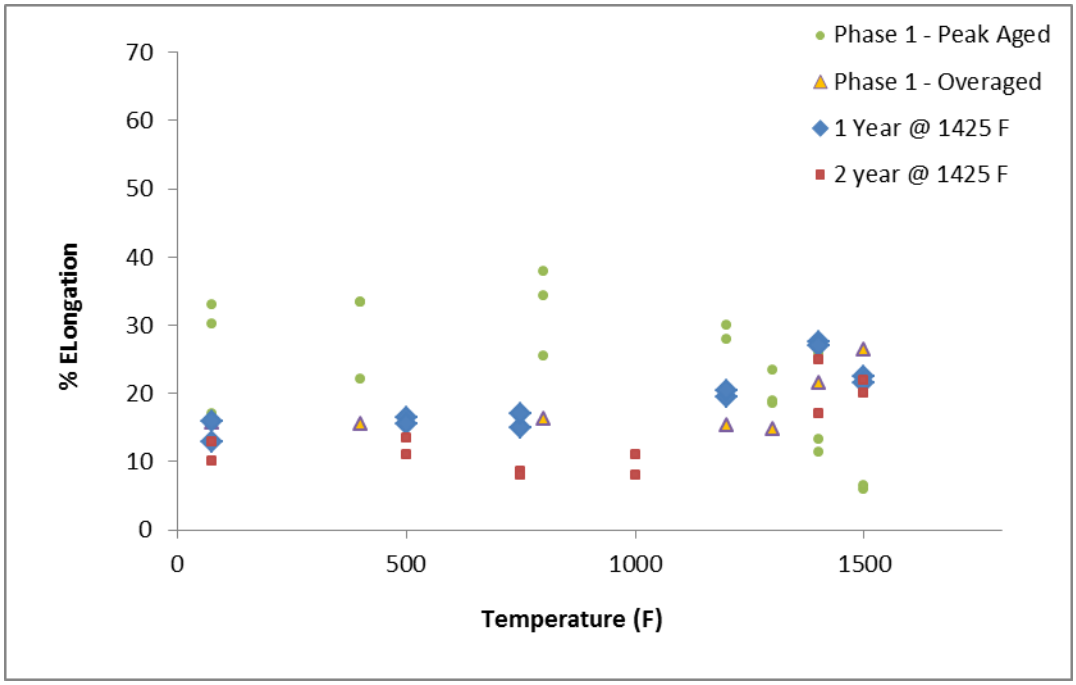

Figure 8: % Elongation in Nimonic 105 after a 1 & 2 year thermal exposure at 1425°F (774°C) [*Longitudinal Orientation*]

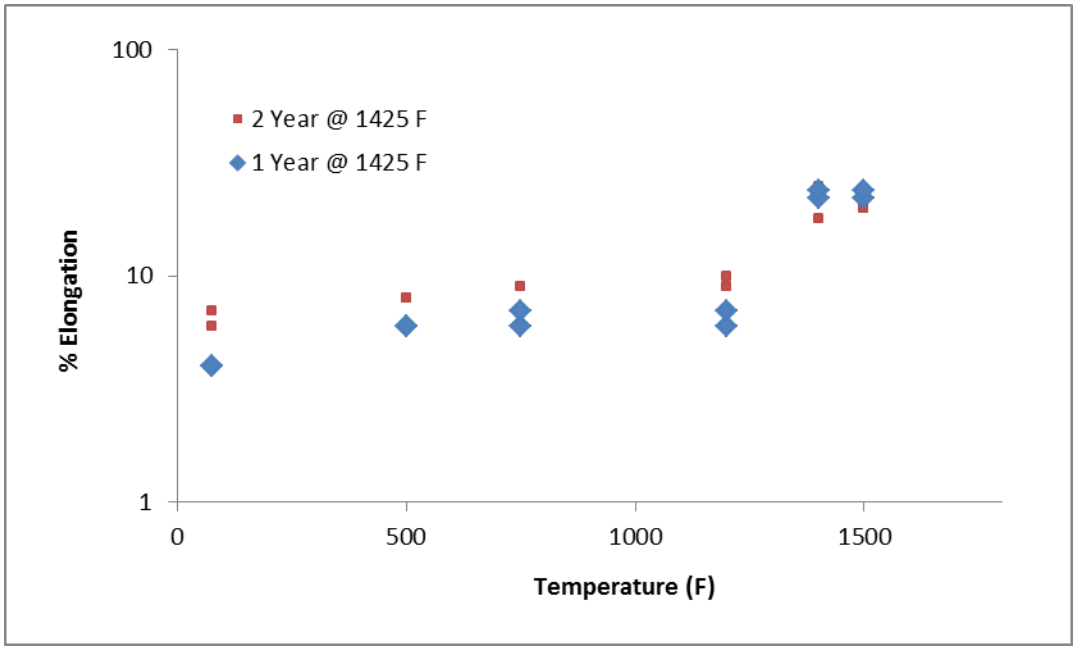

Figure 9: % Elongation in Nimonic 105 after a 1 & 2 year thermal exposure at 1425°F (774°C) [*Transverse Orientation*]

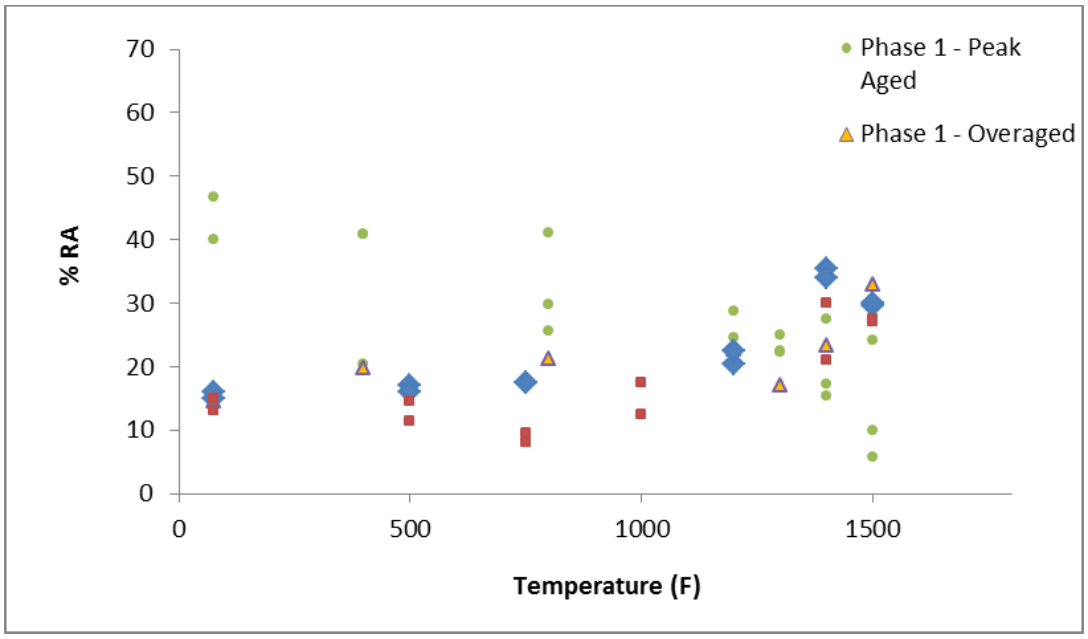

Figure 10: % RA in Nimonic 105 after a 1 & 2 year thermal exposure at 1425°F (774°C) [*Longitudinal Orientation*]

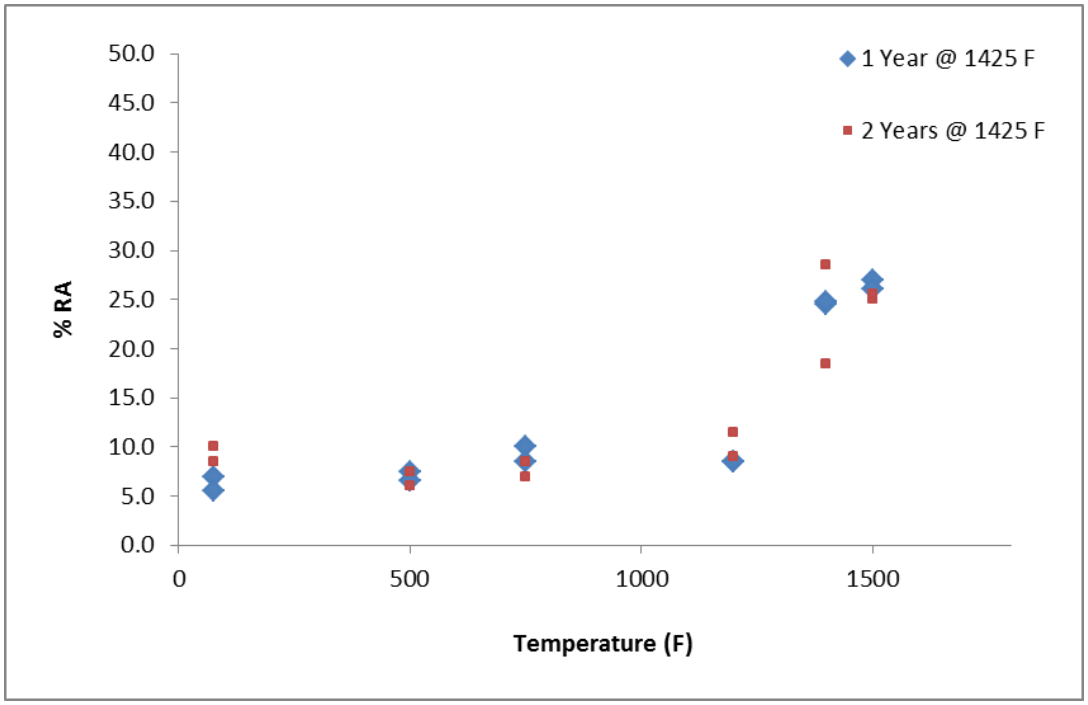

Figure 11: % RA in Nimonic 105 after a 1 & 2 year thermal exposure at 1425°F (774°C) [*Transverse Orientation*]

Multiple specimens were extracted from the bar for fracture toughness testing. The specimens were 0.75" thick [B] and 1.5" Wide [W]. All specimens were side grooved to a depth equal to 20% of the nominal thickness [10% each side]. The

specimens were tested in accordance to ASTM E1820-09. As specimens had a mix of valid and invalid fracture toughness, J1c, Figure 12 plots only the conditional fracture toughness of Nimonic 105 as a function of temperature and thermal exposure. No debit was observed during the thermal exposure of Nimonic 105 over a two year period at 1425°F (774°C).

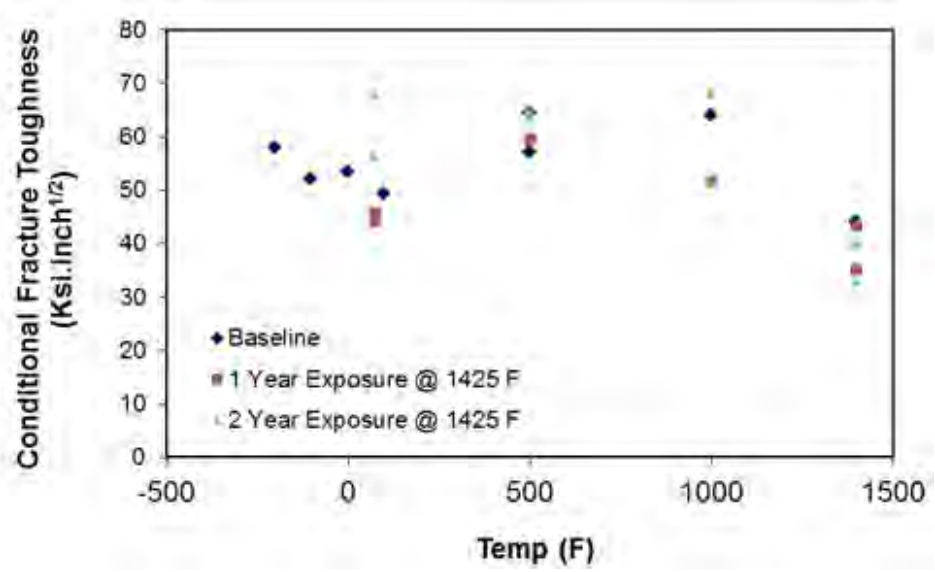

Figure 12: Toughness in Nimonic 105 after a 1 & 2 year thermal exposure at 1425°F (774°C)

Fatigue specimens were machined from the bar [longitudinal orientation only] and subjected to high cycle fatigue tests [in air]. All tests were performed at 1400°F (760°C), 50 Hertz and 10,000,000 cycles runout. Figure 13 shows the plot of alternating stress and cycles to failure for various A ratios.

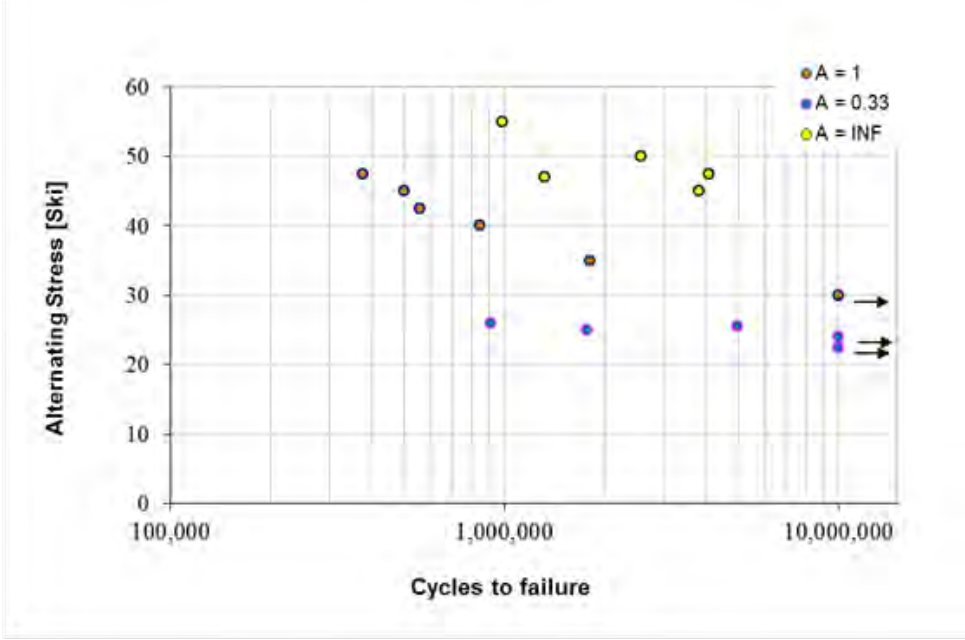

Figure 13: Alternating stress with cycles for Nimonic 105 at various A ratios

Specimens were extracted for the development of fatigue crack growth rates in Nimomic 105 for design intend. All tests were performed in accordance to ASTM

E647-08, Sinusoidal Waveform and 29 Hertz. Figure 14 shows all the tests at 1200, 1300, and 1400°F (649, 704, and 760°C) and various R ratios.

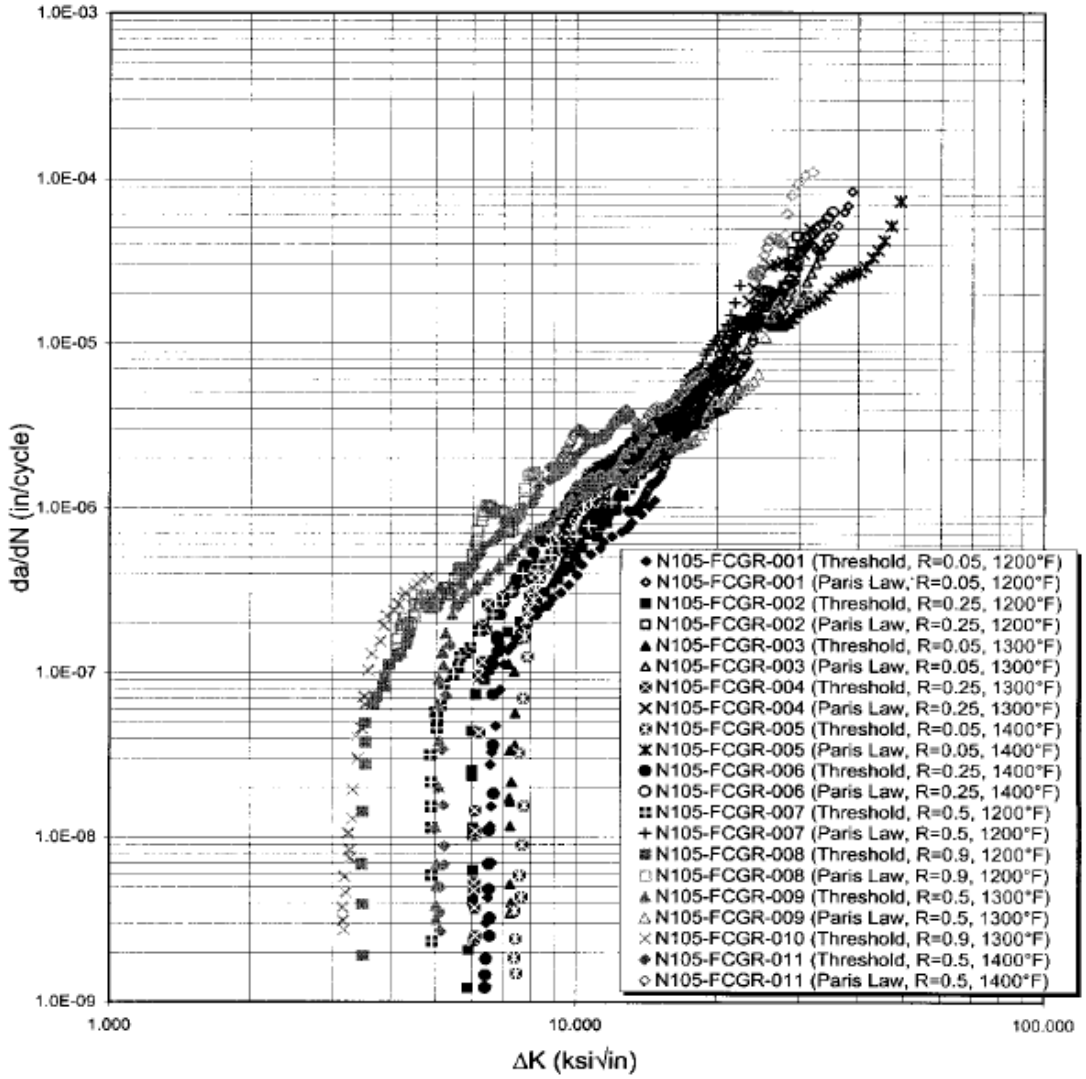

Figure 14: da/dn versus ΔK for Nimonic 105 at various temperatures & load ratio's.

Fatigue threshold data obtained from the tests are documented shown in Figure 15. The difference between the dataset in the 1200 – 1400°F (649 - 760°C) is negligible.

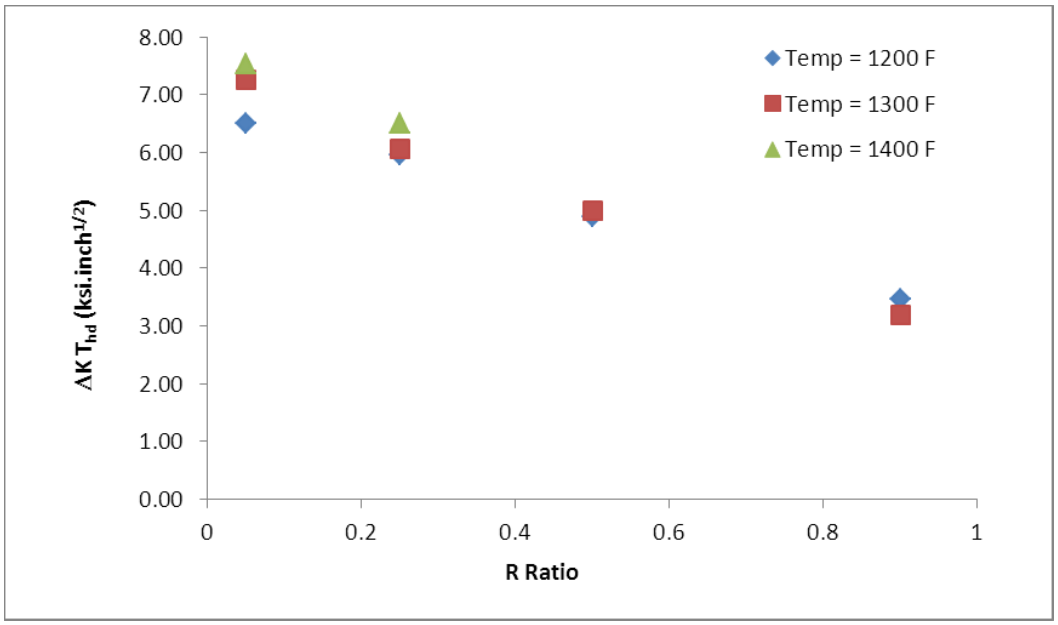

Figure 15: Figure showing fatigue threshold as a function of load ratio and temperature for Nimonic 105

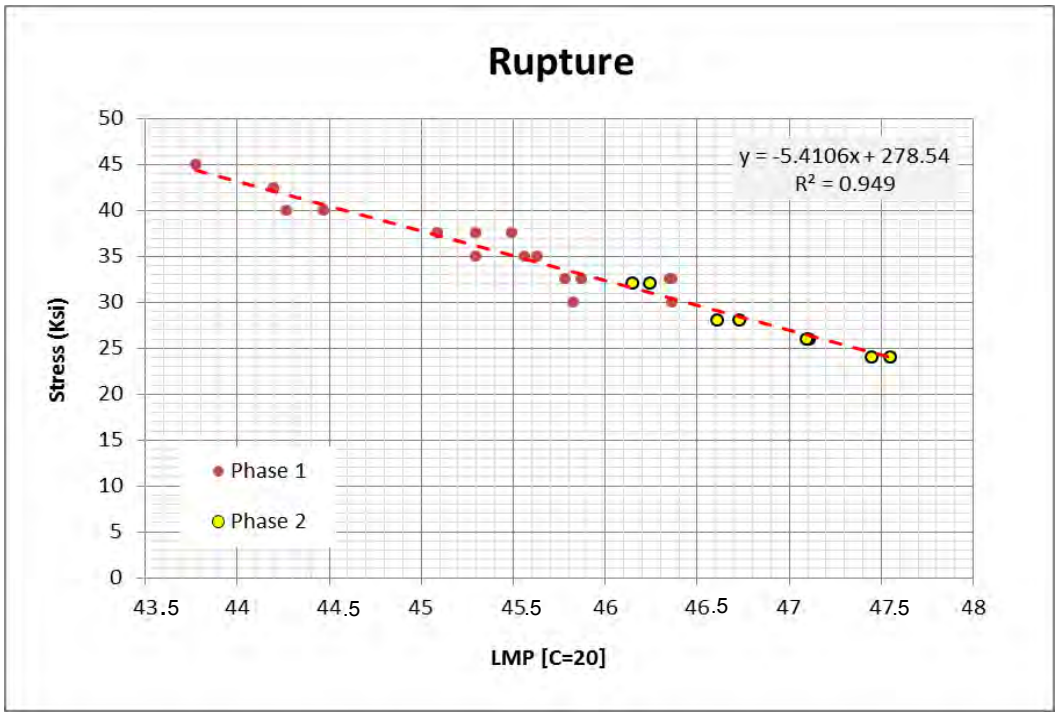

Figure 16: Larson-Miller Parameter (LMP) – Rupture Stress plot of Nimonic 105

Figure 16 shows the rupture data obtained from the long term creep testing of Nimonic 105. The times accumulated ranged from 10,000 – 35,000 hours. The plot also plots the complete dataset obtained from this program and the Phase 1 of the

project**.** Figure 17 plots the strain rate versus time for failure for the specimens tested as a part of this phase. The minimum creep rates obtained from the plot are plotted with time to rupture in Figure 18.

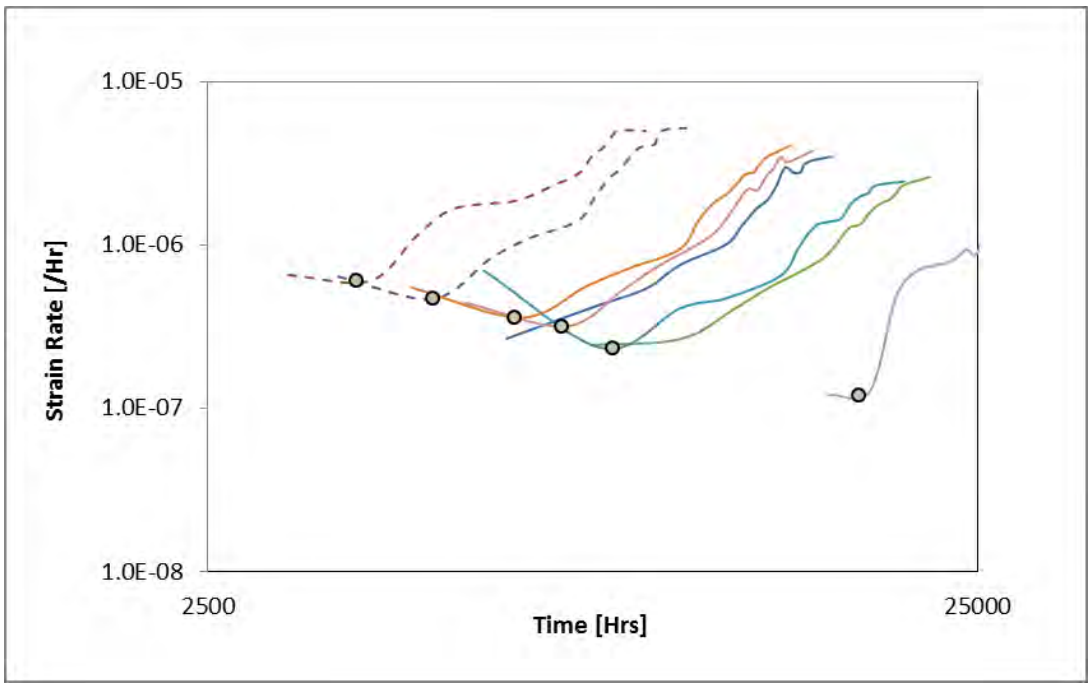

Figure 17: Plots of creep rate as a function of time

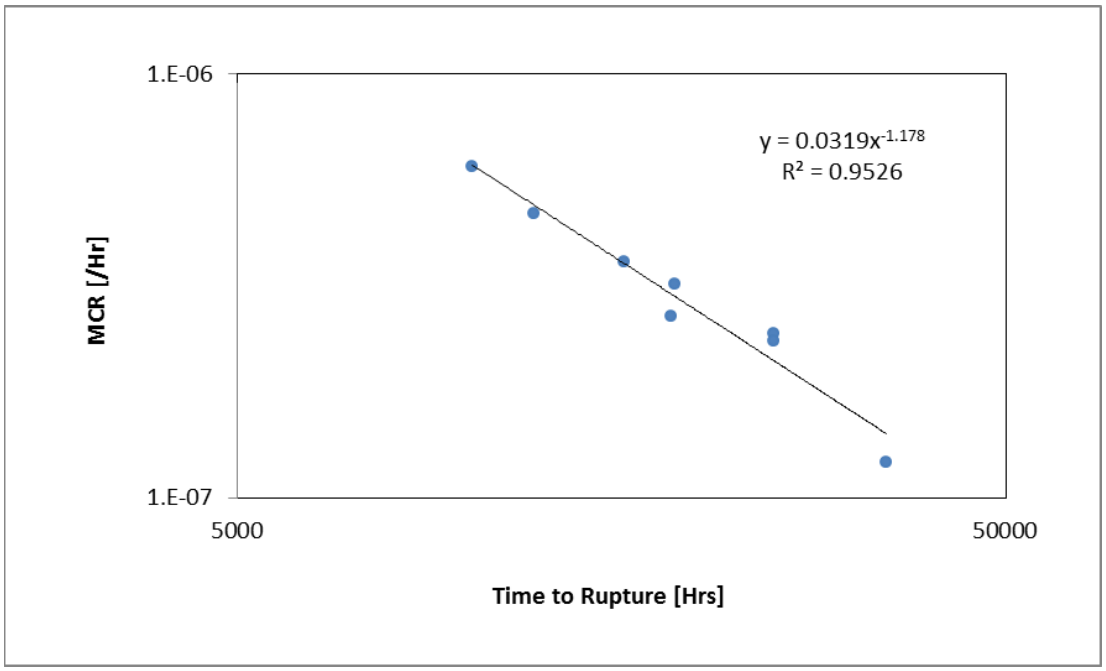

Figure 18: MCR [min. creep rate] versus time to rupture for Nimonic 105

Figure 19 and Figure 20 show the plots of 0.2% creep strain and 1% creep strain in the LMP form. The graphs also include the Phase 1 data as a composite plot covering a broad range of stress.

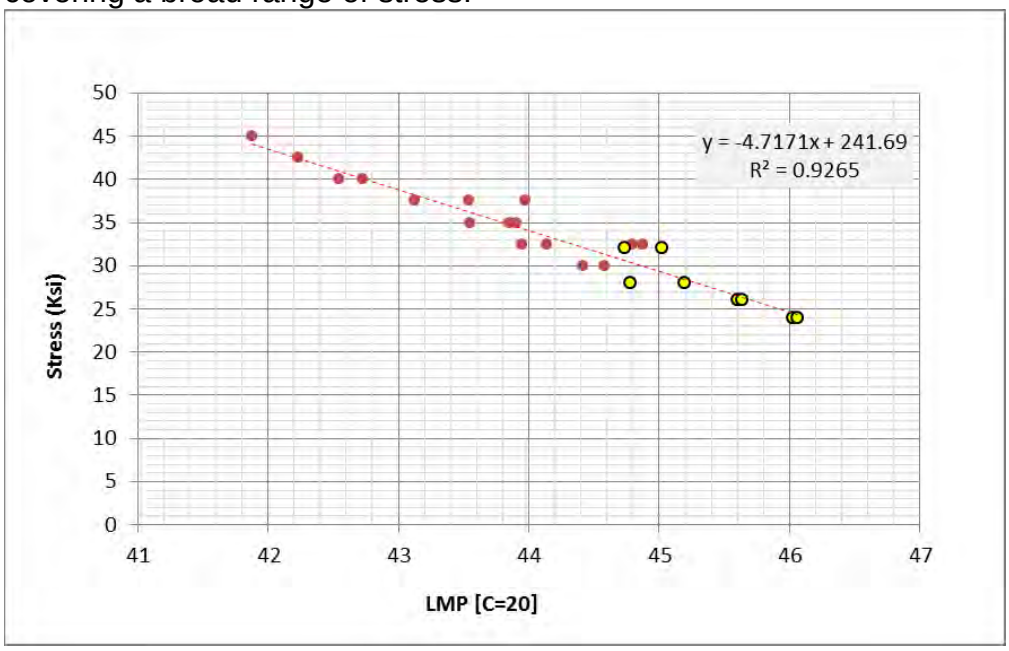

Figure 19: LMP plot of time to reach 0.2% Strain and Stress [Ksi]

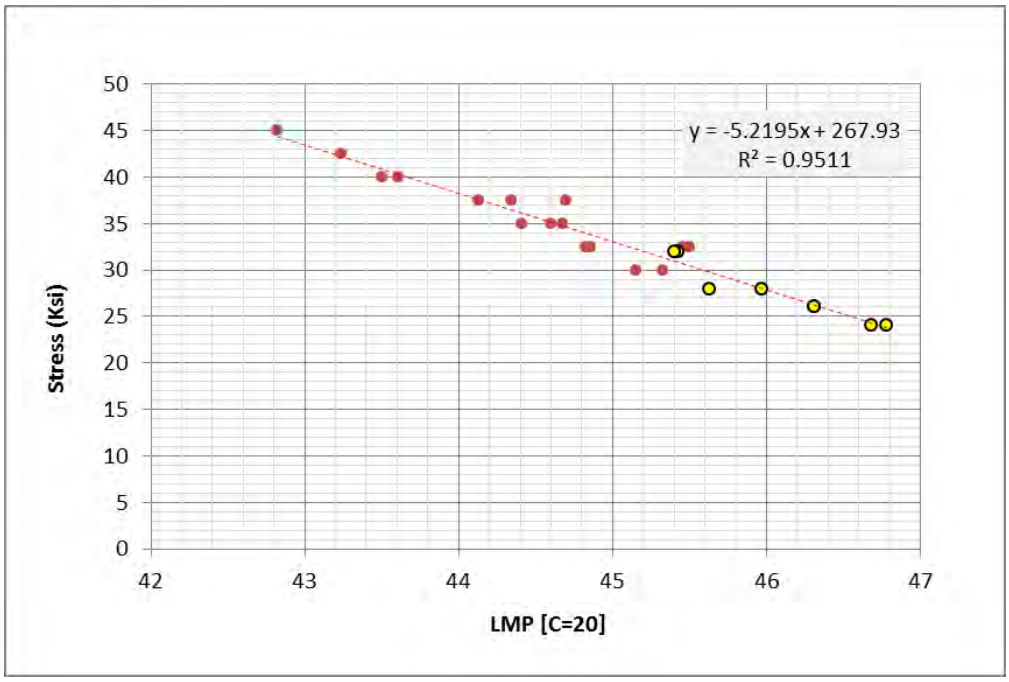

Figure 20: LMP plot of time to reach 1.0% Strain and Stress [Ksi]

The creep specimens from this program were submitted to the GE Global Research Center to ascertain the underlying creep mechanism in the specimens. Figure 21 shows the underlying dominant creep mechanisms in a succinct table.

unpaired dislocations: climb may be present but cannot observe

N105CRP-008 1400F	N105-CRP-007 1425F	N105-CRP-004 1450F	N105-CRP-002 1475F	N105-CRP-001 1500F
high density of continuous faulting/ microtwinning ½<110> pairwise shear unpaired dislocations – cross slip	unpaired dislocations - cross slip, looping ½<110> pairwise shear	unpaired dislocations - cross slip, looping ½<110> pairwise shear shear localization in g channels (formation of long γ channels)	unpaired dislocations - cross slip, looping ½<110> pairwise shear shear localization in g channels (formation of long γ channels) limited continuous faulting	unpaired dislocations – cross slip ½<110> pairwise shear (very less)
planar	wavy	wavy	wavy	wavy
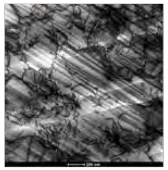 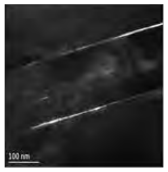	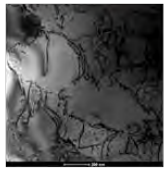 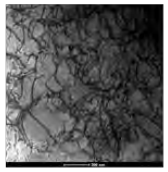	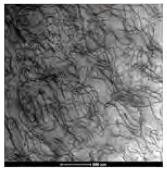 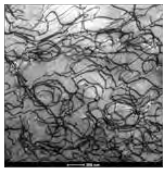	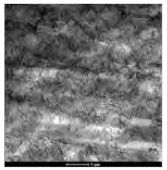 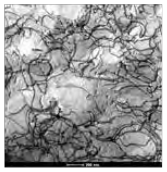	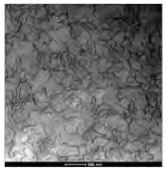 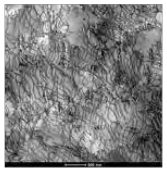

Figure 21: Dominant Creep Mechanism in N105

EVALUATION OF COMMERCIALLY AVAILABLE HAYNES®282®

Pieces of material from Haynes®282® were shipped to NETL for TEM analysis of the microstructure. Figure 22 and Figure 23 show the starting γ' sizes to be in the range of 67 ± 15.5 nm with $Cr_{23}C_6$ primarily decorating the grain boundary.

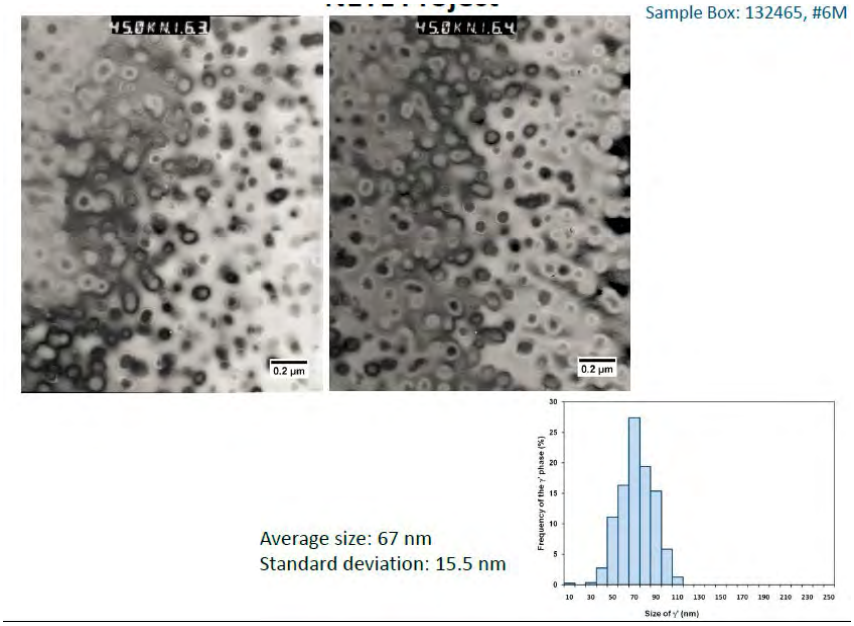

Figure 22: Typical γ' precipitate size of Haynes®282® [67 ± 15.5 nm]. (From NETL)

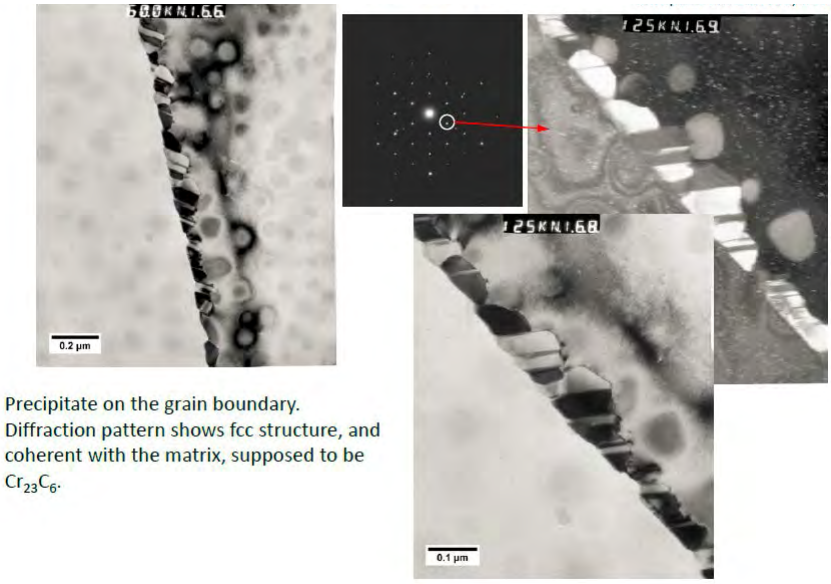

Figure 23: TEM image identifying $Cr_{23}C_6$ as a carbide phase in Haynes®282®. (From NETL)

Pieces from the Haynes®282® were exposed to 1425°F (774°C) for a period of 1 and 2 years and the properties evaluate. Figure 24 - Figure 28 show the properties obtained as a function of thermal exposure.

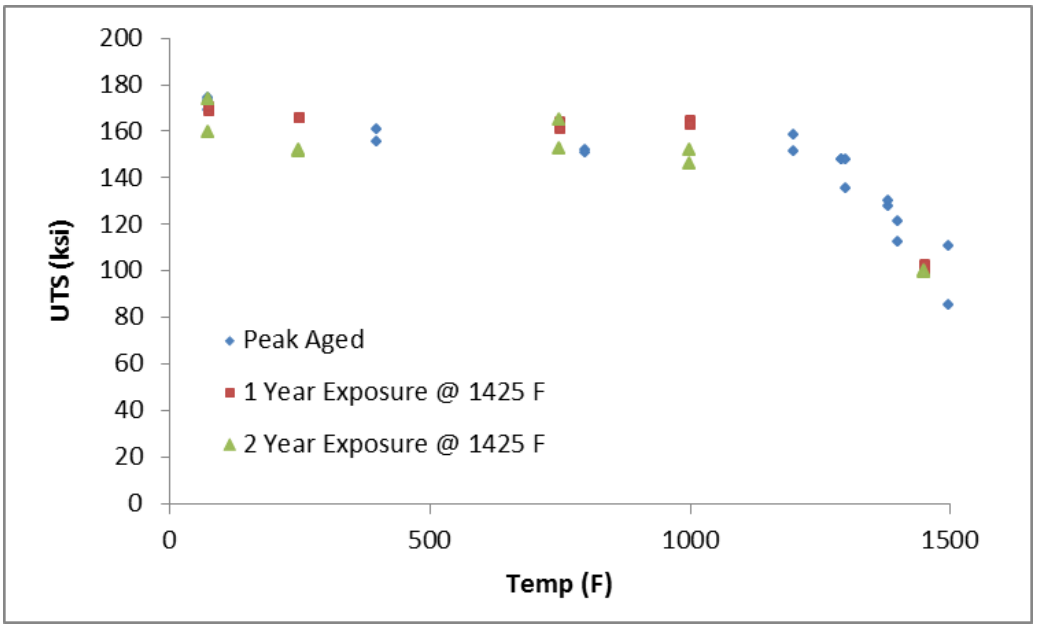

Figure 24: Tensile strength in Haynes®282® after a 1 & 2 year thermal exposure at 1425°F (774°C) [*Longitudinal Orientation*]

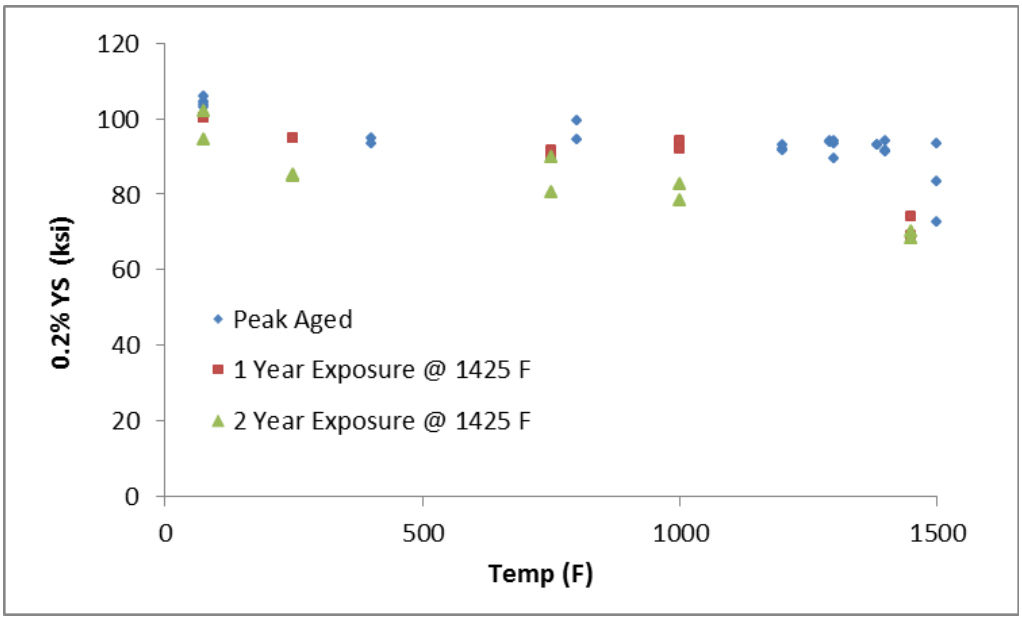

Figure 25: 0.2% Yield Strength in Haynes®282® after a 1 & 2 year thermal exposure at 1425°F (774°C) [*Longitudinal Orientation*]

Negligible drops in tensile properties [UTS and 0.2%YS] were obtained. Similar to the property drops in N105, Haynes®282® exhibited a drop in % Elongation and % RA that plateaued after a year of thermal exposure. The fracture toughness did not exhibit any deterioration in properties.

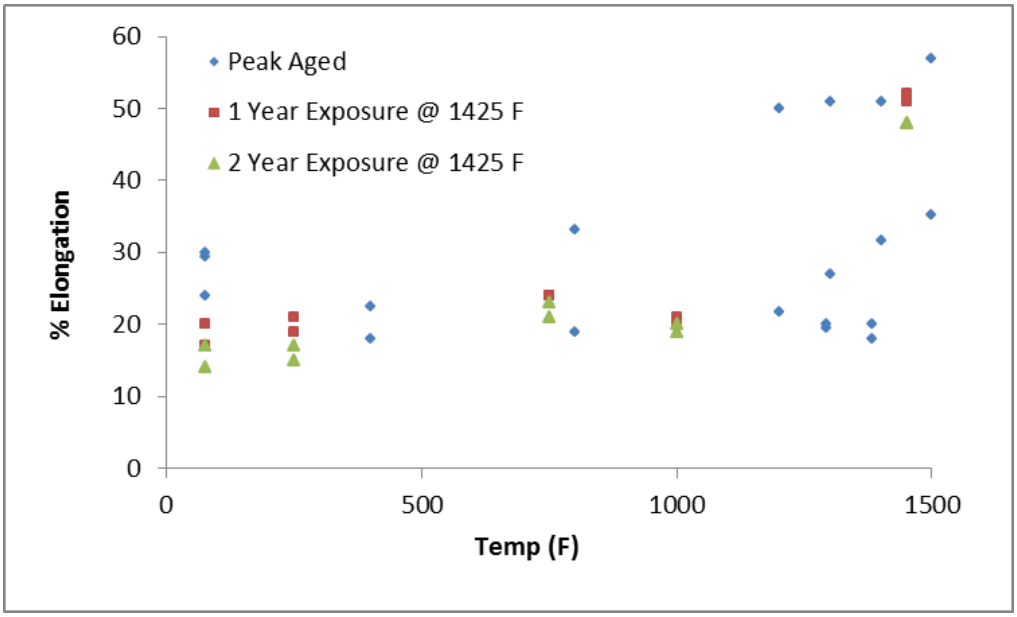

Figure 26: % Elongation in Haynes®28²® after a 1 & 2 year thermal exposure at 1425°F (774°C) [*Longitudinal Orientation*]

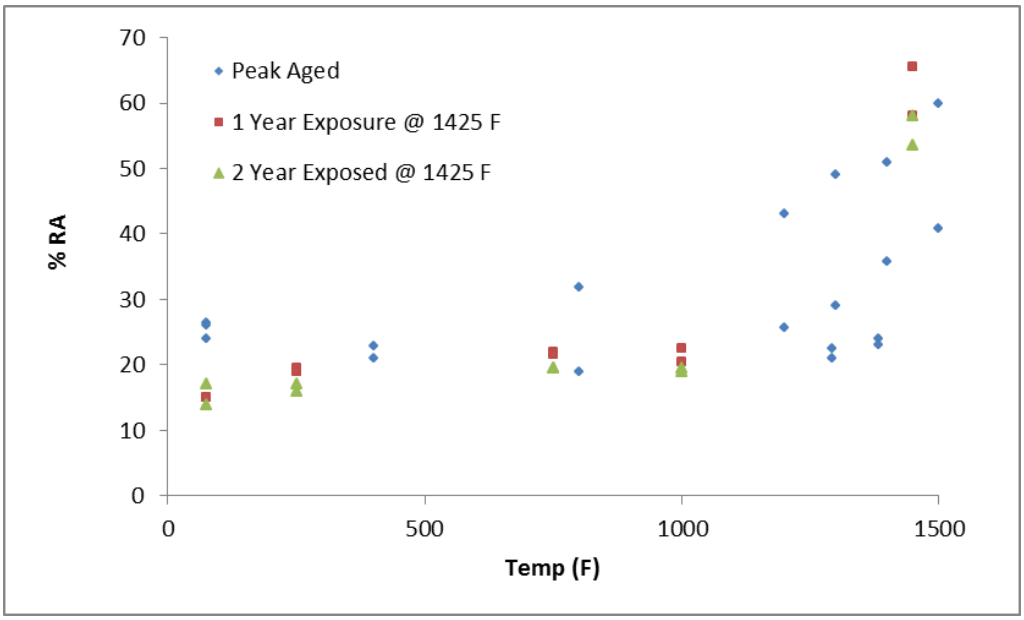

Figure 27: % RA in Haynes®28²® after a 1 & 2 year thermal exposure at 1425°F (774°C) [*Longitudinal Orientation*]

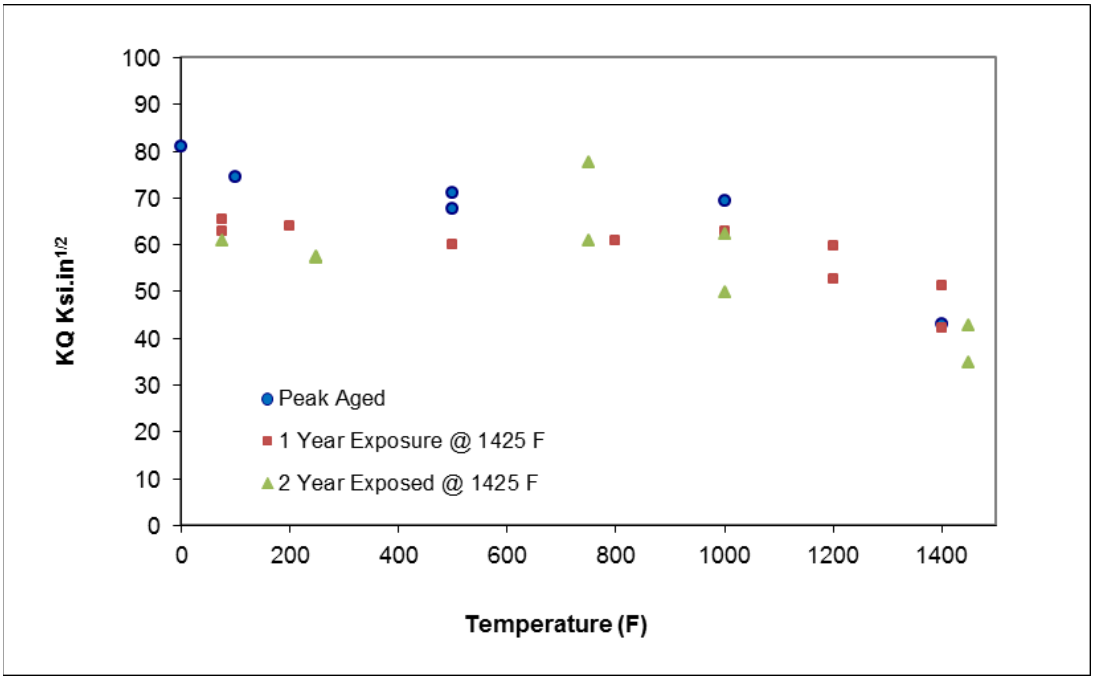

Figure 28: KQ or Conditional Fracture toughness of Haynes®282® after 1 & 2 year thermal exposure at 1425°F (774°C)

Multiple specimens were extracted from the bar for fracture toughness testing. The specimens were 0.75" thick [B] & 1.5" Wide [W]. All specimens were side grooved to a depth equal to 20% of the nominal thickness [10% each side]. The specimens were tested in accordance to ASTM E1820-09. As specimens had a mix of valid and invalid J1c, Figure 28 plots only the conditional fracture toughness of Haynes®282® as a function of temperature and thermal exposure. No debit was observed during the thermal exposure of Haynes®282® over a two year period at 1425 F.

Fatigue specimens were machined from the bar [longitudinal orientation only] and subjected to high cycle fatigue tests [in air]. All tests were performed at 1400°F (760°C), 50 Hertz and 10,000,000 cycles runout. Figure 29 shows the plot of alternating stress and cycles to failure for various A ratios.

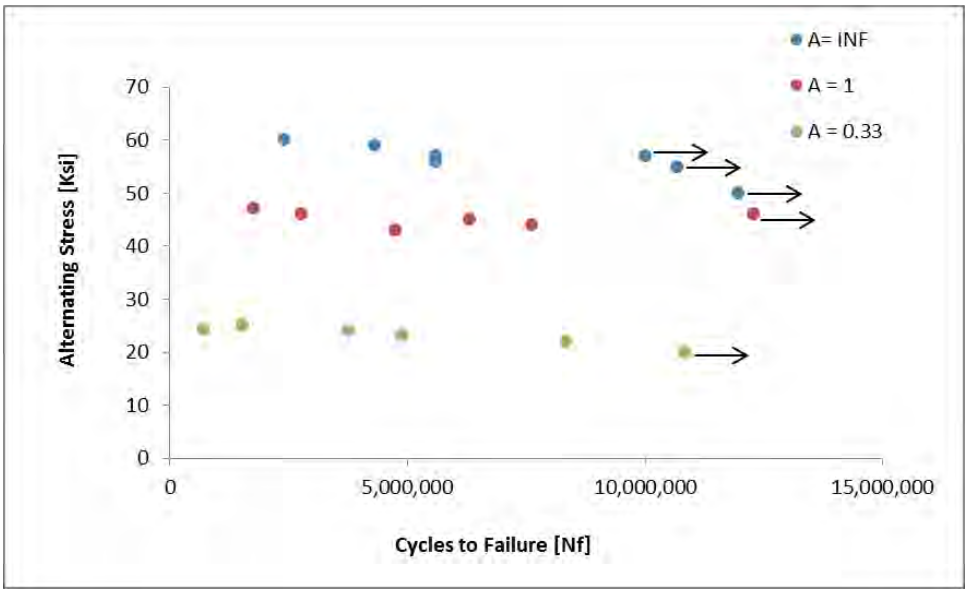

Figure 29: Figure showing alternating stress and cycles to failure at various A ratios

Hold time fatigue tests were performed on the material by hold the fatigue specimens at peak strain [a trapezoid waveform]. Such type of failure mechanism could emanate due a combination of mechanical and thermal stresses at certain locations in a component. Figure 30 shows the debit associated with the hold time fatigue of commercially available material when subjected to a 6 hour hold [plateau in the trapezoid waveform] at peak strain. Baseline data was obtained from Phase 1.

The drop in life associated with an interaction of creep and fatigue is indicative of issues that need to be accounted for during the detailed design of a component.

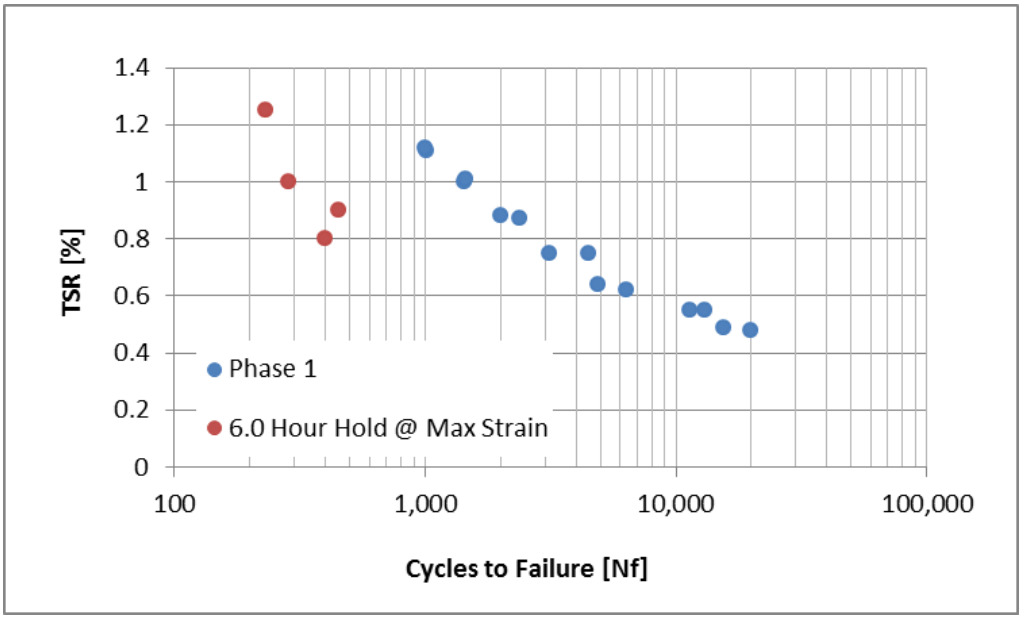

Figure 30: Debit in Hold Time Fatigue of Haynes®282®

FORGEABILITY OF COMMERCIALLY AVAILABLE HAYNES®282® FOR SMALLER FORGINGS

Haynes®282® is also a potential choice for smaller forgings in a turbine [along with Waspaloy, Nimonic 263 and Inconel 740]. The ability to forge an alloy is the determination of the appropriate temperature and strain required to achieve an appropriate grain structure that meets or exceeds the requirements of the component. A cylindrical specimen with 0.5" diameter x 1.00" height was heat treated to 1850°F (1010°C) for 2 hours and air cooled prior to compression testing. Following was the sequence for the generation of flow stress data and the microstructural evolution.

The piece was compression tested at multiple strain rates [0.001 – 3.2 /sec] and multiple temperatures [1600 – 2000°F or 871 - 1093°C].

- All the specimens were heat-treated at 1850F/2hrs + air-cooled prior to compression testing.
- Compression tests have been performed at 5 temperatures - 1600°F, 1700°F, 1800°F, 1900°F and 2000°F (871°C, 927°C, 982°C, 1038°C, and 1093°C).
- Tests have been done at strain rates of 0.001, 0.01, 0.1, 1.0 and 3.2/s for each temperature
- Compression-tested specimens were sectioned axially into four quarters.
- Two quarters from each of the compression tested specimens have been heat-treated at following temperature/time conditions:
    - 1650°F (899°C)/2hrs + air-cool
    - 2150°F (1177°C)/2hrs + air-cool
- Each of these quarters were mounted, polished and etched for microstructure evaluation
- Photomicrographs have been taken at mid-radius/mid-height location of the compression-tested specimen.
- Grain size evaluation was performed by visually comparing the photomicrographs with ASTM Grain Size Chart.

Figure 31 - Figure 35 show the true stress and true strain data at 1600, 1700, 1800, 1900 and 2000°F (871°C, 927°C, 982°C, 1038°C, and 1093°C). Table 1 is a summary of the grain structure obtained as a function of various temperatures and thermal exposure. Based on the dataset, Haynes®282® exhibited evidence of duplex microstructures when re-heated to the lower temperature [< 1800°F or 982°C]. The grain size in the final product can be tailor made based on the combination of the

imparted strain and the final desired microstructures. Some temperature and strain combinations show the tendency of the alloy to exhibited carbide banding.

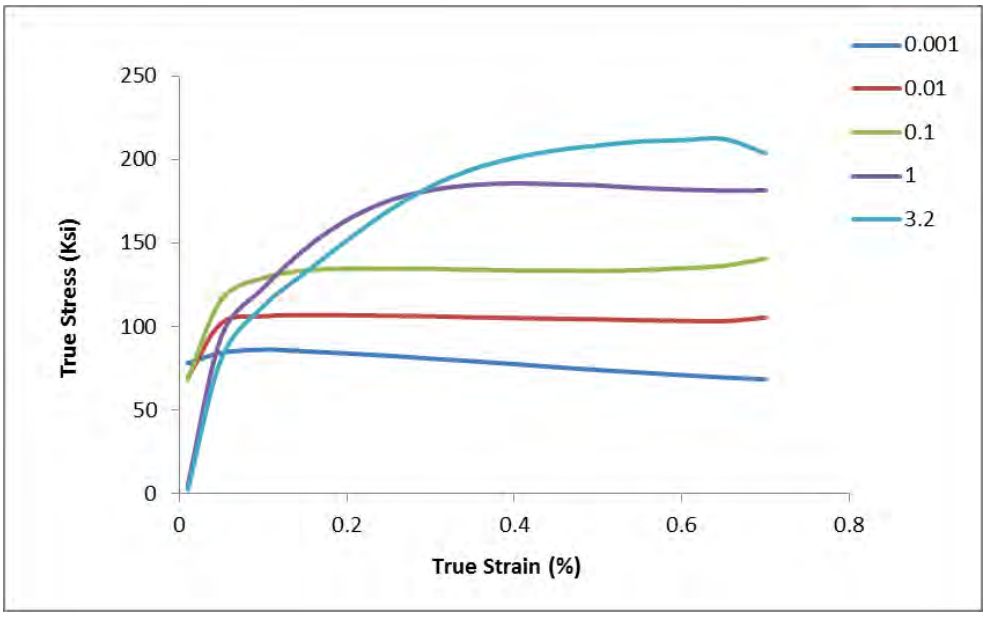

Figure 31: Flow Stress curves of Haynes®282® at 1600°F (871°C)

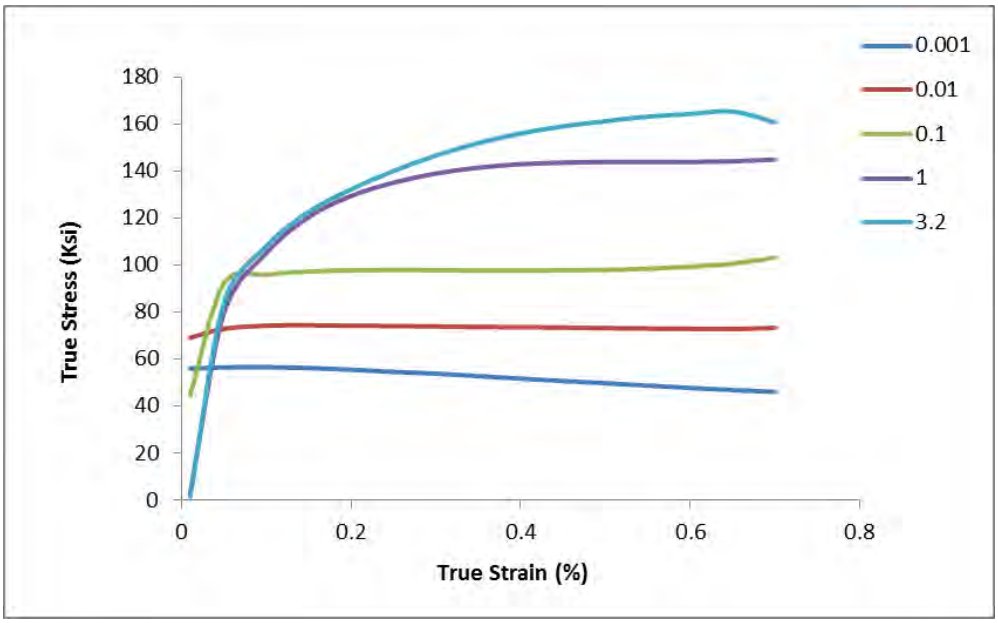

Figure 32: Flow Stress curves of Haynes®282® at 1700°F (927°C)

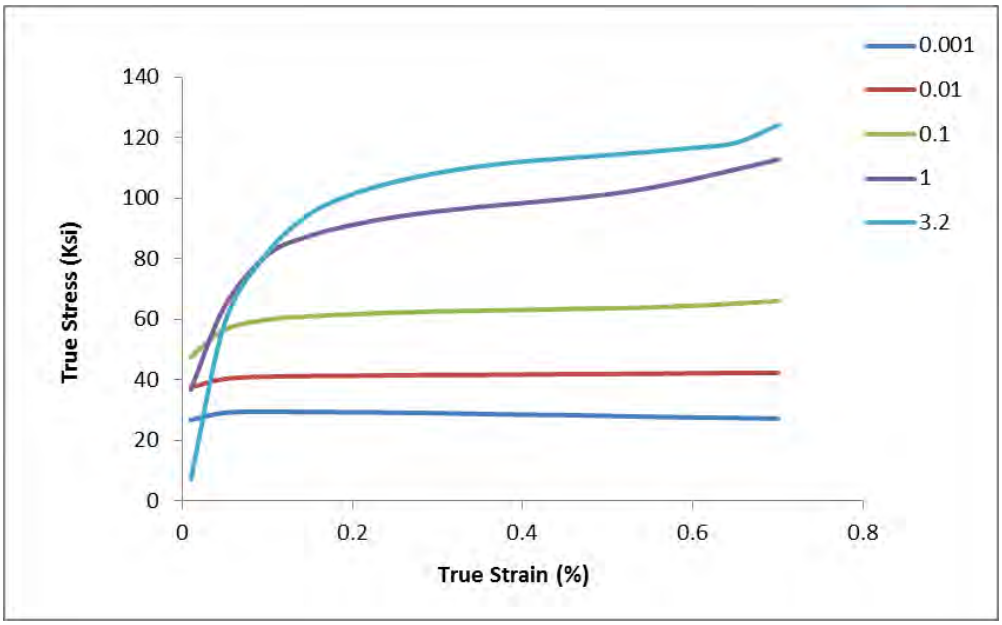

Figure 33: Flow Stress curves of Haynes®282® at 1800°F (982°C)

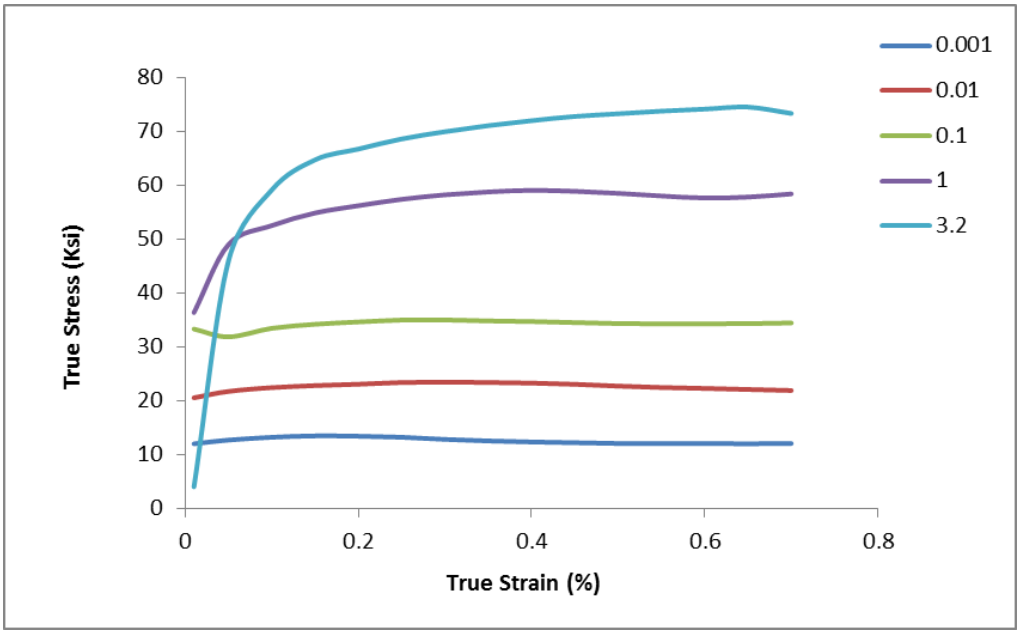

Figure 34: Flow Stress curves of Haynes®282® at 1900°F (1038°C)

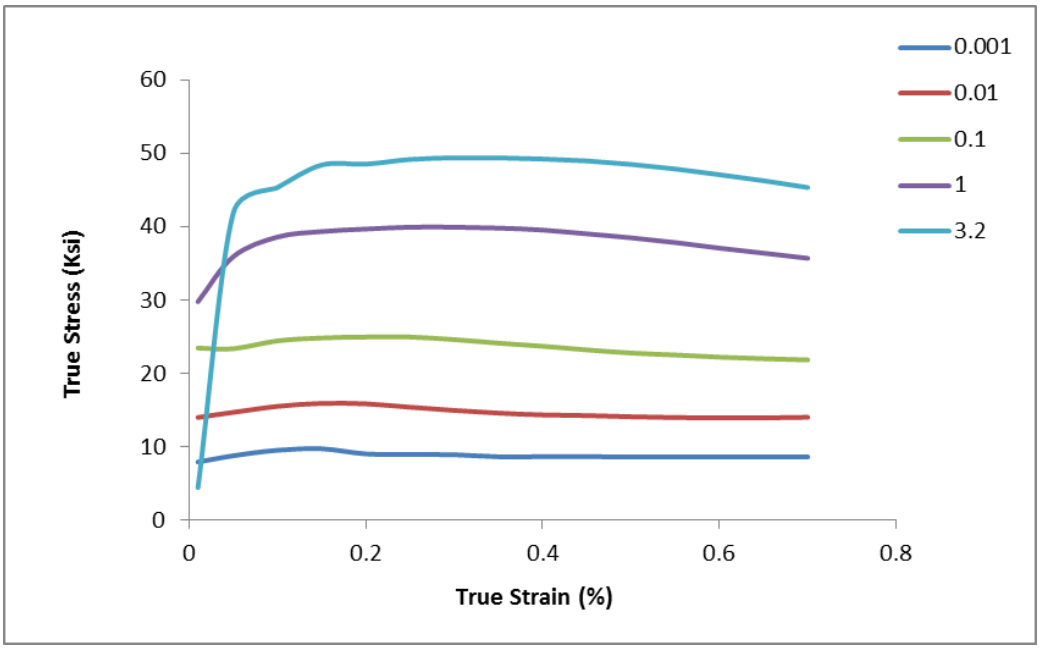

Figure 35: Flow Stress curves of Haynes®282® at 2000°F (1093°C)

Table 1: Grain size after compression tests and exposing the pieces at various temperatures for 2 hours of Hayne®282®

Compression Temperature	Re-heat Temperature (@ 2hours)	Strain Rate (in/in/sec)				
		0.001	0.01	0.1	1	3.2
1600	1650	ASTM 6 ALA 5	ASTM 8.5 ALA 4	ASTM 7 ALA 4	ASTM 5 ALA 4	ASTM 8.5 ALA 3
	1800	ATM 7.5 ALA 6.5	ATM 7.5 ALA 6.5	ASTM 10 ALA 8	ASTM 6 ALA 5	ASTM 8.5 ALA 6
	2150	ASTM 1 ALA 0	ASTM 2 ALA 1	ASTM 1 ALA 00	ASTM 1 ALA 0	ASTM 1 ALA 0
1700	1650	ASTM 5 ALA 4	ASTM 5 ALA 4	ASTM 7.5 ALA 6	ASTM 5 ALA 4	ASTM 7 ALA 6
	1800	ASTM 5 ALA 4	ASTM 5 ALA 4	ASTM 7 ALA 6	ASTM 5 ALA 4	ASTM 7.5 ALA 6
	2150	ASTM 1.5 ALA 0.5	ASTM 2 ALA 1	ASTM 1.5 ALA 0	ASTM 1.5 ALA 1	ASTM 2 ALA 0
1800	1650	ASTM 5.5 ALA 4	ASTM 6 ALA 5.5	ASTM 3.5 ALA 1	ASTM 5 ALA 4	ASTM 7 ALA 6
	1800	ASTM 5.5 ALA 4.5	ASTM 7 ALA 6	ASTM 5 ALA 4	ASTM 6 ALA 5	ASTM 7.5 ALA 6.5
	2150	ASTM 1.5 ALA 1	ASTM 2 ALA 1	ASTM 2.5 ALA 1	ASTM 1.5 ALA 1	ASTM 2 ALA 0.5
1900	1650	ASTM 9 ALA 7	ASTM 11 ALA 4	ASTM 10 ALA 9	ASTM 9 ALA 8	ASTM 9 ALA 3
	1800	ASTM 8.5 ALA 7	ASTM 8 ALA 6	ASTM 9 ALA 8	ASTM 9.5 ALA 8	ASTM 9 ALA 8
	2150	ASTM 1.5 ALA 0	ASTM 2 ALA 1.5	ASTM 2.5 ALA 1	ASTM 2.5 ALA 1.5	ASTM 2 ALA 1
2000	1650	ASTM 6 ALA 5	ASTM 7 ALA 6	ASTM 8 ALA 7	ASTM 7.5 ALA 6	ASTM 7 ALA 5
	1800	ASTM 5 ALA 4	ASTM 6.5 ALA 5.5	ASTM 7 ALA 6	ASTM 7 ALA 6	ASTM 6 ALA 5
	2150	ASTM 2.5 ALA 1	ASTM 1.5 ALA 0.5	ASTM 2 ALA 1	ASTM 1.5 ALA 1	ASTM 1 ALA 0

TRIPLE MELTING OF HAYNES®282® FOR LARGER FORGING

Though alloys such as Haynes®282®, Nimonic 263, Inconel 740, Waspaloy exhibit the requisite creep properties for A-USC conditions, the scalability of these alloys into larger components such as a forging have to be demonstrated. Haynes®282® was primarily developed for non-rotating component and has been processed via a double melt process [VIM-ESR], prior to the interest from this program. The double melt process limits the available starting size for very large diameter disk or forging. Historically, triple melt process is a prerequisite for the manufacture of rotating components and is extensively documented in literature.

Based on the recommendation of the design group, a capability of a final 44" diameter forging would demonstrate the maximum need of a Haynes®282® . Based on this information, it was desired to triple melt 24" diameter ingots [VIM-ESR-VAR] of Haynes®282®. Following was the sequence in the development of the triple melt process

- Two 18" VIM ingots (EX0045PW and EX0046PW) were poured [Figure 36]
  - Chemistries at the head and toe were confirmed to meet the chemistry of Haynes®282® [Table 2]
- The ingots were then ESR melted into 22" diameter ingots [Figure 36]
- ESR ingot EX0045PW was re-melted via VAR into a 24" diameter ingot [Figure 36]
  - The re-melting consisted of three melt rates
  - The ingot was marked for the various conditions during the melting process
  - The ingot was then homogenized based on a temperature cycle determined by NETL. The microstructure after the homogenization cycle are document in Figure 38
  - The ingot was the forged into an 8" diameter bar for maintaining the location of the melt rates [Figure 39] and the resultant microstructure evaluated [Figure 40]
  - The 8" diameter bar was then sectioned and macro-etched with Canada's Etch to reveal segregation tendencies [Figure 41] for various melt conditions.
- The second ESR Ingot EX0046PW was then re-melted via VAR into a 24" diameter ingot with the optimum melt rates determined from the first ingot
  - The ingot was billetized into a 20" diameter ingot [Figure 42]
  - Section from the ingot EX0046PW was cut for macro-segregation (Figure 43) and microstructural analysis (Figure 44)

The 20" diameter ingot was the starting feedstock for the forge ability studies, sub-scale forgings and eventually the large 44" diameter disk of Haynes®282®. All development activities were performed by GE Power and Water and Special Metals.

18” VIM

ESR – 22” Diameter 24” Diameter VAR

Figure 36: Pictures showing the 18” VIM / 22” ESR and the final 24” VAR Ingot.

Table 2: Chemistries obtained from the Hayne®282® ingots

Element	Composition (wt. %)							
	EX0045PW Head			EX0045PW Toe			EX0046PW Head	EX0046PW Toe
	Surface	Mid-Radius	Center	Surface	Mid-Radius	Center		
C	0.065	0.061	0.061	0.056	0.064	0.063	0.061	0.061
Mn	0.034	0.033	0.033	0.033	0.033	0.033	0.033	0.034
Fe	0.849	0.794	0.815	0.767	0.763	0.812	0.49	0.49
S	0.001	0.0008	0.0008	0.0011	0.0011	0.0012	0.0005	0.0004
Si	0.056	0.059	0.057	0.067	0.066	0.064	0.057	0.067
Cu	0.023	0.022	0.022	0.023	0.023	0.024	0.024	0.024
Ni	56.67	57.23	57.07	56.76	56.72	56.54	56.85	56.85
Cr	19.58	19.32	19.42	19.56	19.58	19.42	19.65	19.64
Al	1.62	1.56	1.58	1.58	1.58	1.69	1.57	1.54
Ti	2.14	2.12	2.12	2.18	2.19	2.26	2.11	2.13
Mg	0.001	0.002	0.001	0.001	0.002	0.002	0.0007	0.0008
Co	10.26	10.25	10.26	10.26	10.24	10.25	10.30	10.29
Mo	8.56	8.41	8.43	8.57	8.60	8.70	5.56	8.57
Nb	0.083	0.082	0.080	0.079	0.080	0.081	0.079	0.08
Ta	0.0024	0.0003	0.0009	0.0017	0.0018	0.0018	0.001	0.002
P	0.0027	0.0026	0.0025	0.0026	0.0027	0.0026	0.003	0.003
Ca	0.0009	0.0009	0.0009	0.001	0.001	0.001	0.001	0.001
V	0.012	0.011	0.012	0.012	0.012	0.012	0.012	0.012
W	0.03	0.025	0.027	0.029	0.029	0.029	0.03	0.03
Zr	0.0017	0.0014	0.0014	0.0015	0.0016	0.0018	0.002	0.001
B	0.0040	0.0039	0.0039	0.0038	0.0039	0.0038	0.004	0.0039

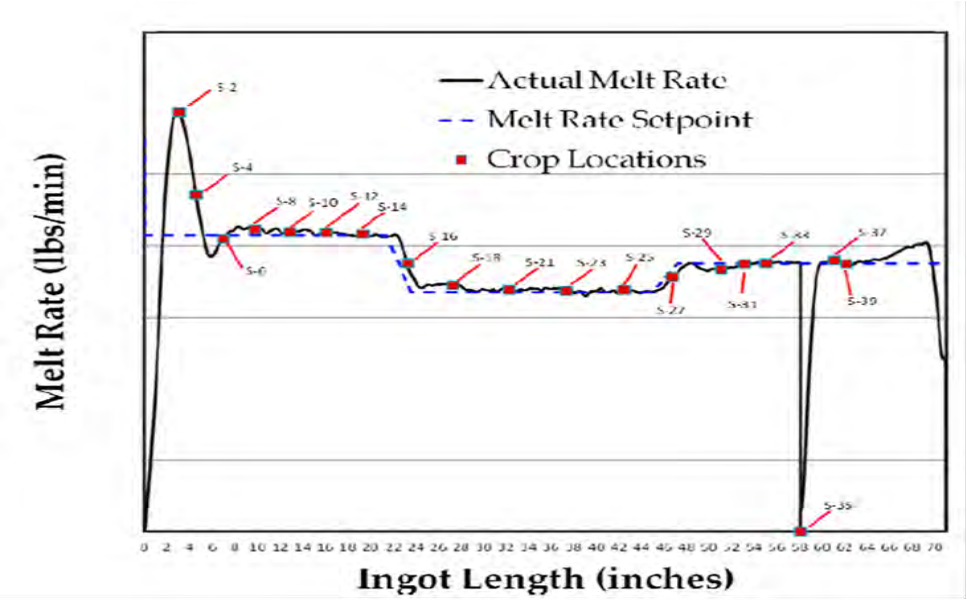

Figure 37: Variation in VAR Melt range [lbs/min] for marco evaluation

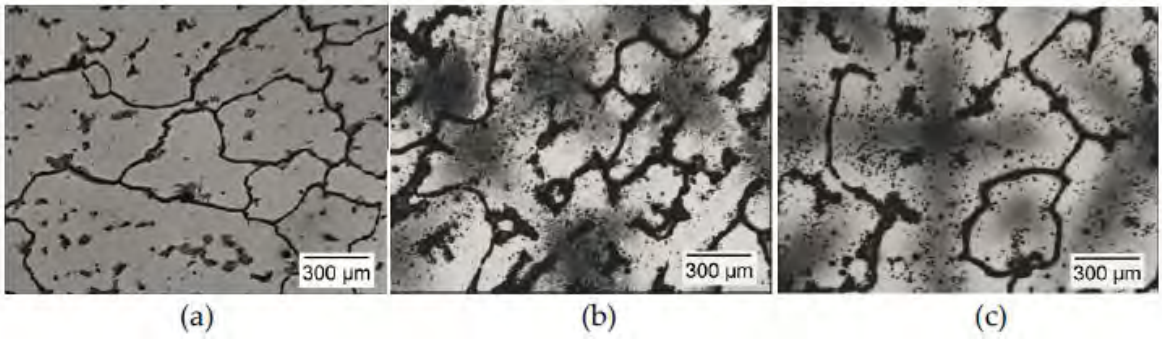

Figure 38: Representative microstructures of 24” ingot EX0045PW after homogenization

Figure 39: EX0045PW was forged into 8” diameter for macro-segregation evaluation

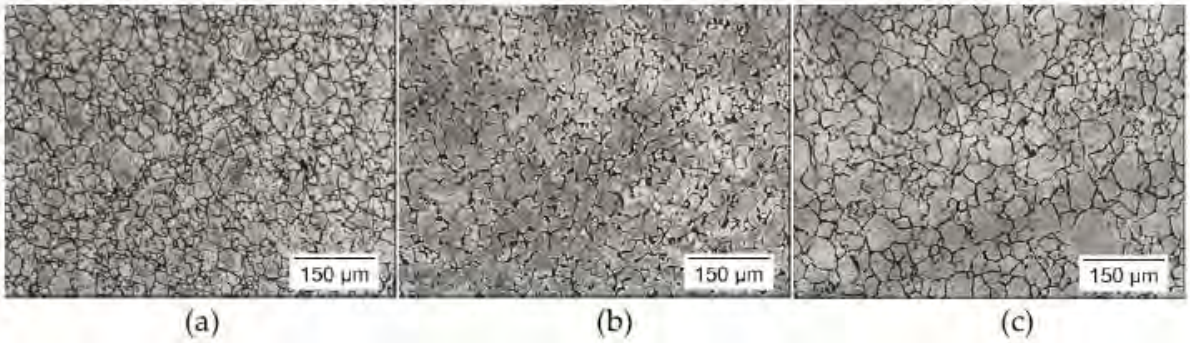

Figure 40: Representative microstructures of ingot EX0045PW after hot working to the 8” diameter bars (a) Surface (b) mid-radius and (c) center locations

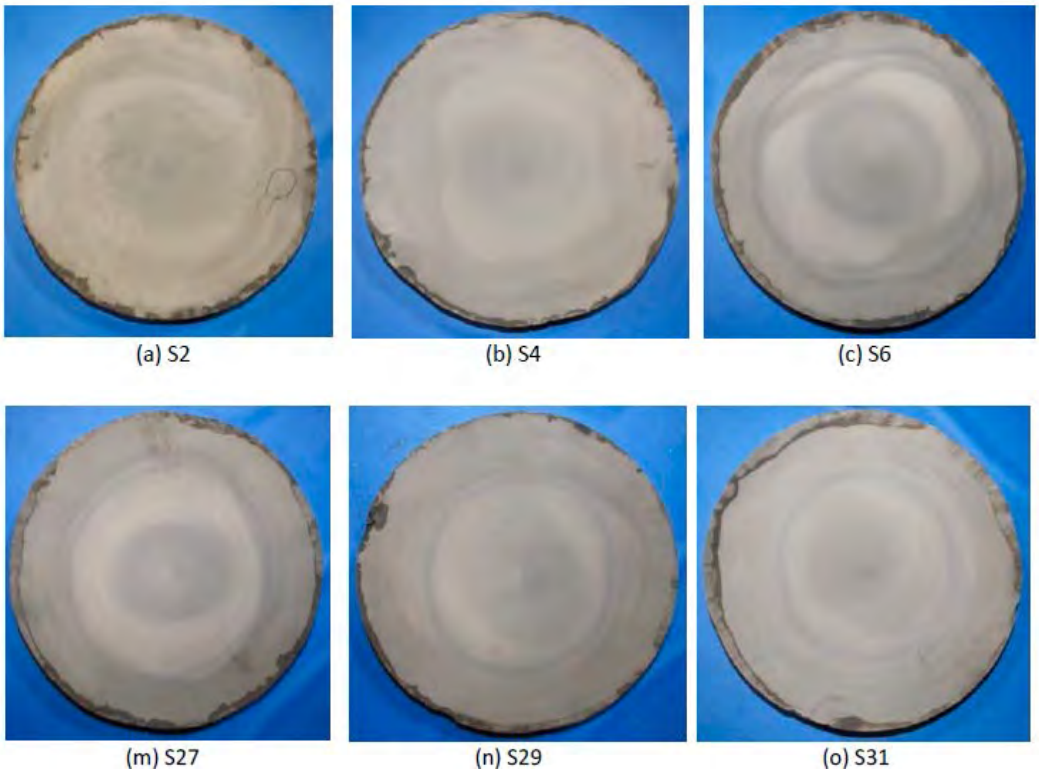

Figure 41: Representative macro slices from EX0045PW and etched with Canada's Etch to reveal segregation tendencies

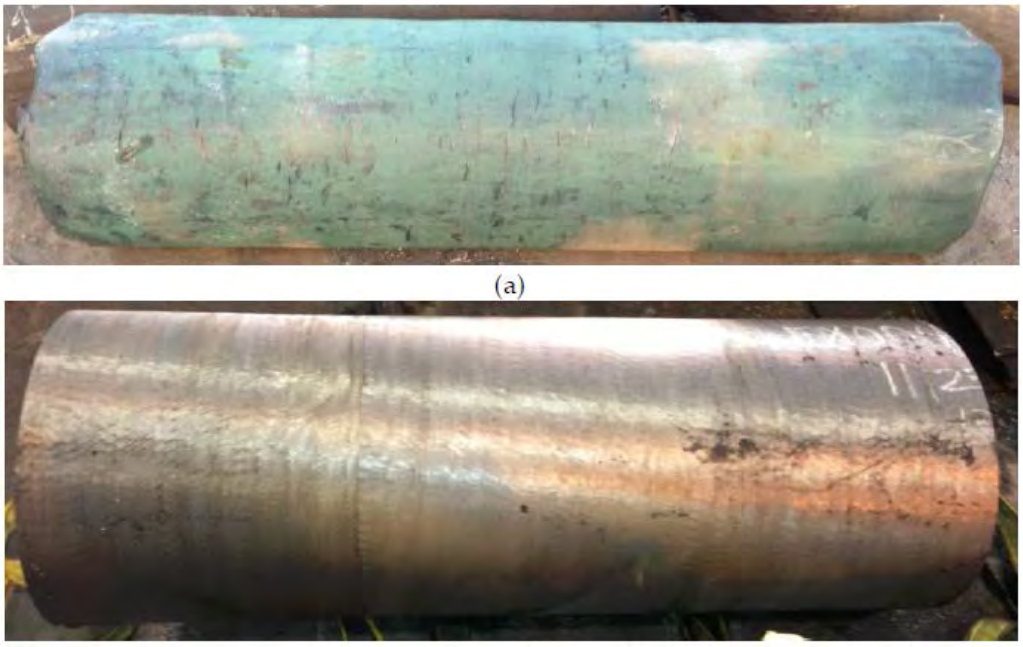

Figure 42 Second ingot EX0046PW billetized in (a) as forged condition and (b) after surface grinding to final diameter

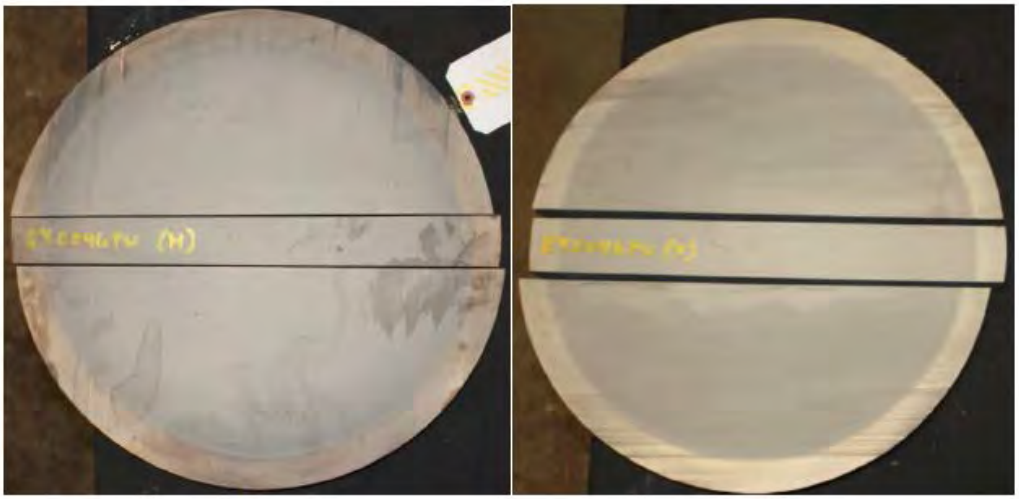

(a) (b)

Figure 43: Second ingot EX0046PW slice revealed no indication of segregation at (a) Head and (b) Toe [2]. Slices shown for microstructures

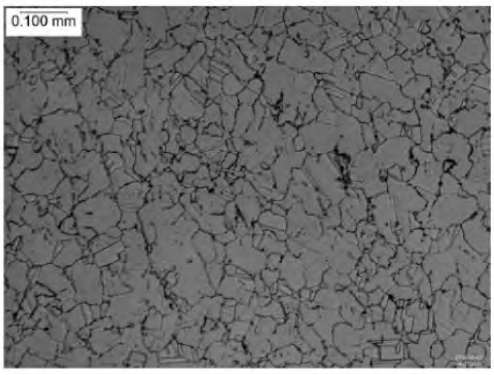

Grain Size ASTM 6 ALA 5

OD

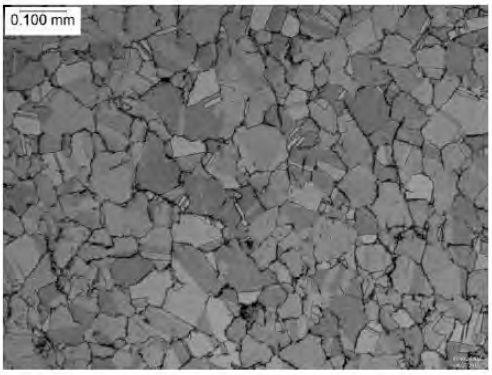

Grain Size ASTM 5

1.5” from OD

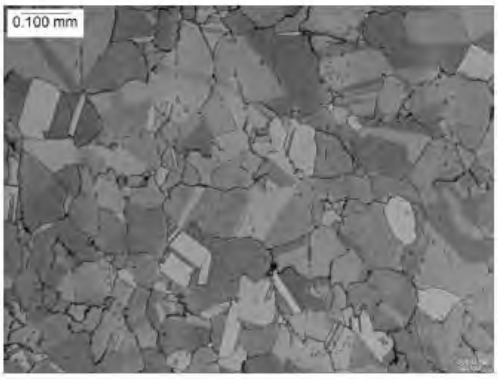

Grain Size ASTM 4 ALA 3

4” from OD

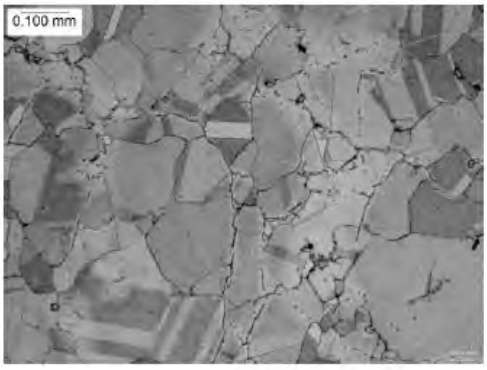

Grain Size ASTM 2.5

ID

Figure 44: Representative micro-graphs showing starting microstructure from the 20” diameter EX0046PW ingot head

LARGE FORGING OF HAYNES®282®

Multiple section of the triple melt forging was machined to characterize the microstructural stability of the alloy at various temperatures. Following were the sequence of steps followed to identify the right forging temperature and the successful demonstration of the large diameter disk of Haynes®282®

- Pieces of the ingot were exposed at various temperatures [1800, 1850, 1900, 1950 and 2000°F or 982, 1010, 1038, 1066, and 1093°C] for 4, 8 and 16 Hours
  - Figure 45and Figure 46 are representative microstructures obtained at various locations as a function of thermal hold.
  - 40 compression test specimens were machined from the billet to determine the flow stress data. The tests were performed at 1700, 1800, 1900 and 2000°F (927, 982, 1038, and 1093°C at various strain rates [0.001, 0.01, 0.1, 1 and 3.2 /sec].

- Two slugs [5" dia X 6.75"] were machined were heated and forged into pancakes in the following sequence
    - The first slug was forged at 1900°F (1038°C) two forge operation
      - Operation 1: 2:1 reduction and air cooled [Final: 6.75" dia x 3.4"]
      - Operation 2: 2:1 reduction and air cooled [Final: 3.4 dia x 1.7"]
    - The second slug was forged at 1900°F (1038°C) in a single operation
      - 4:1 reduction and air cooled [Final: 6.75" x 3.4"]

  - A 1in thick slice was removed through the diameter and a center to edge section metallographically prepared and etched. A 0.5" grid placed across the part and the grain size measured at the intercepts. Figure 47 and Figure 48 show the photomicrographs for the center, mid radius, and outer diameter.

- Based on the data and with an aim grain size of ASTM 8 and finer, the forging was obtained by a triple upset operation at 1900°F (1038°C). Figure 49 is an image showing the successful demonstration of a large diameter Haynes®282® forging.

All microstructural stability studies, sub-scale forgings and the large disk forging were performed by Wyman Gordon [Texas & Massachusetts].

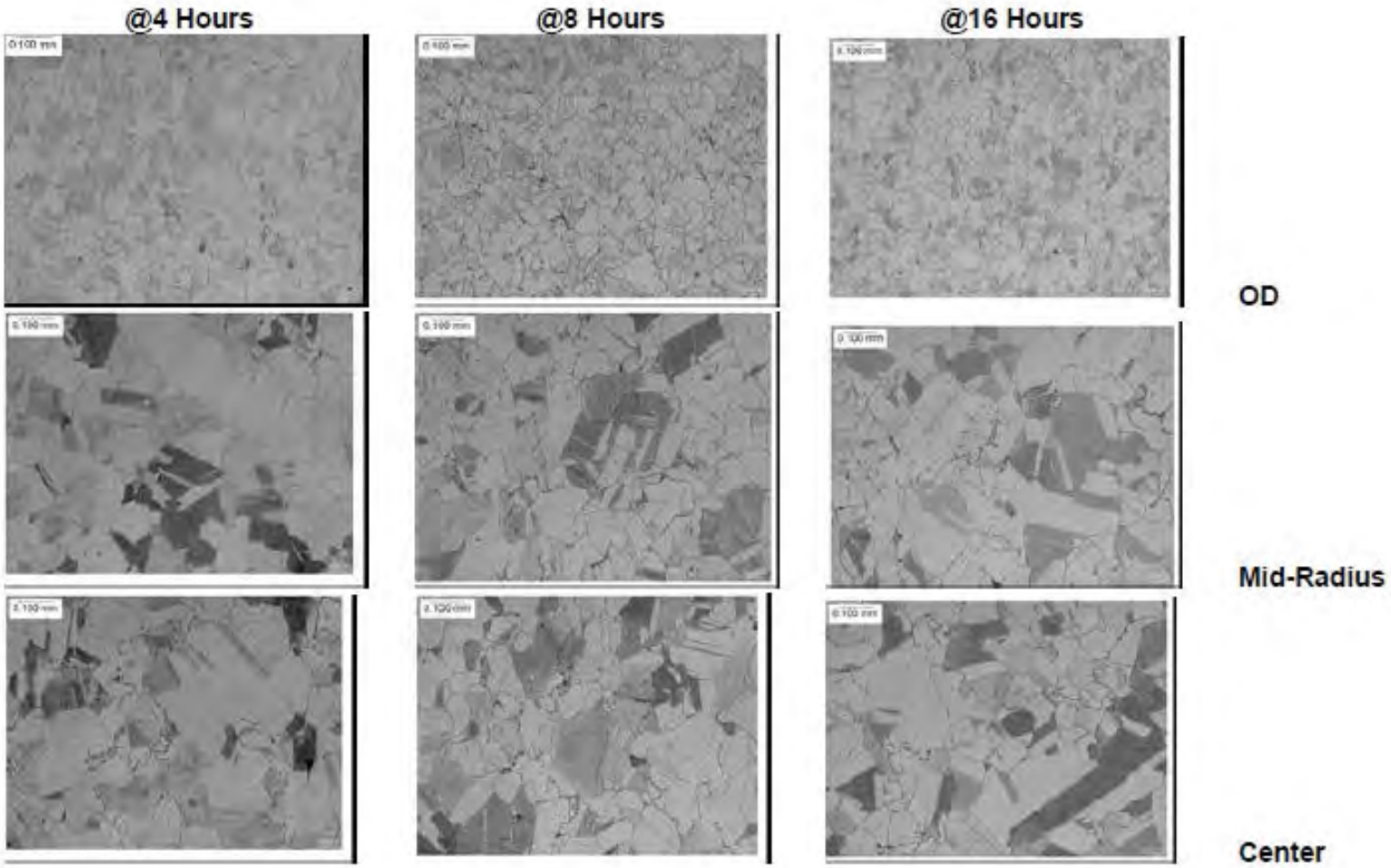

Figure 45: Coarsening studies of starting material exposed at 1800°F (982°C) at various times

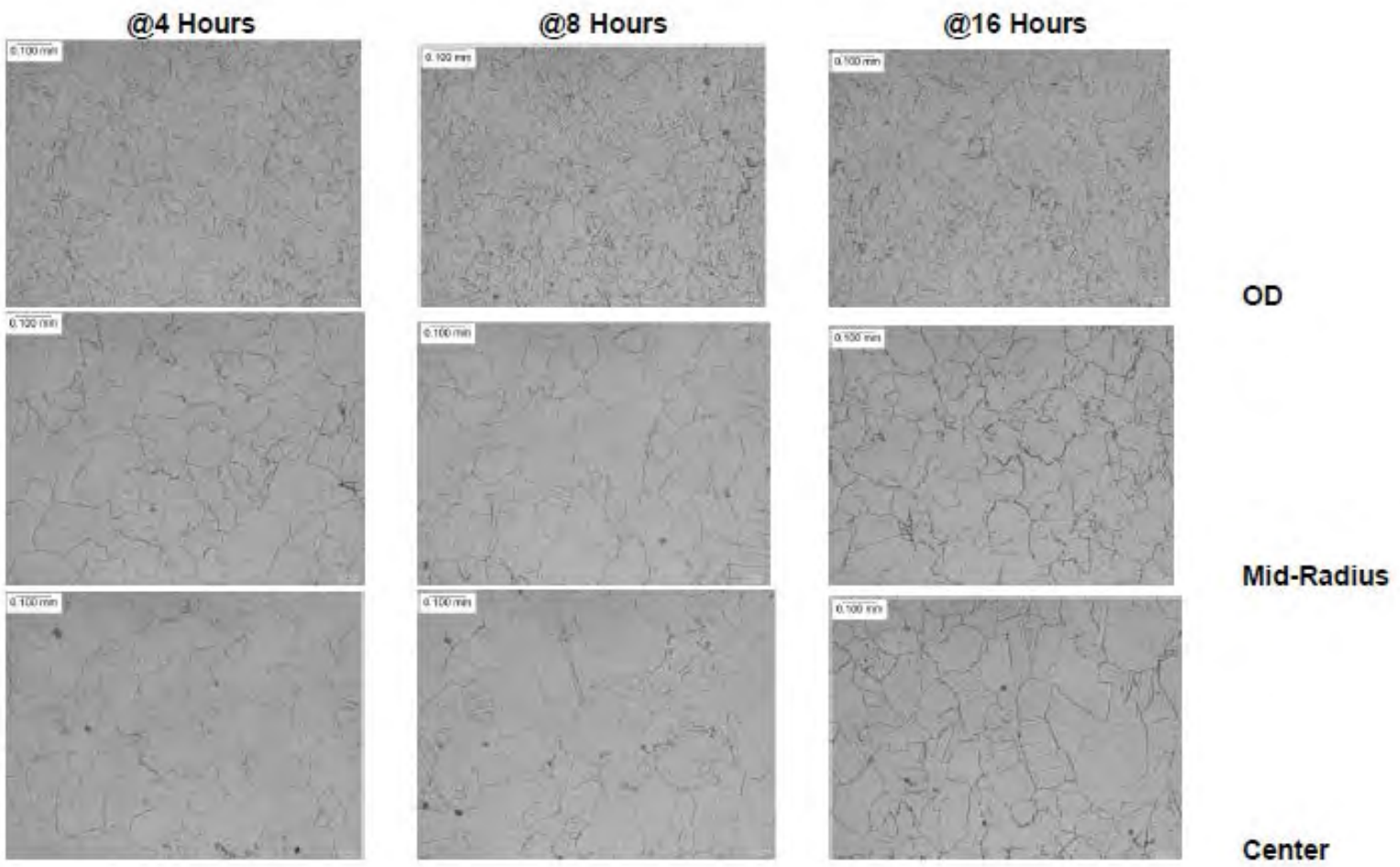

Figure 46: Coarsening studies of starting material exposed at 1900°F (1038°C) at various times

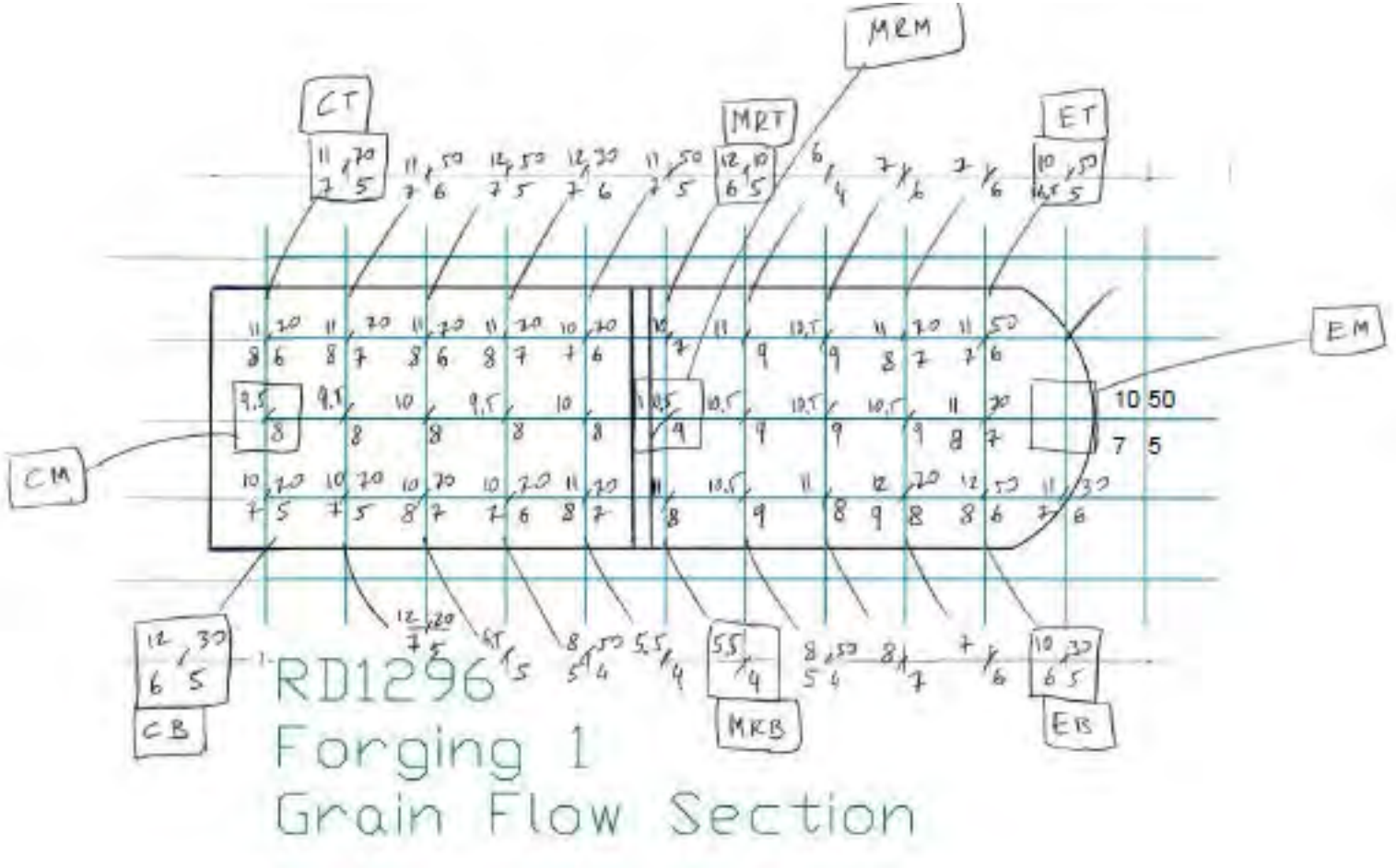

Figure 47: Grain size map of a subscale forging forged in two operations of 2:1 reduction ratio each.

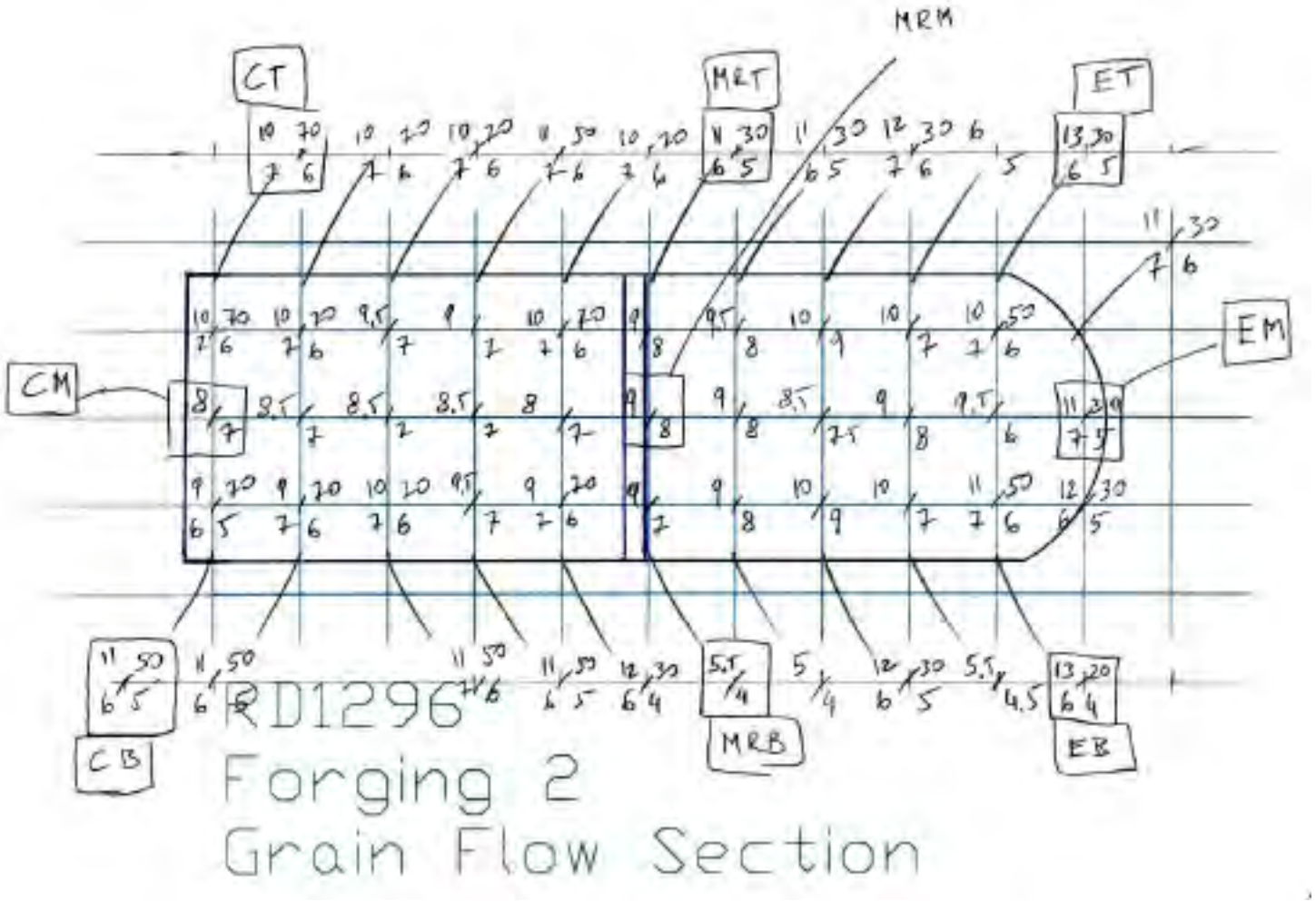

Figure 48: Grain size map of a subscale forging forged in a straight 4:1 reduction ratio.

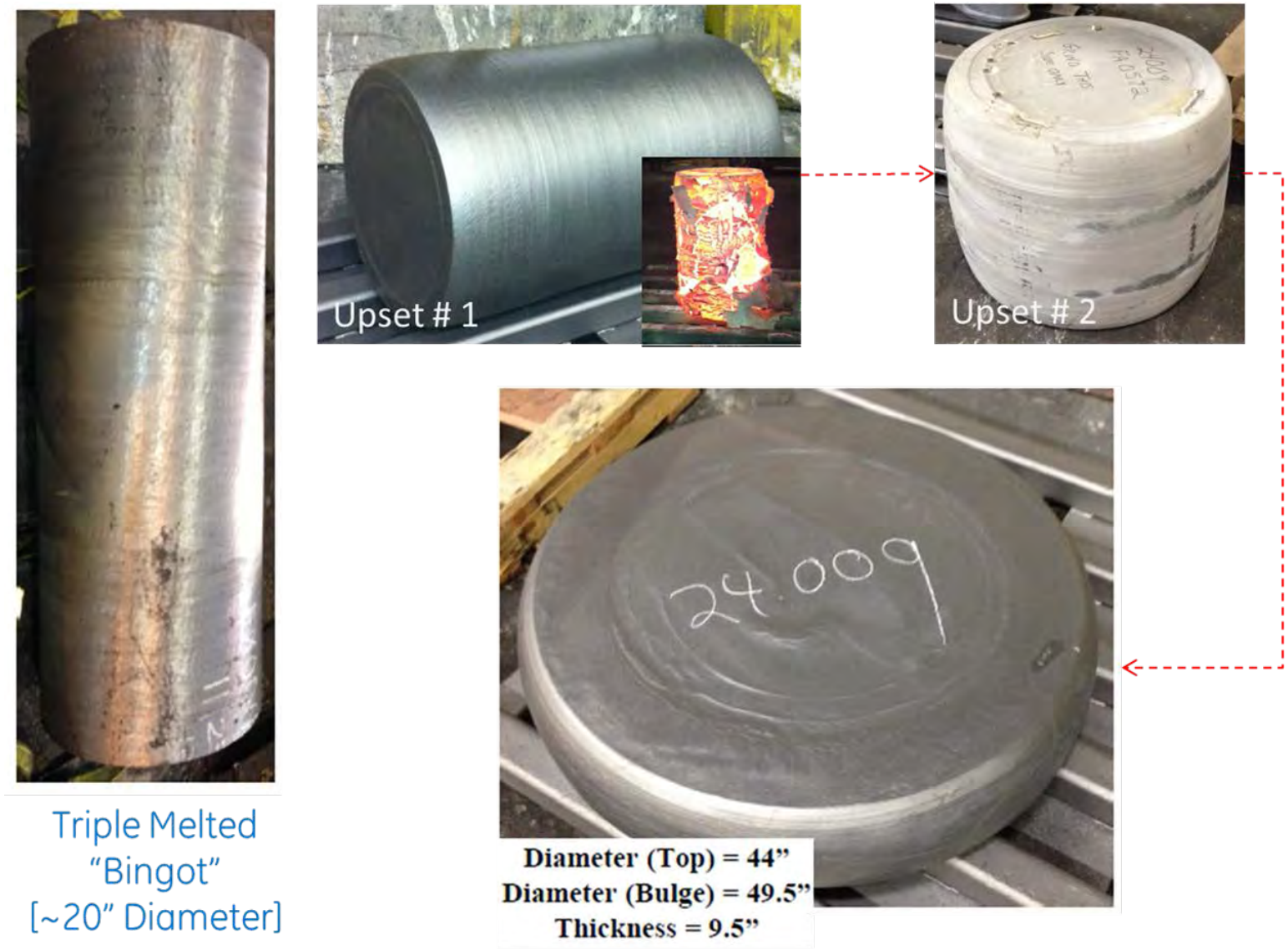

Figure 49: Demonstration of a large diameter Haynes®282® forging

CHARACTERIZATION OF THE LARGE FORGING OF HAYNES®282®

The disk obtained from Wyman Gordon was heat treated with a typical double age process.

Age 1:	1850°F (1010°C) for 2 Hours and air cooled
Age 2:	1450°F (788°C) for 8 Hours and air cooled

Multiple cuts were performed in the disk the microstructure evaluated. Figure 50 shows the typical microstructure obtained from the Haynes®282® forging. The grain size was very fine and typically ASTM 8-9, ALA 4.

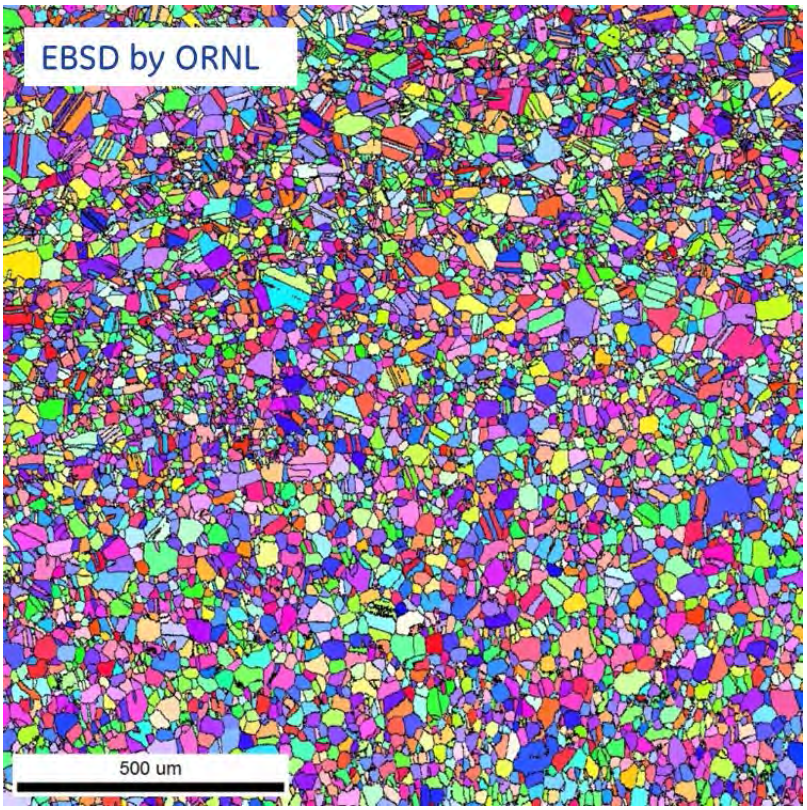

Figure 50: EBSD image of the grain size obtained in the Haynes®282® forging [Courtesy ORNL]. Typical grain size was ASTM 8-9, ALA ASTM 4

The forging was cut and multiple specimens were obtained [at various orientations] to fully characterize the forging. Figure 51 through Figure 54 show the tensile properties obtained from the disk for the radial and tangential orientation.

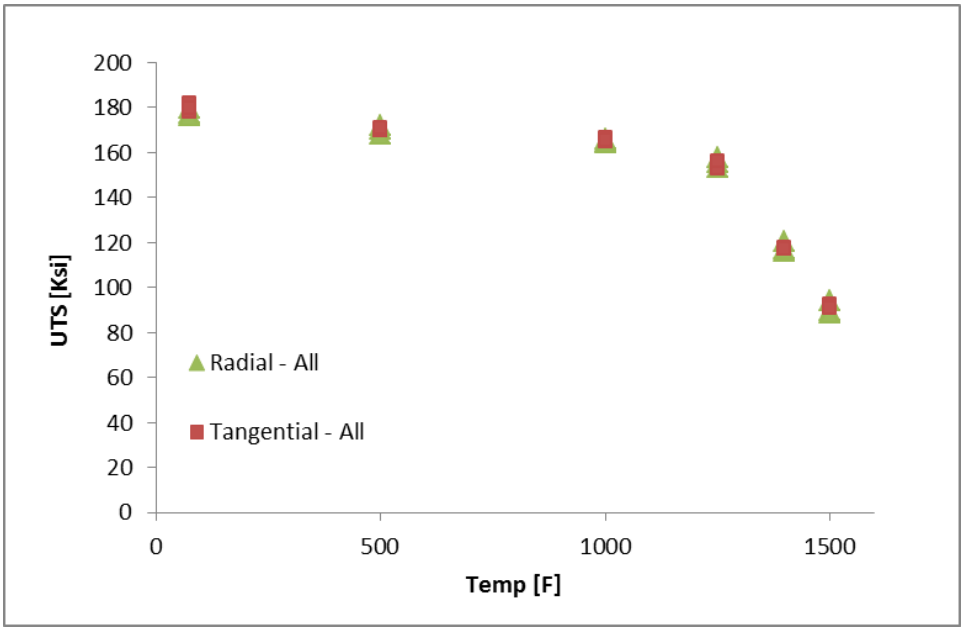

Figure 51: UTS as a function of temperature from Haynes®282® forged disk

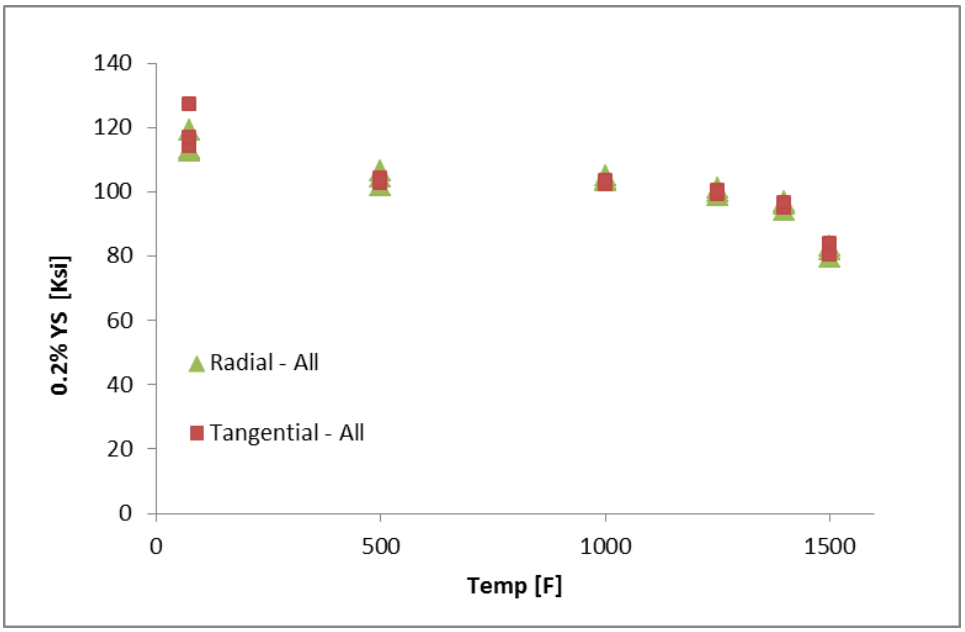

Figure 52: 0.2%YS as a function of temperature from Haynes®282® forged disk

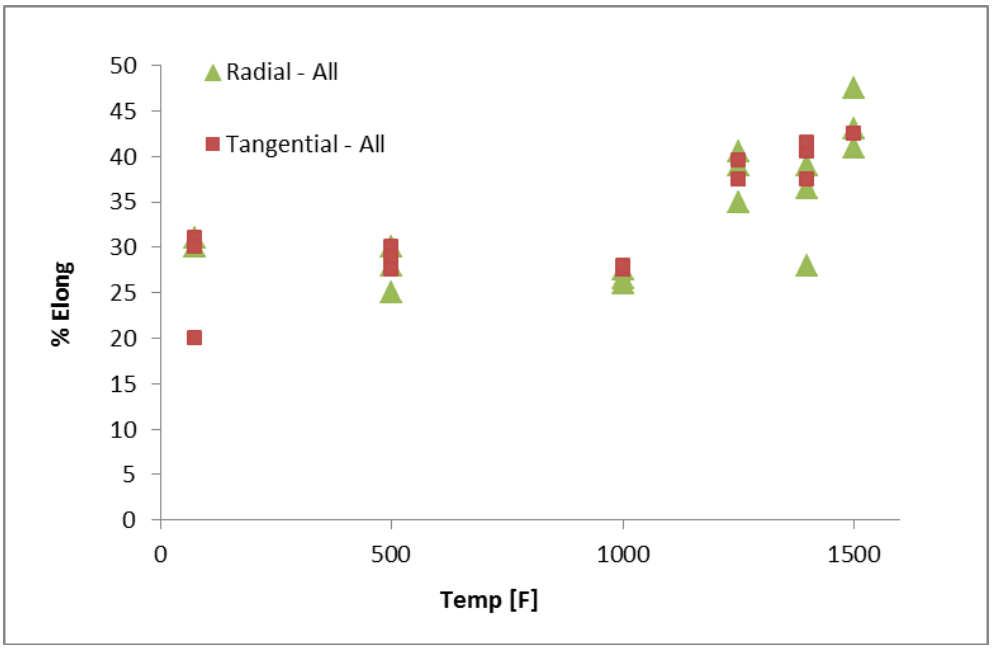

Figure 53: % Elongation a function of temperature from Haynes®282® forged disk

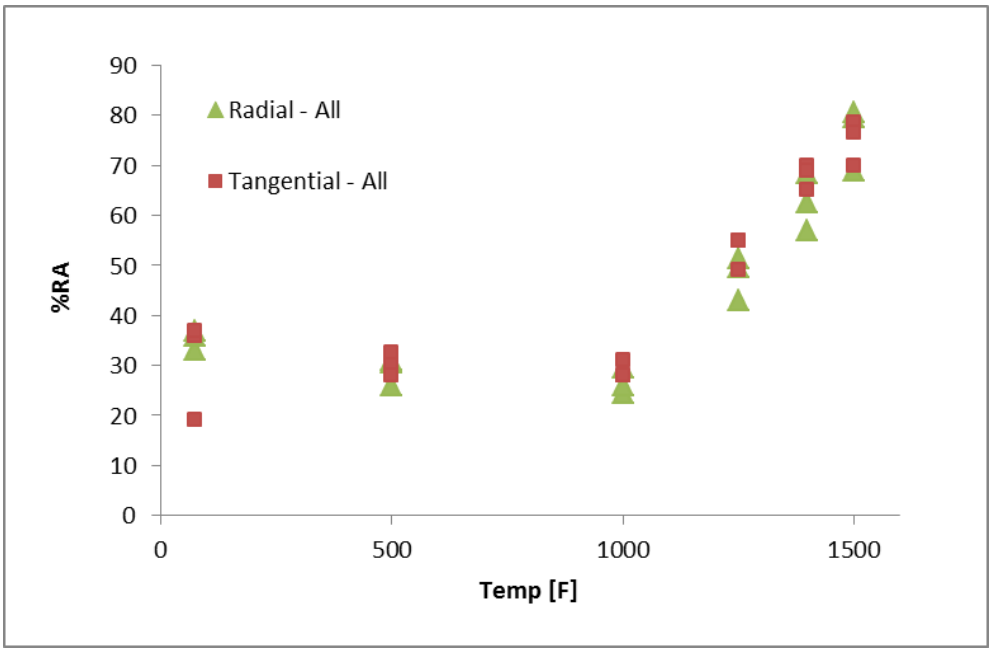

Figure 54: % RA a function of temperature from Haynes®282® forged disk

Figure 55 through Figure 57 show the high cycle fatigue results from Haynes®282® forging. The figures represent various A ratios [A=INF, 1 and 0.5] and all orientations, 1400°F (760°C), A= INF, 50 Hz and Triangular waveform. The data obtained from commercially available Haynes®282® is also plotted for reference.

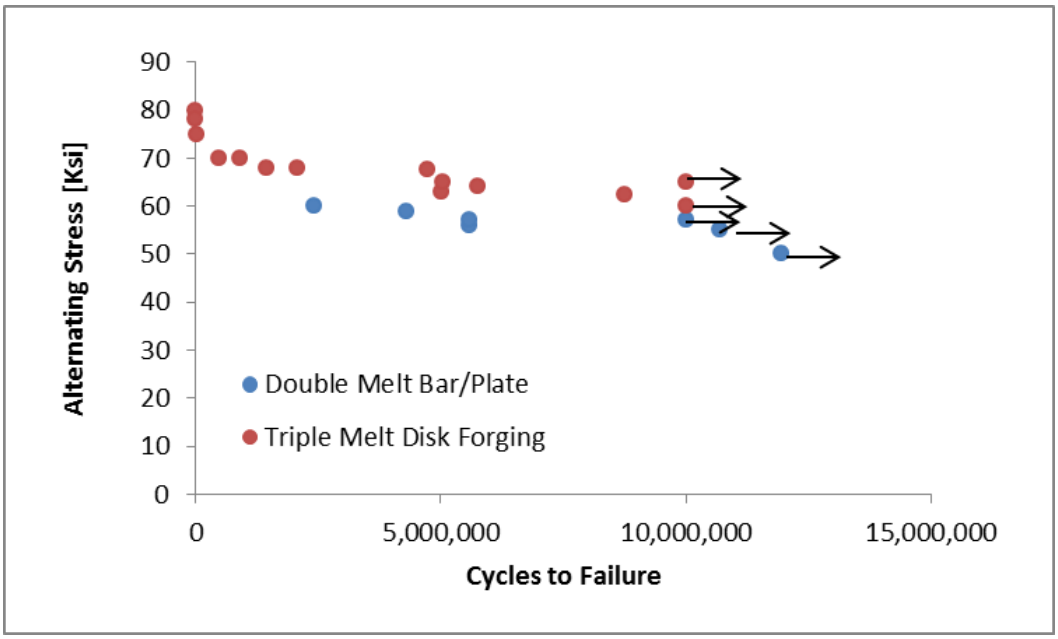

Figure 55: High cycle fatigue data from Haynes®282® disk forging [A=INF]

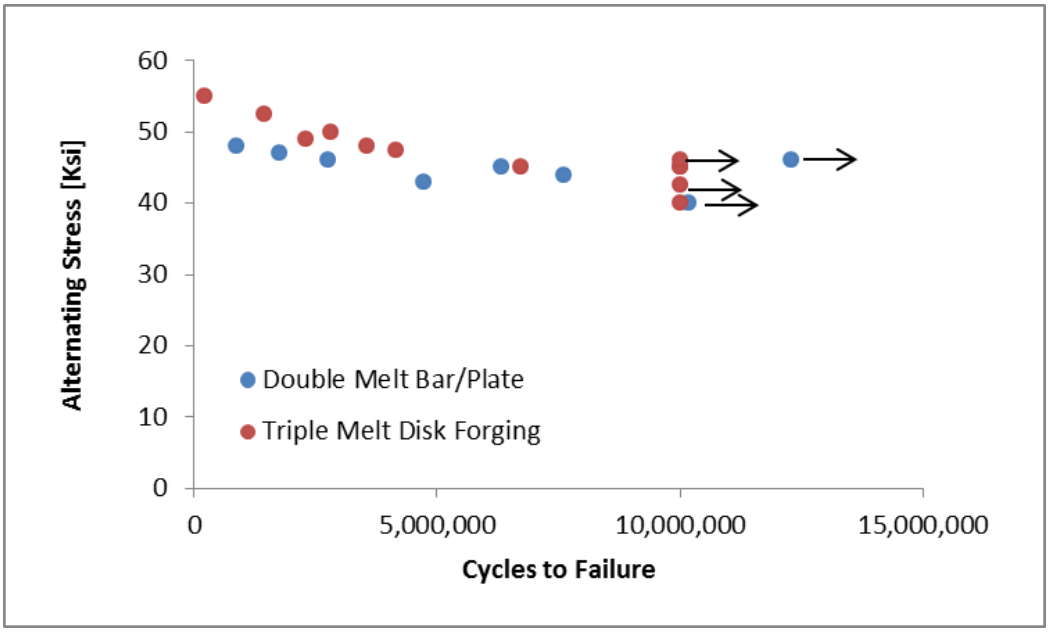

Figure 56: High cycle fatigue data from Haynes®282® disk forging [A=1]

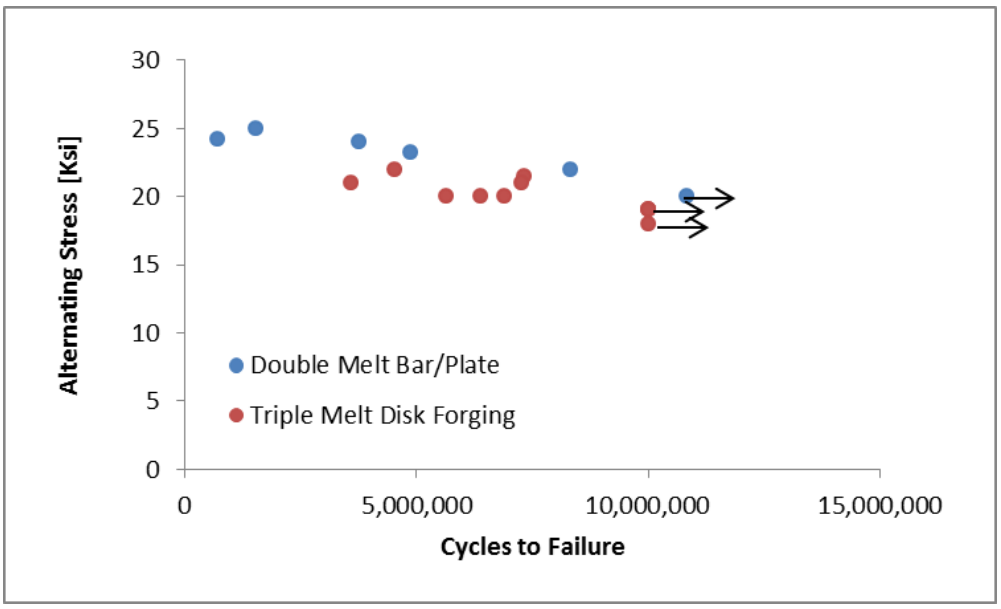

Figure 57: High cycle fatigue data from Haynes®282® disk forging [A= 0.5]

Figure 58 shows the low cycle fatigue behavior of Haynes®282® forging from all orientations, 1400 F, 20 cpm and triangular waveform. All data is compared to commercially available Haynes®282® [Phase 1 report]. The benefits obtained in the fatigue life due to the finer grain, is evident from the figure.

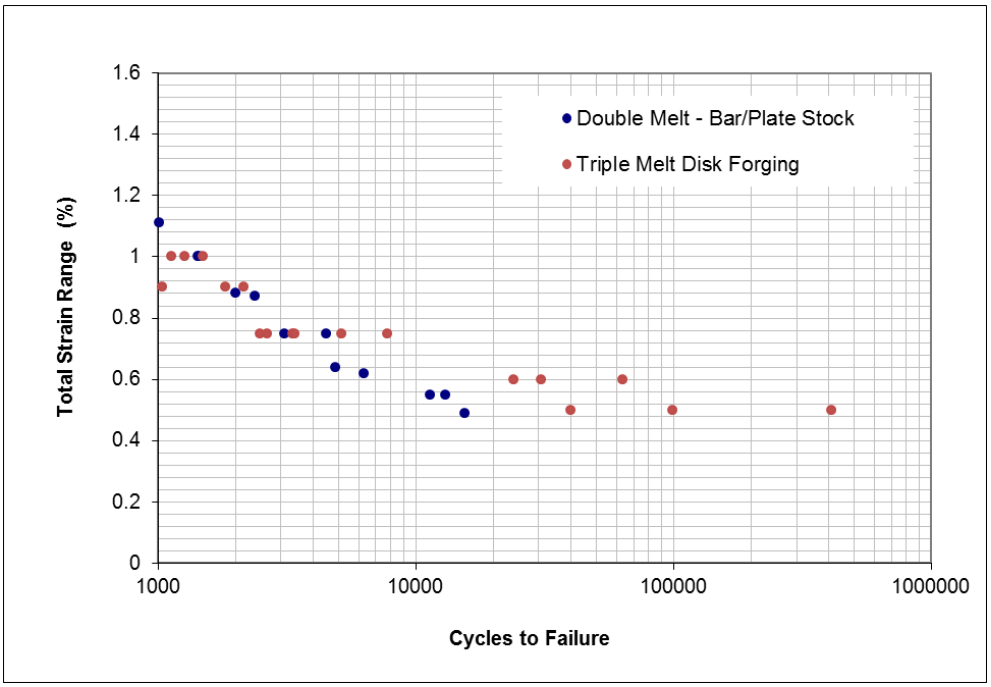

Figure 58: Low cycle fatigue data from Haynes®282® disk forging compared to commercially available Haynes®282® billet/bar

Hold time fatigue tests were performed from the large disk forging similar to the commercially available Haynes®282® billet/bar form [Figure 30]. All hold time fatigue tests were performed at 1400°F (760°) with a trapezoid waveform with a 6 hour and 1 hour hold at peak strain. Figure 59 compares the life obtained and compared to low cycle fatigue in the absence of hold time [Figure 58]. The debit in the hold time fatigue behavior was reduced dramatically by the refined structure.

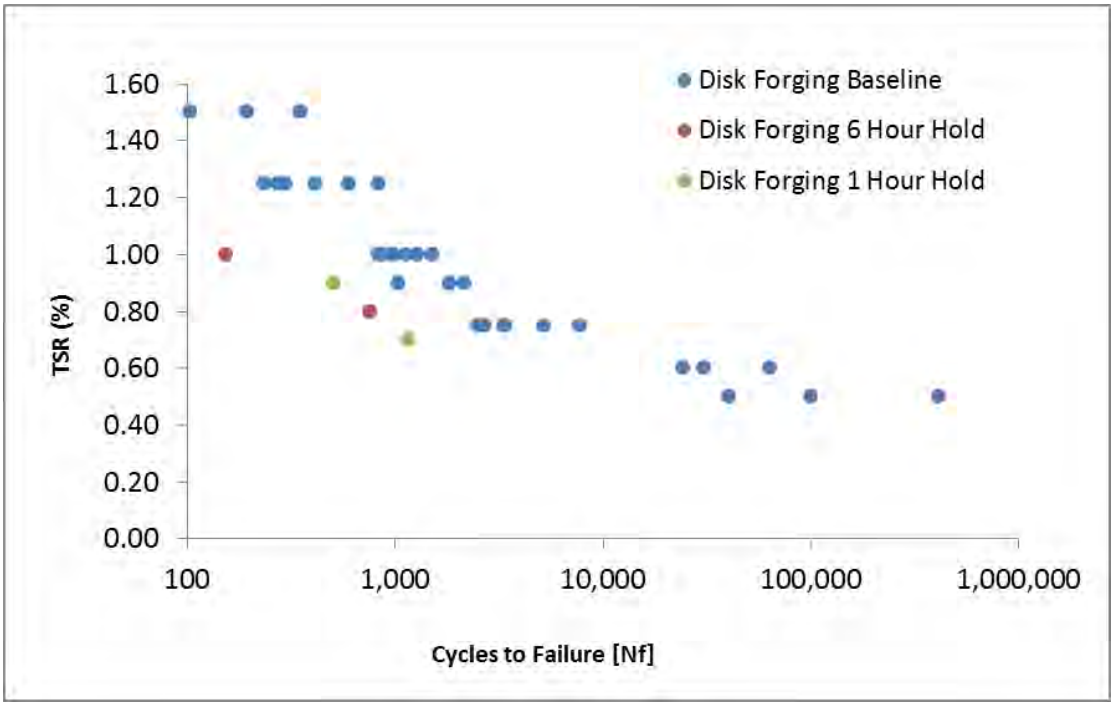

Figure 59: Hold Time Haynes®282® disk forging.

Multiple specimens were extracted from the forging for fracture toughness testing. The specimens were 0.75" thick [B] & 1.5" wide [W]. All specimens were side grooved to a depth equal to 20% of the nominal thickness [10% each side]. The specimens were tested in accordance to ASTM E1820-09. Figure 60 compared the conditional fracture toughness obtained from the fine grained disk to the commercially available Haynes®282® billet/bar. It is also clear from the figure on the gains obtained in the fracture toughness of the alloy due the finer grain size.

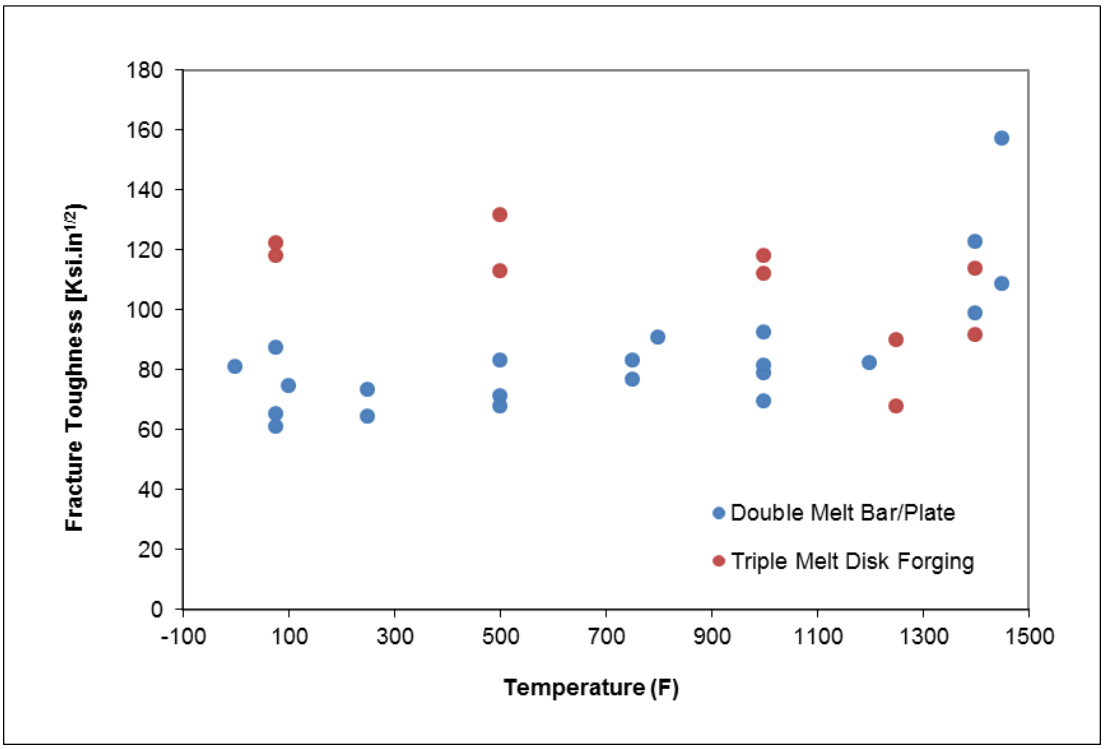

Figure 60: Fracture toughness of Haynes®282® disk forging compared to commercially available Haynes®282® billet/bar

Specimens were extracted for the development of fatigue crack growth rates in the forged Haynes®282®. All tests were performed in accordance to ASTM E647-08, Sinusoidal Waveform and 20 Hertz at room temperature (RT), 1200°F (649°C), 1300°F (704°C) and 1400°F (760°C). Figure 61 shows the curves obtained from the tests. Figure 62

compares the fatigue threshold obtained in the tests as a function of temperature and R ratio.

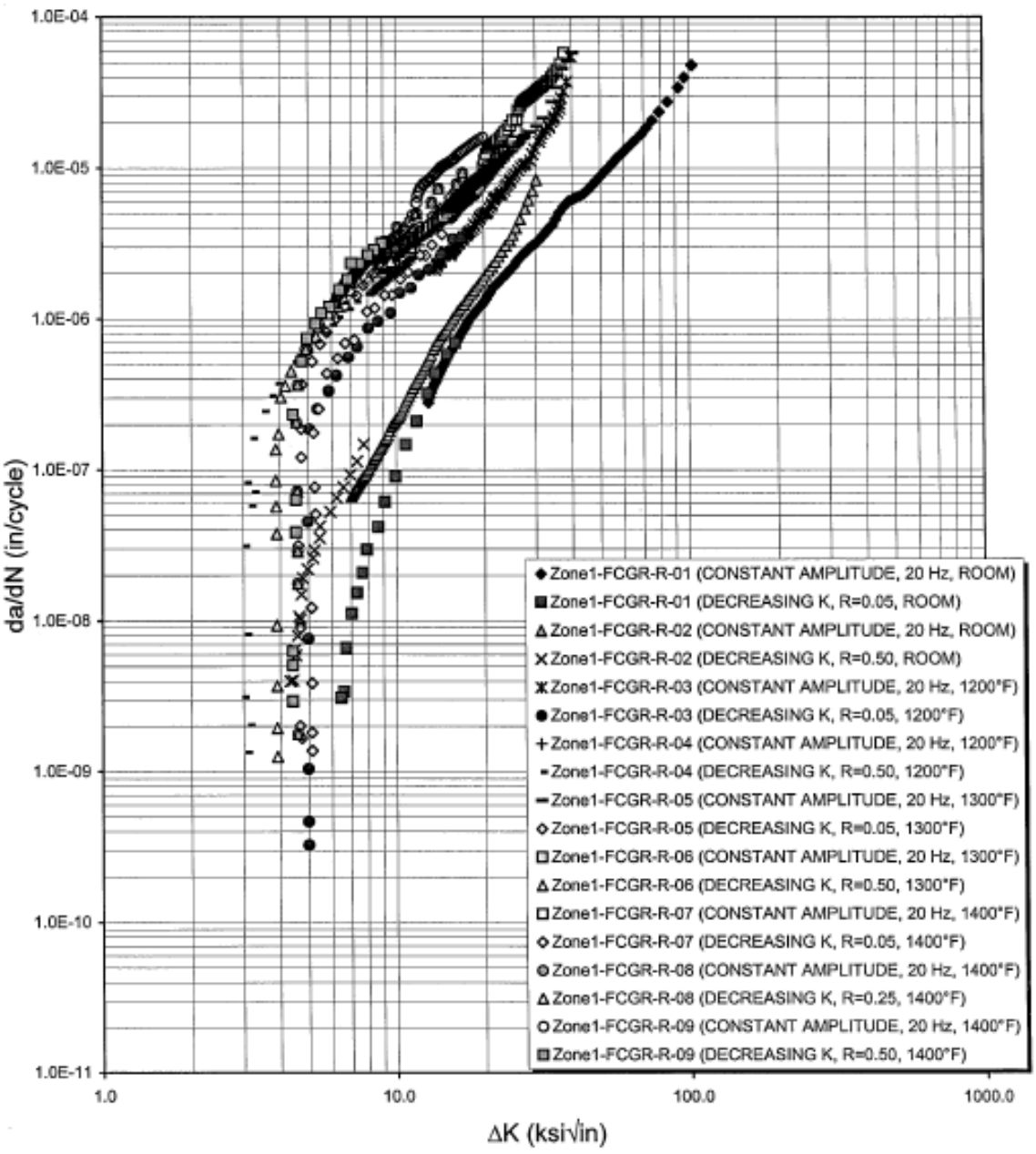

Figure 61: Fatigue crack growth rates in Haynes®282® disk forging

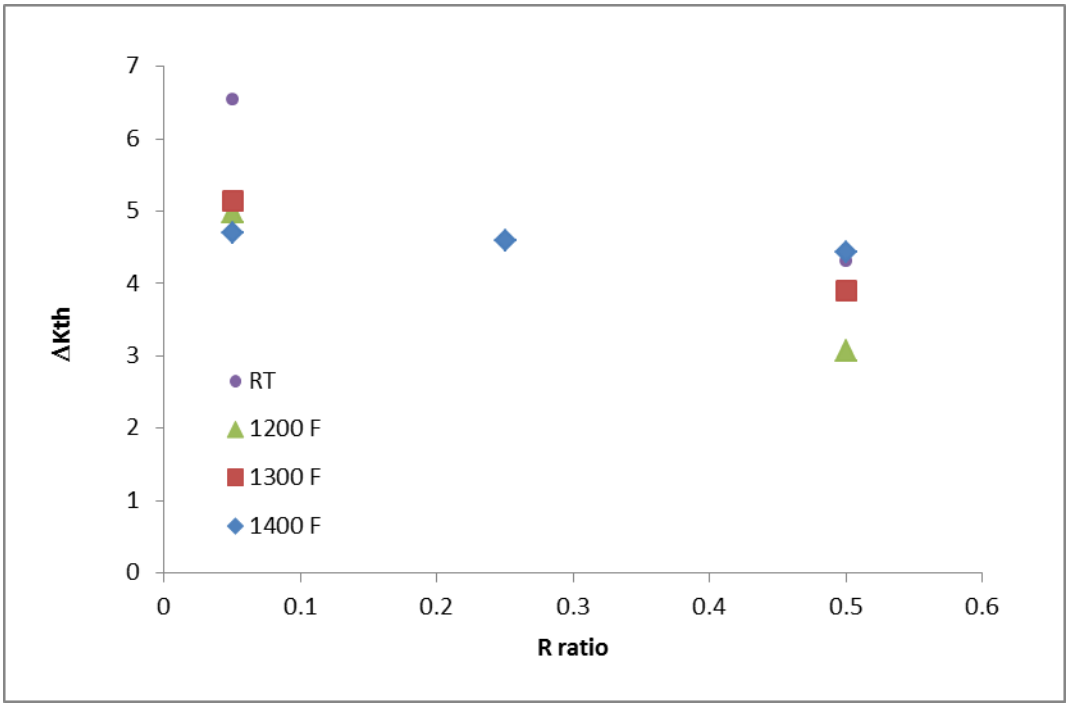

Figure 62: Fatigue threshold in Haynes®282® disk forging as a function of R ratio at various temperatures.

Creep specimens were machined from the disk to evaluate the creep-rupture properties obtained from the forged Haynes®282®disk. Table 3 shows the data obtained from the specimens.

Table 3: Creep-Rupture data obtained from Haynes®282®disk

	Temp	Stress	Time	% Elong.	% RA	% Def.
H282-1	1300	62.5	661	37.8	65.5	27.5
H282-2	1300	55	1307	31.9	63.7	31.6
H282-3	1400	40	477	51.4	79.2	42.9
H282-4	1400	35	872	50.3	76.7	44.4
H282-5	1450	32	264	82.1	83.0	48.5
H282-6	1450	27	590	55.4	79.7	45.6
H282-7	1300	50	2593	43.5	72.6	38.7
H282-10	1400	30	2301	44.9	75.1	39.8
H282-11	1400	25	4655	43.9	63.7	40.4
H282-13	1450	20	2752	57.1	70.3	52.4
H282-8	1300	45	4985	40.6	72.7	33.4
H282-9	1300	40	6771	Stopped Prior to Failure		
H282-12	1400	20	6771			
H282-14	1450	15	6771			
H282-15	1450	10	6771			

Figure 63 is a plot obtained from the fine grained Haynes®282® disk compared to commercially available Haynes®282® material. There is a reduction in life due the fine grained material [approximately 1LMP].

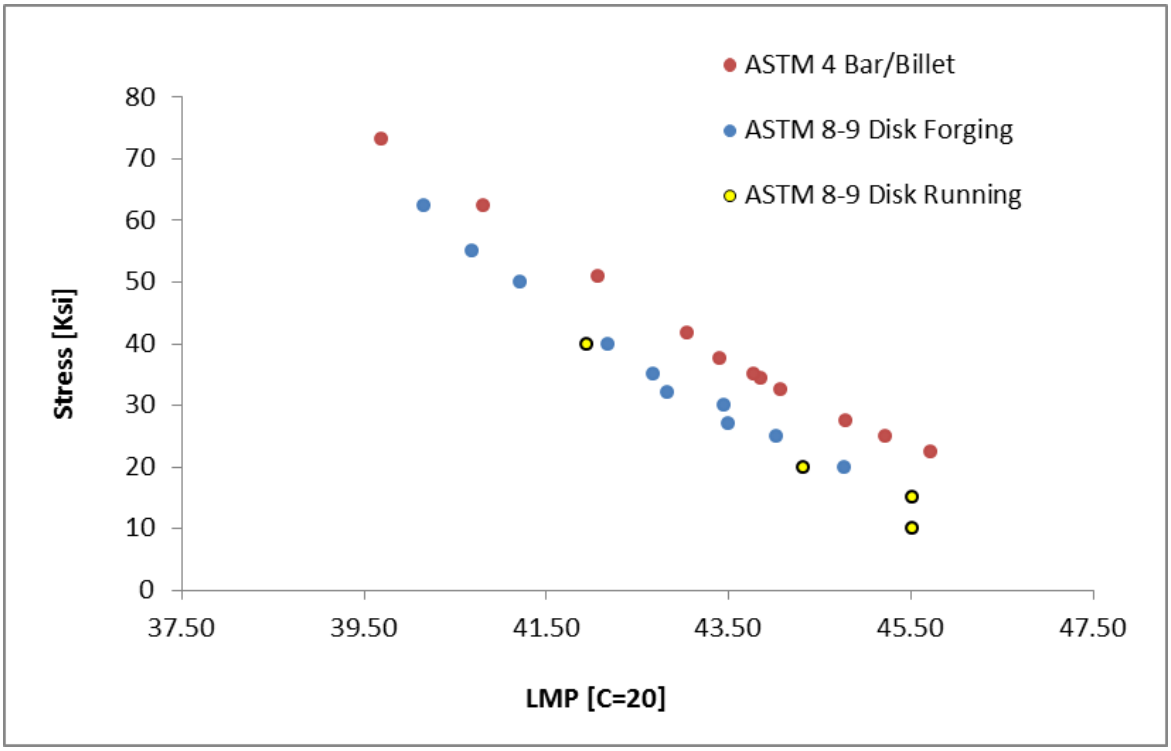

Figure 63: LMP – Rupture Stress plot of Haynes®282® disk forging

The complete dataset from the commercially available Haynes®282® [ASTM 3-4] and the finer grain size disk forging [ASTM 8-9] offer an additional design tradeoff to balance creep and fatigue during the future design process

CONCLUSIONS

Commercially available Nimonic 105 and Haynes®282® were evaluated for microstructural stability by long term thermal exposure studies. Material properties requisite for design such as tensile, creep / rupture, low cycle fatigue, high cycle fatigue, fatigue crack growth rate, hold-time fatigue, fracture toughness, and stress relaxation are documented in this report.

A key requisite for the success of the program was a need to demonstrate the successful scale up of the down-selected alloys, to large components. All property evaluations in the past were performed on commercially available bar/billet forms. Components in power plant equipment such as rotors and castings are several orders in magnitude larger and there is a real need to resolve the scalability issue. Nimonic 105 contains high volume fraction γ' [>50%], and hence the alloy is best suited for smaller forging and valve internals, bolts, smaller blades. Larger Nimonic 105 forgings, would precipitate γ' during the surface cooling during forging, leading to surface cracks. The associated costs in forging Nimonic 105 to larger sizes [hotter dies, press requirements], were beyond the scope of this task and not investigated further. Haynes®282® has 20 - 25% volume fraction γ' was a choice for large components, albeit untested.

A larger ingot diameter is pre-requisite for a larger diameter forging and achieves the "typically" accepted working ratio of 2.5-3:1. However, Haynes®282® is manufactured via a double melt process [VIM-ESR] limited by size [<18-16" diameter], which limited the maximum size of the final forging. The report documents the development of a 24" diameter triple melt ingot, surpassing the current available technology. A second triple melt ingot was manufactured and successfully forged into a 44" diameter disk. The successful developments in triple melting process and the large diameter forging of Haynes®282® resolved the scalability issues and involved the first of its kind attempt in the world for this alloy. The complete characterization of Haynes®282® forging was performed and documented in this report. The dataset from the commercially available Haynes®282® [grain size ASTM 3-4] and the finer grain size disk forging [ASTM 8-9] offer an additional design tradeoff to balance creep and fatigue during the future design process.

TASK 3 APPENDIX: Constitutive Creep Modeling and Deformation Characterization for NIMONIC 105

Monica Soare[1], Chen Shen[1], Mallikarjun Karadge[1], Deepak Saha[2]
[1] GE Global Research, 1 Research Circle, Niskayuna, NY 12309
[2] GE Power and Water, 1 River Road, Schenectady, NY 12345

1. Background

A continuum damage based creep model[1,2] was developed previously under DOE project DE-FE0005859 for the γ' strengthened nickel-base superalloy 282 for Advanced Ultra-Supercritical (A-USC) steam turbine rotor application at temperatures around 1400˚F. The model has been subsequently extended under the DOE project DE-FE0024027 for a broader range of application temperatures. It has been validated for alloy 282 on isothermal creep tests at temperatures between 1375 and 1700˚F, and stresses between 15 and 40Ksi. Depending on the actual temperature and stress in the aforementioned regime, it was observed that the dominating deformation mechanisms in alloy 282 were diffusion creep and dislocations climb-bypassing γ' particles, acting either independently or in a coupled way.

The current study explored the applicability of the model to NIMONIC 105 alloy under A-USC application conditions. The model was tested by using the same analytic forms of the constitutive equations as formulated for alloy 282 but with microstructural parameters, elastic parameters and fitted parameters reflecting NIMONIC 105 properties.

In order to explain in more details the procedure, the general formulation of the creep model is recalled in Section 2. A list of the parameters (fitted or microstructural) specific to NIMONIC 105 is provided in Section 3. The γ' evolution in NIMONIC 105 is summarized in Section 4. Section 5 compares the creep model predictions with experimental data. A few comments on the model limitations and potential paths ahead to address them are included in Section 6. TEM characterization of creep deformation mechanisms is summarized in Section 7.

2. Model equations

In order to capture both diffusion and dislocation mechanisms in a unified creep model the total creep strain, ε^{creep} was considered as a superposition of dislocation component, ε^{disloc}, and diffusion component, $\varepsilon^{diffusion}$:

$$\varepsilon^{creep} = \varepsilon^{disloc} + \varepsilon^{diffusion} \quad (1)$$

2.1. Dislocation component

For dislocation gliding and climb-bypassing precipitates, Dyson *et al*[3-5] proposed a hyperbolic sine dependence of the strain rate, $\dot{\varepsilon}^{disloc}$, on the net stress required to advance a dislocation:

$$\dot{\varepsilon}^{disloc} = \begin{cases} \rho A D_V f(1-f)\left(\sqrt{\frac{\pi}{4f}} - 1\right)\sinh\left(C\frac{\sigma_{eff}-\sigma_B-\sigma_o}{MkT}b^2\lambda\right), & \text{if } \sigma_{eff}-\sigma_B-\sigma_o > 0 \\ 0 & \text{othewise} \end{cases} \quad (2)$$

Where A and C are constant parameters, ρ is the density of dislocations, f is the volume fraction of precipitates, M is Taylor factor, k is Boltzmann constant, T is the absolute temperature, b is the Burgers vector, and λ is the average spacing between precipitates. Since each gliding dislocation encounters a series of obstacles, the net stress that drives the dislocation motion was taken as the local effective stress, σ_{eff}, subtracted by a penalty due to the interaction with other dislocations (forest dislocation strengthening term), σ_o, and a penalty due to the interaction with precipitates (back stress), σ_B. The effective stress, σ_{eff}, is further discussed in Section 2.3.

Using the Taylor law, the dislocation strengthening term is proportional to the square root of dislocation density ρ [6]:

$$\sigma_o = 0.25MG(T)b\sqrt{\rho} \quad (3)$$

where $G = E(T)/2(1+\nu)$ is the shear modulus, and ν the Poisson's ratio.

We considered that dislocation creep proceeds via either climb-bypass or shearing precipitates. For shearing precipitates with weakly coupled dislocation pairs, the back stress can be calculated as [7]:

$$\sigma_{shear} = \frac{\gamma_{APB}}{2b}\left[\left(\frac{12\gamma_{APB}fr}{\pi Gb^2}\right)^{1/2} - f\right] \quad (4)$$

Where γ_{APB} is the anti-phase boundary energy, r is the average size of precipitates. The hypothesis of the weakly coupled dislocations is made on the consideration that the space between the precipitates is large compared with their radius (about three times larger in Alloy 282). However, this may not be the case for NIMONIC 105 since the inter-particle space is significantly smaller. The actual possible mechanisms were studied by TEM image analysis of deformed samples. The TEM observations are included in a separate section.

The analytic form proposed for the back stress for dislocation climb-bypass included the strong dependence of precipitated volume fraction f, dislocation creep strain ε^{disloc}, elastic modulus E and effective stress σ_{eff} [3-5]

$$\sigma_{climb} = \frac{2f}{1+2f}\sigma_{eff}\left[1 - \exp\left(-\frac{1+2f}{2(1-f)}E\frac{\varepsilon^{disloc}}{\sigma_{eff}}\right)\right] \quad (5)$$

For simplicity, the model considered that the creep deformation was driven predominantly by the weaker mechanism, either shearing or climb-bypass at a given time, although there could be a transitional regime where both were active. The back stress was thus taken as:

$$\sigma_B = \min(\sigma_{shear}, \sigma_{climb}) \quad (6)$$

Typically, separate methods are being used (e.g. TEM images based) to identify the evolution of dislocation density. When these are not available, we fit a simple linear dependence followed by a plateau, on creep strain as:

$$\rho = \begin{cases} \rho_i + (\rho_f - \rho_i)\varepsilon/\varepsilon^{crit} & \text{if } \varepsilon \le \varepsilon^{crit}(\sigma_{applied}, T) \\ \rho_f & \text{if } \varepsilon > \varepsilon^{crit}(\sigma_{applied}, T) \end{cases} \quad (7)$$

with $\varepsilon^{crit} = B\ \sigma_{applied}[MPa]$.

2.2. Diffusion component

According to Cocks and Ashby [8,9] the diffusion creep strain rate $\dot{\varepsilon}^{diffusion}$ can be contributed by multiple sources: lattice diffusion $\dot{\varepsilon}^{lattice_diff}$, grain boundary diffusion $\dot{\varepsilon}^{boundary_diff}$, surface diffusion at the grain boundary cavities $\dot{\varepsilon}^{cavity_surface_diff}$, and grain boundary diffusion near cavities $\dot{\varepsilon}^{cavity_boundary_diff}$:

$$\dot{\varepsilon}^{diffusion} = \dot{\varepsilon}^{lattice_diff} + \dot{\varepsilon}^{boundary_diff} + \dot{\varepsilon}^{cavity_boundary_diff} + \dot{\varepsilon}^{cavity_surface_diff} \quad (8)$$

The grain boundary and lattice diffusion components, which do not contribute to the cavity growth, can be written as:

$$\dot{\varepsilon}^{boundary_diff} = 3\pi\xi\left(\frac{l}{d}\right)^3\sigma_{applied}(1+\varepsilon^{creep}) \quad (9)$$

$$\dot{\varepsilon}^{lattice_diff} = \xi\beta\sigma_{applied}(1+\varepsilon^{creep}) \quad (10)$$

where $\beta = \frac{3D_V}{D_B\delta_B}\frac{l^3}{d^2}$ and $\xi = F\frac{4D_B\delta_B}{d^3}\left(\frac{l}{d}\right)^3$

For both alloy 282 and NIMONIC 105 we used the self-diffusivity of Ni: $D_V = 9.2 \times 10^{-5} \exp\left(-\frac{278kJ/mol}{RT}\right) m^2/s$ for bulk diffusion and $D_B\delta_B = 7.7 \times 10^{-14} \exp\left(-\frac{162kJ/mol}{RT}\right) m^3/s$ for grain boundary diffusion[10], and the ratio l/d~0.1, where the grain size was taken as $100\mu m$ for both alloy 282 and NIMONIC 105.

As discussed by Cocks and Ashby [8,9], the growth of cavities through diffusion is associated also with the change in the overall strain rate. The strain rate contribution due to cavities boundary diffusion was taken as:

$$\dot{\varepsilon}^{cavity_boundary_diff} = \xi \frac{l}{d} \frac{\sigma_{applied}}{\ln(1/\varpi_{boundary_diff})} \tag{11}$$

while the strain rate contribution due to cavities surface diffusion was:

$$\dot{\varepsilon}^{cavity_surface_diff} = \xi\alpha \frac{\sqrt{\varpi_{surface_diff}}\sigma_{applied}{}^2}{(1-\varpi_{surface_diff})^3} \tag{12}$$

Where $\alpha = \frac{D_S\delta_S}{D_B\delta_B}\frac{1}{\sqrt{2}}\frac{l^2}{d\gamma}$

2.3. Damage variable evolution and effective stress

Although the governing equation (2) is able to describe a nonlinear increase of creep strain toward later times, tertiary creep and especially the associated grain boundary cavity growth are not well accounted for. For NIMONIC 105 the existence of cavitation mechanisms at the grain boundaries was clearly identified. The optical images included in Figure 12 to Figure 18, at various loading conditions showed clearly multiple grain boundaries cavities and cracks. The density of the cracks appeared to increase in the vicinity of the rupture surface.

The model correlates the nucleation and growth of grain boundaries cavities to a macroscopic change of the effective cross-sectional area of the creep sample, A. Denoting by A_0 the initial cross-sectional area and by ϖ the factor related to its change: $\varpi = 1 - A/A_0$, the effective stress in the gage area of a creep specimen was written as:

$$\sigma_{eff} = \frac{\sigma_{applied}}{(1-\varpi)}(1 + \varepsilon^{creep}) \tag{13}$$

Following[8,9,11] we assumed that the cavities can grow though deformation of the neighboring grains ϖ_{disloc} or diffusion into the neighboring grains ϖ_{diff}

$$\varpi = \varpi_{diff} + \varpi_{disloc} \tag{14}$$

According to [11], the combined effects of diffusion and deformation become relevant at temperatures above half melting temperature (>1200°F) and at stress levels beyond $10^{-3}G$ (where G is the shear modulus).

For simplicity, a simple linear dependence on strain is used for the dislocation component [12,13]:

$$\dot{\varpi}_{disloc} = D\dot{\varepsilon}^{disloc} \tag{15}$$

The diffusion damage variable couples the boundary diffusion component $\varpi_{boundary_diff}$ and cavity surface diffusion component $\varpi_{surface_diff}$:

$$\varpi_{diff} = \varpi_{boundary_diff} + \varpi_{surface_diff} \tag{16}$$

As proposed by Cocks and Ashby[8,9], the boundary diffusion damage variable evolved as:

$$\dot{\varpi}_{boundary_diff} = \frac{\xi}{2}\frac{\sigma_{applied}(1+\varepsilon^{creep})}{\sqrt{\varpi_{boundary_diff}}\ln(1/\varpi_{boundary_diff})} \tag{17}$$

while the surface diffusion damage variable evolved as:

$$\dot{\varpi}_{surface_diff} = \frac{\xi\alpha}{4}\frac{d}{\gamma}\frac{\sqrt{\varpi_{surface_diff}}[\sigma_{applied}(1+\varepsilon^{creep})]^3}{(1-\varpi_{surface_diff})^3} \tag{18}$$

where d is grain size, γ the surface energy, and α a scaling parameter:

$$\alpha = \frac{D_S\delta_S}{D_B\delta_B}\frac{1}{\sqrt{2}}\frac{l^2}{d\gamma} \tag{19}$$

which depends on the surface diffusion coefficient $D_S\delta_S$, boundary diffusion coefficient $D_B\delta_B$, and l, the average distance between two neighboring voids. Based on the reported diffusivities values for various materials [10] we consider $D_S\delta_S$ on the same order of magnitude as $D_B\delta_B$.

Equations (1)-(19) constitute the proposed creep model formulation for capturing the main creep mechanisms of diffusion, dislocation climb-bypass, and to some limited extend, γ' shearing.

3. Model parameters

We divided the model parameters in two categories:

(i) Extrinsic parameters – which have the same expression (either numerical or analytic) for alloy 282 and NIMONIC 105. These are listed in Table 1.

(ii) Intrinsic parameters – which are specific to each alloy type (Table 2). These were divided in two subcategories: microstructural (measurable) and fitted. The parameter fitting was performed at 1400 and 1500˚F.

Table 1: Parameters with similar values or analytic expressions for alloy 282 and NIMONIC 105:

Parameter name	Symbol	Value	Source
Activation volume	Ω	$1.2 \times 10^{-29} m^3$	Thermodynamic calculations
Burgers vector	b	2.54Å	Ni lattice parameter
Taylor Factor	M	3.07	Typical for FCC metal
Void diameter/grain diameter ratio	l/d	0.1	Estimated
Lattice diffusion parameter	β	$\beta = \frac{3D_V}{D_B\delta_B}\frac{l^3}{d^2}$	Ref.[8,9]
Self-diffusion coefficient of Ni	D_V	$9.2 \times 10^{-5} \exp\left(-\frac{278}{RT}\frac{kJ}{mol}\right)\ m^2/s$	Ref.[10]
Bulk diffusion parameter	$D_B\delta_B$	$7.7 \times 10^{-14} \exp\left(-\frac{162}{RT}\frac{kJ}{mol}\right) m^3/s$	Ref.[10]
Diffusion related parameter	ξ	$4D_V/(d^3KT(l/d)^3)$F K Boltzmann constant 1.38e-23J/K T in Kelvin	Ref.[8,9]
Surface Energy	γ	2 J/m^2	Estimated
Anti-phase boundary energy	γ_{APB}	0.15 J/m^2	Estimated
Boundary diffusion parameter	α	$\alpha = \frac{D_S\delta_S}{D_B\delta_B}\frac{1}{\sqrt{2}}\frac{l^2}{d\gamma}$	Ref.[8,9]
Inter-precipitates spacing	λ	$\lambda = 1.6\left(\sqrt{\pi/(4f)} - 1\right)r$	Phase field simulation
Poisson's ratio	ν	0.3	Estimated

Table 2: Parameters updated for NIMONIC 105:

Parameter name	Symbol	Value	Source
Average grain size	d	$\mathbf{100\mu m}$	Characterization
Precipitates volume fraction	f	$\left[0.5 - 27850\ exp\left(-\frac{119.4}{RT}\frac{kJ}{mol}\right)\right] / \left[1 - 27850\ exp\left(-\frac{119.4}{RT}\frac{kJ}{mol}\right)\right]$	Ref.[14]
Precipitate mean radius	r	$k = 2.13e + 11\ exp\left(-\frac{420.75}{RT}\frac{kJ}{mol}\right)$	Ref.[15]

		$r = [0.0002 + kt]^{1/3}$	
Elastic Modulus	E	$-0.0152T^2 - 16.4T + 2.22e+5$ [MPa] T temperature in F	Ref.[13]
Ultimate tensile strength	UTS	$-5.397e-7T^3 + 9.253e-4T^2 - 0.4641T + 1.228$ [MPa] T temperature in F	Ref.[13]
Initial and saturation dislocation densities	ρ_i ρ_f	$0.001 \times 10^{12}/m^2$ $0.00239 \times 10^{12}/m^2$	Estimated Fitted
Creep strain rate coefficient	A	0.97E-3 1/s	Fitted (Same as for alloy 282)
Dislocation density parameter	B	1e-7	Fitted
Creep strain rate parameter	C	1	Not used in the latest version
Damage evolution parameter	D	2	Fitted
Creep diffusion parameter	F	0.0054	Fitted

4. Precipitate (γ') microstructure evolution

The controlling microstructure in NIMONIC 105 under creep conditions is the ordered $L1_2$ γ' precipitates. Compared with alloy 282, NIMONIC 105 has a higher level of γ' content. At 1400-1500˚F the γ' precipitates constitutive about 45% total volume fraction. In Figure 1, the γ' volume fraction by ThermoCalc calculation with TCNI database[16] (version 5) is seen to agree with the experimental measurement by Nembach *et al* [14]. In addition, the TCNI database predicts γ' solvus temperature at 1918˚F. Experimental measurement with differential scanning calorimetry (DSC) found that during cooling γ' started to form at about 1893˚F (Figure 2). Taking into account the typical 20-40˚F of undercooling for γ' nucleation, the predicited γ' solvus is in reasonble agreement with the experimental DSC result. In the creep model we thus took the analytical form of Nembach *et al*[14] for γ' volume fraction.

While the volume fraction stays nearly constant at a given temperature, the size of γ' precipitates continuously increases due to coarsening. Betteridge and Heslop[15] reported an experimental study of γ' growth under isothermal aging conditions between 800 and 1000˚C (1472-1832˚F). The data indicated a well behaved cubic coarsening trend. We therefore adopted a conventional cubic law equation to represent γ' sizes in NIMONIC 105 over the long-term creep times:

$$D^3(t) - D_0^3 = K_0 \exp\left(-\frac{Q}{RT}\right) t \qquad (20)$$

Here D is the average size (equivalent spherical diameter) of γ' at time t, D_0 the initial size, and T the absolute temperature. The pre-factor K_0 and the activation energy Q were determined to be, respectively, $2.134 \times 10^{-7} m^3/s$ and $420.7 kJ/mol$ by fitting the equation to Betteridge and Heslop's data. Figure 3 compares the original experimental data[15] and the fit equation (20).

Finally, the initial γ' microstructure from an untested creep bar is shown in Figure 4. The γ' precipitates are seen in cuboidal shape with average size about 150nm.

5. Model predictions

The model predictions were compared with experiments in terms of creep strain (Figure 5), creep strain rate (Figure 6), and rupture time (Figure 7-Figure 9). The rupture time was estimated as the minimum time when either one of the equations are satisfied:

(i) The effective stress reaches the Ultimate stress value

$$UTS = \frac{\sigma_{applied}}{(1-\varpi(t_c))}(1 + \varepsilon^{creep}(t_c)) \quad (21)$$

or

(ii) The strain rate becomes high (A value of 1e-8/s was calibrated on 1400F, 32Ksi data)

$$\dot{\varepsilon}^{creep}(t_c) = 10^{-8}/s \quad (22)$$

The evolution of damage variable until rupture time is represented in Figure 10.

In order to estimate the accuracy of the model, we used the z-value estimation procedure [17]

$$Z = 10^{2.5\mathrm{Std}[\log(\varepsilon_{predicted})-\log(\varepsilon_{actual})]} \quad (23)$$

which accounts for the standard deviation of the difference between the logarithm of the predicted strain and logarithm of the experimental strain. The data points are collected at various temperatures and stress levels for a given strain value. The model is considered ideal if the z-value is smaller than 2, acceptable if the z-value is between 2 and 4, and unacceptable if the z-value is higher than 4. In order to assess the accuracy of the creep model we computed the z-value for the 8 stress-temperature conditions highlighted in Figure 11. As shown in Figure 11, the z value is smaller than 1.6 for strain values between 0.5% and 2%.

6. Comments and future model development

Visually (Figure 6) and by calculating the z-value (Figure 11) we observed that the recalibration of the damage based creep model, originally developed for alloy 282, predicted fairly well the experiments for NIMONIC 105.

However, we acknowledge that the current version of the model incorporates only diffusion, dislocation climb, and only to some limited extend (the lower boundaries) γ' shear mechanisms. The TEM characterization studies on NIMONIC 105 ruptured samples indicated that additional creep deformation modes, such as micro-twinning and γ' shearing, may have been operative. These mechanisms can be incorporated in the future development. Also, the advancement of micro-cavities measurement techniques may open new possibilities of a better model for cavities growth and coalescence.

7. Creep deformation mechanisms

7.1. Procedure

Transmission electron microscopy (TEM) examination was conducted on crept (to failure) specimens to identify mechanisms of deformation. Creep conditions utilized for obtaining the creep specimens are listed in Table 3. Thin foils were prepared from discs sectioned perpendicular to the stress axis. Foils were mechanically ground to a thickness of ~100 μm from which 3mm disks were punched. Final thinning was achieved on a Fischione jet polishing unit using an electrolyte consisting of 80% methanol and 20% perchloric acid at -40C. Analysis was done on the FEI Osiris TEM operating at 200kV. Defect structures were imaged using two beam diffraction conditions.

It should be noted that TEM examination was conducted on specimens crept to failure, therefore signatures of tertiary creep may well be present within the foils although the foils were sectioned ~10 mm away from the fracture surface.

As received microstructure structure has been discussed in Section 4.

Table 3: Creep testing conditions of specimens for TEM study

heat #	cond.	temp (F)	stress (ksi)	time (h)	strain (%)	elong. (%)	RA (%)	LMP_f
As received	PA	-	-	-	-	-	-	-
N105CRP-008	PA	1400	32	34955	6.118	6.7	11.1	45.65
N105-CRP-007	PA	1425	32	18583	5.386	6	12.3	45.74
N105-CRP-004	PA	1450	26	24950	4.35	4.6	10.6	46.59

N105-CRP-002	PA	1475	24	18363	4.394	4.7	8.9	46.95
N105-CRP-001	PA	1500	24	10122	3.363	6.1	7	47.05

7.2. Observations

A variety of creep deformation mechanisms are possible in γ' strengthened nickel-base superalloys dependent on factors such as temperature, stress, alloy chemistry and microstructure. The typically reported mechanisms, in order of increasing propensity with temperature are: (1) Orowan looping and pairwise APB shearing of γ' precipitates by ½<110> dislocations, (2) shearing by stacking fault formation in the γ' precipitates, (3) planar activity by microtwinning, (4) formation of continuous / extended faults spanning matrix and the precipitates and (5) dislocation climb bypass. Mechanisms 1-4 usually lead to 'planar slip' like microstructural appearance upon deformation with clear signatures observed for the respective mechanisms. Cross-slip and dislocation climb bypass lead to 'wavy slip' like appearance in the deformed microstructure.

A summary of the findings is presented in Table 4. Primary and secondary modes are highlighted in the observations where primary mode is the predominant mode of creep deformation.

Table 4: Deformation modes observed by TEM

specimen	N105CRP-008 (1400F)	N105-CRP-007 (1425F)	N105-CRP-004 (1450F)	N105-CRP-002 (1475F)	N105-CRP-001 (1500F)
primary/predominant mechanism	high density of continuous faulting/ microtwinning	unpaired dislocations : cross slip, looping, climb	unpaired dislocations : cross slip, looping, climb	unpaired dislocations : cross slip, looping, climb	unpaired dislocations : cross slip, climb

secondary observations	½<110> pairwise shear unpaired dislocations –cross slip	½<110> pairwise shear	½<110> pairwise shear shear localization in γ channels (formation of long γ channels)	½<110> pairwise shear shear localization in γ channels (formation of long γ channels) limited continuous faulting	½<110> pairwise shear (very less)
slip type	planar	wavy	wavy	wavy	wavy

7.3. 1400˚F creep

Figure 19(a-c) shows that at 1400˚F, deformation was predominantly planar in nature. Majority of the features were those of continuous stacking faults with some microtwins interspersed in the same orientation both spanning the γ/γ' structure. Apart from this a significant activity of ½<110> matrix dislocations was also observed (Figure 19(d)) indicating cross slip/ climb of dislocations representative of contribution from other mechanisms. These observations point out that, 1400˚F, under the current stress used for creep testing, is more likely to be just above the microtwinning regime as at 1400˚F mixed signatures of continuous faulting, microtwinning and wavy slip activity were observed and that beyond 1400˚F planar slip completely disappeared.

7.4. 1425 – 1500˚F creep

Deformation structures remained similar across the 1425-1500˚F temperature range (Figure 20). The most likely deformation mode is combination of climb and cross-slip with some amount of pair-wise shearing of γ'. The dislocation density was extremely high corresponding to a higher strain achieved (3-5 %) in creep to failure. Within these microstructures one can notice that some amount of looping is present around the γ' precipitates. Additionally intense dislocation activity along continuous γ channels was observed in some specimens (Figure 21). The origin (creep deformation or as-received structure) of these continuous γ channels is unknown. Stacking fault and microtwinning activity was completely absent indicating the typical high temperature creep mechanisms being active.

References

1 Soare, M. & Shen, C. Modeling Long-term Creep Performance for Welded Nickel-base Superalloy Structures for Power Generation Systems: Topical Report: Constitutive Creep Model for Alloy 282. (2015).

2 Shen, C. Modeling Creep-Fatigue-Environment Interactions in Steam Turbine Rotor Materials for Advanced Ultra-supercritical Coal Power Plants, A Final Report. doi:http://dx.doi.org/10.2172/1134364 (2014).

3 Dyson, B. F. Creep and Fracture of metals: mechanisms and mechanics. *Revue de Physique Appliquée* **23**, 605-613 (1988).

4 Dyson, B. F. Microstructure based creep constitutive model for precipitation strengthened alloys: theory and application. *Mat Sci. Tech* **25**, 213-220 (2009).

5 McLean, M. & Dyson, B. F. Modeling the Effects of Damage and Microstructural Evolution on the Creep Behavior of Engineering Alloys. *Journal of Engineering Materials and Technology* **122**, 273-278, doi:10.1115/1.482798 (2000).

6 Kassner, M. E. & Pérez-Prado, M. T. *Fundamentals of Creep in Metals and Alloys*. (Elsevier Science Ltd, 2004).

7 Reed, R. C. *The Superalloys, Fundamentals and Applications*. (Cambridge University Press, 2006).

8 Cocks, A. C. F. & Ashby, M. F. Intergranular fracture during power-law creep under multiaxial stresses. *Metal Science* **14**, 395-402, doi:10.1179/030634580790441187 (1980).

9 Cocks, A. C. F. & Ashby, M. F. On creep fracture by void growth. *Progress in Materials Science* **27**, 189-244, doi:http://dx.doi.org/10.1016/0079-6425(82)90001-9 (1982).

10 Divinski, S. V., Reglitz, G. & Wilde, G. Grain boundary self-diffusion in polycrystalline nickel of different purity levels. *Acta Materialia* **58**, 386-395, doi:http://dx.doi.org/10.1016/j.actamat.2009.09.015 (2010).

11 Needleman, A. & Rice, J. R. Plastic creep flow effects in the diffusive cavitation of grain boundaries. *Acta Metallurgica* **28**, 1315-1332, doi:http://dx.doi.org/10.1016/0001-6160(80)90001-2 (1980).

12 Hayhurst, D. R., Lin, J. & Hayhurst, R. J. Failure in notched tension bars due to high-temperature creep: Interaction between nucleation controlled cavity growth and continuum cavity growth. *International Journal of Solids and Structures* **45**, 2233-2250, doi:http://dx.doi.org/10.1016/j.ijsolstr.2007.11.026 (2008).

13 Perrin, I. J. & Hayhurst, D. R. A method for the transformation of creep constitutive equations. *International Journal of Pressure Vessels and Piping* **68**, 299-309, doi:http://dx.doi.org/10.1016/0308-0161(95)00069-0 (1996).

14 Nembach, E., Pesicka, J. & Langmaack, E. The high-temperature decrease of the yield strength of the γ' -strengthened superalloys NIMONIC PE16 and NIMONIC 105. *Materials Science and Engineering: A* **362**, 264-273, doi:http://dx.doi.org/10.1016/S0921-5093(03)00593-8 (2003).

15 Betteridge, W. & Heslop, J. in *The Nimonic Alloys* (Edward Arnold, London, 1974).

16 TCNI. *TCS Ni-based superalloys database*, <http://www.thermocalc.com/media/23648/dbd_tcni8.pdf> (

17 Holmström, S. & Auerkari, P. Robust prediction of full creep curves from minimal data and time to rupture mode. *Energy Materials, Materials Science & Engineering for Energy Systems* **1**, 249-255 (2006).

Figures:

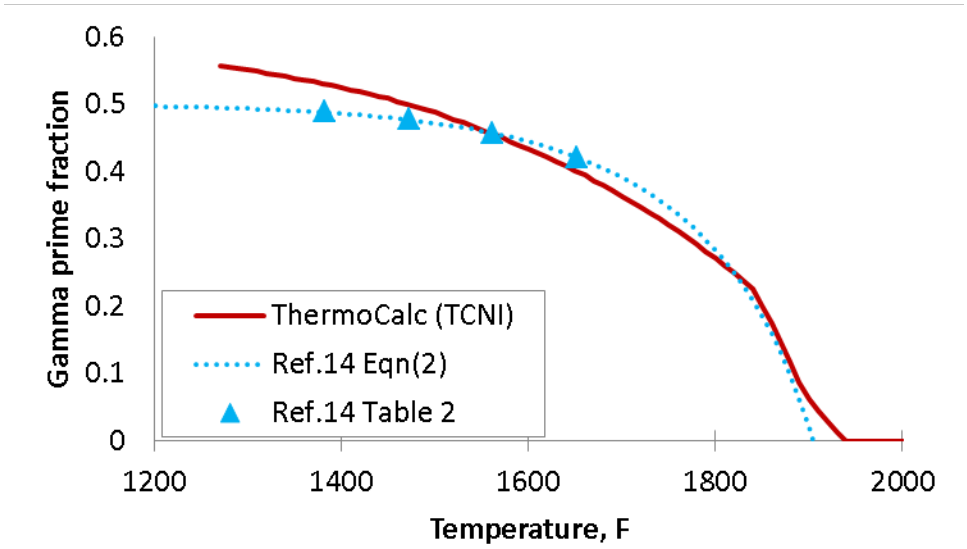

Figure 1: γ' volume fraction in NIMONIC 105. The ThermoCalc calculation (red curve) agrees well with the experimental data of Nembach et al [14]. The blue dotted curve is a parametric fit to the experimental data. The same equation is used in the model and is listed in Table 2.

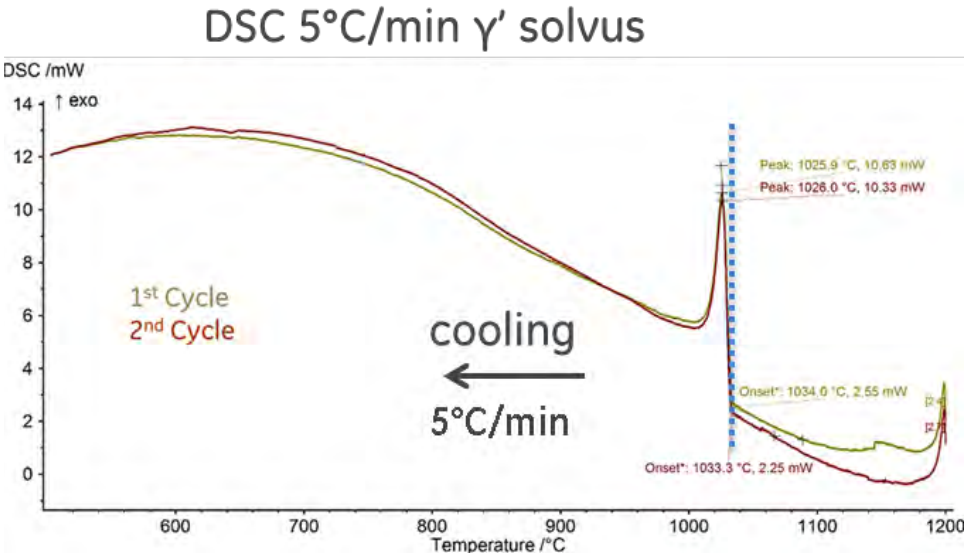

Figure 2: Differential scanning calorimetry (DSC) analysis of NIMONIC 105. The dotted line indicates that γ' starts to form at 1034˚C (1893˚F).

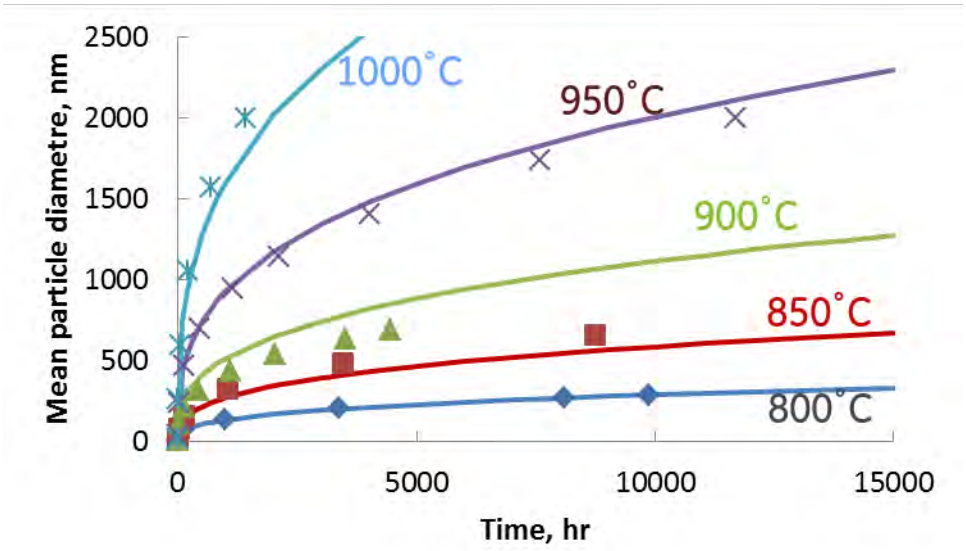

Figure 3: NIMONIC 105 γ' coarsening. Symbols are experimental data (discretized) from [15]. Lines are from Equation (20).

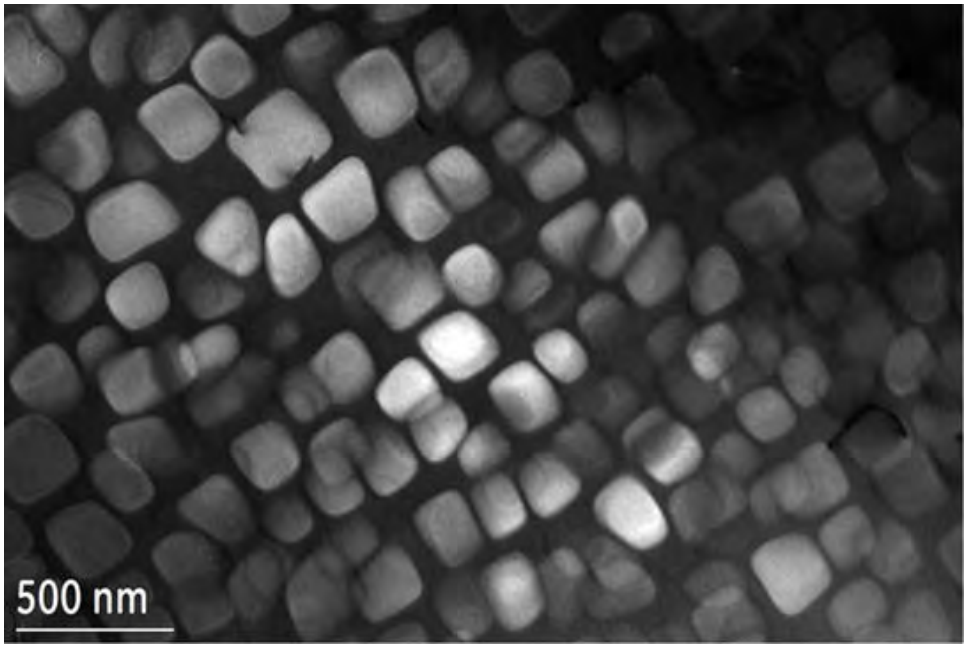

Figure 4: TEM image of the initial γ' microstructure of NIMONIC 105 from an untested creep specimen.

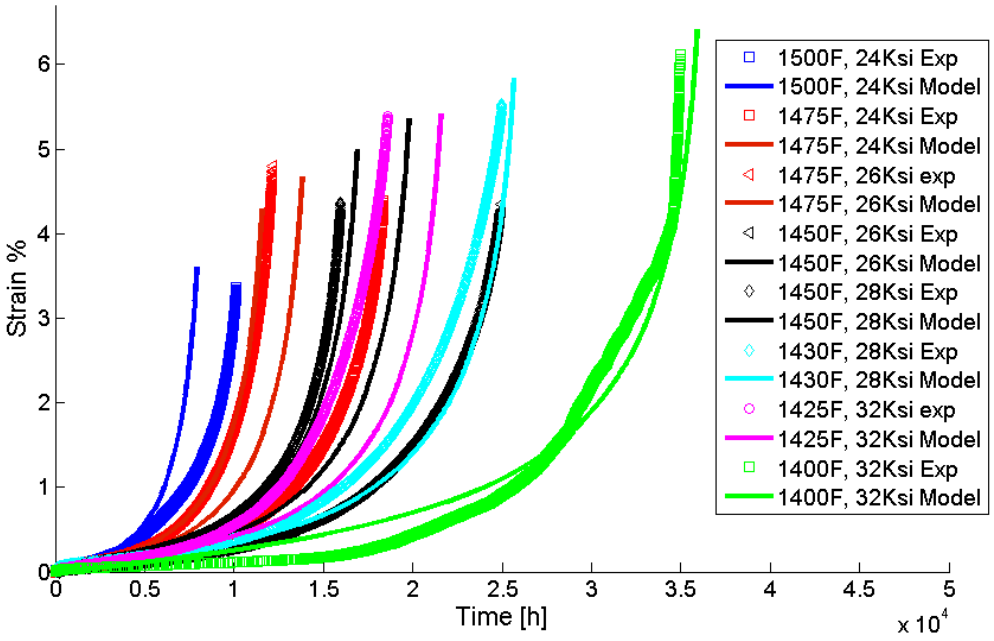

Figure 5: Creep strain evolution with time for various temperatures and stress levels. Experiment (symbols) and model predictions (continuous lines).

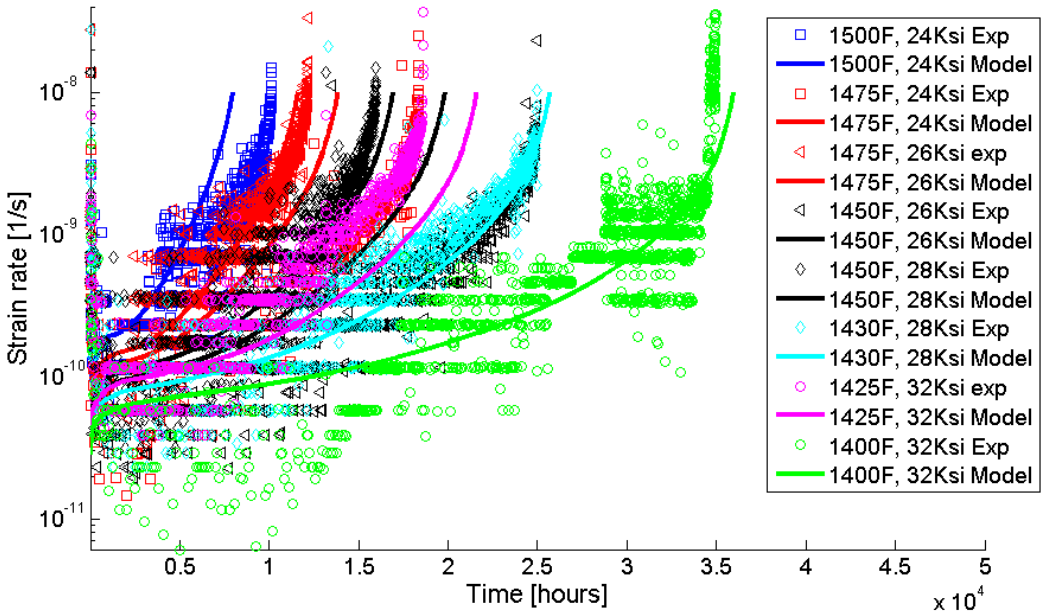

Figure 6: Creep strain rate evolution with time for various temperatures and stress levels. Experiment (symbols) and model predictions (continuous lines).

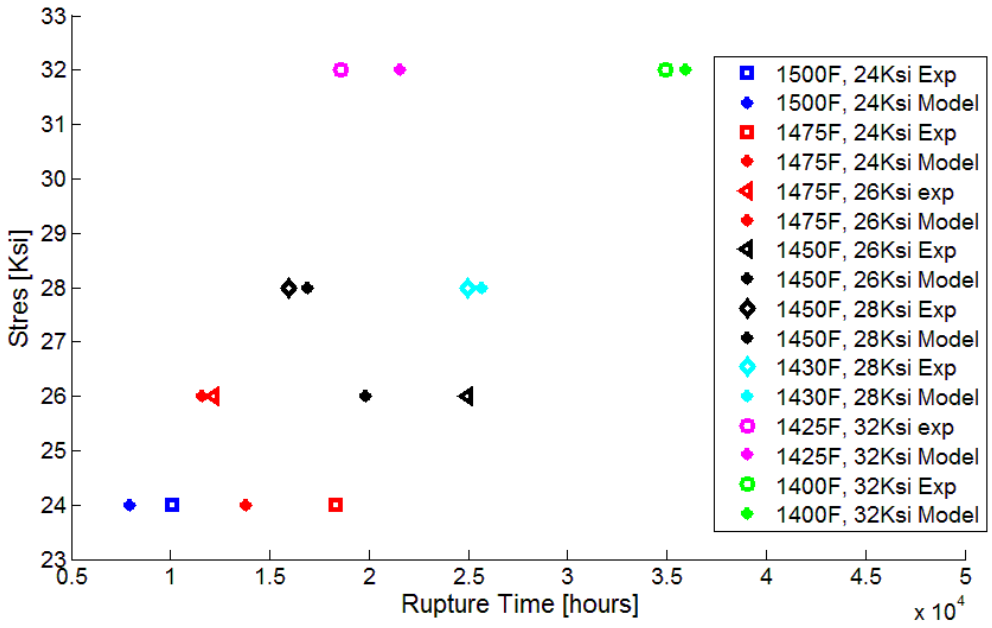

Figure 7: Predicted and experimental rupture time at various stress and temperature conditions.

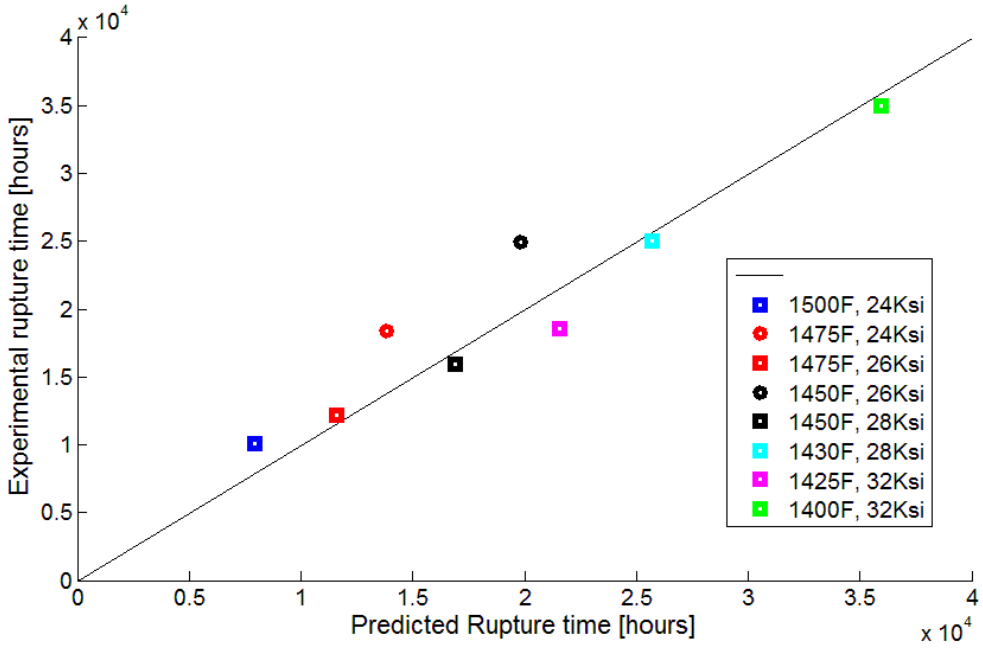

Figure 8: Predicted rupture time compared with experimental rupture time.

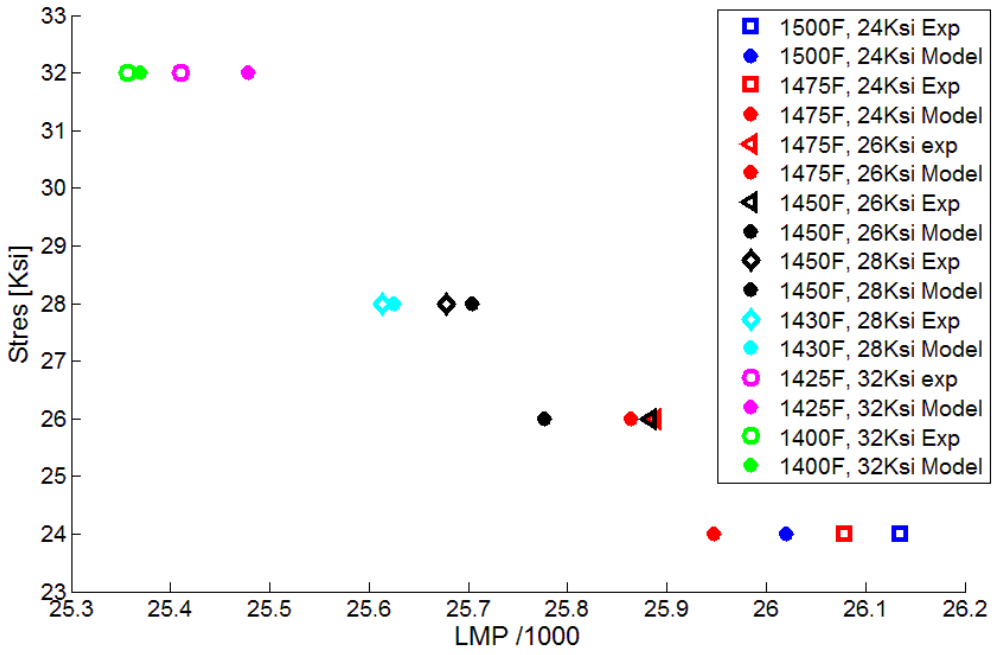

Figure 9: Stress vs normalized LMP parameter: experiment and model results.

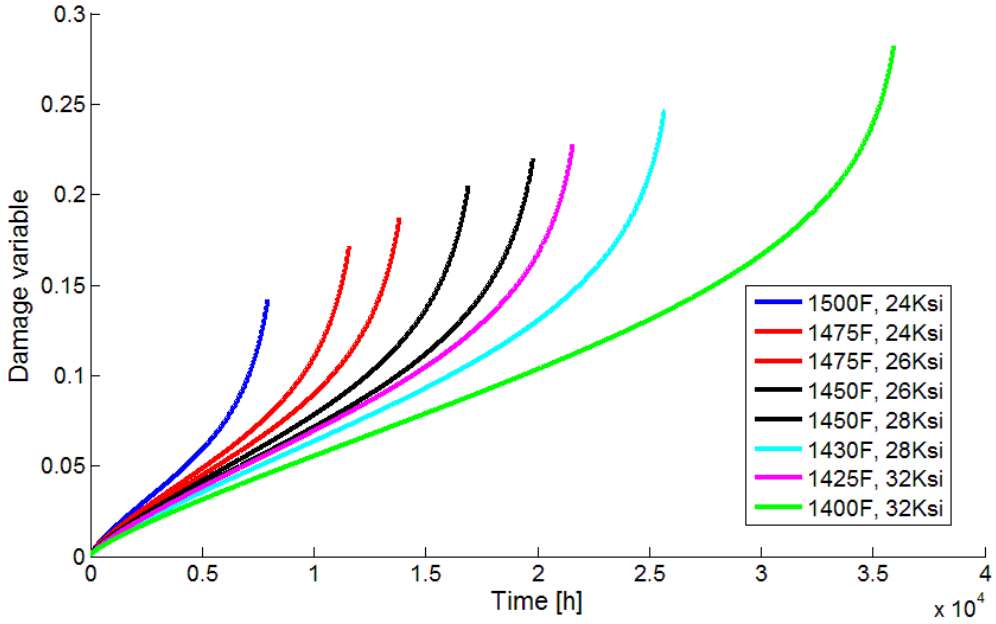

Figure 10: Evolution of damage parameter, as predicted by the model at various temperature-stress conditions.

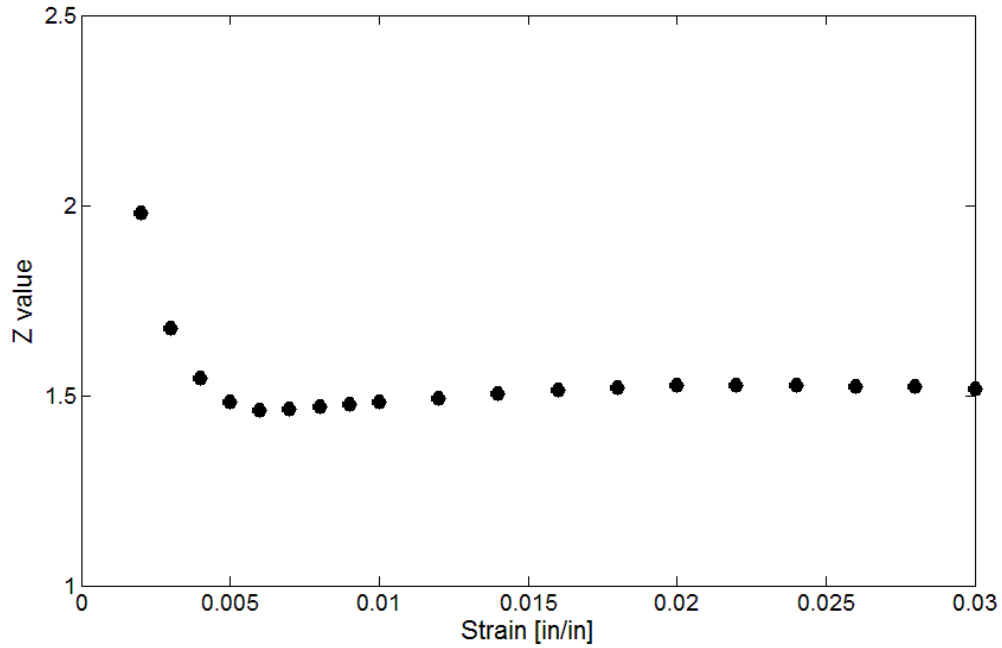

Figure 11: Calculated Z-parameter for creep strain values around 1%. Note the values smaller than 1.6 (good predictions) for strains between 0.5% and 3%.

Figure 12: Optical image of a cross-section of a ruptured sample under creep conditions: 1500F, 24Ksi. (Sample# N105-CRP-001). Note high density of grain boundary cavities, close to the fracture surface (on the top).

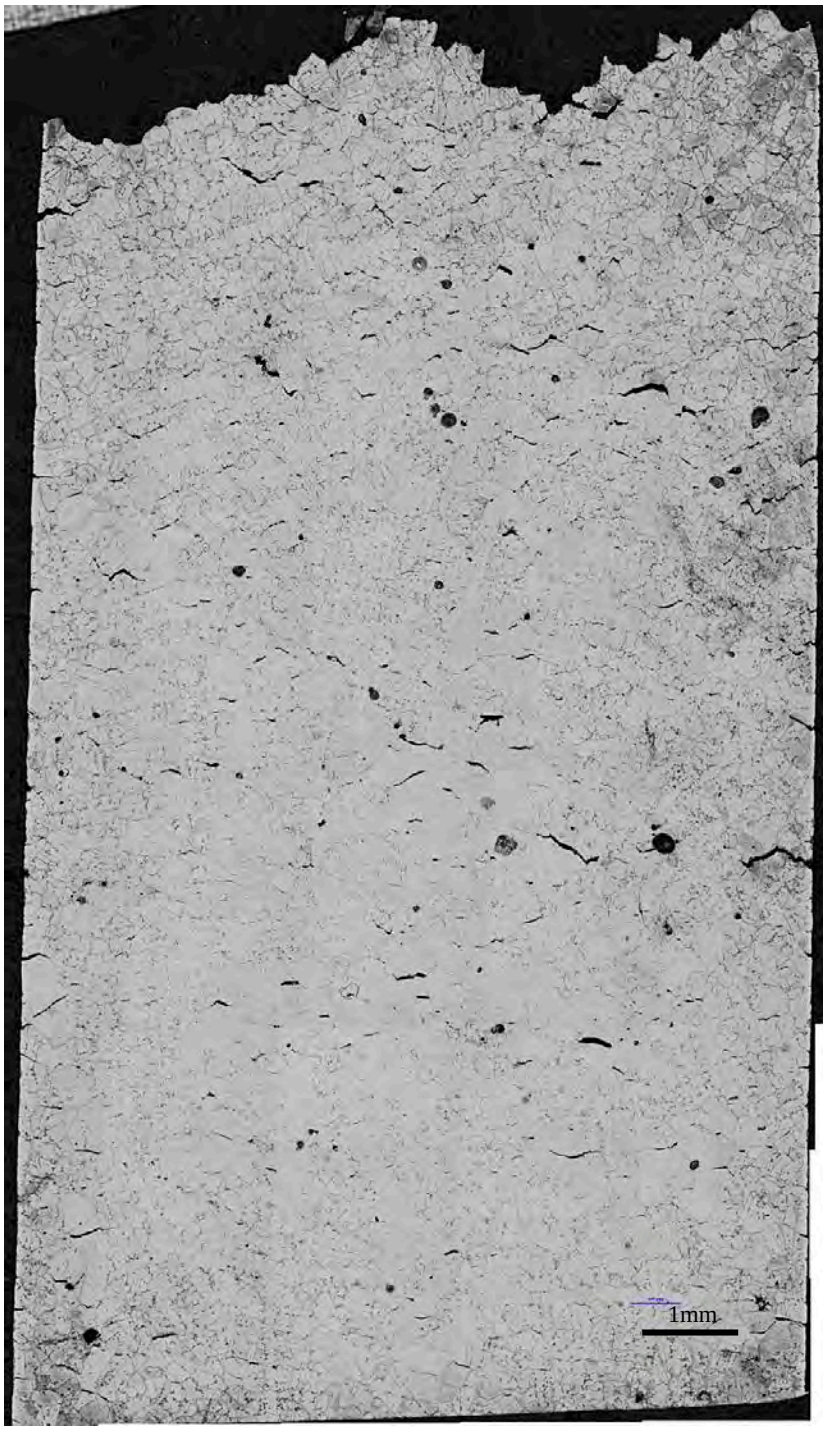

Figure 13: Optical image of a cross-section of a ruptured sample under creep conditions: 1475F, 24Ksi (Sample# N105-CRP-002).

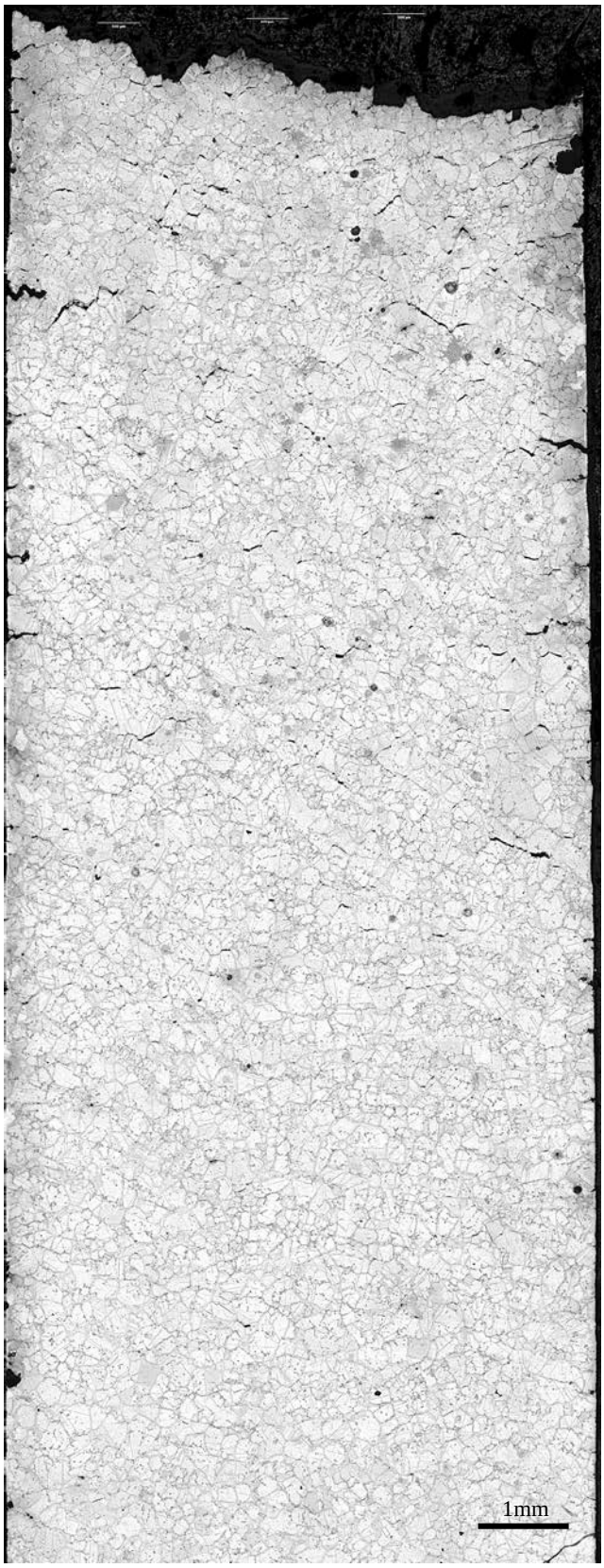

Figure 14: Optical image of a cross-section of a ruptured sample under creep conditions: 1475F, 26Ksi (Sample# N105-CRP-003).

Figure 15: Optical image of a cross-section of a ruptured sample under creep conditions: 1450F, 26Ksi (Sample # N105-CRP-004).

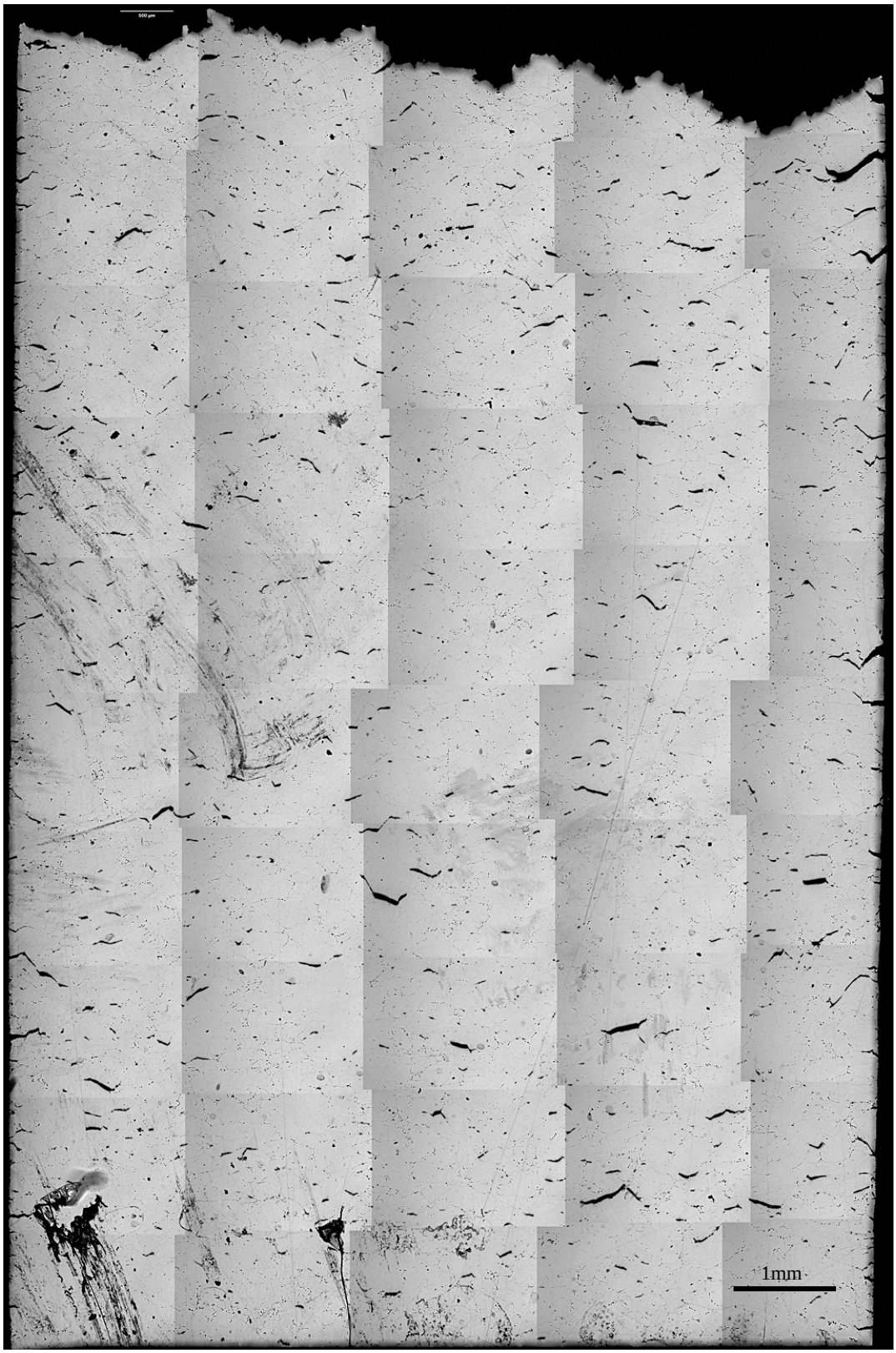

Figure 16: Optical image of a cross-section of a ruptured sample under creep conditions: 1450F, 28Ksi (Sample N105-CRP-005).

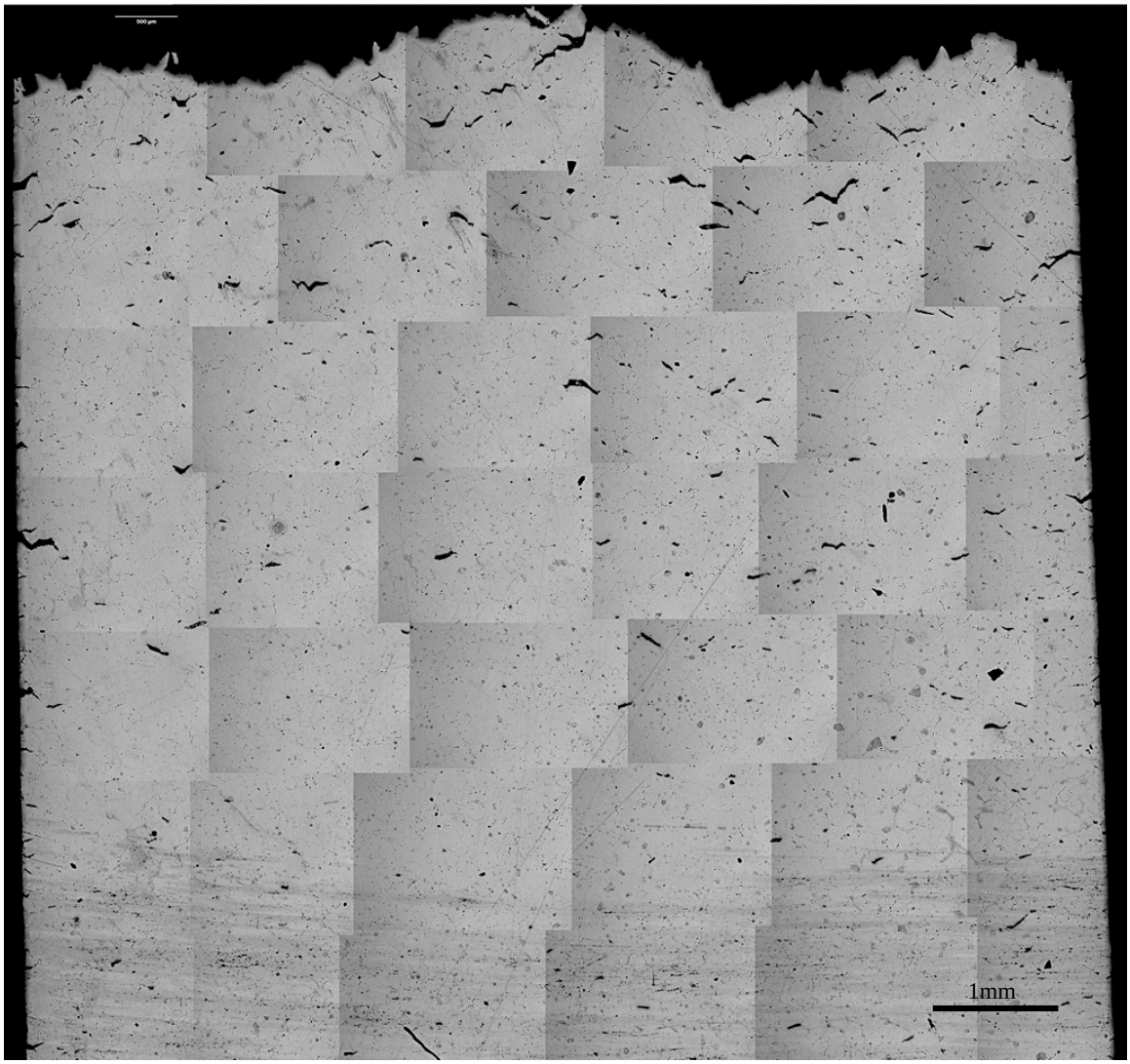

Figure 17: Optical image of a cross-section of a ruptured sample under creep conditions: 1430F, 28Ksi (Sample# N105-CRP-006)

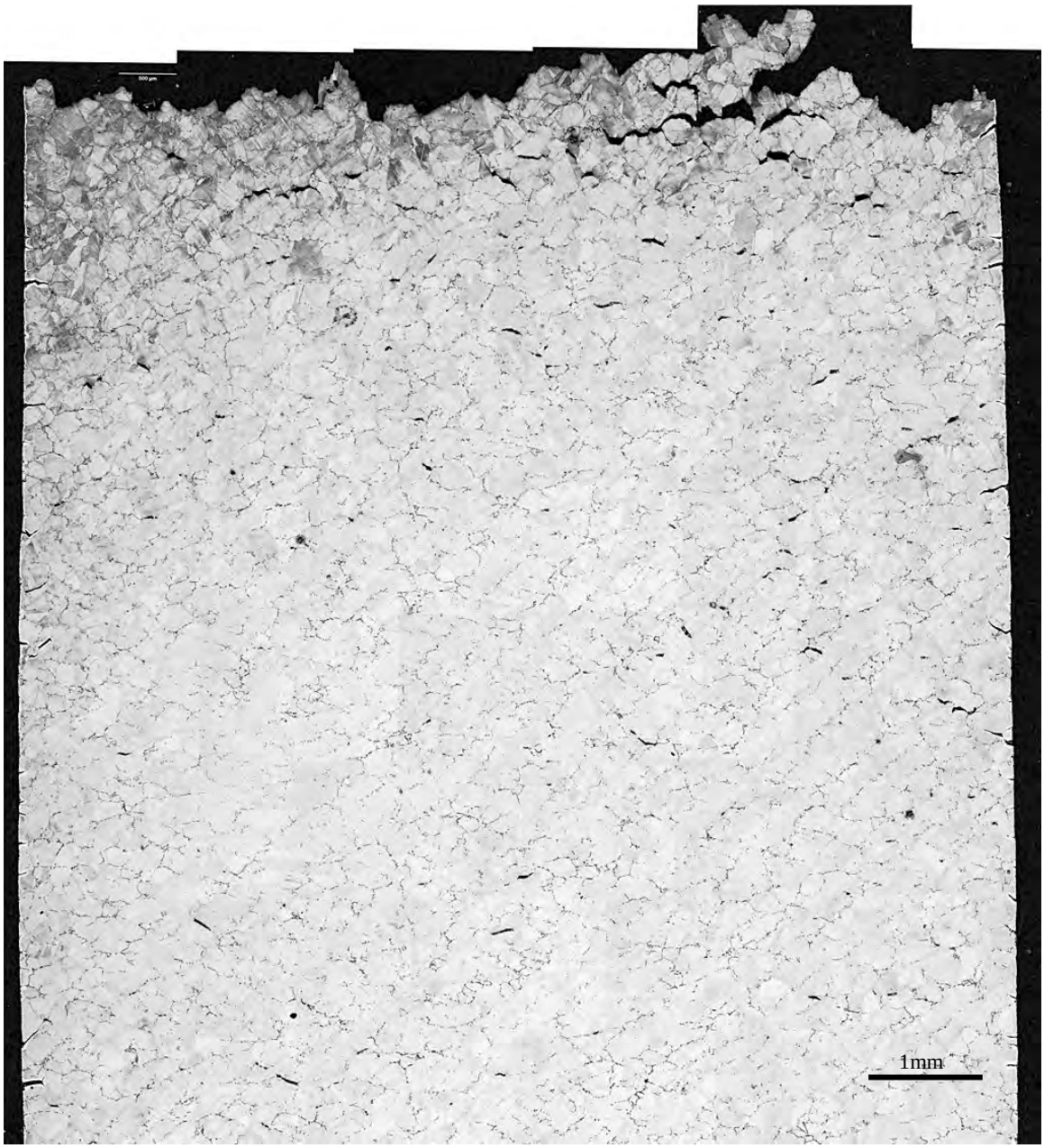

Figure 18: Optical image of a cross-section of a ruptured sample under creep conditions: 1425F, 32Ksi (Sample N105-CRP-007)

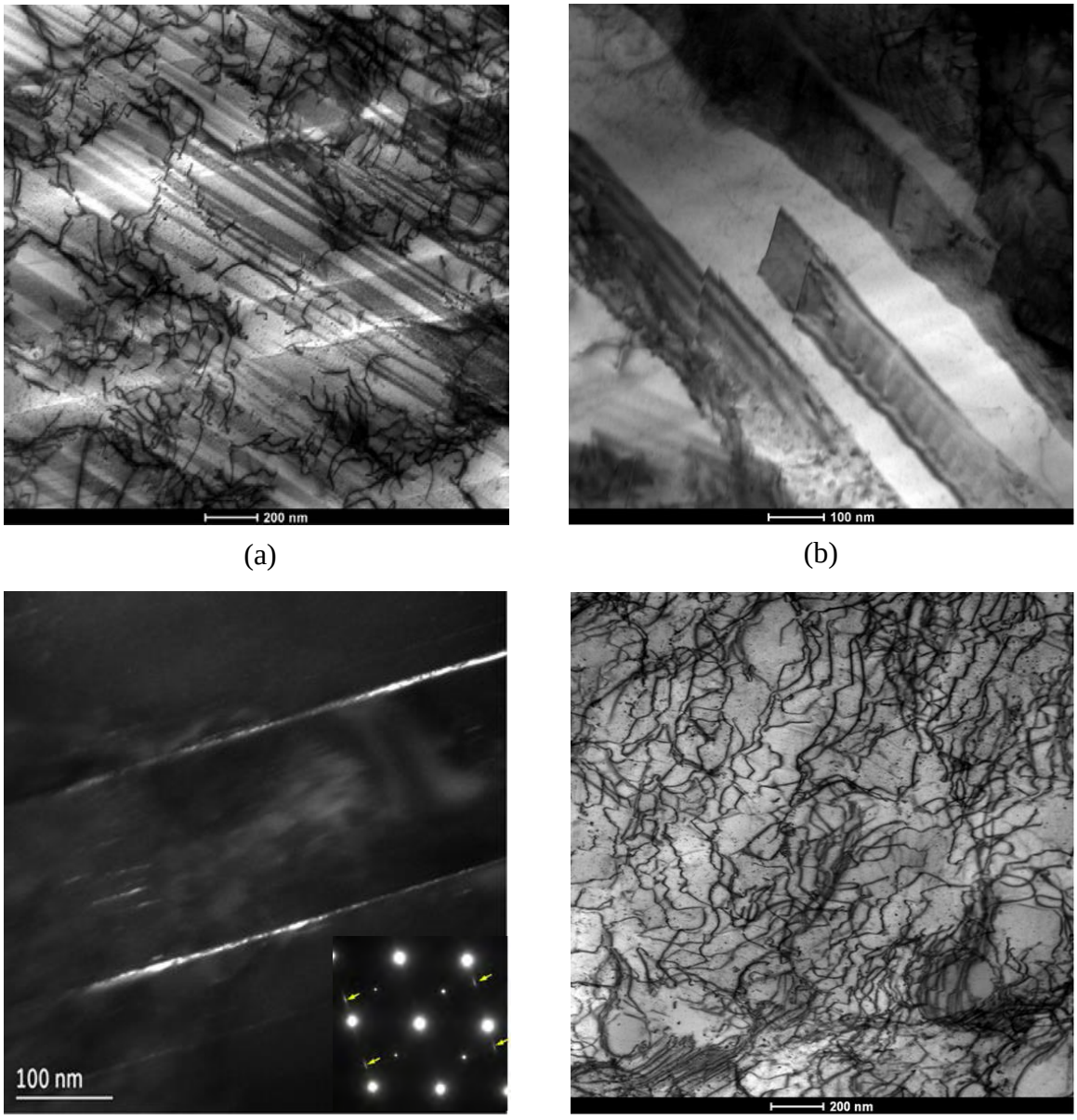

(a) (b)

(c) (d)

Figure 19: Creep deformation at 1400F showing (a, b) continuous planar faulting, (c) microtwins and (d) 1/2<110> matrix dislocations.

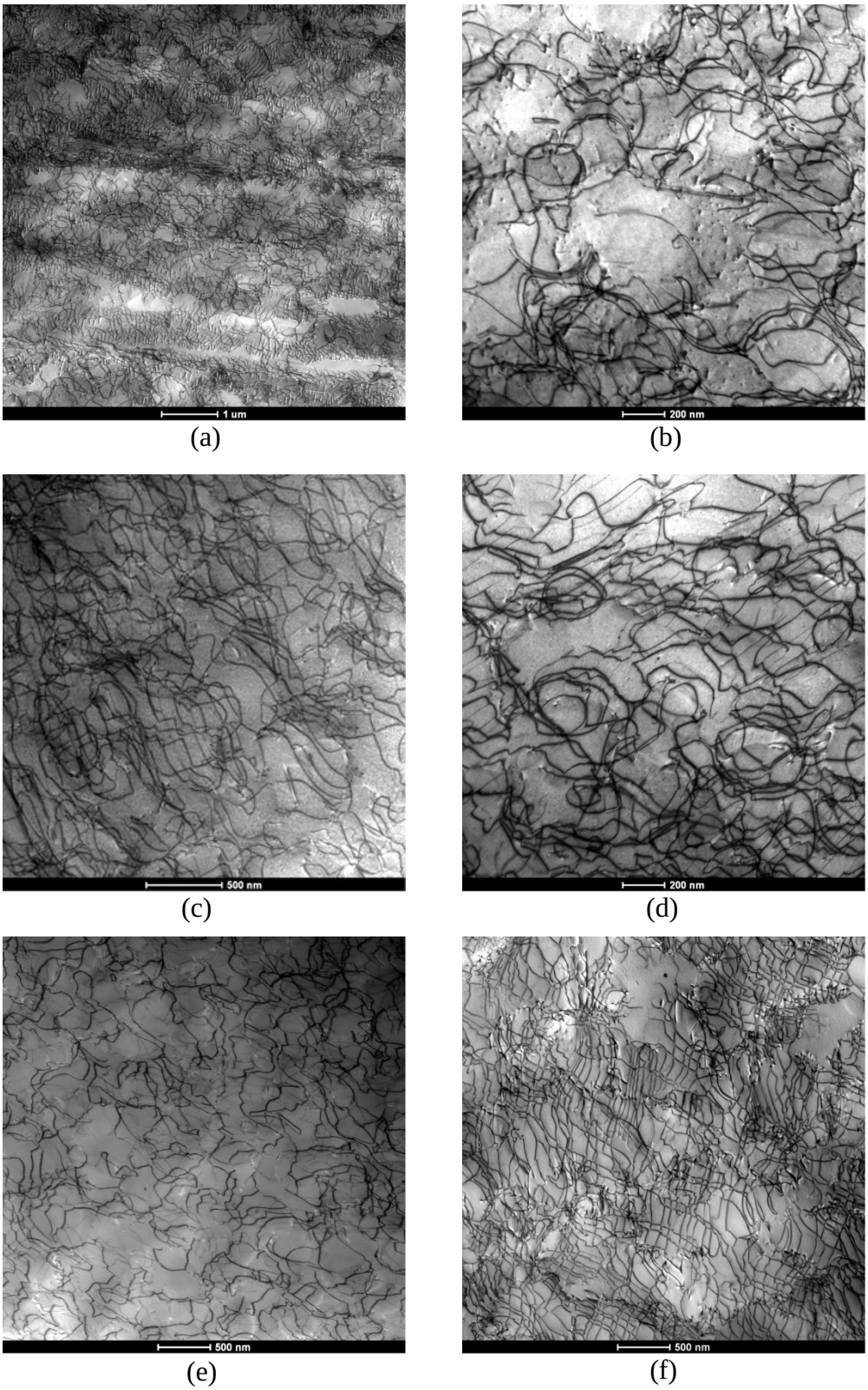

(a) (b)

(c) (d)

(e) (f)

Figure 20: Wavy slip ½<110> activity: (a,b) 1450F, (c,d) 1475F and (e,f) 1500F.

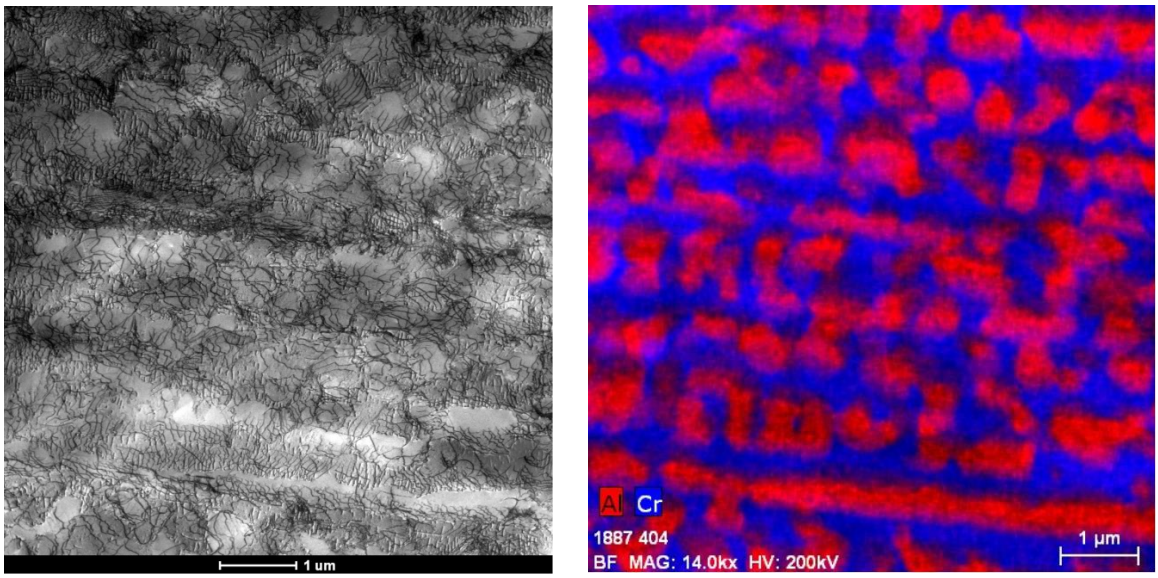

(a) (b)

Figure 21: High dislocation activity along continuous γ channels in specimen crept at 1475F (a) bright field image and (b) STEM image showing γ/γ' structure (Al-red-γ' and Cr-blue-γ).

4. Task 4 - Cast Superalloy Development

Note: this section contains its own numbering and table of contents

ABSTRACT

The Steam Turbine critical stationary structural components are high integrity Large Shell and Valve Casing heavy section Castings, containing high temperature steam under high pressures. Hence to support the development of advanced materials technology for use in an A-USC steam turbine capable of operating with steam conditions of 760°C (1400°F) and 35 MPa (5000 psia), Casting alloy selection and evaluation of mechanical, metallurgical properties and castability with robust manufacturing methods are mandated.

Alloy down selected from Phase 1 based on producability criteria and creep rupture properties tested by NETL-Albany and ORNL directed the consortium to investigate cast properties of Haynes 282 and Haynes 263. The goals of Task 4 in Phase 2 are to understand a broader range of mechanical properties, the impact of manufacturing variables on those properties, and to scale up the size of heats to production levels to facilitate the understanding of the impact of heat and component weight, on metallurgical and mechanical behavior.

GE Power & Water Materials and Processes Engineering for the Phase 2, Task 4.0 Castings work, systematically designed and executed casting material property evaluation, multiple test programs. Starting from 15 lbs. cylinder castings to world's first 17,000 lbs. poured weight, heavy section large steam turbine partial valve Haynes 282 super alloy casting. This has demonstrated scalability of the material for steam Turbine applications.

Activities under Task 4.0, Investigated and characterized various mechanical properties of Cast Haynes 282 and Cast Nimonic 263. The development stages involved were:

1) Small Cast Evaluation: 4 inch diam. Haynes 282 and Nimonic 263 Cylinders. This provided effects of liquidus super heat range and first baseline mechanical data on cast versions of conventional vacuum re-melted and forged Ni based super alloys.

2) Step block castings of 300 lbs. and 600 lbs. Haynes 282 from 2 foundry heats were evaluated which demonstrated the importance of proper heat treat cycles for Homogenization, and Solutionizing parameters selection and implementation.

3) Step blocks casting of Nimonic 263: Carried out casting solidification simulation analysis, NDT inspection methods evaluation, detailed test matrix for Chemical, Tensile, LCF, stress rupture, CVN impact, hardness and J1C Fracture toughness section sensitivity data and were reported.

4) Centrifugal Casting of Haynes 282, weighing 1400 lbs. with hybrid mold (half Graphite and half Chromite sand) mold assembly was cast using compressor casing production tooling. This test provided Mold cooling rates influence on centrifugally cast microstructure and mechanical properties. Graphite mold

section out performs sand mold across all temperatures for 0.2% YS; %Elongation, %RA, UTS at 1400°F. Both Stress-LMP and conditional Fracture toughness plots data were in the scatter band of the wrought alloy.

5) Fundamental Studies on Cooling rates and SDAS test program. Evaluated the influence of 6 mold materials Silica, Chromite, Alumina, Silica with Indirect Chills, Zircon and Graphite on casting solidification cooling rates. Actual Casting cooling rates through Liquidus to Solidus phase transition were measured with 3 different locations based thermocouples placed in each mold. Compared with solidification simulation cooling rates and measurement of SDAS, microstructure features were reported. The test results provided engineered casting potential methods, applicable for heavy section Haynes 282 castings for optimal properties, with foundry process methods and tools.

6) Large casting of Haynes 282 Drawings and Engineering FEM models and supplemental requirements with applicable specifications were provided to suppliers for the steam turbine proto type feature valve casing casting. Molding, melting and casting pouring completed per approved Manufacturing Process Plan during 2014 Q4.

   The partial valve casing was successfully cast after casting methods were validated with solidification simulation analysis and the casting met NDT inspection and acceptance criteria. Heat treated and sectioned to extract trepan samples at different locations comparing with cast on coupons test data. Material properties requisite for design, such as tensile, creep/rupture, LCF, Fracture Toughness, Charpy V-notch chemical analysis testing were carried out. The test results will be presented in the final report. The featured valve section model views and drawing reference were provided in the Appendix 1-F [Large Casting of Haynes 282].

   Research efforts were directed ensuring engineered casting development and material properties evaluation test programs delivering material properties data for turbine design applications.

   The typical Haynes 282 large size Steam Turbine production casting from Order to Delivery foundry schedule with the activity break up is shown below with more details in the report (Figure 129 and Figure 130).

   - **From Purchase Order placement to Casting pouring ~ 26 weeks.**
     1. Sales and commercial review 3
     2. Engineering Drawings models review 4
     3. Pattern and core box manufacturing 6
     4. Casting process engineering review 4
     5. FEM and solidification simulation analysis 4
     6. Gating & Feeder Attachments, Ceramic tiling 2
     7. Molding and coremaking production scheduling 6

8. Melting planning and schedule 3
9. Pouring, cooling and shake out 2

- **From Pouring to casting Delivery ~ 29 weeks**
  10. Shot blast and riser cutting, gates removal 3
  11. Homogenizing , solutionizing HT furnace prep 4
  12. Grinding, Fettling 2
  13. Aging HT Cycle, cooling 2
  14. VT and LPT NDT inspections 2
  15. Radiographic inspection 4
  16. Mechanical testing, Chemical analysis test certs 4
  17. Casting weld repair upgrades and Aging PWHT 4
  18. NDT after weld repairs and casting upgrades 3
  19. Casting Final Inspection and test certs 3
  20. Package and delivery 2

Hence the Total Lead time from P.O to Casting delivery is approximately 55 weeks.

TABLE OF CONTENTS

ABSTRACT 111
LIST OF FIGURES 115
LIST OF TABLES 121
LIST OF ACRONYMS AND ABBREVIATIONS 122
SMALL CAST EVALUATION 123
STEP BLOCK CASTING OF HAYNES 282 138
STEP CASTING OF NIMONIC 263 144
CENTRIFUGAL CASTING OF HAYNES 282 177
FUNDAMENTAL STUDIES ON COOLING RATES AND SDAS 195
LARGE CASTING OF HAYNES 282 209

LIST OF FIGURES

Figure 1: Schematic of the six 4 inch diameter, 4 inch high NETL-Albany cast Nimonic 263 and Haynes 282 cylinder castings..... 123
Figure 2: Super heat influence on N263 Tensile strength at RT and 1400°F 124
Figure 3: Super heat influence on N263- 0.2% YS at RT and 1400°F..... 125
Figure 4: Cast structure influence on N263 Tensile strength at RT and 1400°F..... 125
Figure 5: Cast structure influence on N263 0.2% YS at RT and 1400°F. 126
Figure 6: Super heat influence on H 282 Tensile strength at RT and 1400°F 127
Figure 7: Super heat influence on H 282- 0.2% YS at RT and 1400°F..... 127
Figure 8: Cast structure influence on H 282 Tensile strength at RT and 1400°F..... 128
Figure 9: Cast structure influence on H 282 0.2% YS at RT and 1400°F. 128
Figure 10: Super heat influence on N263 LCF at RT. Higher super heat temperatures of 150°C provides improved LCF properties 129
Figure 11: Cast structure influence on N263 LCF at RT. Columnar as cast structures tend to provide better LCF properties..... 129
Figure 12: Super heat influence on H282 LCF at RT. Higher super heat pour temperatures of 100°C-150°C shows improved LCF properties 130
Figure 13: Cast Structure influence on H 282 LCF at RT. Columnar as cast structures shows improved LCF properties at RT..... 130
Figure 14: Super heat influence on N263 LCF at 1400°F compared with Forged 263. 100°C-150°C super heat pour temperatures shows improved LCF properties at 1400°F 131
Figure 15: Cast structure influence on N263 LCF at 1400°F compared with Forged 263 131
Figure 16: Super heat influence on H 282 LCF at 1400F compared with Forged H282 data. 100°C super heat pours indicate comparable LCF to forged 282 data at 1400°F 132
Figure 17: Cast structure influence on H282 LCF at 1400F compared with Forged H282. Columnar as cast structure provides improved LCF at 1400°F compared with equiaxed cast structure. 132
Figure 18: Schematic of the MetalTek 300 lbs. Haynes 282 step block casting with dimensions..... 138
Figure 19: MetalTek 300 lbs. Haynes 282 step block casting after mold shake out and shot blast cleaning operations. Bottom gated with casting top feeder arrangement shown. 139
Figure 20: Schematic of Flowserve Step block. Top feeder with section modulus controlled feeding..... 140
Figure 21: Optical micrographs from the Flowserve step block (etched with Kallings) 141
Figure 22: Secondary Electron Images (SEM) showing high-Mo, high-Si phases on grain boundaries 142
Figure 23: Optical micrographs from the MetalTek step block (etched with Kallings) 142
Figure 24: Secondary Electron Images (SEM) showing various phases..... 143
Figure 25: Nimonic 263 step block test casting, weighing 605 lbs. Completed optimized Homogenizing and Age hardening heat treatments..... 144

Figure 26: Picture showing the N263 casting and the associated shrink cavity below the rise/feeder section 147
Figure 27: Casting solidification simulation analysis showing the hot spot location and the associated casting shrinkage defect. 148
Figure 28: Nimonic 263 test casting, CAD layout of specimen extraction isometric views from step block cast sections 149
Figure 29: Orientation and specimen layout of various test specimens from N263 test block 150
Figure 30: Test matrix for Tensile, Charpy impact energy and LCF properties with specimen identification 151
Figure 31: Test matrix for Stress rupture, Fracture toughness and Chemical analysis with specimen identification 152
Figure 32: Step block casting thermal center trepanned section chemical analysis. No significant variation in chemistry when compared with casting section Thermal center analysis 153
Figure 33: Homogenizing and Aging Heat treatment cycles Optimized to within +/- 5% of nominal chemistry variation (NETL) 154
Figure 34: UT immersion scans of N263 step block casting 6 inch and 4 inch sections showing the inherent issue of achieving a superior back wall reflection in thick walled super alloy castings 156
Figure 35: Radiographic Scan Plan 157
Figure 36: Radiographic Test Report confirming no other casting defect in other cast sections, except the surface cavity defect in 10 inch section under the casting feeder. 158
Figure 37: UTS plot with temperature and trepanned casting section thickness variation 159
Figure 38: UTS vs temperature plot for 10 inch section CL and DL location trepans .. 160
Figure 39 UTS vs temperature plot for 6 inch section CL and DL location trepans 160
Figure 40: 0.2 % YS vs. Temperature for all N263 step block cast section trepans. The 0.2% YS vs. temperature trend plot shows tighter band trepan CL values at elevated temperatures for all section thicknesses 161
Figure 41: 0.02 % YS vs. Temperature for all N263 step block cast section trepans. The 0.02% YS vs. temperature trend plot shows tighter band at elevated temperatures for all section thicknesses 162
Figure 42: N263 step block cast section trepan samples % Elongation vs. Temperature 163
Figure 43: N263 %RA Vs Temperature plots for all section trepans 164
Figure 44: Nimonic 263 step block casting SDAS measurements with section size 165
Figure 45: N263 Step block 10 inch and 6 inch sections cycles to failure compared at RT, A-ratio 1. The 10 inch section shows a debit in comparison with 6 inch section 167
Figure 46: N263 Step block 10 inch and 6 inch sections cycles to failure compared at 1400°F, A-Ratio 1. The 10 inch section shows increased debit in comparison with 6 inch section, while 6 inch section shows degradation 167
Figure 47: N263 Stress rupture strength vs, LMP (C=20) with section thickness. No significant changes in stress rupture data with section thickness variation 168

Figure 48: Plot showing Kq Fracture toughness value Vs. Temperature for various section sizes. Note that the conditional fracture toughness Kq values are minimum influenced with temperature raise up to 6 inch cast wall thickness 170
Figure 49: 10-J1C-01, J vs. a graph for 10 inch section tested at RT 171
Figure 50: 10-J1C-01, Force vs. COD graph for 10 inch section tested at RT 171
Figure 51: 10-J1C-03, J vs. a graph for 10 inch section tested at 1400°F..... 172
Figure 52: 10-J1C-03, Force vs. COD graph for 10 inch section tested at 1400°F 172
Figure 53: 4-J1C-02, J vs. a graph for 4 inch section tested at 1400°F..... 173
Figure 54: 4-J1C-02, Force vs. COD graph for 4 inch section tested at 1400°F 173
Figure 55: 4-J1C-01, J vs. a graph for 4 inch section tested at RT 174
Figure 56: 4-J1C-01, Force vs. COD graph for 4 inch section tested at RT 174
Figure 57: Charpy V notch Impact energy vs. section size combined data plot 175
Figure 58: N263 Cast hardness values are not section thickness dependent..... 176
Figure 59: Haynes 282 Test program Centrifugal casting..... 177
Figure 60: Sectional view drawing of 282 Centrifugal Casting 179
Figure 61: Haynes282 Centrifugal casting mold assembly comprising half mold Graphite and half mold Chromite sand..... 180
Figure 62: Casting simulation predicted cooling rates for Graphite and Chromite sand side molds..... 180
Figure 63: Picture showing the location of the casting utilized for micro-structural analysis and mechanical testing..... 181
Figure 64: Picture showing the extraction of the slice for heat treatment and micro-structural analysis 181
Figure 65: SDAS along the wall thickness for the two respective mold material..... 182
Figure 66 As cast microstructural evolution across the wall thickness for the two mold material 183
Figure 67 SEM image of grain boundary in as cast specimens. Most precipitates consists of Ti, Mo and Cr rich..... 184
Figure 68: Complete map of specimen extraction from the centrifugally cast Haynes 282. The specimens include tensile, LCF and fracture toughness..... 185
Figure 69: Color codes of specimen type are as shown. All mini specimens are for the thinner wall thickness..... 185
Figure 70: Plots of UTS as a function of temperature [Sand and Graphite mold]. In general, the variation between the thick and thin sections on the sand side has less variability, when compared to the graphite side. Graphite side has better RT properties when compared to the sand. However at 1400°F, all data falls within a very tight band..... 186
Figure 71: Plots of 0.2% YS as a function of temperature for various mold material. Unlike the variation in UTS, the 0.2% YS has a very tight range across all temperatures tested 187
Figure 72: Plots of % Elongation as a function of temperature for various mold material. The plots clearly show a wide variation in % Elongation, with the graphite mold being better than the sand mold across all temperatures..... 188
Figure 73: Plots of % RA as a function of temperature for various mold material. The plots clearly show a wide variation in % RA, and in general, graphite mold out performs sand mold across all temperatures 189

Figure 74: Plots of Cycles to Failure and Total Strain Range (%) for the Sand and Graphite molds at RT and 1400°F. The Graphite side shows a debit at 1400°F, while the sand side does degrade with the same severity 190
Figure 75: Plots of Cycles to Failure and Total Strain Range (%) for the Sand and Graphite molds at RT and 1400°F. The debit in the graphite compared to sand at high strains and 1400°F will need some further investigation 191
Figure 76: Plot of cycles to failure and total strain range from Table 4B-1. The graph clearly shows the better performance of faster cooling rates [finer SDAS in the graphite side] due to higher UTS at 75°F (+10 to15 Ksi increase in UTS on Graphite side]..... 192
Figure 77: Plot of cycles to failure and total strain range from Table 4B-2. The graph clearly shows no performance difference at 1400°F as the tensile properties of both sand and graphite are similar at 1400°F 192
Figure 78: Conditional Fracture toughness (K_Q) of centrifugally cast Haynes 282. The cast data [Sand & Graphite] falls in the scatter of wrought alloy. The wrought data in the figure above consists of PA, and exposed for 1 & 2 years at 1425°F..... 193
Figure 79: Stress-LMP plot of Centrifugal Cast H282 compared to wrought H282 data. The data scatter is in line with the wrought alloy. 194
Figure 80: Enhancing SDAS prediction with casting solidification mold cooling rate studies. Six molds with different mold materials [to simulate different cooling rates] were poured with thermocouples located as shown to measure casting cooling rates 196
Figure 81: Detailed plan of casting solidification cooling rates measurement mold layout assembly..... 197
Figure 82: Sand molds from 5 different mold materials [left] coated with refractory paint and dried [right]. Six mold materials were evaluated: 1. Silica, 2. Chromite, 3. Graphite, 4. Alumina, 5. Zircon, 6. Silica with indirect chills placement. 198
Figure 83: Photograph of chills location in mold pattern prior to molding 199
Figure 84: Thermocouples and extension wire were wrapped with Kaowool thermal insulation. 200
Figure 85: Photograph of thermocouple compensating cables routing within the drag mold 201
Figure 86: Type B Thermocouples, insulators and connectors assembly components 201
Figure 87: Photograph of completed mold ready for pour 202
Figure 88: Photograph showing castings after mold shake out, gating and feeders removal 203
Figure 89: Haynes 282 cylinder castings thermocouple arrangements schematic view. Photograph showing Quartz sheathed Type–B thermocouples located within the molds 204
Figure 90: Casting cooling rates measured and simulated compared for different mold materials during liquidus to solidus transition temperature range..... 204
Figure 91: Casting Solidification Simulation Analysis cooling rates plot from pour to post solidification elevated temperature range for all the mold materials. Data from the 3 thermocouples T1, T2 and T3 vs. casting cooling time are plotted for different molds. 205

Figure 92: Haynes 282 Casting cooling rates during Liquidus to Solidus temperature range for different mold materials..... 206
Figure 93: Mold cooling rates influence on SDAS values 208
Figure 94: Steam turbine half valve casing selected for the large casting trial..... 211
Figure 95: Foundry Casting Pattern and feeder design..... 212
Figure 96: Picture showing Cope, drag molds and the valve body core after refractory coating and drying..... 212
Figure 97: Solidification simulation indicates bottom to top filling (left) and temperature variation during liquidus to solidus transition temperature range (right) 213
Figure 98: Solidification fraction solid cut off indicates no trail of shrinkage..... 214
Figure 99: Assembled mold, hot air dried and purged with Argon prior to pouring [Courtesy-MetalTek MO]..... 214
Figure 100: Induction melted, composition controlled with argon cover during melting and tapping melt quality controlled [Courtesy-MetalTek MO]..... 215
Figure 101: Pouring the mold after deslagging with covered ladles ensuring targeted pouring temperature and pour times..... 216
Figure 102: Casting after in mold cooling and shake out [Courtesy-MetalTek MO]..... 217
Figure 103: Homogenization HT cycle with insert HT step detailed view..... 219
Figure 104: Two step Aging heat treat cycles thermocouple plot..... 220
Figure 105: Thermocouples attached, coated for double Age heat treat cycle..... 221
Figure 106: RT Scan sheet for the partial valve casing..... 222
Figure 107: RT Inspection report for the H282 valve casing 223
Figure 108: Haynes 282 Valve casing Liquid penetrant testing 100% surface area.... 224
Figure 109: LPT inspection pictures on 100 % Cast surface areas..... 226
Figure 110: Niyama criteria per solidification simulation analysis. Niyama indicates potential feeding difficulty zones in the casting with lower (Nẏ) values. This plot is primarily used to avoid sectioning through potential zones for micro shrinkage... 227
Figure 111 : Cast on coupons tensile properties UTS, 0.2% YS and 0.02% YS values with temperature indicate tighter band for the yield strength values for the temperature range..... 230
Figure 112 : UTS trend with temperature for all cast sections, trepans and chilled cast sections compared. Chilled cast section indicates lower tensile properties. 230
Figure 113 : 0.2% YS for cast on coupons indicate higher yield strength values in comparison with chilled cast sections. 0.2% YS values are fairly in tight range… 231
Figure 114 : 0.02% YS values trend cast on coupons, trepan sections and chilled cast sections with temperature 231
Figure 115 : Cast on coupon UTS trend compared with Centrifugal and sand cast trepan tensile values over the temperature range. Cast on coupons UTS values are higher compared with Centrifugal cast tensile properties..... 232
Figure 116 : 0.2% YS values show similar range for sand cast and centrifugal castings 233
Figure 117 : Fracture toughness Kjq shows cast on coupons, and Chilled sections have higher values compared with trepan section values at higher temperatures..... 233
Figure 118 : Conditional Fracture toughness Kq for centrifugal cast indicate, cast on coupons show higher values, however are comparable with sand cast trepan samples..... 234

Figure 119 : Charpy impact values comparing cast on coupons [CD] Section trepans [B,H,K] and Chilled cast section [D]. 235
Figure 120: cast on coupons have higher Charpy impact energy values compared with chilled cast section trepans [D]. Charpy V notch testing as per ASTM E23-12c at RT. 235
Figure 121 : LCF plot comparing Cast on coupons at RT and 1400° F, Nf cycles to failure 236
Figure 122 : Cast on coupons, trepans and chilled section, e-Nf cycles to failure plot for 1400°F 236
Figure 123 : e-N plot at RT comparing sand cast and centrifugal cast H282 Nf cycles to failure. Sand cast trepan and centrifugal cast sections are in similar range..... 237
Figure 124 : Sand cast and centrifugal cast H282 show similar e-N trend, Nf cycles to failure for the strain ranges at 1400°F. 238
Figure 125 : Cast on coupon and Trepan sand cast section DAS compared 238
Figure 126: Cast on Coupons {CA & CC] Dendritic Arm Spacing micrographs at 25X (Top) and 100X image at (Bottom). Average DAS range from 0.0034 to 0.0051 inches..... 240
Figure 127: Trepan cast sections [B & H], DAS measurements are 0.0050 inches, average. 241
Figure 128 : Stress rupture test plot for trepans. Solid fills indicate test completed and non-fill shows testing stopped 242
Figure 129: Schedule from Purchase Order Placement to Casting Pouring ~ 26 weeks 243
Figure 130: Schedule from Pouring to Delivery 30 weeks~ 243

LIST OF TABLES

Table 1: Nimonic263 Cast Cylinder Microstructures (50X) with Superheat Temperature and Structure Variation 134
Table 2: Haynes 282 Cast Cylinder Microstructures (50X) with Superheat Temperature and Structure Variation 135
Table 3: Nimonic263 Cast Cylinder Microstructures (500X) with Superheat Temperature and Structure Variation 136
Table 4: Haynes 282 Cast Cylinder Microstructures (500X) with Superheat Temperature and Structure Variation 137
Table 5: N263 Step block trepan cast sections tensile strength (UTS) vs temperature data 159
Table 6: N263 Step block trepan cast sections 0.2% Yield strength vs temperature data 161
Table 7: N263 Step block trepan cast sections 0.02% Yield strength vs temperature data 162
Table 8: N263 step block trepan section samples % Elongation values 163
Table 9: N263 Step Block section Trepan sample % RA values data 164
Table 10: Nimonic 263 Step block cast sections SDAS Measurements. Consistently in the range of 0.35 to 0.40 mm for 100 to 250 mm cast sections 165
Table 11: Nimonic 263 Step block cast section thermal center trepanned samples SDAS values show independent of casting section thickness and orientation 166
Table 12: Stress rupture test results raw data 168
Table 13: Nimonic 263 Step block sections J-Integral Test results at RT; 1000°F and 1400°F summarized 169
Table 14: Kq Fracture toughness @ RT, `1000°F and 1400°F temperatures vs. section size data 170
Table 15: Charpy V-Notch Impact energy data for 10 inch, 8 inch and 6 inch trepan samples 175
Table 16: N263 Casting section hardness values raw data 176
Table 17: Casting cooling rates, both measured and simulated compared for different mold materials at 3 different locations within each mold 207
Table 18: Mold materials influence on microstructure SDAS values for Graphite, Zircon and Silica sand with indirect chills 207
Table 19: Mold materials influence on SDAS values through casting liquidus to solidus range cooling rates variation 208
Table 20: H282 casting sections and cast on coupons test matrix and specimens identification 228
Table 21 Valve casing cast on coupons and casting trepan sections chemical analysis tabulation 229
Table 22 : DAS values table comparing cast on coupons with trepan sections 239

LIST OF ACRONYMS AND ABBREVIATIONS

UTS……...Ultimate Tensile Strength
0.2YS……0.2% Yield Strength
% Elongation……...% Elongation to failure
%RA……....% Reduction in Area
KQ……..Conditional Fracture Toughness
RT……..Room Temperature
HT……..Heat Treatment
UT……..Ultrasonic Testing
LPT……Liquid Penetrant Testing
LCF……Low Cycle Fatigue
CL……..Center Line
DL……..Drag Line [1 inch above drag mold surface]
CAD……..Computer Aided Design
COD……..Crack Opening Displacement
LMP…….. Larson-Miller Parameter; is a function of time and temperature in the form T(C + log t); where T is the temperature in degrees R, C is a constant and t is the time in hours
NDT……...Non Destructive Testing
SDAS……Secondary Dendritic Arm Spacing
CTQ……..Critical to Quality Characteristic
PQP……..Product Quality Process
MPP……..Manufacturing Process Plan
FMEA……Failure Mode Effects Analysis
FEM……..Finite Element Modeling

SMALL CAST EVALUATION

Haynes 282 and Nimonic 263 alloy were down selected from Phase 1 based on producibility criteria and creep rupture properties from a series of small heats were poured at NETL-Albany. These initial heats showed the effect of liquidus superheat (50°, 100° and 150°C over the liquidus) immediately prior to pouring and also provided the first baseline mechanical data on cast versions of these traditionally vacuum remelted and forged nickel-based alloys.

These six small heats out of NETL-Albany were each 13-15 lb, 4 inch diameter cylinders 4 inches tall. The process used poured the alloy into a graphite mold embedded in sand under argon shrouding per the schematic in Figure 1. The chemical analyses of the 6 castings are provided in Table 1 of Appendix 1-A. The cylinder castings were subjected to following heat treat cycles:

> Nimonic 263HT Cycle: (1) Homogenize for 3 hours at 1100 °C followed directly by 9 hours at 1200 °C, fast cool; (2) Age 8 hours at 800 °C.
>
> Haynes 282 HT Cycle: (1) Homogenize for 3 hours at 1100 °C followed directly by 9 hours at 1200 °C, fast cool; (2) Solutionize for 2 hours at 1010 °C, fast cool, and (3) Age for 8 hours at 788 °C

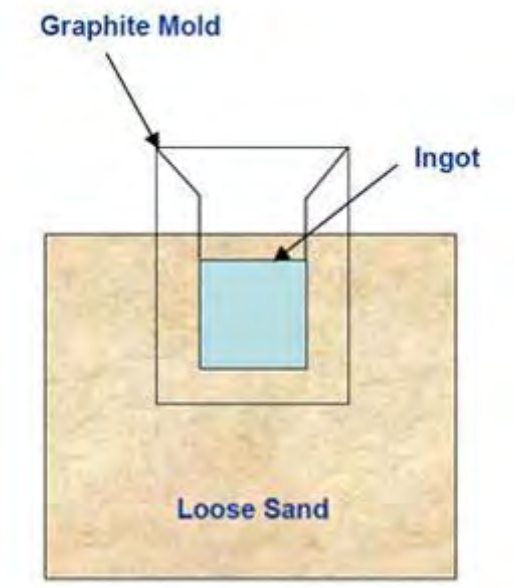

Figure 1: Schematic of the six 4 inch diameter, 4 inch high NETL-Albany cast Nimonic 263 and Haynes 282 cylinder castings

The six small cylinder castings were tested for tensile and LCF to capture the effects of both superheat as well as any impact of grain structure (equiaxed/dendritic and columnar). The castings were radiographed to identify valid test sample areas. Specimens extracted near outer surface, solidified in contact with graphite mold are

marked columnar microstructure and specimens from interior are marked equiaxed grain structure.

The test results showed a few ksi increase in UTS with super heat and no discernable pattern in LCF with super heat. Grain orientation did not appear to impact either of these properties.

Within Appendix 1-A, Tables 2 and 3 provide Cylinder castings tensile properties for Nimonic 263 and Haynes 282 and Tables 4 and 5 provide LCF raw data and Cast microstructure tables

Figure 2 and Figure 3 show the influence of melt super heat temperatures on Nimonic 263 Tensile (UTS) and 0.2% YS, respectively. Differences in Tensile properties at 1400°F are minimal for 100° to 150°C super heat temperatures which are typical foundry casting pouring temperature practices.

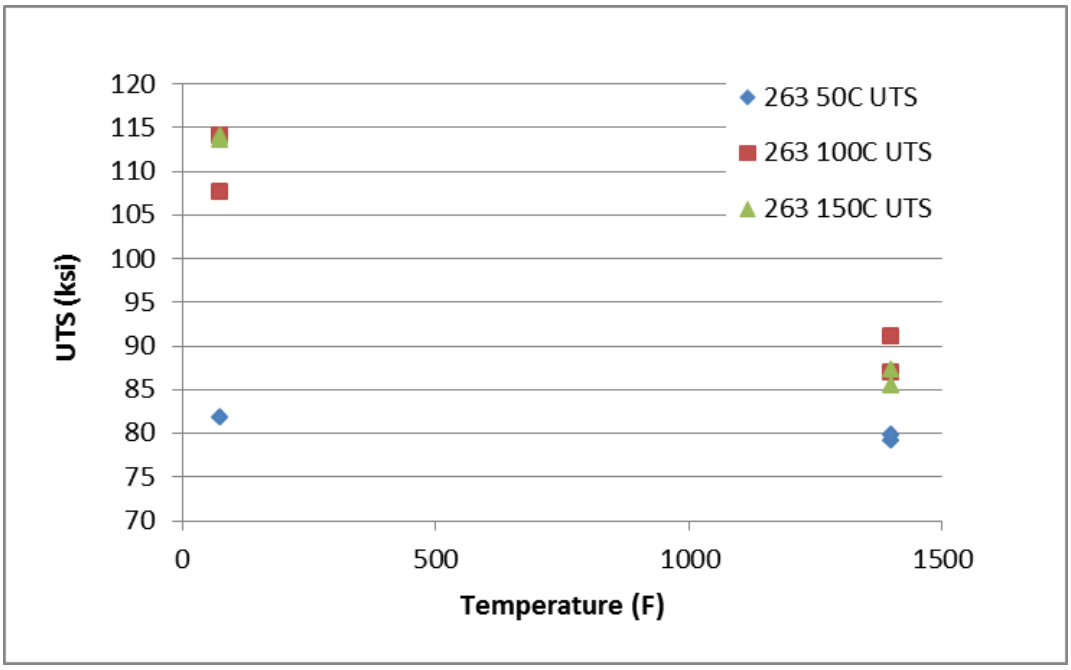

Figure 2: Super heat influence on N263 Tensile strength at RT and 1400°F

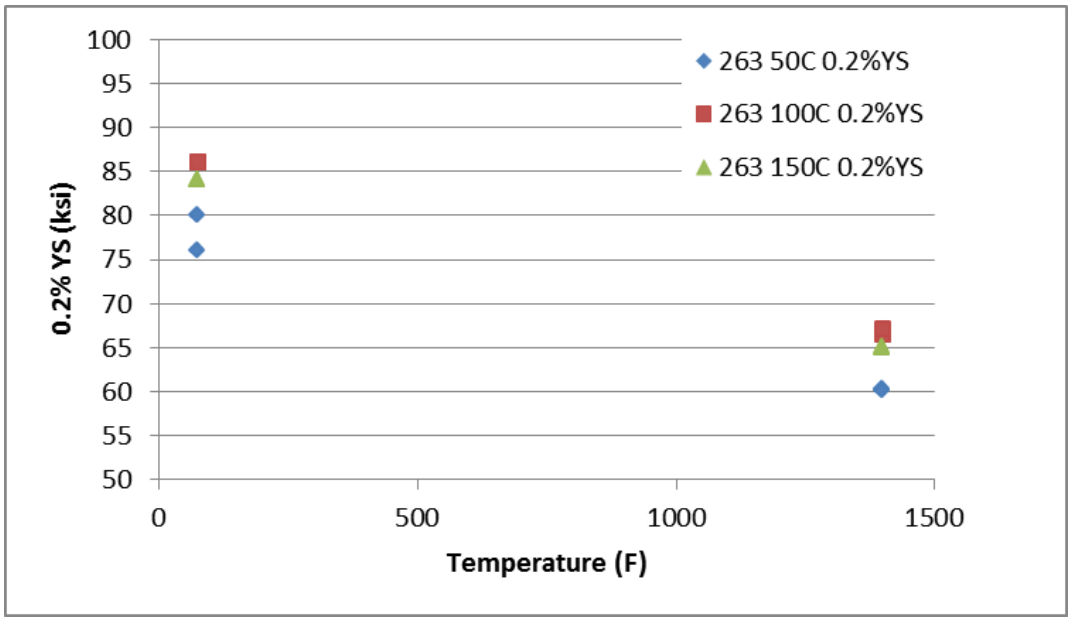

Figure 3: Super heat influence on N263- 0.2% YS at RT and 1400°F.

Figure 4 and Figure 5 show the influence of cast structure on Nimonic 263 Tensile (UTS) and 0.2% YS, respectively. Differences in Tensile and 0.2% YS values at elevated temperature (1400°F) are minimal.

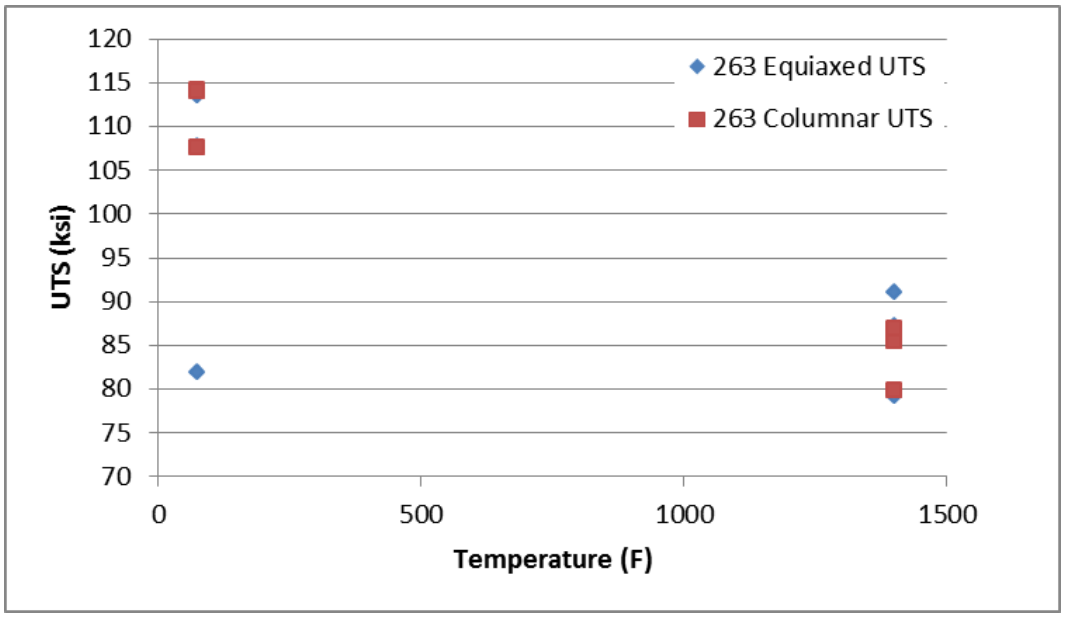

Figure 4: Cast structure influence on N263 Tensile strength at RT and 1400°F

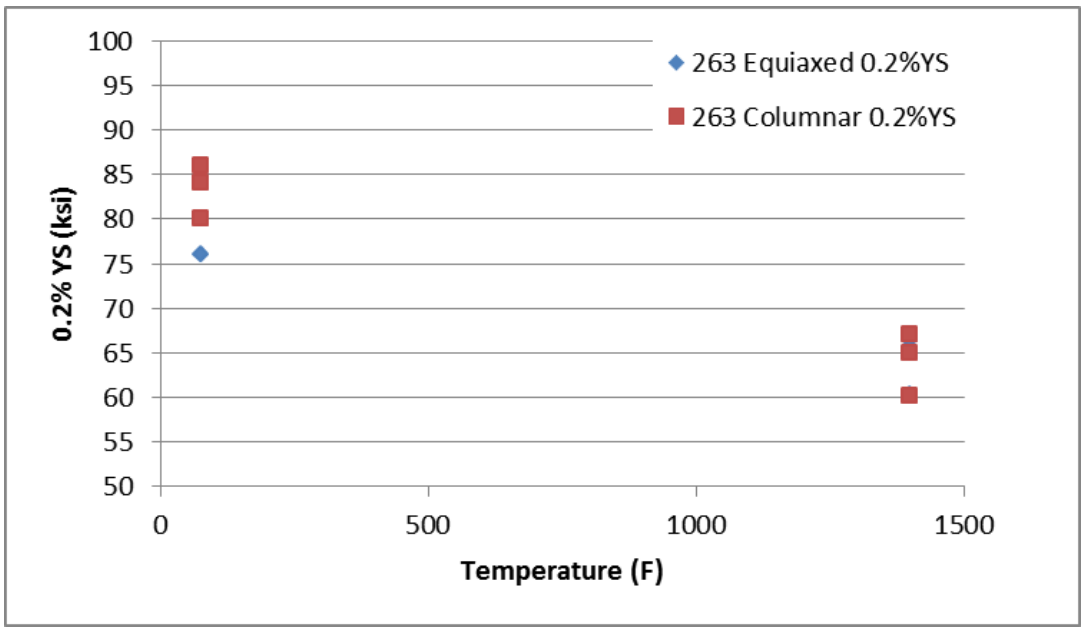

Figure 5: Cast structure influence on N263 0.2% YS at RT and 1400°F.

Figure 6 and Figure 7 show the influence of melt super heat temperatures on Haynes 282 Tensile (UTS) and 0.2% YS, respectively. Differences in Tensile and 0.2% YS properties are minimal for 100°C-150°C, super heat range temperatures, which are typical foundry casting pouring temperature selection practices.

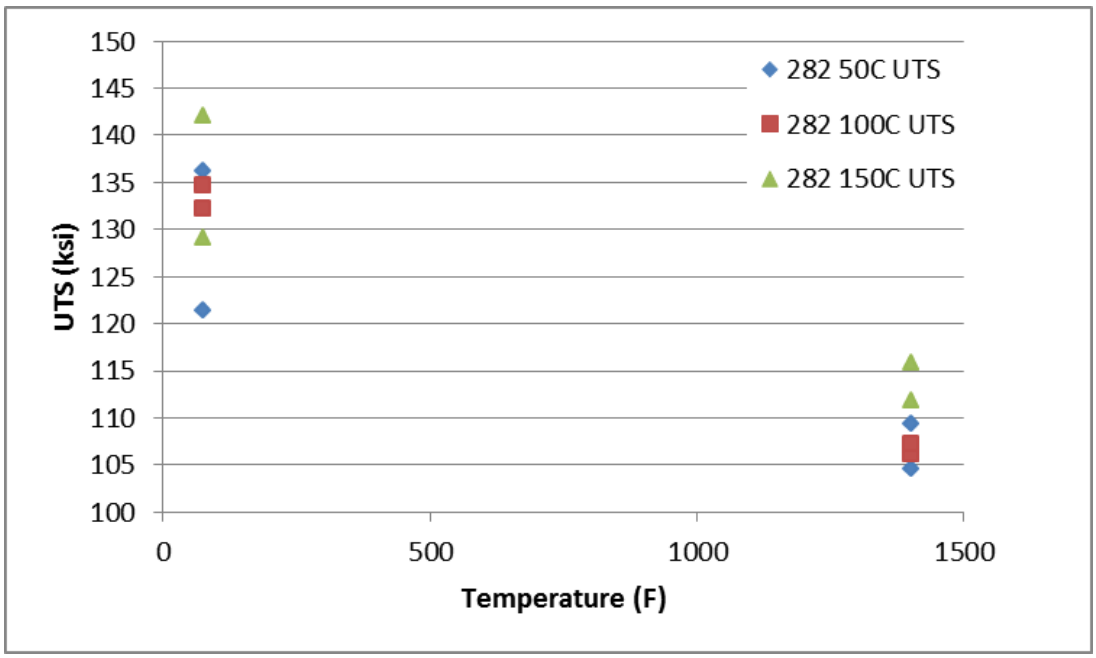

Figure 6: Super heat influence on H 282 Tensile strength at RT and 1400°F

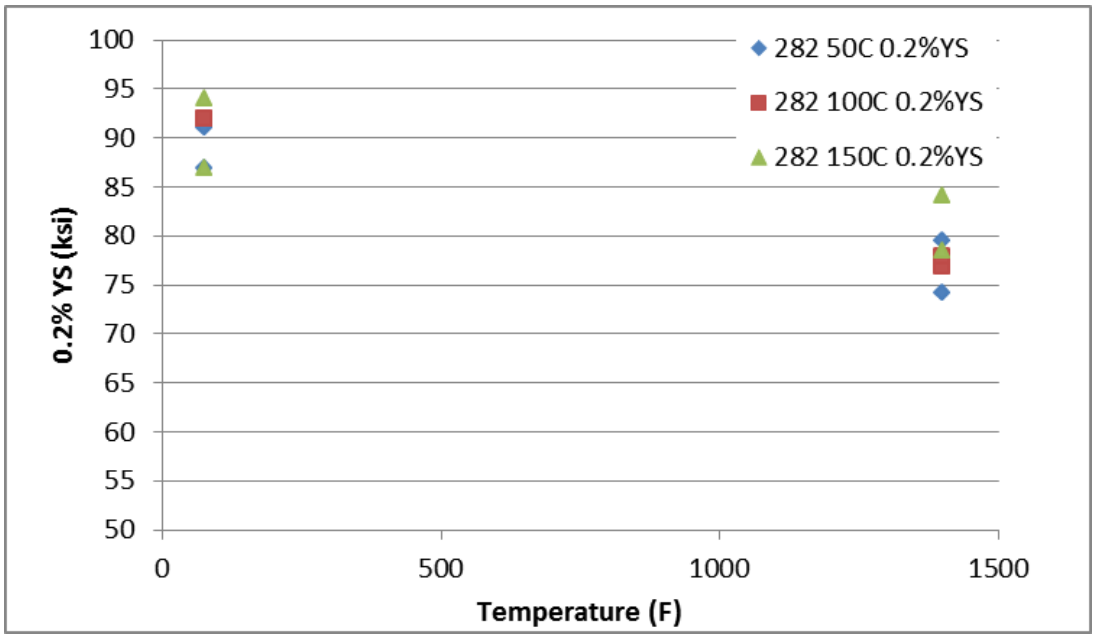

Figure 7: Super heat influence on H 282- 0.2% YS at RT and 1400°F.

Figure 8 and Figure 9 show the influence of cast structure on Haynes 282 Tensile (UTS) and 0.2% YS, respectively. Columnar as cast structures show higher tensile and 0.2% YS values at all temperatures.

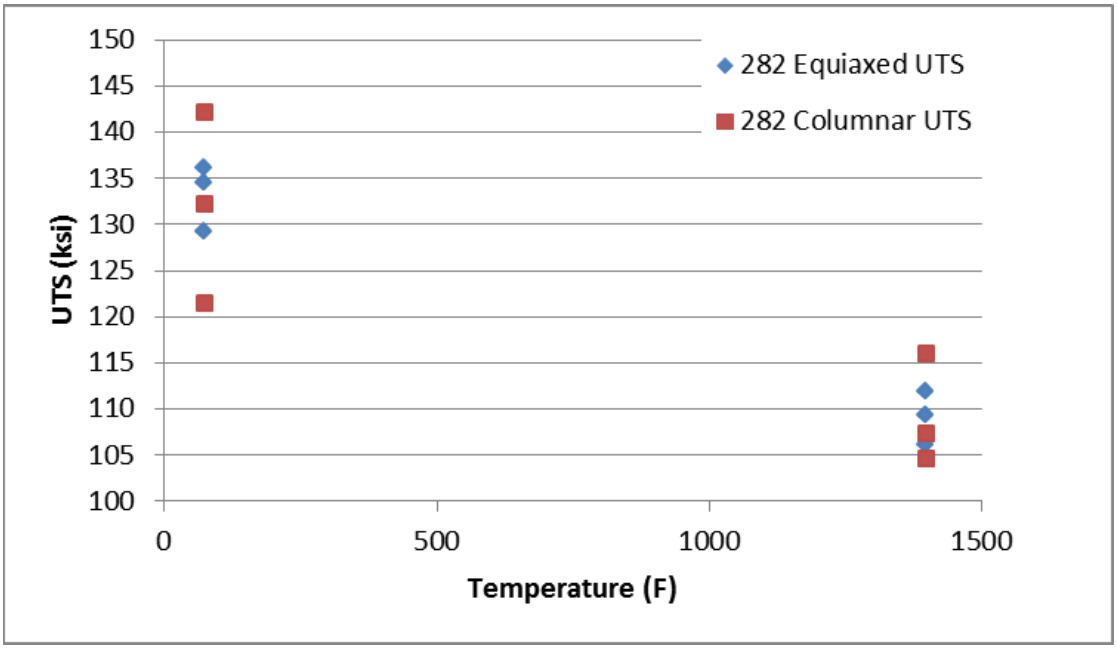

Figure 8: Cast structure influence on H 282 Tensile strength at RT and 1400°F

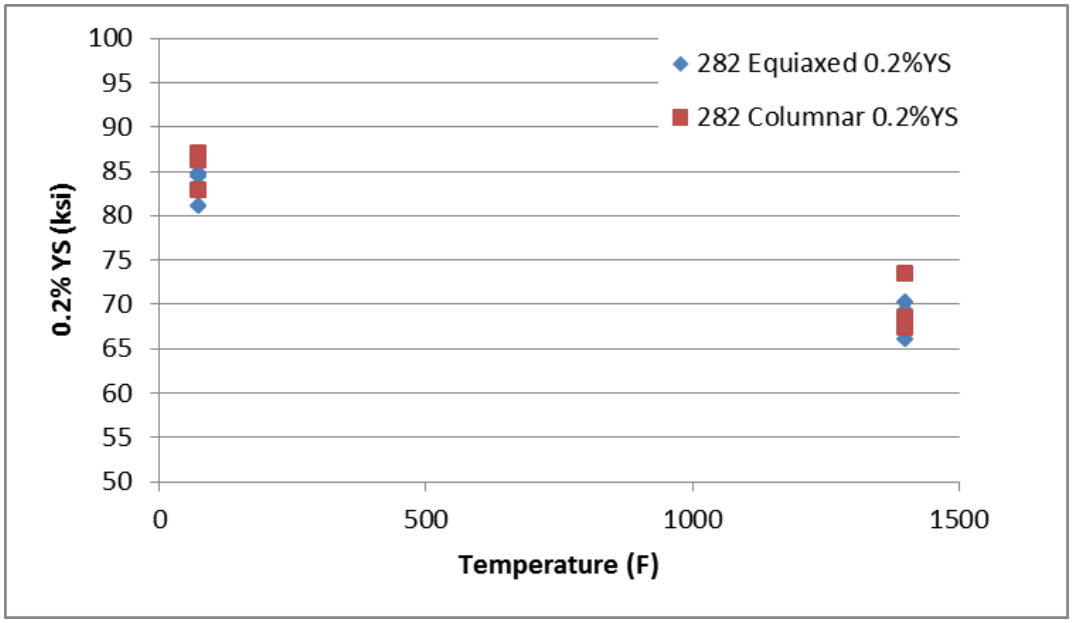

Figure 9: Cast structure influence on H 282 0.2% YS at RT and 1400°F.

Figure 10 and Figure 11 show the influence of Super heat and cast structure on Nimonic 263 LCF properties, respectively.

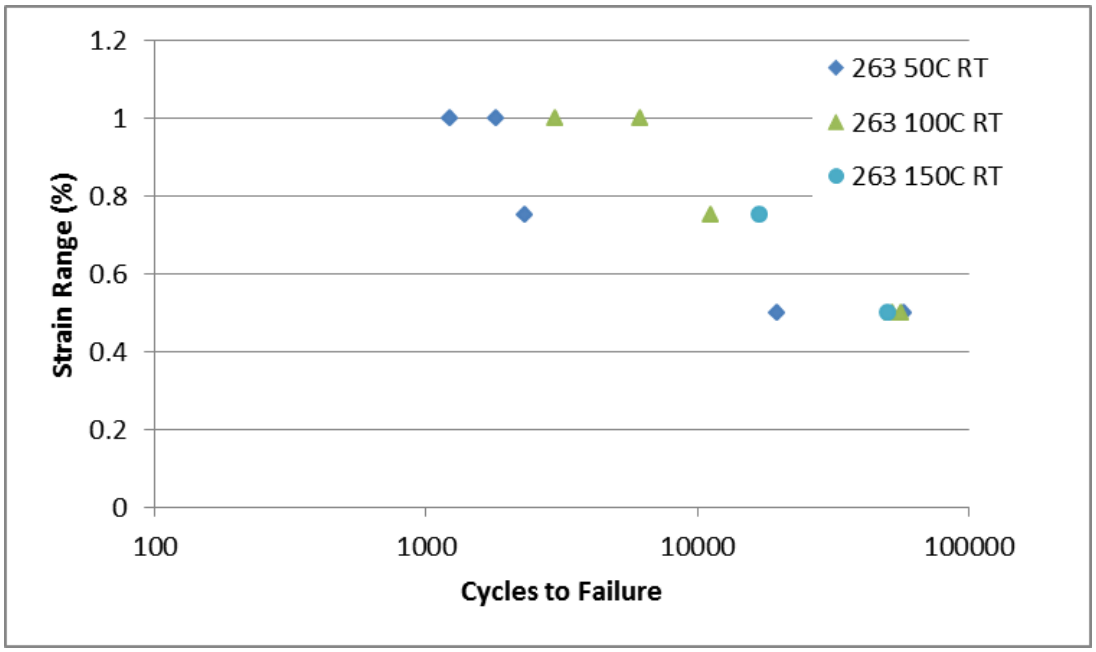

Figure 10: Super heat influence on N263 LCF at RT. Higher super heat temperatures of 150°C provides improved LCF properties

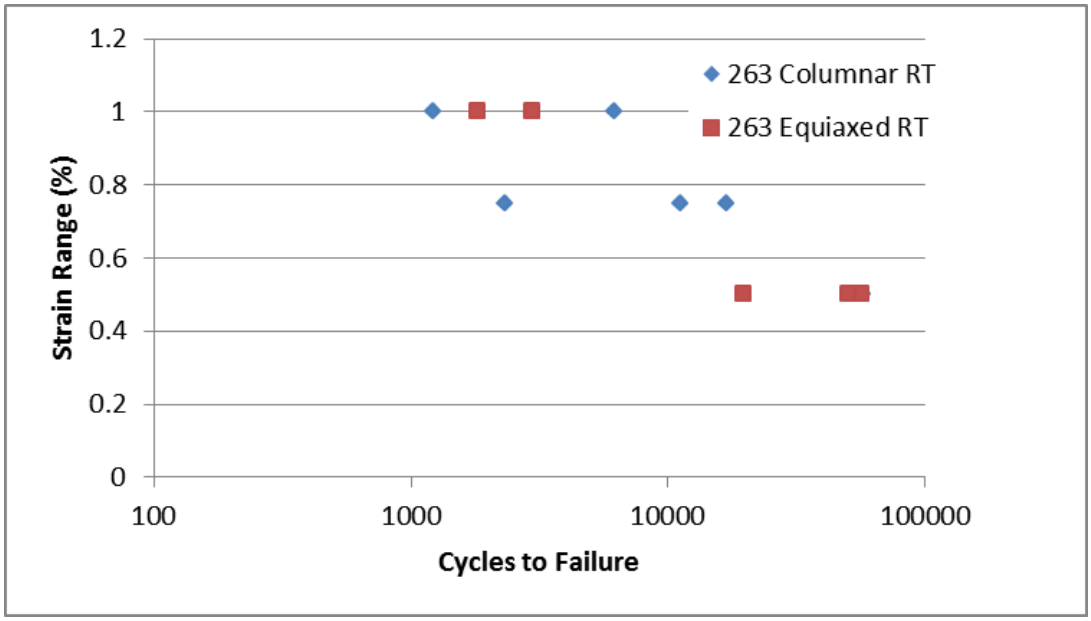

Figure 11: Cast structure influence on N263 LCF at RT. Columnar as cast structures tend to provide better LCF properties.

Figure 12 and Figure 13 show the influence of Super heat and cast structure on Haynes 282 LCF properties, respectively.

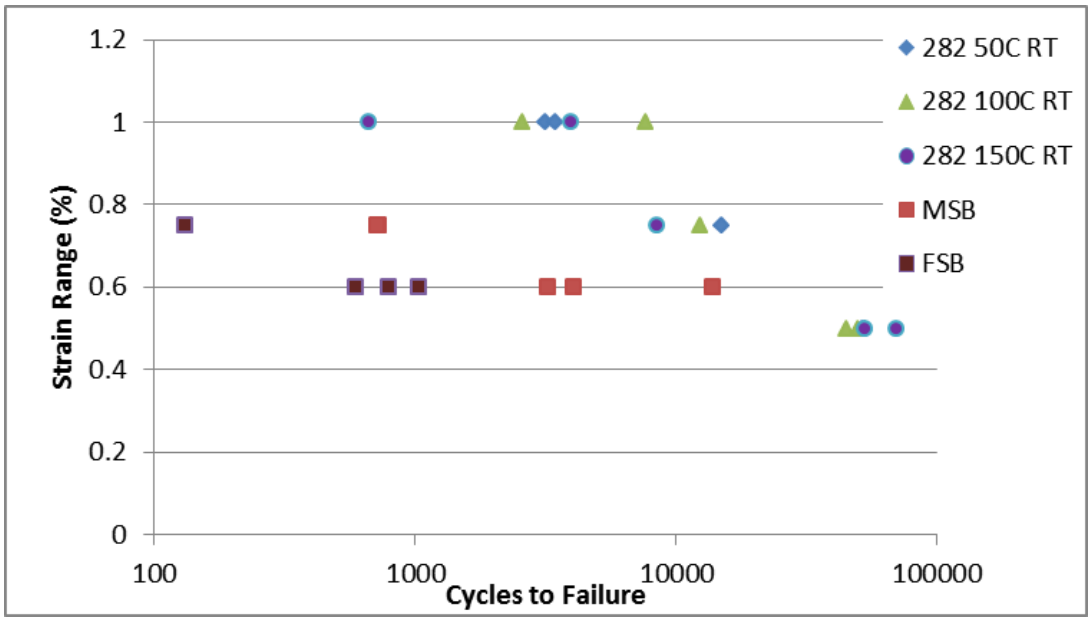

Figure 12: Super heat influence on H282 LCF at RT. Higher super heat pour temperatures of 100°C-150°C shows improved LCF properties

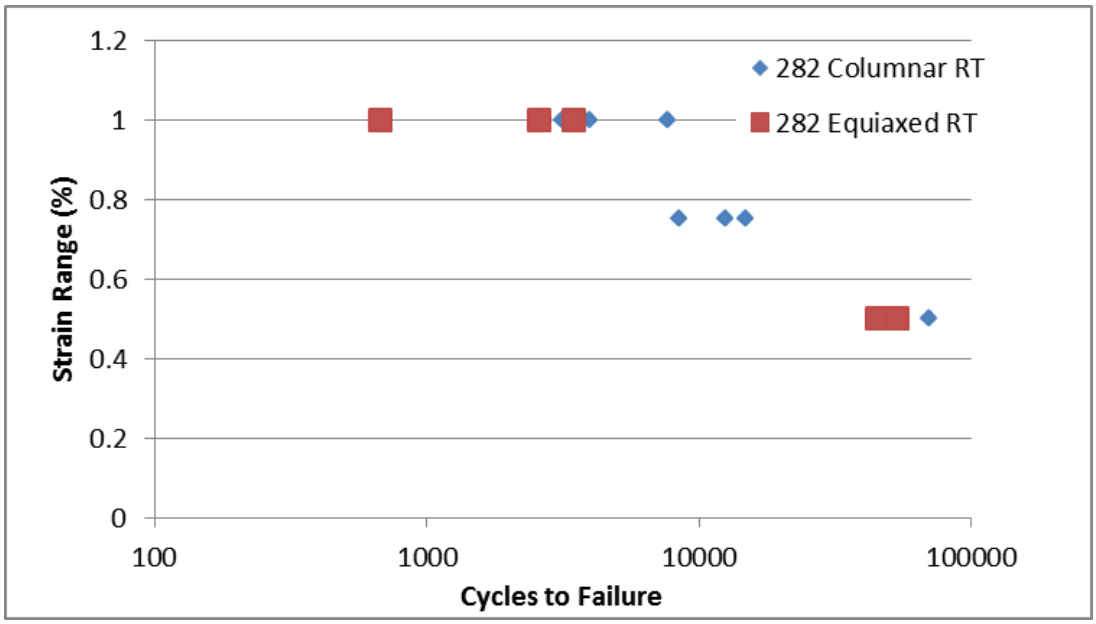

Figure 13: Cast Structure influence on H 282 LCF at RT. Columnar as cast structures shows improved LCF properties at RT.

Figure 14 and Figure 15 show the influence of Super heat and cast structure on Nimonic 263 LCF properties at 1400°F, respectively, compared with forging properties.

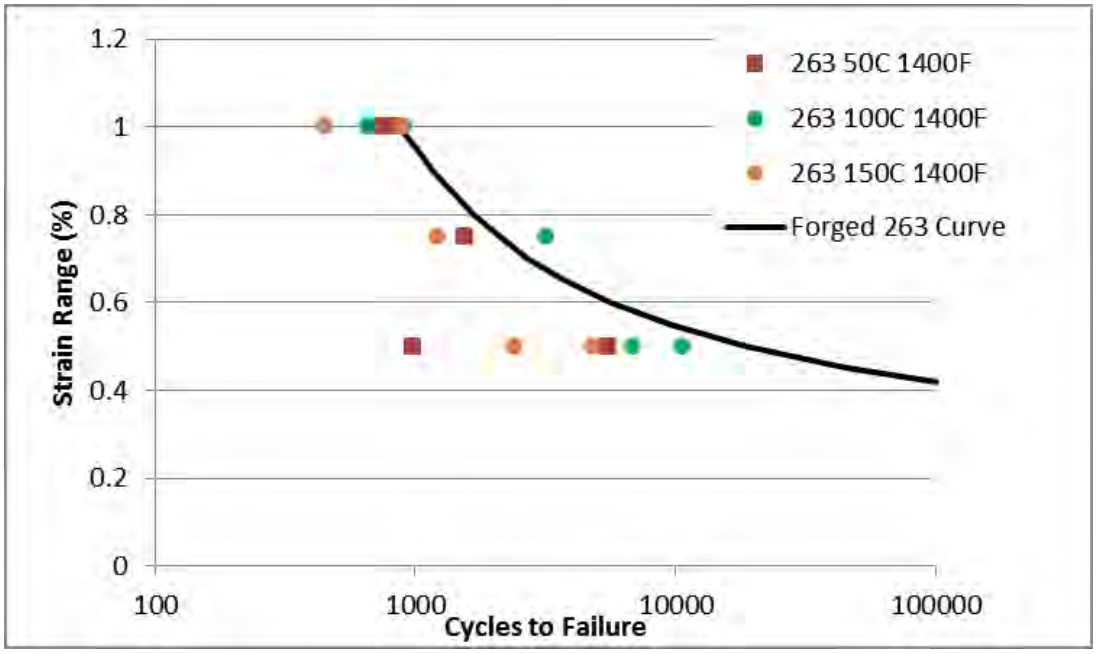

Figure 14: Super heat influence on N263 LCF at 1400°F compared with Forged 263. 100°C-150°C super heat pour temperatures shows improved LCF properties at 1400°F

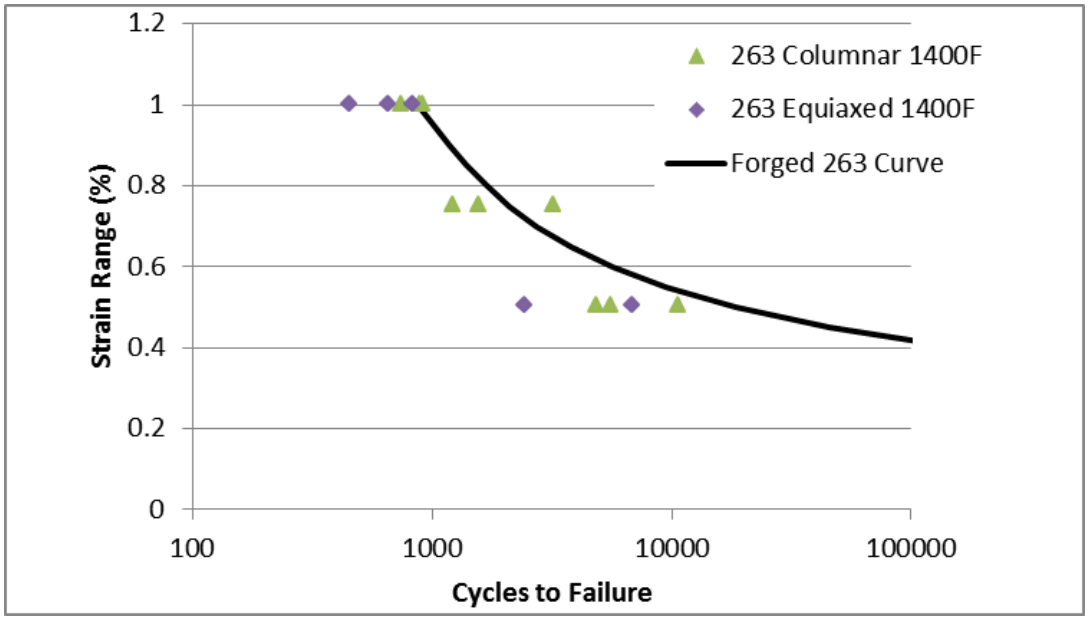

Figure 15: Cast structure influence on N263 LCF at 1400°F compared with Forged 263

Figure 16 and Figure 17 show the influence of Super heat and cast structure on Haynes 282 LCF properties at 1400°F, respectively, compared with forging properties.

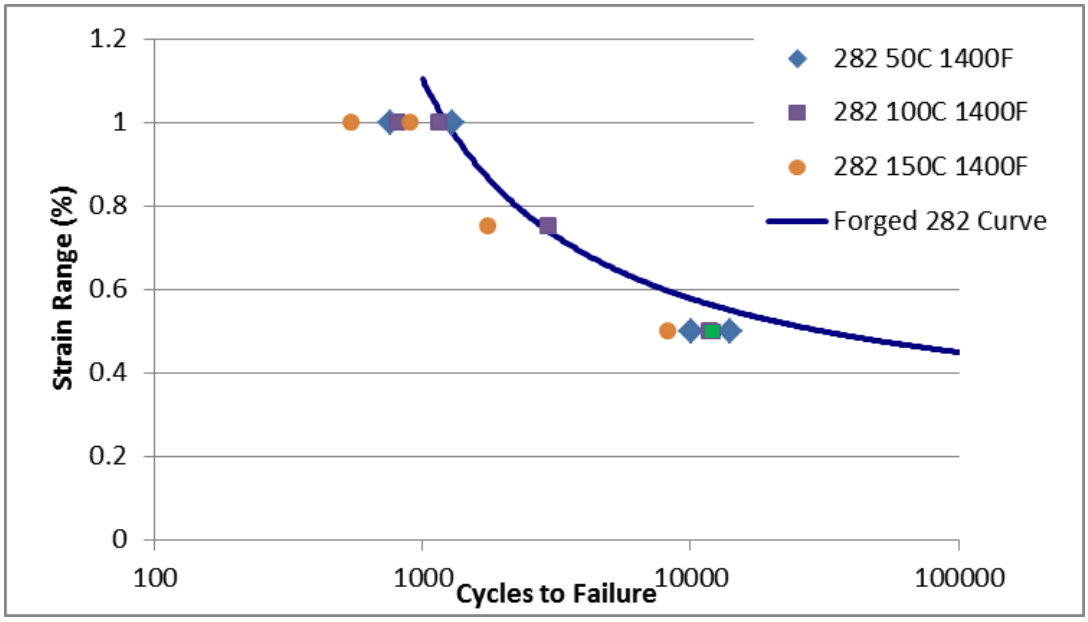

Figure 16: Super heat influence on H 282 LCF at 1400F compared with Forged H282 data. 100°C super heat pours indicate comparable LCF to forged 282 data at 1400°F

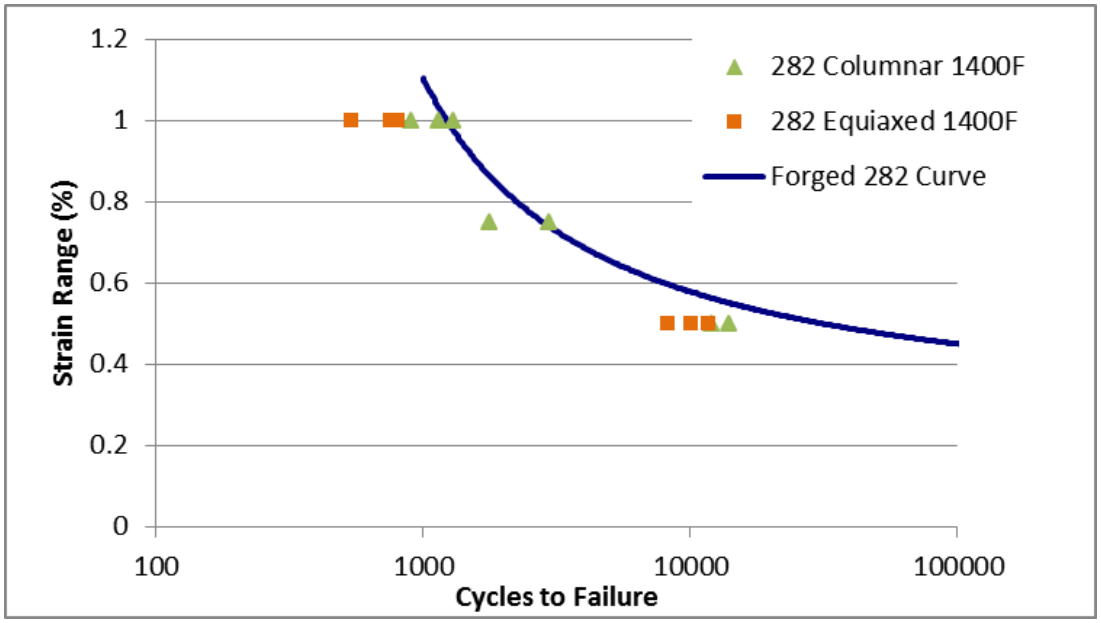

Figure 17: Cast structure influence on H282 LCF at 1400F compared with Forged H282. Columnar as cast structure provides improved LCF at 1400°F compared with equiaxed cast structure.

Conclusion: This test program confirms that 100°C to 150°C Melt super heat temperature is a recommended practice depending on casting geometry for Haynes 282

Table 1: Nimonic263 Cast Cylinder Microstructures (50X) with Superheat Temperature and Structure Variation

50°C Superheat- Columnar	100°C Superheat- Columnar	150°C Superheat- Columnar
	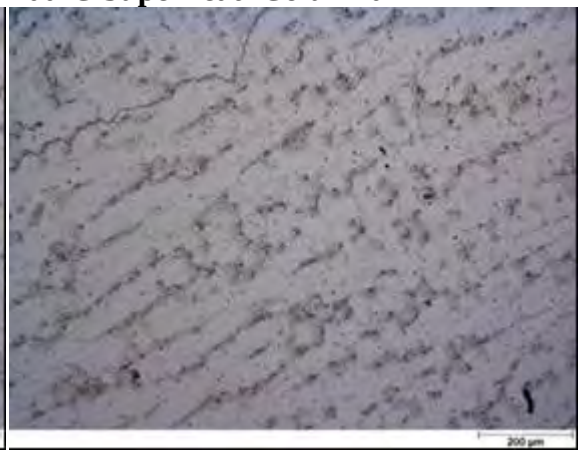	
50°C Superheat- Equiaxed	**100°C Superheat- Equiaxed**	**150°C Superheat- Equiaxed**
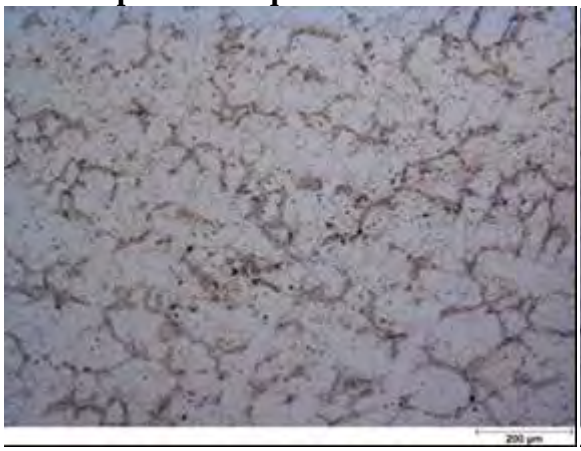	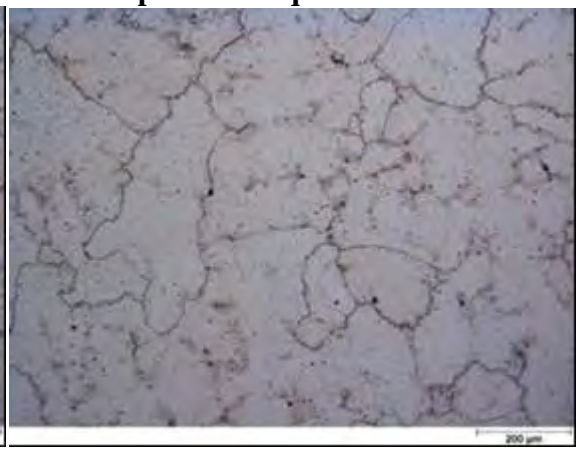	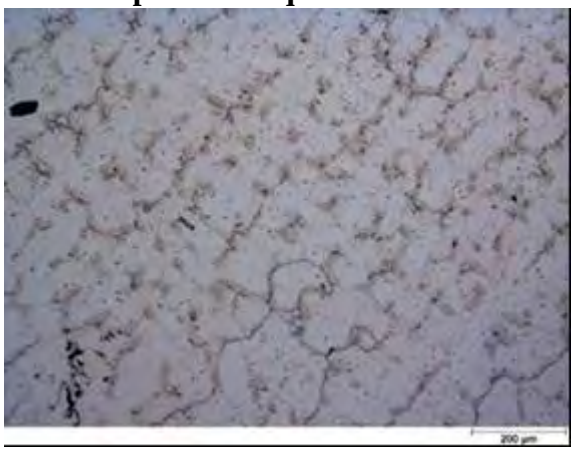

Table 2: Haynes 282 Cast Cylinder Microstructures (50X) with Superheat Temperature and Structure Variation

50°C Superheat- Columnar	100°C Superheat- Columnar	150°C Superheat- Columnar
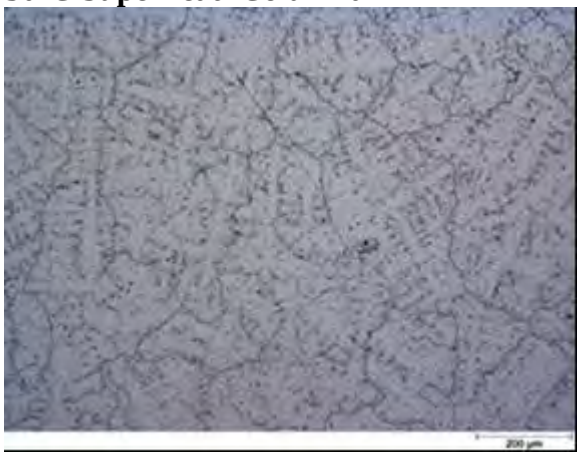	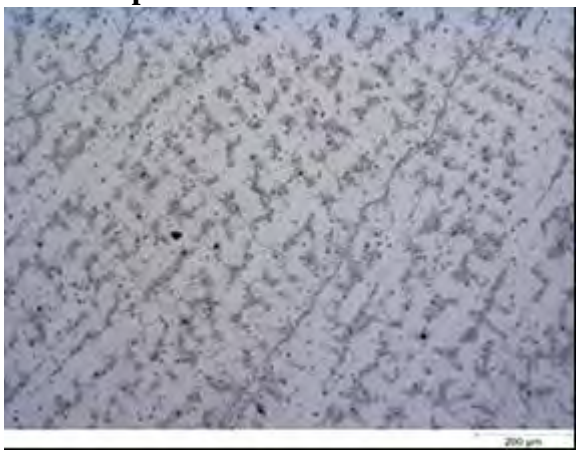	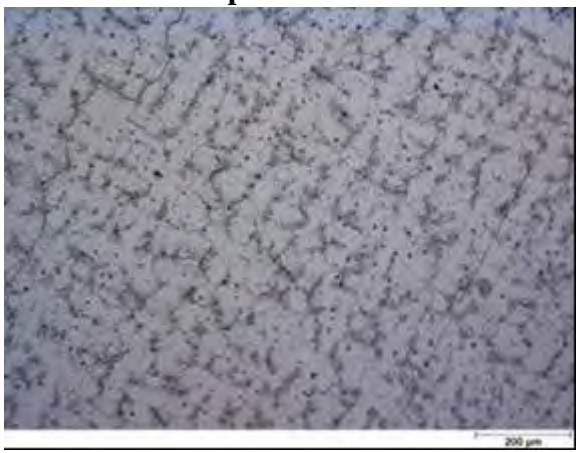
50°C Superheat- Equiaxed	**100°C Superheat- Equiaxed**	**150°C Superheat- Equiaxed**
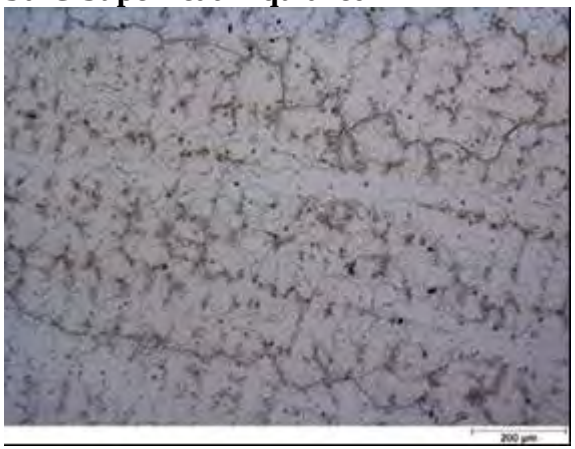	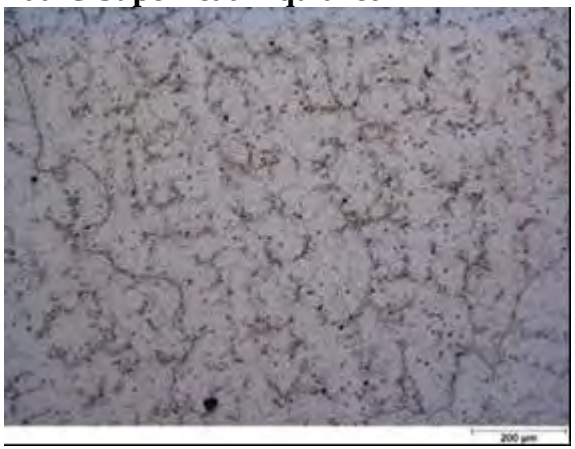	

Table 3: Nimonic263 Cast Cylinder Microstructures (500X) with Superheat Temperature and Structure Variation

50°C Superheat- Columnar	100°C Superheat- Columnar	150°C Superheat- Columnar
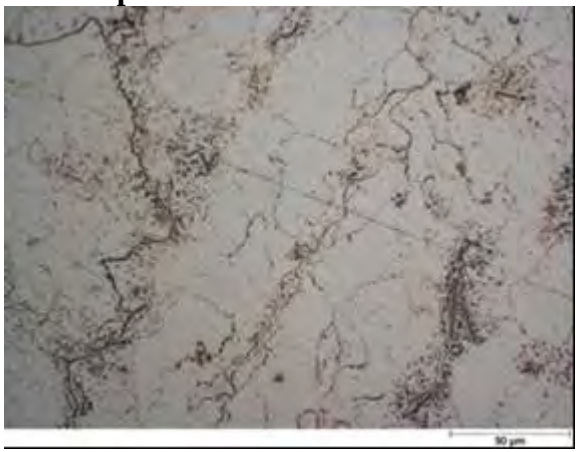	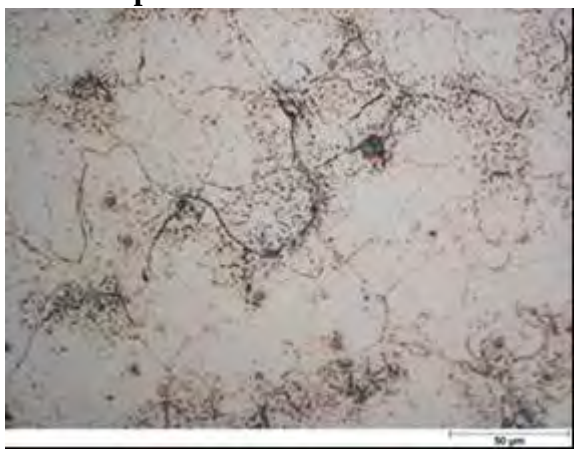	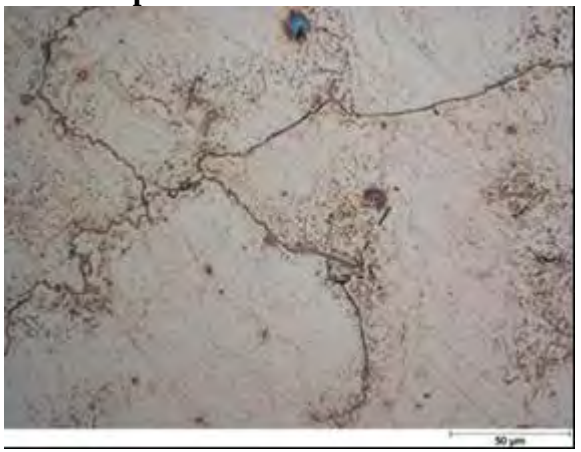
50°C Superheat- Equiaxed	**100°C Superheat- Equiaxed**	**150°C Superheat- Equiaxed**
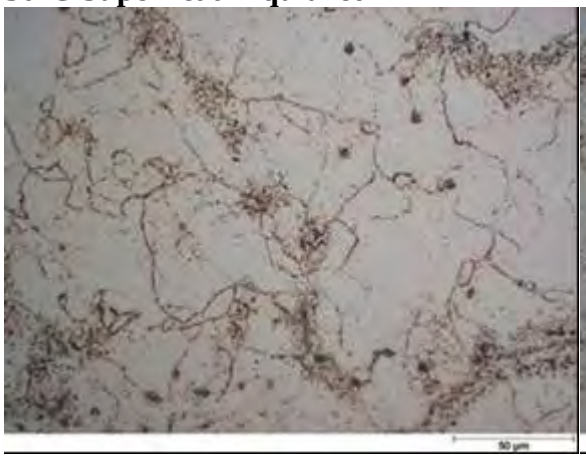	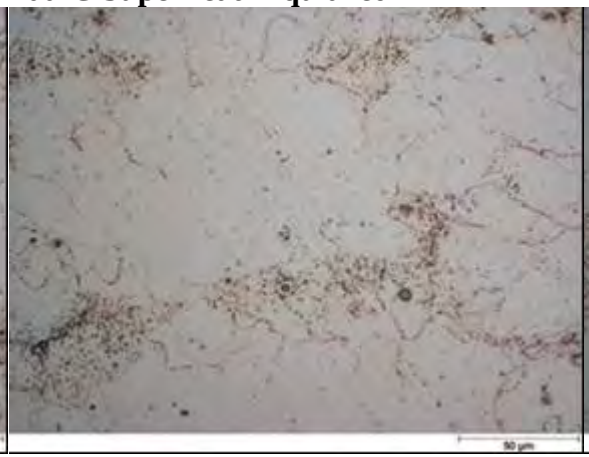	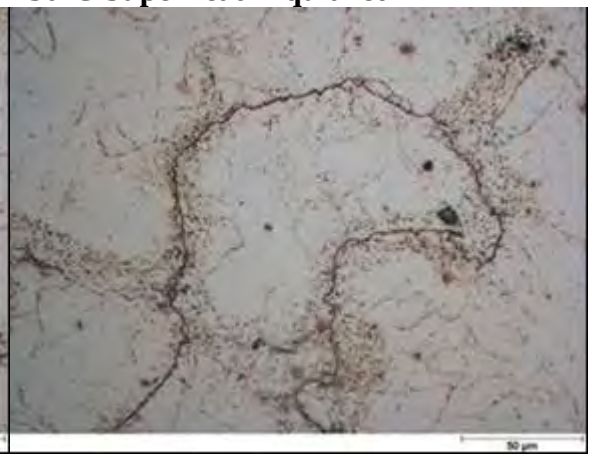

Table 4: Haynes 282 Cast Cylinder Microstructures (500X) with Superheat Temperature and Structure Variation

50 C Superheat Columnar

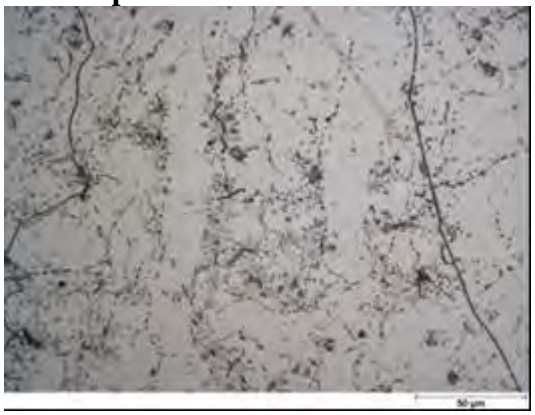

100 C Superheat Columnar

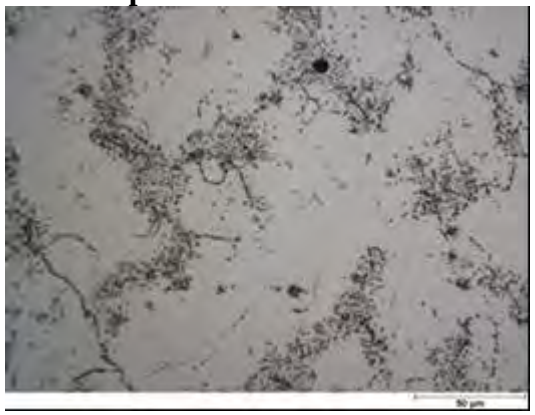

150 C Superheat Columnar

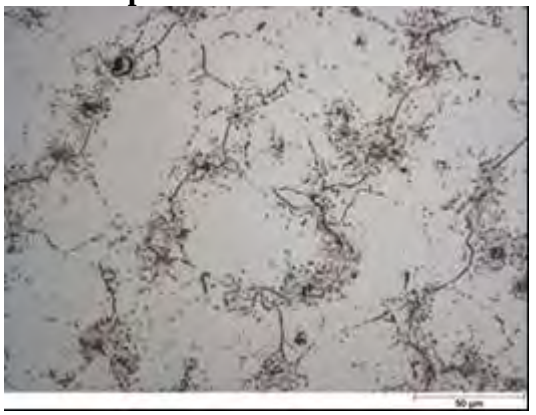

50 C Superheat Equiaxed

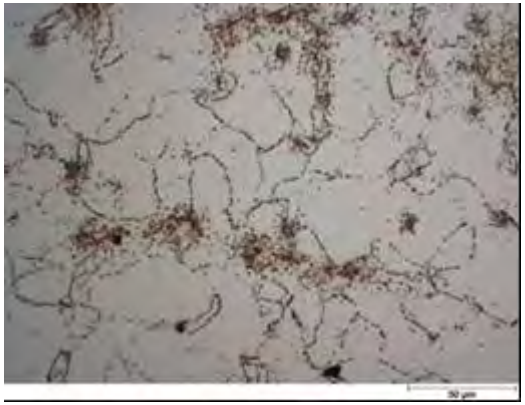

100 C Superheat Equiaxed

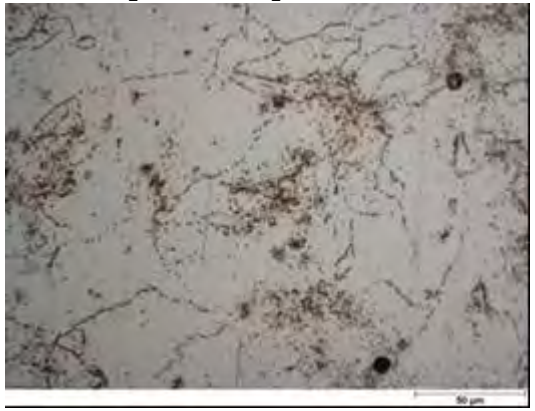

150 C Superheat Equiaxed

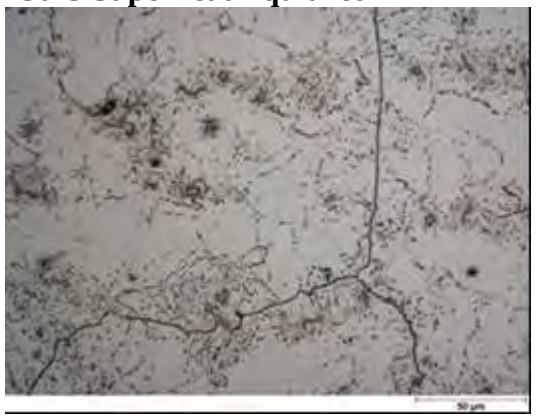

STEP BLOCK CASTING OF HAYNES 282

Two separate Step block castings were poured at two foundry suppliers with different section sizes and casting gating and feeding methods.

MT Foundry Step block dimensions shown in Figure 18 and uses bottom gating and top feeder methods as shown in Figure 19. FS Foundry step block dimensions and horizontal gating method is shown in Figure 20.

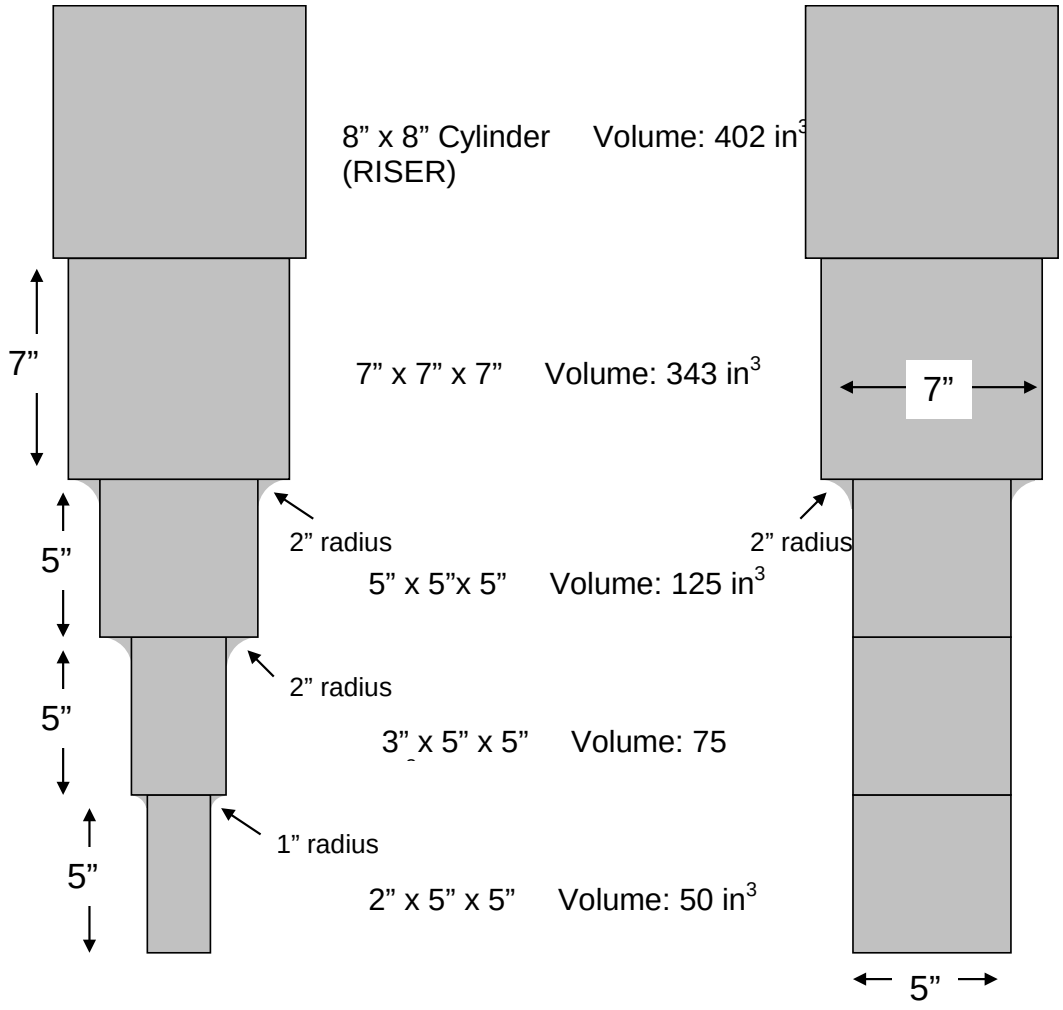

Figure 18: Schematic of the MetalTek 300 lbs. Haynes 282 step block casting with dimensions

Figure 19: MetalTek 300 lbs. Haynes 282 step block casting after mold shake out and shot blast cleaning operations. Bottom gated with casting top feeder arrangement shown.

HT Cycles: To justify the thermal cycle applied to the step blocks, microprobe analysis was performed on the casting as-cast and after a series of homogenization cycles to model the effect of the secondary dendrite arm spacing had on the extent of remaining segregation. Those cycles attempted to optimize a thermal cycle for homogenization while trading over time.

The Step block casting Homogenization, Solution heat treatment and the Aging HT cycles are tabulated in the Appendix 1-B.

The step block section casting trepan samples optical micrographs and SEM images showing high Mo, high Si phases on grain boundaries which are as shown in Appendix 1-B.

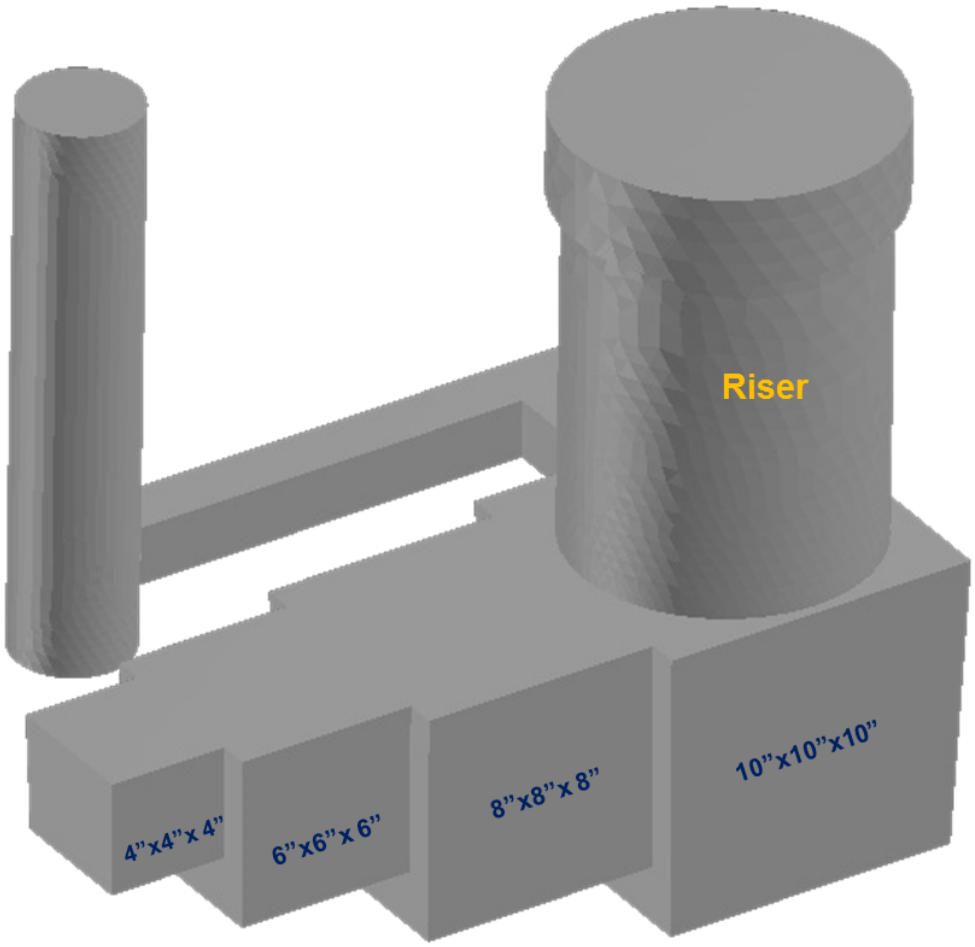

Figure 20: Schematic of Flowserve Step block. Top feeder with section modulus controlled feeding.

The MetalTek and Flowserve step block castings sample sections cut up diagram and the trepan test specimen cut up diagrams are shown in the Appendix 1-B. These core sections were tested for tensile, impact, and LCF properties as a baseline for future studies.

The step block section trepan specimens Tensile properties at RT and 1400°F for the 10 inch Flowserve step section and 7 inch MetalTek step sections are tabulated in Appendix 1-B. Both tensile and ductility values were lower compared with the smaller section cast cylinders data. The debit in mechanical properties are due to the in appropriate homogenization heat treatment cycles for the step block.

The trepanned test specimens from 10 inch and 7 inch step block sections, LCF properties at RT and 1400°F and also the Charpy V-Notch Impact properties are tabulated in Appendix 1-B.

Metallography was performed and both optical micrographs and SEM grain boundary images showing high Moly and high Silicon phases for Flowserve step block are shown in Figure 21 and Figure 22.

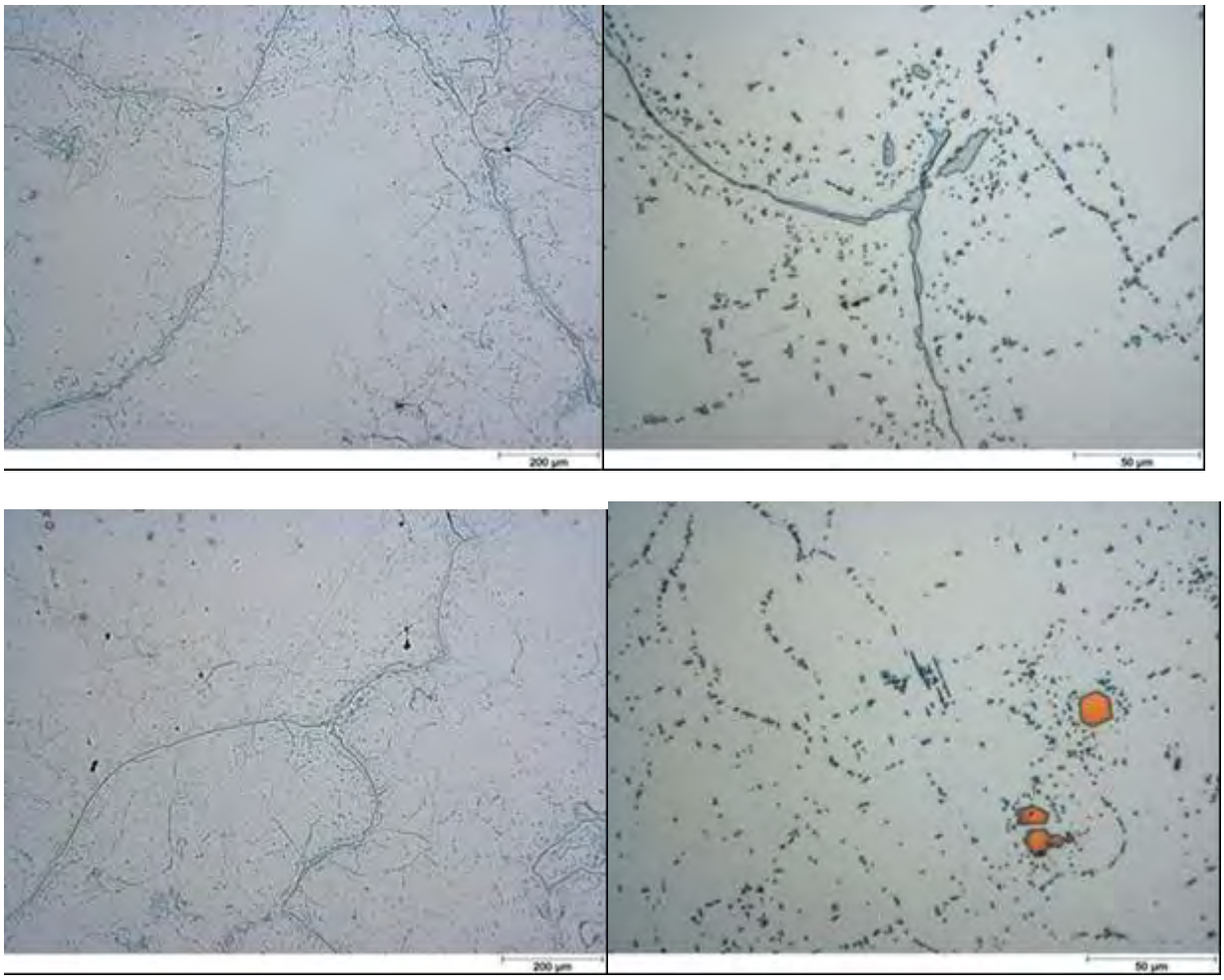

Figure 21: Optical micrographs from the Flowserve step block (etched with Kallings)

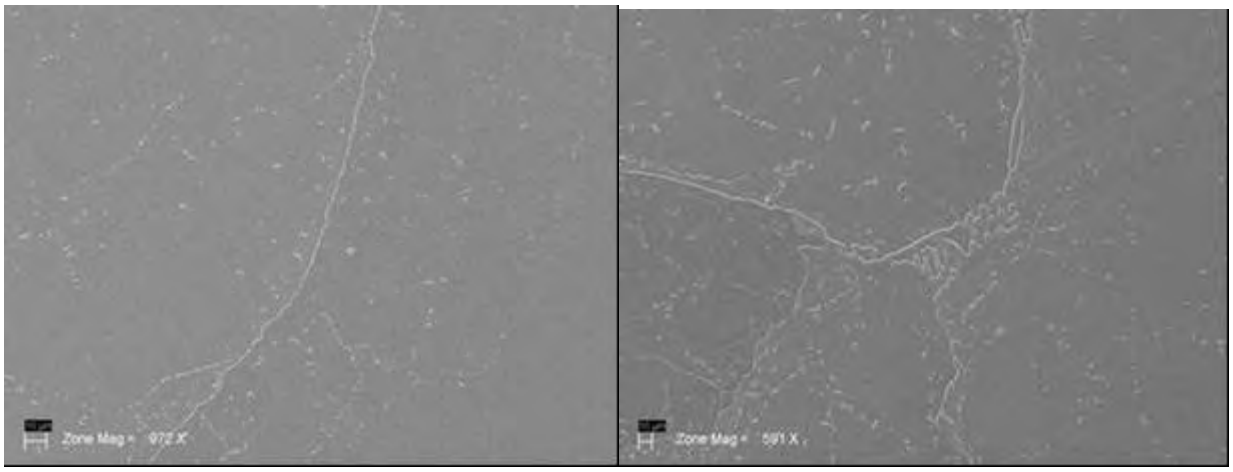

Figure 22: Secondary Electron Images (SEM) showing high-Mo, high-Si phases on grain boundaries

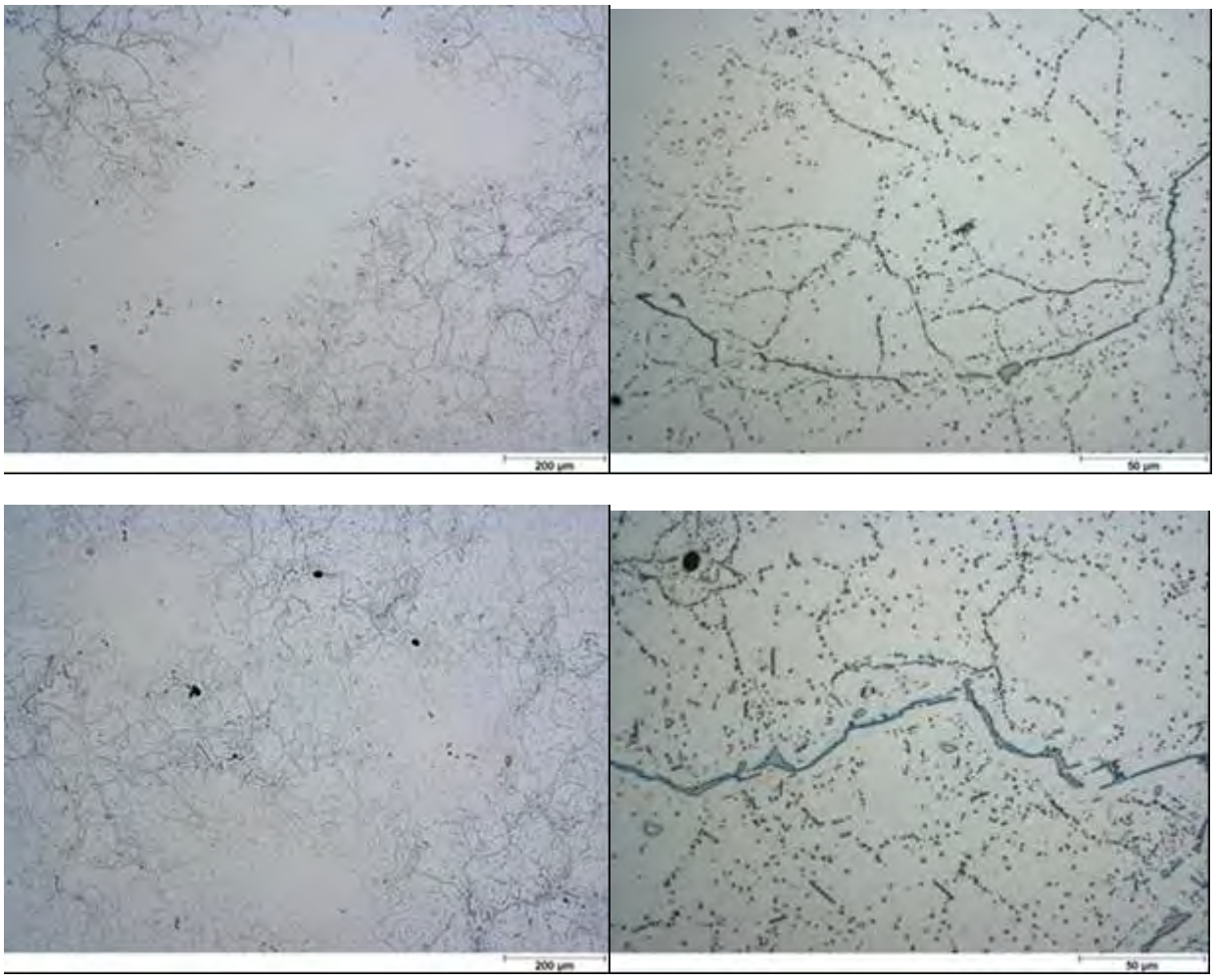

Figure 23: Optical micrographs from the MetalTek step block (etched with Kallings)

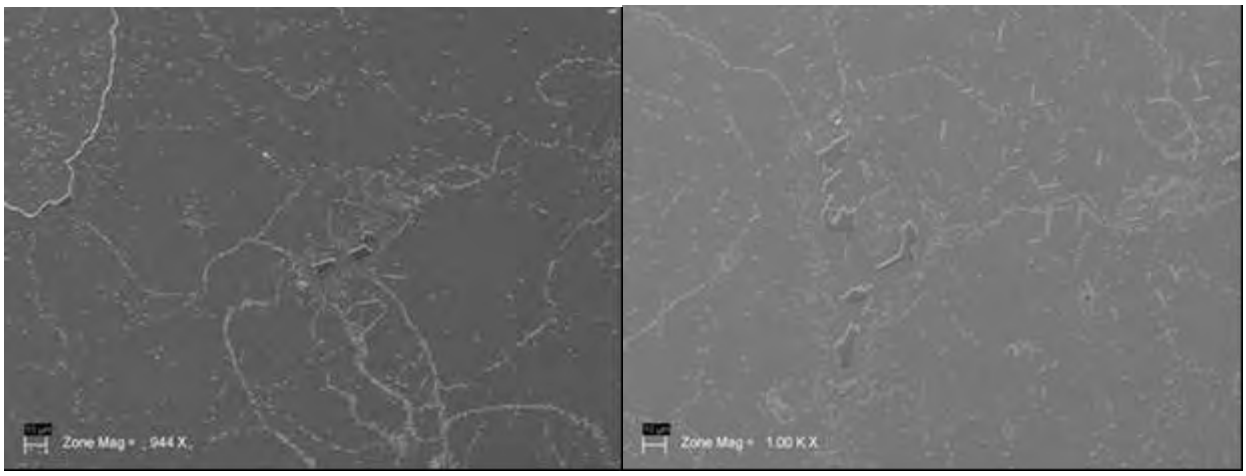

Figure 24: Secondary Electron Images (SEM) showing various phases

Optical micrographs and SEM pictures for MetalTek step block casting are shown in Figure 23 and Figure 24. Both the step block section microstructures showed clusters of carbides near grain boundaries with carbide-denuded zones away from grain boundaries as shown in Appendix 1-B. This may be the result of heat treat cycles specified for the parts.

STEP CASTING OF NIMONIC 263

GE manufactured a large step block (SB) casting of Nimonic 263, with a pour weight of 1280 lbs. cast at Flowserve foundry and carried out multi step Homogenizing and Aging heat treatments followed by casting evaluation test program.

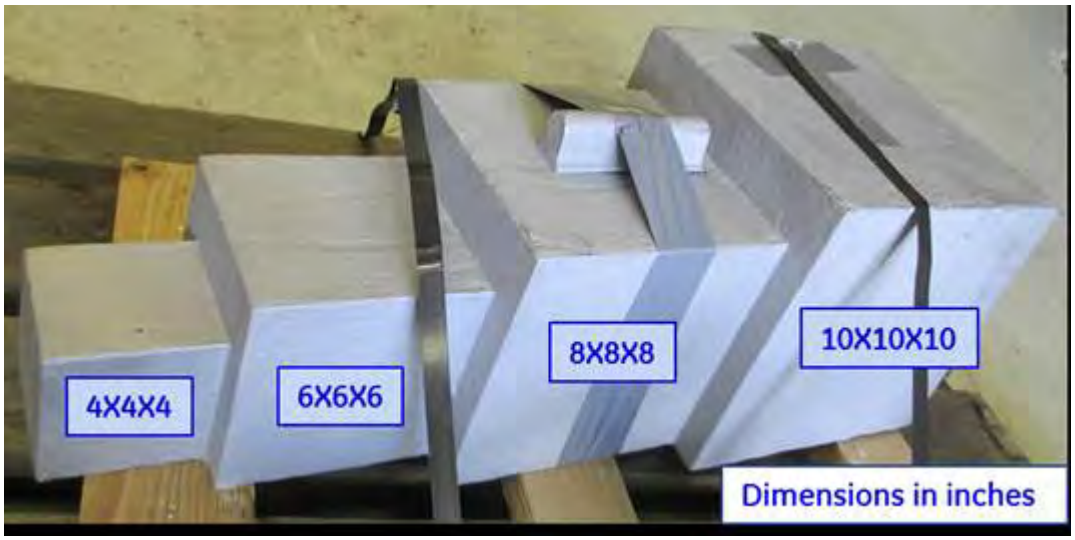

Figure 25: Nimonic 263 step block test casting, weighing 605 lbs. Completed optimized Homogenizing and Age hardening heat treatments

The test program evaluated casting solidification simulation analysis [Figure 27], NDT inspection methods [Figure 34], planned and executed detailed test matrix for chemical, mechanical property section sensitivity studies at RT and at elevated temperatures. Figure 30 and Figure 31 provide the Test matrix**.** Trepan sample extraction location and orientations are provided in Figure 28 and Figure 29. Appendix 1-C provides additional trepan sample cast section views and sample ID and data tables

The test results such as Chemical, Tensile, LCF, stress rupture, CVN impact, hardness, J1C Fracture toughness trend with section size and temperature and microstructural feature SDAS values with section size and cooling rates are provided in this test report.

N263 does not exhibit section sensitivity with respect to UTS, 0.2% YS, Hardness, or stress rupture. However, section thickness influenced the ductility, LCF and Charpy impact energy properties. In addition, casting processing parameters such as gating, feeding, mold and melt processing steps, solidification cooling rate, and heat treatment cycles (Homogenizing & Aging) demonstrated influence on mechanical properties.

The Casting methods, mold, melt, pouring, processing steps and heat treatment are the main foundry process CTQ's:

- Casting gating & feeder methods to ensure free from Shrinkage, porosity-cavity defects.

- Mold zircon refractory coat painting is essential to minimize mold metal interaction related defects. Followed by adequate preheating of molds and ladles to dry refractory
- Argon cover of liquid metal during melt processing and Argon purging of pouring launders, ladles, molds are essential to avoid gas blow hole sub surface casting defects
- Heat treat parameters Solutionizing optimized to within +/- 5% of composition variation recommended, considering the incipient melt temperatures at various stages.

N263 Step Block Casting Findings and Observations Summary:

No significant variation in chemistry when compared with section thermal centers was observed, Figure 32.
Plots of UTS, 0.2% YS, and 0.02% YS as a function of section thickness and temperature were completed. All data falls within a tighter band at 1400F-1500°F elevated temperature range, [Figure 37 - Figure 41].

% Elongation as a function of temperature for various section thicknesses exhibit a wide variation, [Figure 42]

% RA trend in smaller sections show a wide variation at elevated temperatures, [Figure 43].

Hardness variation trend is not section thickness dependent, [Figure 58, Table 16]

CVN spread is larger in 10 inch section in comparison with 8 & 6 inch sections [Figure 57, Table 15]

Plots of cycles to failure and Total strain range (%) for the 10” and 6” thick sections at RT are shown in Figure 45. The 10 inch section shows a debit in comparison with 6 inch section.

Plots of cycles to failure and Total strain range (%) for the 10” and 6” thick sections at 1400 deg. F are shown in Figure 46. The 10 inch section shows increased debit in comparison with 6 inch section, while 6 inch section shows degradation.

No significant changes in stress rupture data with section thickness, [Figure 47, Table 12].

NDT inspection methods are limited to RT, LPT and Acoustic Emission since UT inspection was not effective for the H263 SB casting

Kq the conditional fracture toughness values are minimally influenced by temperature rise up to 6 inch cast wall thickness, [Figure 48, Table 14].

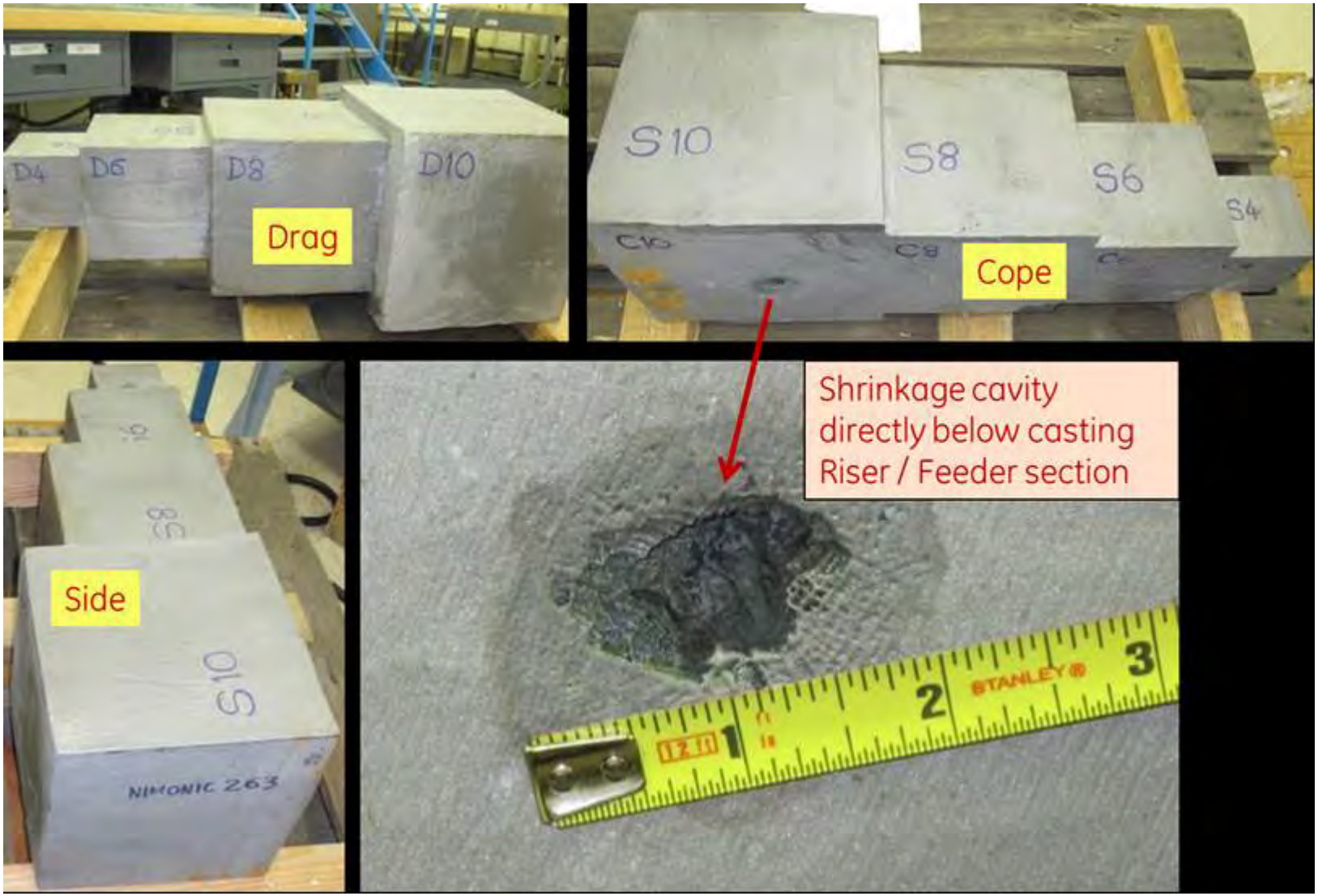

Figure 26: Picture showing the N263 casting and the associated shrink cavity below the rise/feeder section

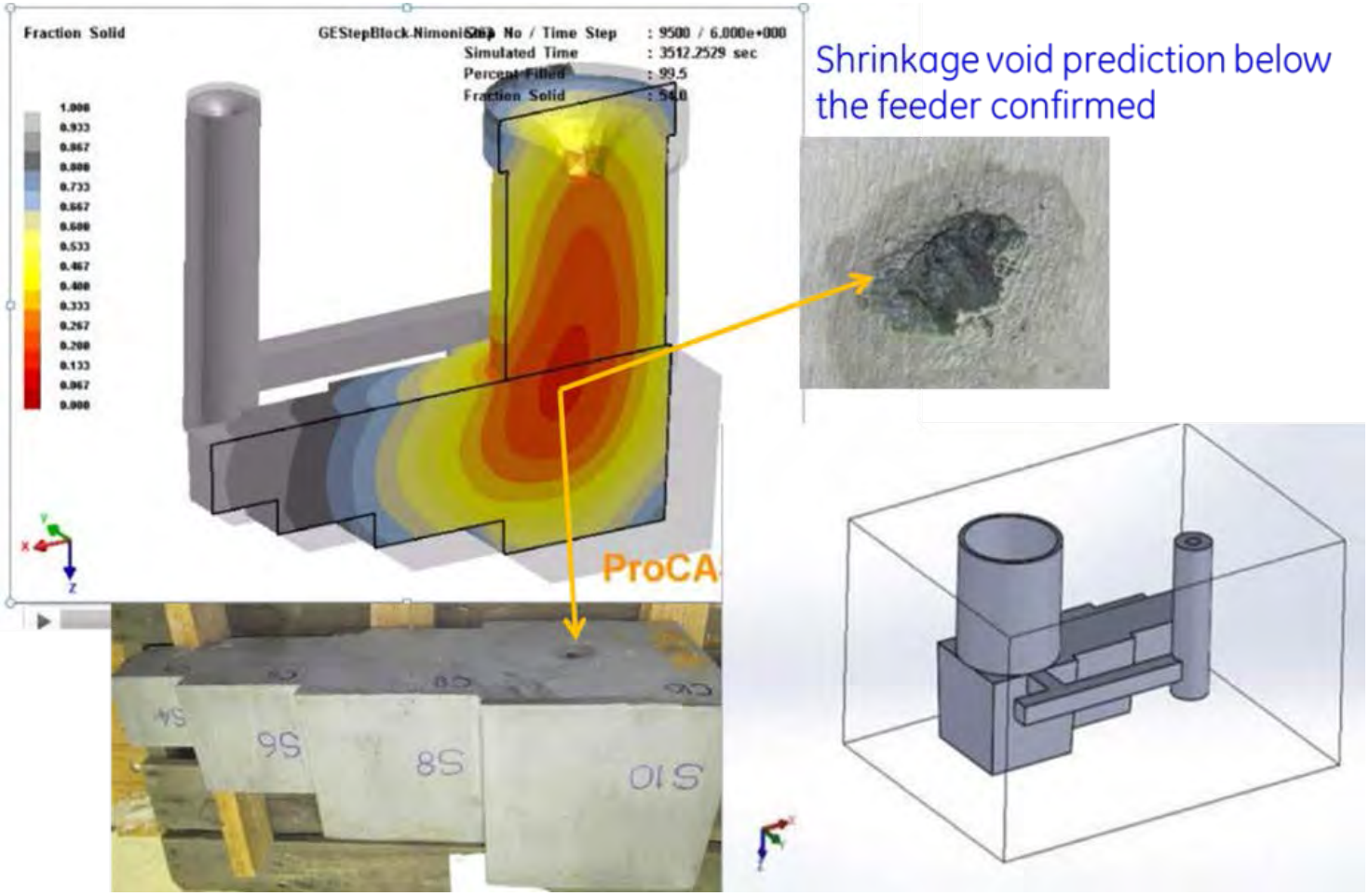

Figure 27: Casting solidification simulation analysis showing the hot spot location and the associated casting shrinkage defect.

Shrinkage associated with Feeder section piping phenomena due to the thermal gradients established

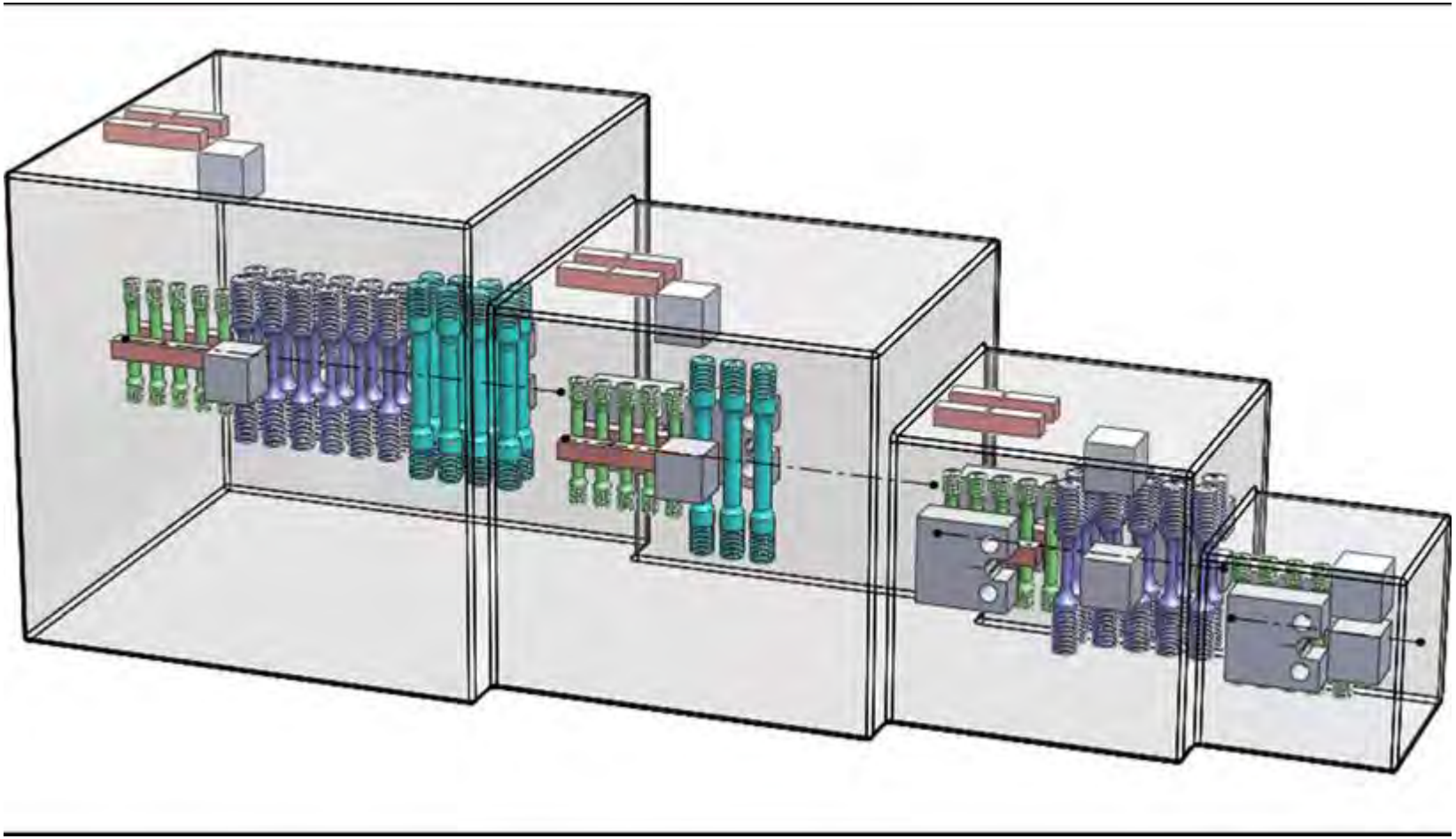

Figure 28: Nimonic 263 test casting, CAD layout of specimen extraction isometric views from step block cast sections

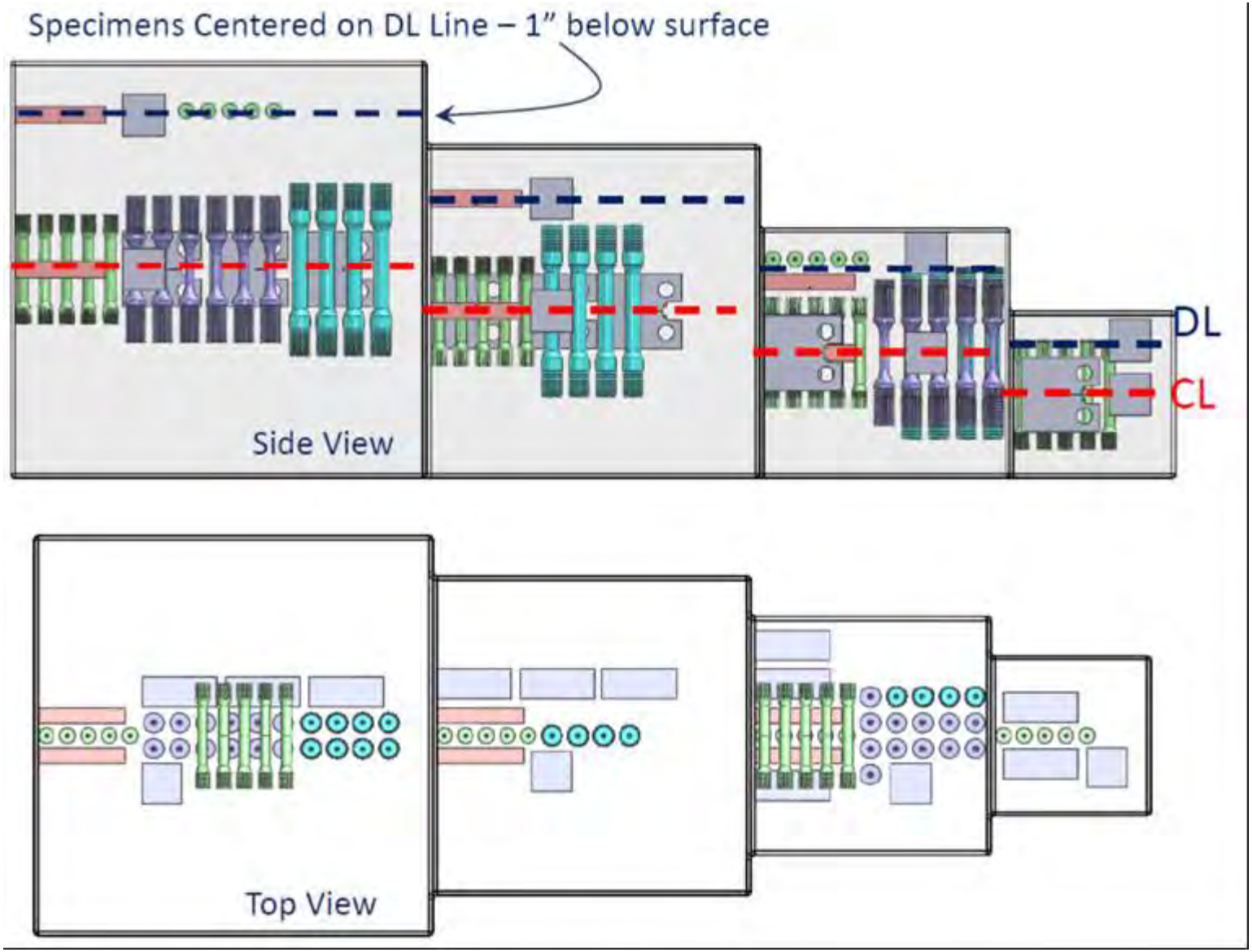

Figure 29: Orientation and specimen layout of various test specimens from N263 test block

Nimonic 263 step block test matrix:					Specimens Identification			
Test #	Test Type	Test condition	Step sections	Total Tests	Specimen ID / Step section			
1	Tensile Test (TS, YS, % EL, %RA) Tensile Specimen: MPE-TNSL-001 P4 30 specimens	Temperature deg.F	10"/8"/6"/4"		10 inch	8 inch	6 inch	4 inch
		RT/ 75 deg. F	1 Test/section in CL plane in vertical orientation	4	10-TN-CL-RT	8-TN-CL-RT	6-TN-CL-RT	4-TN-CL-RT
		500 deg. F		4	10-TN-CL-500	8-TN-CL-500	6-TN-CL-500	4-TN-CL-500
		1000 deg.F		4	10-TN-CL-1000	8-TN-CL-1000	6-TN-CL-1000	4-TN-CL-1000
		1250 deg.F		4	10-TN-CL-1250	8-TN-CL-1250	6-TN-CL-1250	4-TN-CL-1250
		1500 deg F		4	10-TN-CL-1500	8-TN-CL-1500	6-TN-CL-1500	4-TN-CL-1500
		RT/ 75 deg. F	1 Test/section in DL plane in Horizontal orientation (1" above Drag / bottom surface)	2	10-TN-DL-RT	NIL	6-TN-DL-RT	NIL
		500 deg. F		2	10-TN-DL-500	NIL	6-TN-DL-500	NIL
		1000 deg.F		2	10-TN-DL-1000	NIL	6-TN-DL-1000	NIL
		1250 deg.F		2	10-TN-DL-1250	NIL	6-TN-DL-1250	NIL
		1500 deg F		2	10-TN-DL-1500	NIL	6-TN-DL-1500	NIL
2	Charpy V Notch Impact Impact Energy (J); % Shear, Lateral Expansion 12 Specimens	RT/ 75 deg F	2 Tests at Centre CL plane vertical per section	6	10-CVN-RT-C1	8-CVN-RT-C1	6-CVN-RT-C1	NIL
					10-CVN-RT-C2	8-CVN-RT-C2	6-CVN-RT-C2	NIL
			2 Tests at DL horizontal plane per section	6	10-CVN-RT-T1	8-CVN-RT-T1	6-CVN-RT-T1	NIL
					10-CVN-RT-T2	8-CVN-RT-T2	6-CVN-RT-T2	NIL
3	LCF Data Frequency: 20 cpm Waveform: Triangular A Strain 1, TSR% (1.0; 0.90; 0.80; 0.70; 0.60; 0.50) 2 temperatures: RT & 1400 deg. F. Specimen Drg. # 4013195-741 24 specimens	RT/ 75 deg F	A strain / TSR (%)					
			1 / 1.00	2	10-LCF-01	NIL	6-LCF-01	NIL
			1 / 0.90	2	10-LCF-02	NIL	6-LCF-02	NIL
			1 / 0.80	2	10-LCF-03	NIL	6-LCF-03	NIL
			1 / 0.70	2	10-LCF-04	NIL	6-LCF-04	NIL
			1 / 0.60	2	10-LCF-05	NIL	6-LCF-05	NIL
			1 / 0.50	2	10-LCF-06	NIL	6-LCF-06	NIL
		1400 deg F	1 / 1.00	2	10-LCF-07	NIL	6-LCF-07	NIL
			1 / 0.90	2	10-LCF-08	NIL	6-LCF-08	NIL
			1 / 0.80	2	10-LCF-09	NIL	6-LCF-09	NIL
			1 / 0.70	2	10-LCF-10	NIL	6-LCF-10	NIL
			1 / 0.60	2	10-LCF-11	NIL	6-LCF-11	NIL
			1 / 0.50	2	10-LCF-12	NIL	6-LCF-12	NIL

Figure 30: Test matrix for Tensile, Charpy impact energy and LCF properties with specimen identification

Nimonic 263 step block test matrix:					Specimens Identification			
Test #	**Test Type**	**Test condition**	**Step sections**	**Total Tests**	**Specimen ID / Step section**			
		Temperature deg.F	10"/8"/6"/4"		10 inch	8 inch	6 inch	4 inch
4	Stress rupture Specimen per MPE-RUP 003-P3 16 specimens (Creep data not required)	Temperature deg.F	Stress					
		1472	40	1	**10-RUP-01**	NIL	NIL	NIL
		1472	35	1	**10-RUP-02**	NIL	NIL	NIL
		1472	30	1	**10-RUP-03**	NIL	NIL	NIL
		1472	25	1	**10-RUP-04**	NIL	NIL	NIL
		1400	45	3	**10-RUP-05**	**8-RUP-01**	**6-RUP-01**	NIL
		1400	40	3	**10-RUP-06**	**8-RUP-02**	**6-RUP-02**	NIL
		1400	35	3	**10-RUP-07**	**8-RUP-03**	**6-RUP-03**	NIL
		1400	30	3	**10-RUP-08**	**8-RUP-04**	**6-RUP-04**	NIL
5	Fracture Toughness Specimen per # 8024 J1C -11 specimens	RT/ 75 deg. F		4	**10-J1c-01**	**8-J1c-01**	**6-J1c-01**	**4-J1c-01**
		1000 deg.F		3	**10-J1c-02**	**8-J1c-02**	**6-J1c-02**	NIL
		1400 deg F		4	**10-J1c-03**	**8-J1c-03**	**6-J1c-03**	**4-J1c-02**
6	Chemical Analysis 8 Specimens	**Ni,Cr,Co,Mo,Ti,Al,Fe,**	Thermal Center	4	**10-C-1**	**8-C-1**	**6-C-1**	**4-C-1**
		Mn,Si,C,B,P,S & Cu	1" above drag	4	**10-D-1**	**8-D-1**	**6-D-1**	**4-D-1**

Figure 31: Test matrix for Stress rupture, Fracture toughness and Chemical analysis with specimen identification

Chemical Analysis: (Wt. %)	Nimonic 263 N07263 SB - Casting	GJOJ-263-TB-1	Step block casting section locations Chemical composition values (Wt. %)							
			10 inch		8 inch		6 inch		4 inch	
			Thermal-C	Drag-1"	Thermal-C	Drag-1"	Thermal-C	Drag-1"	Thermal-C	Drag-1"
	Flowserve Heat	Cast on coupon	10-C-1	10-D-1	8-C-1	8-D-1	6-C-1	6-D-1	4-C-1	4-D-1
C	0.06	0.01	0.01	0.01	0.01	0.01	0.01	0.01	0.02	0.01
Mn	0.31	0.3	0.29	0.3	0.29	0.3	0.3	0.3	0.3	0.3
Si	0.61*	0.65	0.59	0.66	0.63	0.64	0.66	0.66	0.65	0.66
P	-	<0.010	<0.10	<0.10	<0.10	<0.10	<0.10	<0.10	<0.10	<0.10
S	-	<0.001	<0.001	<0.001	<0.001	<0.001	<0.001	<0.001	<0.001	<0.001
Cr	19.4	20.2	19.97	20.12	20.14	20.07	20.09	20.15	20.12	20.08
Ni	Bal.	50.25	50.23	50.3	50.45	50.5	50.19	50.14	50.18	50.48
Mo	5.8	5.56	5.72	5.67	5.66	5.6	5.8	5.77	5.82	5.55
Co	20.2	19.82	20.14	19.68	19.76	19.67	19.78	19.73	19.67	19.71
Fe	0.45	0.45	0.5	0.48	0.49	0.48	0.46	0.47	0.47	0.48
Cu	0.02	0.02	0.02	0.02	0.02	0.02	0.02	0.02	0.02	0.02
B		0.005	0.005	0.005	0.005	0.005	0.005	0.005	0.005	0.005
Al	0.4	0.34	0.31	0.31	0.32	0.33	0.32	0.32	0.32	0.34
Ti	2.12	2.12	2	2.18	1.97	2.13	2.11	2.16	2.17	2.12

Figure 32: Step block casting thermal center trepanned section chemical analysis. No significant variation in chemistry when compared with casting section Thermal center analysis

Homogenizing Heat Treatment (Note: As-Cast Incipient MP is 2102°F)

- **Part should be loaded into a room temperature furnace with contact thermocouples for recording homogenization HT cycle. Also furnace thermocouples HT cycle record.**
- **Ramp furnace at a rate not exceeding 350^{0}F/Hour**
- **Hold at 1900^{0}F ± 25^{0}F for four hours**
- **Ramp furnace to 1960^{0}F**
- **Hold at 1960^{0}F ± 25^{0}F for four hours.**
- **Ramp furnace to 2012^{0}F.**
- **Hold at 2012^{0}F ± 25^{0}F for ONE hour**
  - **(Note: Theoretical Incipient MP is now 2291°F)**
- **Ramp furnace to 2090°F**
- **Hold at 2090^{0}F ± 10^{0}F for Four hours**
- **Ramp to 2175°F**
- **Hold at 2175^{0}F ± 10^{0}F for 44 Hours**
  - **(Note: Theoretical Incipient MP is now 2410°F)**
- **Forced Air Cool to RT with fans, keeping contact thermocouples attached for measuring cooling rate**

AGING- HT Cycle

- **Ramp furnace at a rate not exceeding 350^{0}F/Hour**
- **Hold at 1472°F ± 25°F for 8 Hours**
- **Forced Air Cool with Fans measuring cooing rate with contact thermocouples attached.**

Figure 33: Homogenizing and Aging Heat treatment cycles Optimized to within +/- 5% of nominal chemistry variation (NETL)

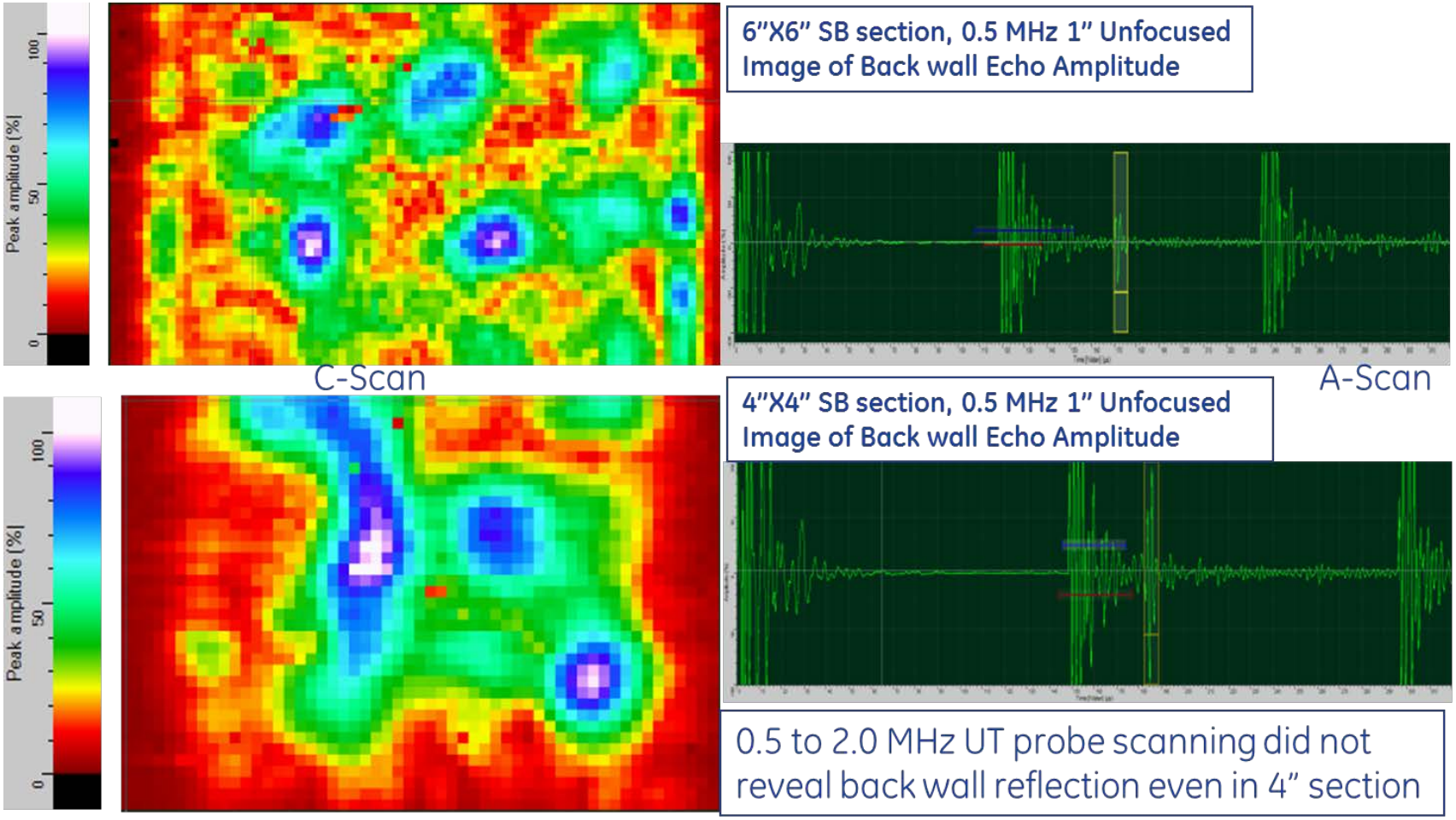

Figure 34: UT immersion scans of N263 step block casting 6 inch and 4 inch sections showing the inherent issue of achieving a superior back wall reflection in thick walled super alloy castings

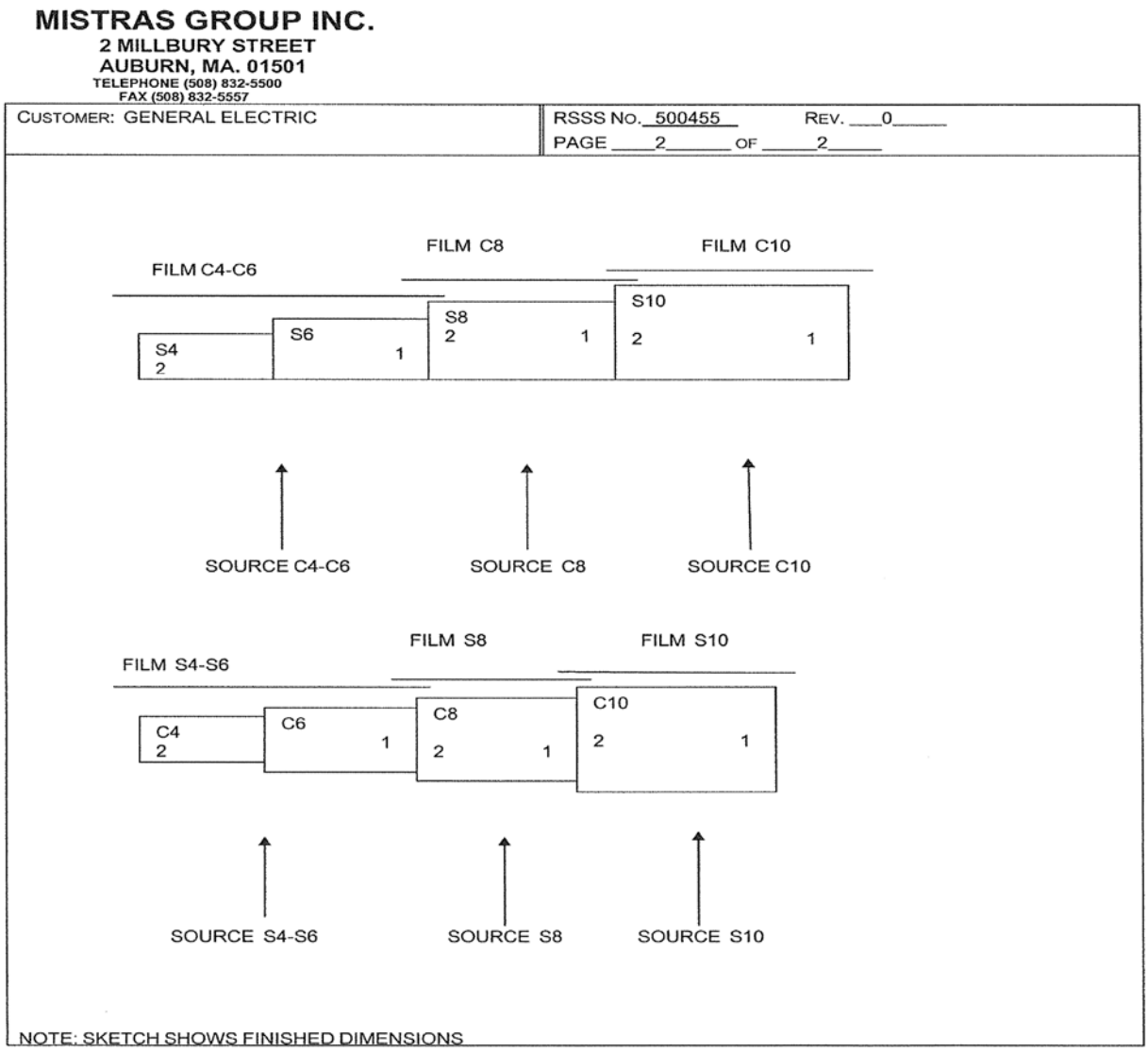

Figure 35: Radiographic Scan Plan

MISTRAS GROUP INC

2 Millbury Street
Auburn, Massachusetts 01501
(508) 832-5500 Fax (508) 832-5557

RADIOGRAPHIC REPORT
PAGE__1__ OF __1_

LOCATIONS NATIONWIDE

BRANCH LABORATORY
SPRINGFIELD, MA.
(413) 734-6648 FAX: (413) 734-2810

Nondestructive Testing - QA/QC Services - Chemical Testing - Mechanical Testing - Metallurgical Testing & Failure Analysis

CASTING☐ WELDMENTS TRANSISTORS☐ DIODES☐ OTHER☐

CUSTOMER: GENERAL ELECTRIC CO. | P.O. NO.: 900473361

ADDRESS: 1 RIVER ROAD SCHENECTADY, NY.

PART NAME: NIMONIC 263 STEP BLOCK	PART NO.: N/A	STAGE OF MFG.: AS CAST	HEAT NO.: N/A

SPEC. NO.: ASTM E94	STANDARD: ASTM E186 & E280	CLASS: NOTE INDICATIONS

TYPE OF MATERIAL:	DATE RADIOGRAPHED: 6-13	GOV'T INSPECTION:	MISTRAS JOB NO.: 500455	FILM TOTAL: 24

SERIAL NO.	VIEW	ACCEPT	REJECT	N.A.D.	FILM SIZE	NO. OF FILM	CODE*						SURFACE	COMMENTS
C4	1-2				14X17	4								GAS ASTM E186 CL 1
S4	1-2				14X17	4								NO APPARENT INDICATIONS
C6	1-2													NO APPARENT INDICATIONS
S6	1-2													NO APPARENT INDICATIONS
C8	1-2				14X17	4								NO APPARENT INDICATIONS, FILM ARTIFACT
S8	1-2				14X17	4								NO APPARENT INDICATIONS, FILM ARTIFACT
C10	1-2				14X17	4								SAND ASTM E280 CLASS 3 & 4 , SURFACE
S10	1-2				14X17	4								SURFACE

MISTRAS GROUP INC. REVIEWER: WAINO GUSTAFSON REVIEWER'S NO.: 42 LEVEL III DATE: 6-14-13

***CODE WELDMENTS AND CASTINGS 509**

1. CRACK
2. SHRINK
3. HOT TEAR
4. SAND INCLUSION
5. INCLUSION
6. GAS INCLUSION
7. POROSITY
8. SEGREGATION
9. UNFUSED CHAPLET
10. INTERNAL CHILL
11. COLD SHUT
12. FOREIGN MAT. LESS DENSE
13. FOREIGN MAT. MORE DENSE
14. SLAG INCLUSION
15. IMCOMPLETE PENETRATION
16. IMCOMPLETE FUSION
17. UNDERCUT
18. BURN THROUGH
19. TUNGSTEN INCLUSION
20. LACK OF BRAZE

* C C D E

31. EXTRANEOUS MATTER
32. EXC. PASTE BUILD-UP
33. PASTE DEPOSITS
34. PASTE FORMATION
35. SOLDER BALL
36. INADEQUATE CLEARANCE
37. MISALIGNED DIODE CRYSTAL
38. CRYSTAL UNDER-CUTTING
39. FUSION CRYSTAL TO CASE
40. DEFECTIVE LEAD WIRE
41. DISPLACED GETTER RING
42. PHYSICAL DAMAGE
43. PASTE EXPULSION
44. DEFORMED DIODE WHISKER
45. LOOPS OR TWIST IN WIRE
46. BENT TERMINAL
47. POOR CONSTRUCTION

This report is not to be construded as a guaranty or warranty of the condition of the materials tested. MISTRAS GROUP INC. is not liable for any misinterpertation of results or conditions, or for any claims or losses attributable to performance of a test. These services are rendered without any warranty. Any liability is limited to the amount paid for the services at issue. All orders are subject to MISTRAS GROUP INC.'s Standard Terms and Conditions of Sale, which are available upon request.

Figure 36: Radiographic Test Report confirming no other casting defect in other cast sections, except the surface cavity defect in 10 inch section under the casting feeder.

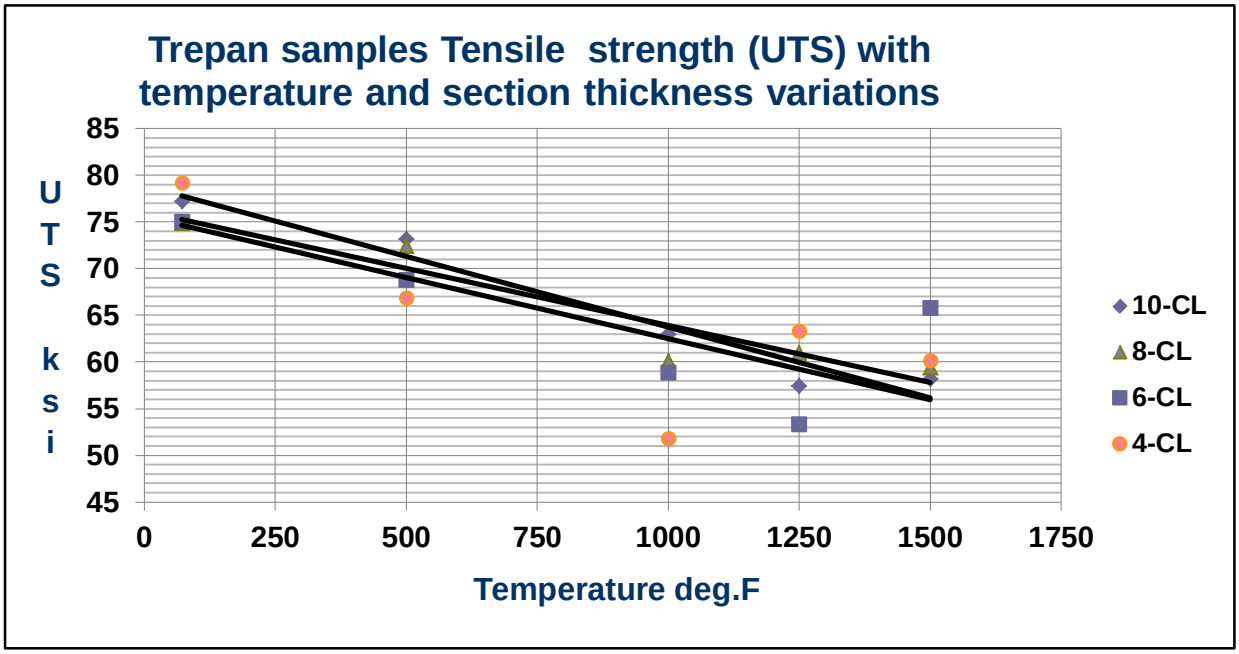

Figure 37: UTS plot with temperature and trepanned casting section thickness variation

Table 5: N263 Step block trepan cast sections tensile strength (UTS) vs temperature data

N263 Step Block trepan cast sections UTS vs. Temperature						
Section thickness (inches)	**10-CL (10)**	**10-DL (10)**	**8-CL (8)**	**6-CL (6)**	**6-DL (6)**	**4-CL (4)**
Temperature °F	(ksi)	(ksi)	(ksi)	(ksi)	(ksi)	(ksi)
72°F	**77.2**	**71.1**	**74.9**	**75**	**70.5**	**79.2**
500°F	**73.2**	**67.3**	**72.4**	**68.8**	**60**	**66.9**
1000°F	**63**	**69.1**	**60.1**	**58.9**	**58.9**	**51.8**
1250°F	**57.4**	**57.6**	**61**	**53.3**	**68.8**	**63.3**
1500°F	**58.2**	**52.4**	**59.4**	**65.8**	**60**	**60.2**

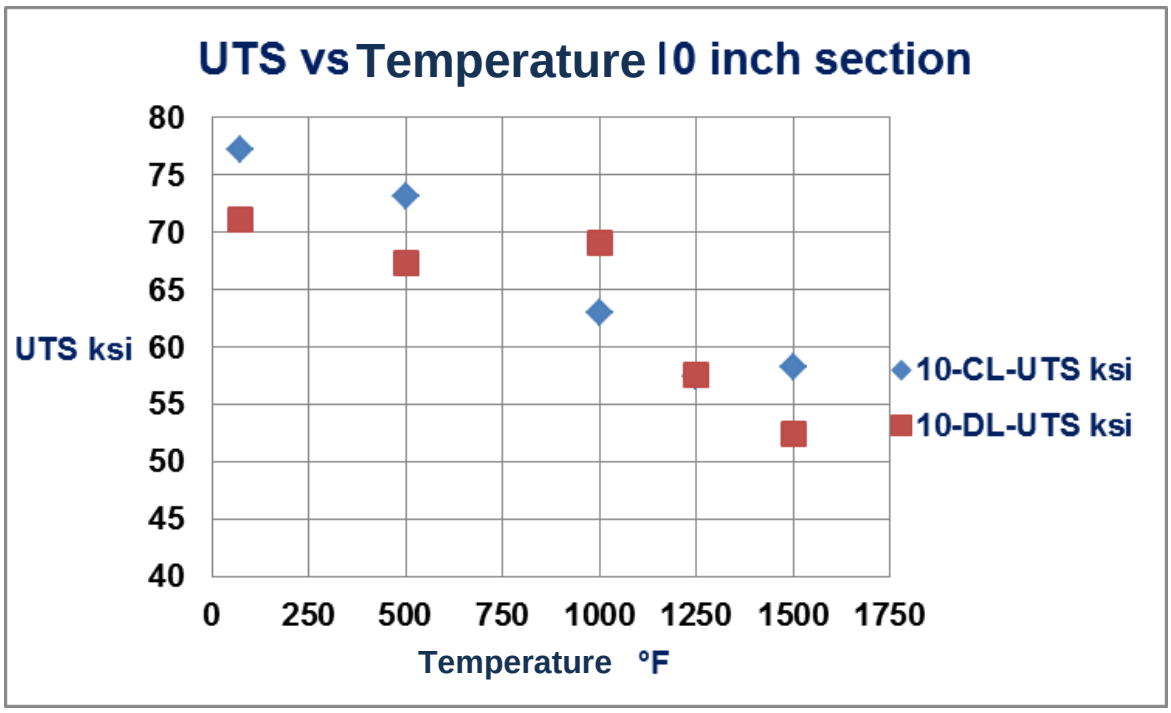

Figure 38: UTS vs temperature plot for 10 inch section CL and DL location trepans

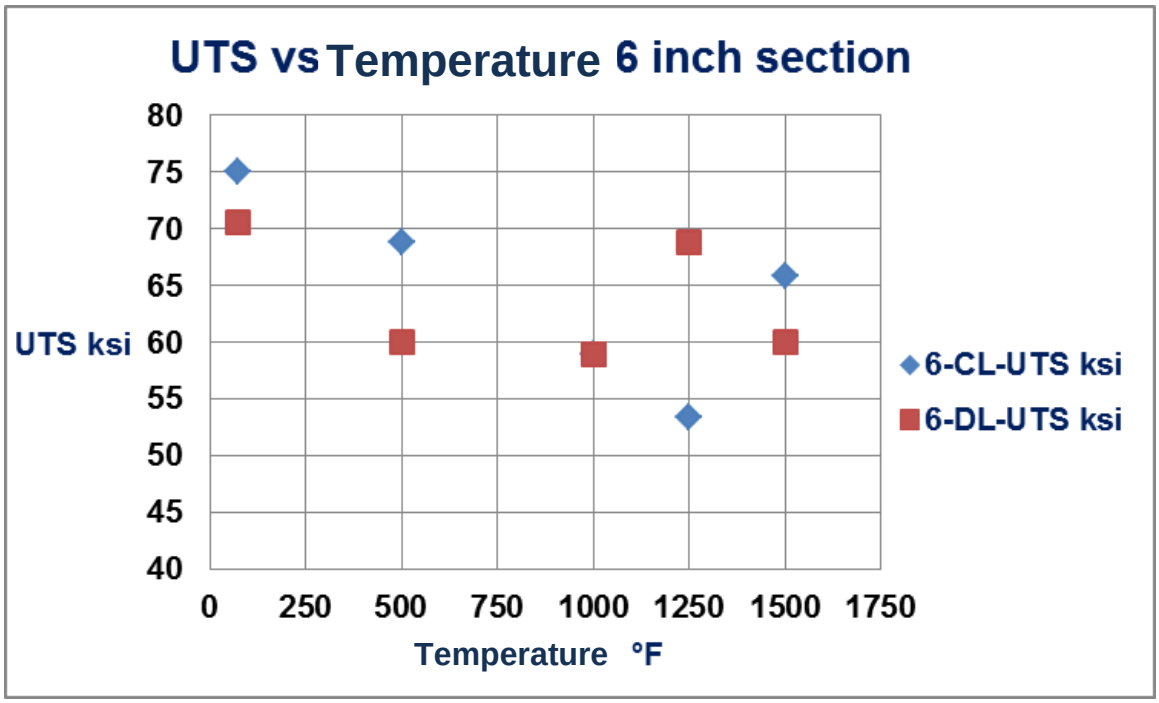

Figure 39 UTS vs temperature plot for 6 inch section CL and DL location trepans

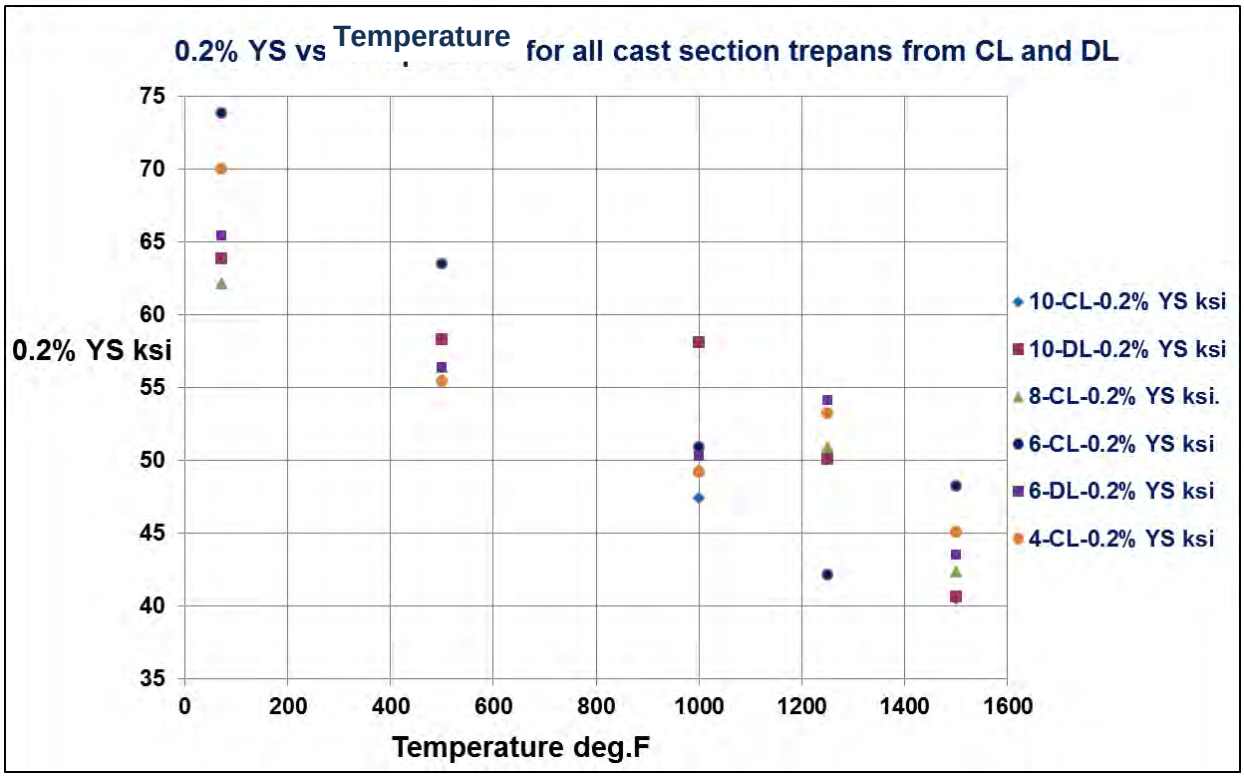

Figure 40: 0.2 % YS vs. Temperature for all N263 step block cast section trepans. The 0.2% YS vs. temperature trend plot shows tighter band trepan CL values at elevated temperatures for all section thicknesses

Table 6: N263 Step block trepan cast sections 0.2% Yield strength vs temperature data

N263 Step Block trepan cast sections 0.2% YS vs. Temperature						
Section thickness (inches)	**10-CL (10)**	**10-DL (10)**	**8-CL (8)**	**6-CL (6)**	**6-DL (6)**	**4-CL (4)**
Temperature °F	(ksi)	(ksi)	(ksi)	(ksi)	(ksi)	(ksi)
72°F	**70**	**63.8**	**62.1**	**73.8**	**65.4**	**70**
500°F	**55.5**	**58.3**	**56.4**	**63.5**	**56.4**	**55.4**
1000°F	**47.4**	**58.1**	**49.3**	**50.9**	**50.3**	**49.2**
1250°F	**50.2**	**50.1**	**50.9**	**42.1**	**54.1**	**53.2**
1500°F	**40.5**	**40.6**	**42.3**	**48.2**	**43.5**	**45.1**

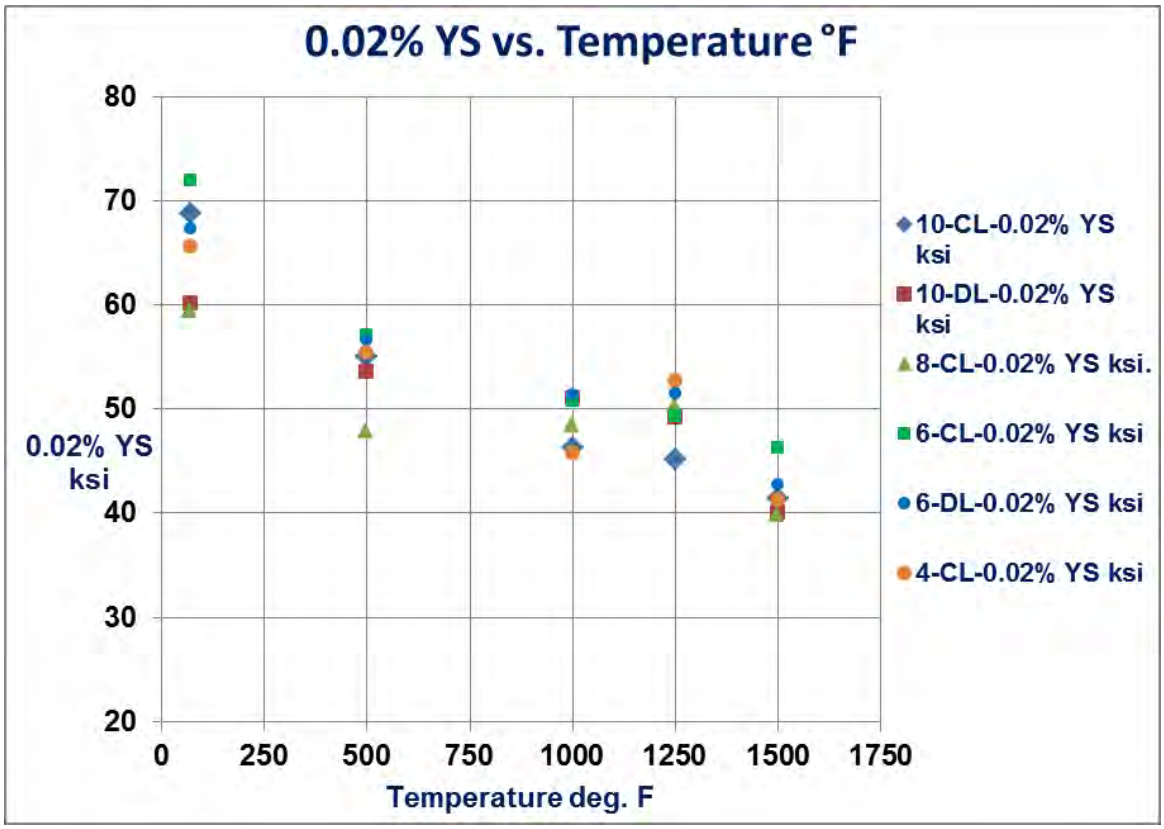

Figure 41: 0.02 % YS vs. Temperature for all N263 step block cast section trepans. The 0.02% YS vs. temperature trend plot shows tighter band at elevated temperatures for all section thicknesses

Table 7: N263 Step block trepan cast sections 0.02% Yield strength vs temperature data

N263 Step Block trepan cast sections 0.02% YS vs. Temperature						
Section thickness (inches)	**10-CL (10)**	**10-DL (10)**	**8-CL (8)**	**6-CL (6)**	**6-DL (6)**	**4-CL (4)**
Temperature °F	(ksi)	(ksi)	(ksi)	(ksi)	(ksi)	(ksi)
72°F	**68.8**	**60.1**	**59.4**	**71.9**	**67.3**	**65.6**
500°F	**55**	**53.6**	**47.8**	**57.1**	**56.6**	**55.4**
1000°F	**46.3**	**51**	**48.4**	**50.7**	**51.4**	**45.8**
1250°F	**45.1**	**49.2**	**50.3**	**49.3**	**51.5**	**52.7**
1500°F	**41.4**	**40**	**39.8**	**46.3**	**42.7**	**41.3**

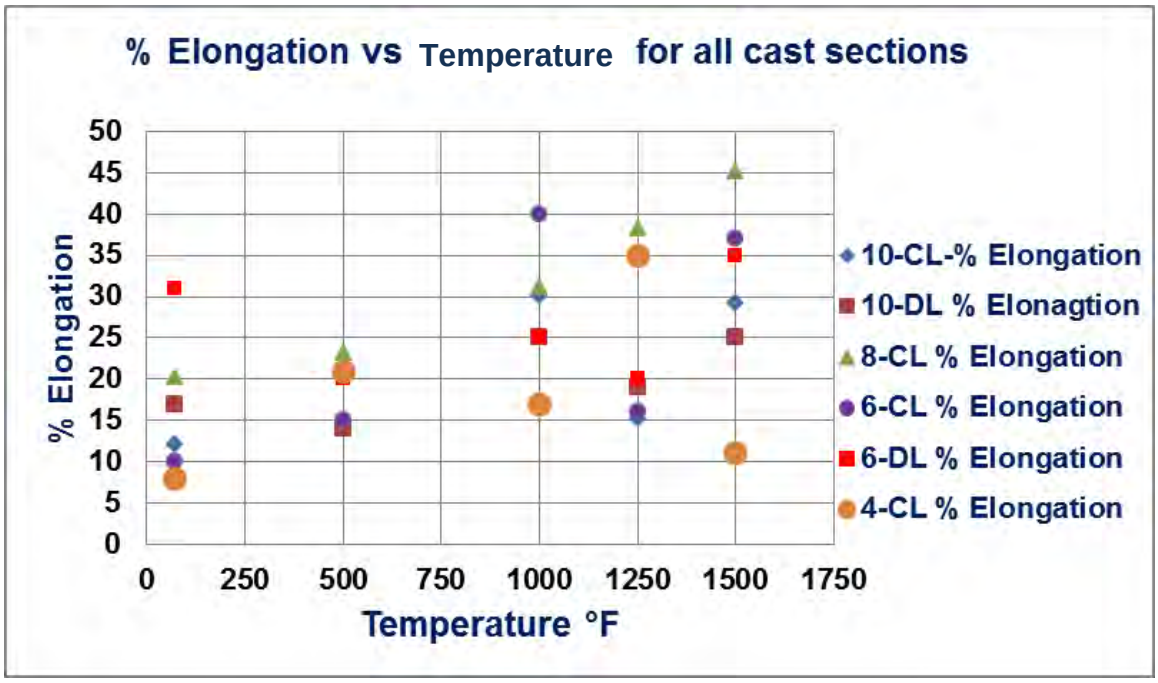

Figure 42: N263 step block cast section trepan samples % Elongation vs. Temperature

Table 8: N263 step block trepan section samples % Elongation values

Trepan sample % Elongation with temperature and section size						
Temperature	**10-CL**	**10-DL**	**8-CL**	**6-CL**	**6-DL**	**4-CL**
(deg. F)	**(%)**	**(%)**	**(%)**	**(%)**	**(%)**	**(%)**
72	**12**	**17**	**20**	**10**	**31**	**8**
500	**21**	**14**	**23**	**15**	**20**	**21**
1000	**30**	**25**	**31**	**40**	**25**	**17**
1250	**15**	**19**	**38**	**16**	**20**	**35**
1500	**29**	**25**	**45**	**37**	**35**	**11**

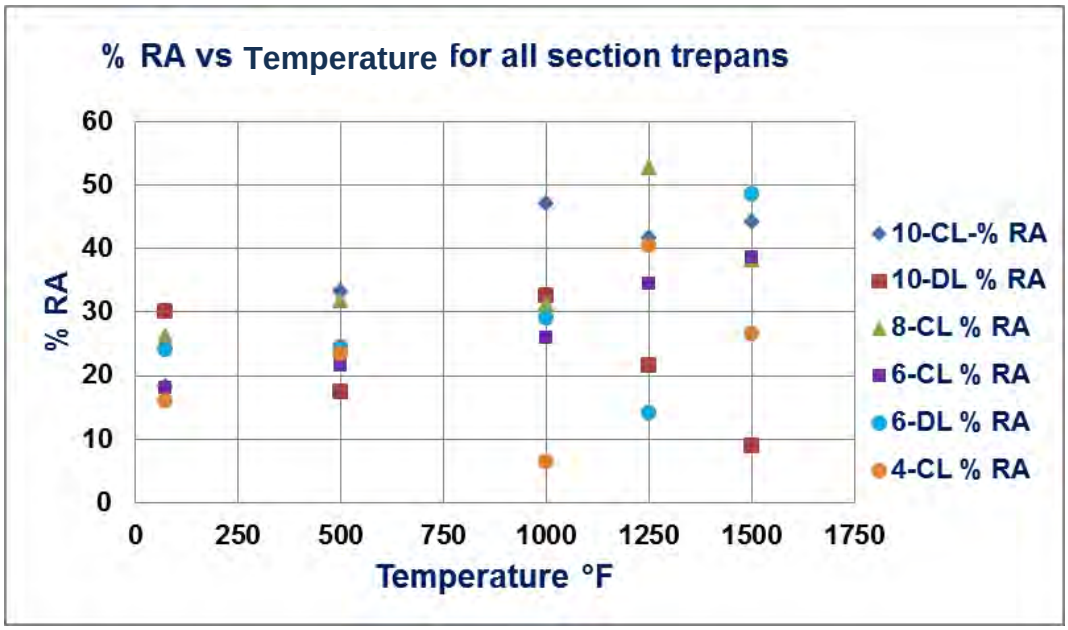

Figure 43: N263 %RA Vs Temperature plots for all section trepans

Table 9: N263 Step Block section Trepan sample % RA values data

Trepan sample % RA values with temperature and section size						
Temperature	**10-CL**	**10-DL**	**8-CL**	**6-CL**	**6-DL**	**4-CL**
(deg. F)	**(%)**	**(%)**	**(%)**	**(%)**	**(%)**	**(%)**
72	**18**	**30**	**26**	**18**	**24**	**16**
500	**33**	**17.5**	**31.5**	**21.5**	**24.5**	**23.5**
1000	**47**	**32.5**	**31**	**26**	**29**	**6.5**
1250	**41.5**	**21.5**	**52.5**	**34.5**	**14**	**40.5**
1500	**44**	**9**	**38**	**38.5**	**48.5**	**26.5**

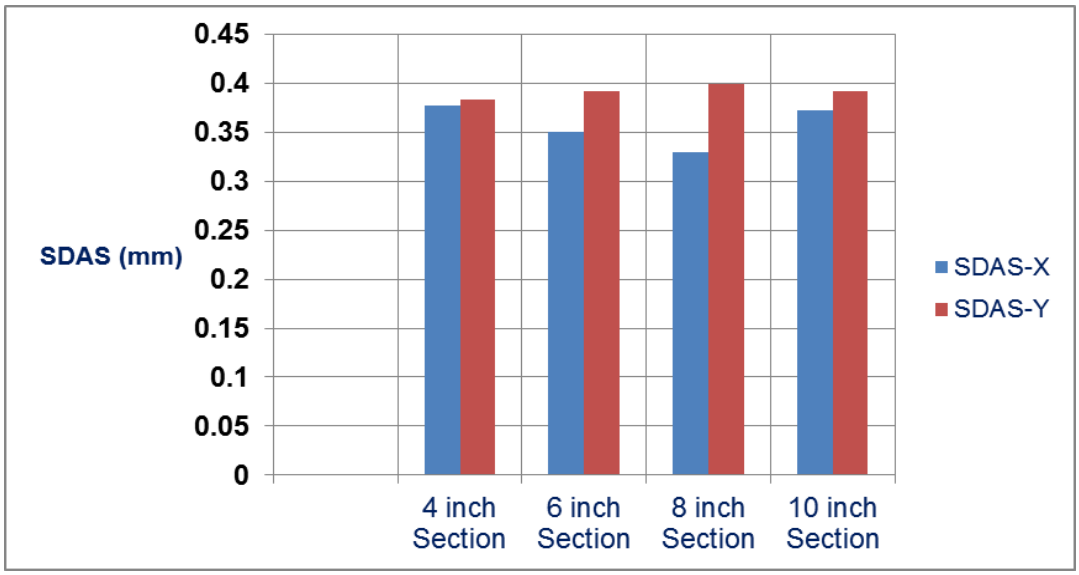

Figure 44: Nimonic 263 step block casting SDAS measurements with section size

Table 10: Nimonic 263 Step block cast sections SDAS Measurements. Consistently in the range of 0.35 to 0.40 mm for 100 to 250 mm cast sections

N263 SB Casting SDAS Measurements				
	SDAS Counts #		SDAS Average value (mm)	
Section thickness	X	Y	SDAS-X	SDAS-Y
4 inch Section	32	29	0.38	0.38
6 inch Section	25	30	0.35	0.39
8 inch Section	27	27	0.33	0.40
10 inch Section	27	25	0.37	0.39

SDAS measurements across the casting section thicknesses and orientation are not influenced by section size.

Table 11: Nimonic 263 Step block cast section thermal center trepanned samples SDAS values show independent of casting section thickness and orientation

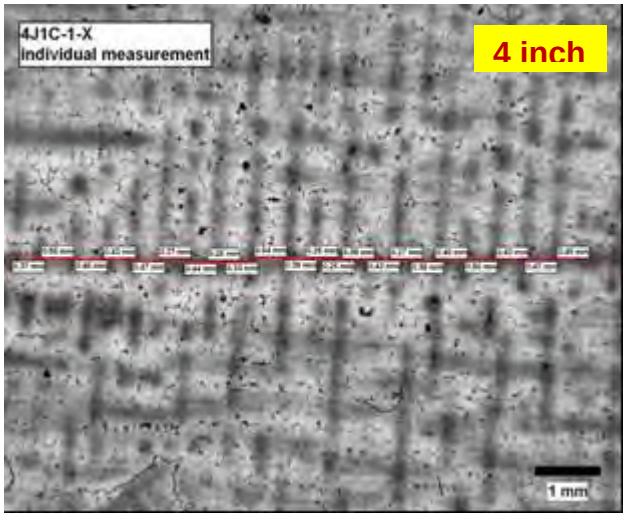

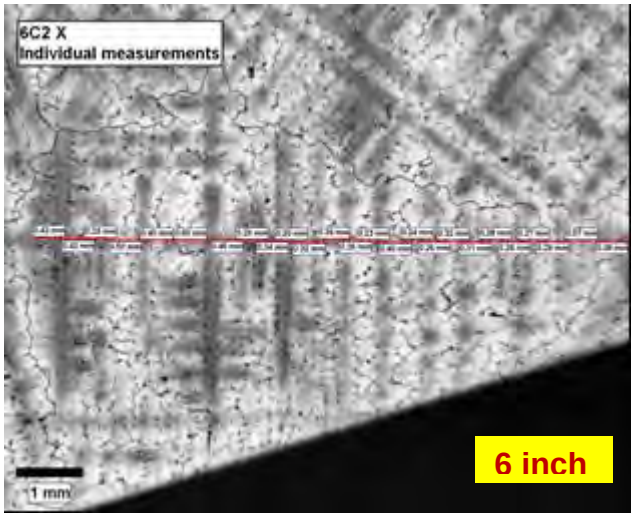

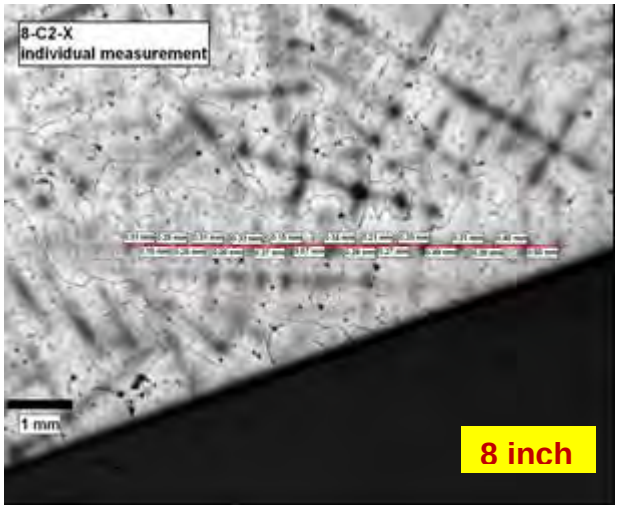

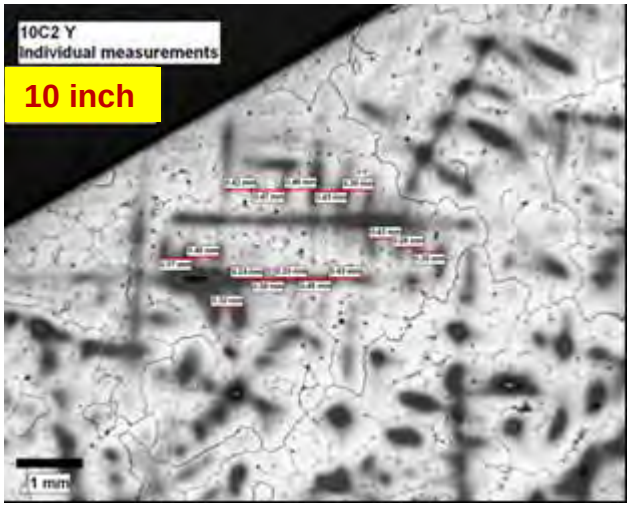

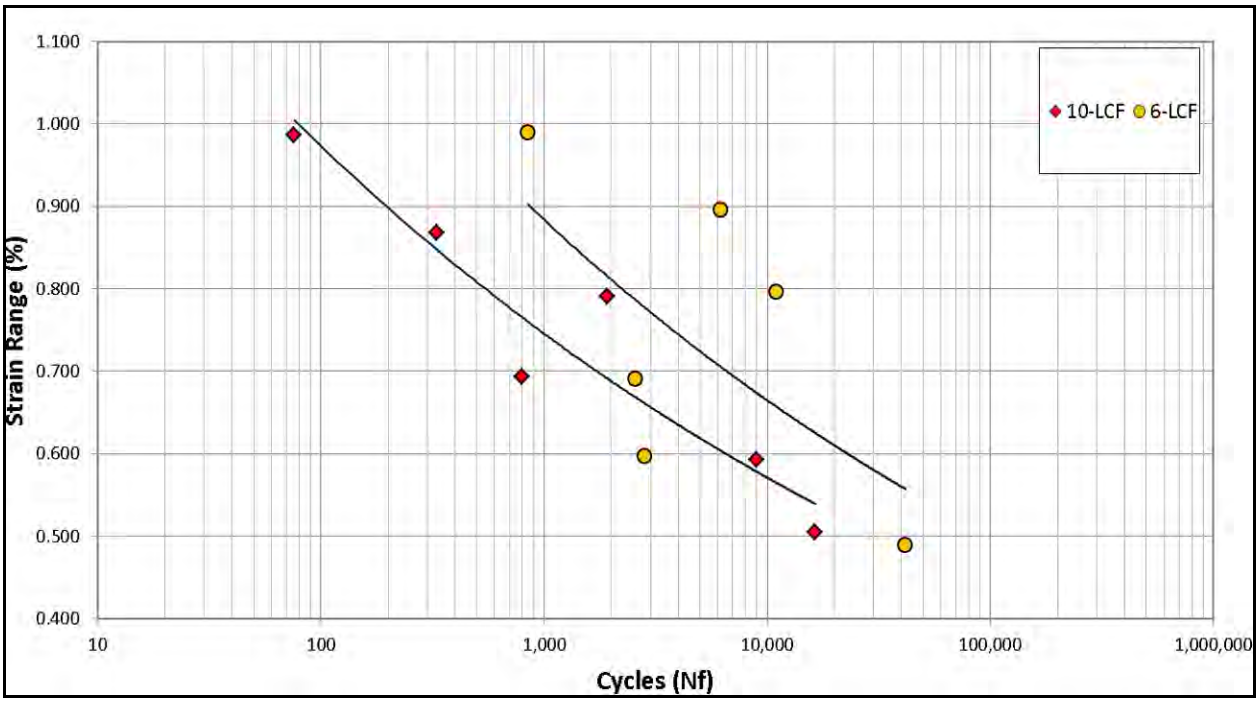

Figure 45: N263 Step block 10 inch and 6 inch sections cycles to failure compared at RT, A-ratio 1. The 10 inch section shows a debit in comparison with 6 inch section

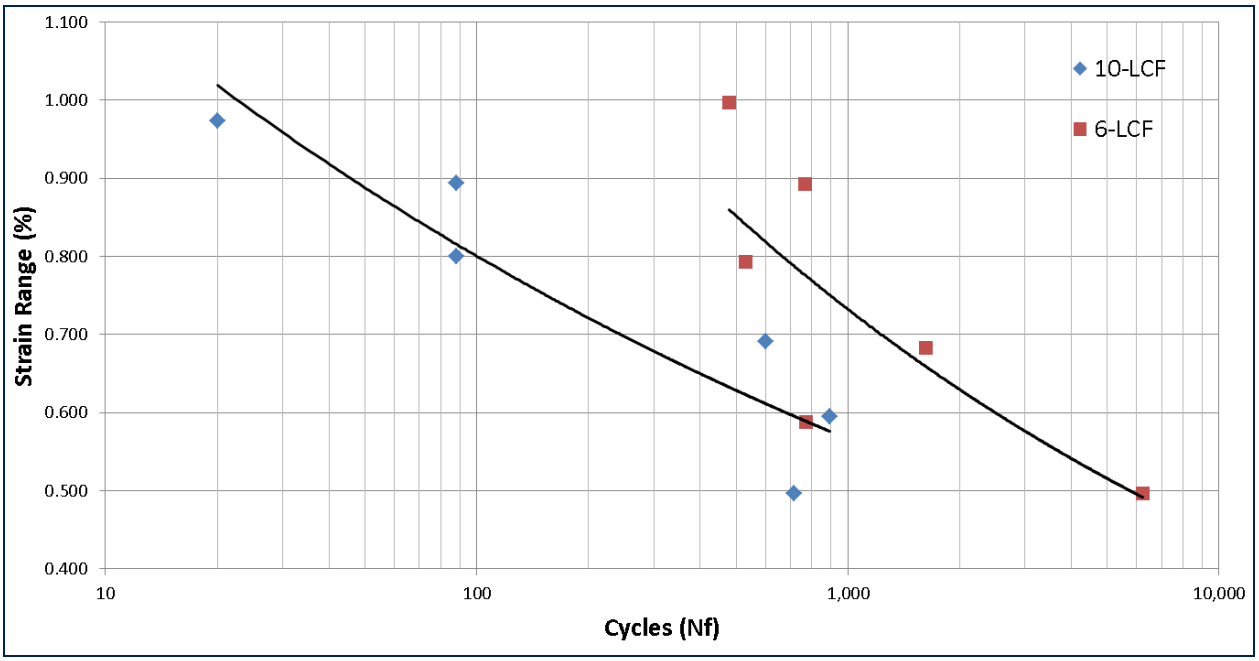

Figure 46: N263 Step block 10 inch and 6 inch sections cycles to failure compared at 1400°F, A-Ratio 1. The 10 inch section shows increased debit in comparison with 6 inch section, while 6 inch section shows degradation

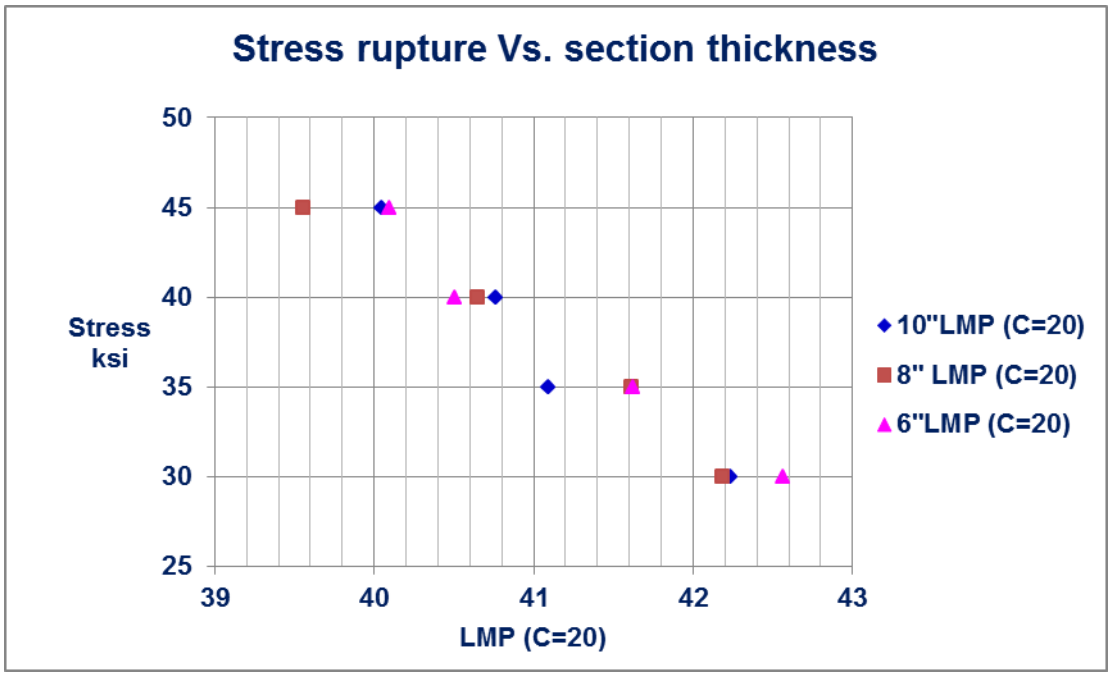

Figure 47: N263 Stress rupture strength vs, LMP (C=20) with section thickness. No significant changes in stress rupture data with section thickness variation

Table 12: Stress rupture test results raw data

Sample ID	Temp. °F	Time (hrs)	Elong %	RA %	Stress (ksi)	LMP
10-RUP-01	1472	1.8	9.3	19.2	40	39.13
10-RUP-02	1472	35.2	21.2	39.0	35	41.63
10-RUP-03	1472	49.2	14.5	27.6	30	41.91
10-RUP-04	1472	209.8	19.0	34.4	25	43.13
10-RUP-05	1400	33.9	15.7	14.4	45	40.05
10-RUP-06	1400	82.5	12.9	22.0	40	40.76
10-RUP-07	1400	123.6	11.3	22.3	35	41.09
10-RUP-08	1400	508.1	16.9	30.4	30	42.23
8-RUP-01	1400	18.4	15.3	41.2	45	39.55
8-RUP-02	1400	71.8	12.4	23.2	40	40.65
8-RUP-03	1400	235.5	15.3	18.1	35	41.61
8-RUP-04	1400	479.9	17.9	38.2	30	42.19
6-RUP-01	1400	36.0	12.8	17.9	45	40.09
6-RUP-02	1400	59.7	13.6	39.0	40	40.50
6-RUP-03	1400	238.3	11.7	14.9	35	41.62
6-RUP-04	1400	761.8	9.0	27.3	30	42.56

Table 13: Nimonic 263 Step block sections J-Integral Test results at RT; 1000°F and 1400°F summarized

Specimen	Testlog Number	Temperature	J_Q (in lb/in^2)	K_{JQ} (ksi$\sqrt{in}$)	K_{Ic} Determination (Annex 5)		Unstable
					P_Q (lb)	K_Q (ksi$\sqrt{in}$)	
10-JIC-01	T46793	Room	273.85	102.67	5046.9	62.3	No
8-JIC-01	T46794	Room	623.19	146.56	4402.0	48.8	No
6-JIC-01	T46795	Room	327.07	105.57	4017.5	49.4	No
4-JIC-01	T46796	Room	531.87	136.16	4765.0	56.0	No
10-JIC-02	T46797	1000°F	479.30	119.34	3313.4	39.3	No
8-JIC-02	T46798	1000°F	642.31	139.60	4542.9	50.7	No
6-JIC-02	T46799	1000°F	467.36	113.85	3779.3	49.0	No
10-JIC-03	T46800	1400°F	272.22	83.74	3236.6	38.7	No
8-JIC-03	T46801	1400°F	621.48	123.59	3707.6	41.8	No
6-JIC-03	T46802	1400°F	336.48	90.25	3855.4	47.9	No
4-JIC-02	T46803	1400°F	550.07	115.68	4371.5	51.4	No

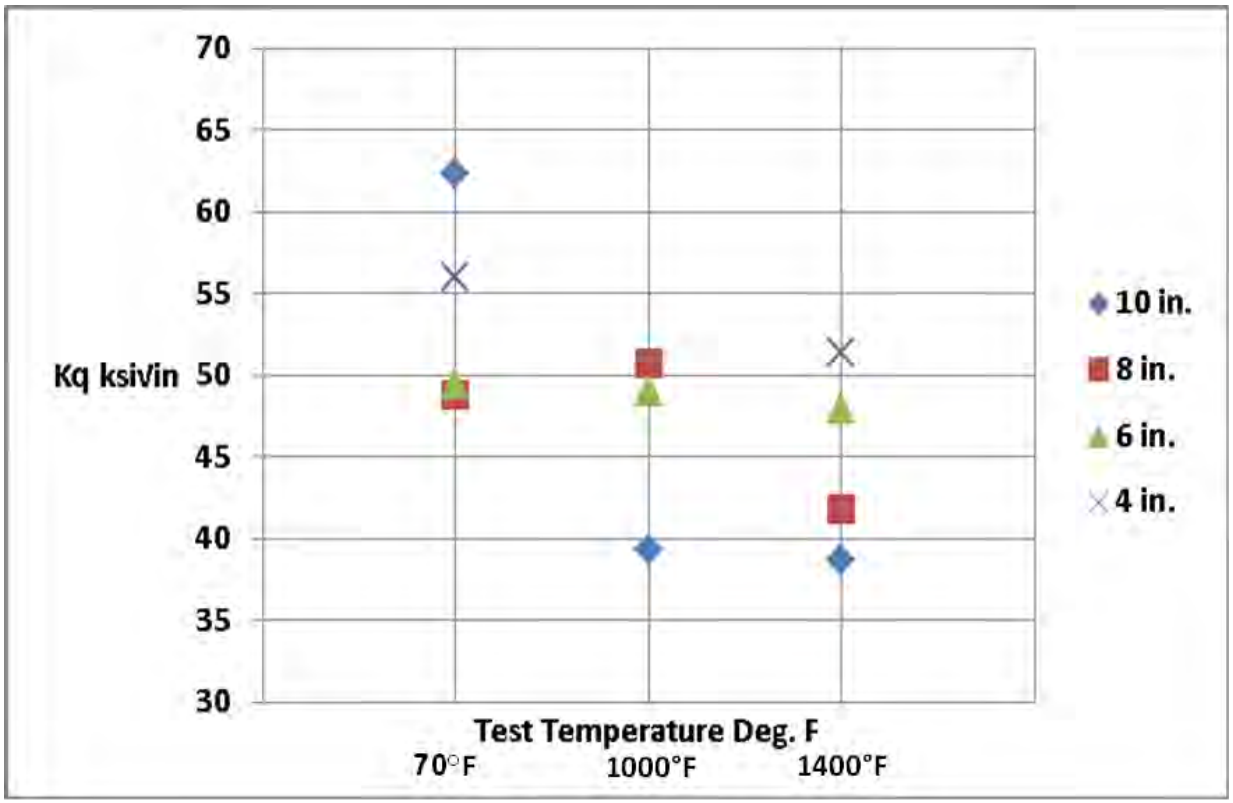

Figure 48: Plot showing Kq Fracture toughness value Vs. Temperature for various section sizes. Note that the conditional fracture toughness Kq values are minimum influenced with temperature raise up to 6 inch cast wall thickness

Table 14: Kq Fracture toughness @ RT, `1000°F and 1400°F temperatures vs. section size data

Kq ksiVin Fracture toughness plot			
SB Section	**70°F**	**1000°F**	**1400°F**
10 in.	**62.3**	**39.3**	**38.7**
8 in.	**48.8**	**50.7**	**41.8**
6 in.	**49.4**	**49**	**47.9**
4 in.	**56**		**51.4**

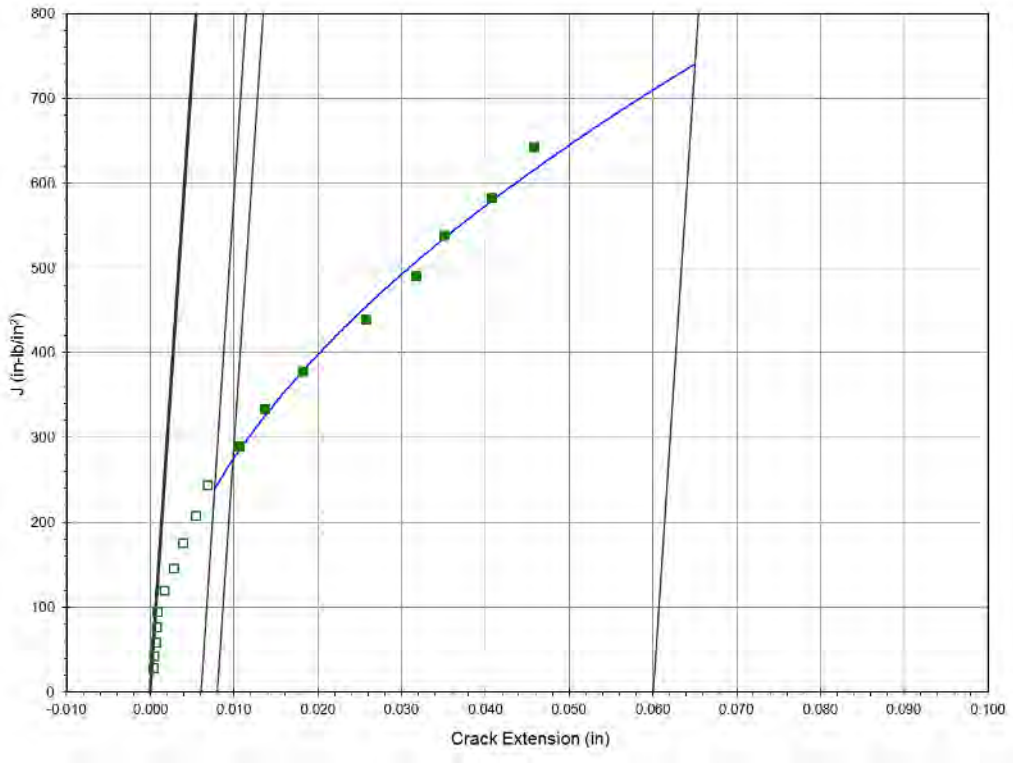

Figure 49: 10-J1C-01, J vs. a graph for 10 inch section tested at RT

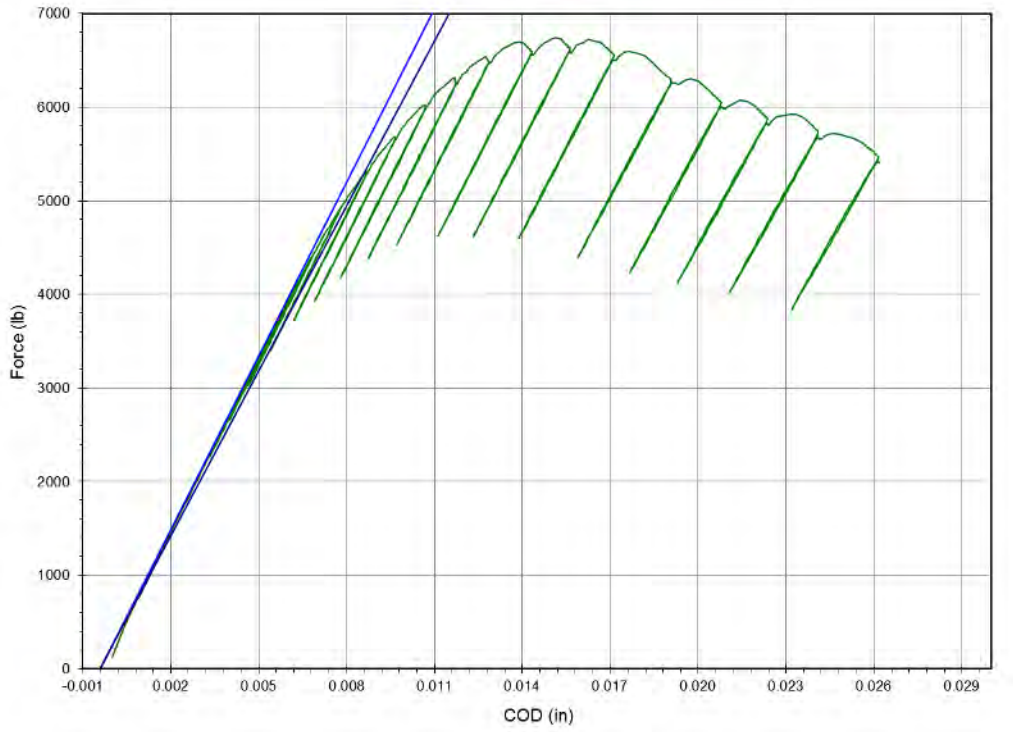

Figure 50: 10-J1C-01, Force vs. COD graph for 10 inch section tested at RT

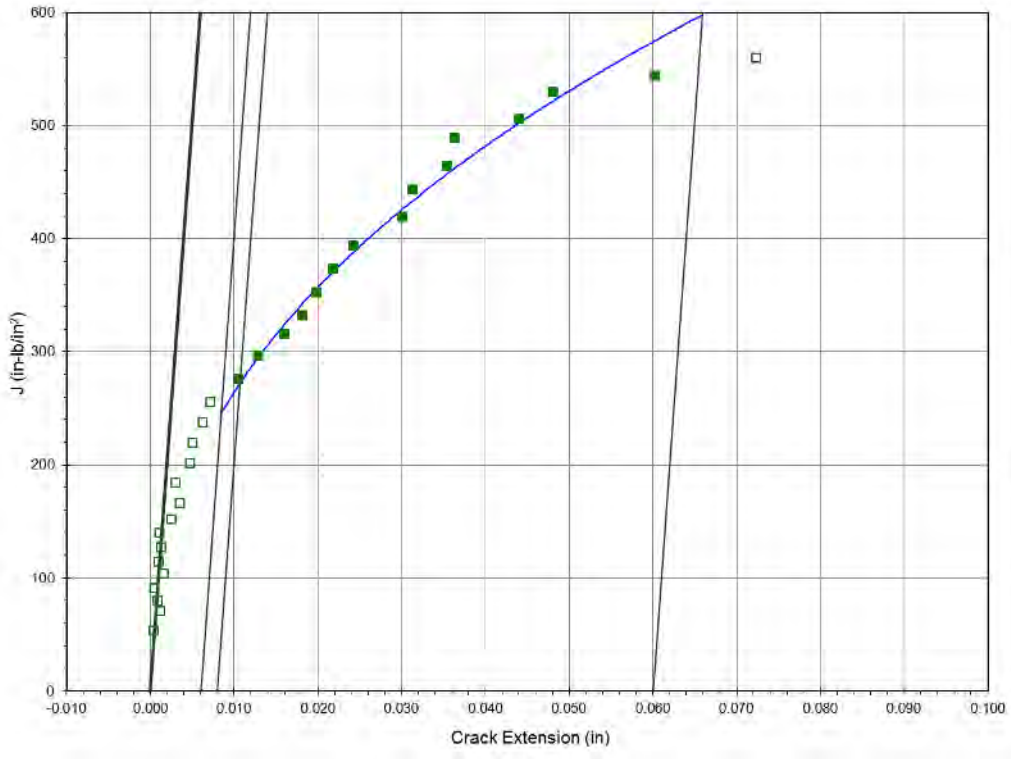

Figure 51: 10-J1C-03, J vs. a graph for 10 inch section tested at 1400°F

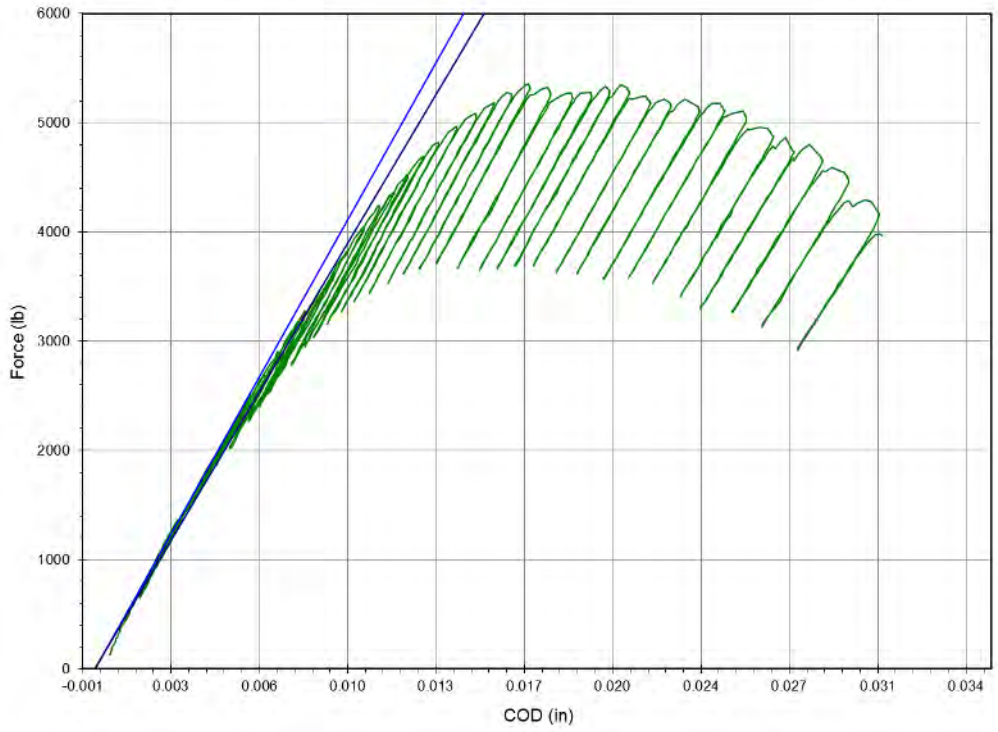

Figure 52: 10-J1C-03, Force vs. COD graph for 10 inch section tested at 1400°F

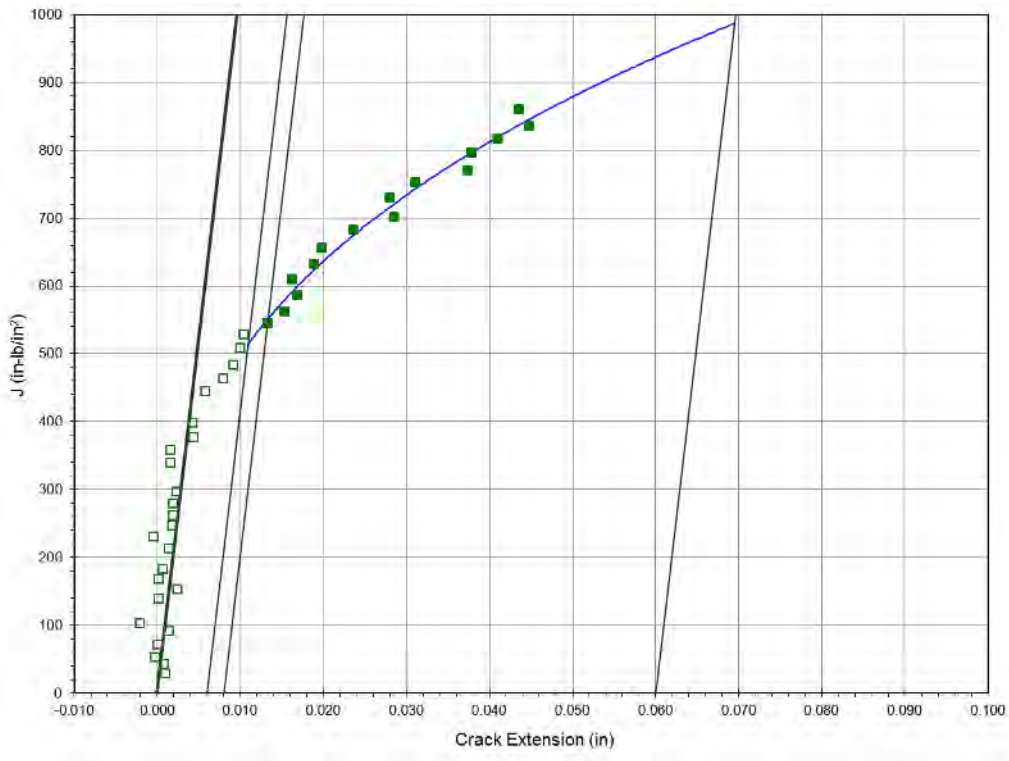

Figure 53: 4-J1C-02, J vs. a graph for 4 inch section tested at 1400°F

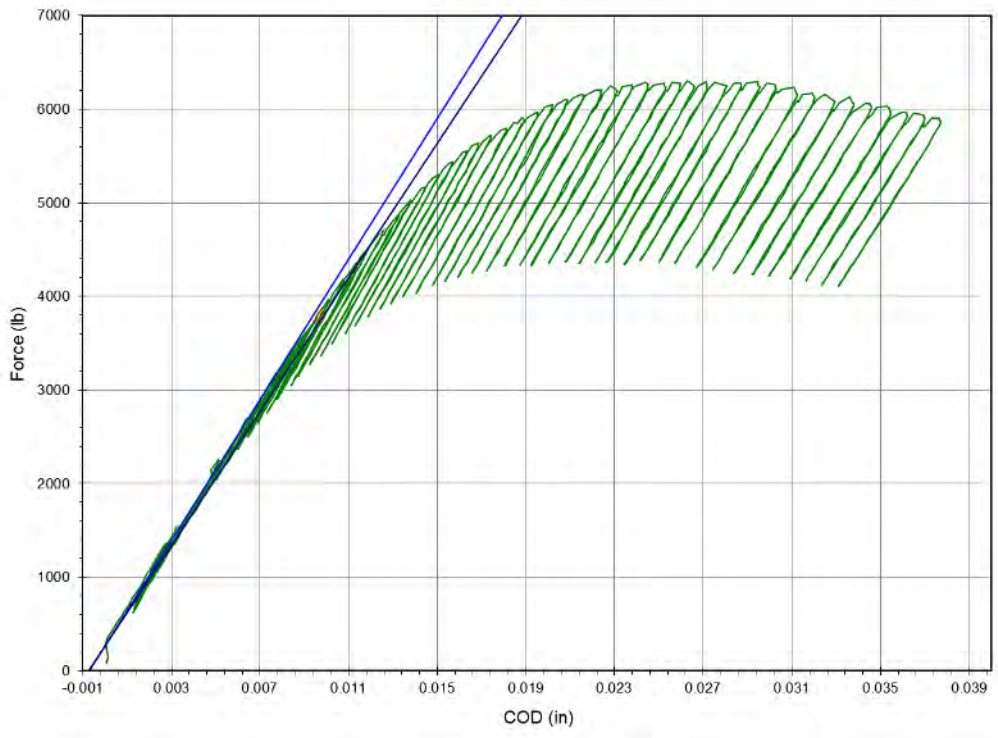

Figure 54: 4-J1C-02, Force vs. COD graph for 4 inch section tested at 1400°F

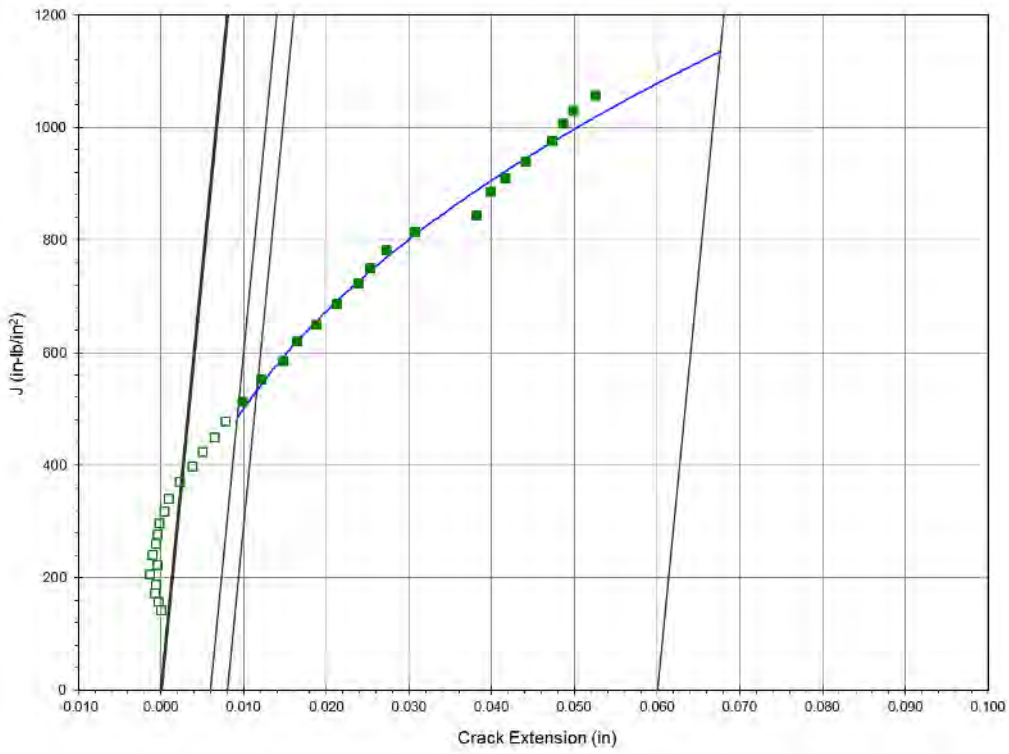

Figure 55: 4-J1C-01, J vs. a graph for 4 inch section tested at RT

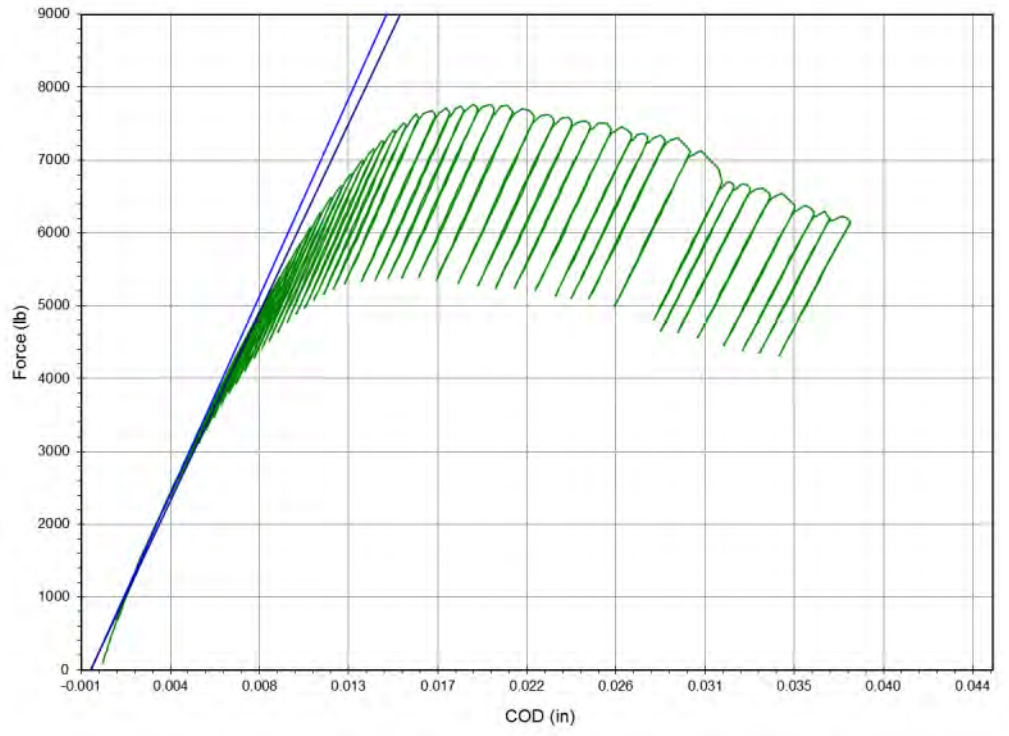

Figure 56: 4-J1C-01, Force vs. COD graph for 4 inch section tested at RT

Table 15: Charpy V-Notch Impact energy data for 10 inch, 8 inch and 6 inch trepan samples

Sample ID	Temp	Energy		Mils
	°F\°C	ft-lbs	Joules	Lat Exp
10-CVN-RT-C1	70/21	48	65.1	51
8-CVN-RT-C1	70/21	39	52.9	41
6-CVN-RT-C1	70/21	30	40.7	22
10-CVN-RT-C2	70/21	37	50.2	33
8-CVN-RT-C2	70/21	40	54.2	32
6-CVN-RT-C2	70/21	36	48.8	43
10-CVN-RT-T1	70/21	67	90.8	46
8-CVN-RT-T1	70/21	46	62.4	56
6-CVN-RT-T1	70/21	24	32.5	15
10-CVN-RT-T2	70/21	42	56.9	24
8-CVN-RT-T2	70/21	52	70.5	52
6-CVN-RT-T2	70/21	30	40.7	22

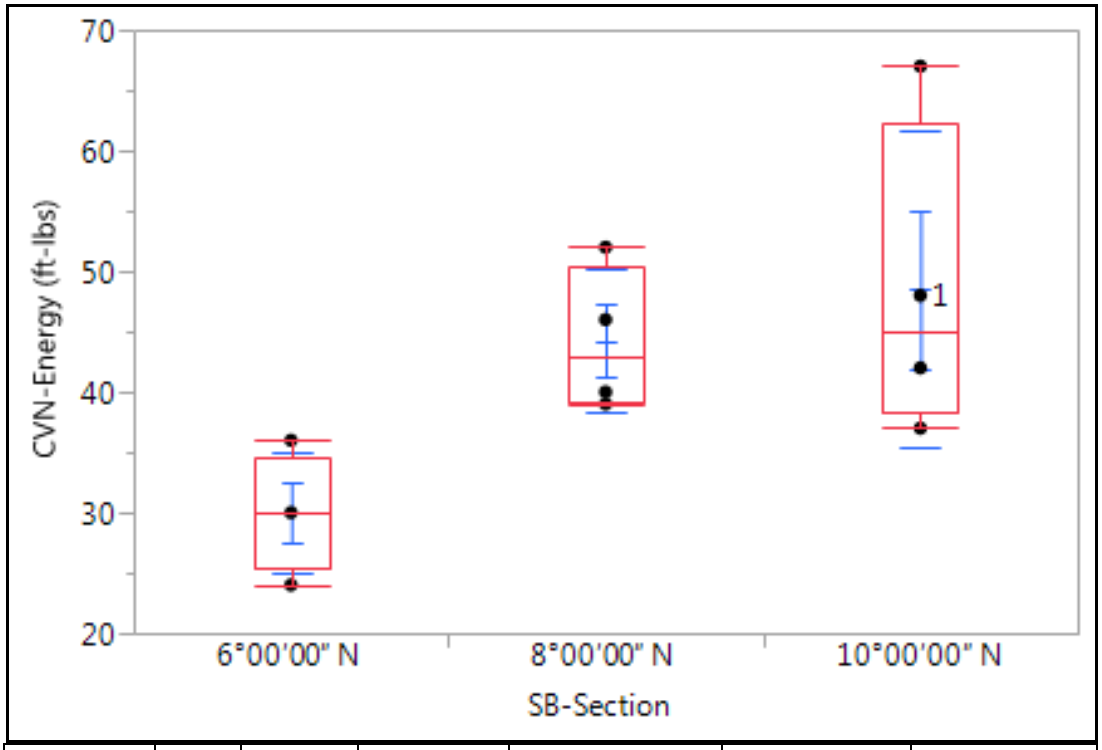

Section	No.	Mean	Std Dev	Std Err Mean	Lower 95%	Upper 95%
6 inch	4	30	4.899	2.4495	22.205	37.795
8 inch	4	44.25	6.0208	3.0104	34.67	53.83
10 inch	4	48.5	13.1276	6.5638	27.611	69.389

Figure 57: Charpy V notch Impact energy vs. section size combined data plot

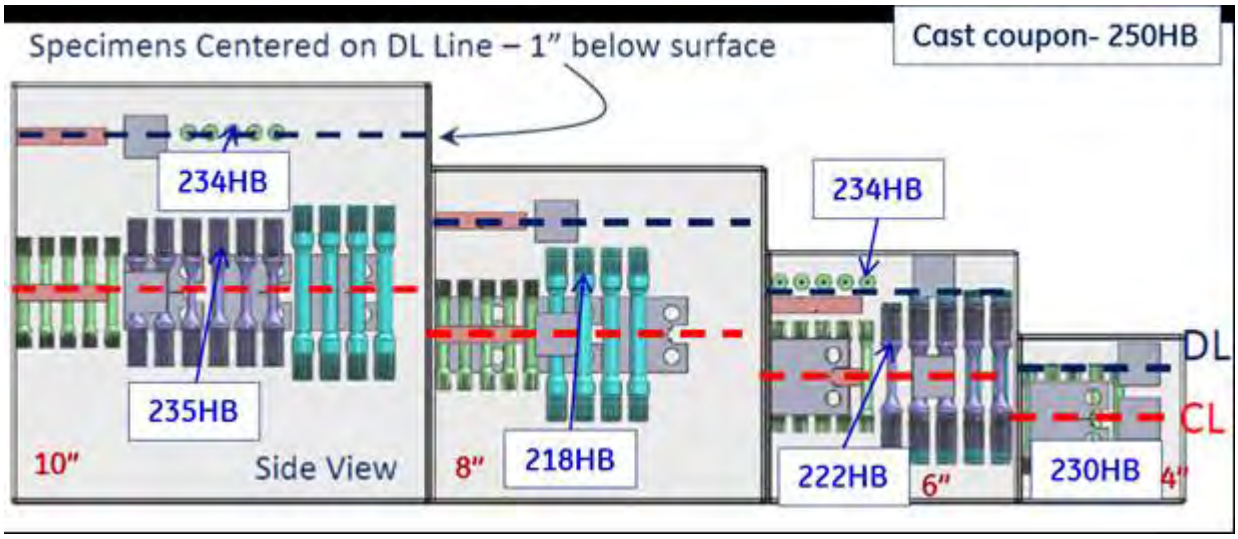

Figure 58: N263 Cast hardness values are not section thickness dependent

Table 16: N263 Casting section hardness values raw data

Sample ID	Hardness (HRBW/HRC)	Conversion (HBW)
10-TN-CL-RT-H	98.98 HRBW *	235 HBW
8-TN-CL-RT-H	96.58 HRBW *	218 HBW
6-TN-CL-RT-H	97.21 HRBW *	222 HBW
4-TN-CL-RT-H	98.36 HRBW *	230 HBW
10-TN-DL-RT-H	99.27 HRBW *	234 HBW
6-TN-DL-RT-H	20.82 HRC *	234 HBW
GJOJ-263-TB-RT-H	23.91 HRC *	250 HBW

CENTRIFUGAL CASTING OF HAYNES 282

A Vertically Spun Centrifugal Casting of Haynes 282, weighing 1400 lbs. with hybrid mold (half Graphite and half Chromite sand) mold assembly was cast at MetalTek WI, with vertical centrifugal casting process, see Figure 59.

The 26 inch OD and 21 inch height casting sectional view is shown in Figure 60. The mold is based in on a GE AE compressor casing for the CF34. This hybrid mold design was selected to illustrate the influence of different cast cooing rates during Centrifugal casting solidification and also the varied cast wall part dimensions influence on microstructural features.

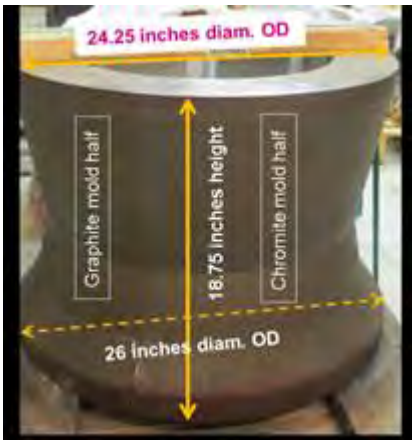

Figure 59: Haynes 282 Test program Centrifugal casting

The Haynes 282 ingots were induction melted in air under Argon cover protection. Necessary aluminum and titanium additions were made to the melt to compensate for the melt losses. The centrifugal die was purged with Argon prior to pour and 35 G forces were maintained with die rotational rpm during casting and solidification process. Mold assembly view shown in Figure 61.

Casting solidification simulation analysis was carried out for cooling rate estimates. The surface indication on the casting ID on the chromite sand mold side matched well with the FEM based solidification simulation analysis. Figure 62 provides simulation predicted casting cooling rates. Additional casting solidification simulation test results are in the Appendix 1-D.

X-ray Radiographic inspections were reported clean except the visual ID surface, mid height level shrink that appeared primarily on the Chromite sand side mold. This is due to the differential thermal cooling rates caused by the hybrid mold materials since Graphite heat extraction rate is faster than Chromite and was per solidification simulation test results Appendix 1-D. The heat treatment cycles homogenizing and aging were determined by NETL based on the average SDAS of 70 µm.

The trepan specimen extraction lay out map of the centrifugally cast Haynes 282 casting wall is as shown in Figure 68 and Figure 69. The specimens include tensile, LCF and fracture toughness and the mechanical properties tabulation are provided in the Appendix 1-D.

Raw Tensile data tables of Haynes 282 casting at the thick location [5S = 5 inch wall thickness] and thin location [2S=2 inch wall thickness] from the side of the casting that solidified in a sand mold and from the side solidified in Graphite mold are tabulated in the Appendix 1-D.

Centrifugal Casting Trial Heat Mechanical Properties Conclusions:

In general it is observed that Graphite mold out performs sand mold across all temperatures for 0.2% YS; %Elongation, %RA and UTS at 1400°F when compared with Chromite sand mold section. The Stress-LMP plot of Centrifugal Cast H282 compared to wrought H282 data. The data scatter is in line with the wrought alloy Figure 79. Also the conditional Fracture toughness Kq plot for the Haynes 282 cast data [Sand & Graphite] falls in the scatter of wrought alloy as shown in Figure 78.

Figure 70 to Figure 73 show the tensile properties and Figure 74 to Figure 77 show LCF.

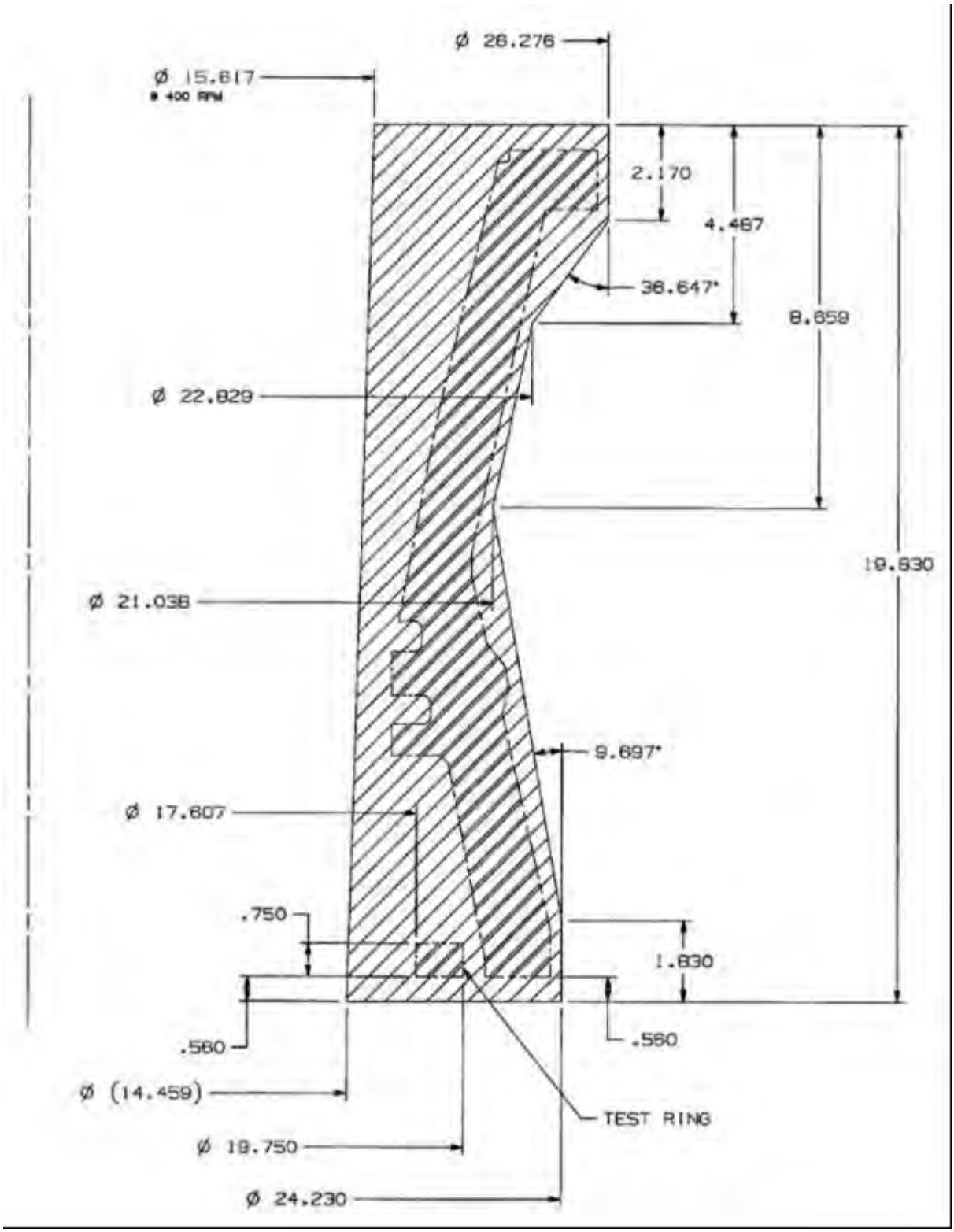

Figure 60: Sectional view drawing of 282 Centrifugal Casting

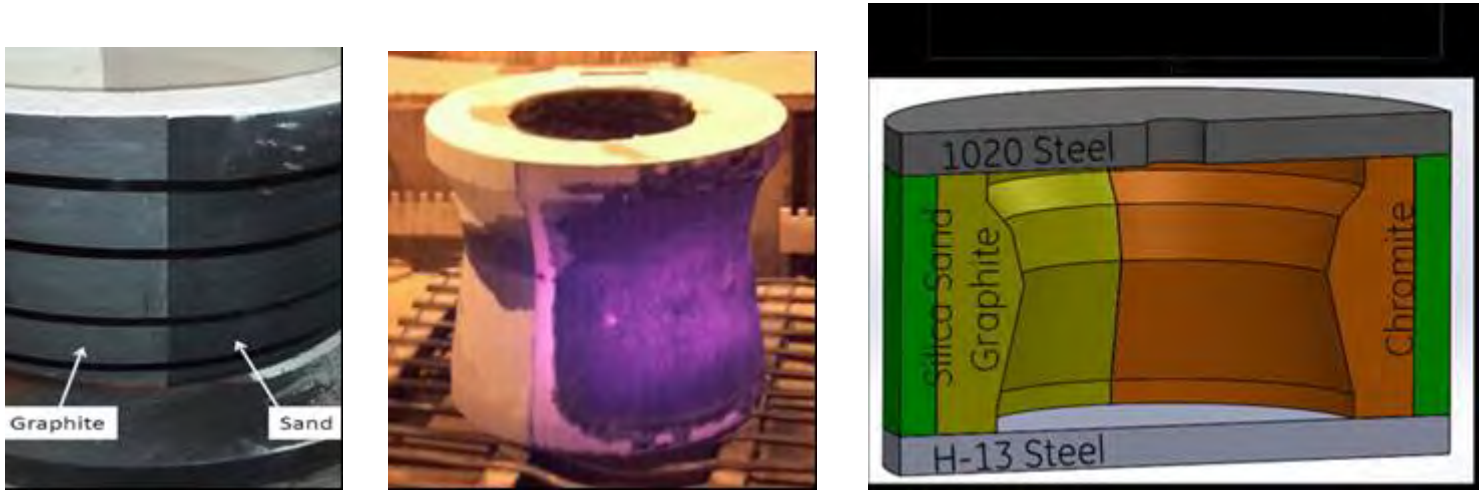

Figure 61: Haynes282 Centrifugal casting mold assembly comprising half mold Graphite and half mold Chromite sand

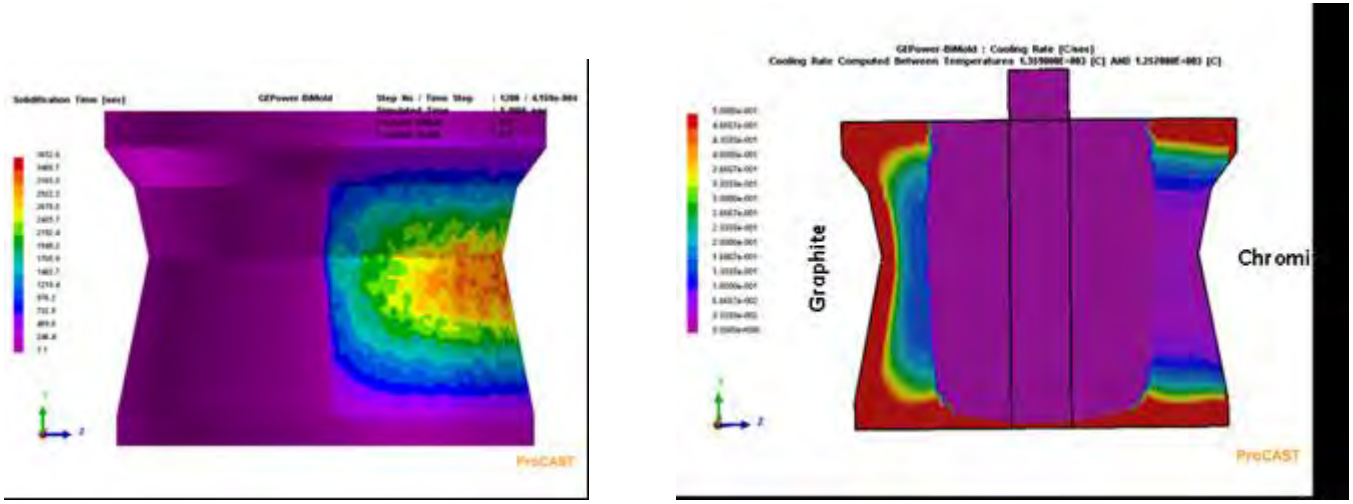

Figure 62: Casting simulation predicted cooling rates for Graphite and Chromite sand side molds

The casting sectioning and Heat treat sample extraction views are shown in Figures 63 and 64.

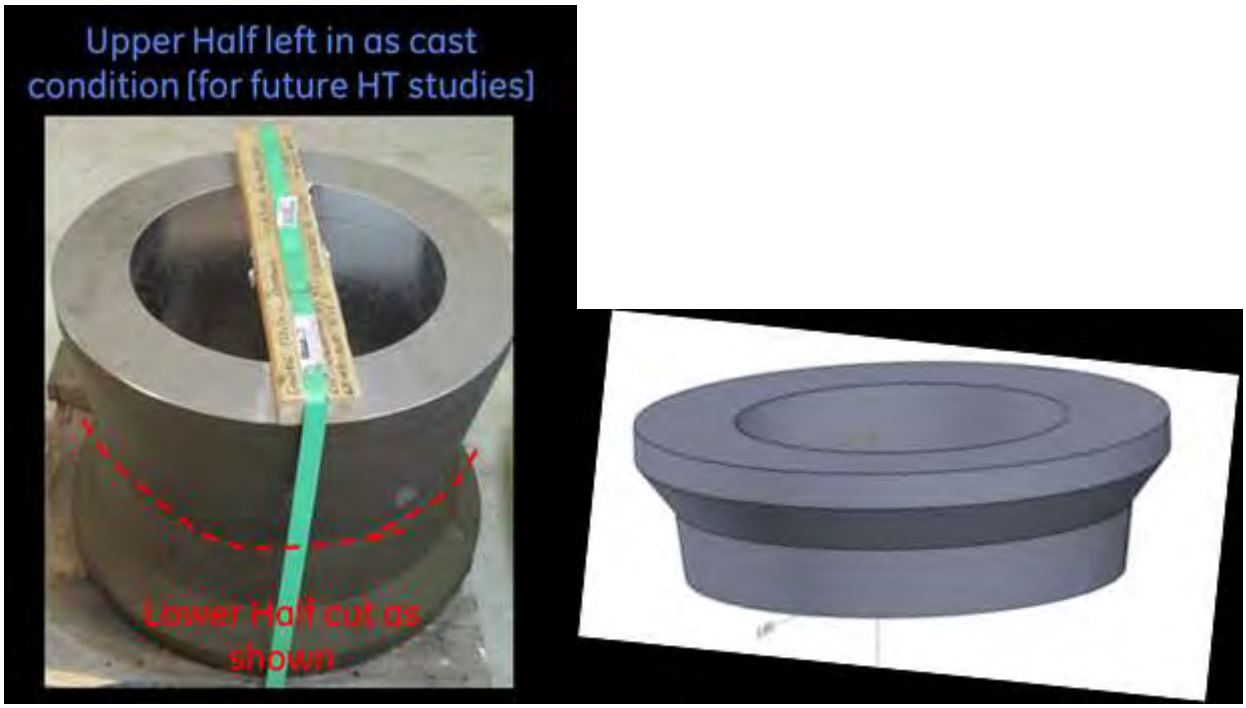

Figure 63: Picture showing the location of the casting utilized for micro-structural analysis and mechanical testing**.**

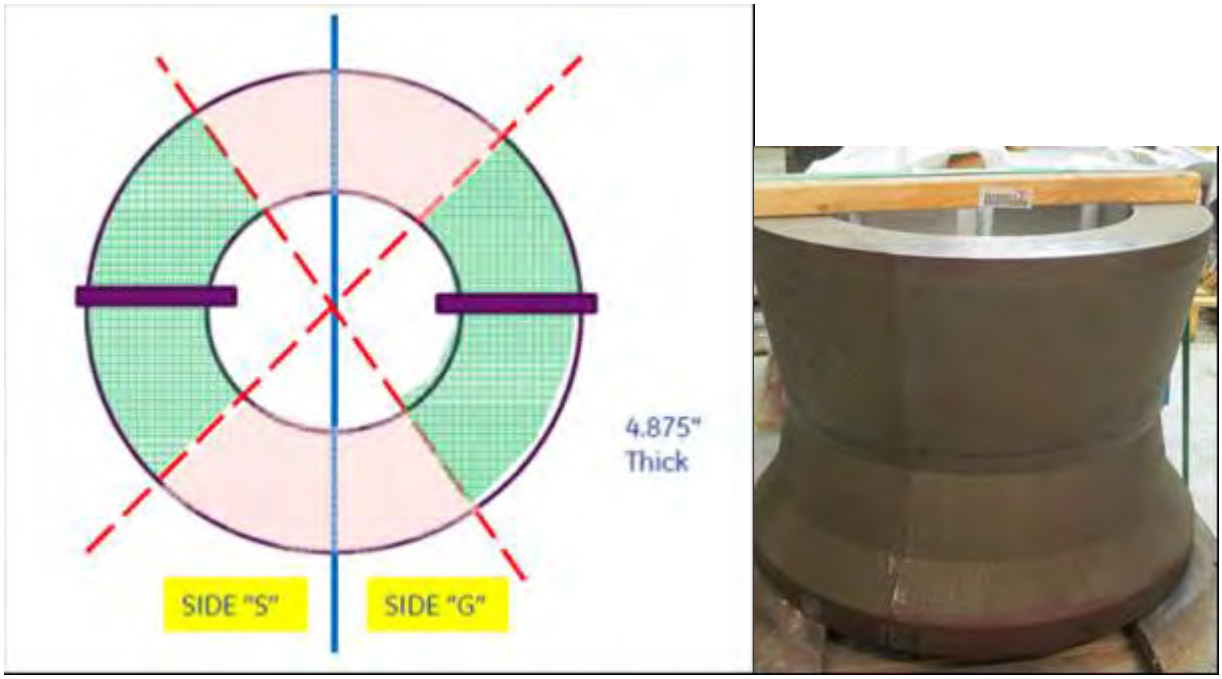

Figure 64: Picture showing the extraction of the slice for heat treatment and micro-structural analysis

The final heat treatment cycle on the centrifugal casting is shown in the Appendix 1-D [Centrifugal Castings of Haynes 282].

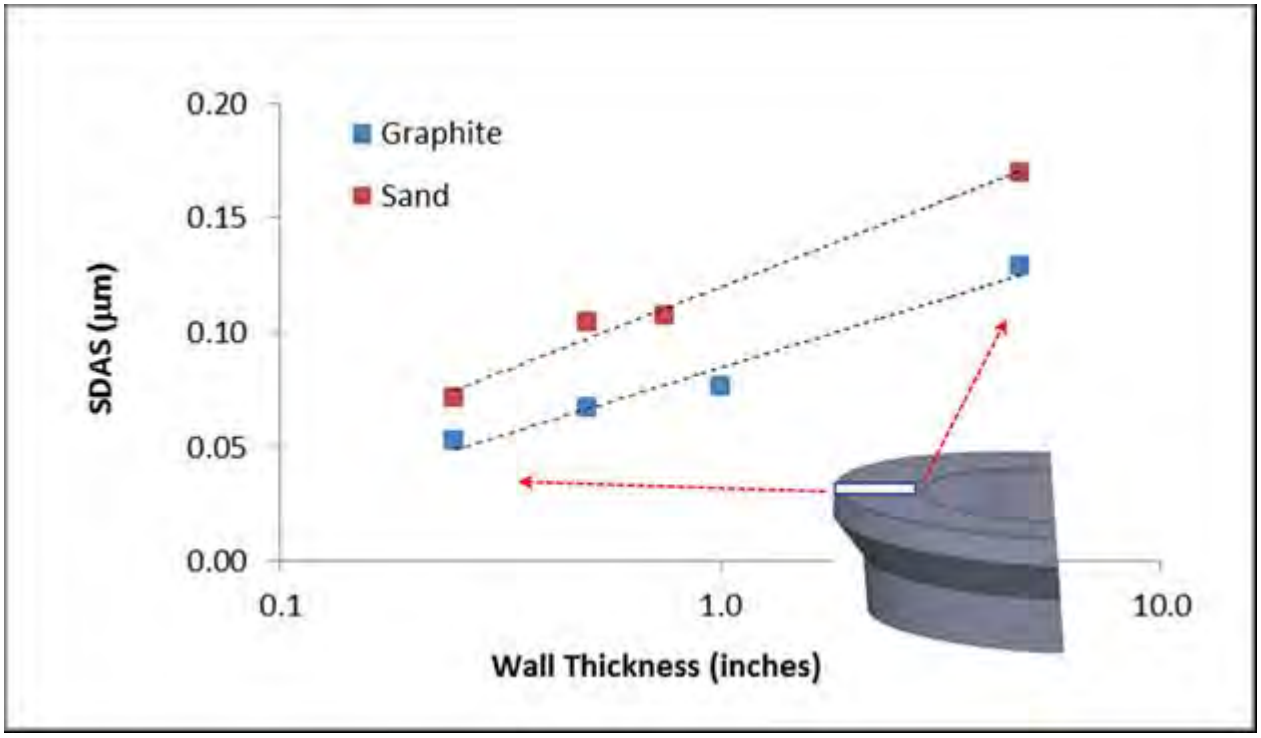

Figure 65: SDAS along the wall thickness for the two respective mold material.

The Microstructure evolution as a function of mold cooling rates for centrifugal castings are clearly established with Haynes 282 hybrid mold casting trials and the SDAS values for both Graphite mold and Chromite sand molds were plotted with ID (Hotter surface) to OD (Cooler mold interfaced surface) distance measurements as shown in Figures 65 and 66.
The Grain boundary regions in as cast condition as shown in Figure 67 (SEM), indicating Ti, Cr and Mo rich precipitates.

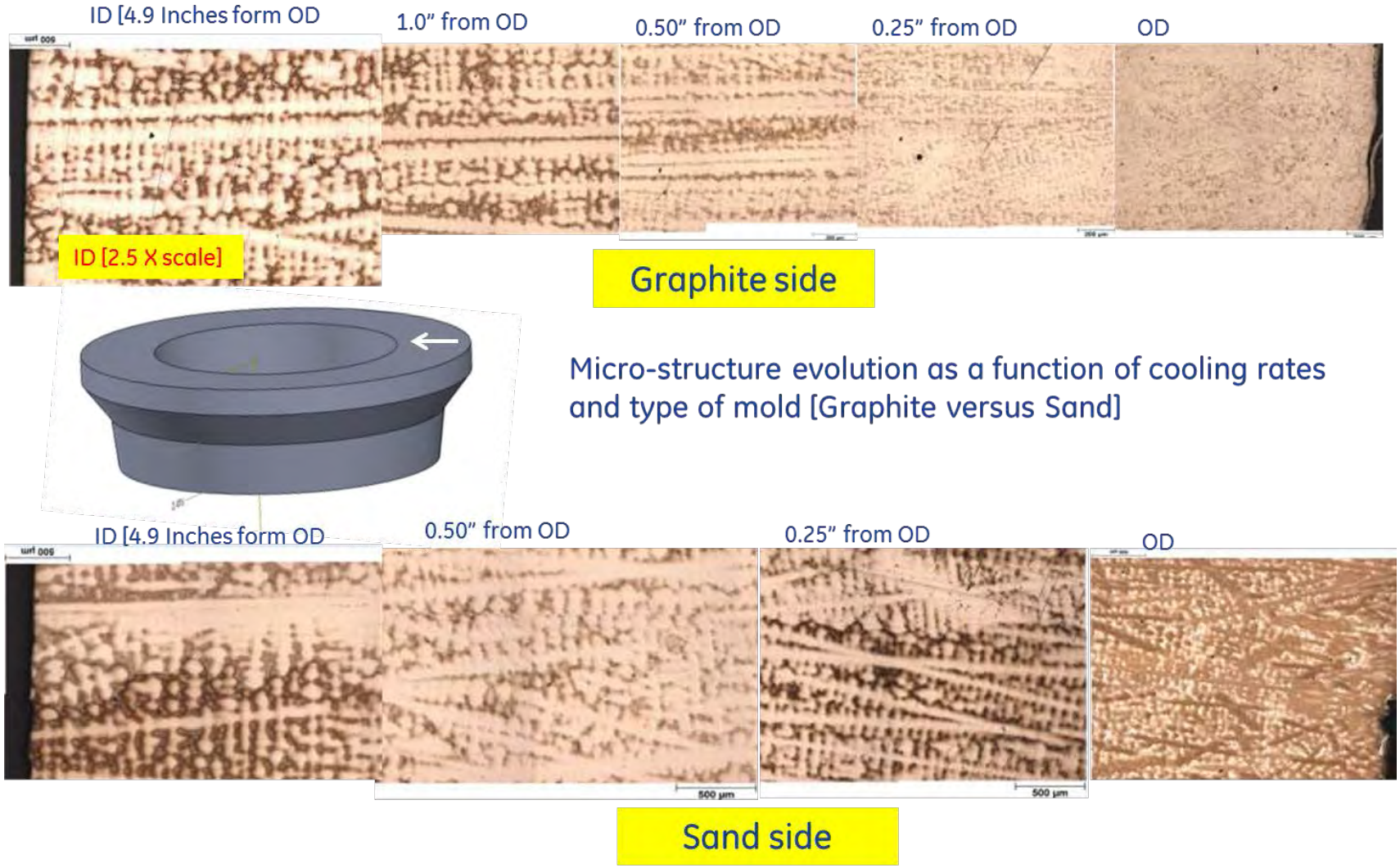

Figure 66 As cast microstructural evolution across the wall thickness for the two mold material

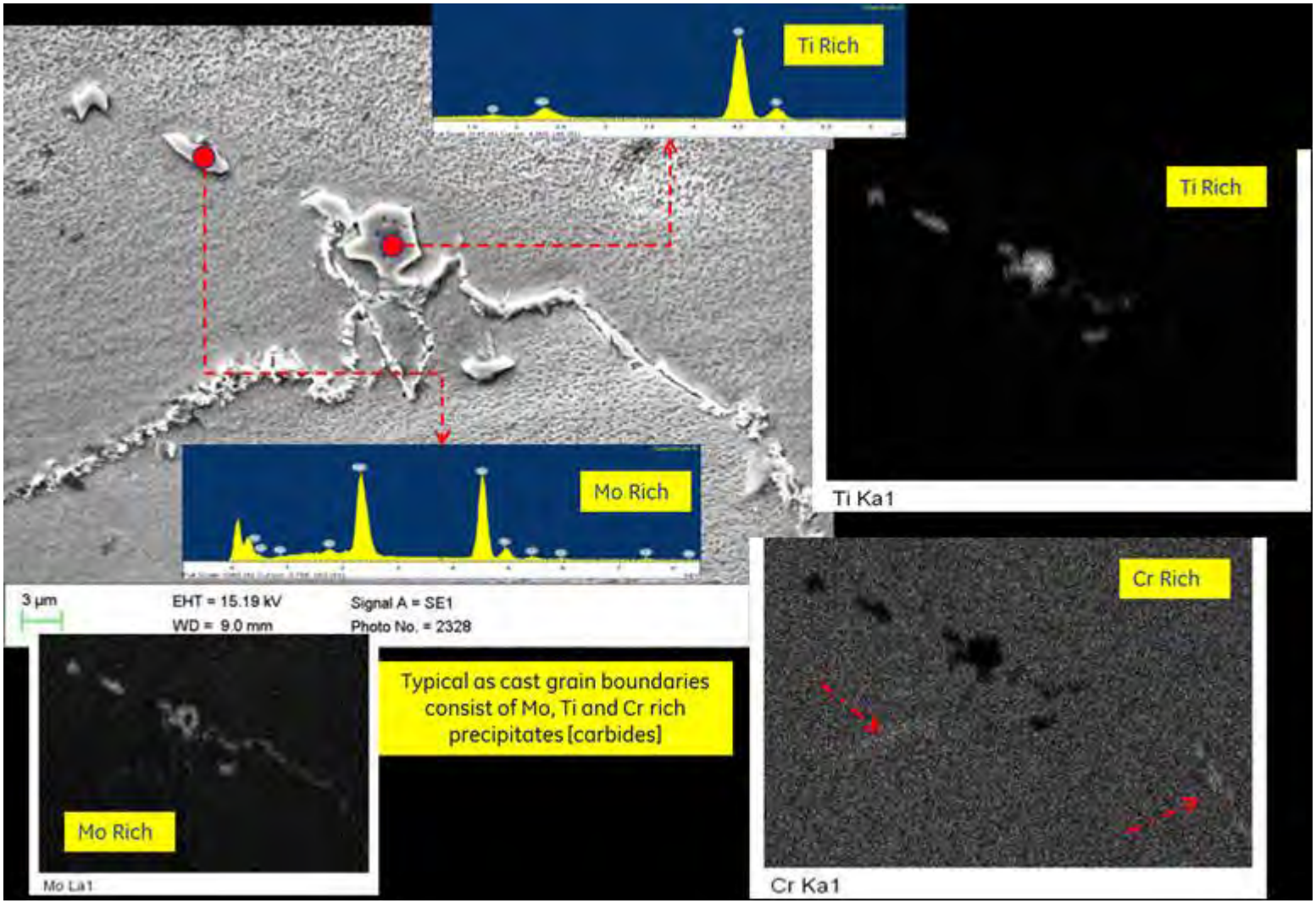

Figure 67 SEM image of grain boundary in as cast specimens. Most precipitates consists of Ti, Mo and Cr rich

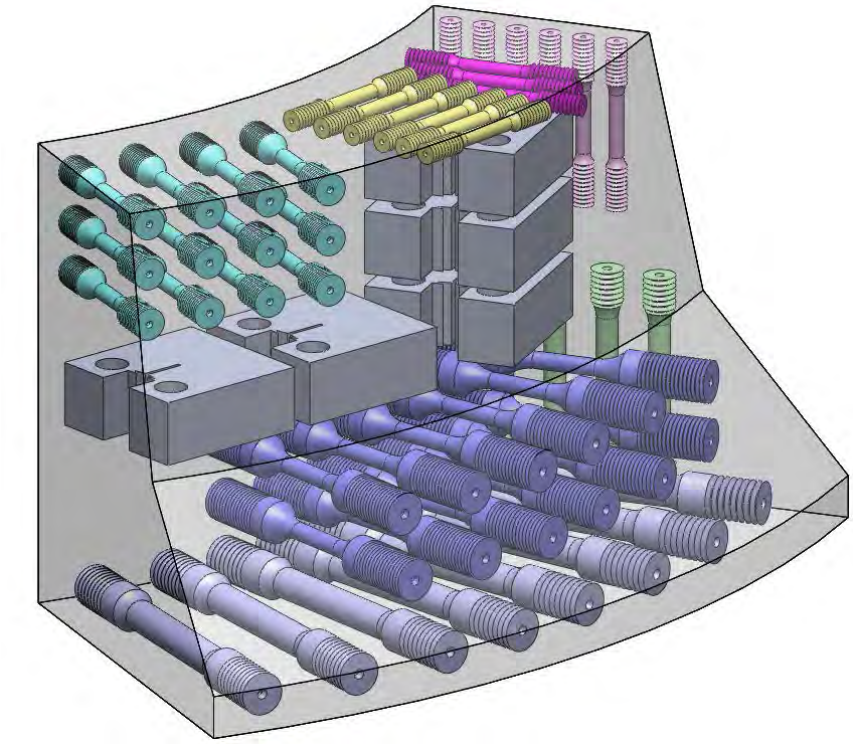

Figure 68: Complete map of specimen extraction from the centrifugally cast Haynes 282. The specimens include tensile, LCF and fracture toughness

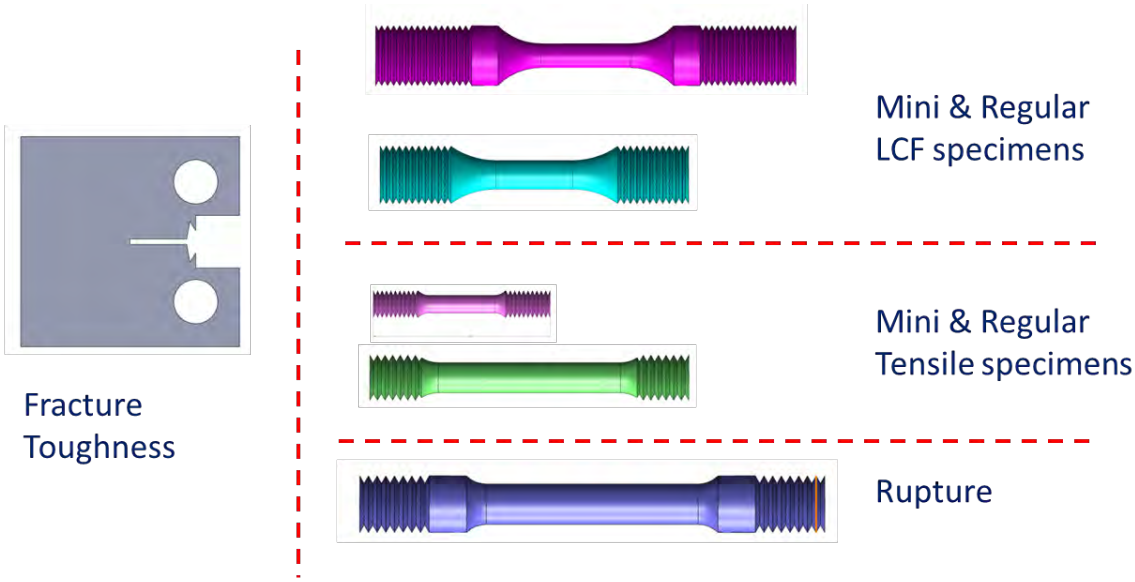

Figure 69: Color codes of specimen type are as shown. All mini specimens are for the thinner wall thickness

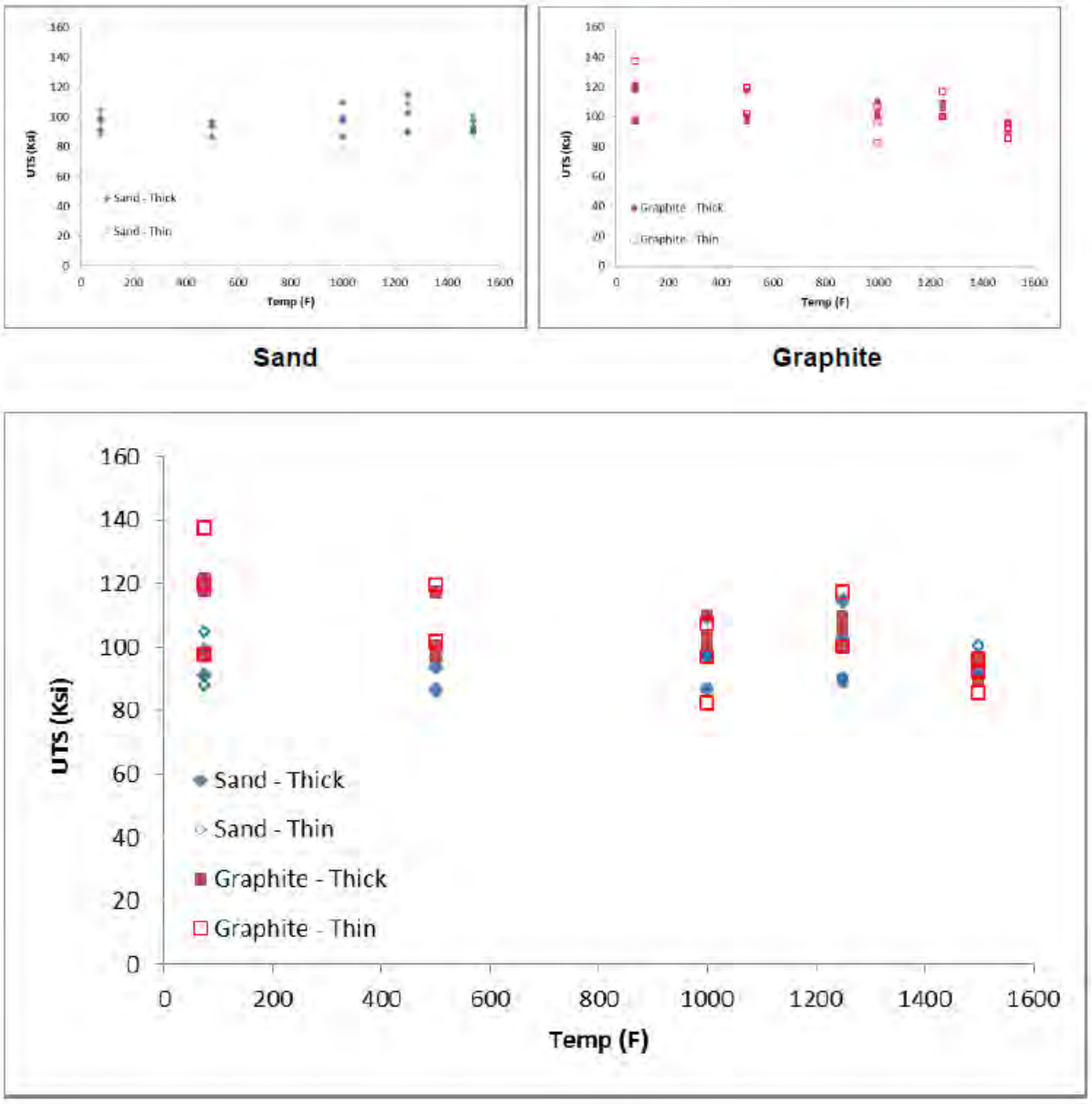

Figure 70: Plots of UTS as a function of temperature [Sand and Graphite mold]. In general, the variation between the thick and thin sections on the sand side has less variability, when compared to the graphite side. Graphite side has better RT properties when compared to the sand. However at 1400°F, all data falls within a very tight band.

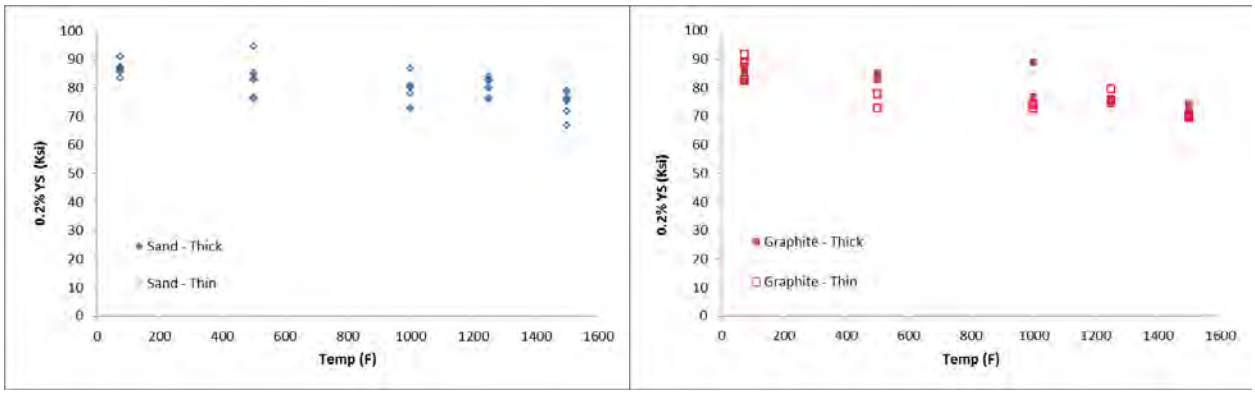

Sand mold **Graphite mold**

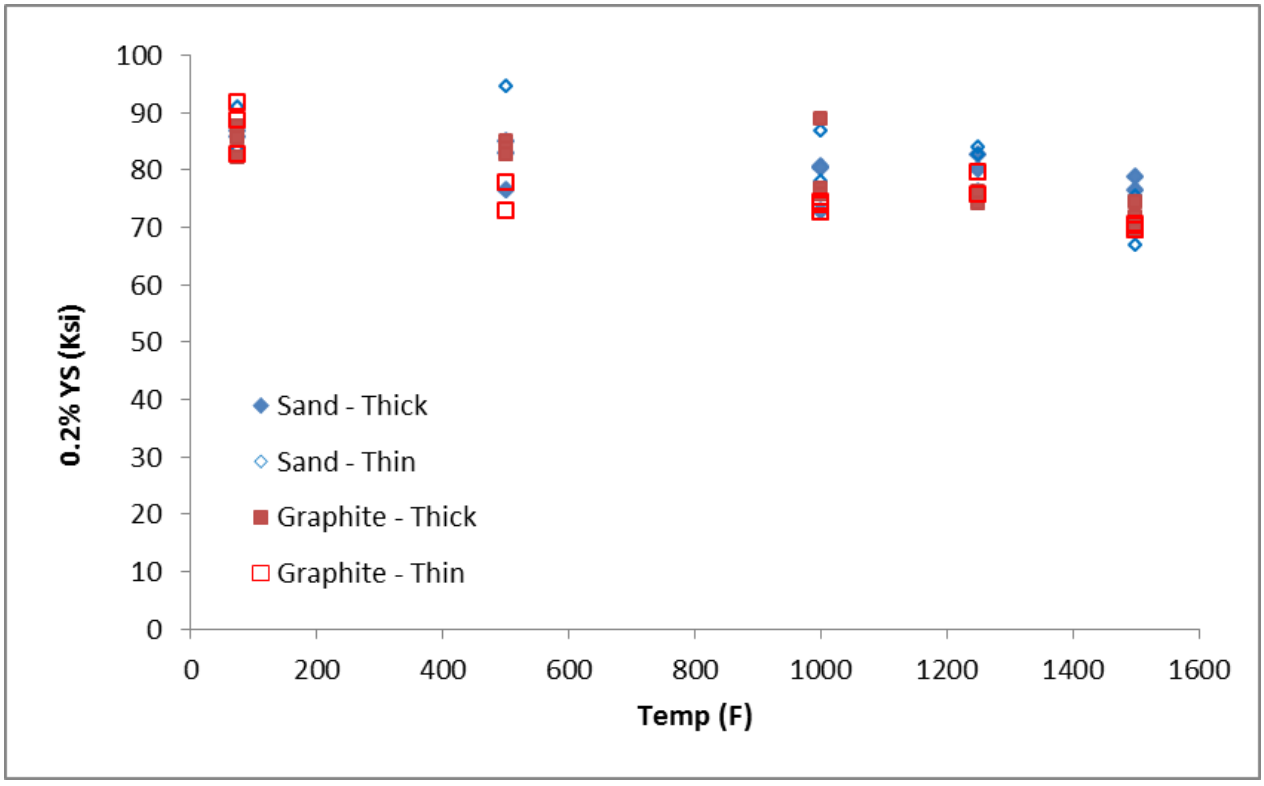

Figure 71: Plots of 0.2% YS as a function of temperature for various mold material. Unlike the variation in UTS, the 0.2% YS has a very tight range across all temperatures tested

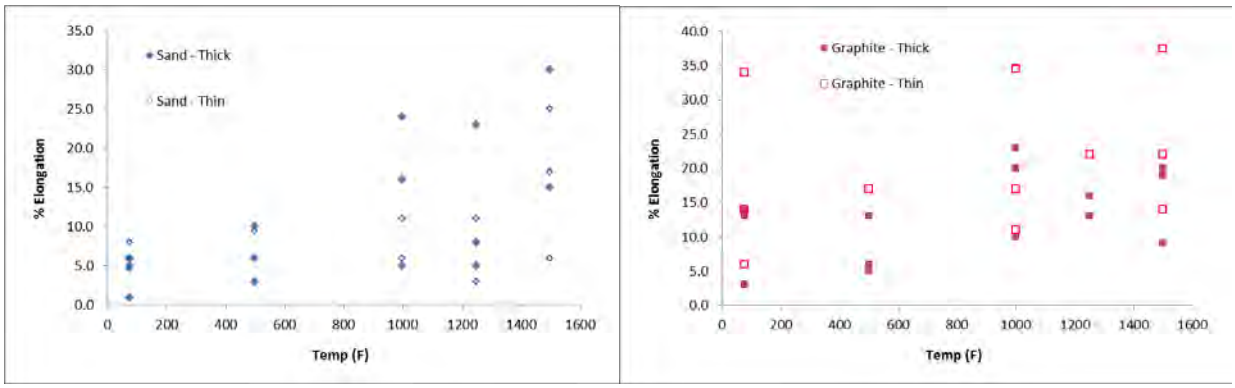

Sand mold **Graphite mold**

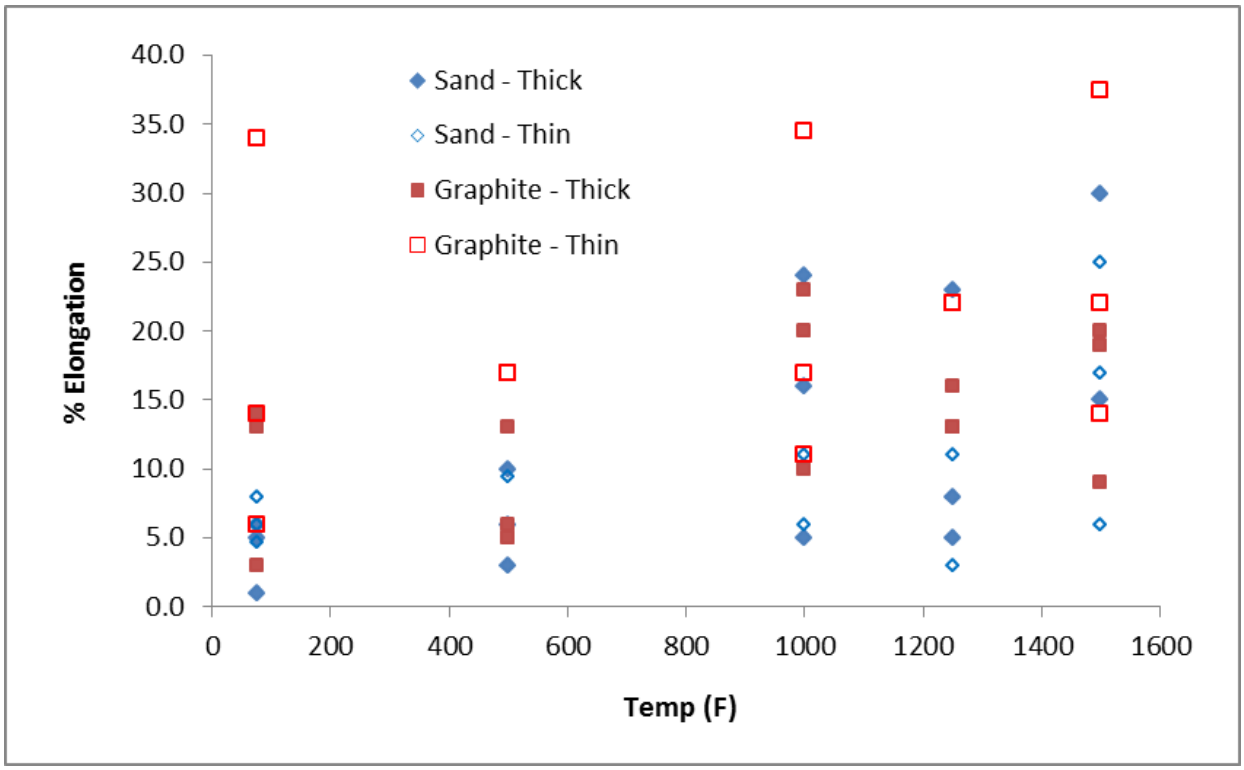

Figure 72: Plots of % Elongation as a function of temperature for various mold material. The plots clearly show a wide variation in % Elongation, with the graphite mold being better than the sand mold across all temperatures

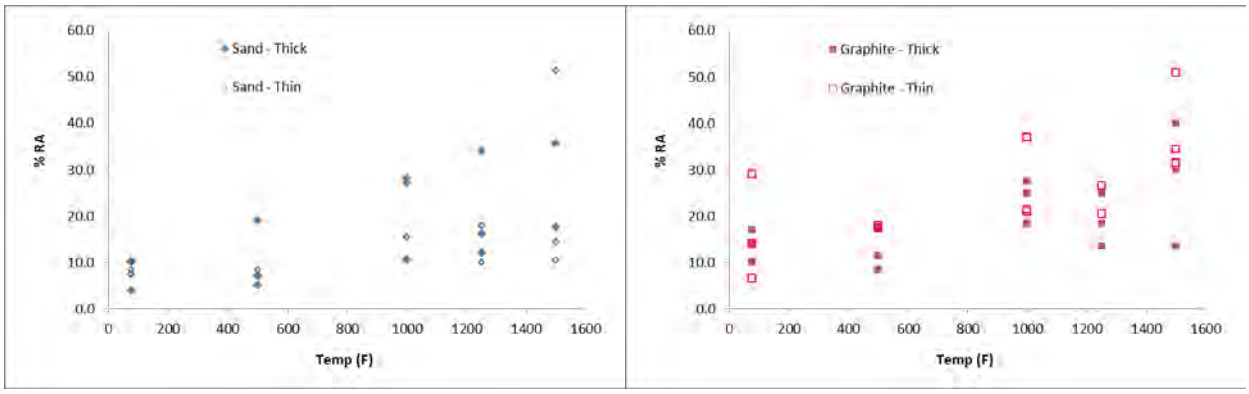

Sand mold **Graphite mold**

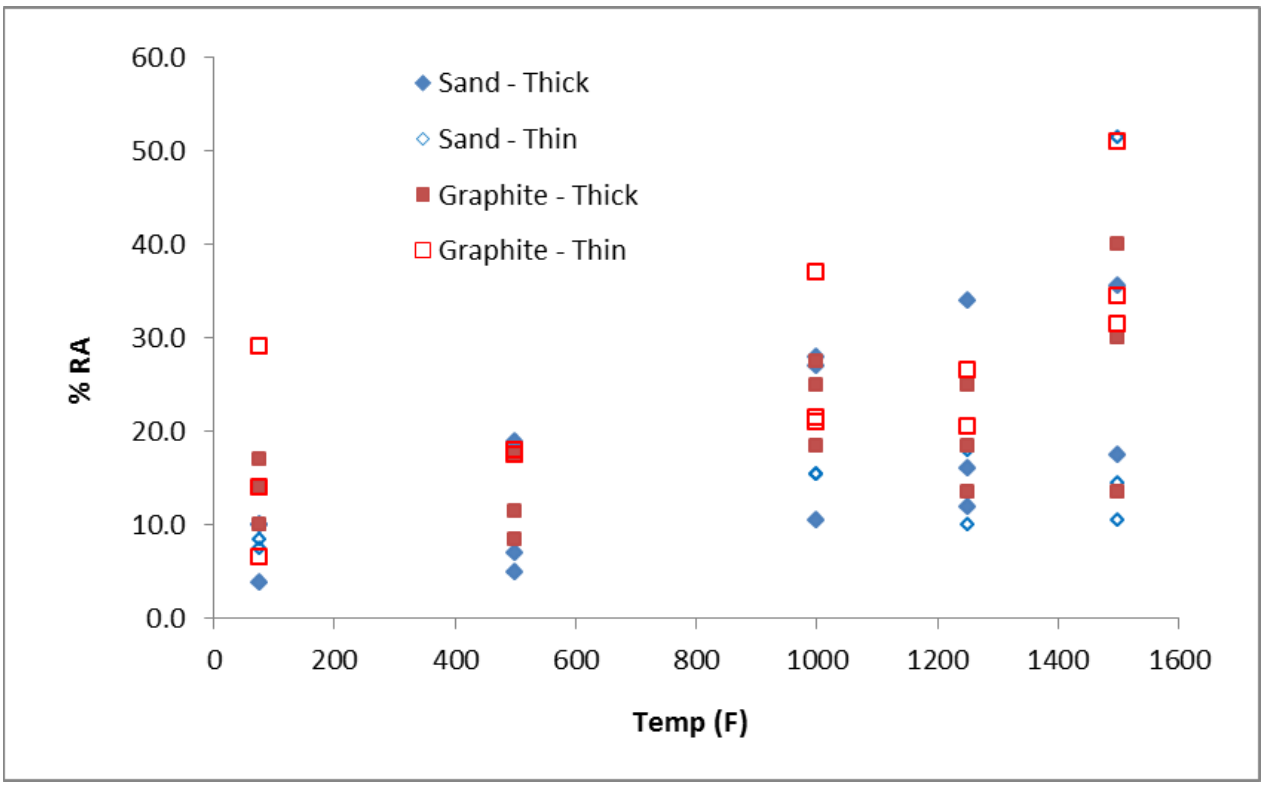

Figure 73: Plots of % RA as a function of temperature for various mold material. The plots clearly show a wide variation in % RA, and in general, graphite mold out performs sand mold across all temperatures

LCF results of specimens extracted from the Sand (S) and Graphite (G) side of the centrifugal cast H282 alloy are tabulated in Appendix 1-D [Centrifugal Castings of Haynes 282].

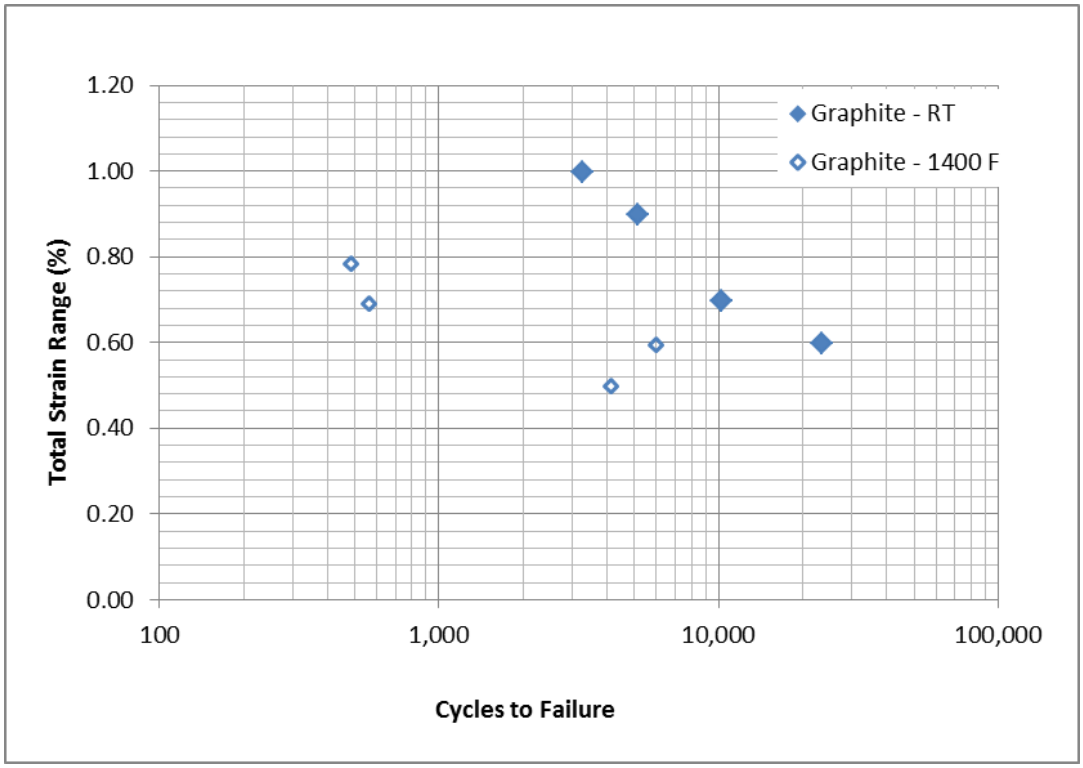

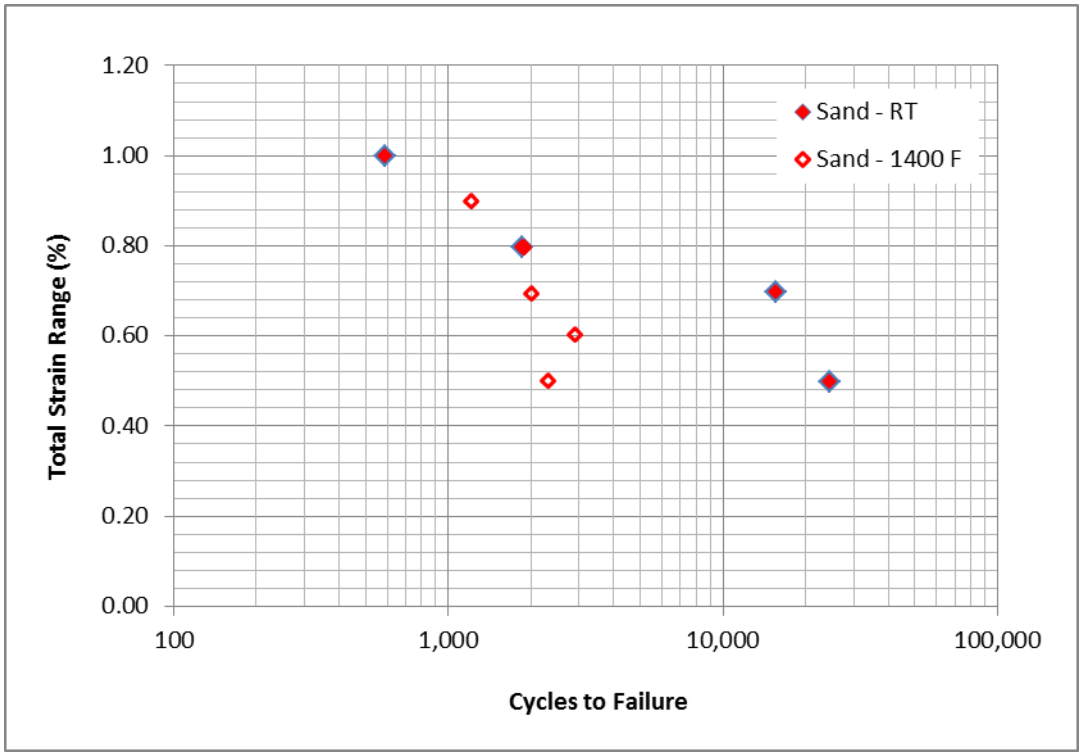

Figure 74: Plots of Cycles to Failure and Total Strain Range (%) for the Sand and Graphite molds at RT and 1400°F. The Graphite side shows a debit at 1400°F, while the sand side does degrade with the same severity

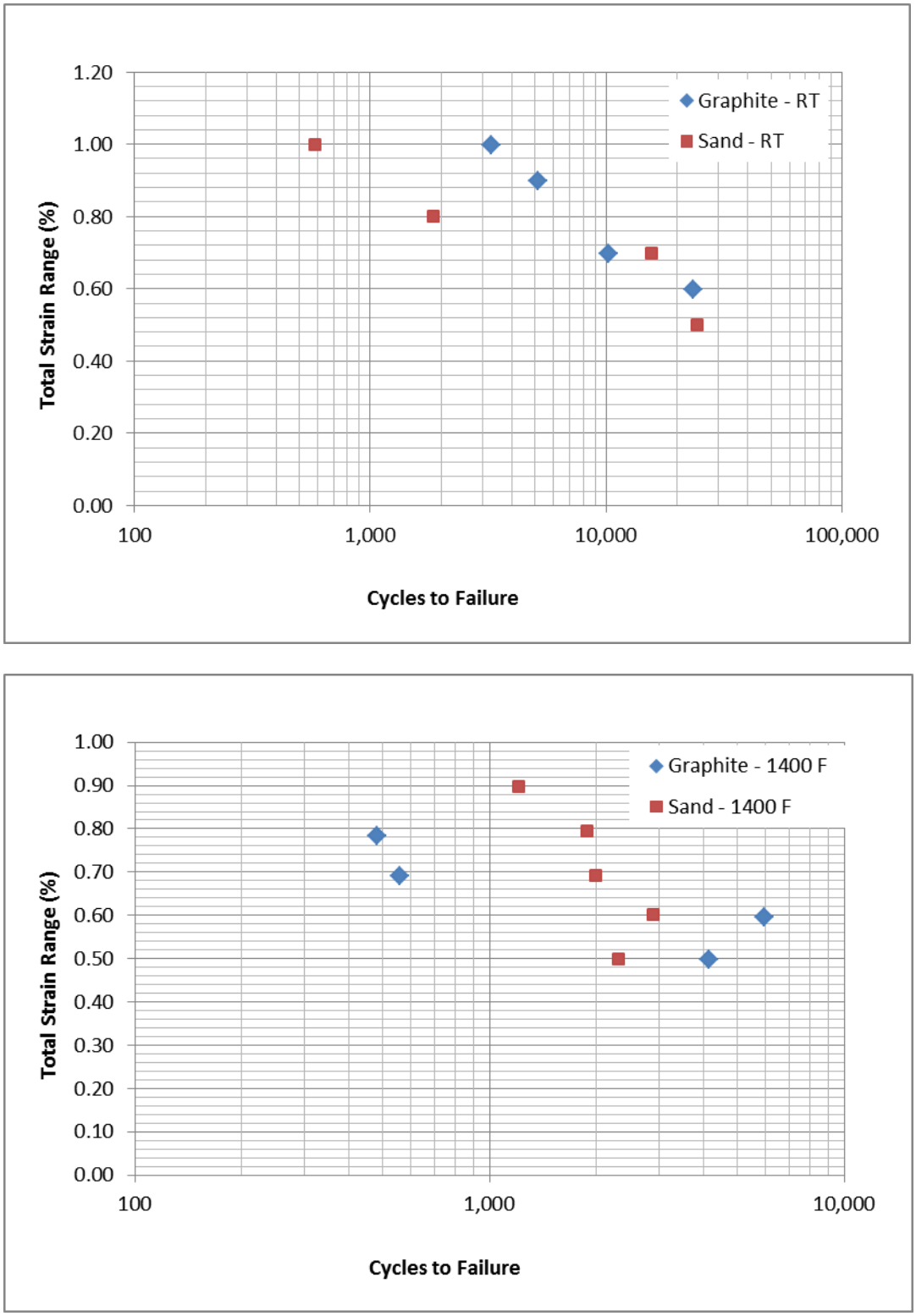

Figure 75: Plots of Cycles to Failure and Total Strain Range (%) for the Sand and Graphite molds at RT and 1400°F. The debit in the graphite compared to sand at high strains and 1400°F will need some further investigation

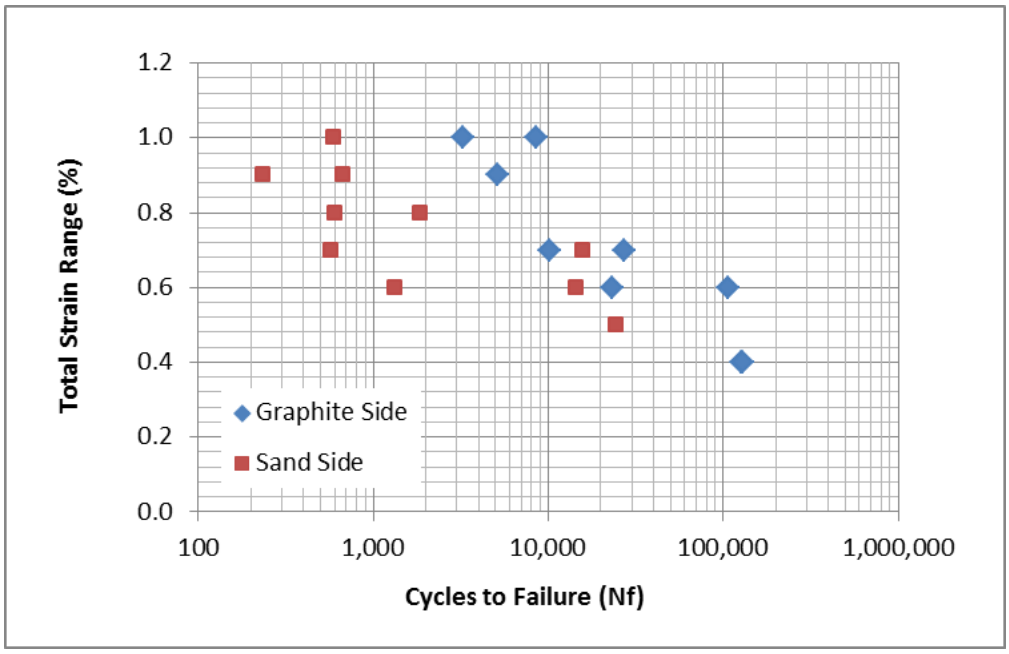

Figure 76: Plot of cycles to failure and total strain range from Table 4B-1. The graph clearly shows the better performance of faster cooling rates [finer SDAS in the graphite side] due to higher UTS at 75°F (+10 to15 Ksi increase in UTS on Graphite side]

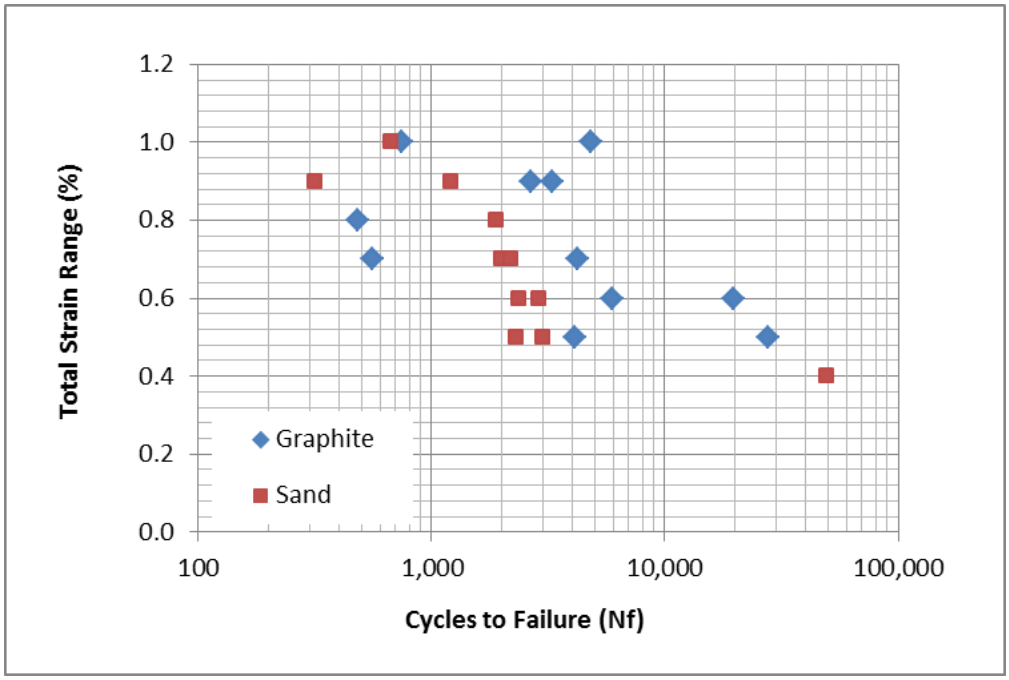

Figure 77: Plot of cycles to failure and total strain range from Table 4B-2. The graph clearly shows no performance difference at 1400°F as the tensile properties of both sand and graphite are similar at 1400°F

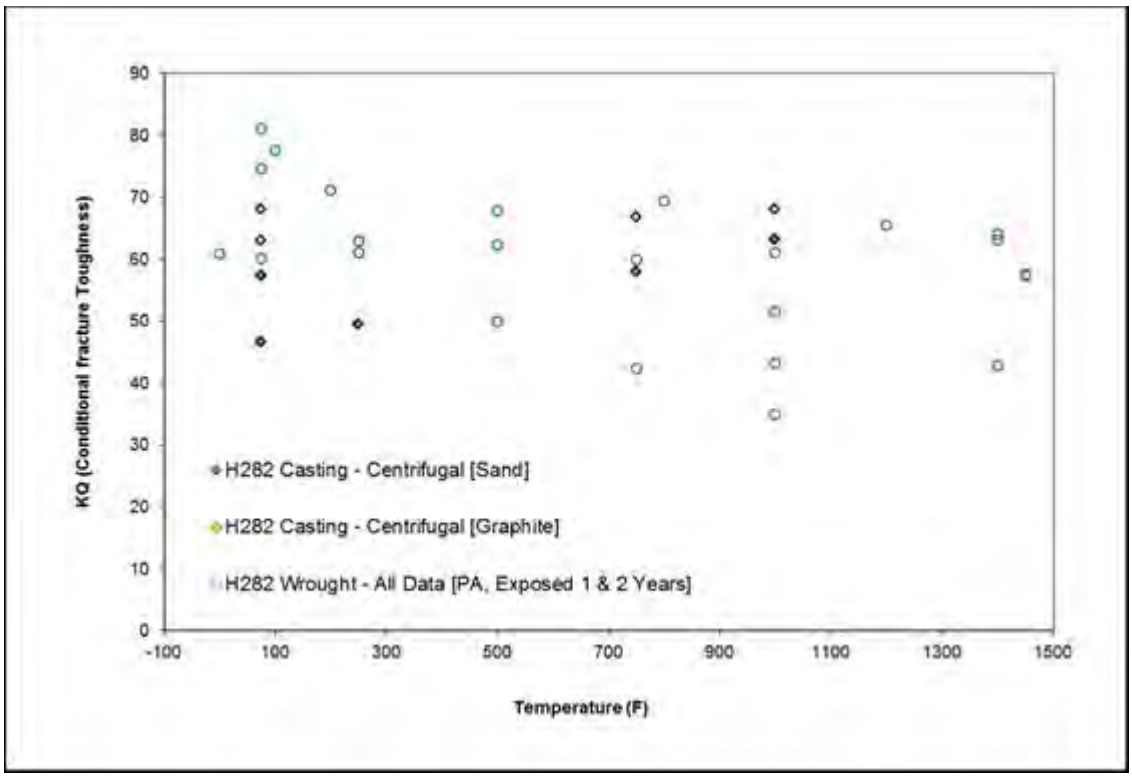

Figure 78: Conditional Fracture toughness (K_Q) of centrifugally cast Haynes 282. The cast data [Sand & Graphite] falls in the scatter of wrought alloy. The wrought data in the figure above consists of PA, and exposed for 1 & 2 years at 1425°F

The Table showing the short term creep rupture test results from Centrifugal Cast H282 is provided in the Appendix 1-D [Centrifugal Castings of Haynes 282].

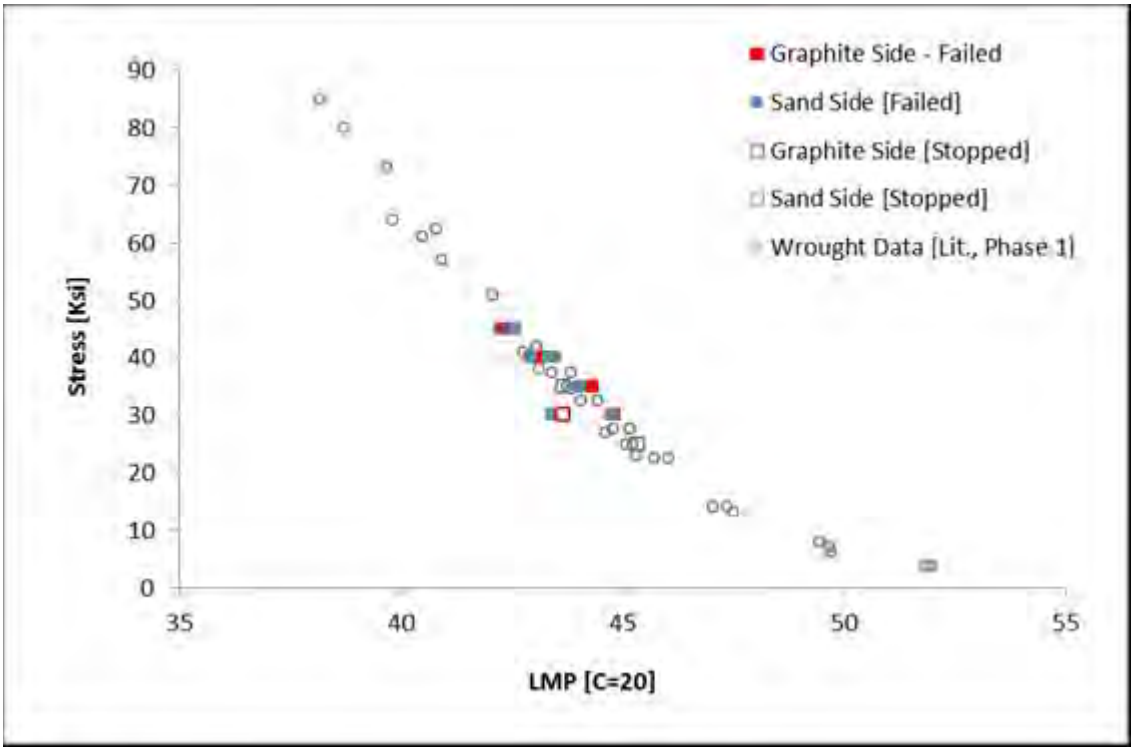

Figure 79: Stress-LMP plot of Centrifugal Cast H282 compared to wrought H282 data. The data scatter is in line with the wrought alloy.

FUNDAMENTAL STUDIES ON COOLING RATES AND SDAS

The objective was to study the effect of mold material on casting cooling rates and to characterize the effect on SDAS spacing in the cast wall section as shown in schematic sketch, Figure 80.

Hence in this test program, evaluated the influence of 6 mold materials Silica, Chromite, Alumina, Silica with Indirect Chills, Zircon and Graphite on casting solidification cooling rates as shown in Figure 82 and Figure 83. The molds layout schematic is shown in Figure 81. The molds assembly, thermocouples cable layout are shown in Figure 84 - Figure 87. The thermocouples relative location in each mold is shown in Figure 89.

Actual Casting cooling rates through Liquidus to Solidus phase transition were measured with 3 different locations based thermocouples placed in each mold, Figure 91.

Compared with solidification simulation cooling rates and measurement of SDAS, microstructure features were reported, Figure 93 and simulation vs. measured cooling rates compared in Table 17 and Table 19 provide the SDAS measurements. Additional details and data tables are provided in Appendix 1-E.

The test results provided engineered casting potential methods, applicable for heavy section Haynes 282 castings for optimal properties, with foundry process methods and tools.

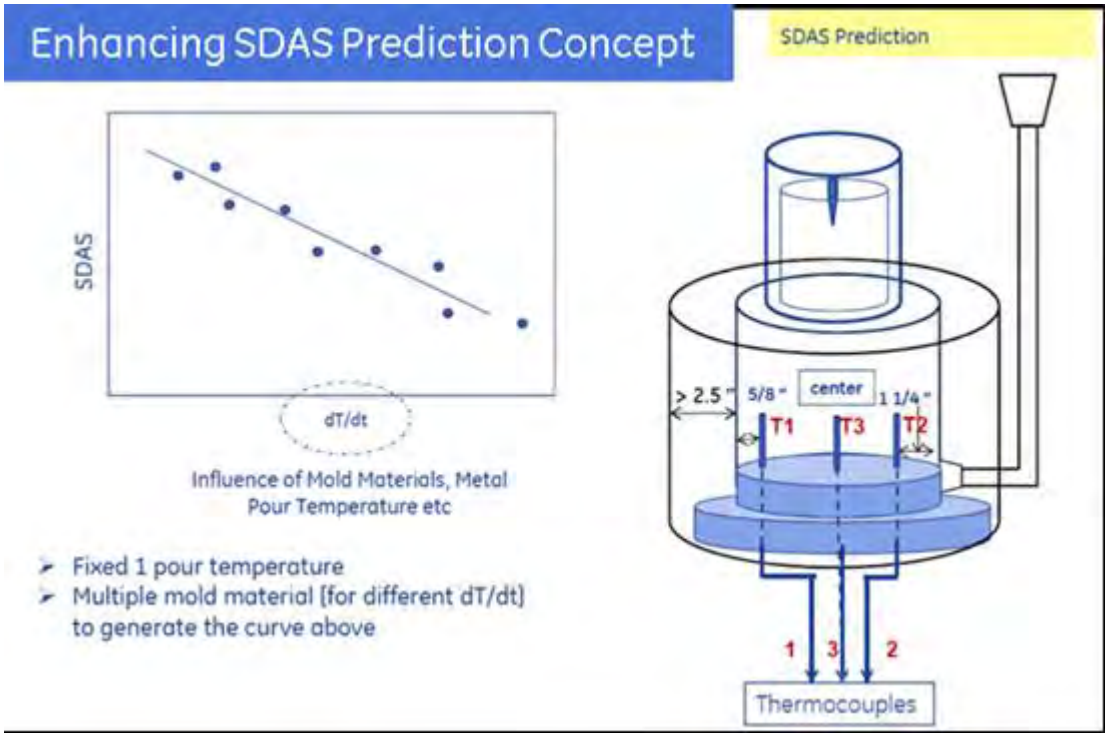

Figure 80: Enhancing SDAS prediction with casting solidification mold cooling rate studies. Six molds with different mold materials [to simulate different cooling rates] were poured with thermocouples located as shown to measure casting cooling rates

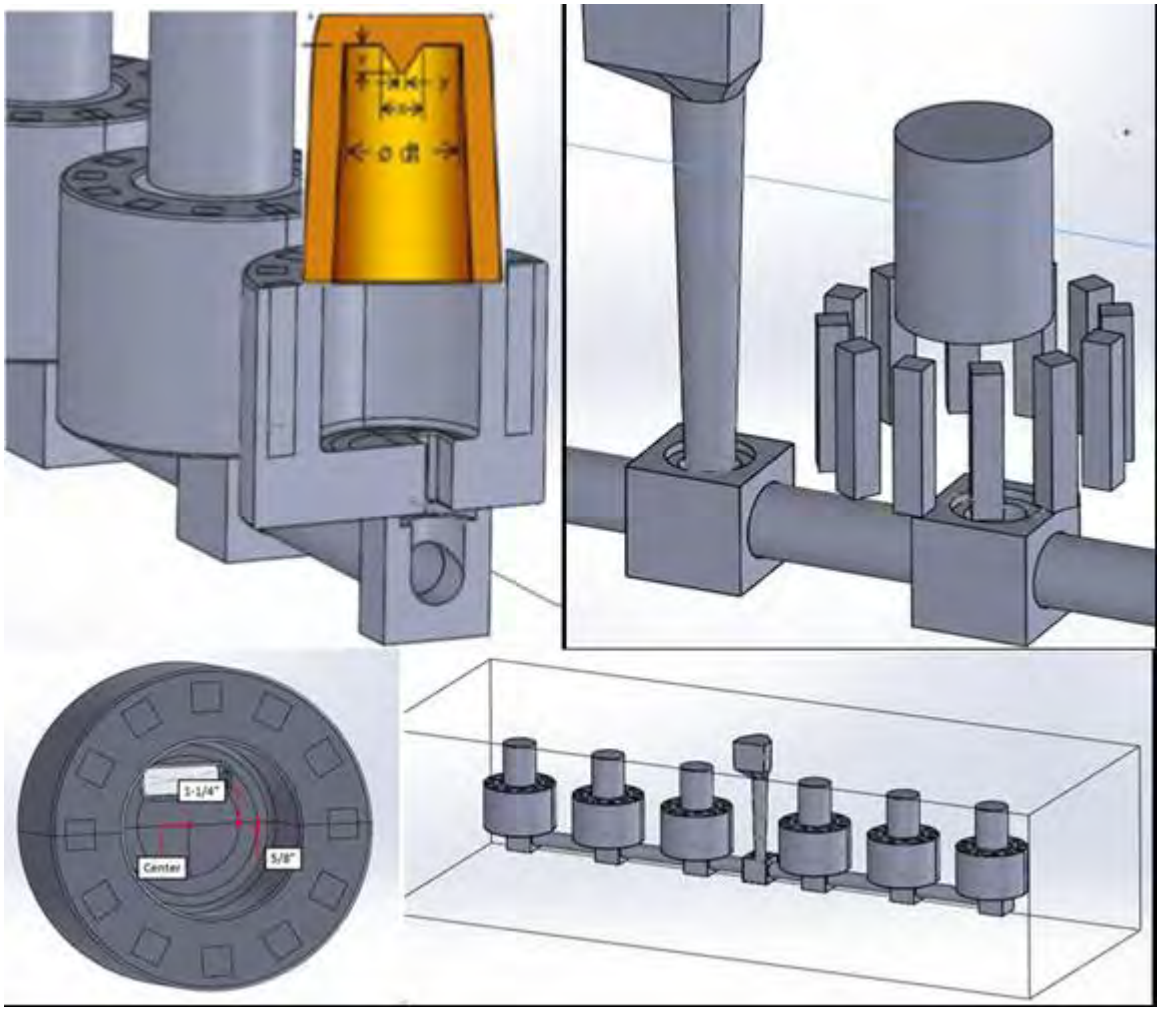

Figure 81: Detailed plan of casting solidification cooling rates measurement mold layout assembly

Figure 82: Sand molds from 5 different mold materials [left] coated with refractory paint and dried [right]. Six mold materials were evaluated: 1. Silica, 2. Chromite, 3. Graphite, 4. Alumina, 5. Zircon, 6. Silica with indirect chills placement.

Figure 83: Photograph of chills location in mold pattern prior to molding

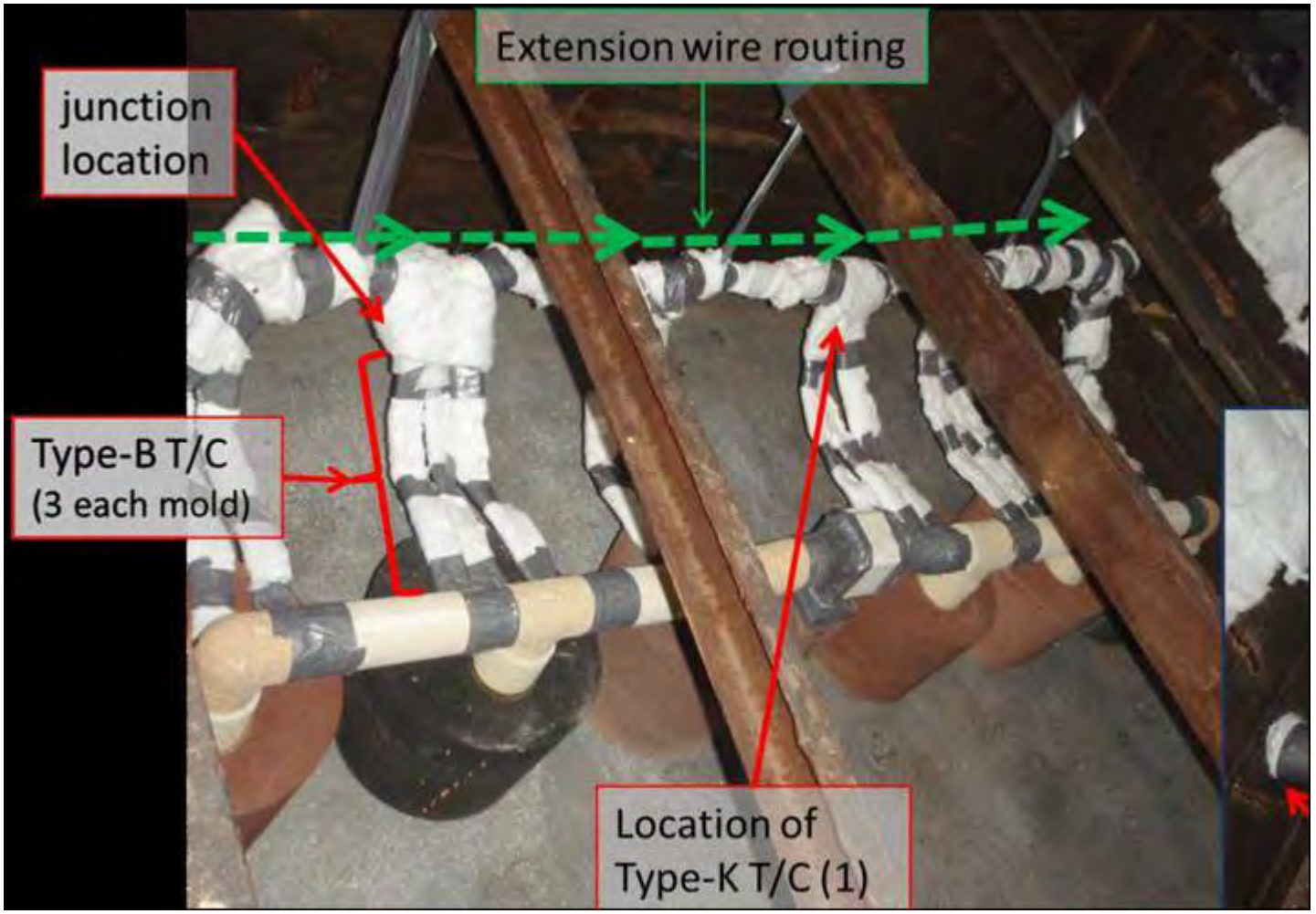

Figure 84: Thermocouples and extension wire were wrapped with Kaowool thermal insulation.

Figure 85: Photograph of thermocouple compensating cables routing within the drag mold

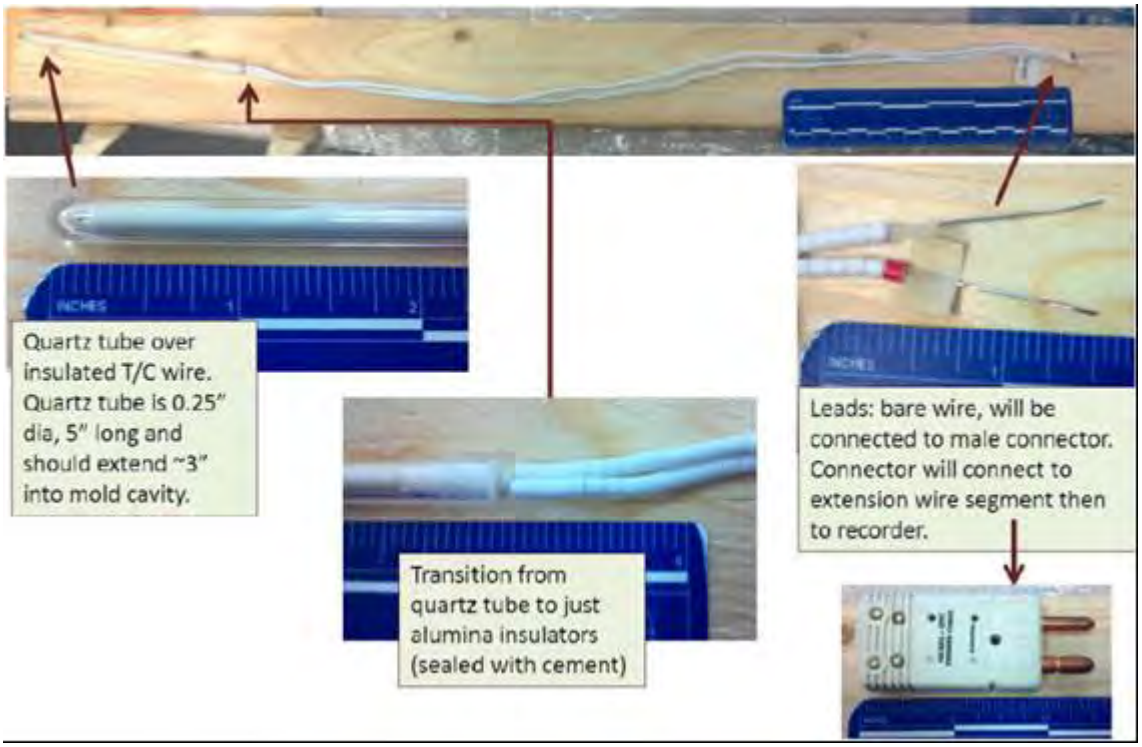

Figure 86: Type B Thermocouples, insulators and connectors assembly components

Figure 87: Photograph of completed mold ready for pour

Figure 88: Photograph showing castings after mold shake out, gating and feeders removal

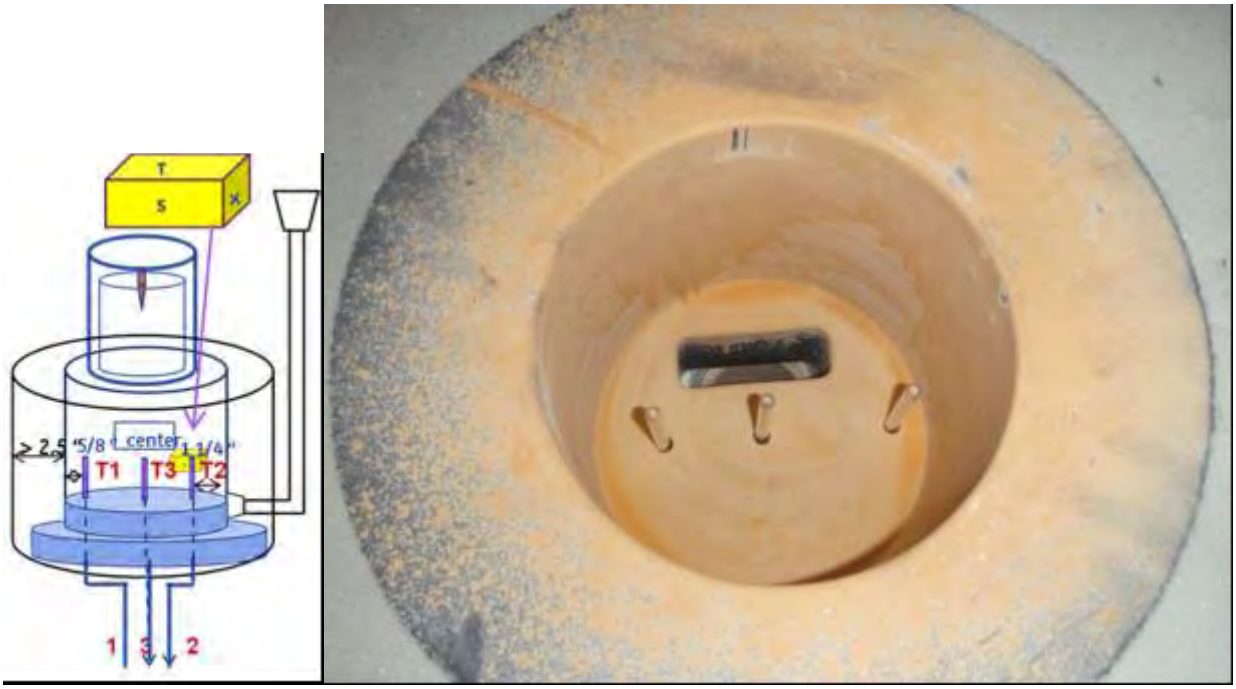

Figure 89: Haynes 282 cylinder castings thermocouple arrangements schematic view. Photograph showing Quartz sheathed Type–B thermocouples located within the molds

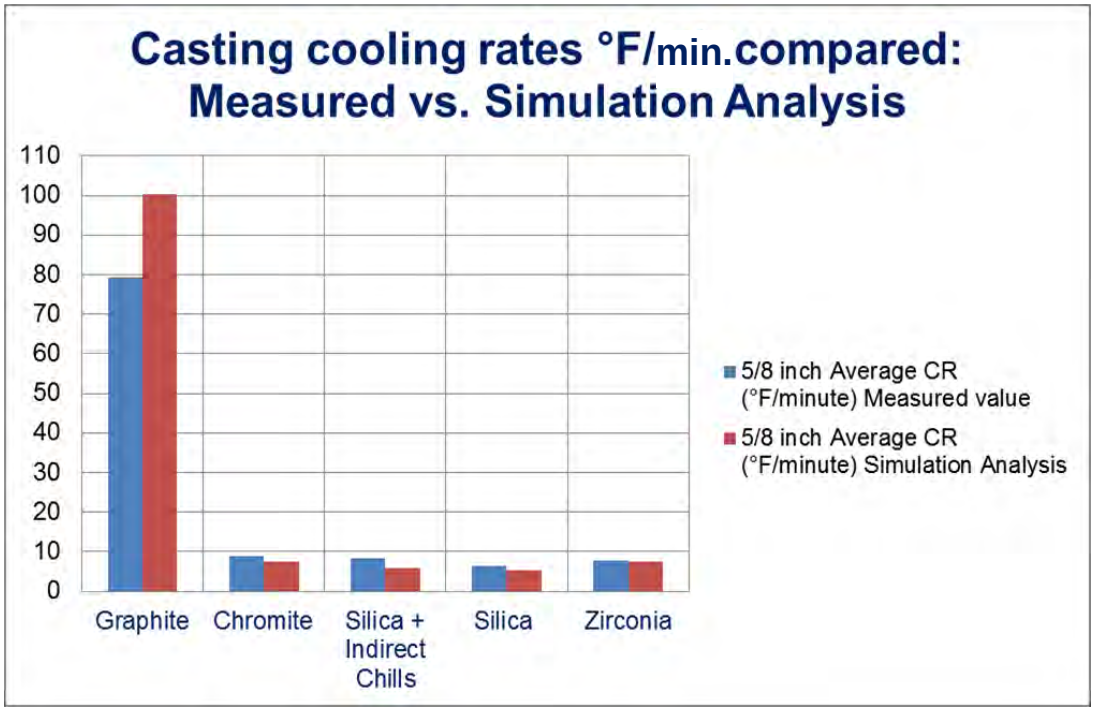

Figure 90: Casting cooling rates measured and simulated compared for different mold materials during liquidus to solidus transition temperature range

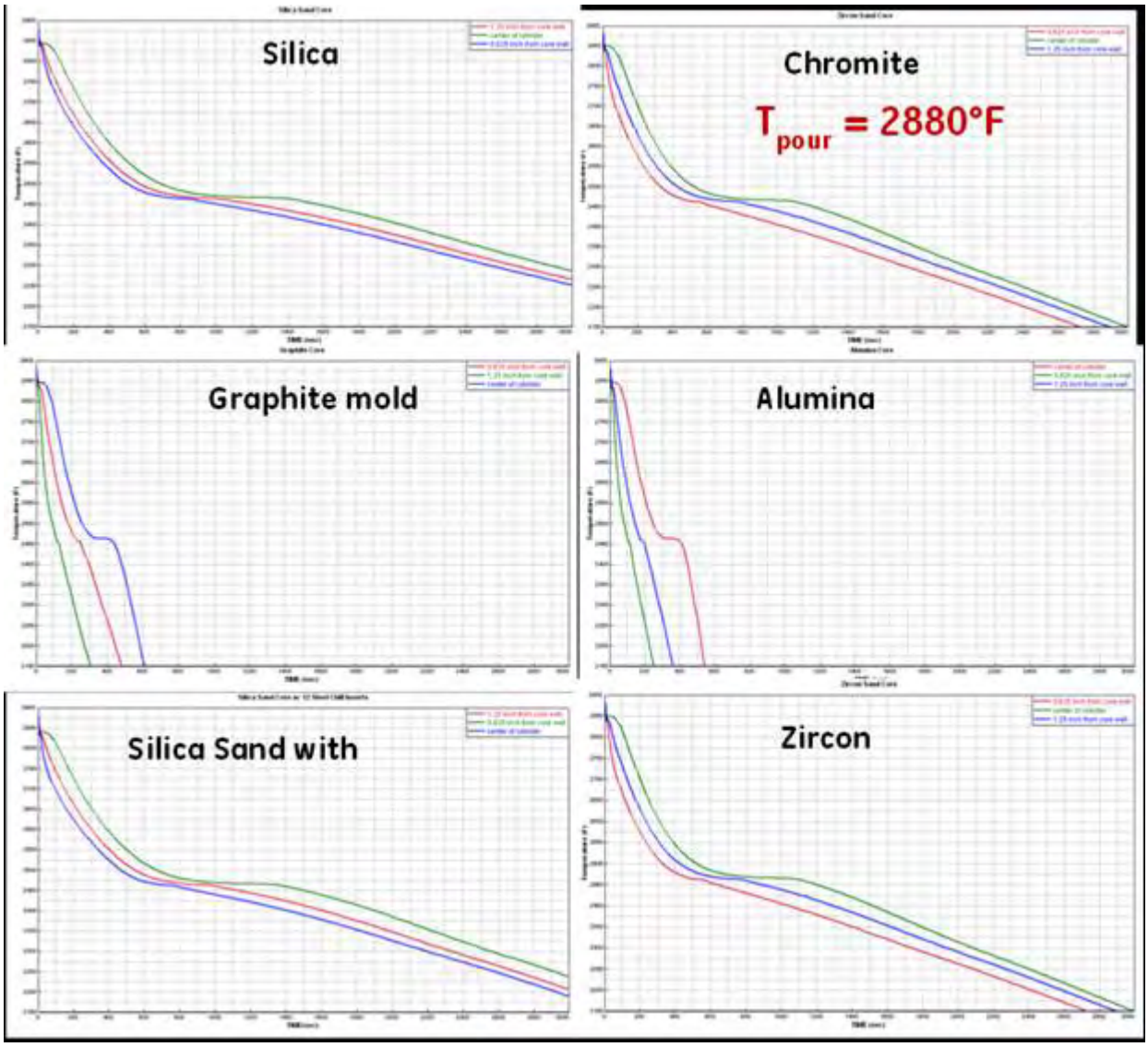

Figure 91: Casting Solidification Simulation Analysis cooling rates plot from pour to post solidification elevated temperature range for all the mold materials. Data from the 3 thermocouples T1, T2 and T3 vs. casting cooling time are plotted for different molds.

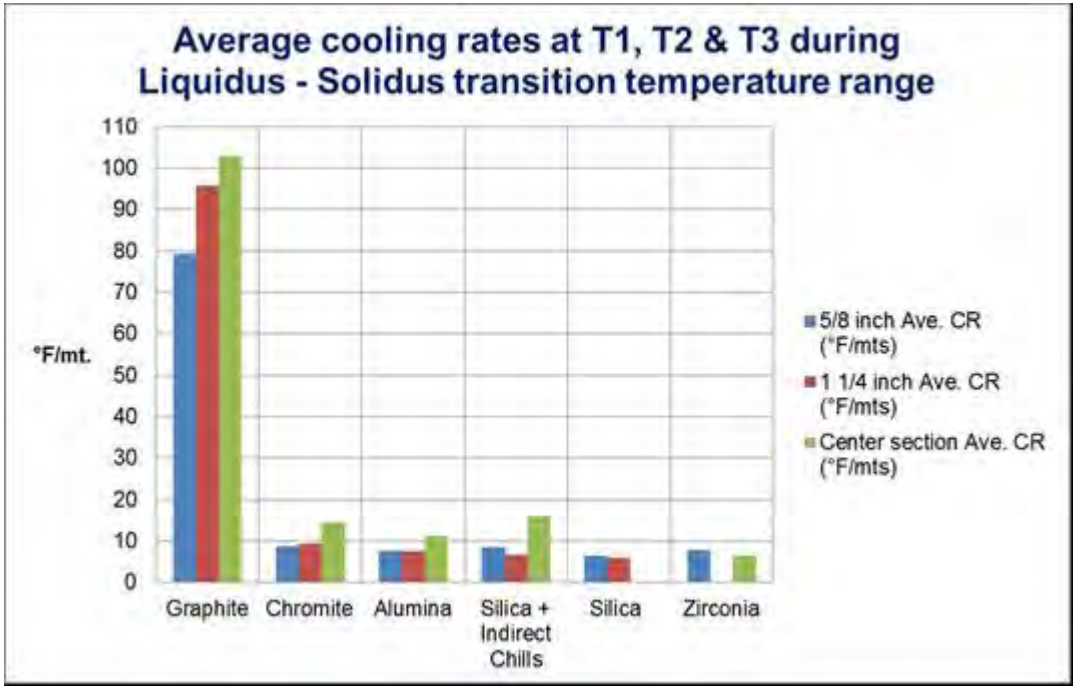

Figure 92: Haynes 282 Casting cooling rates during Liquidus to Solidus temperature range for different mold materials

Table 17: Casting cooling rates, both measured and simulated compared for different mold materials at 3 different locations within each mold

Mold material	5/8 inch Average CR (°F/minute)		1 1/4 inch Average CR (°F/minute)		Center Average CR (°F/minute)	
	Measured	Simulation	Measured	Simulation	Measured	Simulation
Graphite	79.3	100.16	95.74	62.82	102.86	41.44
Chromite	8.85	7.592	9.42	7.61	14.44	6.8
Silica + Indirect Chills	8.41	5.97	6.67	5.82	15.91	5.82
Silica	6.34	5.23	5.98	5.12	NA	5.09
Zirconia	7.73	7.46	NA	7.01	6.43	6.91

Table 18: Mold materials influence on microstructure SDAS values for Graphite, Zircon and Silica sand with indirect chills

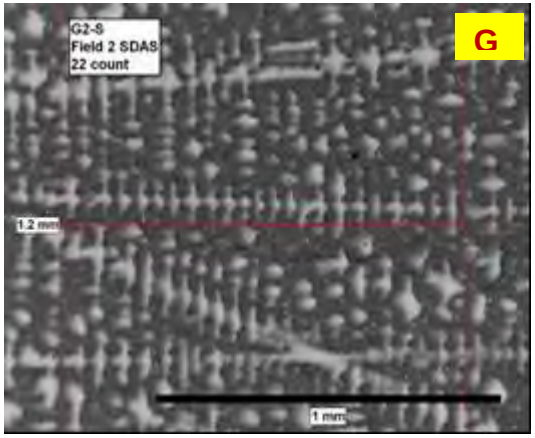

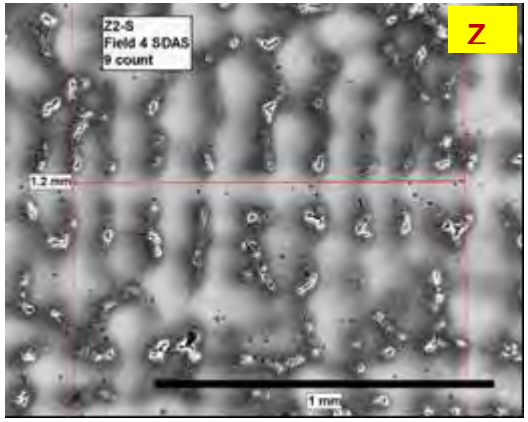

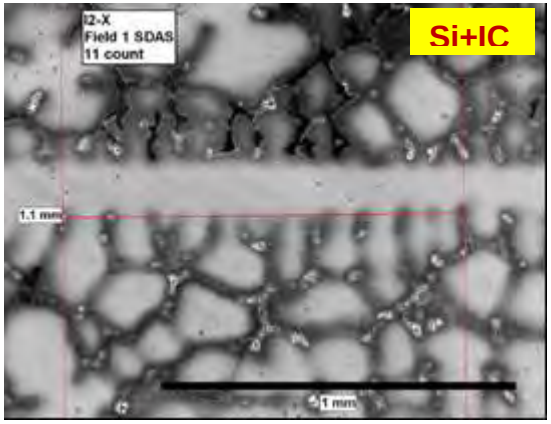

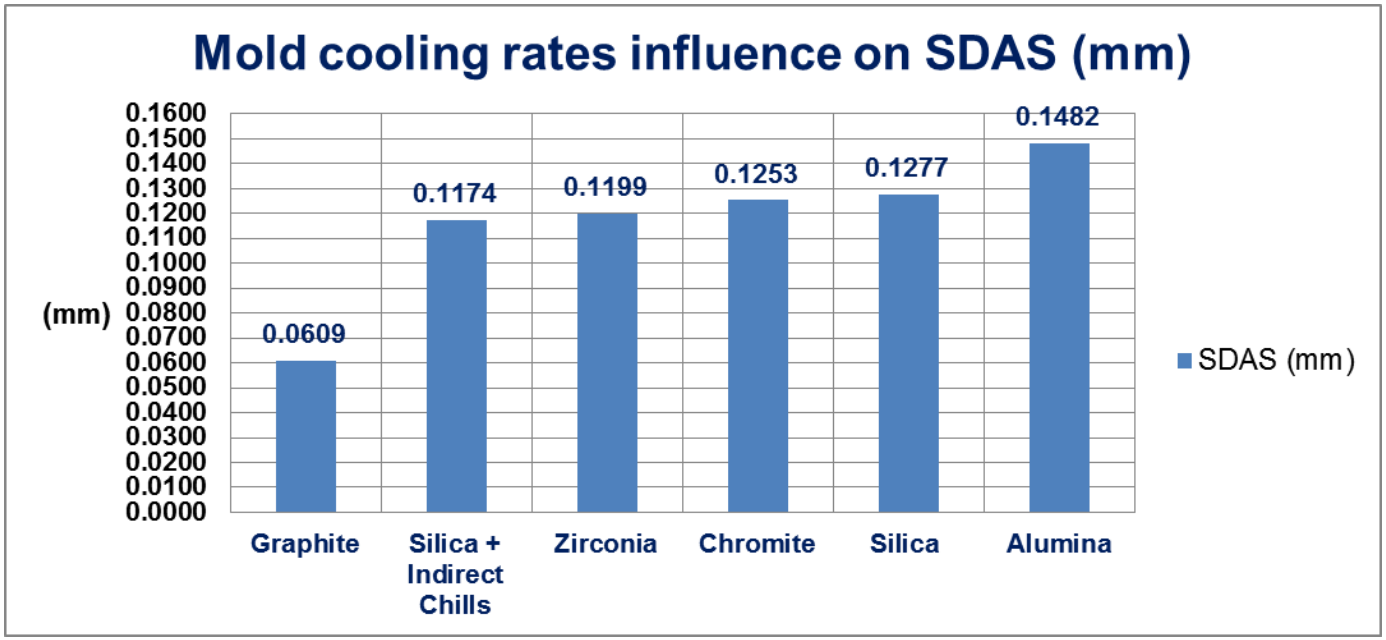

Figure 93: Mold cooling rates influence on SDAS values

Table 19: Mold materials influence on SDAS values through casting liquidus to solidus range cooling rates variation

Mold material	SDAS (mm)	SDAS Count #
Graphite	**0.0609**	**274**
Silica + Indirect Chills	0.1174	138
Zirconia	0.1199	146
Chromite	0.1253	128
Silica	0.1277	137
Alumina	0.1482	106

LARGE CASTING OF HAYNES 282

The key requisite for the success of the program was the need to demonstrate the successful scale up of the Haynes 282 for Steam Turbine Application large size castings. Hence the real need to resolve the scalability issue. GE Design engineering provided Production size prototype valve casing FEM model and drawings for this application.

As the original Valve body casting required 24,000 lbs., a partial casting was scheduled based on the available material for a pour weight of 17,000 lbs. Hence a partial valve casing was selected maintaining the actual cast dimensions, wall thicknesses inlet pipe dimensions and geometry. The gating was mimicked in such a way so that the solidification will be similar to an actual full size valve body. Engineering FEM models and supplemental requirements with applicable specifications provided to suppliers and discussed the casting quality acceptance criteria and NDT inspection requirements and key processing parameters.

Casting methods and process quality inspection plans were reviewed and FMEA carried out. FEM based Casting solidification simulation analysis test results reviewed [Figure 97 and Figure 98 and in Figure 110 for Niyama criteria] and casting methods validated prior to molding, melting and pouring. Haynes 282 valve casing was successfully cast after casting methods were validated and the casting met NDT inspection and acceptance criteria.

Heat treated and sectioned to extract trepan samples at different locations comparing with cast on coupons test data. The H282 casting sections and cast on coupons test matrix and specimen identification is provided in Table 20.

Material properties requisite for design, such as tensile, creep/rupture, LCF, Fracture Toughness, Charpy V-notch chemical analysis testing were carried out. The test results are presented in this report. The featured valve section model views and drawing reference were provided in the Appendix 1-F.

The prototype casting features are provided in Figure 94 and pattern and cope and drag mold views are provided in Figure 95 and Figure 96, with assembled mold, induction melting and pouring shown in Figure 99 - Figure 101. The casting pictures after mold shake out are shown in Figure 102.

The casting heat treat cycles per NETL recommendation and the Homogenizing and Aging HT cycles records are shown in Figure 103 - Figure 105 and are contained in Appendix 1-F.
The casting NDT inspection test results for 100% RT shown in Figure 106 and Figure 107 and 100% surface area Liquid Penetrant Testing are shown in Figure 108 and Figure 109.

The casting sections cast on coupons ID and the test matrix are provided in Table 20. The order to delivery casting manufacturing schedules are provided in Figure 129 and Figure 130. Typical time frame could be 55 weeks or better, depending on components design and upfront preparation as recommended in the review of learning for Comtest program speed up.

Additional details and the raw data obtained from the tests are contained in Appendix 1-F.

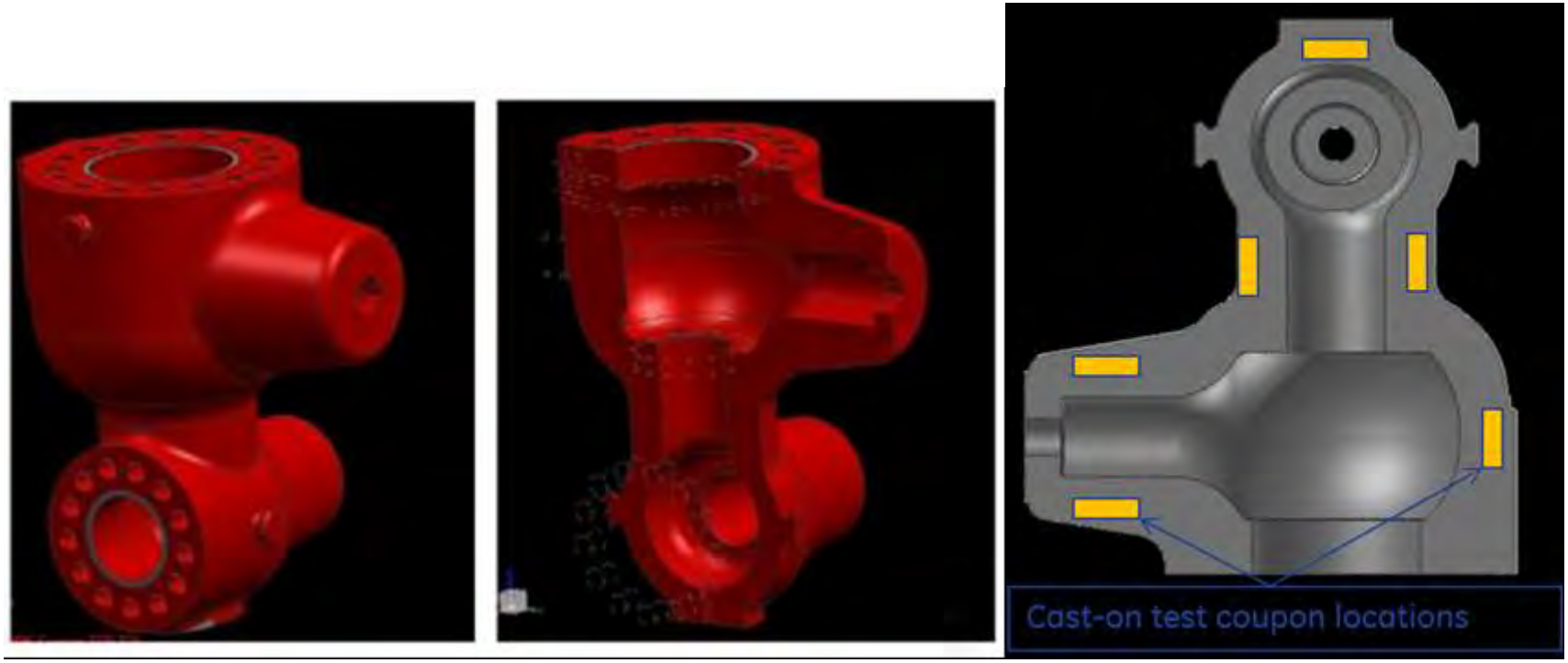

Figure 94: Steam turbine half valve casing selected for the large casting trial

Figure 95: Foundry Casting Pattern and feeder design

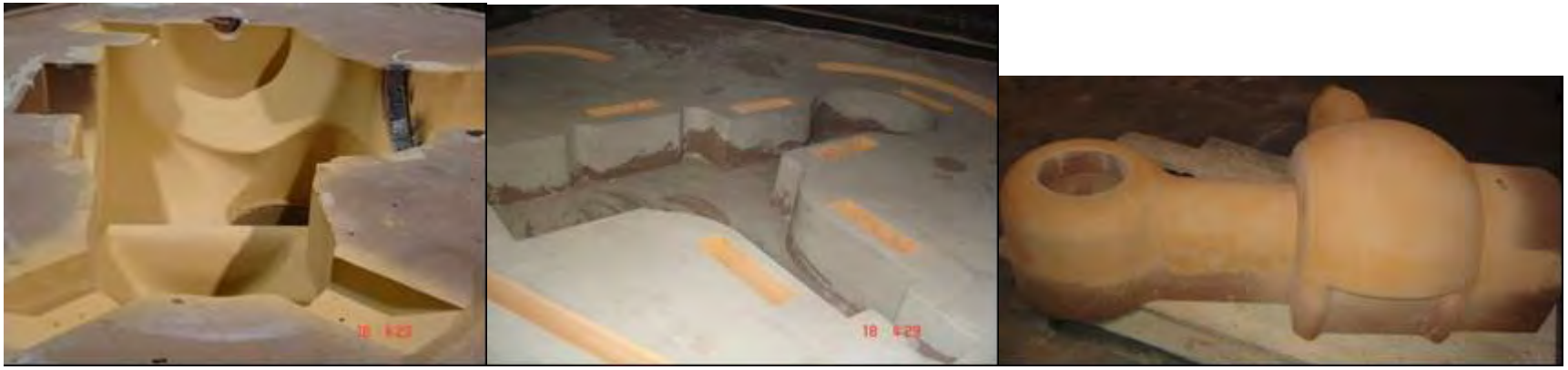

Figure 96: Picture showing Cope, drag molds and the valve body core after refractory coating and drying.

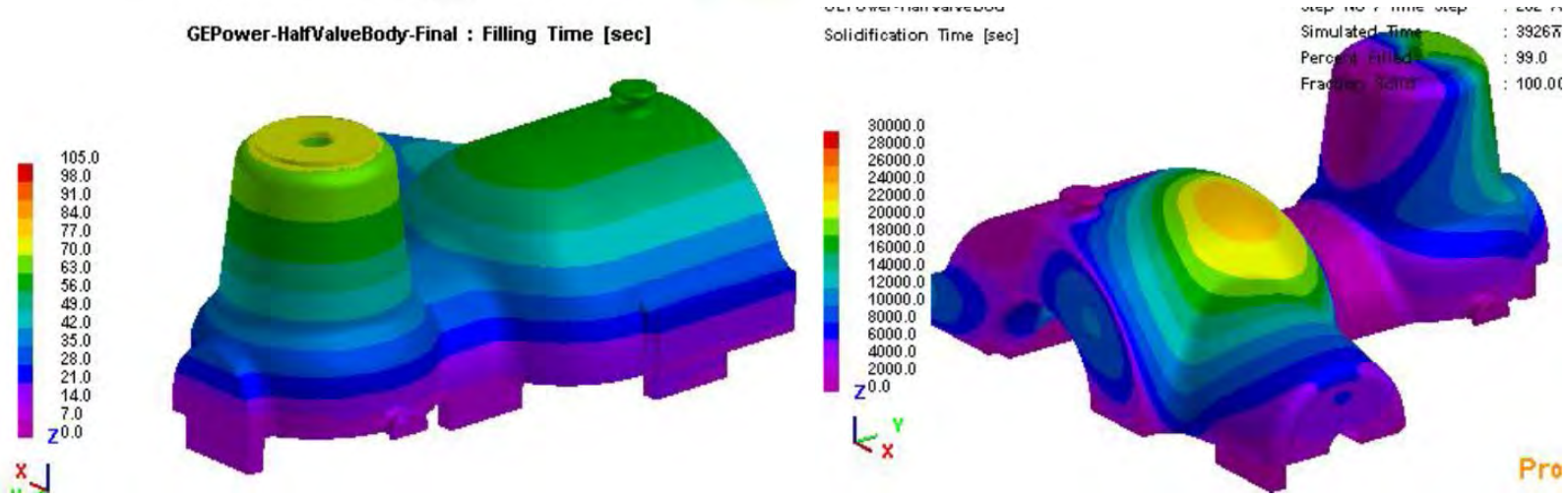

Figure 97: Solidification simulation indicates bottom to top filling (left) and temperature variation during liquidus to solidus transition temperature range (right)

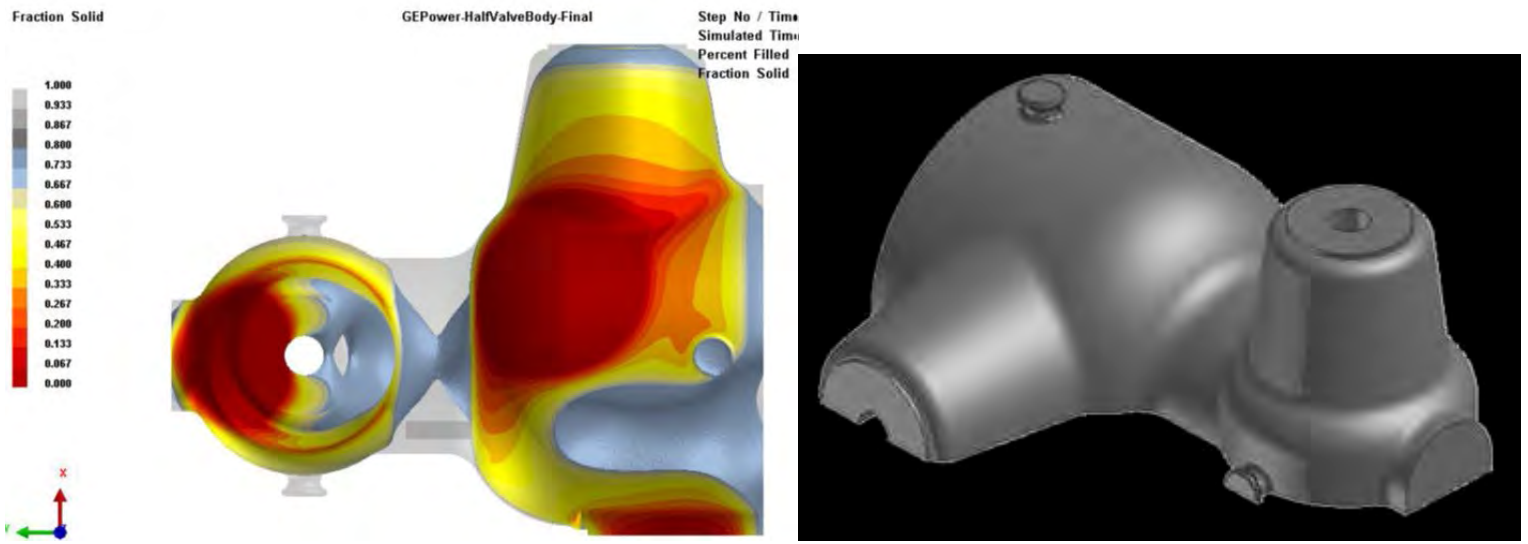

Figure 98: Solidification fraction solid cut off indicates no trail of shrinkage

Figure 99: Assembled mold, hot air dried and purged with Argon prior to pouring [Courtesy-MetalTek MO]

Figure 100: Induction melted, composition controlled with argon cover during melting and tapping melt quality controlled [Courtesy-MetalTek MO]

Figure 101: Pouring the mold after deslagging with covered ladles ensuring targeted pouring temperature and pour times

Figure 102: Casting after in mold cooling and shake out [Courtesy-MetalTek MO]

A. Homogenizing Heat Treatment Steps

- **Casting Preparation**: Coat all casting surfaces, including the cast on coupons with AO Smith CG-11 Ceram-Guard Coating or similar HT coat application.
- Part should be loaded into a room temperature furnace with **Contact thermocouples attached** for recording stepped Homogenization HT cycle. Along with Furnace thermocouples - HT cycle record required.

1. **Ramp furnace at a rate not exceeding 350^{0}F/Hour**
    - **Hold at 2040^{0}F ± 25^{0}F for 3 hours**
2. **Ramp furnace to 2130^{0}F**
    - **Hold at 2130^{0}F ± 10^{0}F for 3 hours**
3. **Ramp furnace to 2147^{0}F.**
    - **Hold at 2147^{0}F ± 10^{0}F for 3 hours**
4. **Ramp furnace to 2174°F**
    - **Hold at 2174^{0}F ± 10^{0}F for 8 hours**
5. **Ramp to 2205°F**
    - **Hold at 2205^{0}F ± 10^{0}F for 12 hours**
6. **Ramp to 2228°F**
    - **Hold at 2228^{0}F ± 10^{0}F for 24 hours**
7. **Ramp to 2237°F**
    - **Hold at 2237^{0}F ± 10^{0}F for 24 hours**

- **Forced Air Cool** to RT with fans, keeping contact thermocouples attached for measuring cooling rate

B. Double Age Heat Treatment Steps

1. **Ramp furnace to 1850°F at a rate not exceeding 350^{0}F/hour**
    - **Hold at 1850°F ± 10°F for 2 Hours**
2. **Forced air cool** with fans measuring cooling rate with contact thermocouples attached
3. **Ramp furnace to 1450°F**
    - **Hold at 1450°F ± 10°F for 8 Hours (plus add ½ hour for through heating)**

Still Air Cool to Room Temperature upon completion of the heat treatment measuring cooing rate with contact thermocouples attached

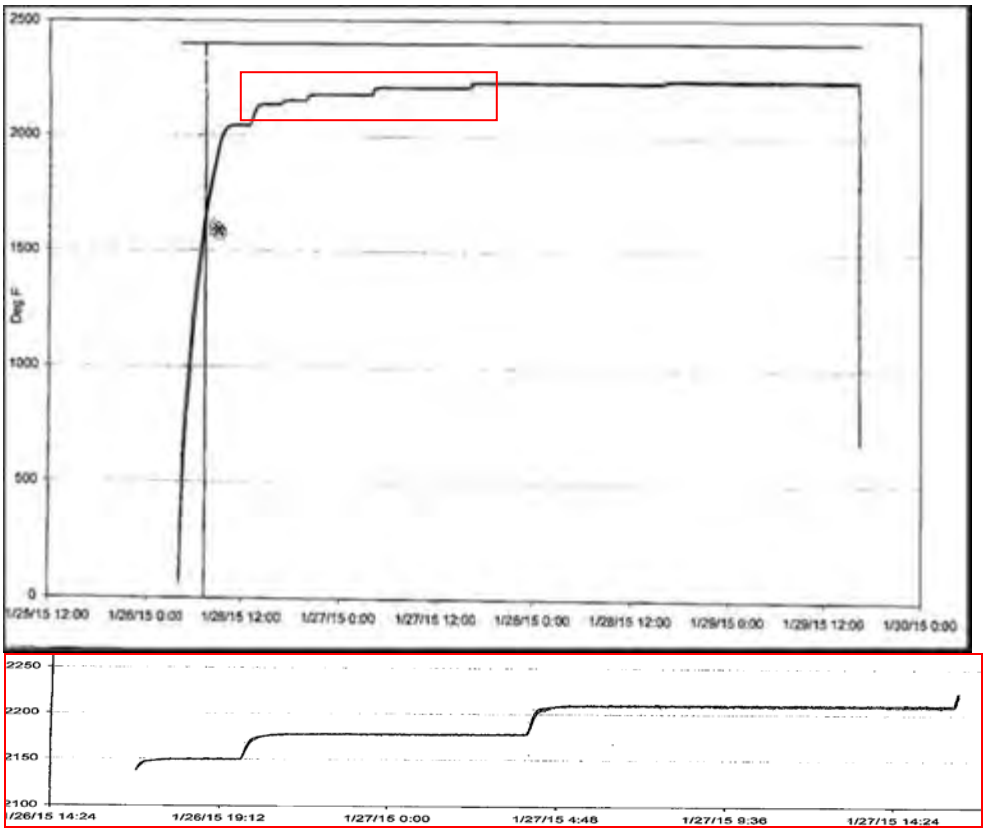

Figure 103: Homogenization HT cycle with insert HT step detailed view

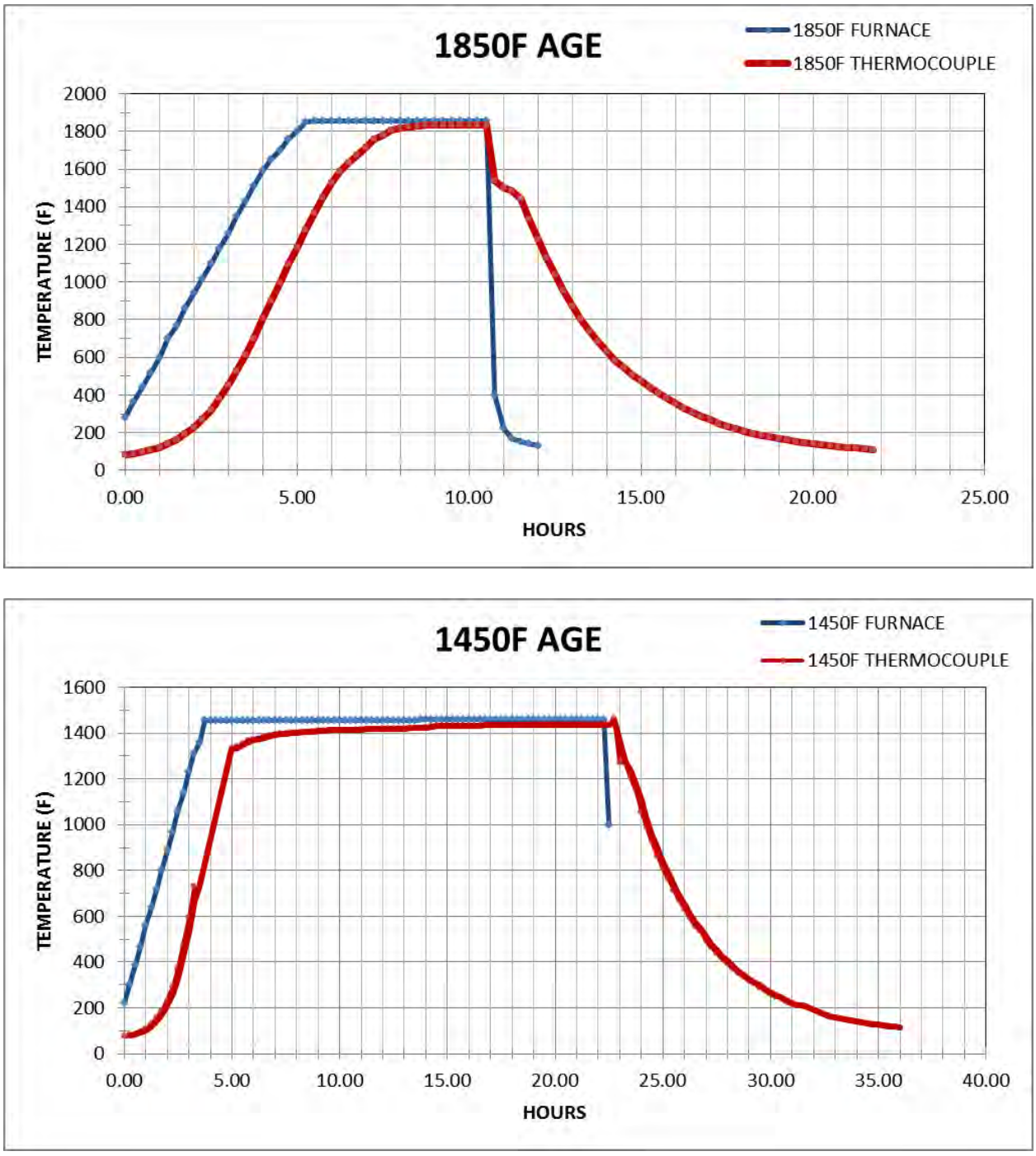

Figure 104: Two step Aging heat treat cycles thermocouple plot

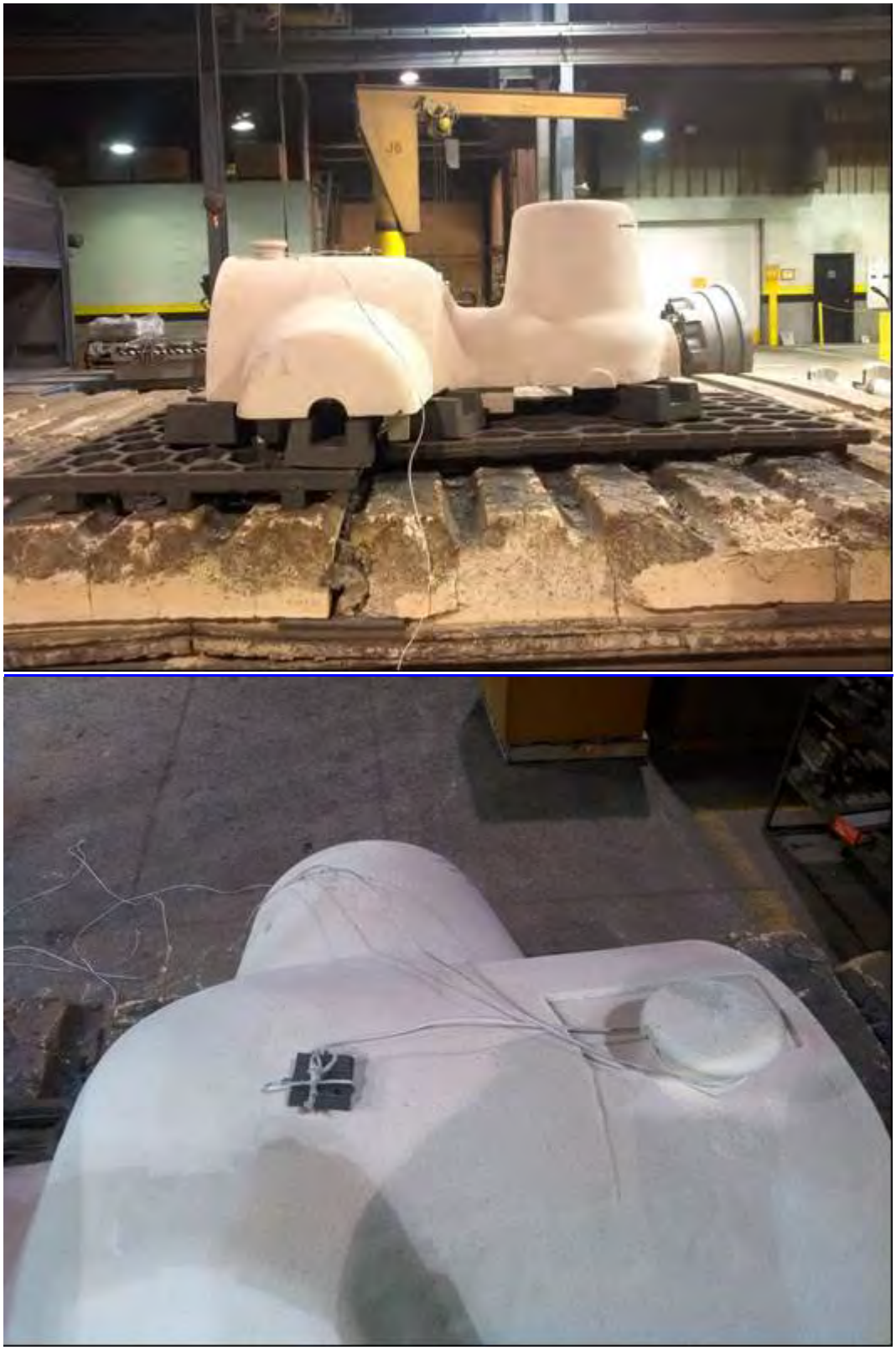

Figure 105: Thermocouples attached, coated for double Age heat treat cycle

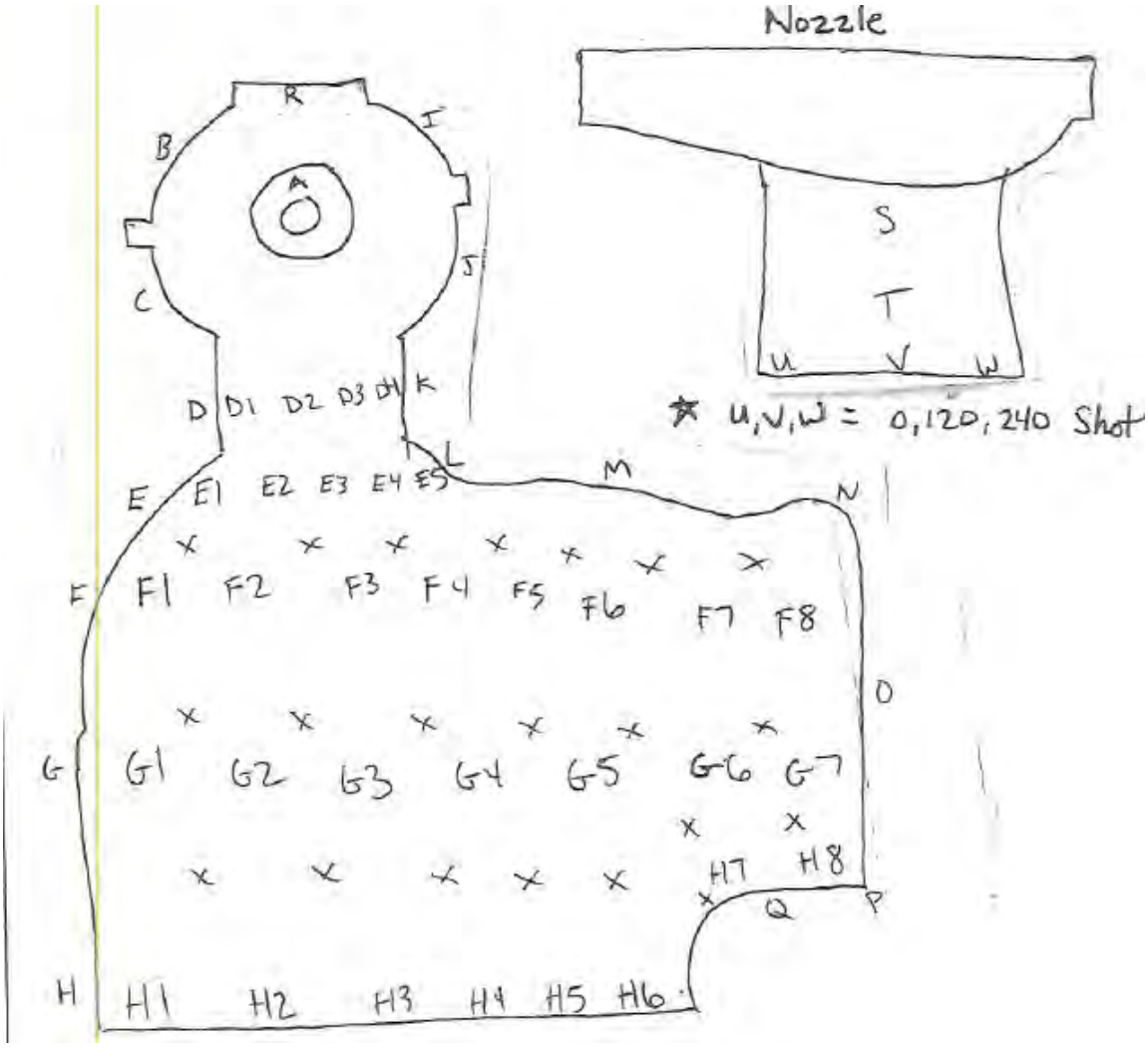

Figure 106: RT Scan sheet for the partial valve casing

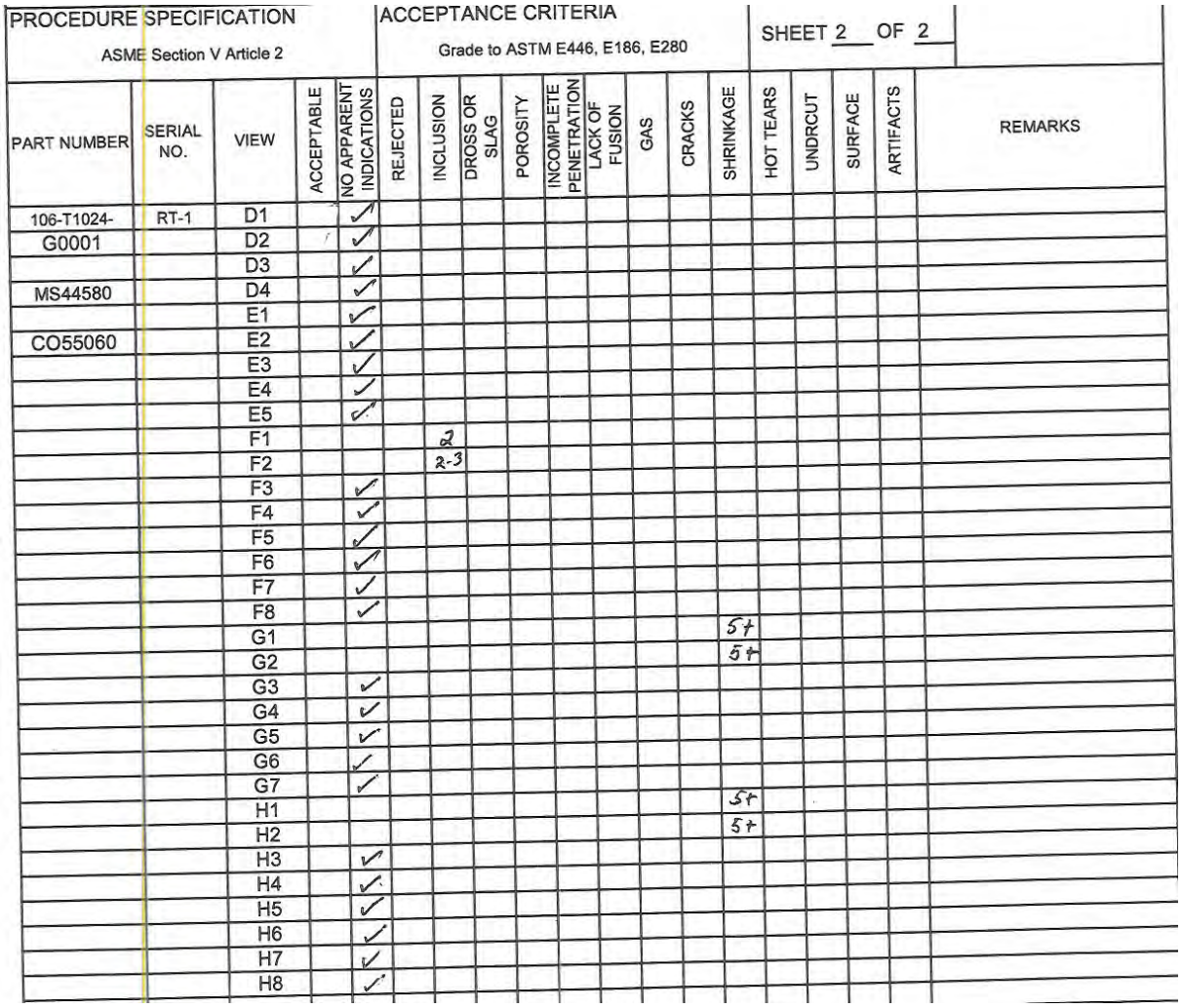

PROCEDURE SPECIFICATION: ASME Section V Article 2

ACCEPTANCE CRITERIA: Grade to ASTM E446, E186, E280

SHEET 2 OF 2

PART NUMBER	SERIAL NO.	VIEW	ACCEPTABLE	NO APPARENT INDICATIONS	REJECTED	INCLUSION	DROSS OR SLAG	POROSITY	INCOMPLETE PENETRATION	LACK OF FUSION	GAS	CRACKS	SHRINKAGE	HOT TEARS	UNDRCUT	SURFACE	ARTIFACTS	REMARKS
106-T1024-	RT-1	D1		✓														
G0001		D2		✓														
		D3		✓														
MS44580		D4		✓														
		E1		✓														
CO55060		E2		✓														
		E3		✓														
		E4		✓														
		E5		✓														
		F1				2												
		F2				2-3												
		F3		✓														
		F4		✓														
		F5		✓														
		F6		✓														
		F7		✓														
		F8		✓														
		G1											5+					
		G2											5+					
		G3		✓														
		G4		✓														
		G5		✓														
		G6		✓														
		G7		✓														
		H1											5+					
		H2											5+					
		H3		✓														
		H4		✓														
		H5		✓														
		H6		✓														
		H7		✓														
		H8		✓														

Figure 107: RT Inspection report for the H282 valve casing

Figure 108: Haynes 282 Valve casing Liquid penetrant testing 100% surface area.

The six cast on coupons, attached to the casting wall mid sections are shown in Figures 108 and 109.

Figure 109: LPT inspection pictures on 100 % Cast surface areas

Two of the cast on coupons were later sectioned and evaluated to determine as cast dendritic arm spacing, SDAS values for solutionizing and aging heat treat cycles determination.

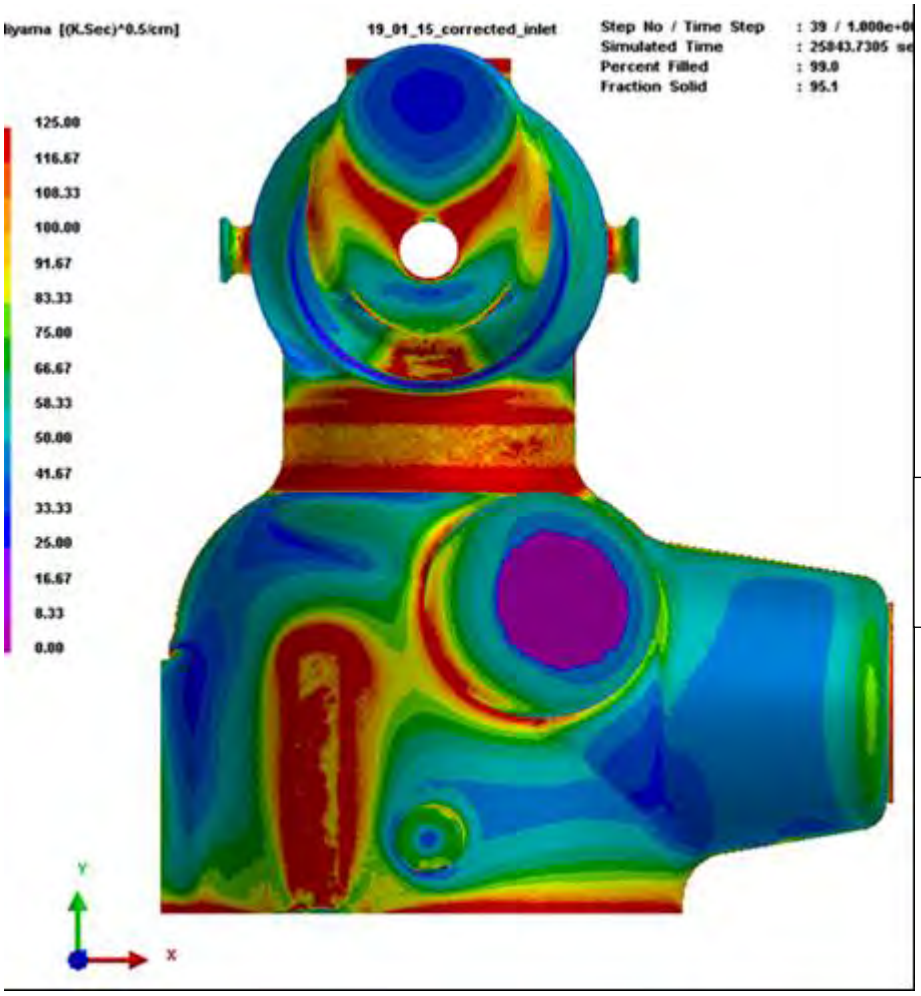

$$Ny = \frac{G}{\sqrt{\dot{T}}}$$

Figure 110: Niyama criteria per solidification simulation analysis. Niyama indicates potential feeding difficulty zones in the casting with lower (Nẏ) values. This plot is primarily used to avoid sectioning through potential zones for micro shrinkage

Table 20: H282 casting sections and cast on coupons test matrix and specimens identification

Haynes 282 casting test matrix:					Specimens Identification (ID)							
Test #	Test Type	Test condition	Step sections	Total Tests	Cast-on coupon ID (*1)		Cast Sections ID (*2)					
		Temperature deg.F			CA	CC	H	D	B	C	E	K
1	Tensile Test (UTS, 0.2% & 0.02% YS, % EL, %RA) Tensile Specimen: MPE-TNSL-001 P4 36 specimens	RT/ 75 deg. F	1 Test/section in CL plane	6	CA-T-75	CC-T-75	HT-75	DT-75	BT-75	CT-75		
		500 deg. F		6	CA-T-500	CC-T-500	HT-500	DT-500	BT-500	CT-500		
		1000 deg.F		6	CA-T-1000	CC-T-1000	HT-1000	DT-1000	BT-1000	CT-1000		
		1250 deg.F		6	CA-T-1250	CC-T-1250	HT-1250	DT-1250	BT-1250	CT-1250		
		1400 deg.F		6	CA-T-1400	CC-T-1400	HT-1400	DT-1400	BT-1400	CT-1400		
		1500 deg F		6	CA-T-1500	CC-T-1500	HT-1500	DT-1500	BT-1500	CT-1500		
2	Charpy V Notch Impact Impact Energy (J); % Shear, Lateral Expansion 12 Specimens	RT/ 75 deg F	2 Tests per section	6	CB-CV-1	CD-CV-1	H-CV-01	D-CV-01	B-CV-01			K-CV-01
				6	CB-CV-2	CD-CV-2	H-CV-02	D-CV-02	B-CV-02			K-CV-02
		A strain / TSR (%)			CB	CD	H	D	B	C	E	J
3	LCF Data Frequency: 20 cpm Waveform: Triangular A Strain 1, TSR% (1.0; 0.90; 0.80; 0.70; 0.60; 0.50) 2 temperatures: RT & 1400 deg. F. Specimen Drg. # 4013195-741 48 specimens	RT/ 75 deg F	1 / 1.00	4	CB-LCF-01	CD-LCF-01		D-LCF-01			E-LCF-01	
			1 / 0.90	4	CB-LCF-02	CD-LCF-02		D-LCF-02			E-LCF-02	
			1 / 0.80	4	CB-LCF-03	CD-LCF-03		D-LCF-03			E-LCF-03	
			1 / 0.70	4	CB-LCF-04	CD-LCF-04		D-LCF-04			E-LCF-04	
			1 / 0.60	4	CB-LCF-05	CD-LCF-05		D-LCF-05			E-LCF-05	
			1 / 0.50	4	CB-LCF-06	CD-LCF-06		D-LCF-06			E-LCF-06	
		1400 deg F	1 / 1.00	4		CD-LCF-07		D-LCF-07	B-LCF-07	C-LCF-07		
			1 / 0.90	4		CD-LCF-08		D-LCF-08	B-LCF-08	C-LCF-08		
			1 / 0.80	4		CD-LCF-09		D-LCF-09	B-LCF-09	C-LCF-09		
			1 / 0.70	4		CD-LCF-10		D-LCF-10	B-LCF-10	C-LCF-10		
			1 / 0.60	4		CD-LCF-11		D-LCF-11	B-LCF-11	C-LCF-11		
			1 / 0.50	4		CD-LCF-12		D-LCF-12	B-LCF-12	C-LCF-12		
4	Stress rupture Specimen per MPE-RUP 003-P3 12 specimens Creep data required	Temperature deg.F	Stress (ksi)			CC	H		B		E	
		1450	37.5	1			H-SR-01					
		1400	45.0	1			H-SR-02					
		1300	67.5	1			H-SR-03					
		1450	35.0	1					B-SR-01			
		1400	42.5	1					B-SR-02			
		1300	62.5	1					B-SR-03			
		1450	40.0	1		CC-SR-01						
		1400	47.5	1		CC-SR-02						
		1300	70.0	1		CC-SR-03						
		1450	33.5	1							E-SR-01	
		1400	40.0	1							E-SR-02	
		1300	58.0	1							E-SR-03	
5	Fracture Toughness Specimen per # 8024 ASTM E1820-11 Kq; J1C -16 specimens	RT/ 75 deg. F		4		CD-Kq-01		D-KQ-01	B-Kq-01			J-Kq-01
		1000 deg.F		4		CD-Kq-02		D-KQ-02	B-Kq-02			J-Kq-02
		1300 deg.F		4		CD-Kq-03		D-KQ-03	B-Kq-03			J-Kq-03
		1400 deg F		4		CD-Kq-04		D-KQ-04	B-Kq-04			J-Kq-04
6	Chemical Analysis 8 Specimens	Ni,Cr,Co,Mo,Ti,Al,Fe, Mn,Si,C,B,P,S, Cu, Co,Nb, W, Zr, N(ppm), O (ppm)	Thermal Center	1 test section	CA	CD	H	D	B			K

Table 21 Valve casing cast on coupons and casting trepan sections chemical analysis tabulation

Valve Casing Casting-Trepan Sample Chemical Analysis							
By Weight [%]	Appended Cast on Coupons		Chilled Section	Cast Section Trepan Samples Chemical Analysis			
Element (%)	CA	CD	D	H	B	K	E
Carbon	0.08	0.09	0.07	0.06	0.06	0.12	0.06
Manganese	0.04	0.04	0.04	0.04	0.04	0.04	0.03
Iron	0.25	0.56	0.3	0.28	0.26	0.28	0.21
Sulfur	0.002	0.002	0.002	0.002	0.002	0.003	0.001
Silicon	0.25	0.19	0.25	0.25	0.25	0.27	0.32
Copper	0.01	0.01	0.01	0.01	0.01	0.01	0.01
Nickel	REM	REM	REM	REM	REM	REM	REM
Chromium	19.17	19.49	19.47	19.54	19.38	19.3	18.48
Aluminum	1.51	1.51	1.5	1.53	1.53	1.53	1.52
Titanium	2.39	2.36	2.49	2.38	2.41	2.43	2.33
Cobalt	10.02	10.08	9.92	10	9.91	9.94	10.03
Molybdenum	8.37	8.22	8.43	8.12	8.31	8.41	8.43
Niobium	0.05	0.06	0.05	0.05	0.05	0.05	0.05
Phosphorus	<0.01	<0.01	<0.01	<0.01	<0.01	<0.01	<0.01
Tungsten	<0.06	<0.06	<0.06	<0.06	<0.06	<0.06	<0.10
Zirconium	0.02	0.02	0.02	0.02	0.02	0.02	0.02
Boron	0.005	0.005	0.005	0.005	0.005	0.005	0.006
Nitrogen	87 ppm	116 ppm	127 ppm	53 ppm	116 ppm	75 ppm	118 ppm
Oxygen	21 ppm	19 ppm	22 ppm	18 ppm	24 ppm	24 ppm	30 ppm

Table 21 clearly shows no significant variation in cast section trepan samples chemical analysis.

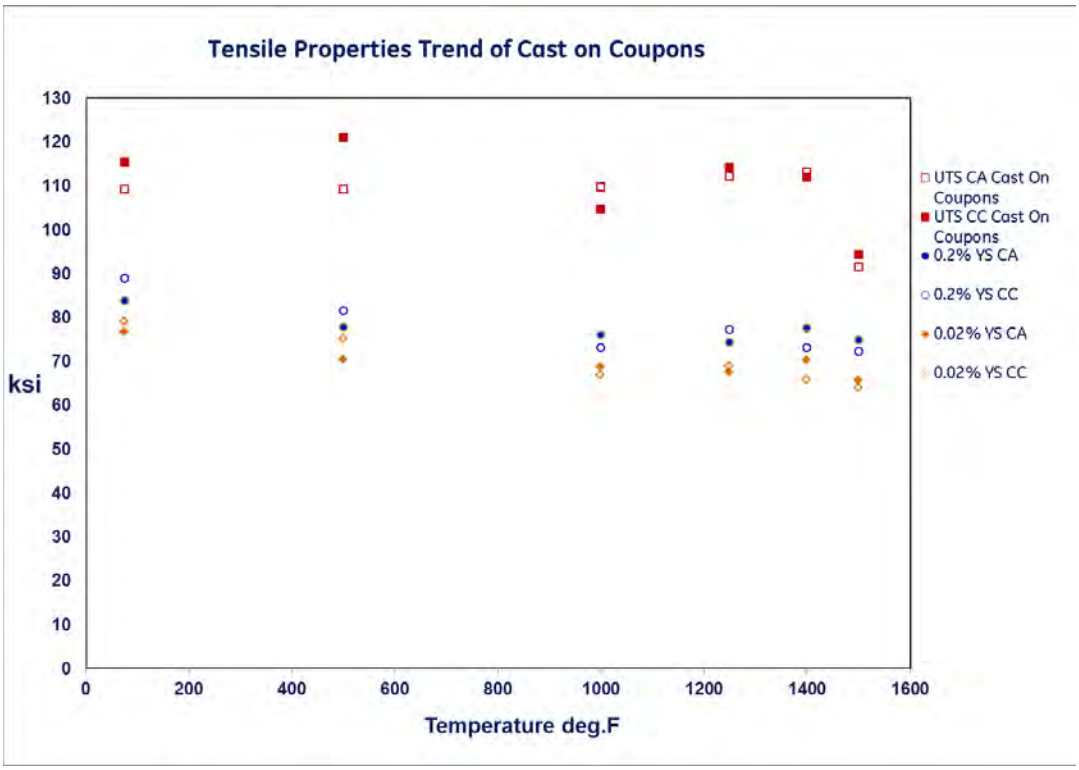

Figure 111 : Cast on coupons tensile properties UTS, 0.2% YS and 0.02% YS values with temperature indicate tighter band for the yield strength values for the temperature range.

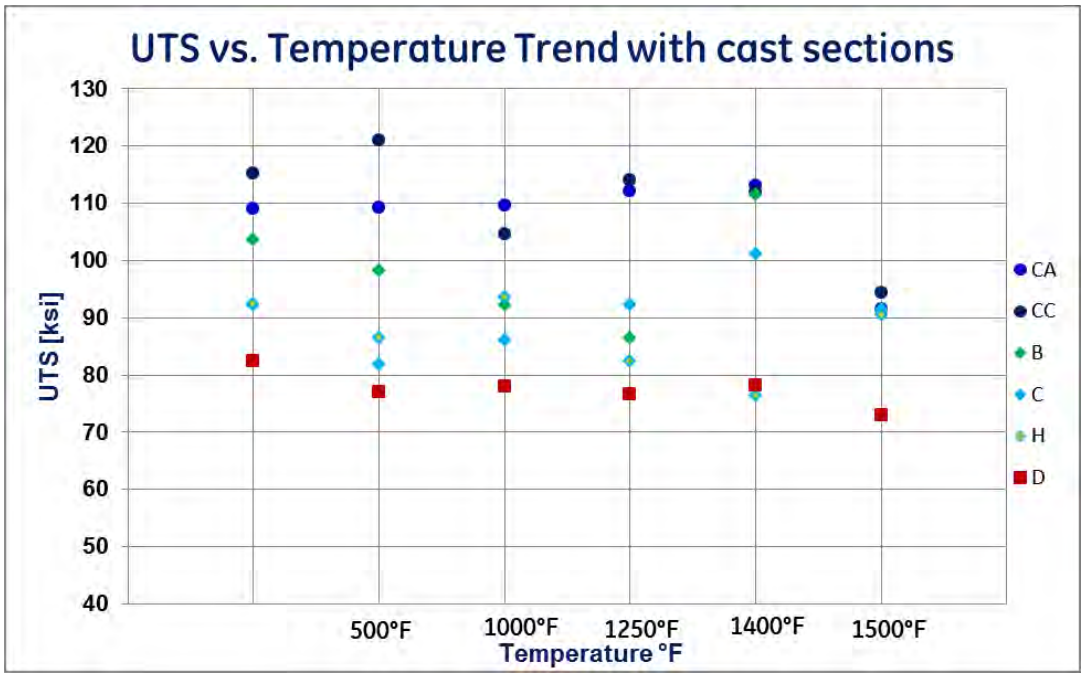

Figure 112 : UTS trend with temperature for all cast sections, trepans and chilled cast sections compared. Chilled cast section indicates lower tensile properties.

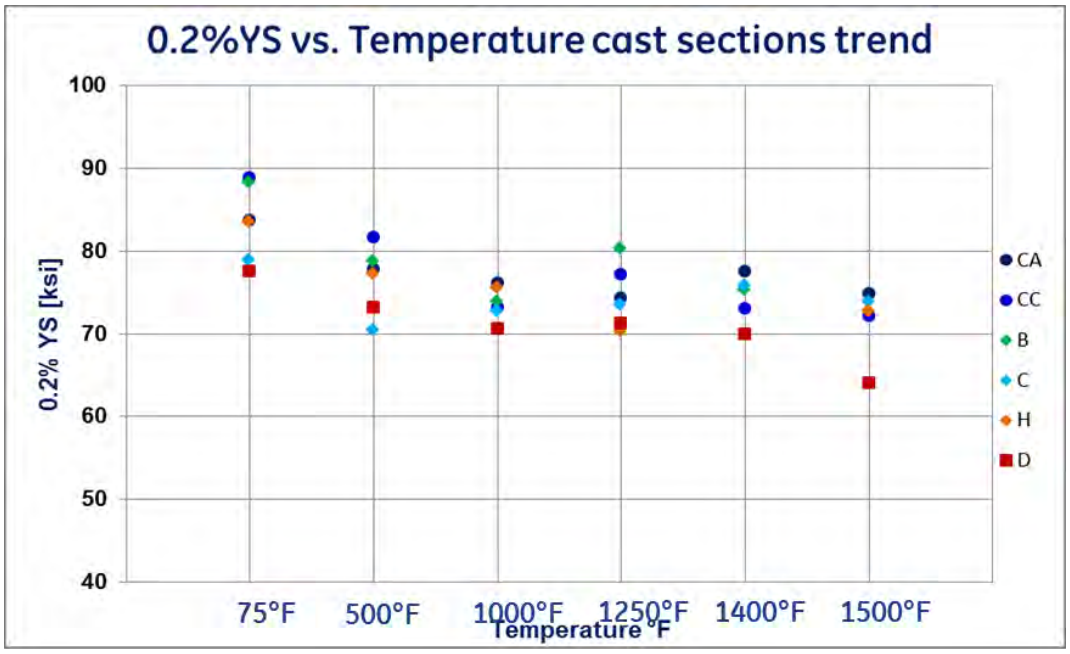

Figure 113 : 0.2% YS for cast on coupons indicate higher yield strength values in comparison with chilled cast sections. 0.2% YS values are fairly in tight range.

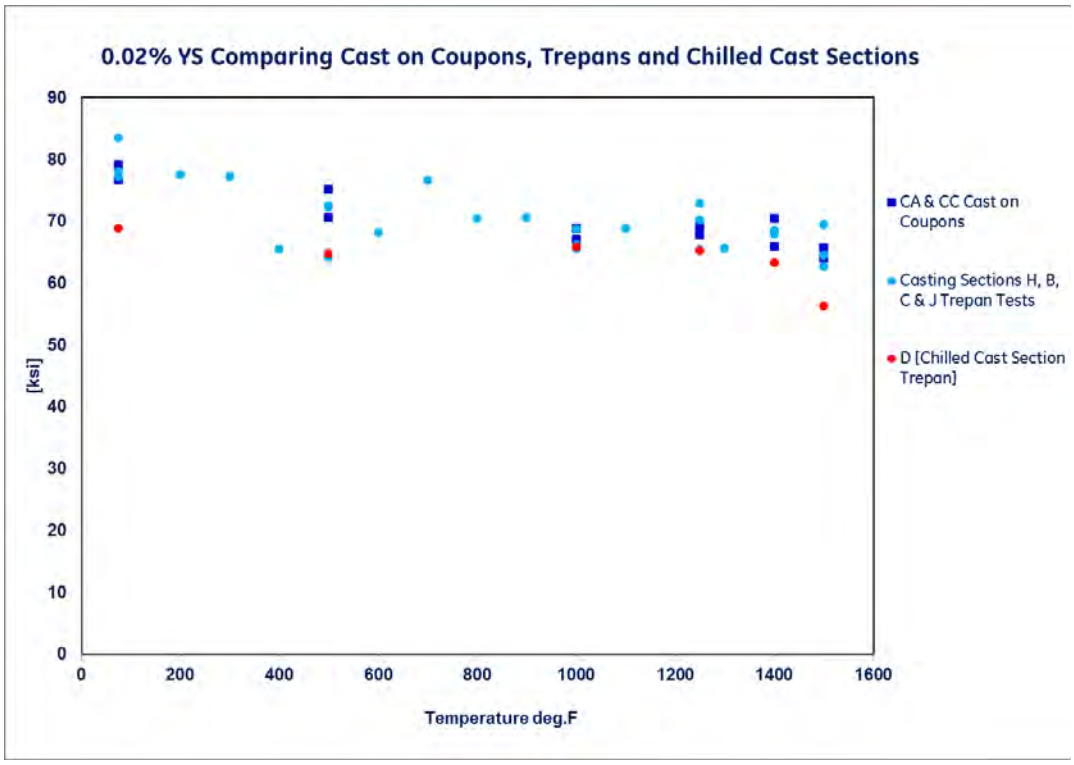

Figure 114 : 0.02% YS values trend cast on coupons, trepan sections and chilled cast sections with temperature

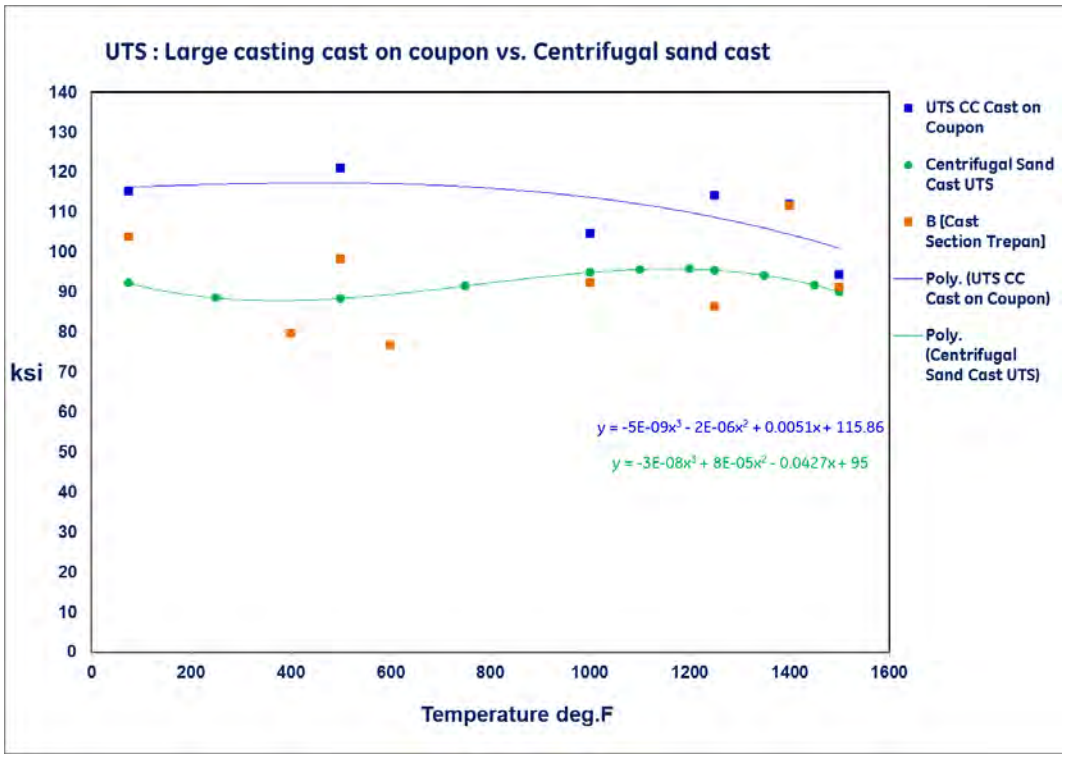

Figure 115 : Cast on coupon UTS trend compared with Centrifugal and sand cast trepan tensile values over the temperature range. Cast on coupons UTS values are higher compared with Centrifugal cast tensile properties.

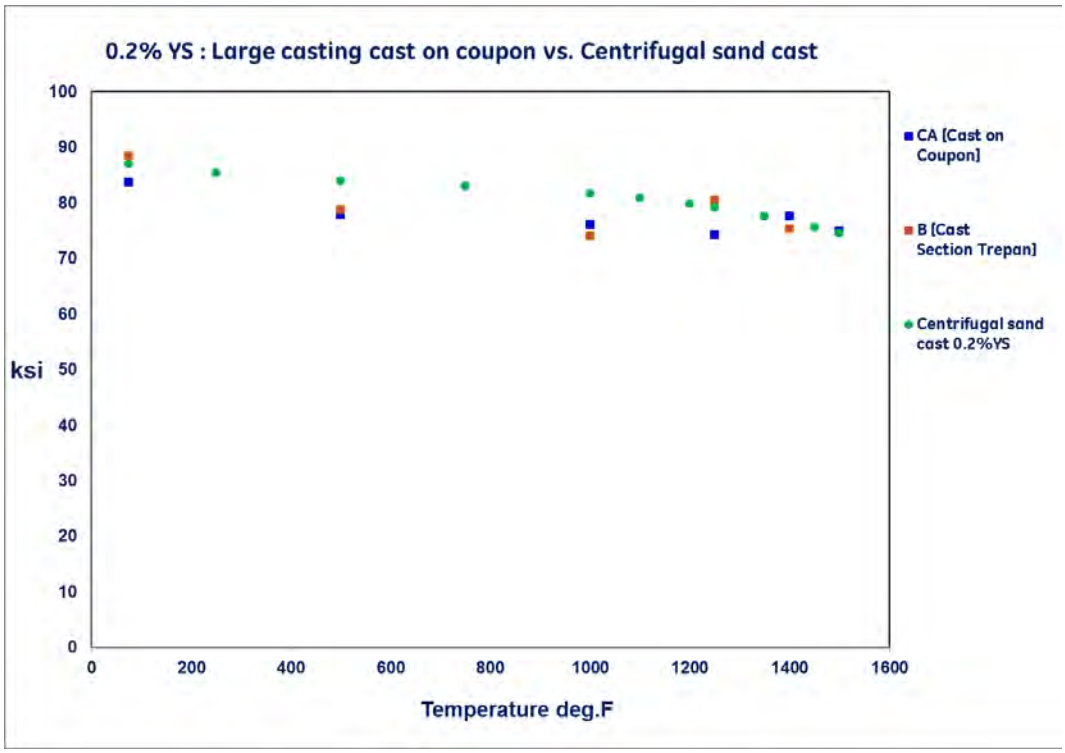

Figure 116 : 0.2% YS values show similar range for sand cast and centrifugal castings

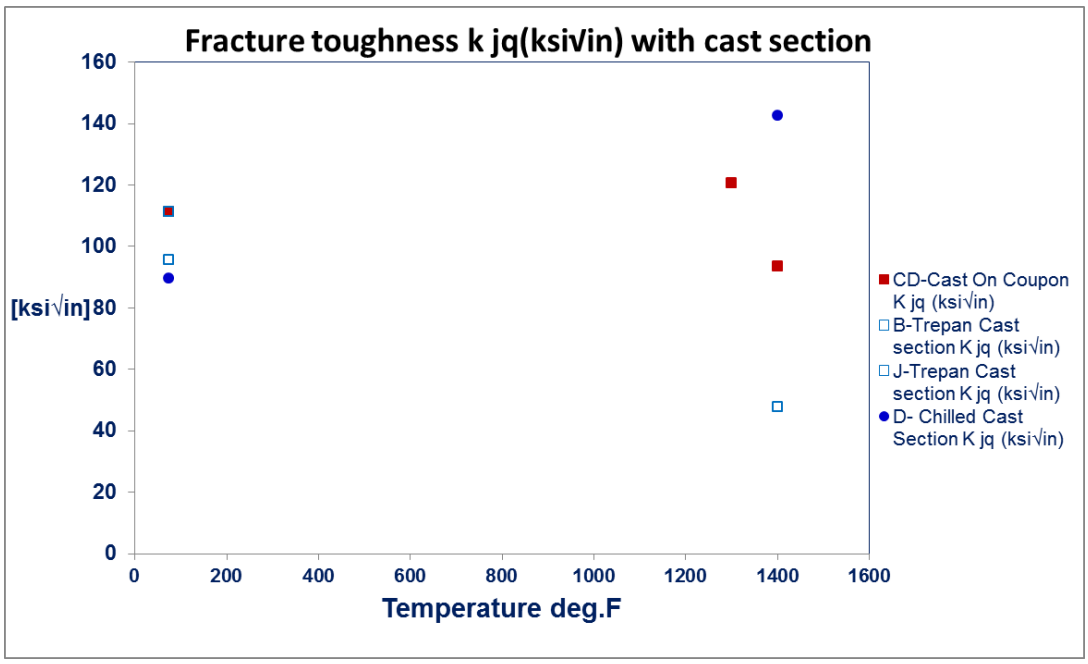

Figure 117 : Fracture toughness Kjq shows cast on coupons, and Chilled sections have higher values compared with trepan section values at higher temperatures

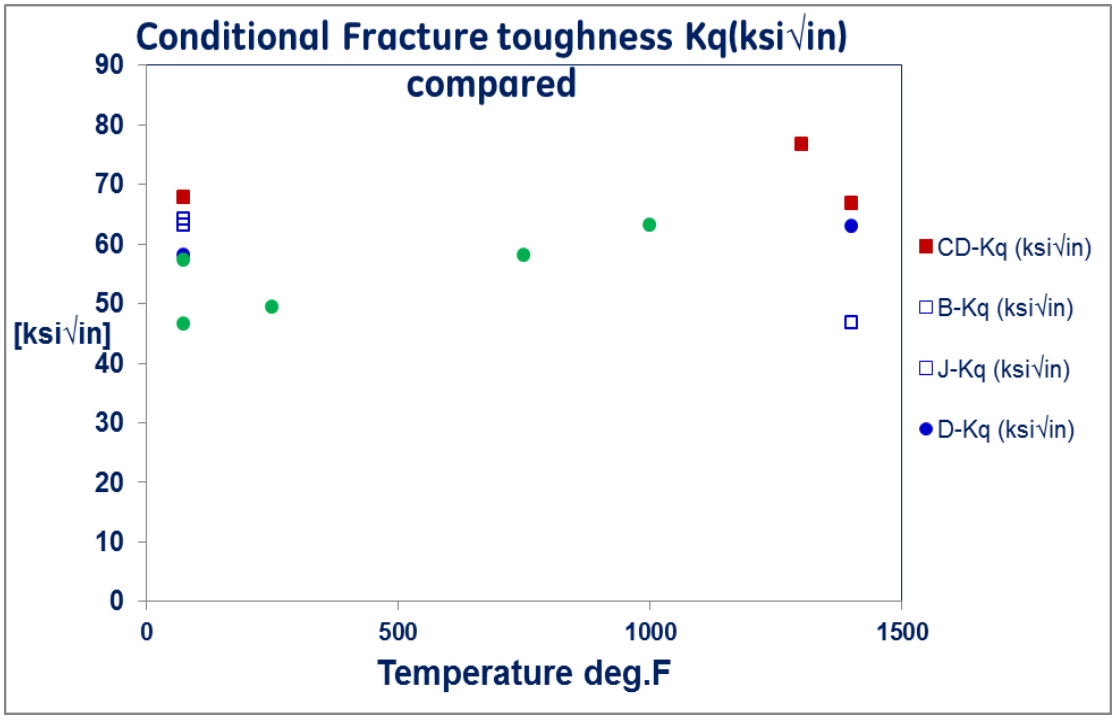

Figure 118 : Conditional Fracture toughness Kq for centrifugal cast indicate, cast on coupons show higher values, however are comparable with sand cast trepan samples

Eight CT specimens were extracted from cast on coupons, section trepans for J-Integral fracture toughness testing per ASTM E1820-11. Specimens were machined to a nominal width measuring 1.60 in, fatigue precracked to a final (a/W) of 0.50 and side grooved to a depth equal to 20% of the nominal thickness [10% per side].

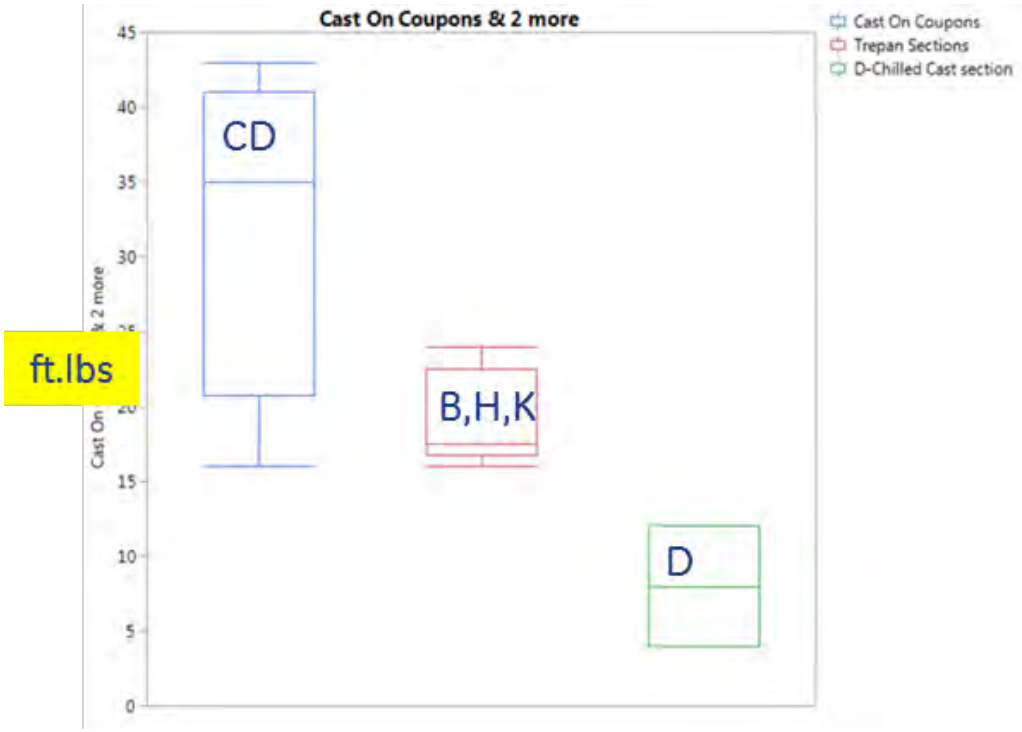

Figure 119 : Charpy impact values comparing cast on coupons [CD] Section trepans [B,H,K] and Chilled cast section [D].

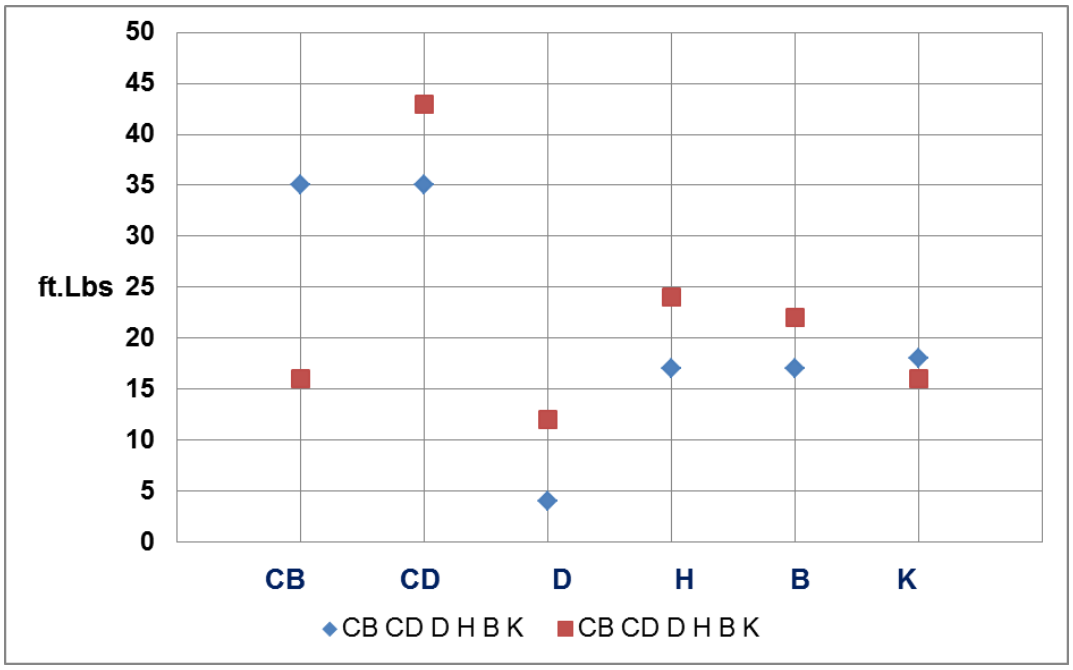

Figure 120: cast on coupons have higher Charpy impact energy values compared with chilled cast section trepans [D]. Charpy V notch testing as per ASTM E23-12c at RT.

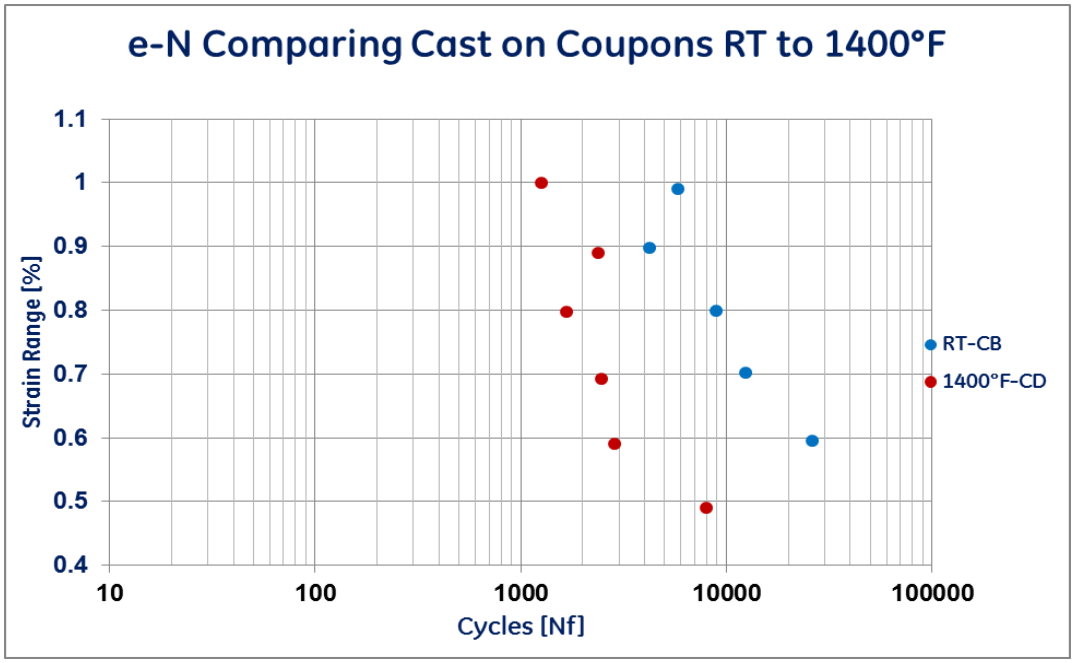

Figure 121 : LCF plot comparing Cast on coupons at RT and 1400° F, Nf cycles to failure

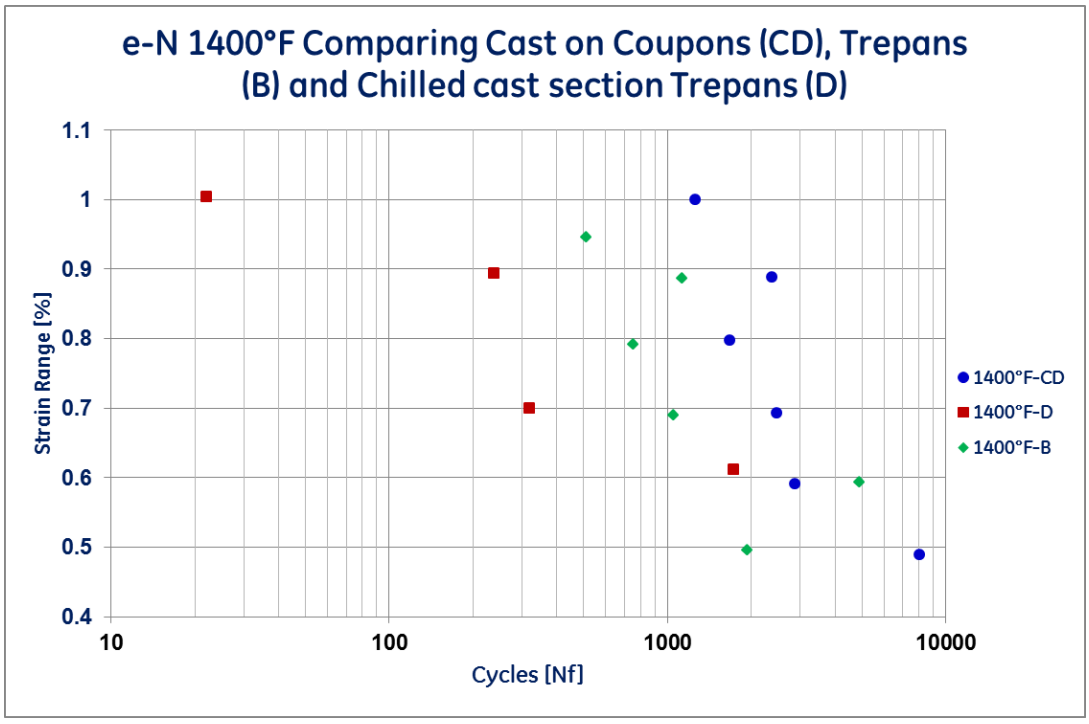

Figure 122 : Cast on coupons, trepans and chilled section, e-Nf cycles to failure plot for 1400°F

Cast on coupon LCF properties at RT and 1400°F performing better than chilled cast section trepan samples. LCF specimens trepanned from cast sections were tested at RT and at 1400°F using triangular wave form with a frequency of 20cpm. Specimens were tested with an A-ratio of +1. Tested per ASTM E 606-12. The raw data from the tests are contained in Appendix 1-F.

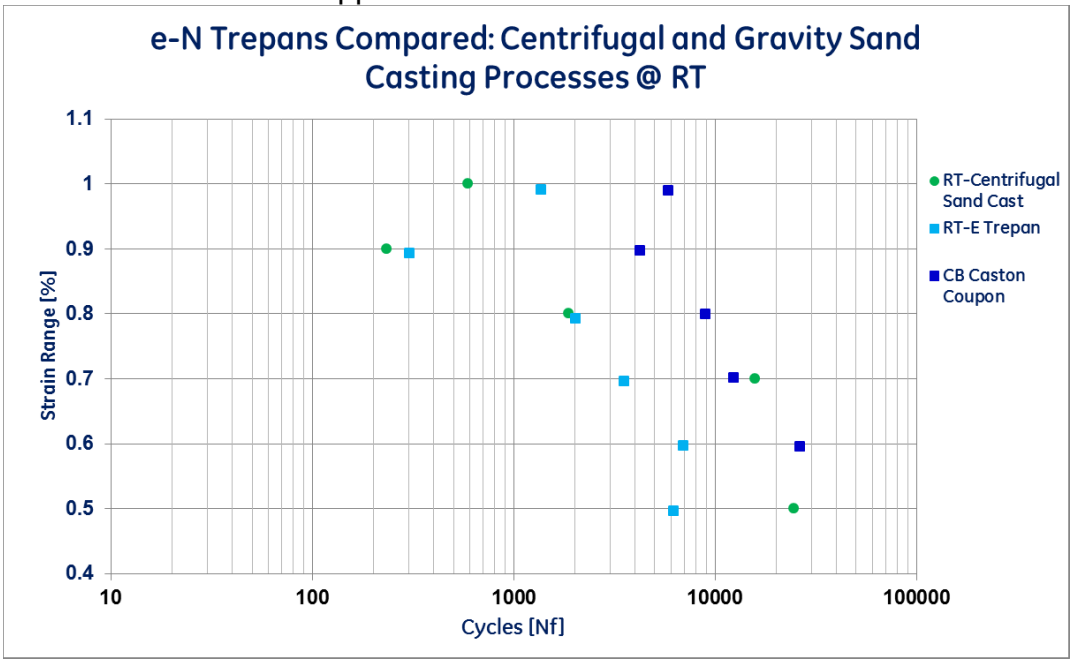

Figure 123 : e-N plot at RT comparing sand cast and centrifugal cast H282 Nf cycles to failure. Sand cast trepan and centrifugal cast sections are in similar rang**e**

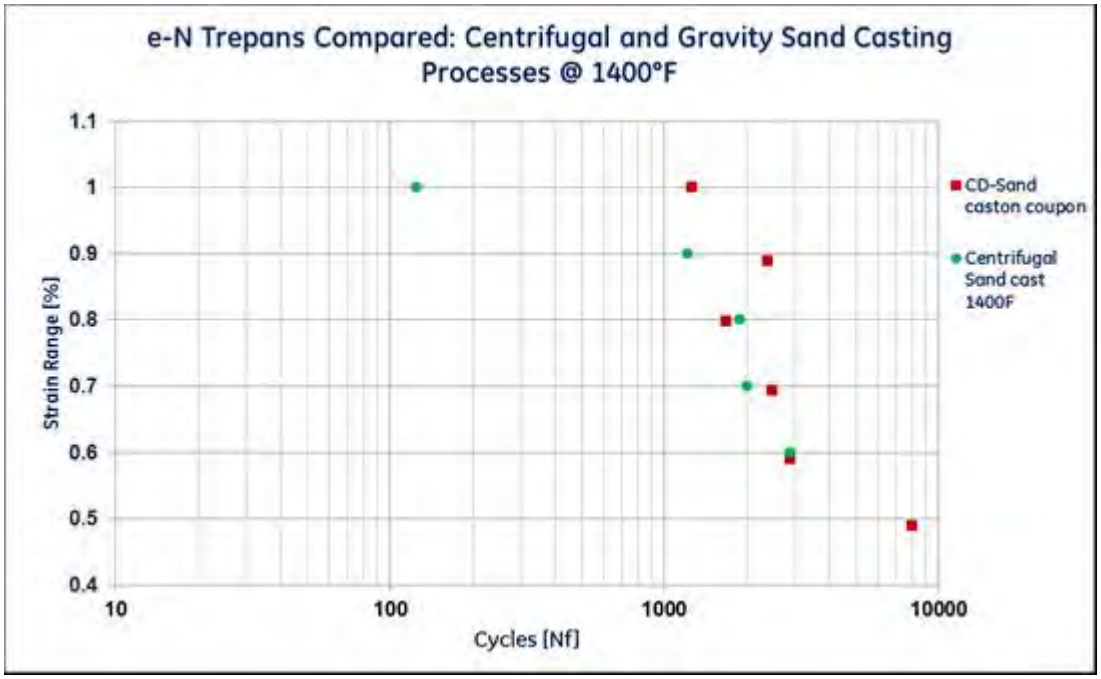

Figure 124 : Sand cast and centrifugal cast H282 show similar e-N trend, Nf cycles to failure for the strain ranges at 1400°F.

At higher strains > 0.8% TSR, sand cast LCF shows better performance over centrifugal casting test specimens.

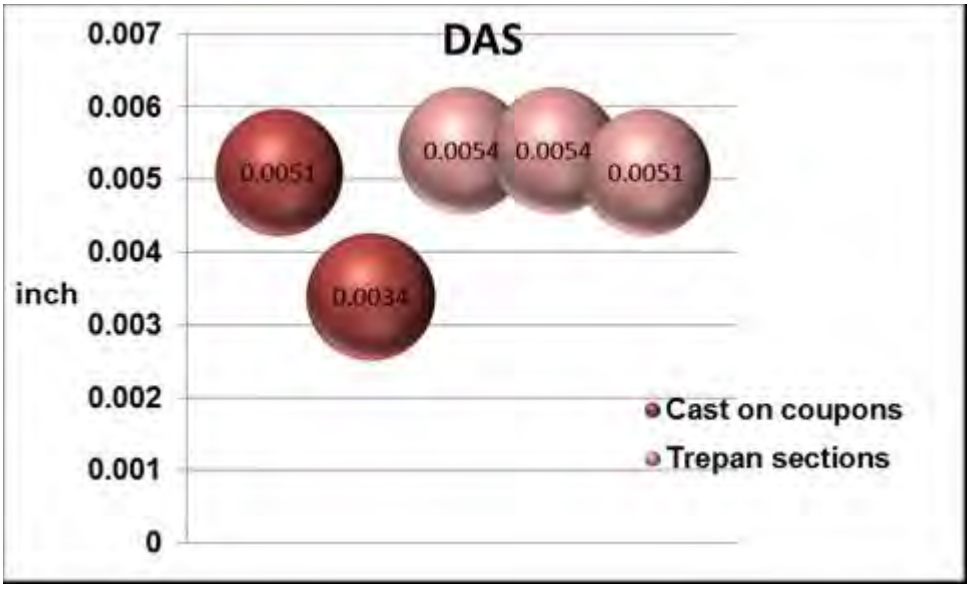

Figure 125 : Cast on coupon and Trepan sand cast section DAS compared

Table 22 : DAS values table comparing cast on coupons with trepan sections

DAS Dendritic Arm Spacing [inch]		
Specimen ID	**Cast on coupons**	**Trepan sections**
CA	**0.0051**	
CC	**0.0034**	
H		**0.0054**
B		**0.0054**
C		**0.0051**

Microstructure examination DAS-ARP 1947. Etchant : $HCL+H_2O+H_2O_2$.

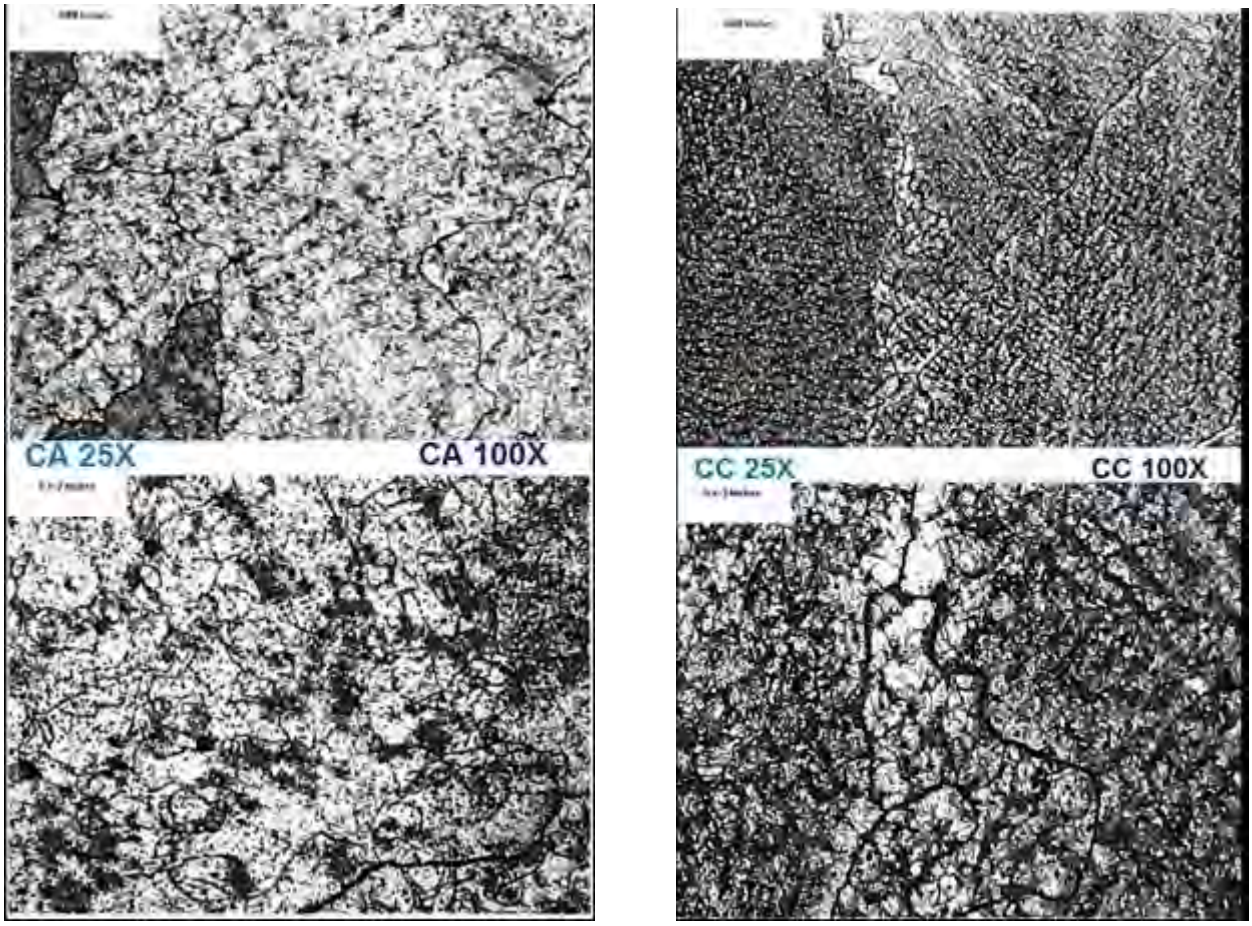

Figure 126: Cast on Coupons {CA & CC] Dendritic Arm Spacing micrographs at 25X (Top) and 100X image at (Bottom). Average DAS range from 0.0034 to 0.0051 inches.

Microstructure examination DAS-ARP 1947. Etchant : $HCL+H_2O+H_2O_2$.

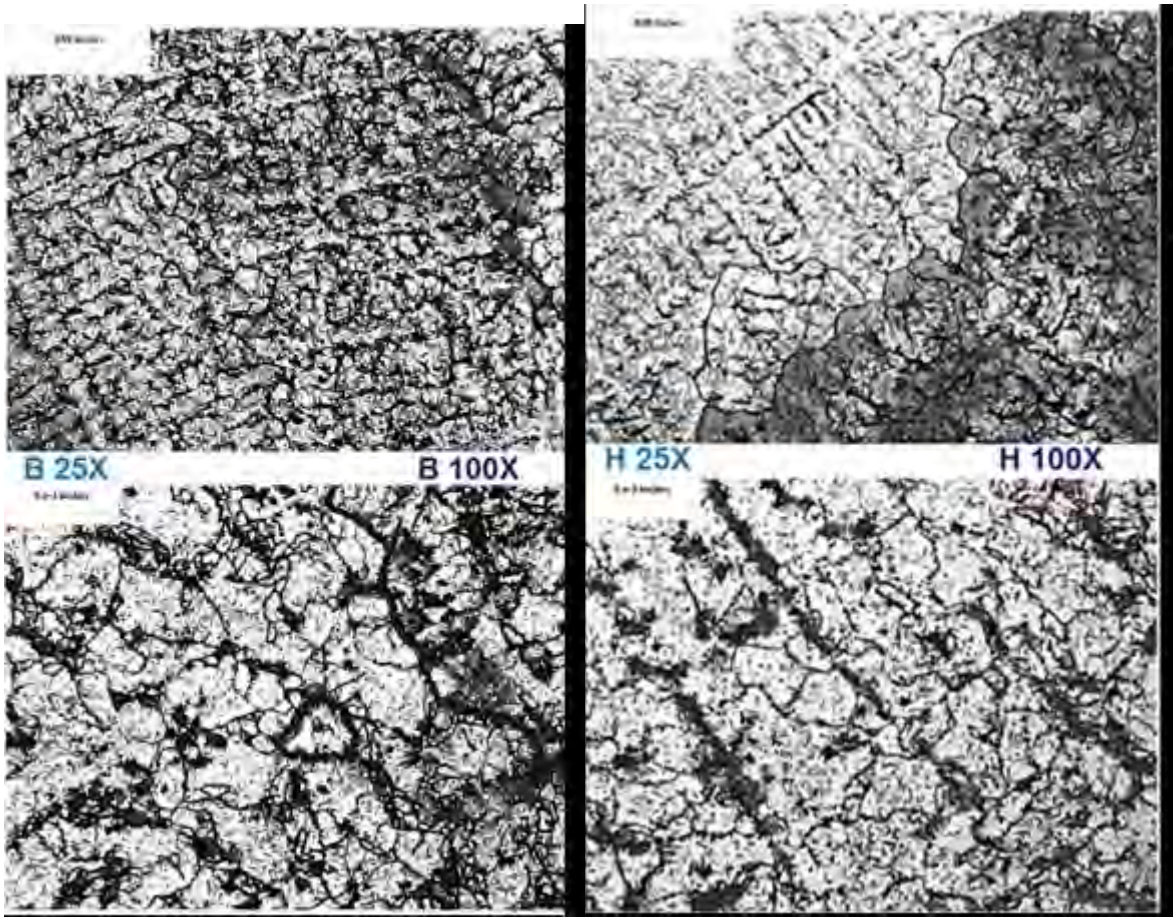

Figure 127: Trepan cast sections [B & H], DAS measurements are 0.0050 inches, average.

25X (Top) and 100X image at (Bottom).
Microstructure examination DAS-ARP 1947. Etchant : $HCL+H_2O+H_2O_2$.

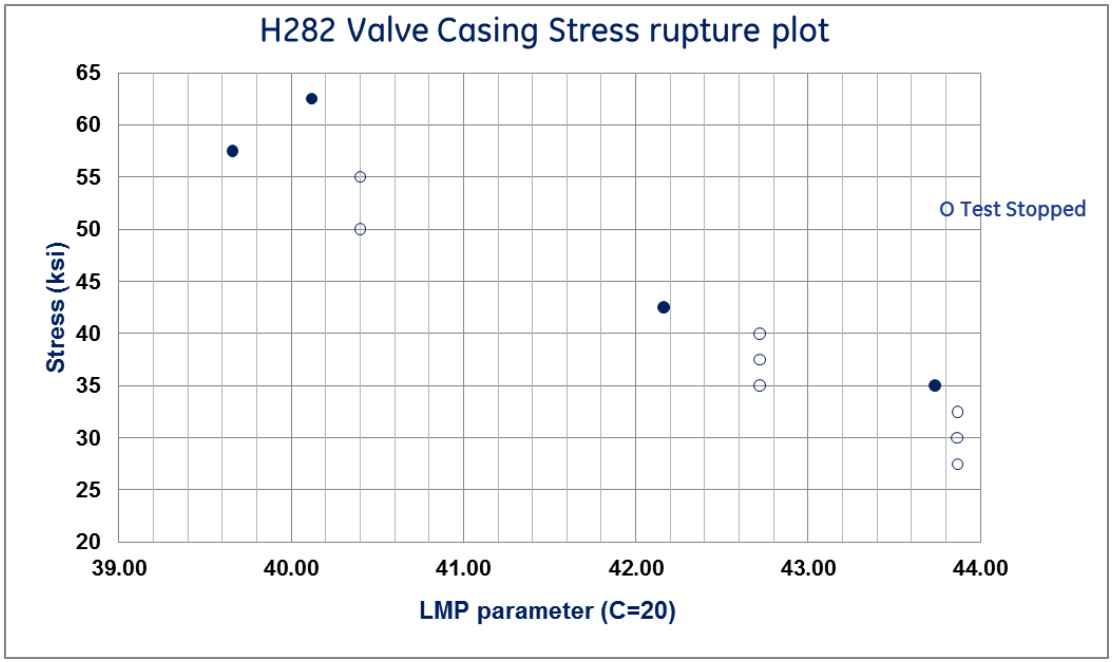

Figure 128 : Stress rupture test plot for trepans. Solid fills indicate test completed and non-fill shows testing stopped

Location	Sample ID	Status	Temp. °F	Stress ksi	Time hrs.	LMP [C=20]	% Elongation	% RA
CC Cast on Coupon	CC-SR-01	Stopped	1450	30	932.11	43.86		
	CC-SR-02	Stopped	1400	35	936.96	42.72		
	CC-SR-03	Stopped	1300	50	911.02	40.40		
H Cast section trepan	H-SR-01	Test Completed	1450	35	799.9	43.74	17.5	37.3
	H-SR-02	Test Completed	1400	42.5	469.63	42.16	22.7	24.1
	H-SR-03	Test Completed	1300	62.5	627.78	40.12	16.6	42.9
B Cast section trepan	B-SR-01	Stopped	1450	27.5	937.62	43.87		
	B-SR-02	Stopped	1400	40	936.08	42.72		
	B-SR-03	Test Completed	1300	57.5	344.4	39.66	7.8	6
E Cast section trepan	E-SR-01	Stopped	1450	32.5	938.28	43.87		
	E-SR-02	Stopped	1400	37.5	936.39	42.72		
	E-SR-03	Stopped	1300	55	910.91	40.40		

Typical Haynes 282 large size steam turbine Casting Order to Delivery Activity Schedule

#	Description	# Weeks	1	2	3	4	5	6	7	8	9	10	12	13	14	15	16	17	18	19	20	21	22	23	24	25	26
1	Sales and commercial review	3	X	X	X																						
2	Engineering Drawings_models review	4			X	X	X	X																			
3	Pattern and core box manufacturing	6							X	X	X	X	X	X													
4	Casting process engineering review	4							X	X	X	X															
5	FEM and solidifcation simualtion analysis	4										X	X	X	X												
6	Gating & Feeder Attachments, Ceramic tiling	2													X	X											
7	Molding and coremaking production scheduling	6															X	X	X	X	X	X					
8	Melting planning and schedule	3																					X	X	X		
9	Pouring, cooling and shake out	2																								X	X

Figure 129: Schedule from Purchase Order Placement to Casting Pouring ~ 26 weeks

		Weeks	27	28	29	30	31	32	33	34	35	36	37	38	39	40	41	42	43	44	45	46	47	48	49	50	51	52	53	54	55
10	Shot blast and riser cutting, gates removal	3	X	X	X																										
11	Homogenizing , solutionizing HT furnace prep	4				X	X	X	X																						
12	Grinding, Fettling	2								X	X																				
13	Aging HT Cycle, cooling	2										X	X																		
14	VT and LPT NDT inspections	2												X	X																
15	Radiographic inspection	4														X	X	X	X												
16	Mechanical testing, Chemical anlysis test certs	4												X	X	X	X														
17	Casting weld repair upgrdaes and Aging PWHT	4																		X	X	X	X								
18	NDT after weld repairs and casting upgrades	3																						X	X	X					
19	Casting Final Inspection and testcerts	3																									X	X	X		
20	Package and delivery	2																												X	X
		#REF!																													
Total 55-56 Weeks lead time from Order to Delivery																															

Figure 130: Schedule from Pouring to Delivery 30 weeks~

The key learnings that can be applied to the ComTest project to ensure it is successful considering technical achievement, scheduling, budget, etc. are:

1. Casting drawings, solid models and machined casting finish dimension drawings all needs to be prepared and reviewed well in advance for pattern, core boxes and foundry tooling manufacturing. Foundry tooling schedules involves ~4 to 5 weeks.
2. Casting material and process specifications along with NDT inspection and acceptance criteria specifications have to be provided early for suppler evaluation and preparation of casting manufacturing process plans, MPP and PQP.
3. Detailed vendor technical discussions, heat treatment cycle clarifications and heat treat furnace qualifications to be carried out upfront. Since the homogenizing cycles involve stepped furnace temperature ramp ups to avoid incipient melting.
4. Casting upgrade methods / weld repair process and post weld heat treat methods, specifications and weld inspection NDT procedure specs all have to be issued upfront for foundry manufacturing process plans and PQP development
5. Casting manufacturing schedule is multi stage process with ~56 week lead time
6. Selection of machine shops capable of machining super alloy castings and fit in to production schedule to be done in advance prior to pouring of the casting itself.

Appendix-1-A [SMALL CAST EVALAUATION]

Table 1: Nimonic 263 and Haynes 282 Cylinder Casting Heats Chemical Analysis and Superheat Temperatures (°C)

Superheat (°C)	**50**	**100**	**150**	**50**	**100**	**150**
Chemistry	**263-B2**	**263-E**	**263-H**	**282-D2**	**282-I**	**282-J**
C	0.08	0.08	0.08	0.08	0.08	0.08
Mn	0.48	0.50	0.51	0.25	0.25	0.25
Si	0.34	0.33	0.32	0.14	0.15	0.14
Cr	19.69	19.67	19.69	19.24	19.24	19.25
Ni	Rem	Rem	Rem	Rem	Rem	Rem
Mo	5.79	5.77	5.79	8.42	8.45	8.48
Co	19.73	19.92	19.92	9.90	9.87	9.84
Ti	2.09	2.16	2.09	2.05	2.08	2.10
Al	0.31	0.38	0.38	1.41	1.49	1.41
B	--	--	--	0.01	0.01	0.01
N (ppm)	127	62	66	53	73	67
O (ppm)	439	41	53	16	65	37

Table 2: Nimonic 263 Cylinder Casting Heats Tensile properties at RT and 1400 (°F) with Superheat Temperatures (°C) and Structure

Alloy	Heat	Superheat (C)	Structure	Temperature (F)	UTS (ksi)	0.02% YS (ksi)	0.2% YS (ksi)	%EL	%RA
263	**B2**	50	equiaxed	75	81.9	76.4	76	0.7**	2.5
263	**B2**	50	equiaxed	1400	79.2	52.9	60.4	13.9	21.8
263	**B2**	50	columnar	75	107.6	73.4	80	13.6	19.5
263	**B2**	50	columnar	1400	79.8	56.1	60.1	23.8	25.9
263	**H**	150	equiaxed	75	113.5	77.7	84	16.9	19.8
263	**H**	150	equiaxed	1400	87.3	60.6	65.2	24.3	31.4
263	**H**	150	columnar	75	114.1	77	84	16.9	21.3
263	**H**	150	columnar	1400	85.4	51.1	65	22.1	25.3
263	**E**	100	equiaxed	75	107.7	76.5	86	9.4	15.2
263	**E**	100	equiaxed	1400	91.1	58.5	66.5	17.9	24.1
263	**E**	100	columnar	75	114	79.1	86	12.8	20.1
263	**E**	100	columnar	1400	86.9	60.4	67.1	25.6	29

** Broke in the thread

Table 3: Haynes 282 Cylinder Casting Heats Tensile properties at RT and 1400(°F) with Superheat Temperatures (°C) and Structure

Alloy	*Heat*	*Superheat (C)*	*Structure*	*Temperature (F)*	*UTS (ksi)*	*0.02% YS (ksi)*	*0.2% YS (ksi)*	*%EL*	*%RA*
282	***I***	*100*	*equiaxed*	*75*	*134.6*	*84.7*	*92*	*10.9*	*16.8*
282	***I***	*100*	*equiaxed*	*1400*	*106.2*	*66*	*76.9*	*31.2*	*52.2*
282	***I***	*100*	*columnar*	*75*	*132.2*	*86.2*	*92*	*8.7*	*13.9*
282	***I***	*100*	*columnar*	*1400*	*107.3*	*68.4*	*77.9*	*23.5*	*39.1*
282	***D2***	*50*	*equiaxed*	*75*	*136.2*	*84.5*	*91*	*13.9*	*17.4*
282	***D2***	*50*	*equiaxed*	*1400*	*109.4*	*70.2*	*79.6*	*25.5*	*32.6*
282	***D2***	*50*	*columnar*	*75*	*121.4*	*82.9*	*87*	*10.1*	*11.6*
282	***D2***	*50*	*columnar*	*1400*	*104.6*	*67.4*	*74.2*	*12.9*	*40.2*
282	***J***	*150*	*equiaxed*	*75*	*129.2*	*81.1*	*87*	*14.5*	*17.8*
282	***J***	*150*	*equiaxed*	*1400*	*111.9*	*69.3*	*78.5*	*12.4*	*20*
282	***J***	*150*	*columnar*	*75*	*142.1*	*87*	*94*	*11.1*	*16.1*
282	***J***	*150*	*columnar*	*1400*	*115.9*	*73.5*	*84.1*	*17.4*	*24.4*

Table 4: Nimonic 263 Cylinder Casting Heats LCF Data at RT and 1400 (°F) with Superheat Temperatures (°C) and Structure

Alloy	Heat	Grain	Super-heat (C)	Temp (F)	RT MOD (MSI)	RANGE	MAX	MIN	NF-CYCLE	
263	B2	Columnar	50	75	27.3	1	0.5	-0.5	1221	Fractured
263	B2	Columnar	50	75	28.1	0.75	0.375	-0.375	2319	Fractured
263	B2	Columnar	50	75	27.6	0.5	0.25	-0.25	57607	Runout
263	B2	Columnar	50	1400	26.7	1	0.5	-0.5	739	Fractured
263	B2	Columnar	50	1400	27.4	0.75	0.375	-0.375	1554	Fractured
263	B2	Columnar	50	1400	27.8	0.5	0.25	-0.25	5535	Fractured
263	B2	Equiaxed	50	75	34.1	1	0.5	-0.5	1810	Fractured
263	B2	Equiaxed	50	75	29.5	0.5	0.25	-0.25	19618	Fractured
263	B2	Equiaxed	50	1400	30.7	1	0.5	-0.5	821	Fractured
263	B2	Equiaxed	50	1400	34.6	0.5	0.25	-0.25	985	Fractured
263	E	Columnar	100	75	25.9	1	0.5	-0.5	6194	Fractured
263	E	Columnar	100	75	27.7	0.75	0.375	-0.375	11180	Fractured
263	E	Columnar	100	75	26.1	0.5	0.25	-0.25	52074	Runout
263	E	Columnar	100	1400	25.7	1	0.5	-0.5	906	Fractured
263	E	Columnar	100	1400	24.8	0.75	0.375	-0.375	3196	Fractured
263	E	Columnar	100	1400	25.4	0.5	0.25	-0.25	10668	Fractured
263	E	Equiaxed	100	75	30.1	1	0.5	-0.5	2977	Fractured
263	E	Equiaxed	100	75	29.5	0.5	0.25	-0.25	56490	Runout
263	E	Equiaxed	100	1400	28.2	0.5	0.25	-0.25	6854	Fractured
263	E	Equiaxed	100	1400	29.5	1	0.5	-0.5	657	Fractured
263	H	Columnar	150	75	27.5	0.75	0.375	-0.375	16956	Fractured
263	H	Columnar	150	75	27.6	0.5	0.25	-0.25	50191	Fractured
263	H	Columnar	150	1400	28.1	1	0.5	-0.5	881	Fractured
263	H	Equiaxed	150	75	28.9	0.5	0.25	-0.25	50598	Fractured
263	H	Equiaxed	150	1400	32.2	1	0.5	-0.5	451	Fractured
263	H	Columnar	150	1400	29.6	0.75	0.375	-0.375	1213	Fractured
263	H	Columnar	150	1400	26.7	0.5	0.25	-0.25	4819	Fractured
263	H	Equiaxed	150	1400	30.8	0.5	0.25	-0.25	2419	Fractured

Table 5: Haynes 282 Cylinder Casting Heats LCF Data at RT and 1400 (°F) with Superheat Temperatures (°C) and Structure

Alloy	Heat	Grain	Super-heat (C)	Temp (F)	RT MOD (MSI)	RANGE	MAX	MIN	NF-CYCLE	
282	D2	Columnar	50	75	25.1	1	0.5	-0.5	3152	Fractured
282	D2	Columnar	50	75	24.3	0.75	0.375	-0.375	14876	Fractured
282	D2	Columnar	50	75	24.4	0.5	0.25	-0.25	52859	Runout
282	D2	Equiaxed	50	75	29.9	1	0.5	-0.5	3442	Fractured
282	D2	Equiaxed	50	75	26.8	0.5	0.25	-0.25	51778	Runout
282	I	Columnar	100	75	25.7	1	0.5	-0.5	7634	Fractured
282	I	Columnar	100	75	25.9	0.75	0.375	-0.375	12441	Fractured
282	I	Columnar	100	75	26.5	0.5	0.25	-0.25	50000	Runout
282	I	Equiaxed	100	75	29.3	1	0.5	-0.5	2595	Fractured
282	I	Equiaxed	100	75	29.2	0.5	0.25	-0.25	44932	Fractured
282	J	Columnar	150	75	27.2	1	0.5	-0.5	3945	Fractured
282	J	Columnar	150	75	29.6	0.75	0.375	-0.375	8416	Fractured
282	J	Columnar	150	75	28.3	0.5	0.25	-0.25	69802	Runout
282	J	Equiaxed	150	75	30.4	1	0.5	-0.5	670	Fractured
282	J	Equiaxed	150	75	24.2	0.5	0.25	-0.25	53096	Runout
282	D2	Columnar	50	1400	25.4	1	0.5	-0.5	1299	Fractured
282	D2	Columnar	50	1400	26.4	0.5	0.25	-0.25	13977	Fractured
282	D2	Equiaxed	50	1400	30.1	1	0.5	-0.5	759	Fractured
282	D2	Equiaxed	50	1400	23.5	0.5	0.25	-0.25	10045	Fractured
282	I	Columnar	100	1400	25.9	1	0.5	-0.5	1150	Fractured
282	I	Columnar	100	1400	25.2	0.75	0.375	-0.375	2947	Fractured
282	I	Columnar	100	1400	27.1	0.5	0.25	-0.25	12047	Fractured
282	I	Equiaxed	100	1400	25	0.5	0.25	-0.25	11782	Fractured
282	I	Equiaxed	100	1400	28.8	1	0.5	-0.5	806	Fractured
282	J	Equiaxed	150	1400	29.5	1	0.5	-0.5	541	Fractured
282	J	Equiaxed	151	1400	29.8	0.5	0.25	-0.25	8301	Fractured
282	J	Columnar	152	1400	29.8	1	0.5	-0.5	903	Fractured
282	J	Columnar	153	1400	27	0.75	0.375	-0.375	1764	Fractured

Table 6: Nimonic263 Cast Cylinder Microstructures (50X) with Superheat Temperature and Structure Variation

50°C Superheat- Columnar	100°C Superheat- Columnar	150°C Superheat- Columnar
50°C Superheat- Equiaxed	**100°C Superheat- Equiaxed**	**150°C Superheat- Equiaxed**
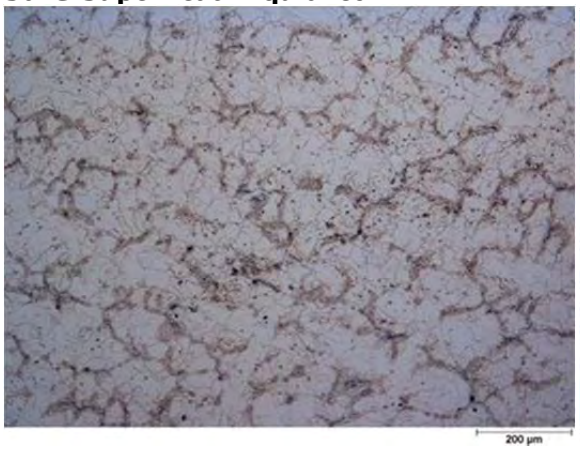	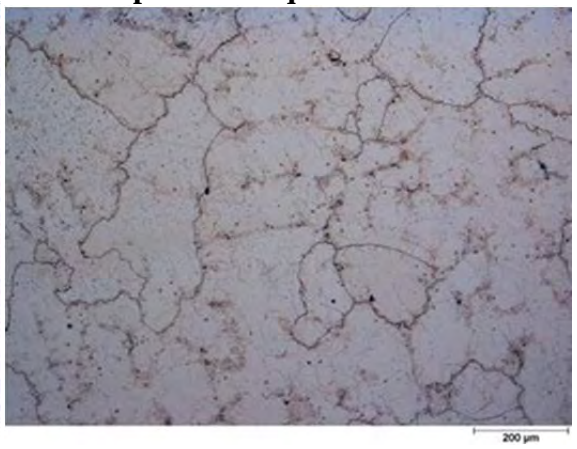	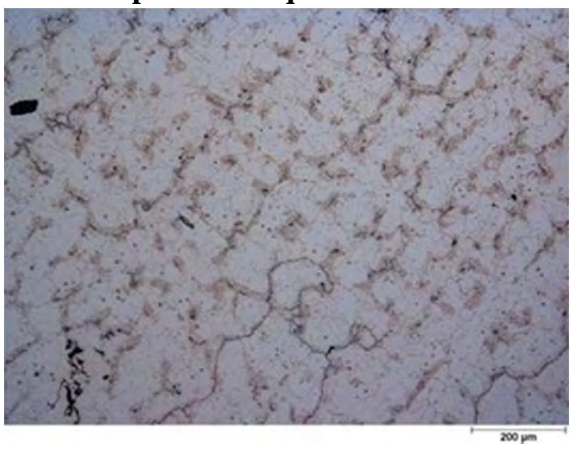

Table 7: Haynes 282 Cast Cylinder Microstructures (50X) with Superheat Temperature and Structure Variation

50°C Superheat- Columnar

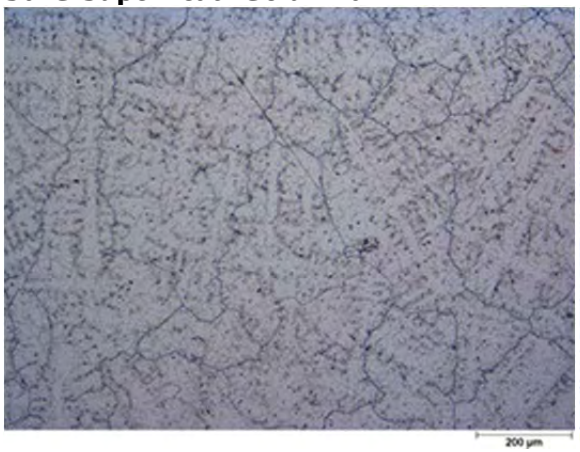

100°C Superheat- Columnar

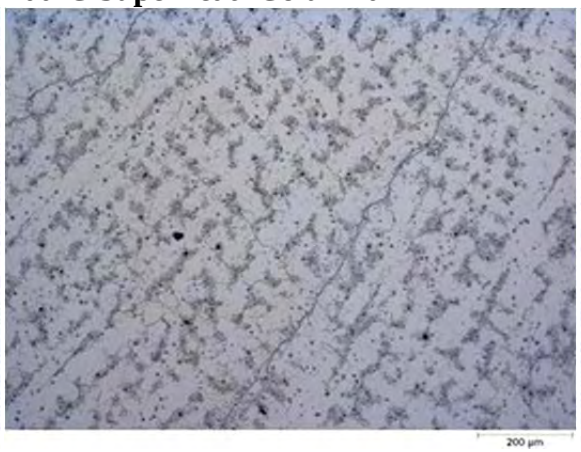

150°C Superheat- Columnar

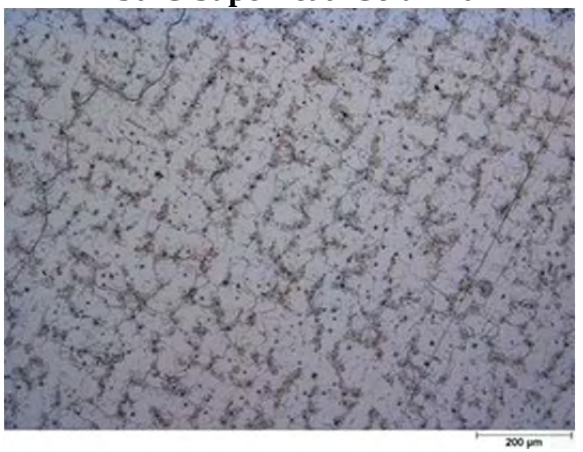

50°C Superheat- Equiaxed

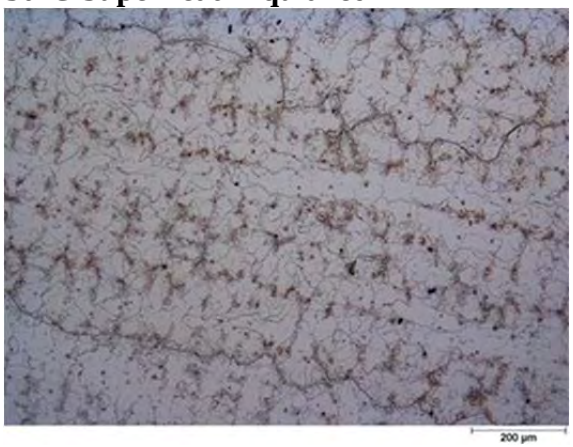

100°C Superheat- Equiaxed

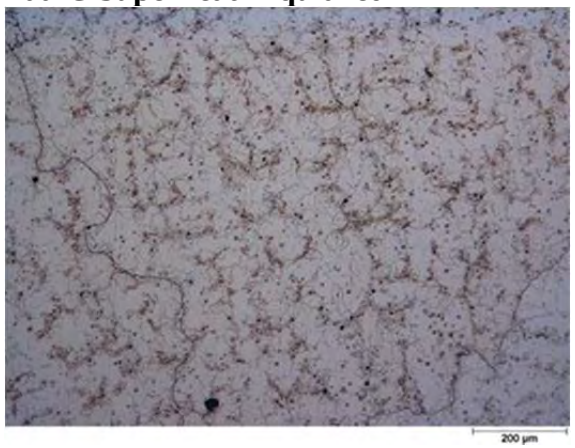

150°C Superheat- Equiaxed

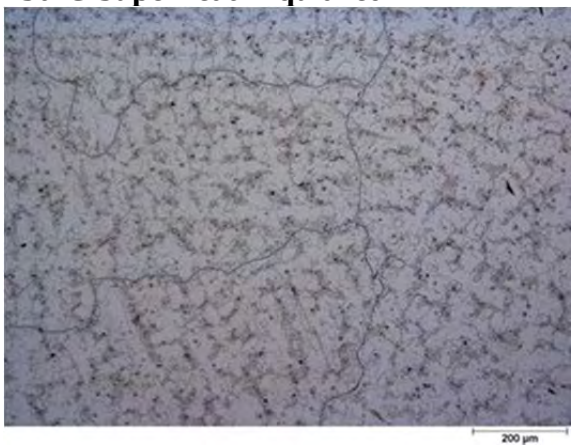

Table 8: Nimonic263 Cast Cylinder Microstructures (500X) with Superheat Temperature and Structure Variation

50°C Superheat- Columnar

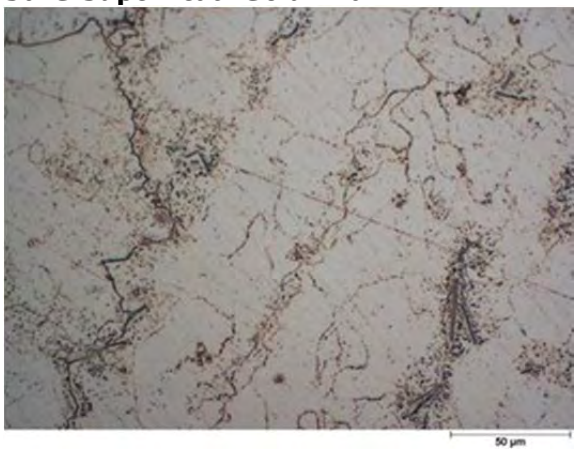

100°C Superheat- Columnar

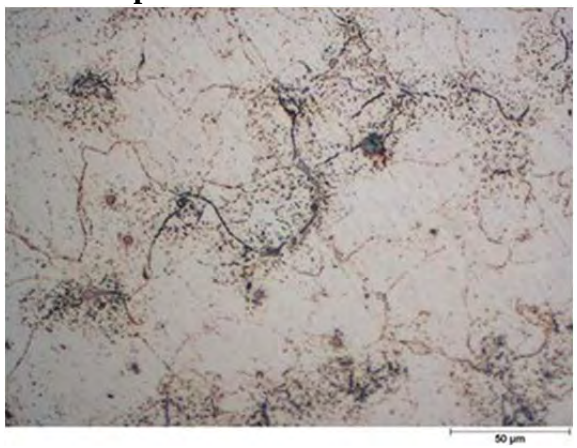

150°C Superheat- Columnar

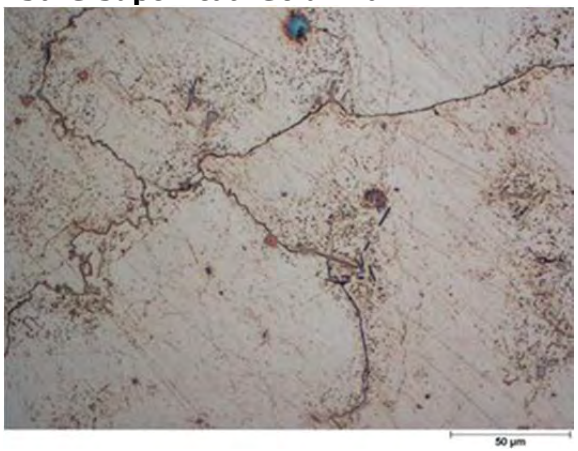

50°C Superheat- Equiaxed

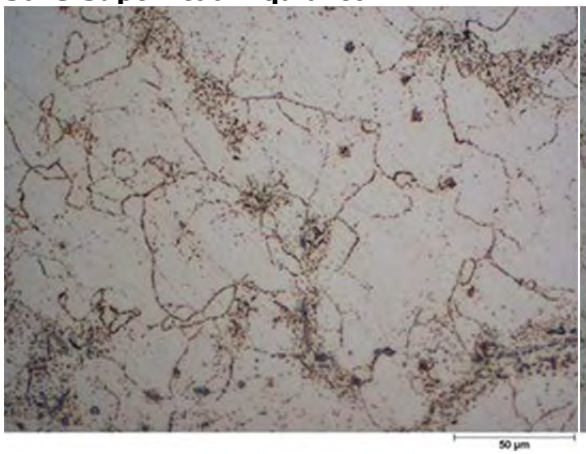

100°C Superheat- Equiaxed

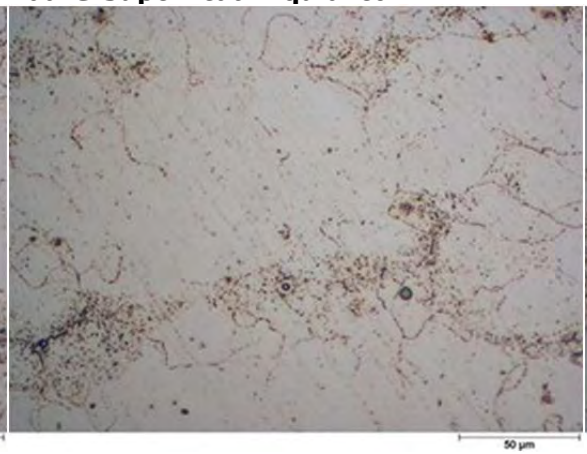

150°C Superheat- Equiaxed

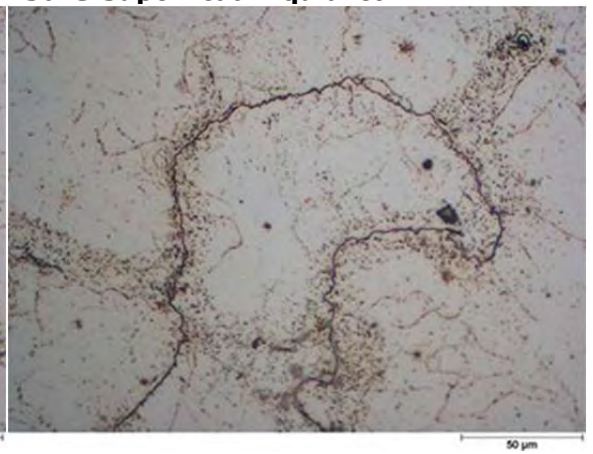

Table 9: Haynes 282 Cast Cylinder Microstructures (500X) with Superheat Temperature and Structure Variation

50 C Superheat Columnar

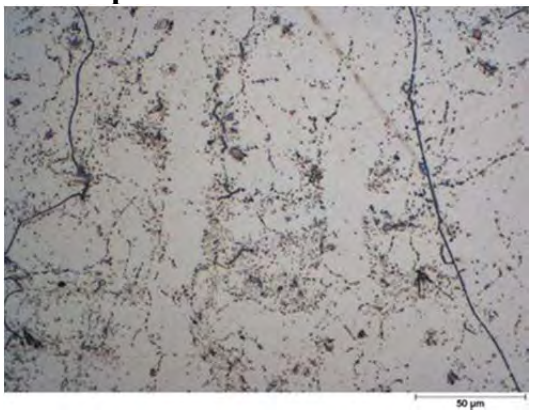

100 C Superheat Columnar

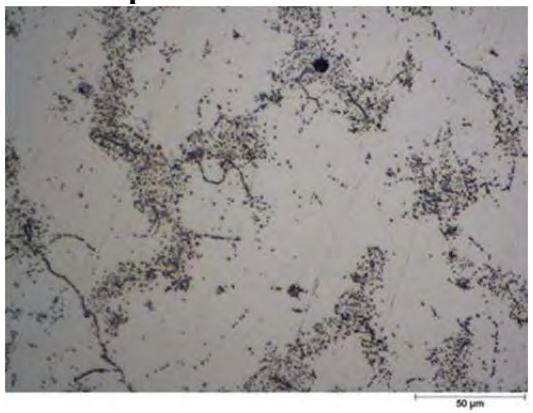

150 C Superheat Columnar

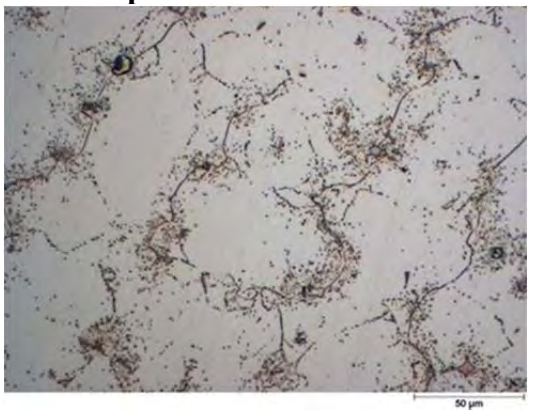

50 C Superheat Equiaxed

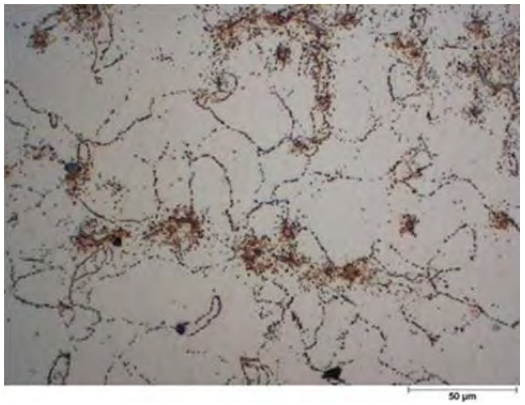

100 C Superheat Equiaxed

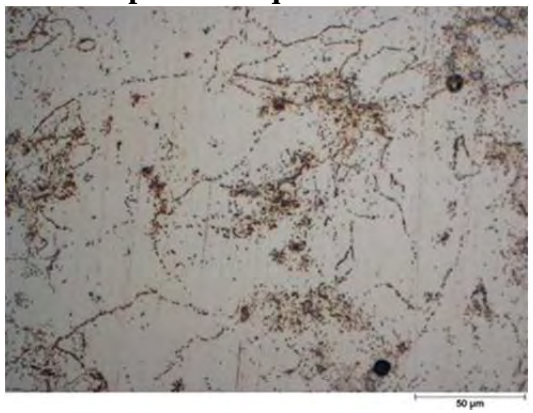

150 C Superheat Equiaxed

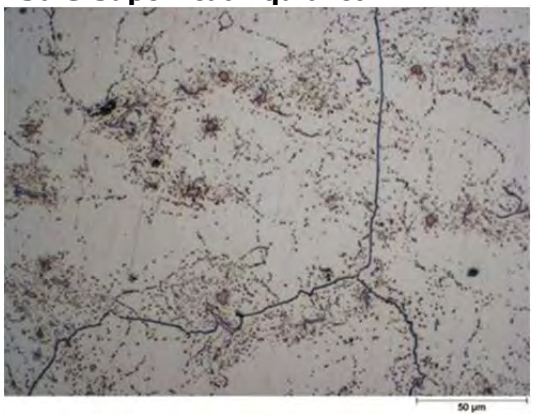

Appendix 1-B [Step block Casting of Haynes 282]

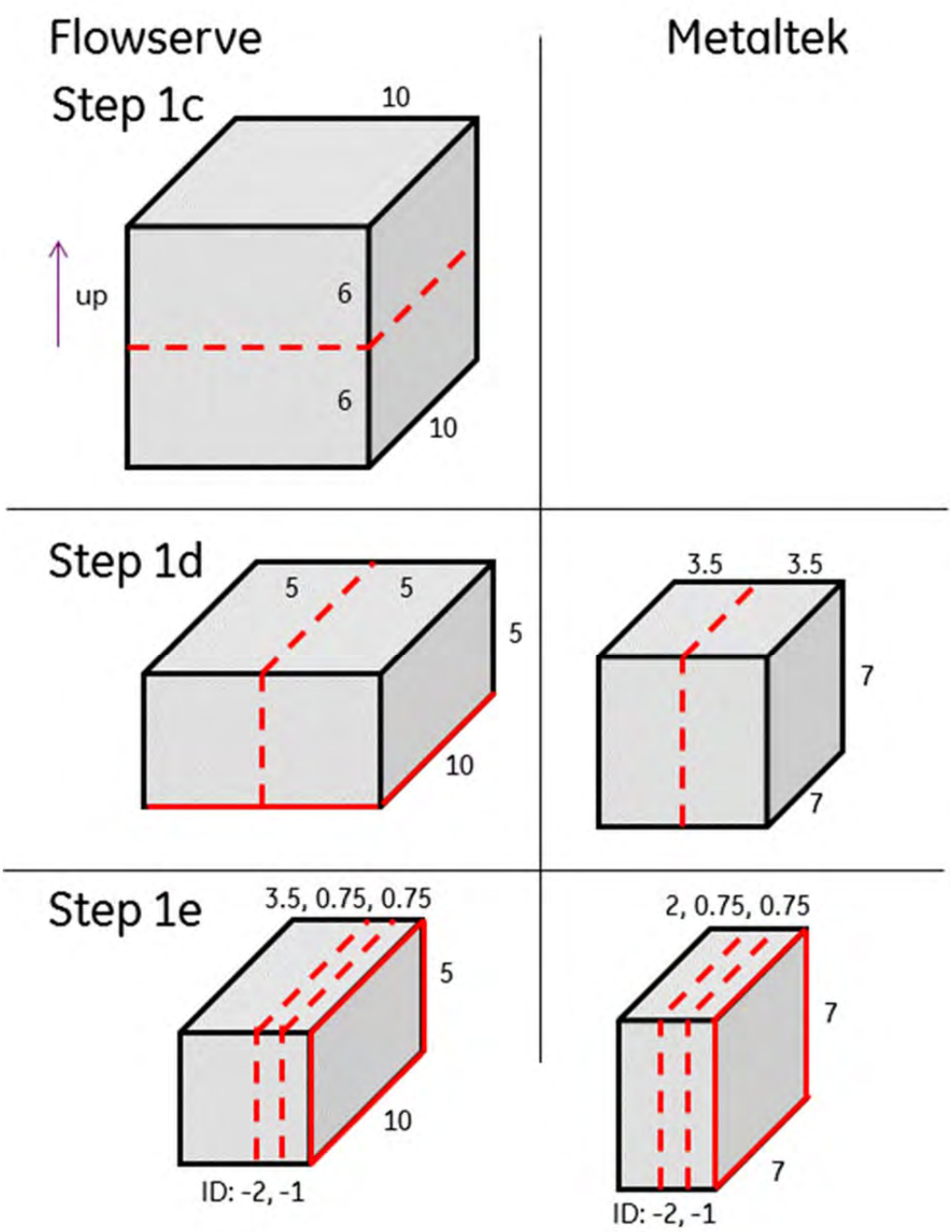

Figure 1: Flowserve and MetalTek step block casting sample sections cut up diagram

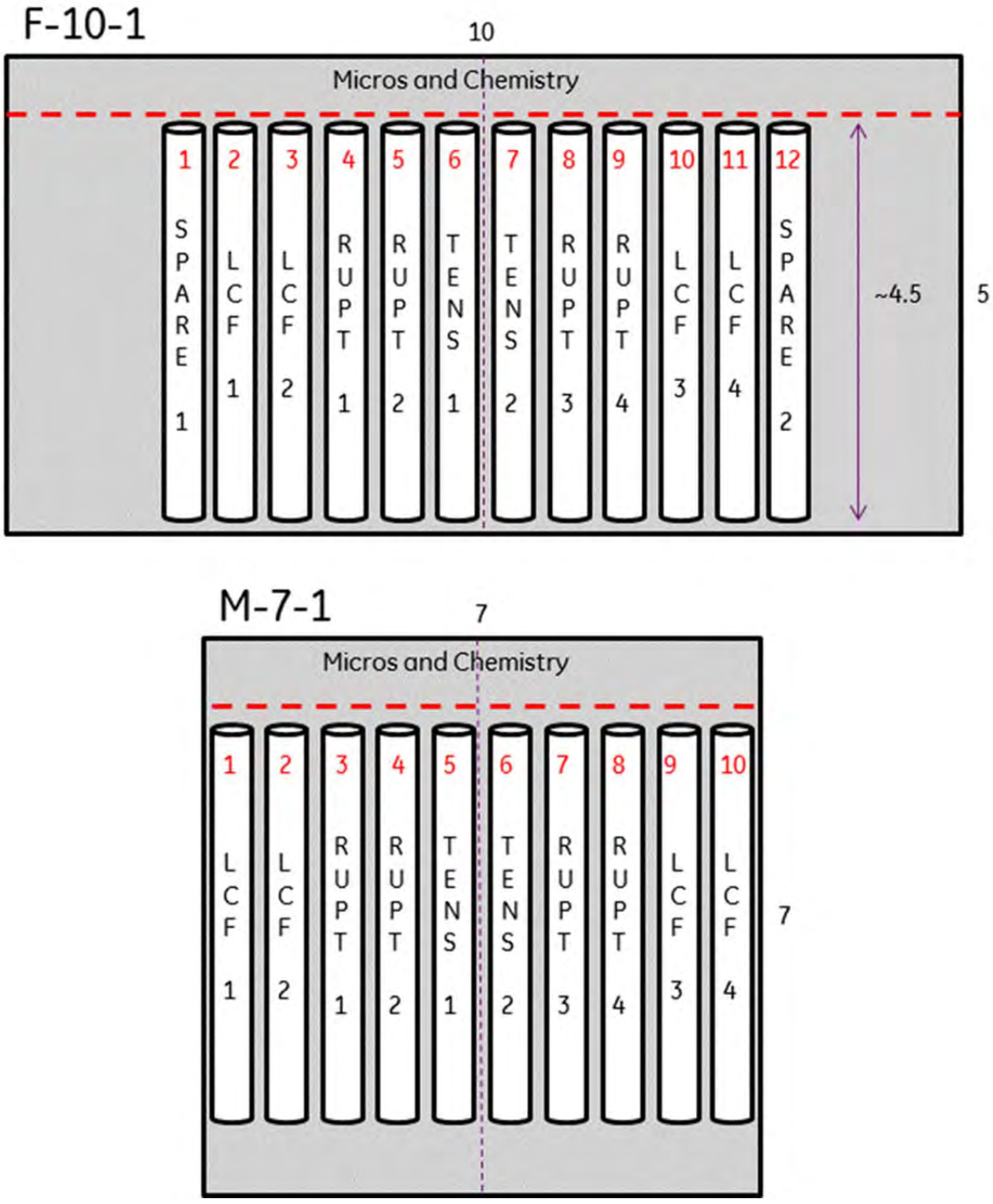

Figure 2: Flowserve and MetalTek step block castings test specimens cut up diagram

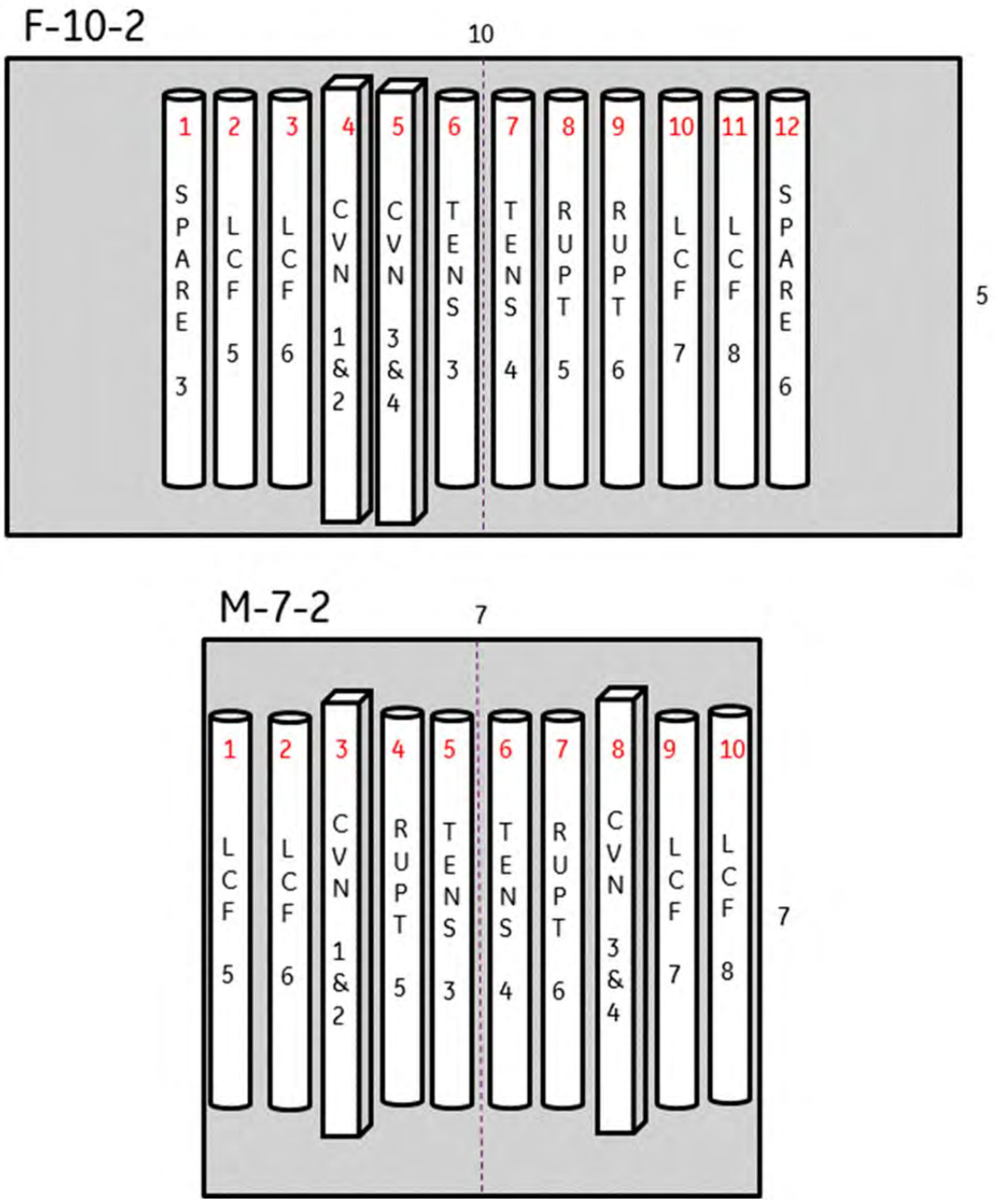

Figure 3: Flowserve and MetalTek step block casting test specimens cut up diagram

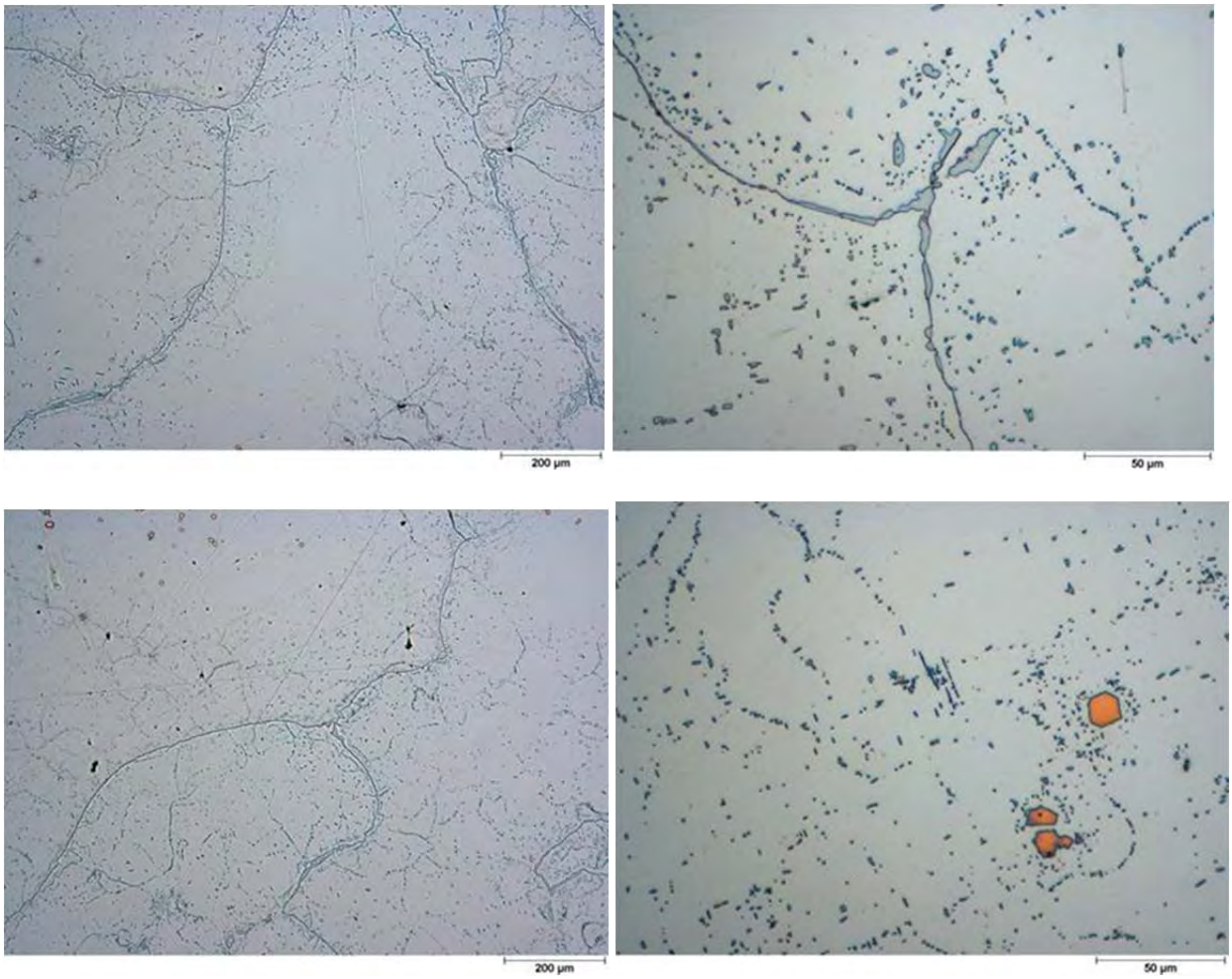

Figure 4: Optical micrographs from the Flowserve step block (etched with Kallings)

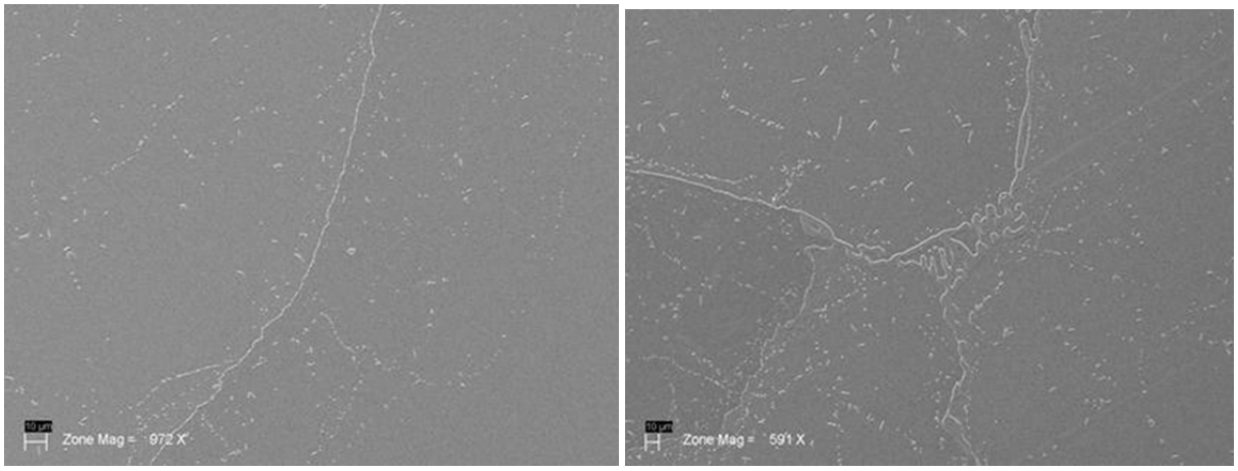

Figure 5: Secondary Electron Images (SEM) showing high-Mo, high-Si phases on grain boundaries

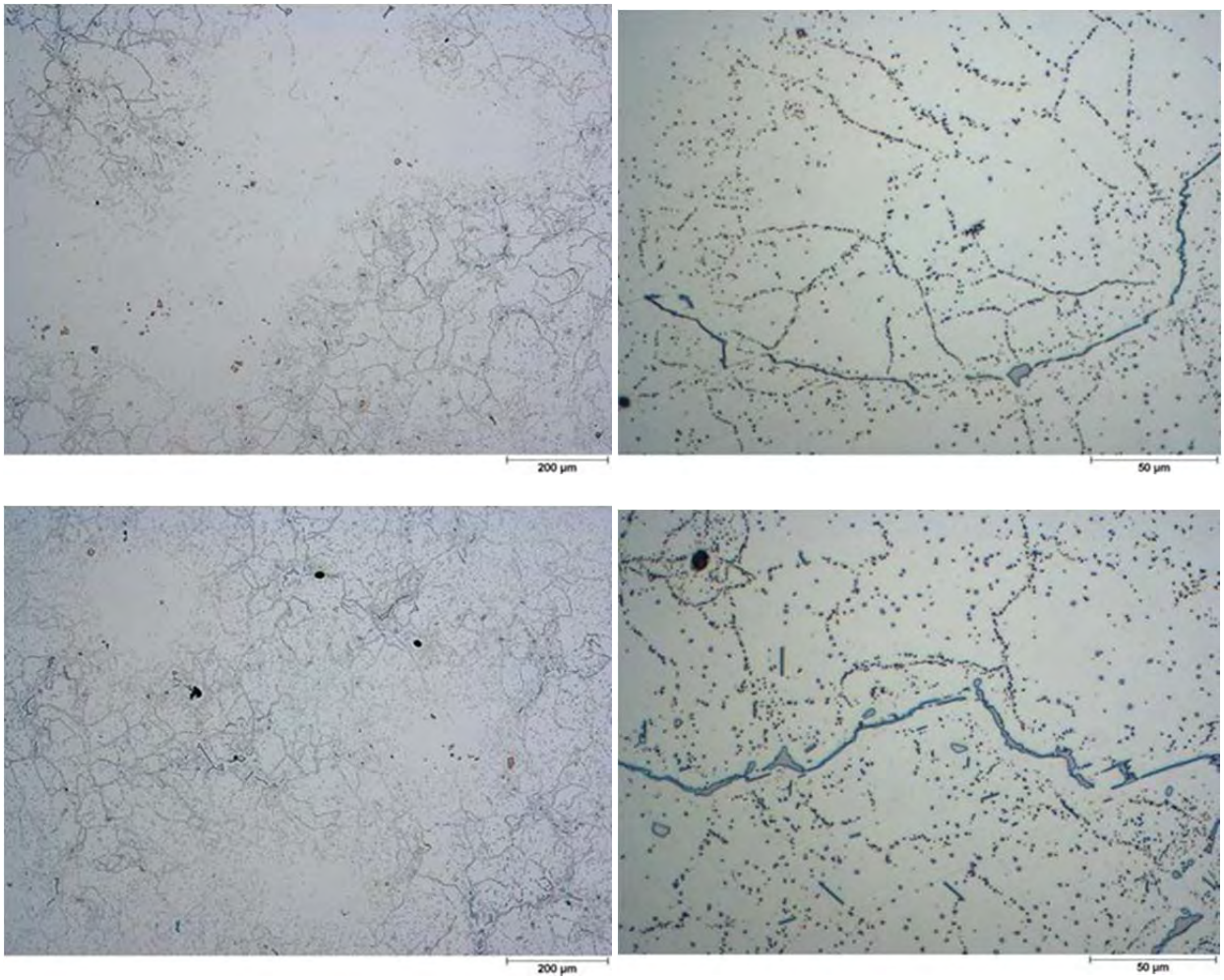

Figure 6: Optical micrographs from the MetalTek step block (etched with Kallings)

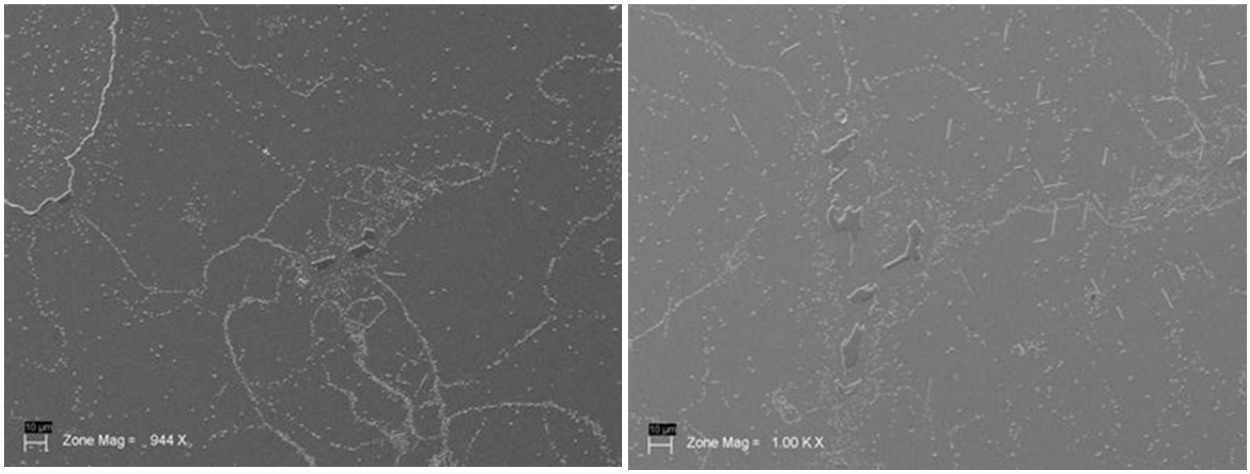

Figure 7: Secondary Electron Images (SEM) showing vartious phases

Table 1: Microprobe measurements at zones showing high Mo and low Mo before and after the homogenization cycle. The reported numbers are the average of five measurements taken from Mo peak and valley concentrations from a Microprobe traverse.

	Al	Ni	Co	Cr	Ti	Mo	Fe	Si	Mn
As-Cast High Mo	**1.6**	**54.8**	**9.8**	**19.5**	**2.5**	**10.3**	**0.1**	**0.2**	**0.25**
As-Cast Low Mo	**1.8**	**57.9**	**10.8**	**19.6**	**1.6**	**7.2**	**0.1**	**0.05**	**0.20**
Homogenized High Mo	**1.8**	**56.5**	**10.1**	**18.9**	**2.4**	**9.0**	**0.1**	**0.1**	**0.2**
Homogenized Low Mo	**1.9**	**57.4**	**10.8**	**19.4**	**1.9**	**7.4**	**0.1**	**0.08**	**0.2**
Nominal	**1.71**	**57.85**	**9.92**	**19.53**	**2.26**	**8.14**	**0.14**	**0.08**	**0.22**

Table 2: Raw data from the microprobe measurements taken from homogenized sections of the Metaltek 282 step casting

11PDJ125	**A**	**Al**	**Ni**	**Co**	**Cr**	**Ti**	**Mo**	**Fe**	**Si**	**Mn**
Max	1	1.82	55.97	9.43	18.73	2.96	9.73	0.11	0.16	0.25
Max	2	1.55	54.7	9.97	19.86	2.19	10.34	0.12	0.2	0.25
Max	3	1.74	55.31	9.73	19.42	2.76	9.64	0.11	0.18	0.27
Max	4	1.46	54.11	9.95	19.7	2.12	10.86	0.1	0.22	0.24
Max	5	1.45	54.22	9.89	19.75	2.26	10.85	0.11	0.21	0.25
Average		**1.6**	**54.86**	**9.79**	**19.49**	**2.46**	**10.28**	**0.11**	**0.2**	**0.25**
11PDJ125	**A**	**Al**	**Ni**	**Co**	**Cr**	**Ti**	**Mo**	**Fe**	**Si**	**Mn**
Min	1	1.92	56.84	10.21	19.65	2.34	8.12	0.13	0.09	0.25
Min	2	1.79	58.43	11.05	19.71	1.34	6.78	0.13	0.04	0.2
Min	3	1.83	57.84	10.82	19.35	1.59	7.19	0.14	0.05	0.2
Min	4	1.8	58.3	11.06	19.66	1.35	6.86	0.13	0.04	0.19
Min	5	1.8	58.3	11.06	19.66	1.35	6.86	0.13	0.04	0.19
Average		**1.83**	**57.94**	**10.84**	**19.61**	**1.59**	**7.16**	**0.13**	**0.05**	**0.2**
11PDJ126		**Al**	**Ni**	**Co**	**Cr**	**Ti**	**Mo**	**Fe**	**Si**	**Mn**
Max	1	1.73	56.58	10.04	18.99	2.4	9.12	0.12	0.13	0.22
Max	2	1.76	56.58	10.19	19.07	2.24	8.76	0.12	0.1	0.22
Max	3	1.78	56.51	10.17	18.89	2.43	8.99	0.11	0.13	0.23
Max	4	1.76	56.63	10.24	18.91	2.37	8.87	0.11	0.12	0.24
Max	5	1.73	56.4	10	18.84	2.34	9.1	0.11	0.12	0.23
Average		**1.75**	**56.54**	**10.13**	**18.94**	**2.36**	**8.97**	**0.11**	**0.12**	**0.23**
11PDJ126		**Al**	**Ni**	**Co**	**Cr**	**Ti**	**Mo**	**Fe**	**Si**	**Mn**
Min	1	1.9	57.49	10.94	19.66	1.7	7.06	0.14	0.07	0.21
Min	2	1.85	57.41	10.7	19.5	1.88	7.45	0.13	0.07	0.21
Min	3	1.87	57.58	10.69	19.19	1.89	7.52	0.13	0.07	0.21
Min	4	1.89	57.34	10.71	19.4	1.9	7.49	0.13	0.07	0.22
Min	5	1.89	57.23	10.74	19.25	2	7.62	0.13	0.09	0.23
Average		**1.88**	**57.41**	**10.76**	**19.4**	**1.87**	**7.42**	**0.13**	**0.08**	**0.22**

Table 3: Graphs of thermodynamicly predicted volume fractions of various phases in alloy 282 when homogenized to the same levels as in Tables 10 and 11.

High Molybdenum:

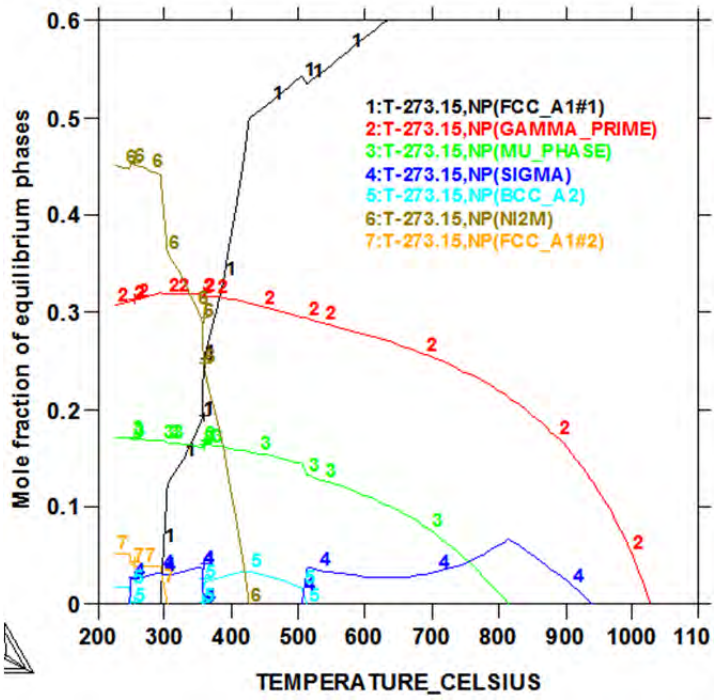

Low Molybdenum:

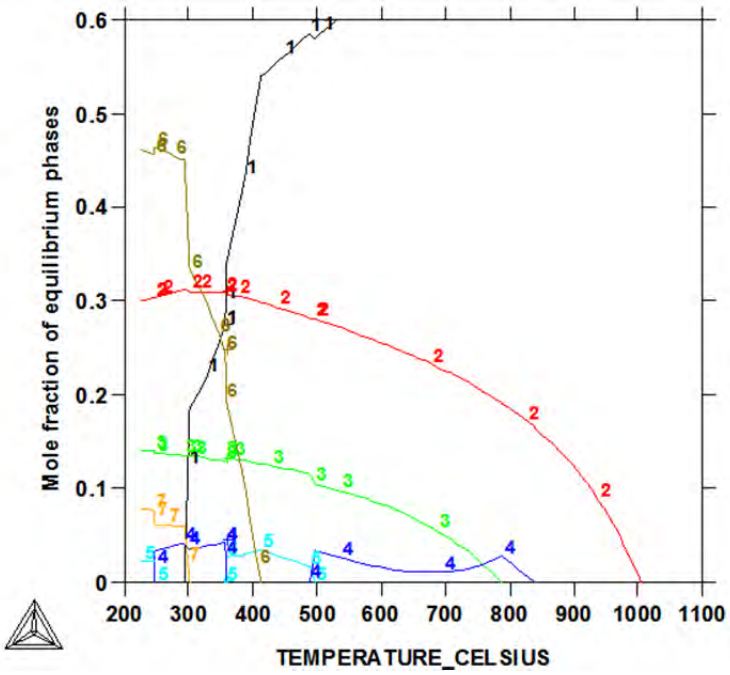

Table 4: MetalTek Step block heat treatment cycle

Material:	Haynes 282
Part:	Carondelet Step Casting
Test Material:	Single keel bars (4) plus riser segment
Casting Preparation:	Coat all casting surfaces with AO Smith CG-11 Ceram-Guard Coating.
Quality:	Independent thermocouple in attached to the casting.
	Heat treat chart to customer
Cooling Requirement:	Still cool to room temperature.
Heat Treatment: (This treatment is a three temperature heat treatment)	Charge into a cold furnace and heat load to temperature.
	Hold load at 2066°F (1130°C) +/- 25F – 3 hours minimum (plus add 1 hour for through heating. Begin counting time when the thermocouple on the casting has reached 2060 – 2070F);
	Heat load to 2192°F (1200°C) +5/-15F – hold at temperature for 3 hours minimum (plus add ½ to 1 hour for through heating. Begin counting time when the thermocouple on the casting reaches 2185 – 2195F);
	Heat load to 2210°F (1210°C) +25/-5°F – hold for 14 hours minimum (plus add ½ hour for through heating)
	Still cool the load to room temperature upon completion of the heat treatment.

Table 5: Flowserve Step block heat treatment cycle

Homogenizing Heat Treatment for ' step test casting, riser, and gate .'	Part should be loaded into a room temperature furnace.
	Ramp furnace at a rate not exceeding 200°C/Hour
	Hold at 1130°C ± 10°C for six hours
	Ramp furnace to 1160°C and hold for six hours.
	Ramp furnace to 1200°C.
	Hold at 1200°C ± 10°C for 48 hours
	Still Air Cool
Solution Heat Treatment	Part should be loaded into a room temperature furnace.
	Ramp furnace at a rate not exceeding 200°C/Hour
	1105°C ± 5°C for 12 Hours (Force Air Cool or Quench)
Aging	Part should be loaded into a room temperature furnace.
	Ramp furnace at a rate not exceeding 200°C/Hour
	790°C ± 10°C for 16 Hours (Still or Forced Air Cool) NOTE riser was water quenched.

Table 6: Haynes 282 Step Block Tensile properties

Heat	ID	Temp (F)	Temp (C)	UTS (ksi)	0.2% YS (ksi)	%EL	%RA
Flowserve Step Block	F-10-2-7	75	25	76	74.5	2.2	3.1
Flowserve Step Block	F-10-2-6	1400	760	74	69.0	6.0	9.0
Flowserve Step Block	F-10-1-6	75	25	84.5	80.0	4.4	9.0
Flowserve Step Block	F-10-1-7	1400	760	67.5	62.5	6.5	9.0
Metaltek Step Block	M-7-2-6	75	25	93	89.0	2.3	7.5
Metaltek Step Block	M-7-2-5	1400	760	83.5	79.0	6.0	8.5
Metaltek Step Block	M-7-1-5	75	25	89.5	84.5	6.0	6.0
Metaltek Step Block	M-7-1-6	1400	760	97.5	78.0	10.0	10.0

Table 7: Haynes 282 Step Block Charpy V notch Impact properties

Heat	ID	Temp (F)	Temp (C)	Impact Energy (ft-lbs)	Impact Energy (J)	Percent Shear	Lateral Expansion
Flowserve Step Block	F-10-2-4a	75	25	22	30.	50	0.023
Flowserve Step Block	F-10-2-4b			7	9.5	5	0.007
Flowserve Step Block	F-10-1-5a			17	23	40	0.018
Flowserve Step Block	F-10-1-5b			7	9.5	5	0.006
Metaltek Step Block	M-7-2-3a			18	24	55	0.013
Metaltek Step Block	M-7-2-3b			9	12	20	0.011
Metaltek Step Block	M-7-1-8a			14	19	20	0.013
Metaltek Step Block	M-7-1-8b			10	14	10	0.010

*Note: “a” specimens extracted from the thermal top of the sliced section and “b” specimens came from the bottom.

Table 8: Haynes 282 Step Block LCF properties

Heat	ID	Temp (F)	Temp (C)	Frequency (CPM)	Strain Ratio (A)	Strain Range	Ni	Nf
Flowserve Step Block	F-10-1-2	75	25	20	∞	0.75	--	152
	F-10-1-3	75	25	20	∞	0.6	--	593
	F-10-1-10	1400	760	20	∞	0.75	125	132
	F-10-1-11	1400	760	20	∞	0.6		1036
	F-10-2-2	75	25	20	∞	0.6	386	800
	F-10-2-3	75	25	20	∞	0.75	136	137
	F-10-2-10	1400	760	20	∞	0.6		
	F-10-2-11	1400	760	20	∞	0.75		
Metaltek Step Block	M-7-1-1	75	25	20	∞	0.75	408	472
	M-7-1-2	75	25	20	∞	0.6	12734	13913
	M-7-1-9	1400	760	20	∞	0.75	674	728
	M-7-1-10	1400	760	20	∞	0.6	2352	3246
	M-7-2-1	75	25	20	∞	0.6	--	4071*
	M-7-2-2	75	25	20	∞	0.75	3838	4720
	M-7-2-9	1400	760	20	∞	0.6	1190	1198
	M-7-2-10	1400	760	20	∞	0.75	716	718

*This test is void because of a failure in the fixture.

Appendix 1-C [Step Block casting of Nimonic 263]

STEP CASTING OF NIMONIC 263

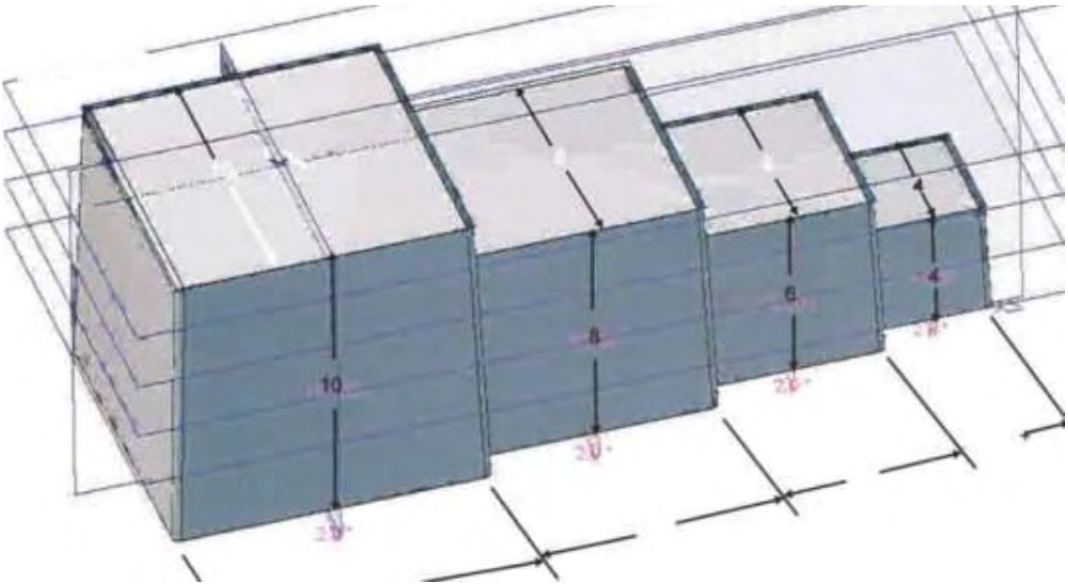

Figure 1: Schematic of the Nimonic 263 step block test casting pattern with 2 degree pattern draft and 3/8 inch shrink rule applied

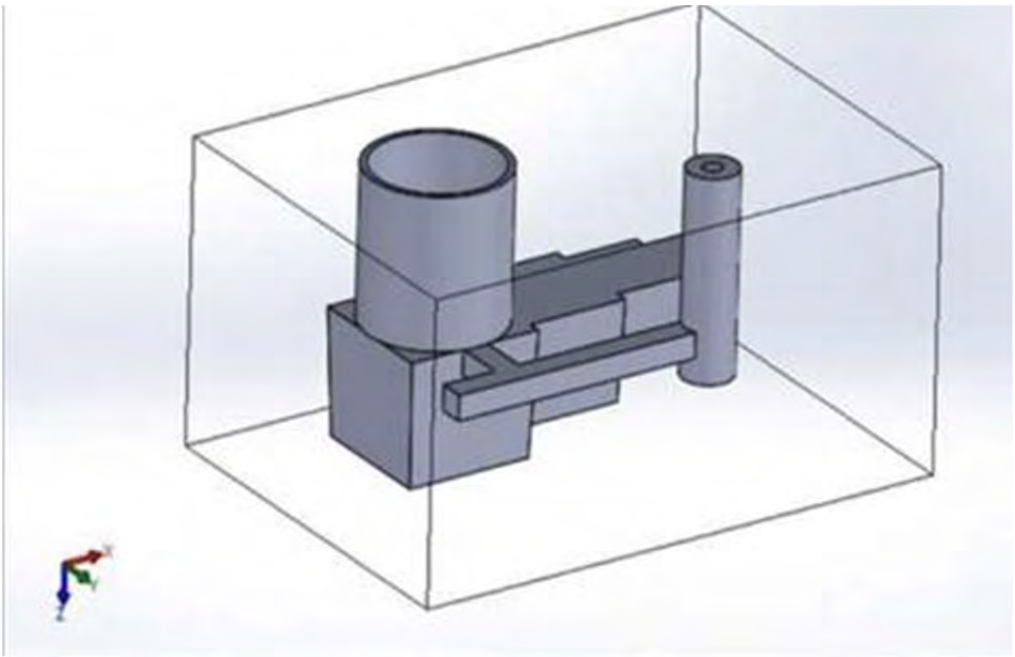

Figure 2: Nimonic 263 step block test casting gating and feeder casting methods

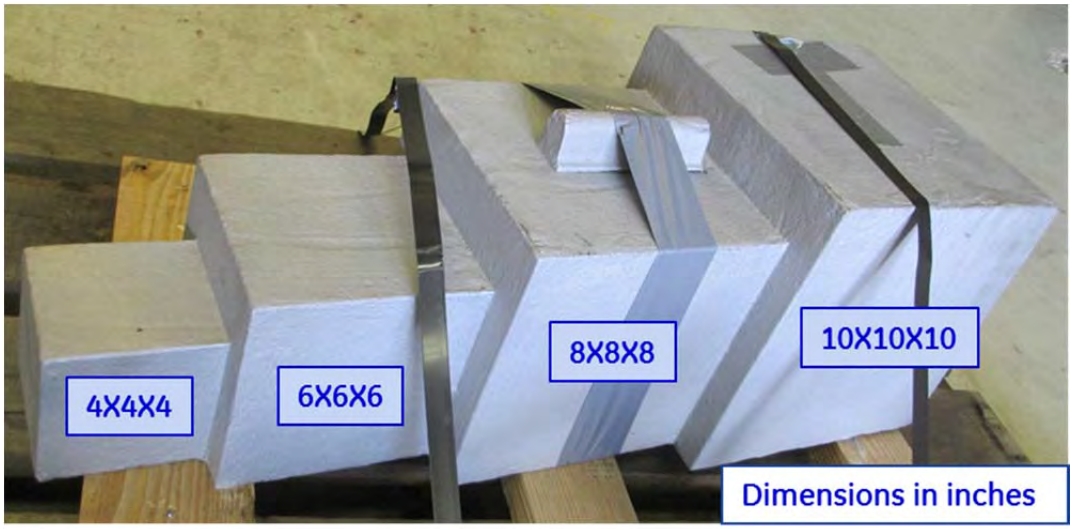

Figure 3: Nimonic 263 step block test casting, weighing 605 lbs. after optimized Homogenizing and Age hardening heat treatments

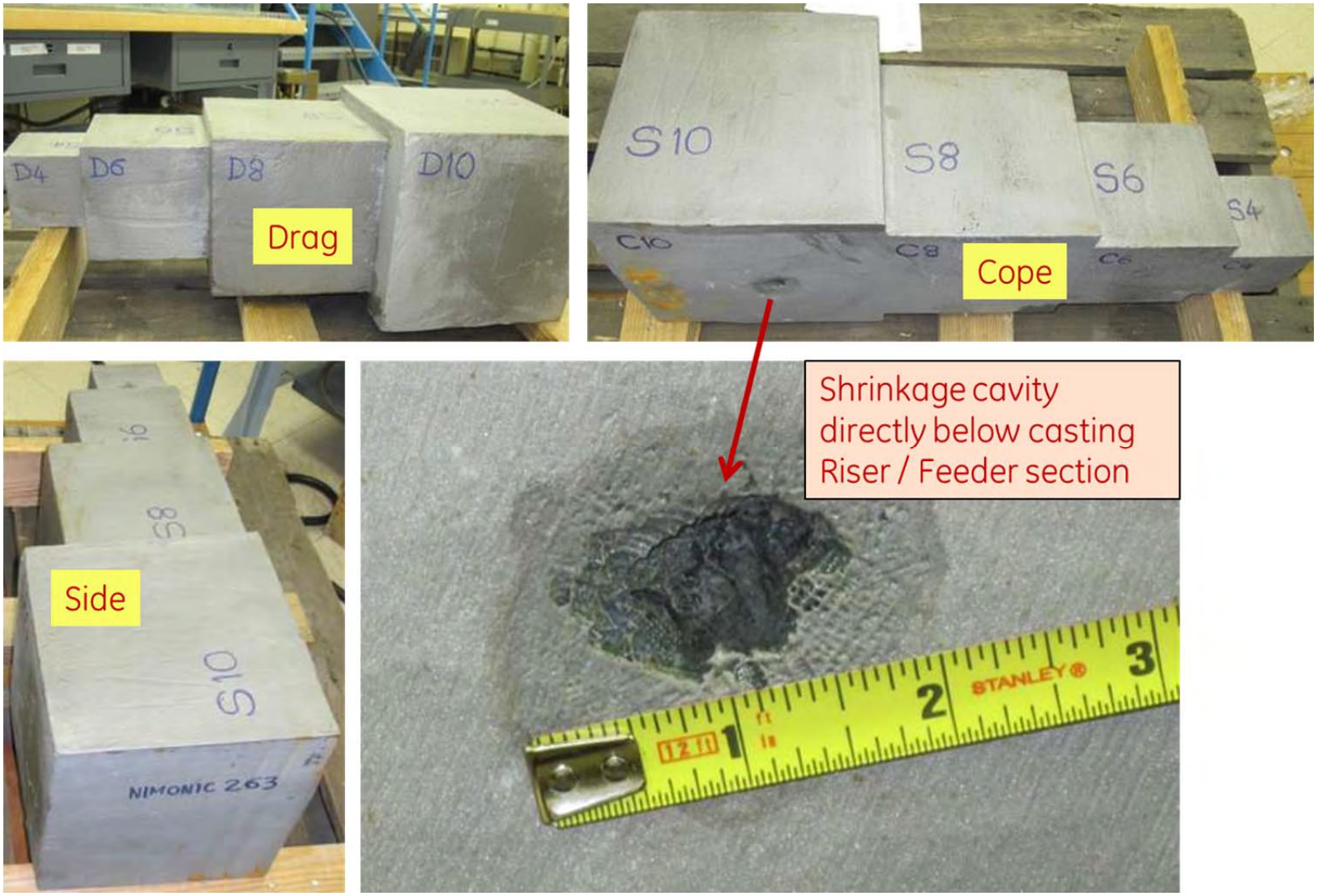

Figure 4: Picture showing the N263 casting and the associated shrink cavity below the rise/feeder section

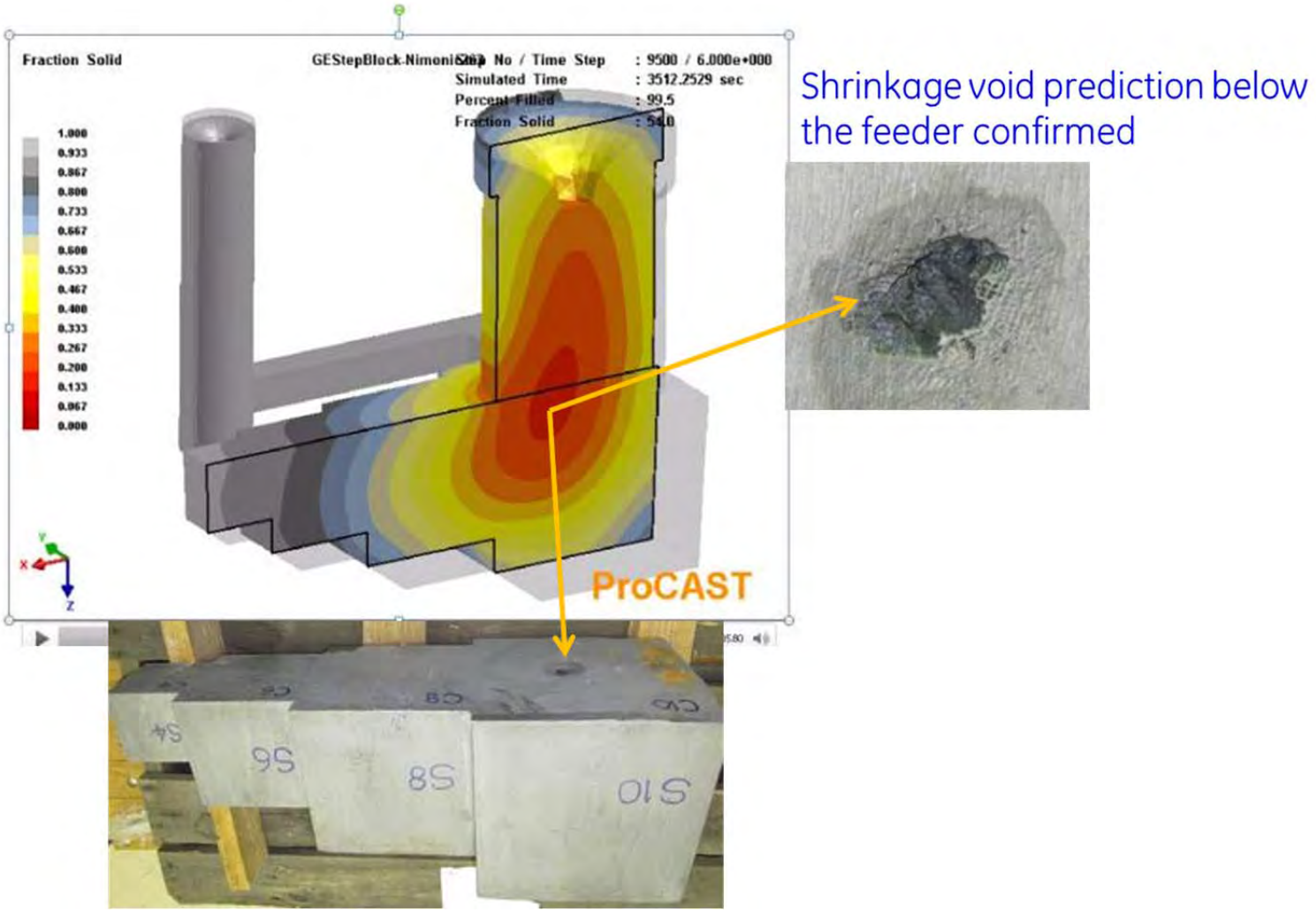

Figure 5: Casting solidification simulation analysis showing the hot spot location and the associated casting defect

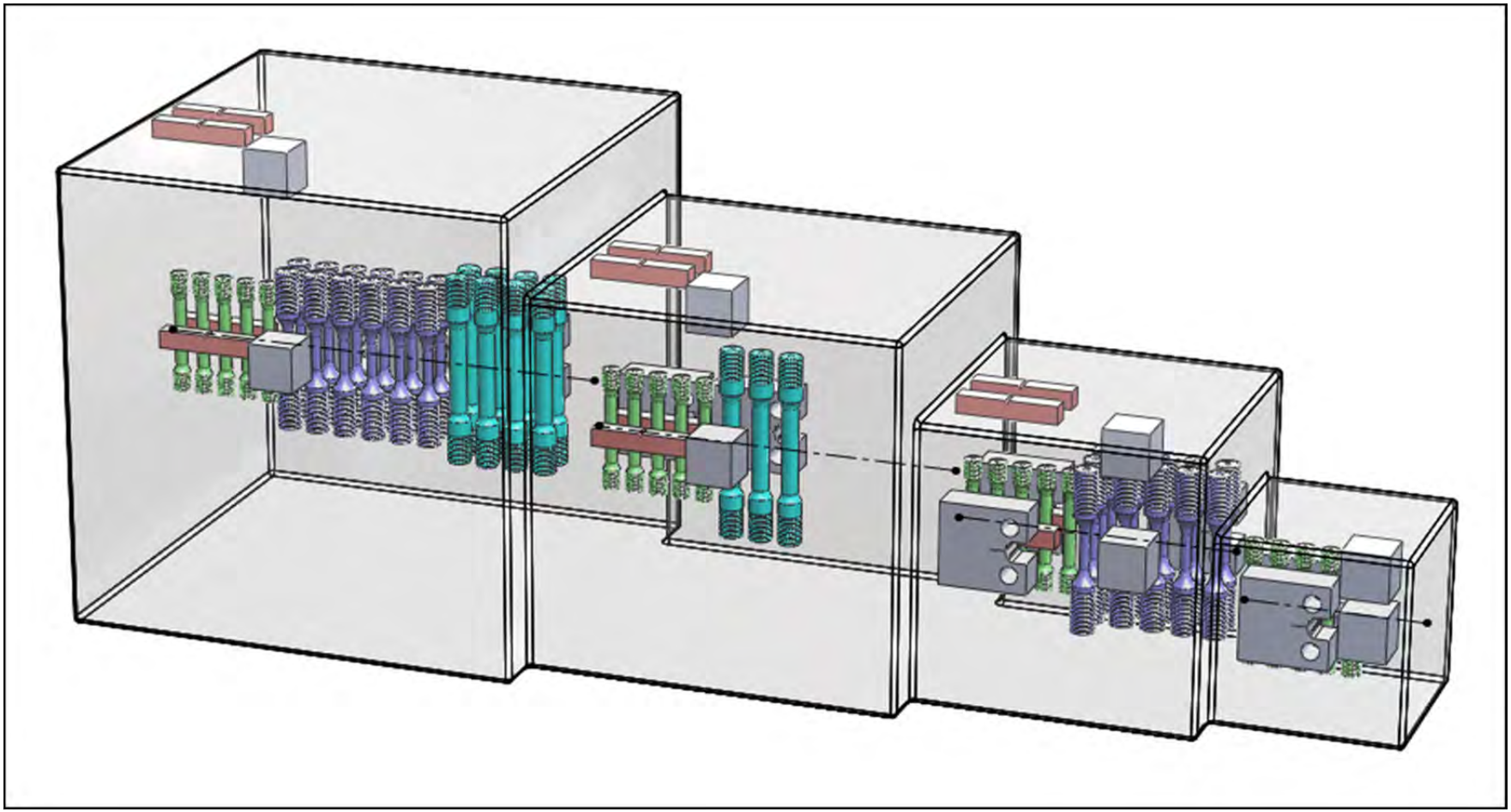

Figure 6: Nimonic 263 test casting,CAD layout of specimen extraction isometric views from step block cast sections

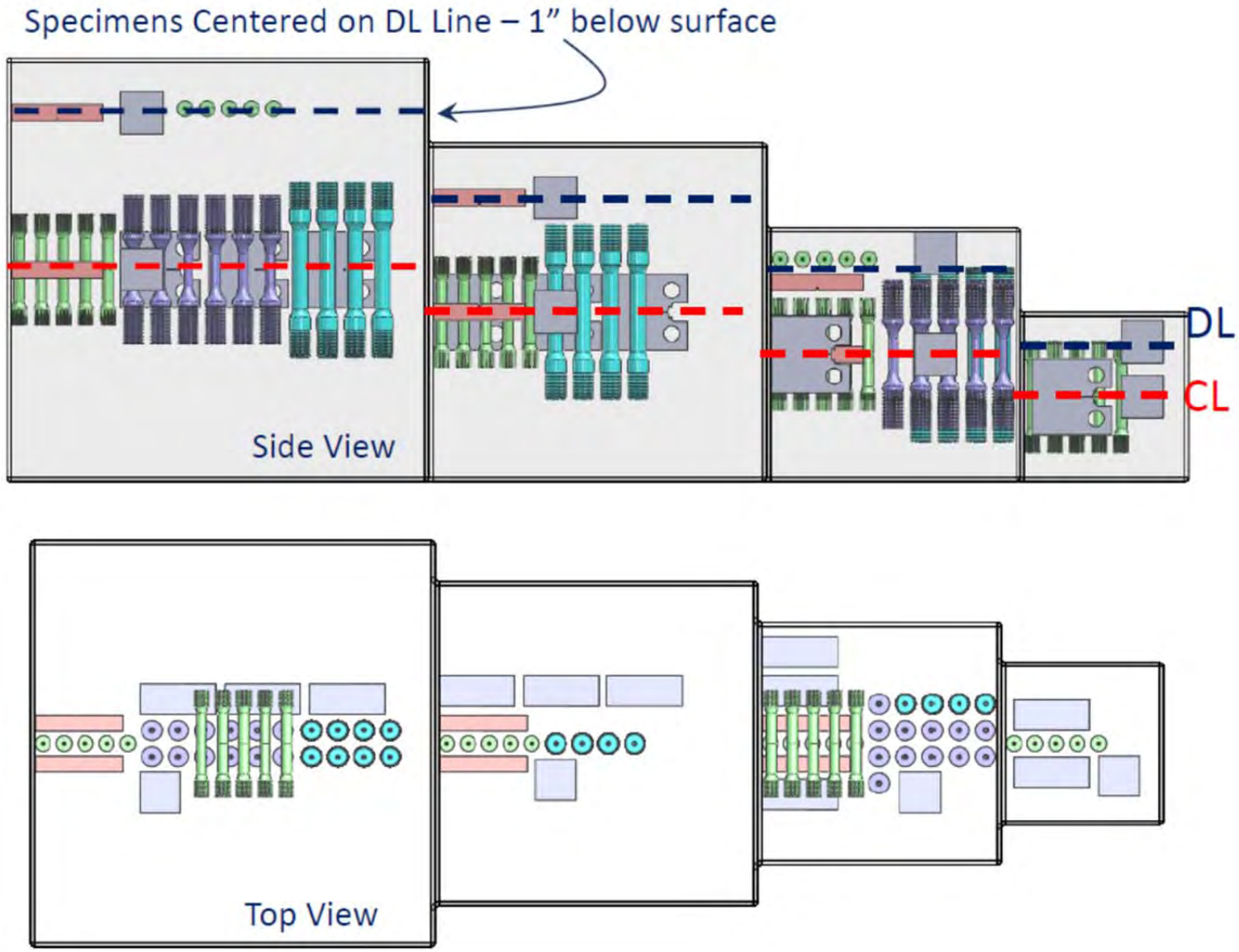

Figure 7: Orientation and specimen layout of various test specimens from N263 test block

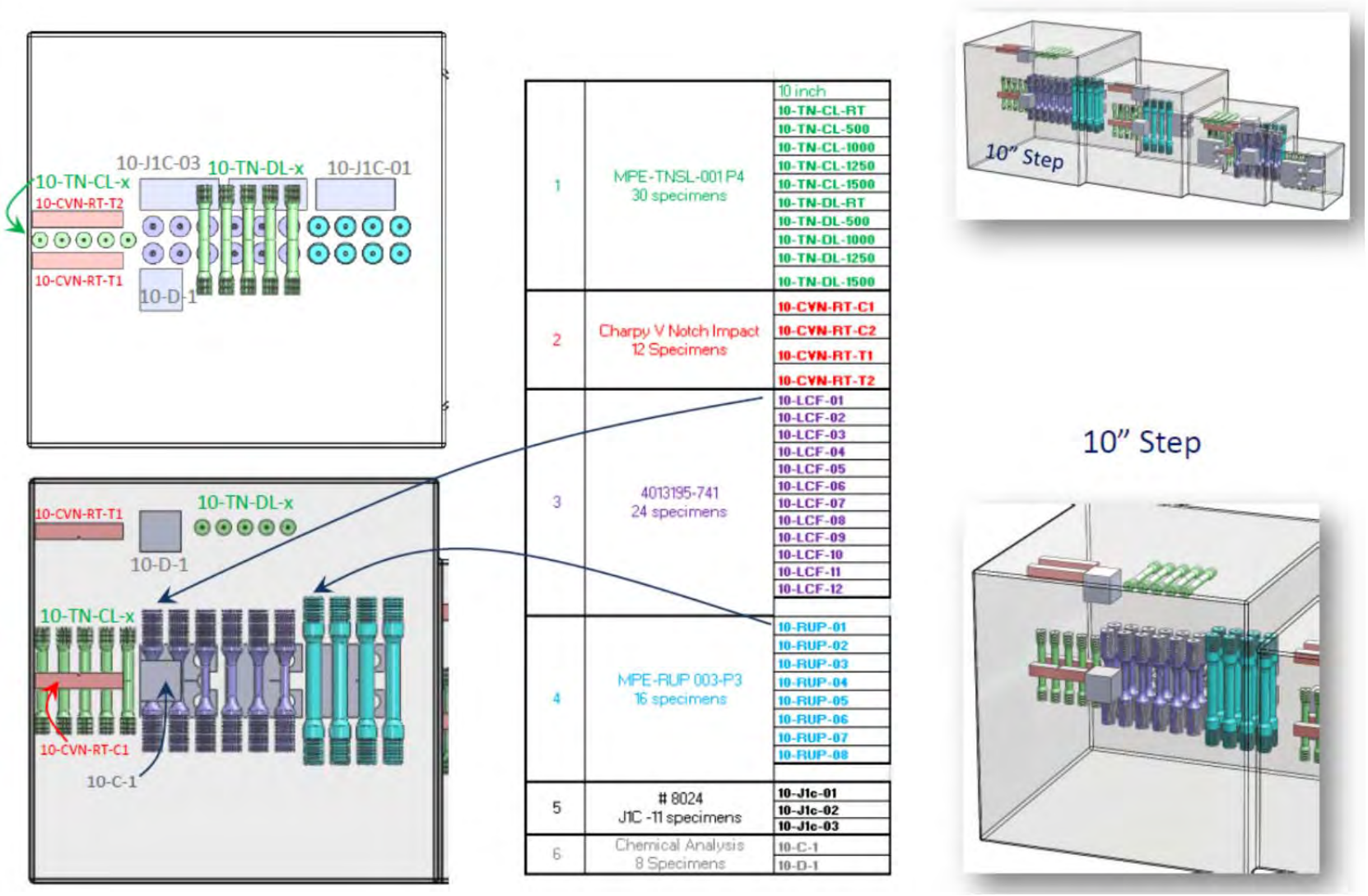

Figure 8: Color coded map of various specimens from the 10" Block [Green – Tensile, Red – Charpy, Purple –LCF, Blue – Rupture and Grey – J1c specimens]

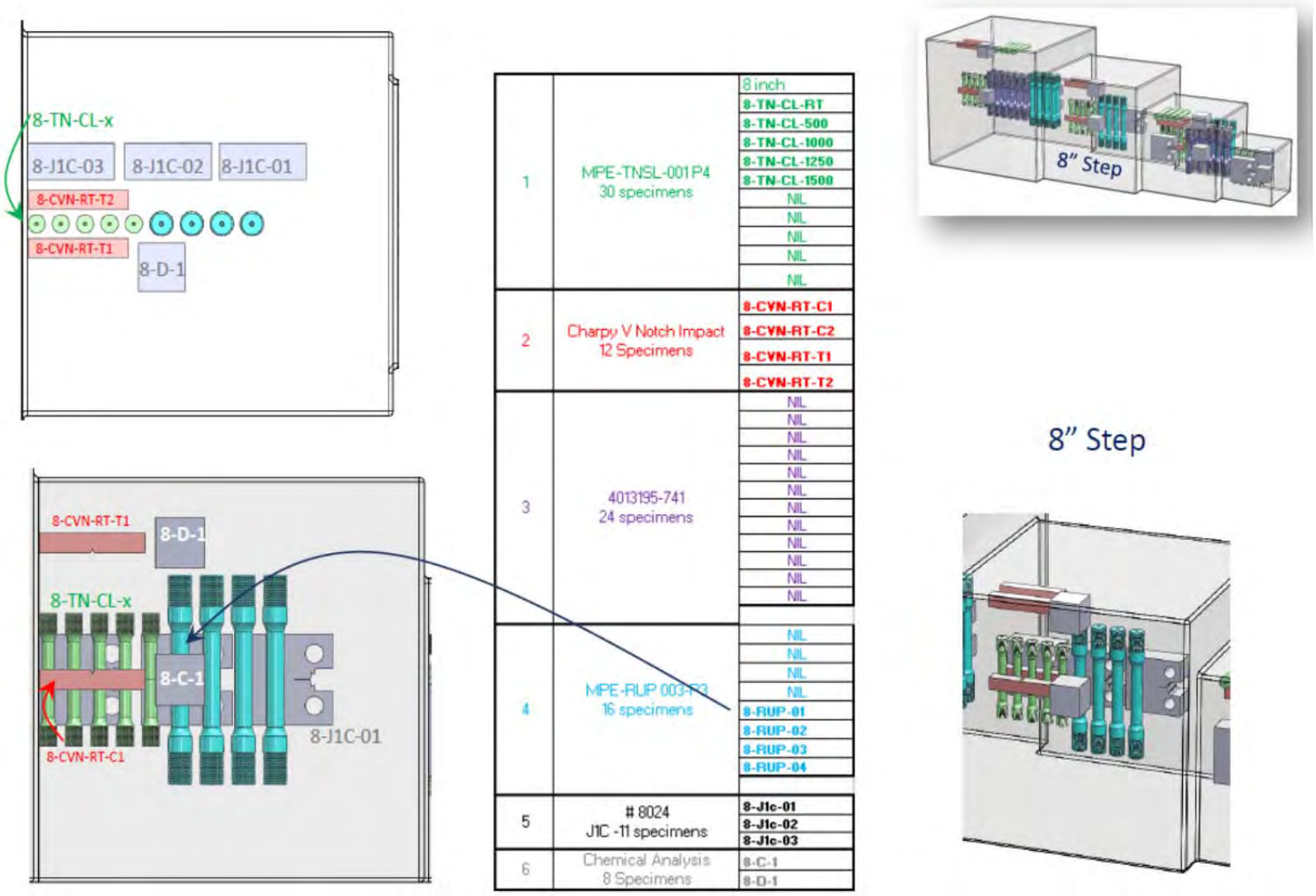

Figure 9: Color coded map of various specimens from the 8" Block [Green – Tensile, Red – Charpy, Purple –LCF, Blue – Rupture and Grey – J1c specimens]

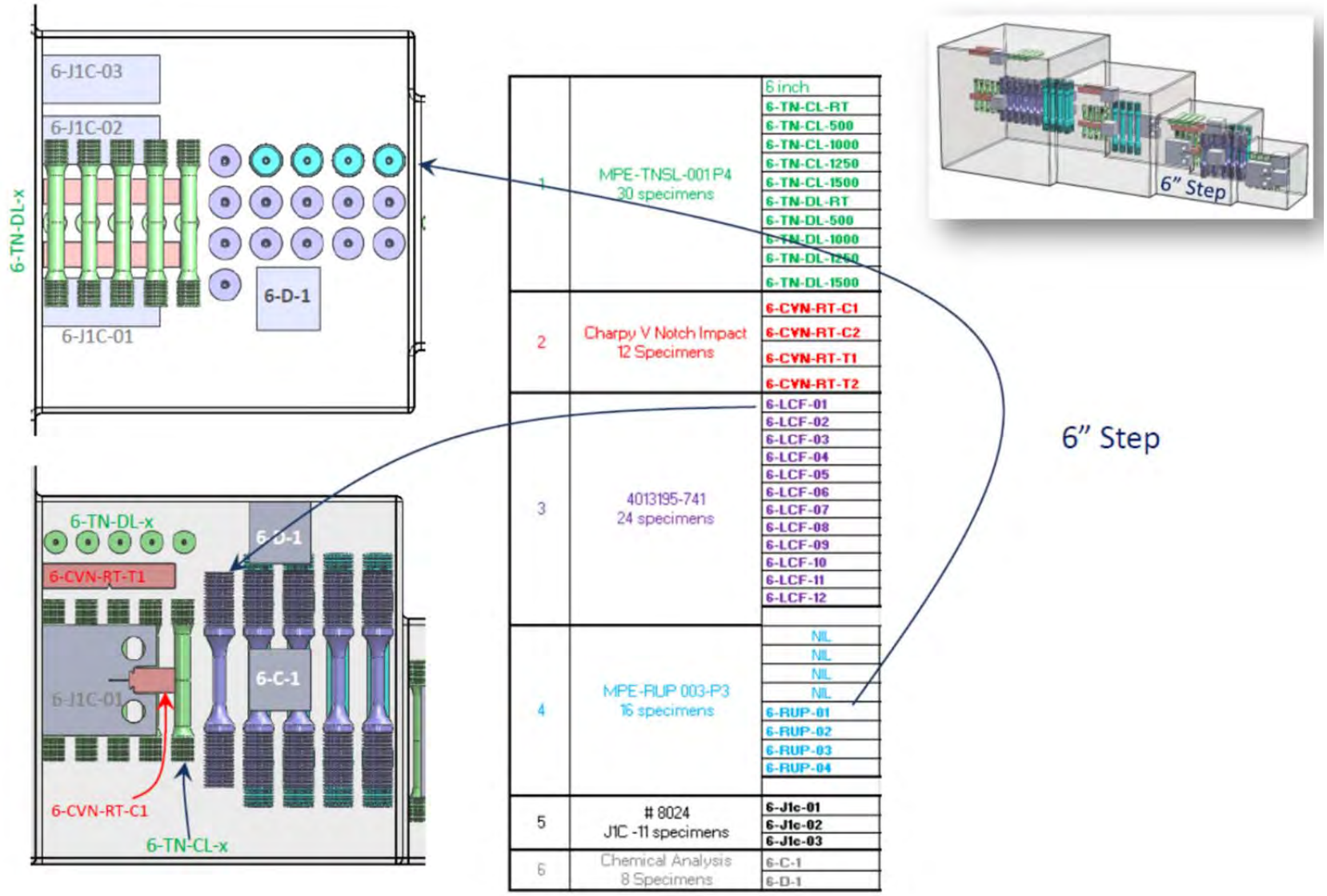

Figure 10: Color coded map of various specimens from the 6" Block [Green – Tensile, Red – Charpy, Purple –LCF, Blue – Rupture and Grey – J1c specimens]

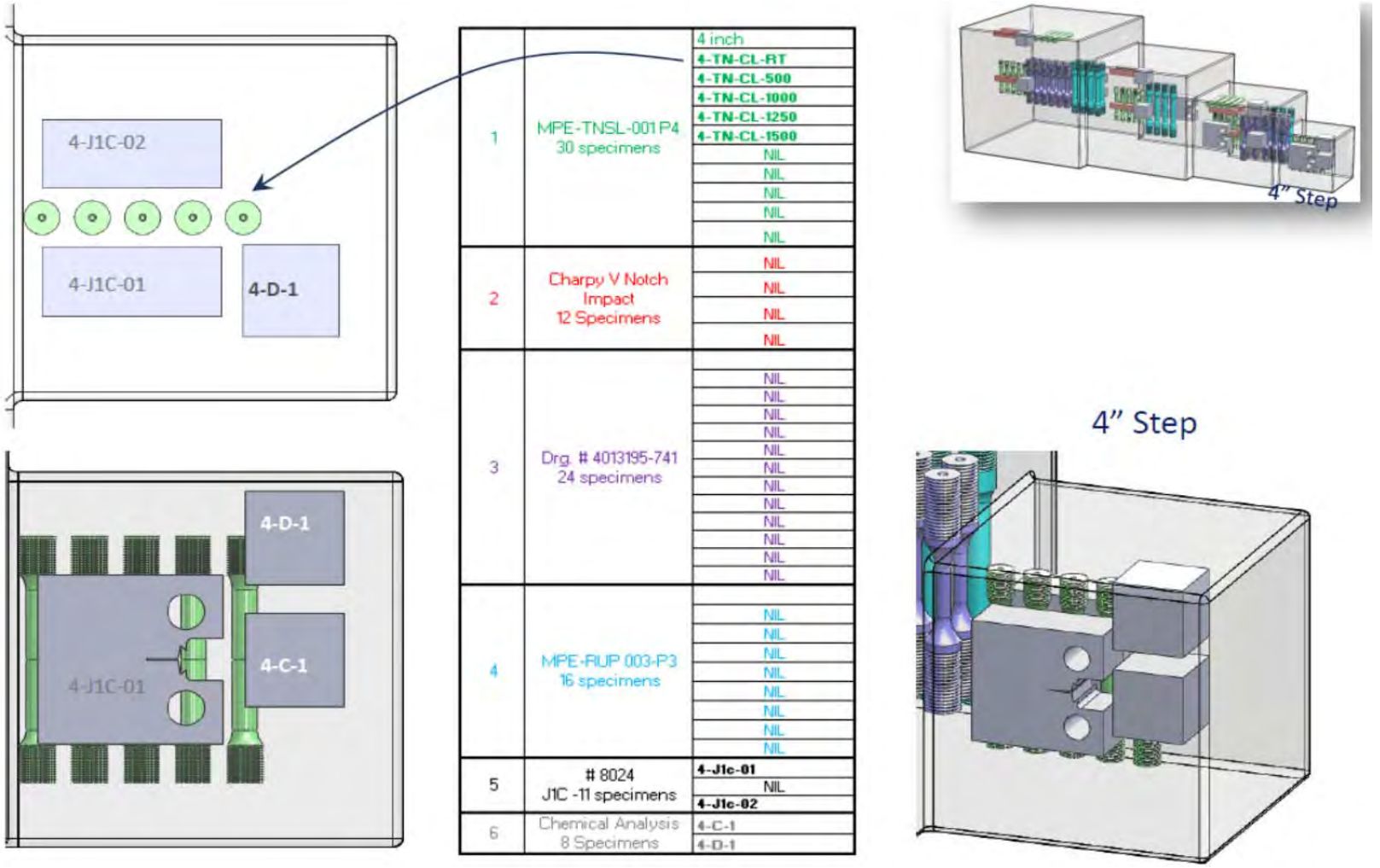

Figure 11: Color coded map of various specimens from the 4" Block [Green – Tensile and Grey – J1c specimens]

Nimonic 263 step block test matrix:					Specimens Identification			
Test #	Test Type	Test condition	Step sections	Total Tests	Specimen ID / Step section			
		Temperature deg.F	10"/8"/6"/4"		10 inch	8 inch	6 inch	4 inch
1	Tensile Test (TS, YS, % EL, %RA) Tensile Specimen: MPE-TNSL-001 P4 30 specimens	RT/ 75 deg. F	1 Test/section in CL plane in vertical orientation	4	10-TN-CL-RT	8-TN-CL-RT	6-TN-CL-RT	4-TN-CL-RT
		500 deg. F		4	10-TN-CL-500	8-TN-CL-500	6-TN-CL-500	4-TN-CL-500
		1000 deg.F		4	10-TN-CL-1000	8-TN-CL-1000	6-TN-CL-1000	4-TN-CL-1000
		1250 deg.F		4	10-TN-CL-1250	8-TN-CL-1250	6-TN-CL-1250	4-TN-CL-1250
		1500 deg F		4	10-TN-CL-1500	8-TN-CL-1500	6-TN-CL-1500	4-TN-CL-1500
		RT/ 75 deg. F	1 Test/section in DL plane in Horizontal orientation (1" above Drag / bottom surface)	2	10-TN-DL-RT	NIL	6-TN-DL-RT	NIL
		500 deg. F		2	10-TN-DL-500	NIL	6-TN-DL-500	NIL
		1000 deg.F		2	10-TN-DL-1000	NIL	6-TN-DL-1000	NIL
		1250 deg.F		2	10-TN-DL-1250	NIL	6-TN-DL-1250	NIL
		1500 deg F		2	10-TN-DL-1500	NIL	6-TN-DL-1500	NIL
2	Charpy V Notch Impact Impact Energy (J); % Shear, Lateral Expansion 12 Specimens	RT/ 75 deg F	2 Tests at Centre CL plane vertical per section	6	10-CVN-RT-C1	8-CVN-RT-C1	6-CVN-RT-C1	NIL
					10-CVN-RT-C2	8-CVN-RT-C2	6-CVN-RT-C2	NIL
			2 Tests at DL horizontal plane per section	6	10-CVN-RT-T1	8-CVN-RT-T1	6-CVN-RT-T1	NIL
					10-CVN-RT-T2	8-CVN-RT-T2	6-CVN-RT-T2	NIL
3	LCF Data Frequency: 20 cpm Waveform: Triangular A Strain 1, TSR% (1.0; 0.90; 0.80; 0.70; 0.60; 0.50) 2 temperatures: RT & 1400 deg. F. Specimen Drg. # 4013195-741 24 specimens		A strain / TSR (%)					
		RT/ 75 deg F	1 / 1.00	2	10-LCF-01	NIL	6-LCF-01	NIL
			1 / 0.90	2	10-LCF-02	NIL	6-LCF-02	NIL
			1 / 0.80	2	10-LCF-03	NIL	6-LCF-03	NIL
			1 / 0.70	2	10-LCF-04	NIL	6-LCF-04	NIL
			1 / 0.60	2	10-LCF-05	NIL	6-LCF-05	NIL
			1 / 0.50	2	10-LCF-06	NIL	6-LCF-06	NIL
		1400 deg F	1 / 1.00	2	10-LCF-07	NIL	6-LCF-07	NIL
			1 / 0.90	2	10-LCF-08	NIL	6-LCF-08	NIL
			1 / 0.80	2	10-LCF-09	NIL	6-LCF-09	NIL
			1 / 0.70	2	10-LCF-10	NIL	6-LCF-10	NIL
			1 / 0.60	2	10-LCF-11	NIL	6-LCF-11	NIL
			1 / 0.50	2	10-LCF-12	NIL	6-LCF-12	NIL

Figure 12: Test matrix for Tensile, Charpy impact energy and LCF properties with specimen identification

Nimonic 263 step block test matrix:					Specimens Identification			
Test #	Test Type	Test condition	Step sections	Total Tests	Specimen ID / Step section			
		Temperature deg.F	10"/8"/6"/4"		10 inch	8 inch	6 inch	4 inch
4	Stress rupture Specimen per MPE-RUP 003-P3 16 specimens (Creep data not required)	Temperature deg.F	Stress					
		1472	40	1	10-RUP-01	NIL	NIL	NIL
		1472	35	1	10-RUP-02	NIL	NIL	NIL
		1472	30	1	10-RUP-03	NIL	NIL	NIL
		1472	25	1	10-RUP-04	NIL	NIL	NIL
		1400	45	3	10-RUP-05	8-RUP-01	6-RUP-01	NIL
		1400	40	3	10-RUP-06	8-RUP-02	6-RUP-02	NIL
		1400	35	3	10-RUP-07	8-RUP-03	6-RUP-03	NIL
		1400	30	3	10-RUP-08	8-RUP-04	6-RUP-04	NIL
5	Fracture Toughness Specimen per # 8024 J1C -11 specimens	RT/ 75 deg. F		4	10-J1c-01	8-J1c-01	6-J1c-01	4-J1c-01
		1000 deg.F		3	10-J1c-02	8-J1c-02	6-J1c-02	NIL
		1400 deg F		4	10-J1c-03	8-J1c-03	6-J1c-03	4-J1c-02
6	Chemical Analysis 8 Specimens	Ni,Cr,Co,Mo,Ti,Al,Fe,	Thermal Center	4	10-C-1	8-C-1	6-C-1	4-C-1
		Mn,Si,C,B,P,S & Cu	1" above drag	4	10-D-1	8-D-1	6-D-1	4-D-1

Figure 13: Test matrix for Stress rupture, Fracture toughness and Chemical analysis with specimen identification

Chemical Analysis: (Wt. %)	Nimonic 263 N07263 SB - Casting	GJOJ-263-TB-1	Step block casting section locations Chemical composition values (Wt. %)							
			10 inch		8 inch		6 inch		4 inch	
			Thermal-C	Drag-1"	Thermal-C	Drag-1"	Thermal-C	Drag-1"	Thermal-C	Drag-1"
	Flowserve Heat	Cast on coupon	10-C-1	10-D-1	8-C-1	8-D-1	6-C-1	6-D-1	4-C-1	4-D-1
C	0.06	0.01	0.01	0.01	0.01	0.01	0.01	0.01	0.02	0.01
Mn	0.31	0.3	0.29	0.3	0.29	0.3	0.3	0.3	0.3	0.3
Si	0.61*	0.65	0.59	0.66	0.63	0.64	0.66	0.66	0.65	0.66
P	-	<0.010	<0.10	<0.10	<0.10	<0.10	<0.10	<0.10	<0.10	<0.10
S	-	<0.001	<0.001	<0.001	<0.001	<0.001	<0.001	<0.001	<0.001	<0.001
Cr	19.4	20.2	19.97	20.12	20.14	20.07	20.09	20.15	20.12	20.08
Ni	Bal.	50.25	50.23	50.3	50.45	50.5	50.19	50.14	50.18	50.48
Mo	5.8	5.56	5.72	5.67	5.66	5.6	5.8	5.77	5.82	5.55
Co	20.2	19.82	20.14	19.68	19.76	19.67	19.78	19.73	19.67	19.71
Fe	0.45	0.45	0.5	0.48	0.49	0.48	0.46	0.47	0.47	0.48
Cu	0.02	0.02	0.02	0.02	0.02	0.02	0.02	0.02	0.02	0.02
B		0.005	0.005	0.005	0.005	0.005	0.005	0.005	0.005	0.005
Al	0.4	0.34	0.31	0.31	0.32	0.33	0.32	0.32	0.32	0.34
Ti	2.12	2.12	2	2.18	1.97	2.13	2.11	2.16	2.17	2.12

Figure 14: Step block casting thermal center trepanned section chemical analysis. No significant variation in chemistry when compared with casting section Thermnal center analysis

Homogenizing Heat Treatment (Note: As-Cast Incipient MP is 2102°F)

- **Part should be loaded into a room temperature furnace with contact thermocouples for recording homogenization HT cycle. Also furnace thermocouples HT cycle record.**
- **Ramp furnace at a rate not exceeding 350^{0}F/Hour**
- **Hold at 1900^{0}F ± 25^{0}F for four hours**
- **Ramp furnace to 1960^{0}F**
- **Hold at 1960^{0}F ± 25^{0}F for four hours.**
- **Ramp furnace to 2012^{0}F.**
- **Hold at 2012^{0}F ± 25^{0}F for ONE hour**
  - **(Note: Theoretical Incipient MP is now 2291°F)**
- **Ramp furnace to 2090°F**
- **Hold at 2090^{0}F ± 10^{0}F for Four hours**
- **Ramp to 2175°F**
- **Hold at 2175^{0}F ± 10^{0}F for 44 Hours**
  - **(Note: Theoretical Incipient MP is now 2410°F)**
- **Forced Air Cool to RT with fans, keeping contact thermocouples attached for measuring cooling rate**

AGING- HT Cycle

- **Ramp furnace at a rate not exceeding 350^{0}F/Hour**
- **Hold at 1472°F ± 25°F for 8 Hours**
- **Forced Air Cool with Fans measuring cooing rate with contact thermocouples attached.**

Figure 15: Homogenizing and Aging Heat treatment cycles Optimized to within +/- 5% of nominal chemistry variation (NETL)

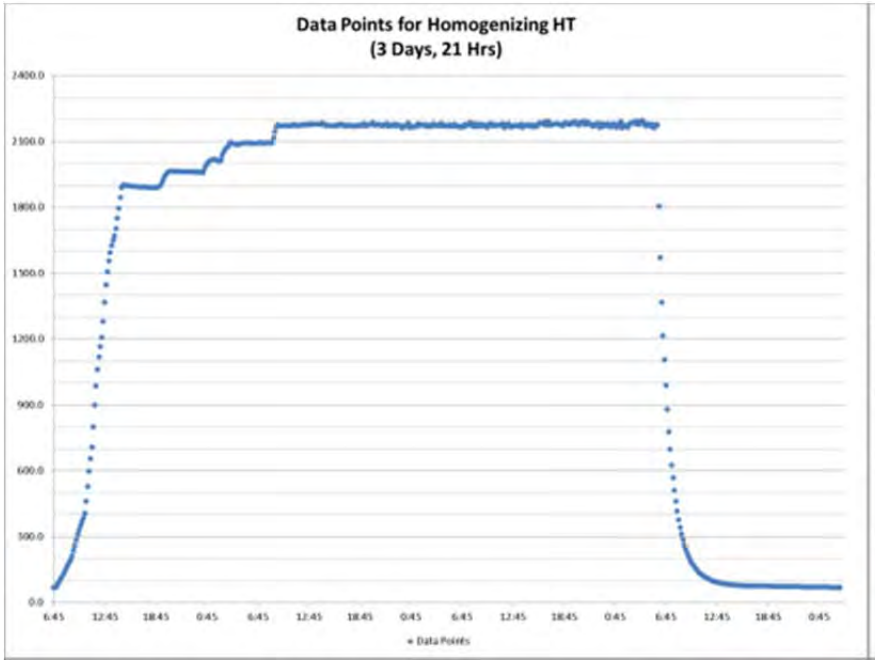

Figure 16: Homogenization Cycle

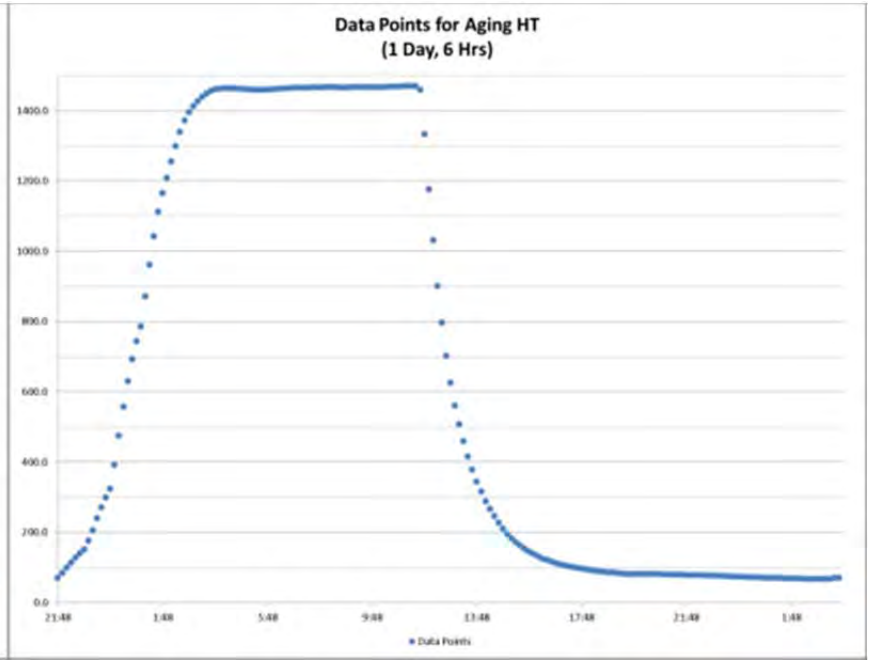

Figure 17: Aging Cycle

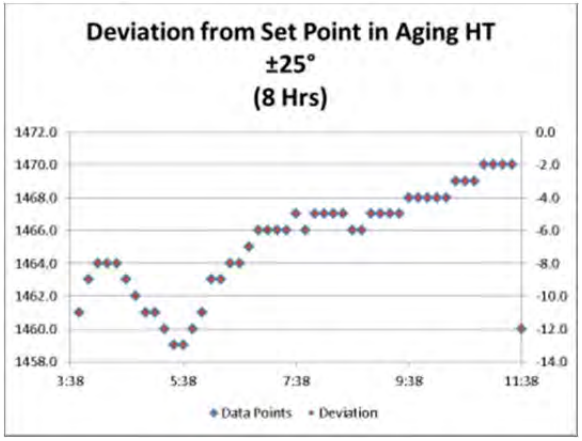

Figure 18: Plot showing deviation from set point in aging HT cycle

4 Inch Specimen Data	6 Inch Specimen Data
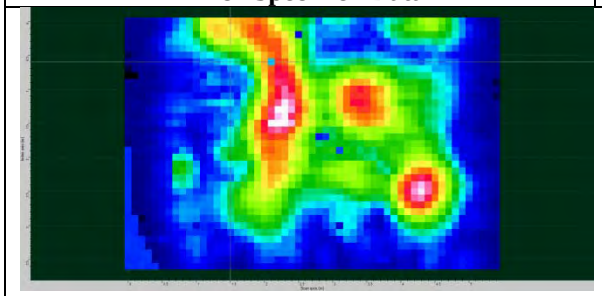 4 Inch Specimen – C Scan at Backwall Linear Color Scale	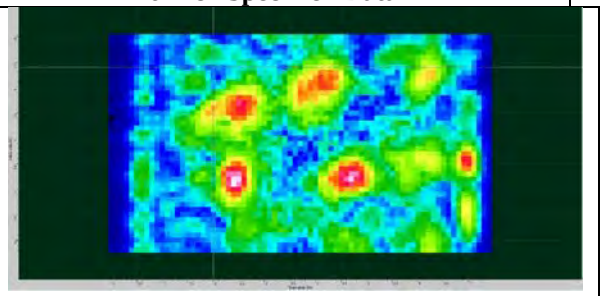 6 Inch Specimen – C Scan at Backwall Linear Color Scale
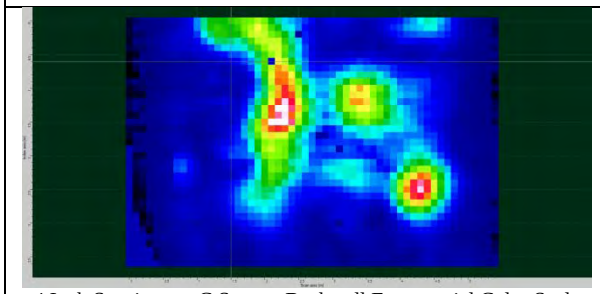 4 Inch Specimen – C Scan at Backwall Exponential Color Scale	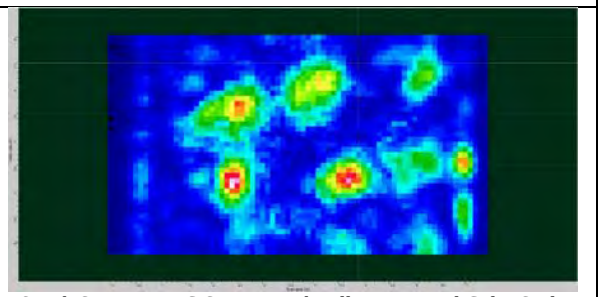 6 Inch Specimen – C Scan at Backwall Exponential Color Scale
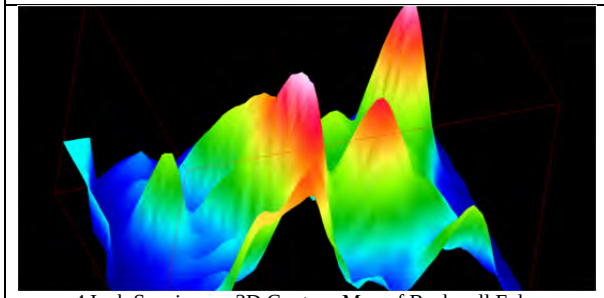 4 Inch Specimen - 3D Contour Map of Backwall Echo	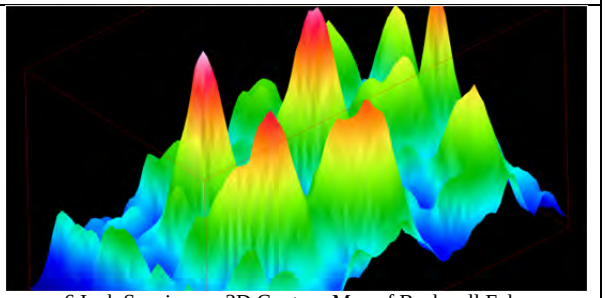 6 Inch Specimen - 3D Contour Map of Backwall Echo
Nimonic 263 step block 4 inch section UT scans	Nimonic 263 step block 6 inch section UT scans

Figure 19: Ultrasonic immersion testing to map back wall echoes as a measure of relative attenuation for 4 inch and 6 inch N263 step block casting sections

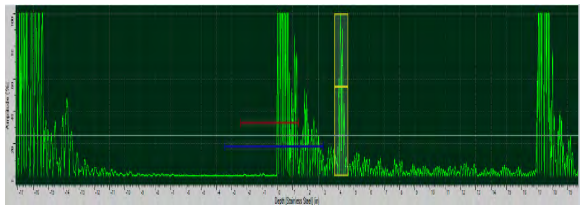

4 Inch Specimen – Maximum amplitude of Backwall Echo

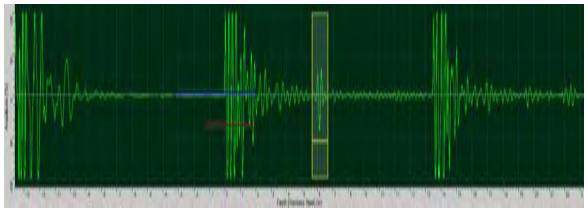

6 Inch Specimen – Maximum amplitude of Backwall Echo (Relative to 4” Specimen)

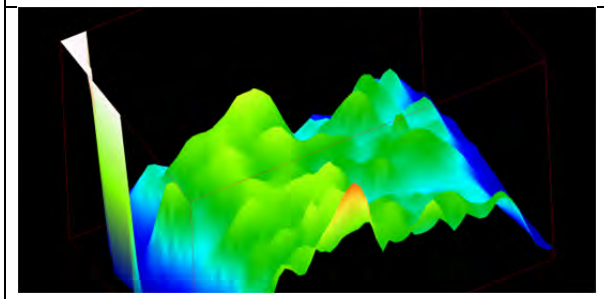

4 Inch Specimen - 3D Contour Map of Noise Preceding the Backwall Echo

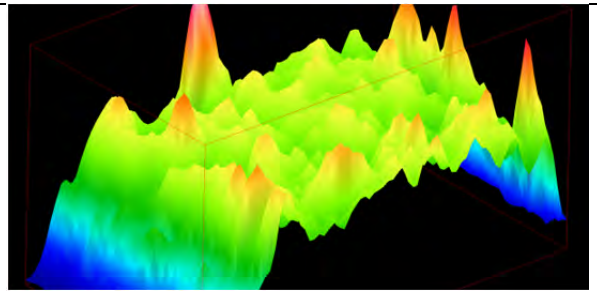

6 Inch Specimen - 3D Contour Map of Noise Preceding the Backwall Echo

Figure 20: Ultrasonic Immersion scan data 3D contour map compilation

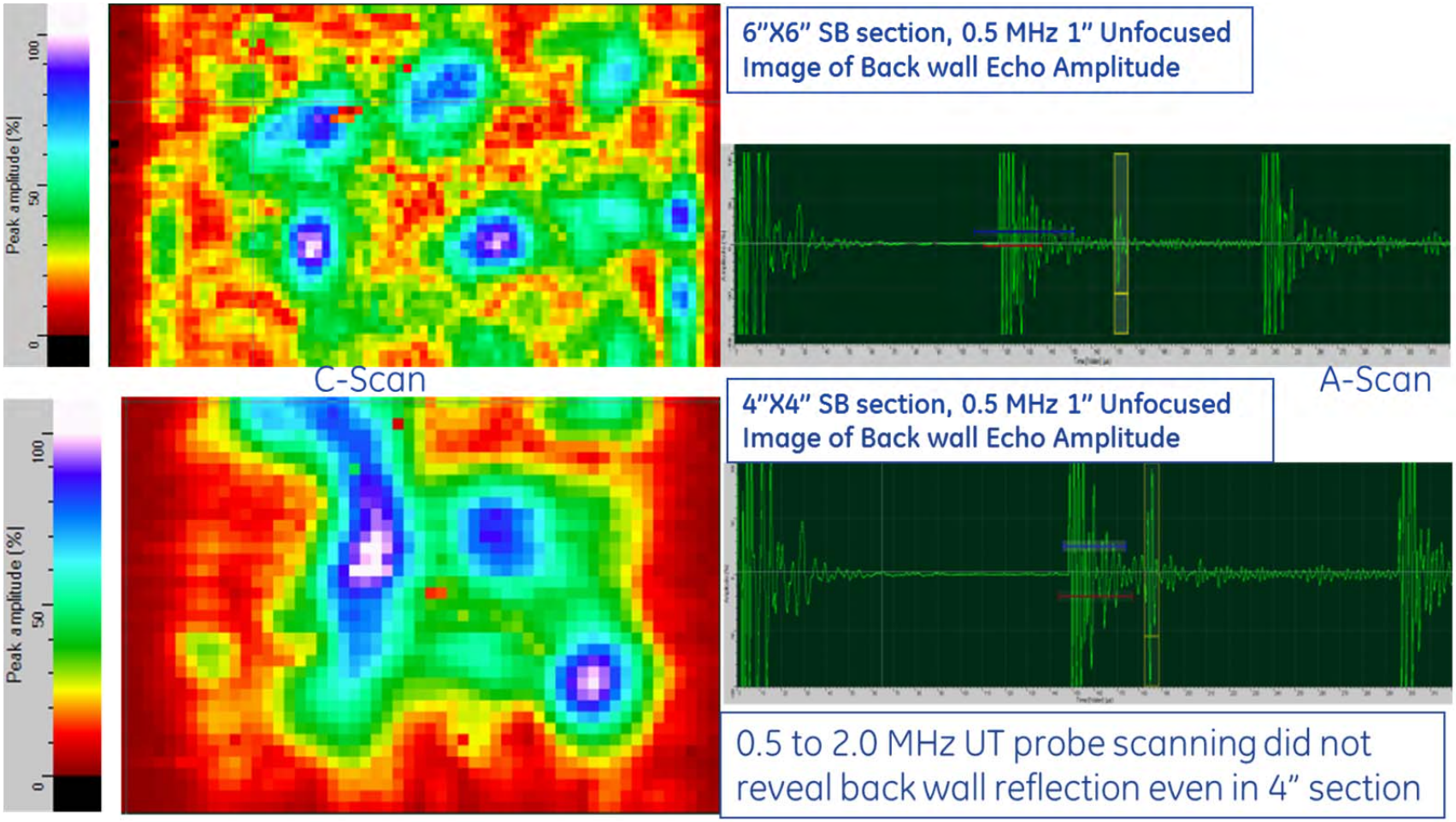

Figure 21: UT immersion scans showing the inherent issue of achieving a superior back wall reflection in thick walled super alloy castings

MISTRAS GROUP INC.
2 MILLBURY STREET
AUBURN, MA. 01501
TELEPHONE (508) 832-5500
FAX (508) 832-5557

CUSTOMER: GENERAL ELECTRIC

RSSS NO. 500455 REV. 0

PAGE 2 OF 2

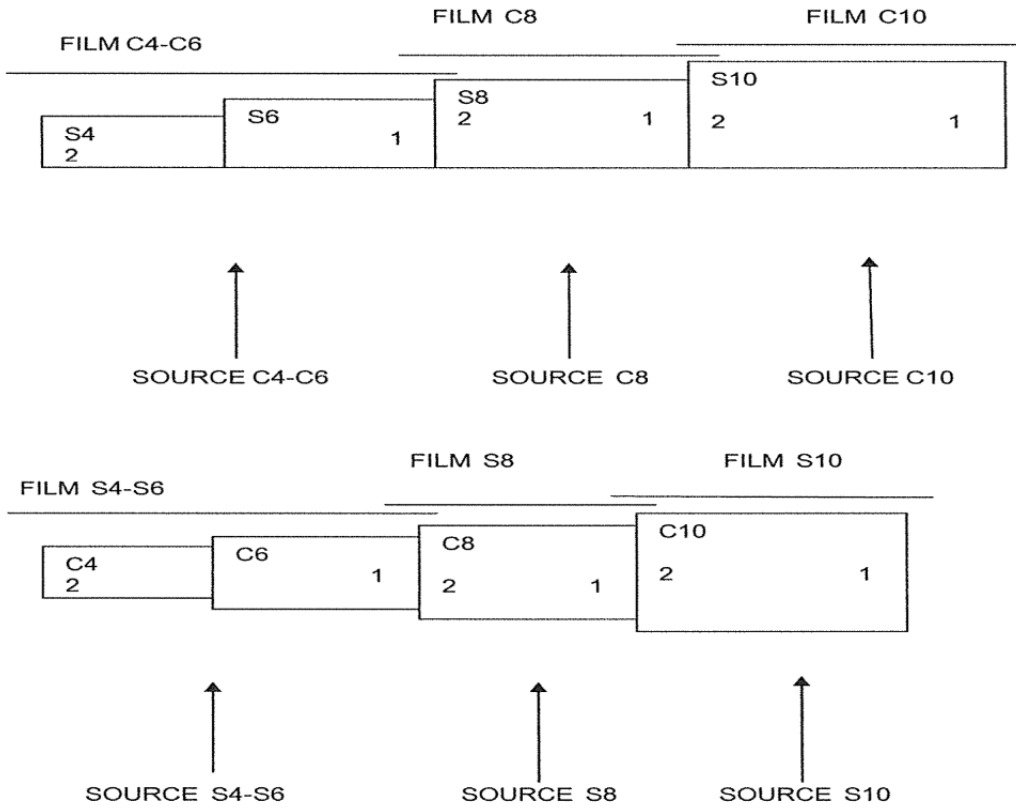

NOTE: SKETCH SHOWS FINISHED DIMENSIONS

Figure 22: Radiographic Scan Plan

MISTRAS GROUP INC

2 Millbury Street
Auburn, Massachusetts 01501
(508) 832-5500 Fax (508) 832-5557

RADIOGRAPHIC REPORT
PAGE__1__ OF __1_

LOCATIONS NATIONWIDE

BRANCH LABORATORY
SPRINGFIELD, MA.
(413) 734-6648 FAX: (413) 734-2810

Nondestructive Testing - QA/QC Services - Chemical Testing - Mechanical Testing - Metallurgical Testing & Failure Analysis

CASTING☐ WELDMENTS TRANSISTORS☐ DIODES☐ OTHER☐

CUSTOMER: GENERAL ELECTRIC CO. | P.O. NO.: 900473361

ADDRESS: 1 RIVER ROAD SCHENECTADY, NY.

PART NAME: NIMONIC 263 STEP BLOCK	PART NO.: N/A	STAGE OF MFG.: AS CAST	HEAT NO.: N/A

SPEC. NO.: ASTM E94	STANDARD: ASTM E186 & E280	CLASS: NOTE INDICATIONS

TYPE OF MATERIAL:	DATE RADIOGRAPHED: 6-13	GOV'T INSPECTION:	MISTRAS JOB NO.: 500455	FILM TOTAL: 24

SERIAL NO.	VIEW	ACCEPT	REJECT	N.A.D.	FILM SIZE	NO. OF FILM	CODE*						SURFACE	COMMENTS
C4	1-2				14X17	4								GAS ASTM E186 CL 1
S4	1-2				14X17	4								NO APPARENT INDICATIONS
C6	1-2													NO APPARENT INDICATIONS
S6	1-2													NO APPARENT INDICATIONS
C8	1-2				14X17	4								NO APPARENT INDICATIONS, FILM ARTIFACT
S8	1-2				14X17	4								NO APPARENT INDICATIONS, FILM ARTIFACT
C10	1-2				14X17	4								SAND ASTM E280 CLASS 3 & 4 , SURFACE
S10	1-2				14X17	4								SURFACE

MISTRAS GROUP INC. REVIEWER: WAINO GUSTAFSON Waino Gustafson REVIEWER'S NO.: 42 LEVEL III DATE: 6-14-13

***CODE WELDMENTS AND CASTINGS 509**

1. CRACK
2. SHRINK
3. HOT TEAR
4. SAND INCLUSION
5. INCLUSION
6. GAS INCLUSION
7. POROSITY
8. SEGREGATION
9. UNFUSED CHAPLET
10. INTERNAL CHILL
11. COLD SHUT
12. FOREIGN MAT. LESS DENSE
13. FOREIGN MAT. MORE DENSE
14. SLAG INCLUSION
15. IMCOMPLETE PENETRATION
16. IMCOMPLETE FUSION
17. UNDERCUT
18. BURN THROUGH
19. TUNGSTEN INCLUSION
20. LACK OF BRAZE

* CODE
31. EXTRANEOUS MATTER
32. EXC. PASTE BUILD-UP
33. PASTE DEPOSITS
34. PASTE FORMATION
35. SOLDER BALL
36. INADEQUATE CLEARANCE
37. MISALIGNED DIODE CRYSTAL
38. CRYSTAL UNDER-CUTTONG
39. FUSION CRYSTAL TO CASE
40. DEFECTIVE LEAD WIRE
41. DISPLACED GETTER RING
42. PHYSICAL DAMAGE
43. PASTE EXPULSION
44. DEFORMED DIODE WHISKER
45. LOOPS OR TWIST IN WIRE
46. BENT TERMINAL
47. POOR CONSTRUCTION

This report is not to be construded as a guaranty or warrenty of the condition of the materials tested. MISTRAS GROUP INC. is not liable for any misinterpertation of results or conditions, or for any claims or losses attributable to performance of a test. These services are rendered without any warranty. Any liability is limited to the amount paid for the services at isue. All orders are subject to MISTRAS GROUP INC.'s Standard Terms and Conditions of Sale, which are available upon request.

Figure 23: Radiographic Test Report

MISTRAS GROUP INC.
2 MILLBURY STREET
AUBURN, MA. 01501
TELEPHONE (508) 832-5500
FAX (508) 832-5557

RADIOGRAPHIC STANDARD SHOOTING SKETCH

CUSTOMER: GENERAL ELECTRIC			RSSS NO. 500455 REV. 0 PAGE 1 OF 2					
PART NAME: TEST BLOCK			PART NUMBER: NIMONIC 263					
RADIOGRAPHY OF CASTING		MATERIAL		A/C	X	S/M		M
SPECIFICATION: ASTM E94			STANDARD: ASTM E186 & E280 NOTE INDICATIONS					
FILM PROCESSING METHOD: AUTOMATIC		CHEM. MFG.: AGFA			CASSETTE TYPE: FLEX			
EXPOSURE NO.	1 & 2	3 & 4	5&6					
REFERENCE MARKERS	S4 –S6 1-2 & C4 –C6 1-2	S8 1-2 & C8 1-2	S10 1-2 & C10 1-2					
SOURCE TYPE	XRAY	XRAY	XRAY					
SOURCE SIZE	1.0 MM	1.0 MM	1.0 MM					
CURIES OR KV	4.0 MEV	4.0 MEV	4.0 MEV					
AMPERAGE	250 MA	250 MA	250 MA					
FOCAL FILM DISTANCE	77"	77"	77"					
MACHINE NUMBER	VARIAN 4.0	VARIAN 4.0	VARIAN 4.0					
EXPOSURE TIME	500 COUNT	1800 COUNT	8000 COUNT					
MATERIAL THICKNESS	4"	8"	10"					
PENE (S) ON PIECE	80	160	200					
PENE (S) ON BLOCKS	N/A	N/A	N/A					
PENE BLOCK (S) THKS.	N/A	N/A	N/A					
PENE (S) ON SHIM	N/A	N/A	N/A					
PENE SHIM (S) THKS.	N/A	N/A	N/A					
MATERIAL TYPE / GROUP	I	I	I					
FILM SIZE & QUANTITY	14X17 8	14X17 8	14X17 8					
FILM TYPE (S) AGFA	D7/5/4/7	D7/5/4/7	D7/5/4/7					
SCREEN PB. FRONT	.010"	.010"	.010"					
SCREEN PB CENTER	N/A	N/A	N/A					
SCREEN PB. BACK	.010"	.010"	.010"					
QUALITY LEVEL	2-2T	2-2T	2-2T					
NO. OF EXP. IN EACH COLUMN	2	2	2					
DENSITIES: 1.5-4.0 SFT. & DFT.				DATE:6-14-13				
COMMENTS:								
VENDOR APPROVAL (AS REQUIRED:)								
SIGNATURE LEVEL III APPROVAL:								

Figure 24: Radiographic Technique Sheet Nimonic 263 Step block casting

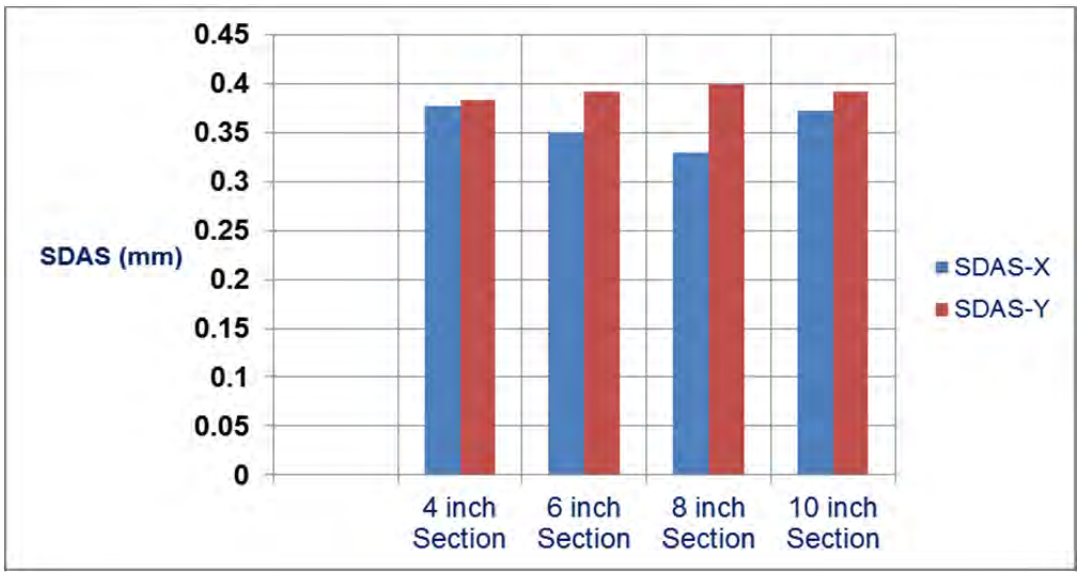

Figure 25: **Nimonic 263 step block casting SDAS measurements with section size**

Table 1: **Nimonic 263 Step block cast sections SDAS Measurements. Consistently in the range of 0.35 to 0.40 mm for 100 to 250 mm cast sections.**

N263 SB Casting SDAS Measurements				
	SDAS Counts #		SDAS Average value (mm)	
Section thickness	X	Y	SDAS-X	SDAS-Y
4 inch Section	32	29	0.38	0.38
6 inch Section	25	30	0.35	0.39
8 inch Section	27	27	0.33	0.40
10 inch Section	27	25	0.37	0.39

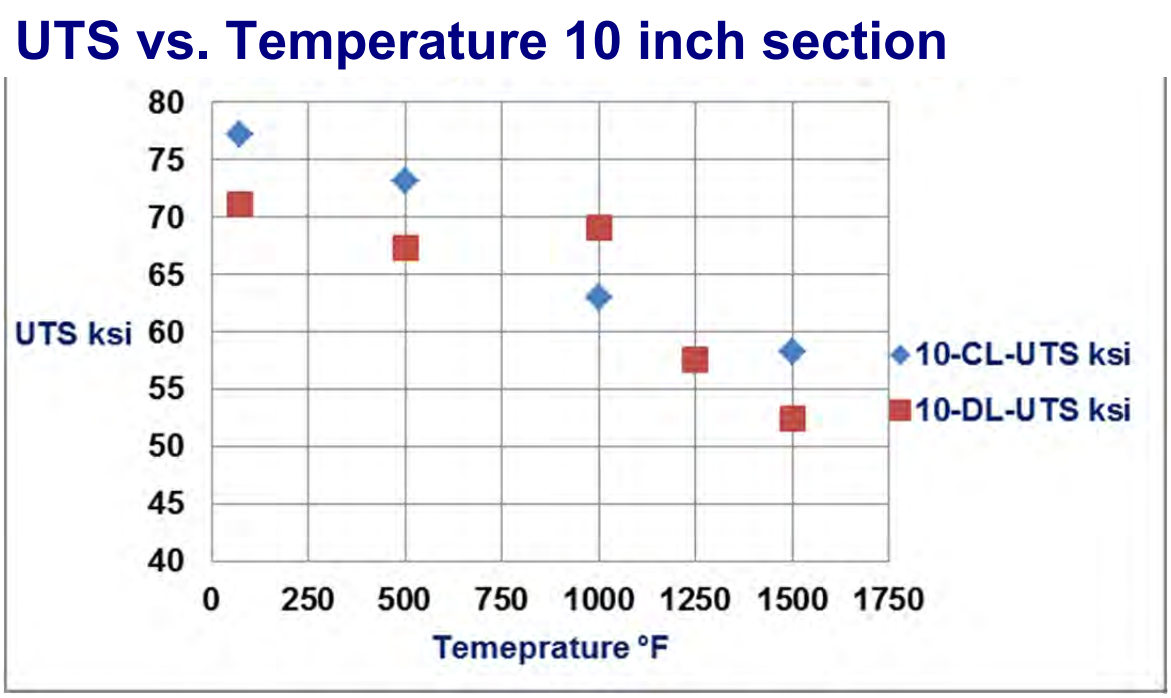

Figure 26: UTS vs temperature plot for 10 inch section CL and DL location trepans

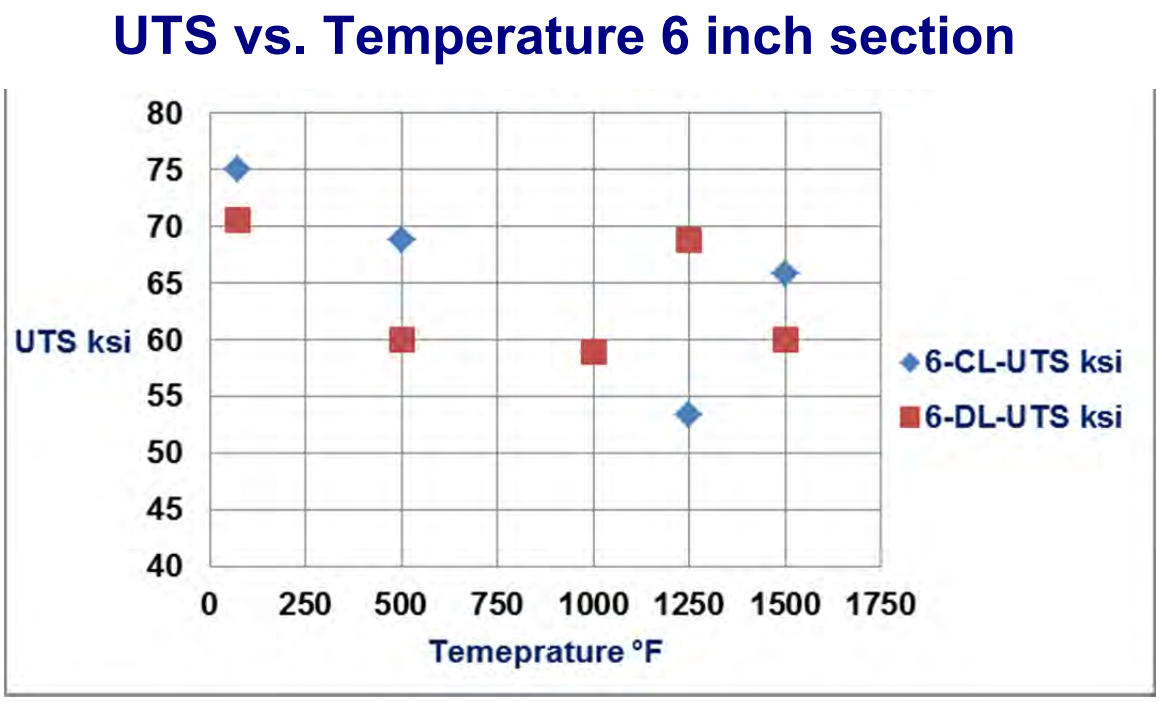

Figure 27 UTS vs temperature plot for 6 inch section CL and DL location trepans

0.2% YS vs. Temperature for all cast section trepans from CL and DL

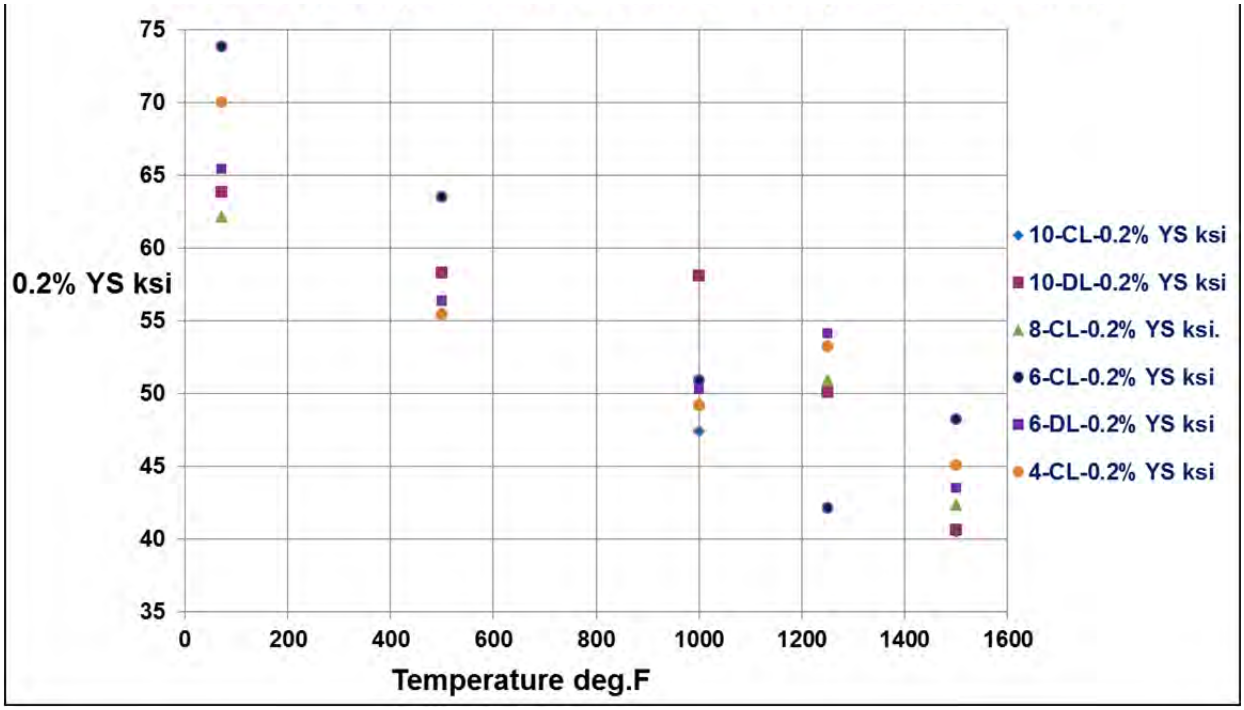

Figure 28: 0.2 % YS vs. Temperature for all N263 step block cast section trepans. The 0.2% YS vs. temperature trend plot shows tighter band trepan CL values at elevated temperatures for all section thicknesses

Table 2: N263 Step block trepan cast sections 0.2% Yield strength vs temperature data

N263 Step Block trepan cast sections 0.2% YS vs. Temperature						
Section thickness (inches)	**10-CL (10)**	**10-DL (10)**	**8-CL (8)**	**6-CL (6)**	**6-DL (6)**	**4-CL (4)**
Temperature °F	(ksi)	(ksi)	(ksi)	(ksi)	(ksi)	(ksi)
72°F	70	63.8	62.1	73.8	65.4	70
500°F	55.5	58.3	56.4	63.5	56.4	55.4
1000°F	47.4	58.1	49.3	50.9	50.3	49.2
1250°F	50.2	50.1	50.9	42.1	54.1	53.2
1500°F	40.5	40.6	42.3	48.2	43.5	45.1

0.2% YS vs. Temperature for 6" section trepans from CL and DL

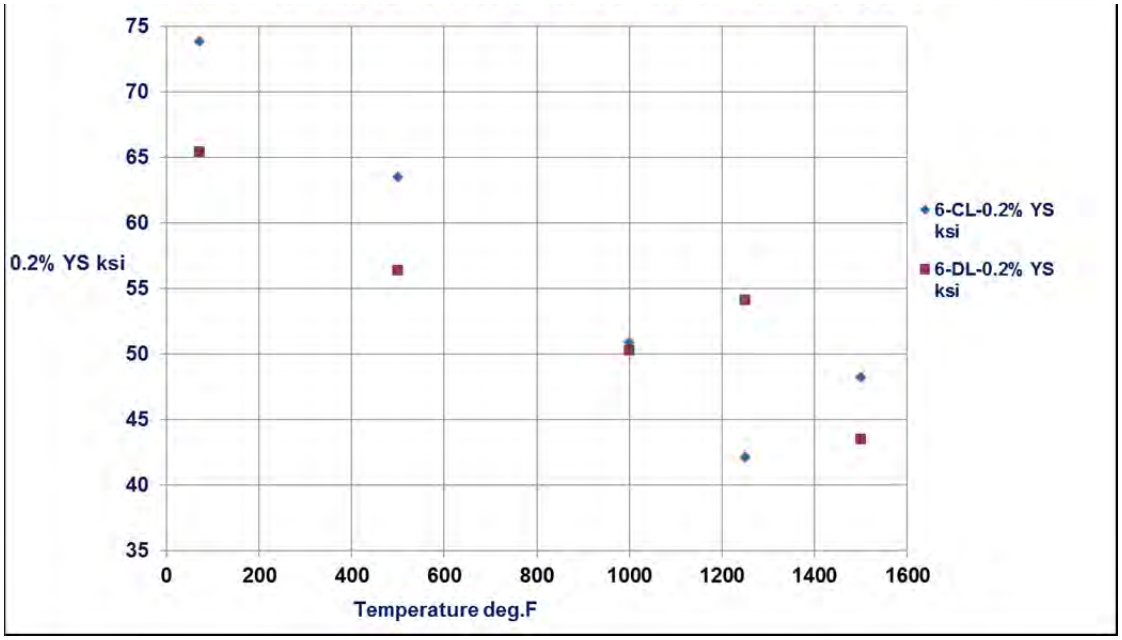

Figure 29: 0.2% YS with temperature for 6 inch section CL and DL location trepans

0.2% YS vs. Temperature for 10" section trepans from CL and DL

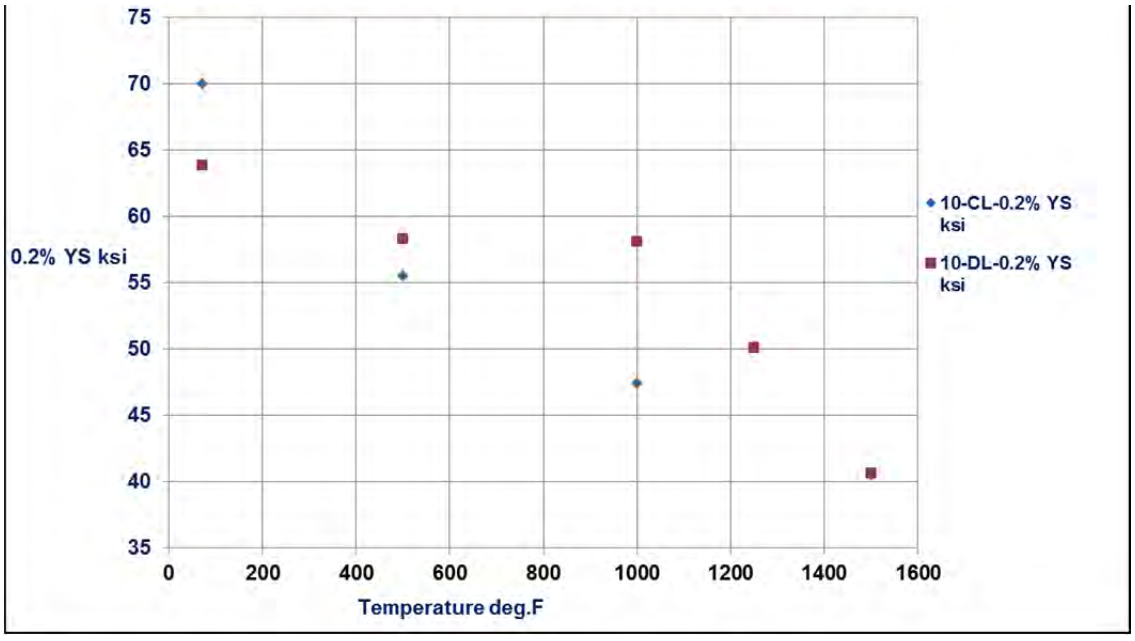

Figure 30: 0.2% YS with temperature for 10 inch section CL and DL location trepans

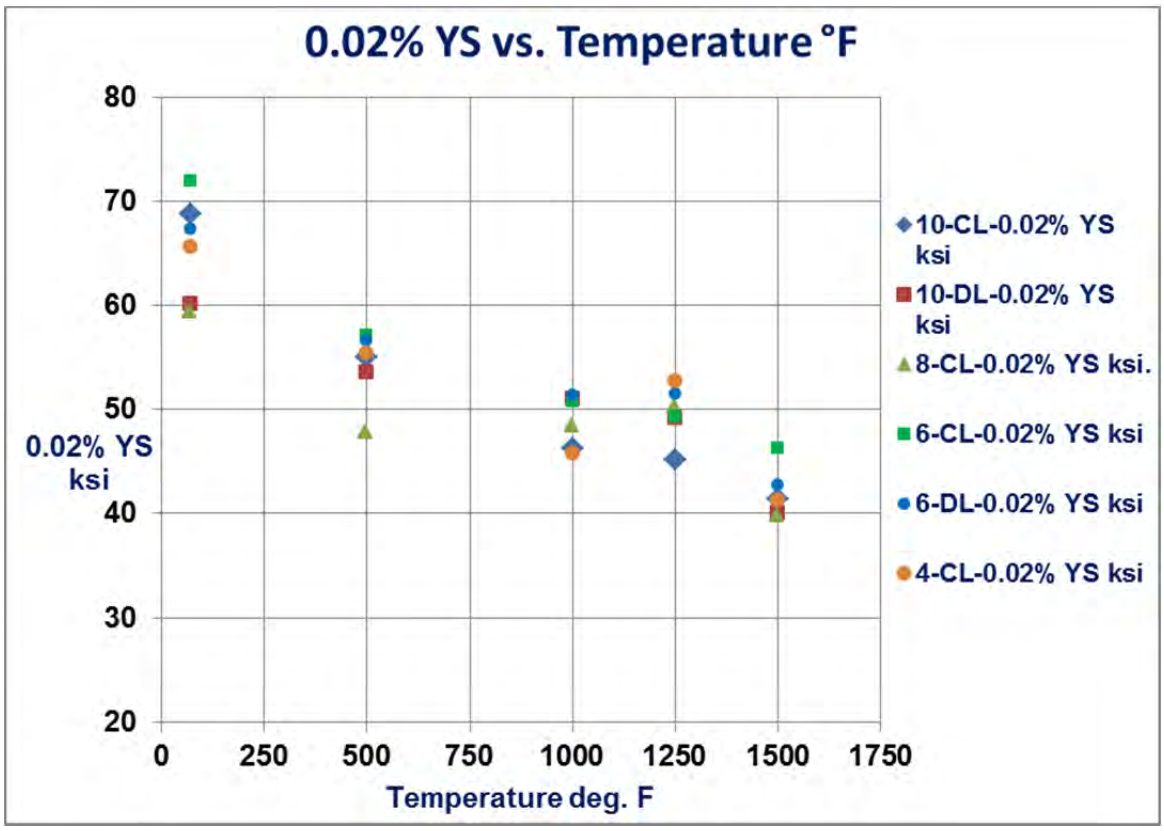

Figure 31: 0.02 % YS vs. Temperature for all N263 step block cast section trepans. The 0.02% YS vs. temperature trend plot shows tighter band at elevated temperatures for all section thicknesses

Table 3: N263 Step block trepan cast sections 0.02% Yield strength vs temperature data

N263 Step Block trepan cast sections 0.02% YS vs. Temperature						
Section thickness (inches)	**10-CL (10)**	**10-DL (10)**	**8-CL (8)**	**6-CL (6)**	**6-DL (6)**	**4-CL (4)**
Temperature °F	(ksi)	(ksi)	(ksi)	(ksi)	(ksi)	(ksi)
72°F	**68.8**	**60.1**	**59.4**	**71.9**	**67.3**	**65.6**
500°F	**55**	**53.6**	**47.8**	**57.1**	**56.6**	**55.4**
1000°F	**46.3**	**51**	**48.4**	**50.7**	**51.4**	**45.8**
1250°F	**45.1**	**49.2**	**50.3**	**49.3**	**51.5**	**52.7**
1500°F	**41.4**	**40**	**39.8**	**46.3**	**42.7**	**41.3**

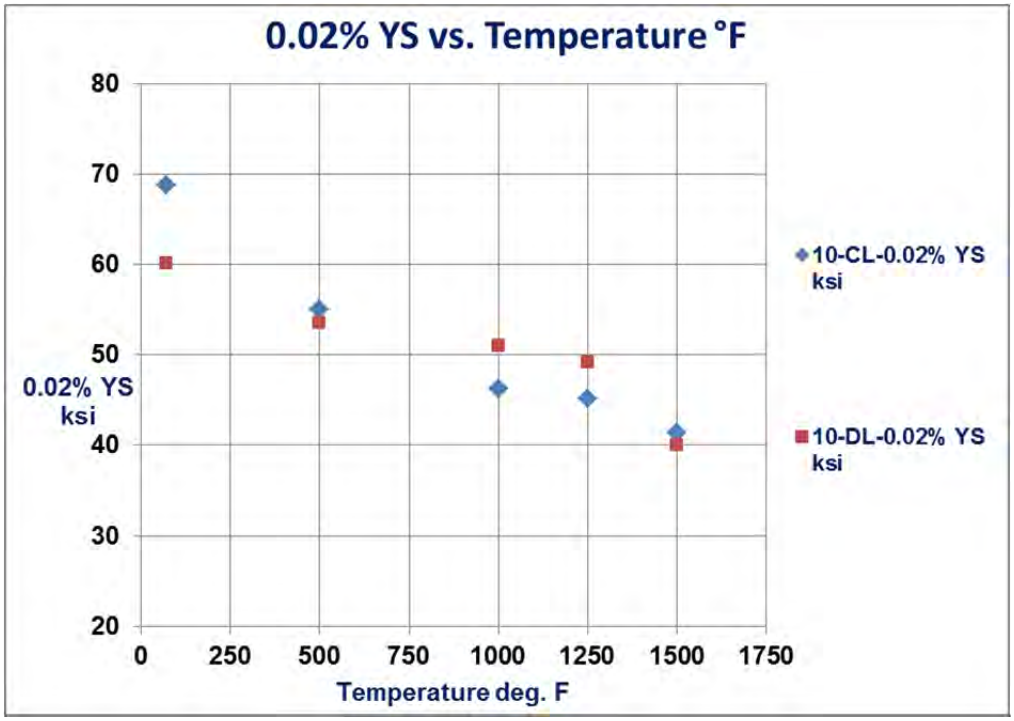

Figure 32: 0.02% YS vs temperature for 10 inch section CL and DL trepans

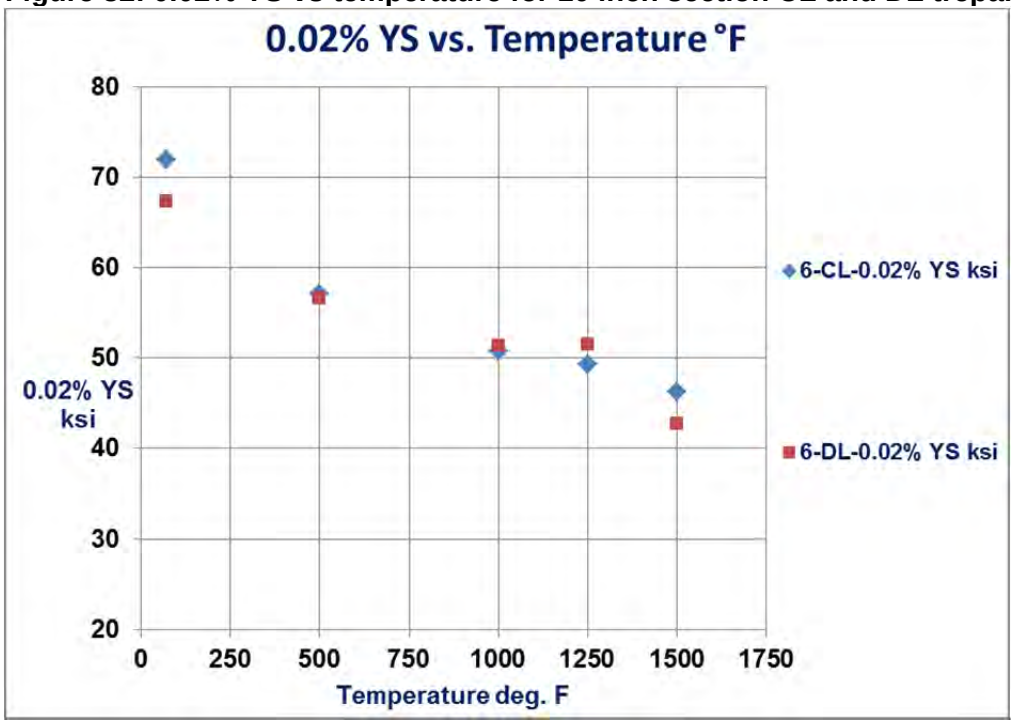

Figure 33: 0.02% YS vs temperature for 6 inch section CL and DL trepans

% Elongation vs Temperature for all cast sections

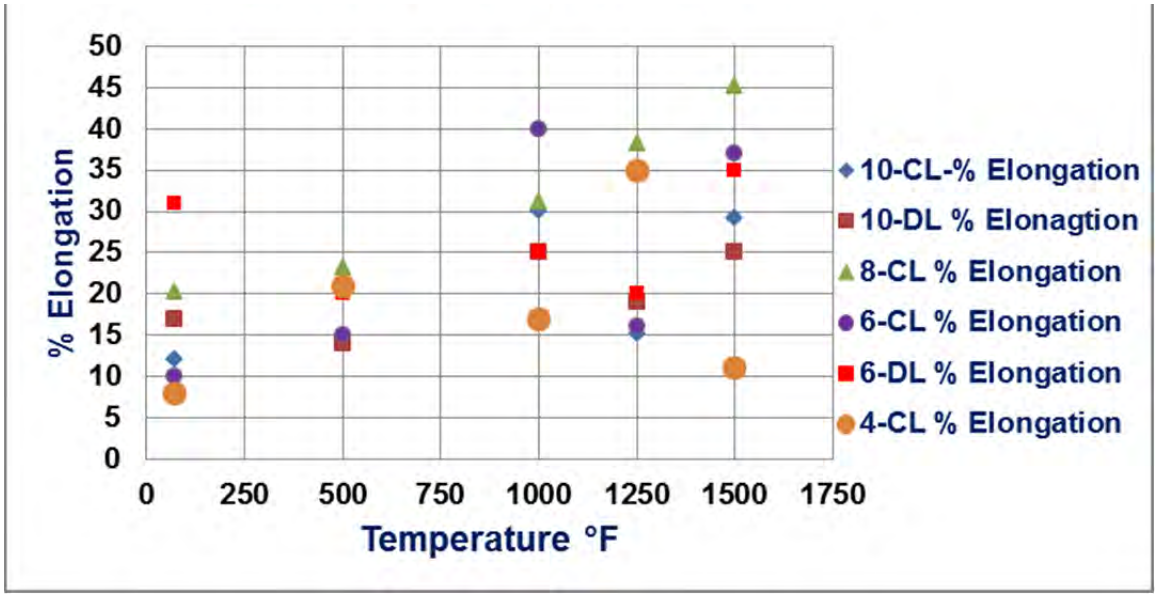

Figure 34: N263 step block cast section trepan samples % Elongation vs. Temperature

Table 4: N263 step block trepan section samples % Elongation values

Trepan sample % Elongation with tempearture and section size						
Temperature	**10-CL**	**10-DL**	**8-CL**	**6-CL**	**6-DL**	**4-CL**
(deg. F)	**(%)**	**(%)**	**(%)**	**(%)**	**(%)**	**(%)**
72	**12**	**17**	**20**	**10**	**31**	**8**
500	**21**	**14**	**23**	**15**	**20**	**21**
1000	**30**	**25**	**31**	**40**	**25**	**17**
1250	**15**	**19**	**38**	**16**	**20**	**35**
1500	**29**	**25**	**45**	**37**	**35**	**11**

% Elongation vs Temperature for all cast sections

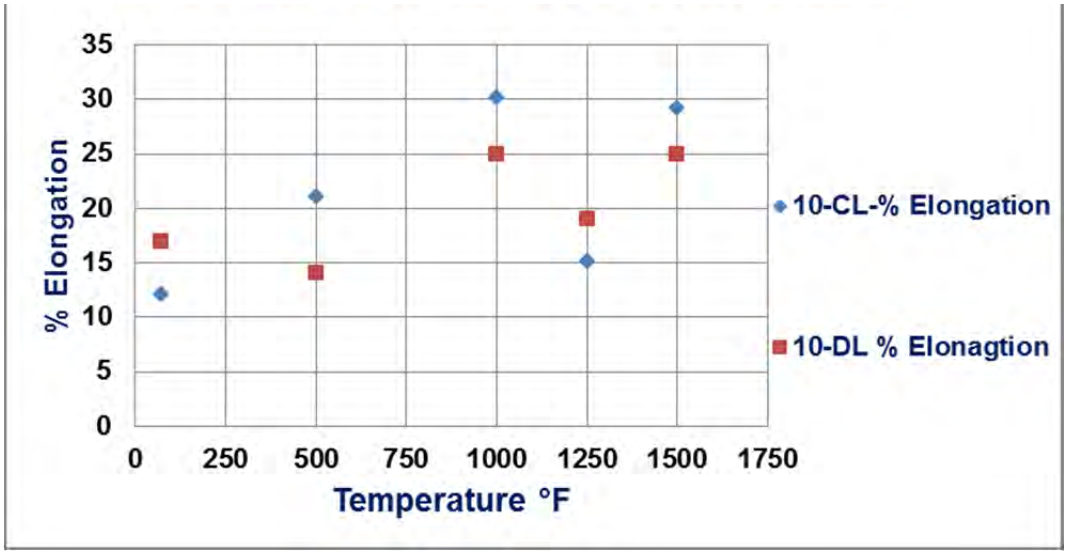

Figure 35: N263 step block 10 inch section CL and DL trepan location % Elongation vs Temperature °F plot.

% Elongation vs Temperature for all cast sections

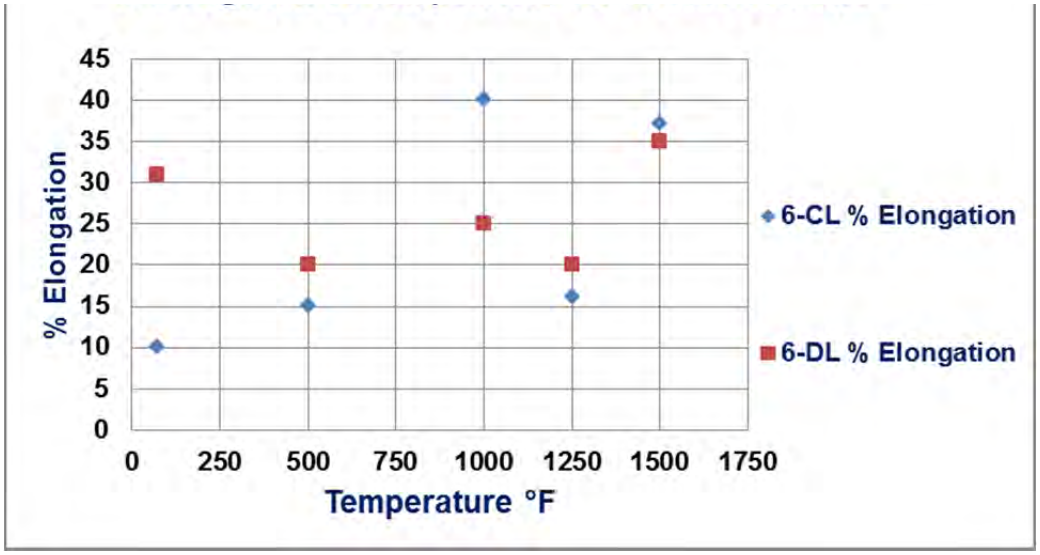

Figure 36: N263 step block 6 inch section CL and DL trepan location % Elongation vs Temperature °F plot

% RA vs. Temperature for 10" section trepans from CL and DL

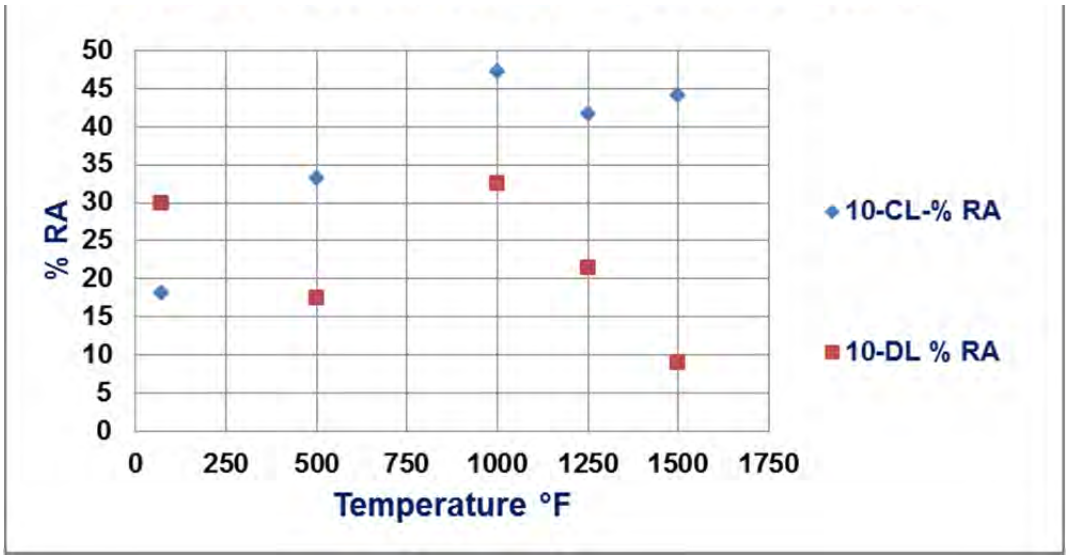

Figure 37: % RA vs Temperature for 10 inch CL and DL trepan sections

% RA vs. Temperature for 6" section trepans from CL and DL

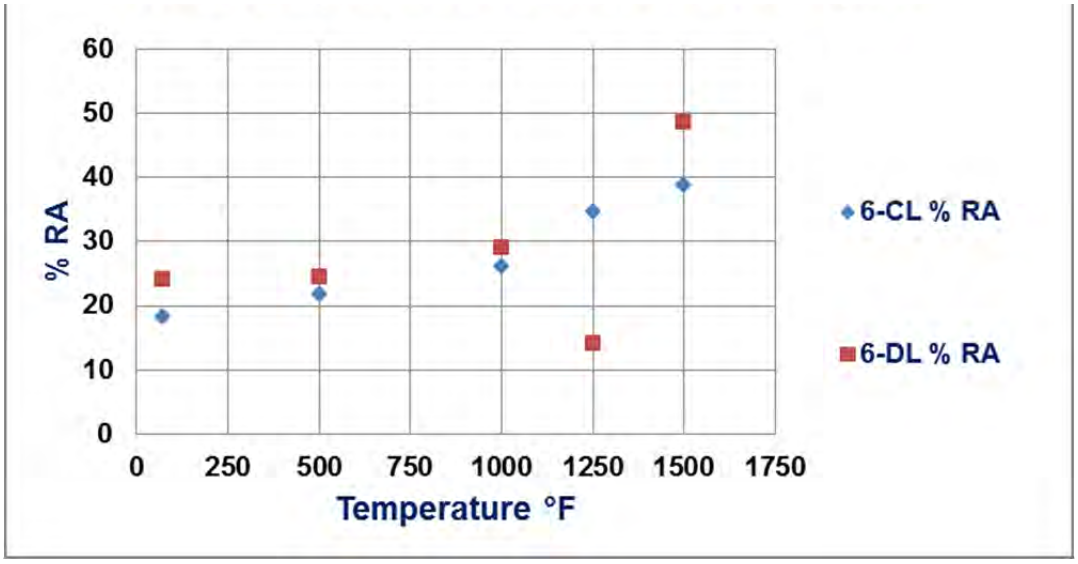

Figure 38: % RA vs Temperature for 6 inch CL and DL trepan sections

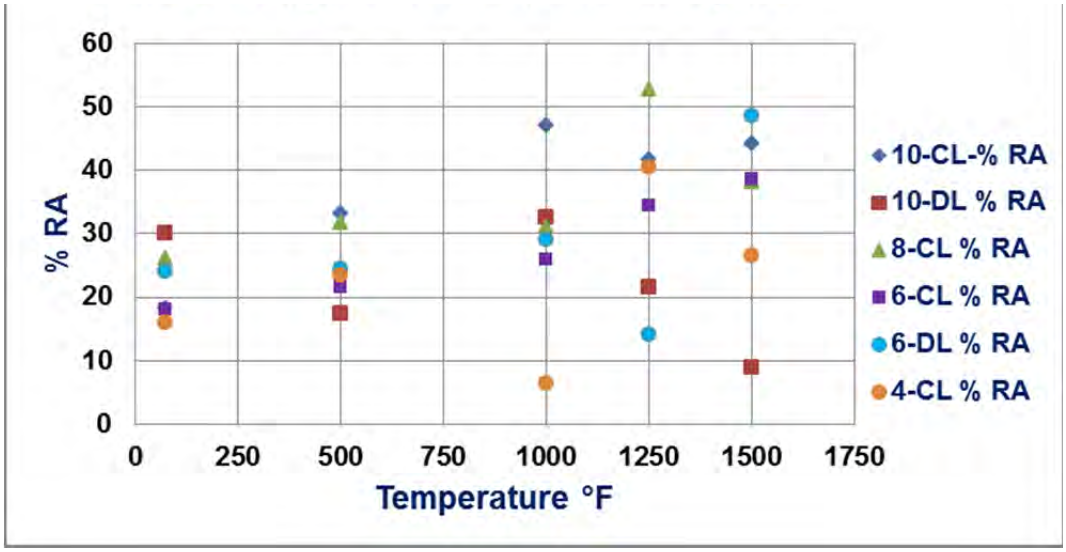

Figure 39: N263 %RA Vs Temperature plots for all section trepans

Table 5: N263 Step Block section Trepan sample % RA values data

Trepan sample % RA values with temperature and section size						
Temperature	10-CL	10-DL	8-CL	6-CL	6-DL	4-CL
(deg. F)	(%)	(%)	(%)	(%)	(%)	(%)
72	18	30	26	18	24	16
500	33	17.5	31.5	21.5	24.5	23.5
1000	47	32.5	31	26	29	6.5
1250	41.5	21.5	52.5	34.5	14	40.5
1500	44	9	38	38.5	48.5	26.5

Table 6: Nimonic 263 Step block cast section thermal center trepanned samples SDAS values show independent of casting section thickness and orientation

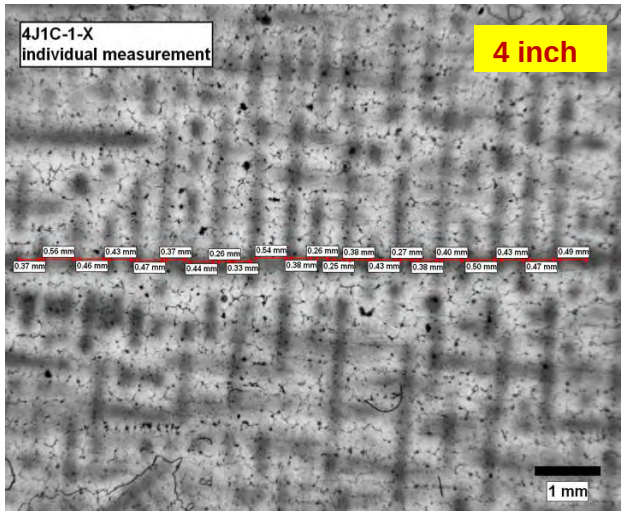

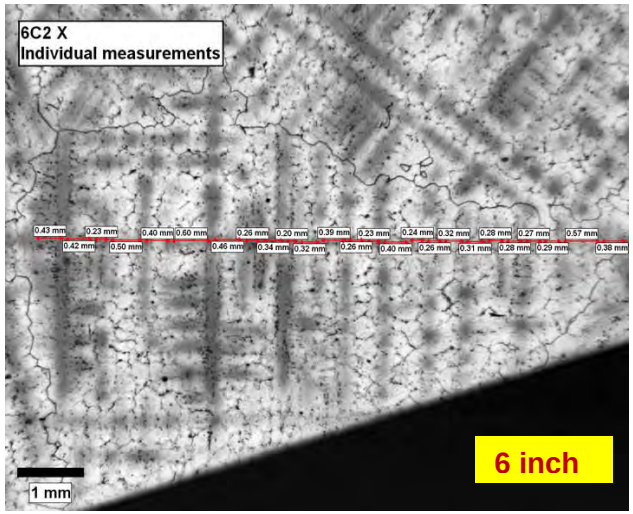

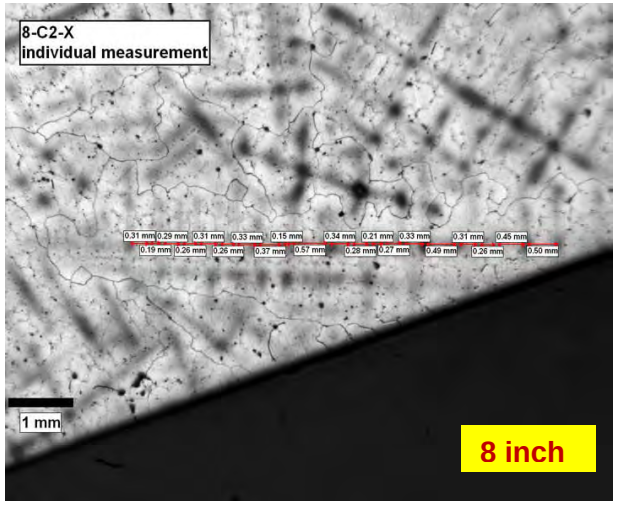
8-C2-X
individual measurement
1 mm
8 inch

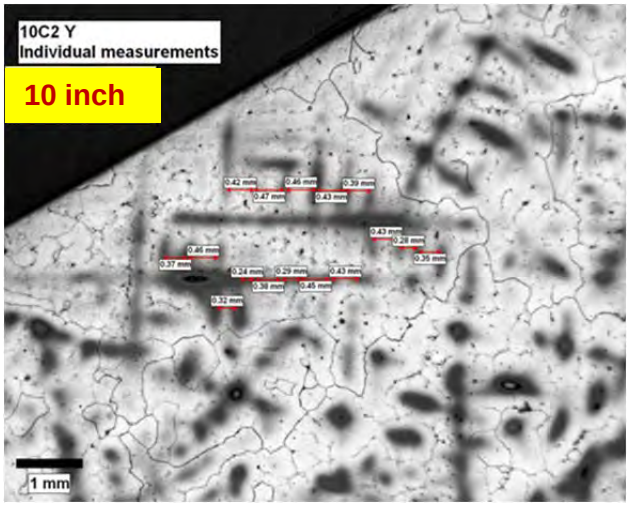
10C2 Y
Individual measurements
10 inch
1 mm

Table 7: Nimonic 263 Step block LCF Data for 10 inch and 6 inch cast sections at RT and 1400°F

SPECIMEN I.D.	TEST TEMP.	Strain RATIO	MAX. STRESS	MIN. STRESS	TOTAL STRAIN RANGE	ELASTIC STRAIN RANGE	PLASTIC STRAIN CALC.	PLASTIC STRAIN MEAS.	Ni	Nf	FRACTURE	FRACTURE INITIATION
TEST ID.	°F	"A"	KSI	KSI	%	%	%	%	CYCLES	CYCLES	LOCATION	SITE
10-LCF-01 (1.00 TSR%)	Room	1	72.1	-72.8	0.987	0.524	0.437	0.463	56	76	IX	S
10-LCF-02 (0.90 TSR%)	Room	1	71.4	-74.3	0.868	0.524	0.363	0.344	253	330	IX	S
10-LCF-03 (0.80 TSR%)	Room	1	73.8	-75.6	0.791	0.572	0.235	0.219	1,385	1,929	OX	S
10-LCF-04 (0.70 TSR%)	Room	1	69.2	-67.9	0.694	0.523	0.173	0.171	750	800	OX	S
10-LCF-05 (0.60 TSR%)	Room	1	71.3	-70.1	0.593	0.503	0.093	0.090	8,753	8,917	IX	S
10-LCF-06 (0.50 TSR%)	Room	1	66.8	-50.9	0.505	0.505	0.005	0.000	13,049	16,437	IX	S
6-LCF-01 (1.00 TSR%)	Room	1	78.0	-80.3	0.990	0.591	0.389	0.399	838	847	OX	S
6-LCF-02 (0.90 TSR%)	Room	1	80.5	-76.7	0.897	0.748	0.142	0.149	5,144	6,176	IX	S
6-LCF-03 (0.80 TSR%)	Room	1	73.2	-72.0	0.796	0.675	0.119	0.121	8,755	10,914	IX	S
6-LCF-04 (0.70 TSR%)	Room	1	77.5	-73.2	0.691	0.588	0.117	0.103	2,554	2,554	IX	S
6-LCF-05 (0.60 TSR%)	Room	1	74.7	-76.0	0.597	0.490	0.104	0.107	2,788	2,818	OX	S
6-LCF-06 (0.50 TSR%)	Room	1	66.0	-51.7	0.490	0.482	0.009	0.008	39,344	41,457	OX	S
10-LCF-07 (1.00 TSR%)	1400	1	56.8	-63.0	0.974	0.446	0.525	0.528	10	20	IX	S
10-LCF-08 (0.90 TSR%)	1400	1	57.1	-61.2	0.893	0.534	0.353	0.359	61	88	IX	S
10-LCF-09 (0.80 TSR%)	1400	1	54.1	-50.9	0.800	0.558	0.241	0.242	88	88	OX	S
10-LCF-10 (0.70 TSR%)	1400	1	53.0	-54.0	0.691	0.497	0.164	0.194	519	602	IX	S
10-LCF-11 (0.60 TSR%)	1400	1	50.6	-49.1	0.595	0.474	0.119	0.121	783	896	IX	S
10-LCF-12 (0.50 TSR%)	1400	1	46.6	-48.5	0.497	0.433	0.035	0.064	325	716	IX	S
6-LCF-07 (1.00 TSR%)	1400	1	66.1	-64.0	0.997	0.789	0.210	0.208	379	478	IX	S
6-LCF-08 (0.90 TSR%)	1400	1	55.5	-52.4	0.893	0.710	0.188	0.183	571	767	IX	S
6-LCF-09 (0.80 TSR%)	1400	1	52.1	-55.8	0.793	0.580	0.200	0.213	515	531	IX	S
6-LCF-10 (0.70 TSR%)	1400	1	46.8	-48.4	0.683	0.428	0.257	0.255	1,241	1,621	IX	S
6-LCF-11 (0.60 TSR%)	1400	1	53.1	-55.0	0.588	0.433	0.157	0.155	745	770	OX	S
6-LCF-12 (0.50 TSR%)	1400	1	40.1	-38.6	0.497	0.434	0.063	0.063	5,996	6,231	IX	S

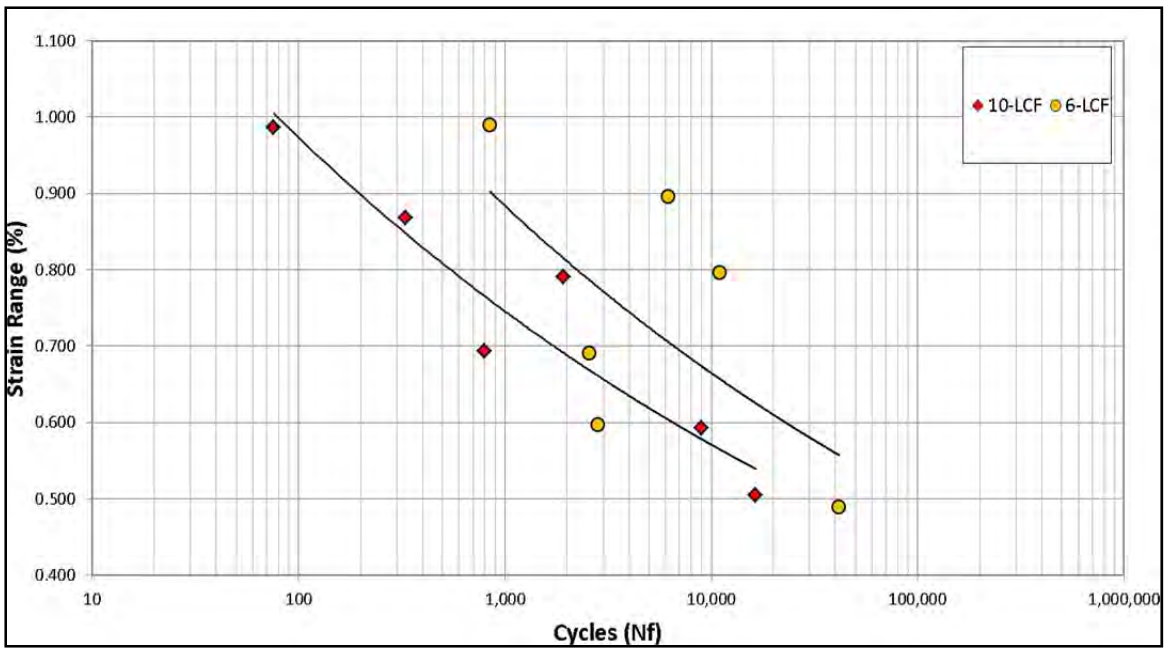

Figure 40: N263 Step block 10 inch and 6 inch sections cycles to failure compared at RT, A-ratio 1. The 10 inch section shows a debit in comparison with 6 inch section

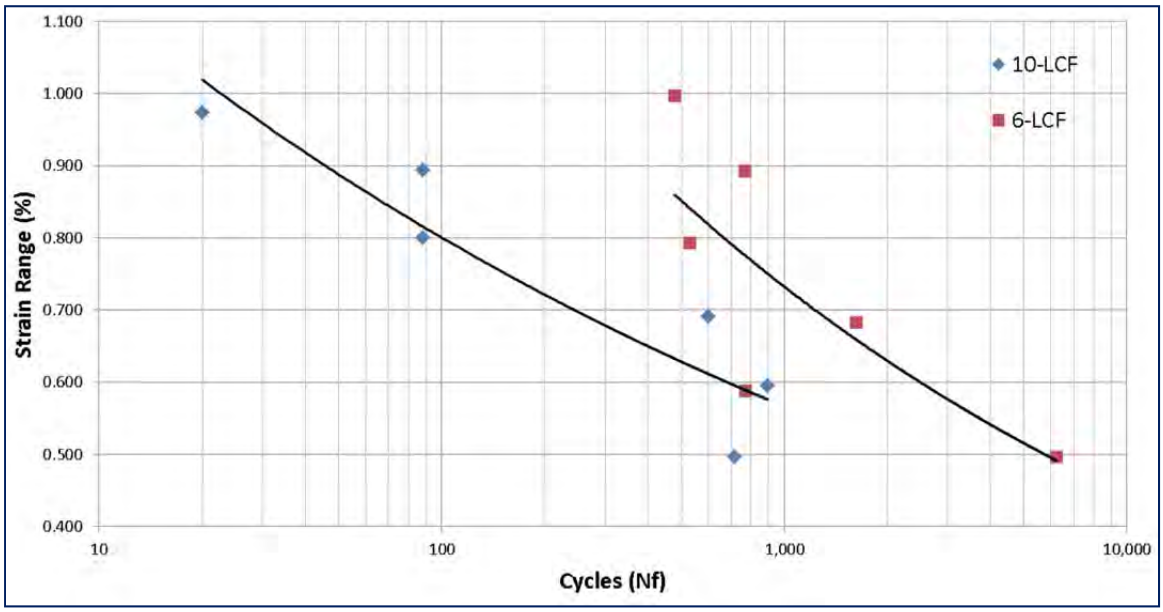

Figure 41: N263 Step block 10 inch and 6 inch sections cycles to failure compared at 1400°F , A-Ratio 1. The 10 inch section shows increased debit in comparison with 6 inch section, while 6 inch section shows degradation

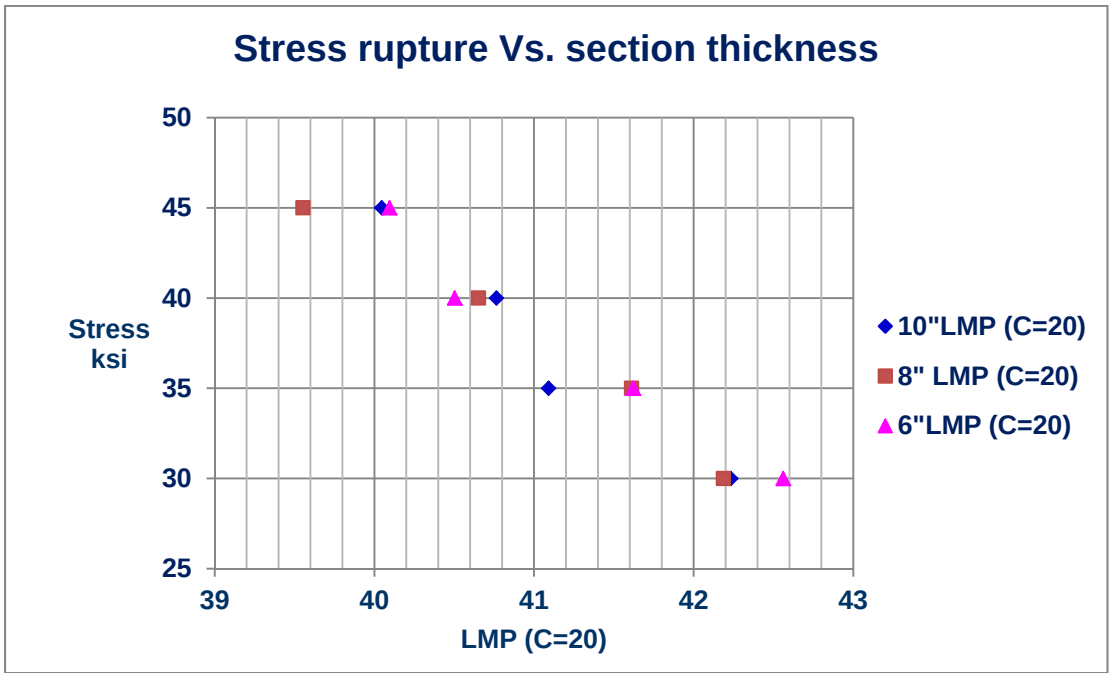

Figure 42: N263 Stress rupture strength vs, LMP (C=20) with section thickness. No significant changes in stress rupture data with section thickness variation

Table 8: Stress rupture test results raw data

Sample ID	Temp. °F	Time (hrs)	Elong %	RA %	Stress (ksi)	LMP
10-RUP-01	1472	1.8	9.3	19.2	40	39.13
10-RUP-02	1472	35.2	21.2	39.0	35	41.63
10-RUP-03	1472	49.2	14.5	27.6	30	41.91
10-RUP-04	1472	209.8	19.0	34.4	25	43.13
10-RUP-05	1400	33.9	15.7	14.4	45	40.05
10-RUP-06	1400	82.5	12.9	22.0	40	40.76
10-RUP-07	1400	123.6	11.3	22.3	35	41.09
10-RUP-08	1400	508.1	16.9	30.4	30	42.23
8-RUP-01	1400	18.4	15.3	41.2	45	39.55
8-RUP-02	1400	71.8	12.4	23.2	40	40.65
8-RUP-03	1400	235.5	15.3	18.1	35	41.61
8-RUP-04	1400	479.9	17.9	38.2	30	42.19
6-RUP-01	1400	36.0	12.8	17.9	45	40.09
6-RUP-02	1400	59.7	13.6	39.0	40	40.50
6-RUP-03	1400	238.3	11.7	14.9	35	41.62
6-RUP-04	1400	761.8	9.0	27.3	30	42.56

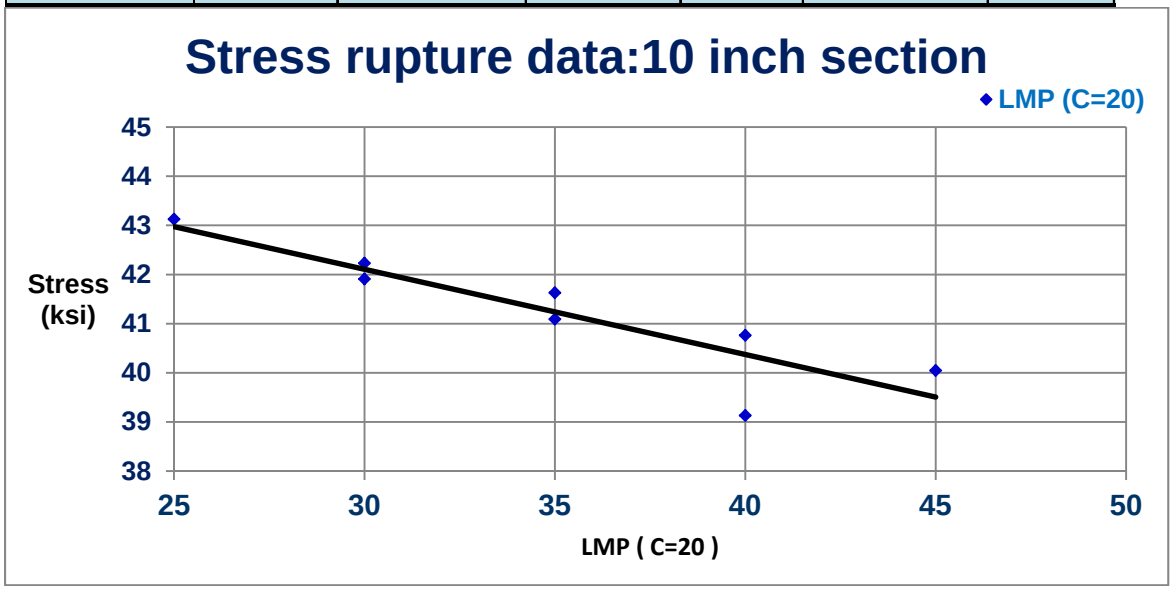

Figure 43: N263 stress rupture plot for 10 inch cast section

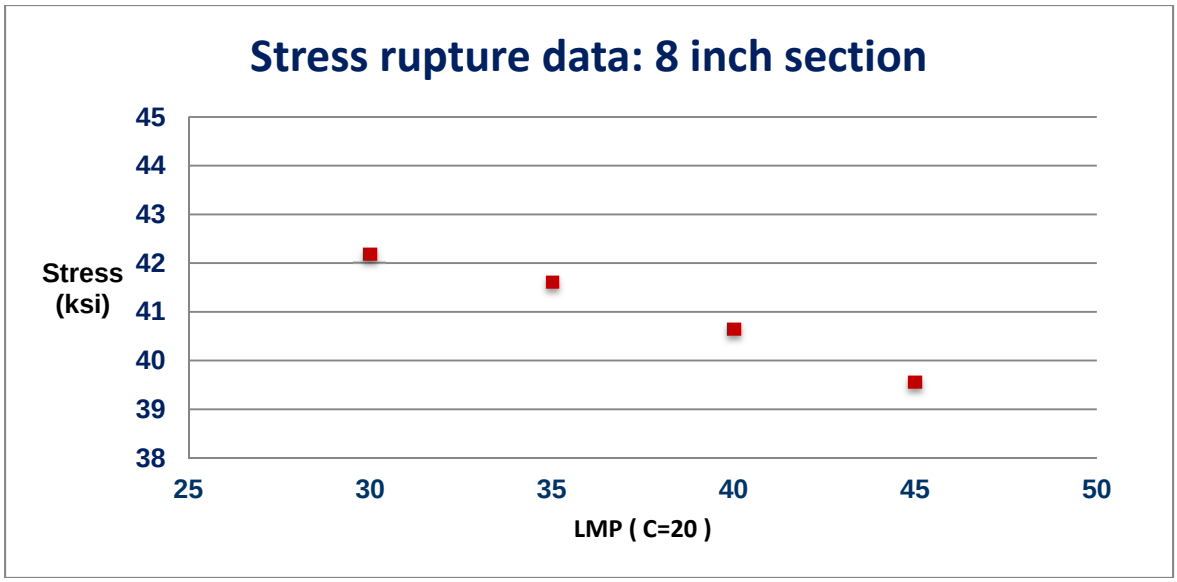

Figure 44: N263 stress rupture plot for 8 inch cast section

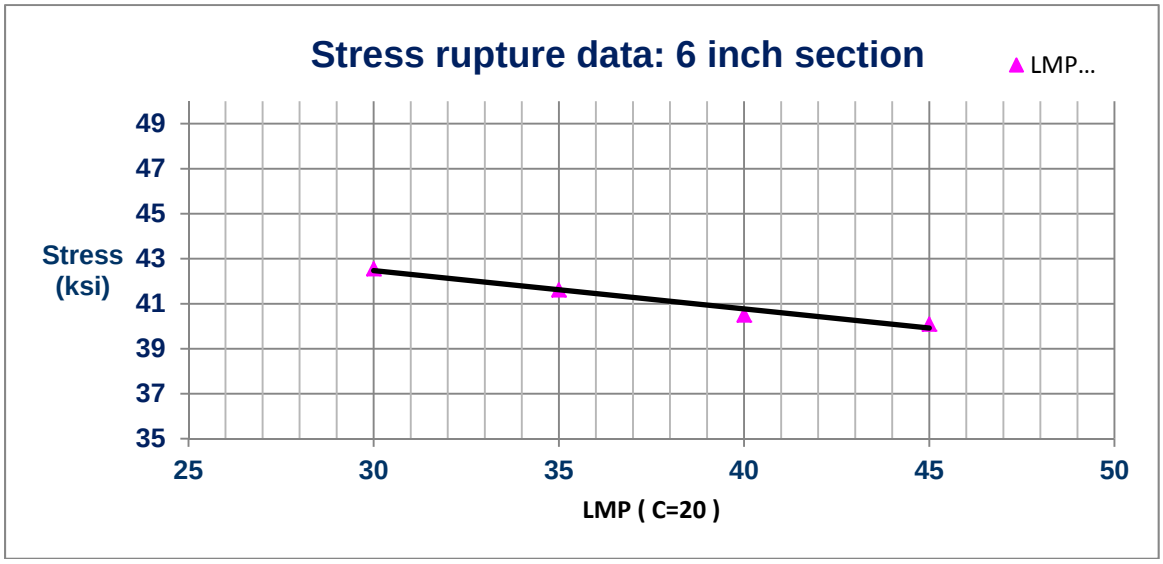

Figure 45: N263 stress rupture plot for 6 inch cast section

Table 9: Nimonic 263 Step block sections J-Integral Test results at RT; 1000°F and 1400°F summarized

Specimen	Testlog Number	Temperature	J_Q (in lb/in^2)	K_{JQ} (ksi$\sqrt{in}$)	K_{Ic} Determination (Annex 5)		Unstable
					P_Q (lb)	K_Q (ksi$\sqrt{in}$)	
10-JIC-01	T46793	Room	273.85	102.57	5046.9	62.3	No
8-JIC-01	T46794	Room	623.19	146.56	4402.0	48.8	No
6-JIC-01	T46795	Room	327.07	105.57	4017.5	49.4	No
4-JIC-01	T46796	Room	531.87	136.16	4765.0	56.0	No
10-JIC-02	T46797	1000°F	479.30	119.34	3313.4	39.3	No
8-JIC-02	T46798	1000°F	642.31	139.60	4542.9	50.7	No
6-JIC-02	T46799	1000°F	467.36	113.85	3779.3	49.0	No
10-JIC-03	T46800	1400°F	272.22	83.74	3236.6	38.7	No
8-JIC-03	T46801	1400°F	621.48	123.59	3707.6	41.8	No
6-JIC-03	T46802	1400°F	336.48	90.25	3855.4	47.9	No
4-JIC-02	T46803	1400°F	550.07	115.68	4371.5	51.4	No

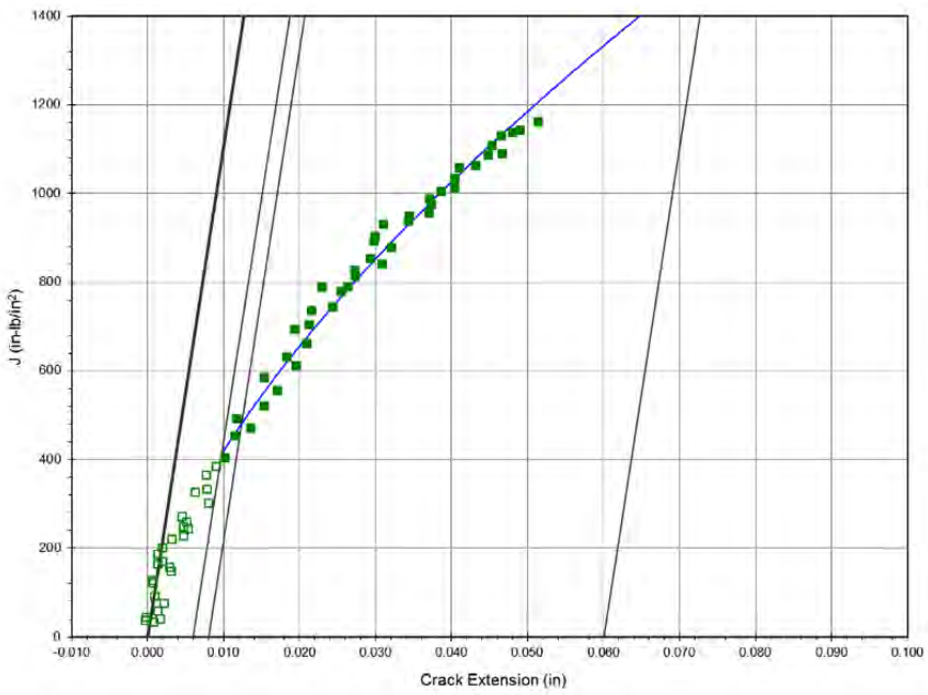

Figure 46: Nimonic 263 step block 10 inch section J vs. a Graph tested at 1000°F

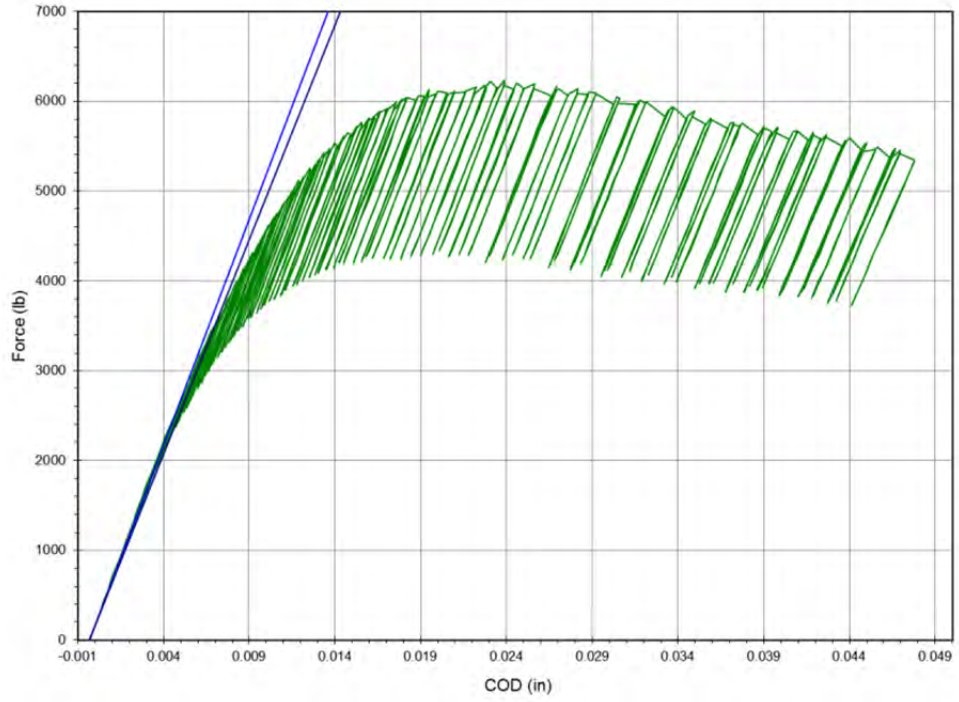

Figure 47: Nimonic 263 step block 10 inch section Force vs. COD Graph tested at 1000°F.

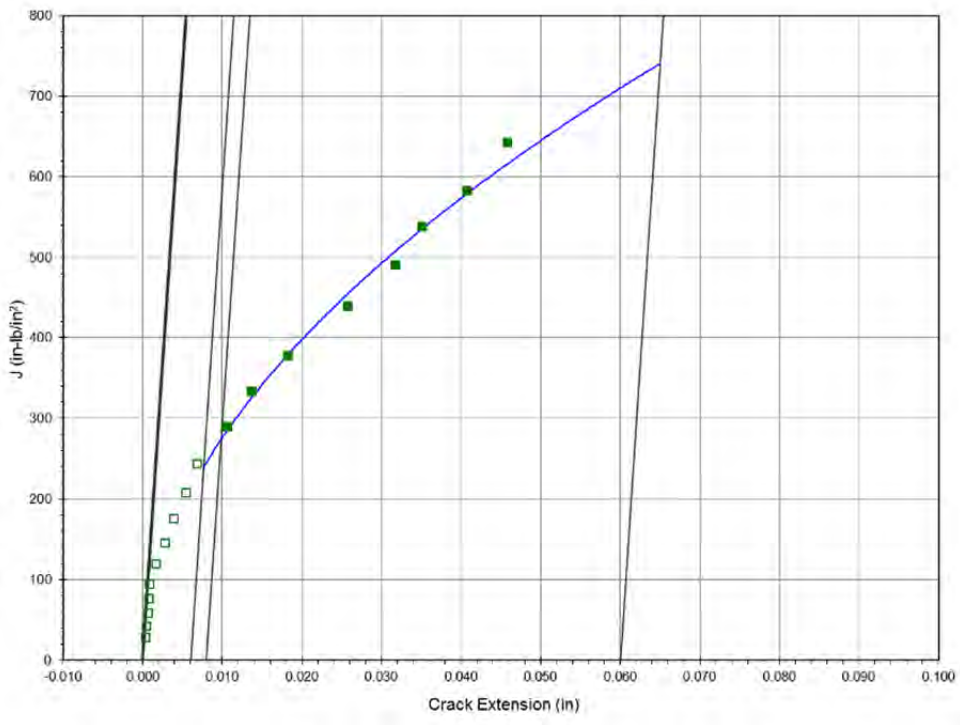

Figure 48: 10-J1C-01, J vs. a graph for 10 inch section tested at RT

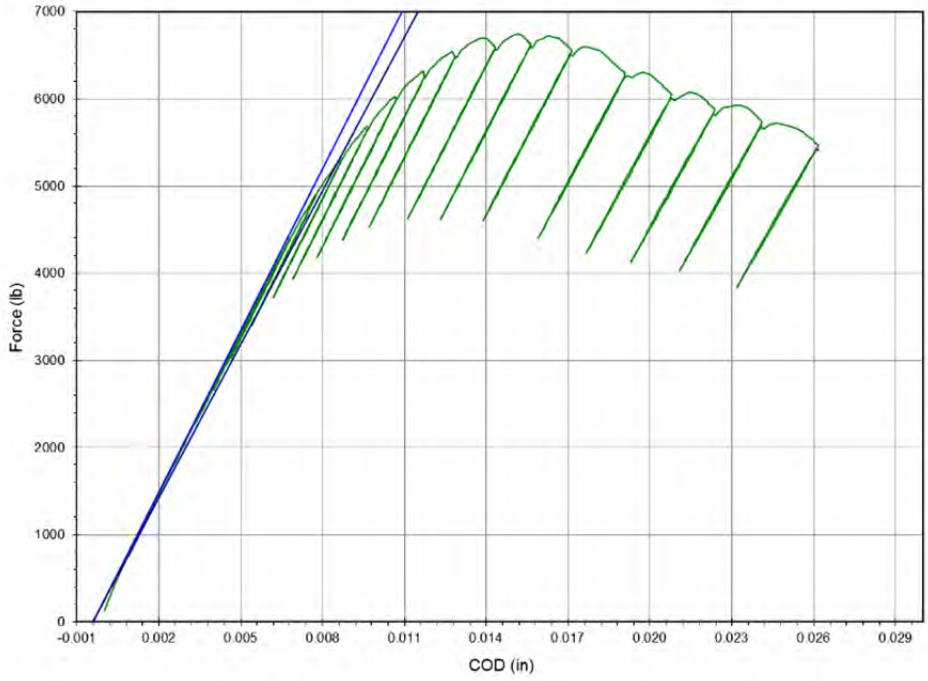

Figure 49: 10-J1C-01, Force vs. COD graph for 10 inch section tested at RT

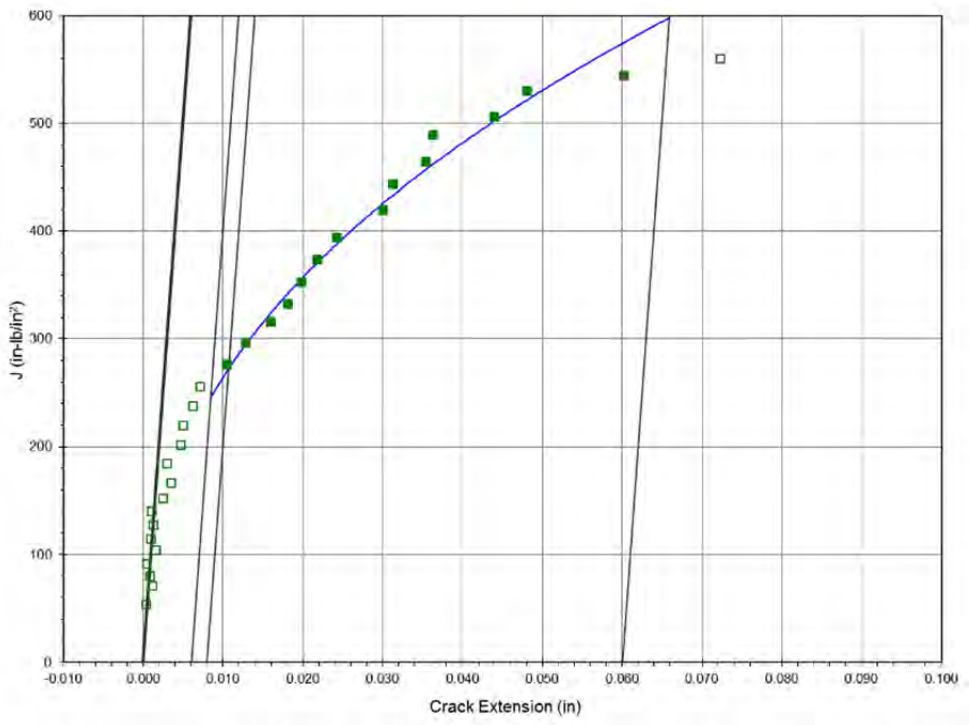

Figure 50: 10-J1C-03, J vs. a graph for 10 inch section tested at 1400°F

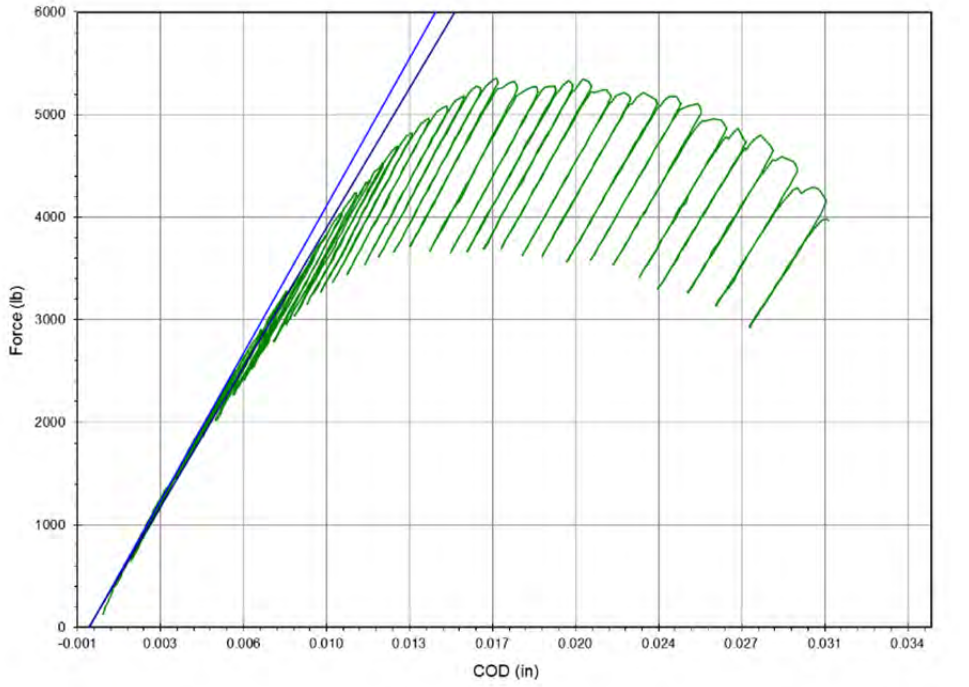

Figure 51: 10-J1C-03, Force vs. COD graph for 10 inch section tested at 1400°F

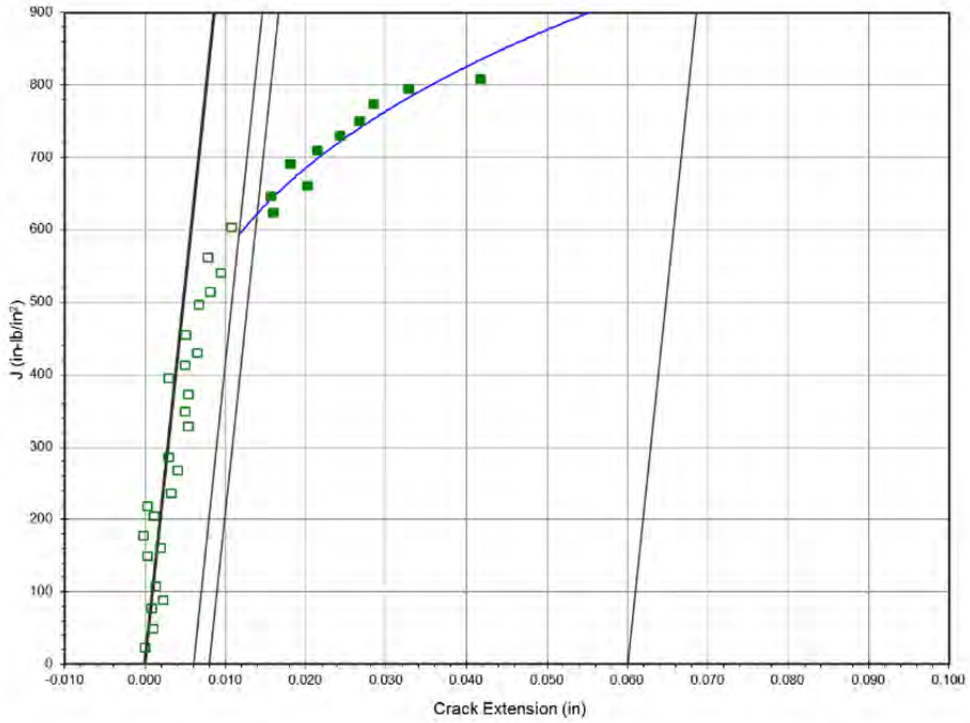

Figure 52: 8-J1C-03, J vs. a graph for 8 inch section tested at 1400°F

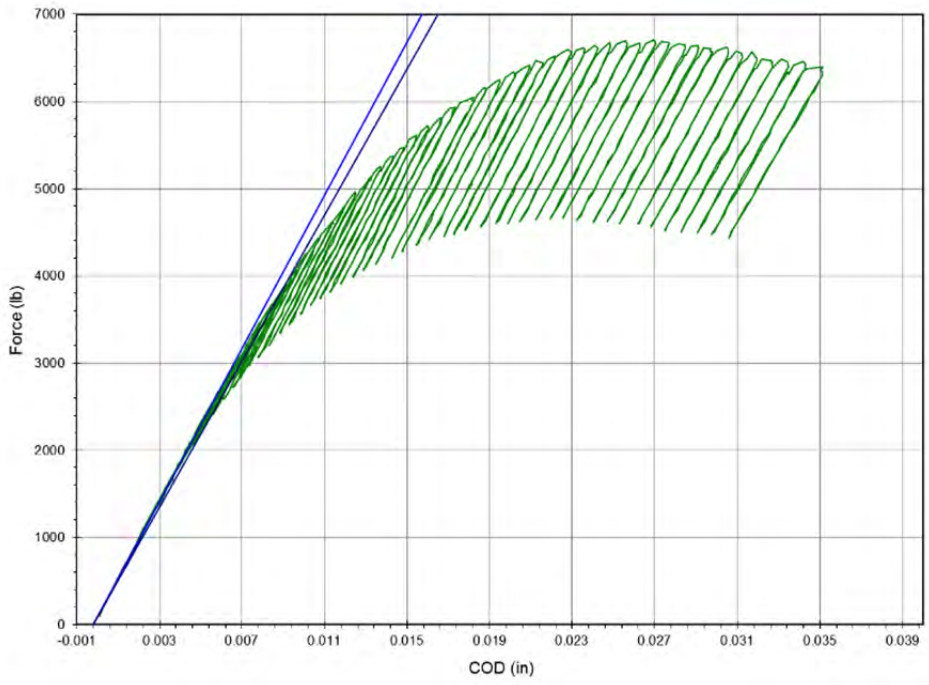

Figure 53: 8-J1C-03, Force vs. COD graph for 8 inch section tested at 1400°F

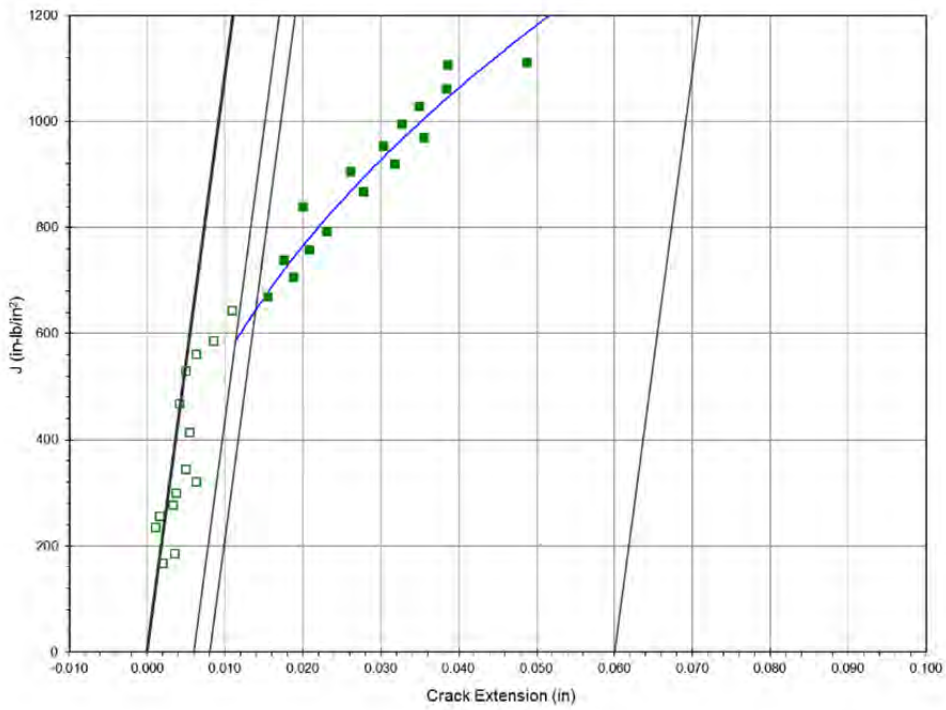

Figure 54: 8-J1C-02, J vs. a graph for 8 inch section tested at 1000°F

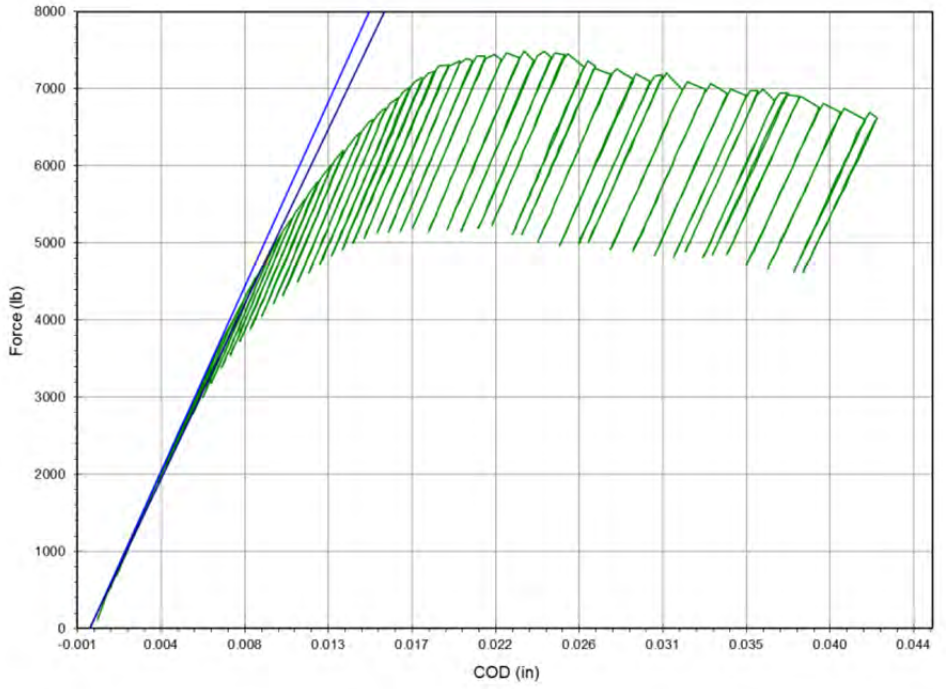

Figure 55: 8-J1C-02, Force vs. COD graph for 8 inch section tested at 1000°F

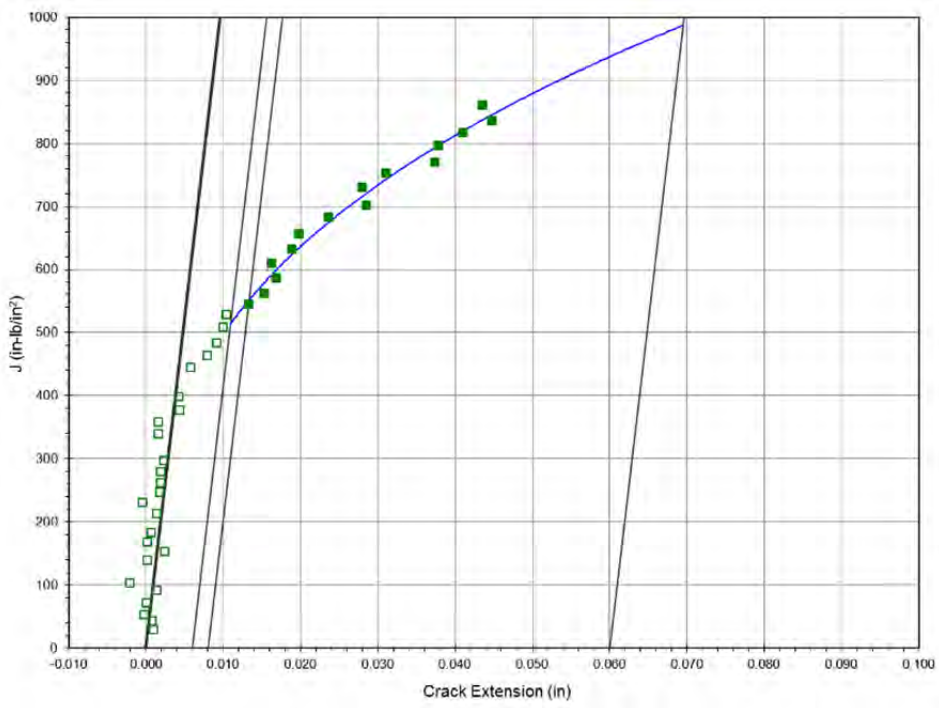

Figure 56: 4-J1C-02, J vs. a graph for 4 inch section tested at 1400°F

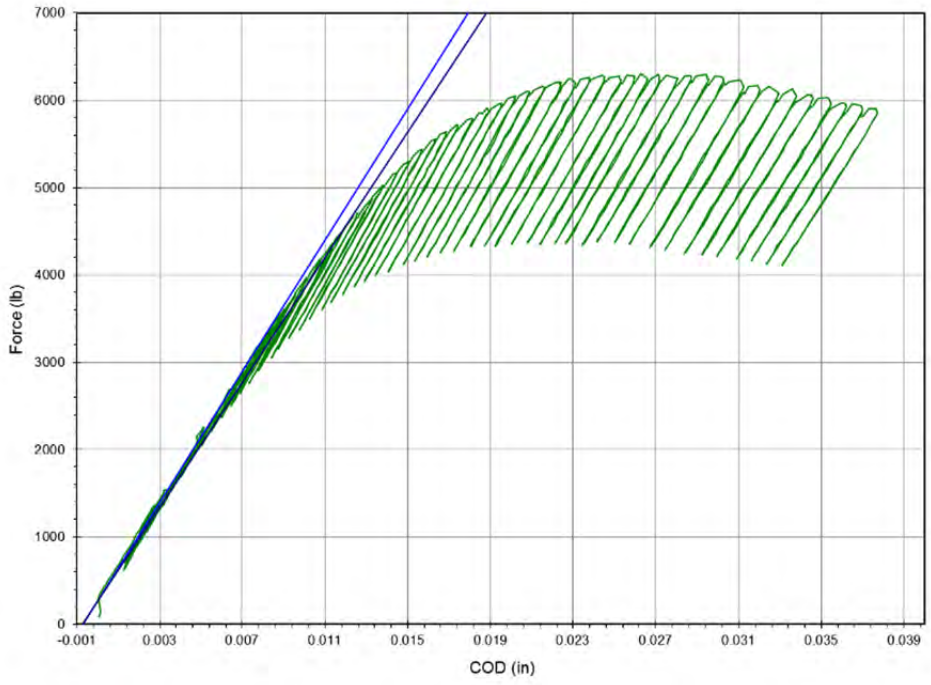

Figure 57: 4-J1C-02, Force vs. COD graph for 4 inch section tested at 1400°F

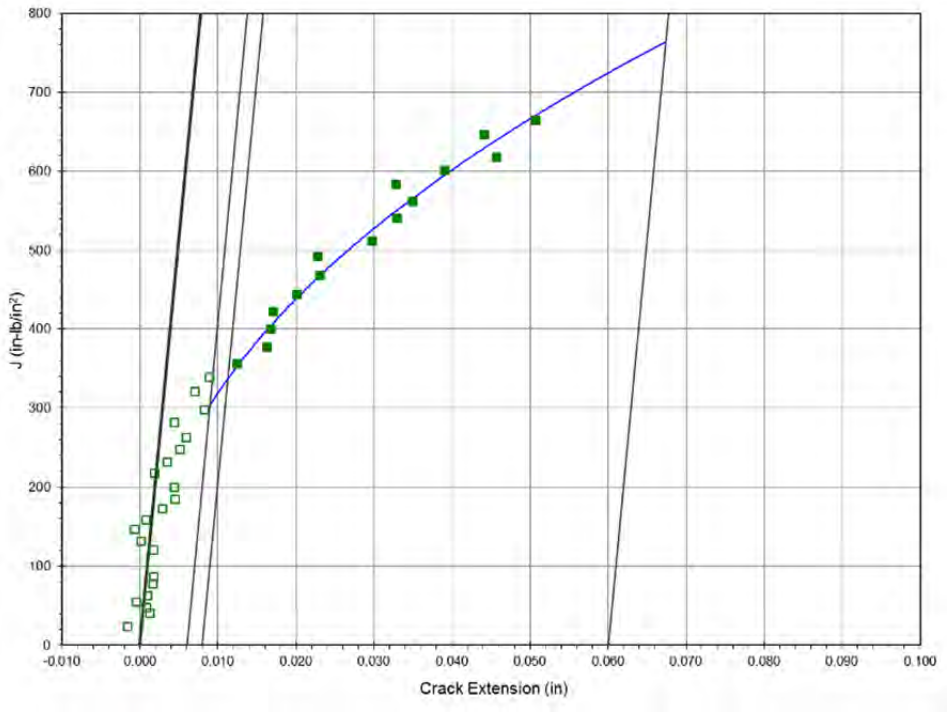

Figure 58: 6-J1C-03, J vs. a graph for 6 inch section tested at 1400°F

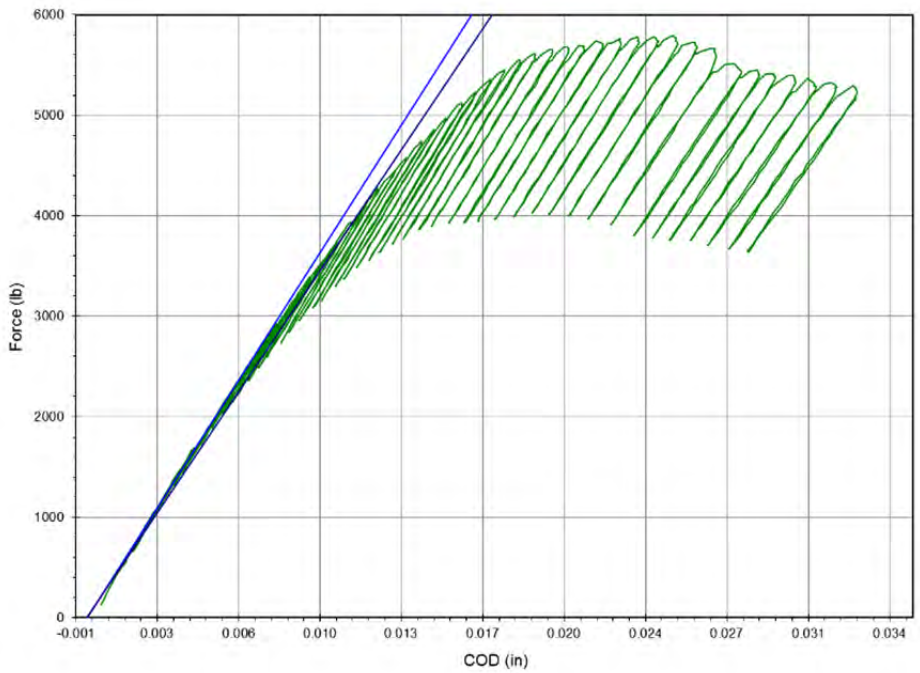

Figure 59: 6-J1C-03, Force vs. COD graph for 6 inch section tested at 1400°F

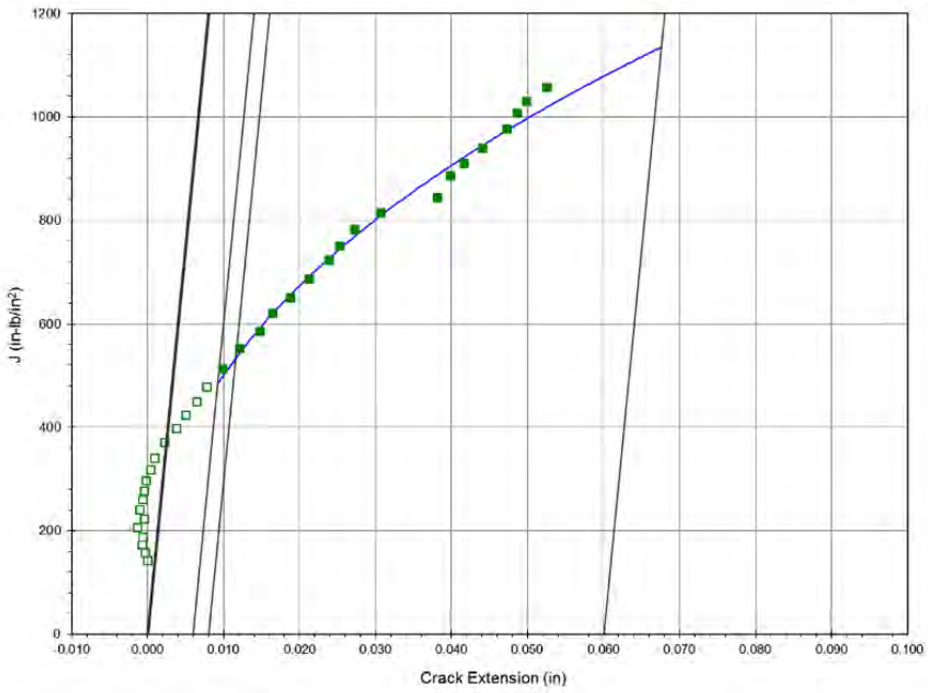

Figure 60: 4-J1C-01, J vs. a graph for 4 inch section tested at RT

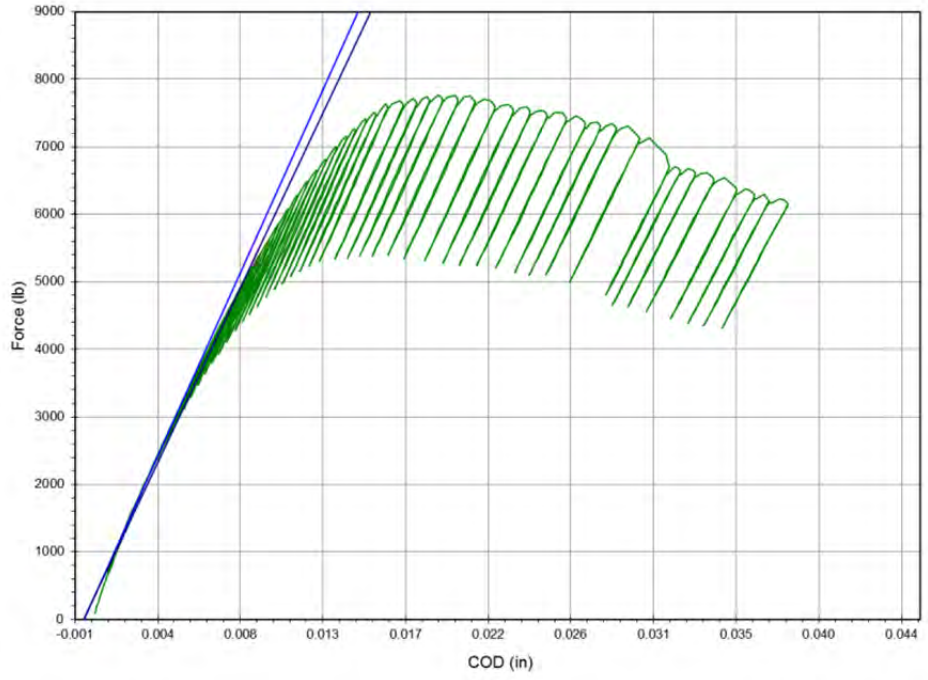

Figure 61: 4-J1C-01, Force vs. COD graph for 4 inch section tested at RT

Table 10: Charpy V-Notch Impact energy data for 10 inch,8 inch and 6 inch trepan samples

Sample ID	Temp	Energy		Mils
	°F\°C	ft-lbs	Joules	Lat Exp
10-CVN-RT-C1	70/21	48	65.1	51
8-CVN-RT-C1	70/21	39	52.9	41
6-CVN-RT-C1	70/21	30	40.7	22
10-CVN-RT-C2	70/21	37	50.2	33
8-CVN-RT-C2	70/21	40	54.2	32
6-CVN-RT-C2	70/21	36	48.8	43
10-CVN-RT-T1	70/21	67	90.8	46
8-CVN-RT-T1	70/21	46	62.4	56
6-CVN-RT-T1	70/21	24	32.5	15
10-CVN-RT-T2	70/21	42	56.9	24
8-CVN-RT-T2	70/21	52	70.5	52
6-CVN-RT-T2	70/21	30	40.7	22

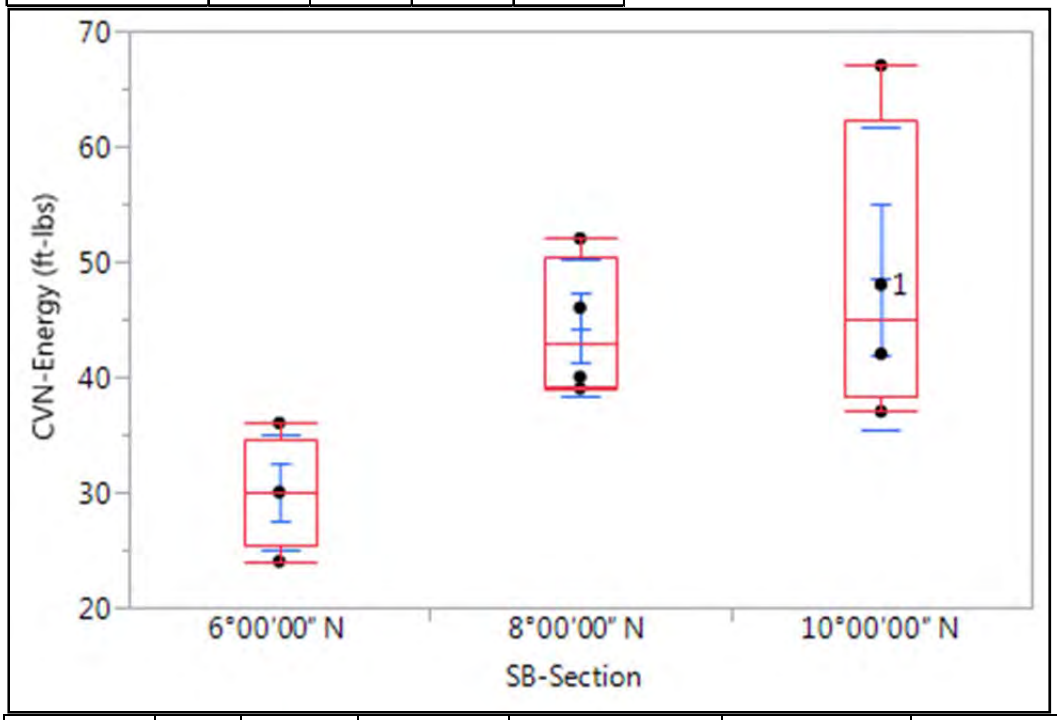

Section	No.	Mean	Std Dev	Std Err Mean	Lower 95%	Upper 95%
6 inch	4	30	4.899	2.4495	22.205	37.795
8 inch	4	44.25	6.0208	3.0104	34.67	53.83
10 inch	4	48.5	13.1276	6.5638	27.611	69.389

Figure 62: Charpy V notch Impact energy vs. section size combined data plot

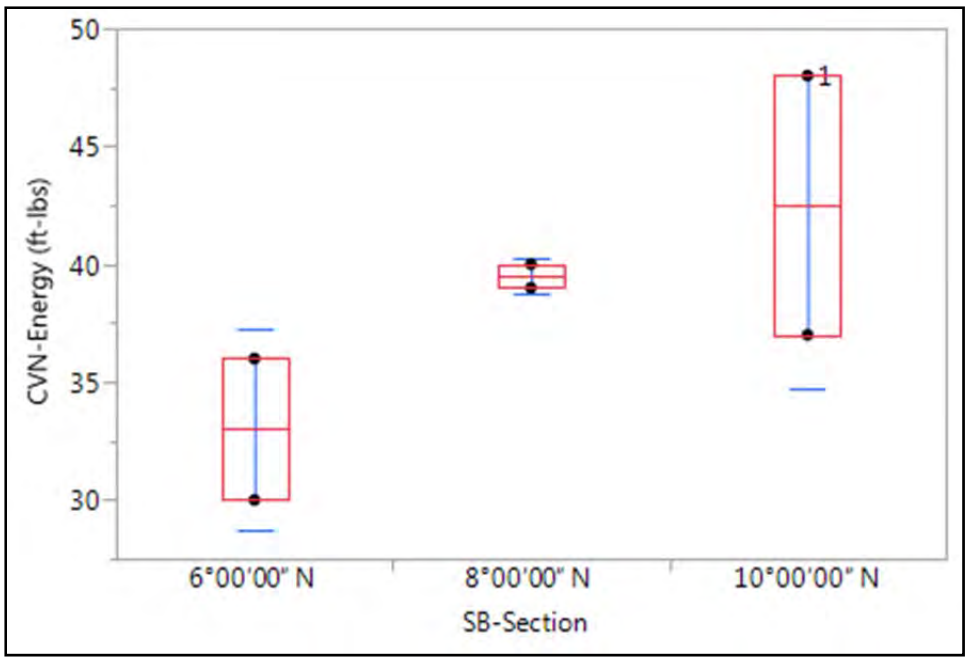

Figure 63: CL plane trepan samples Charp V-notch Impact energy vs. Section size plot

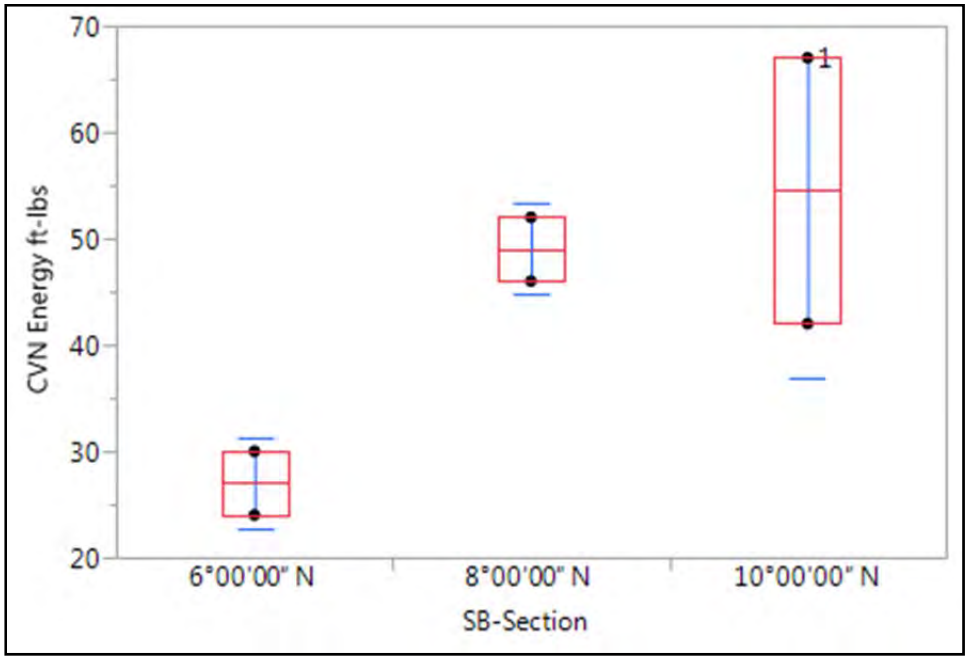

Figure 64: DL plane trepan samples Charp V-notch Impact energy vs. Section size plot

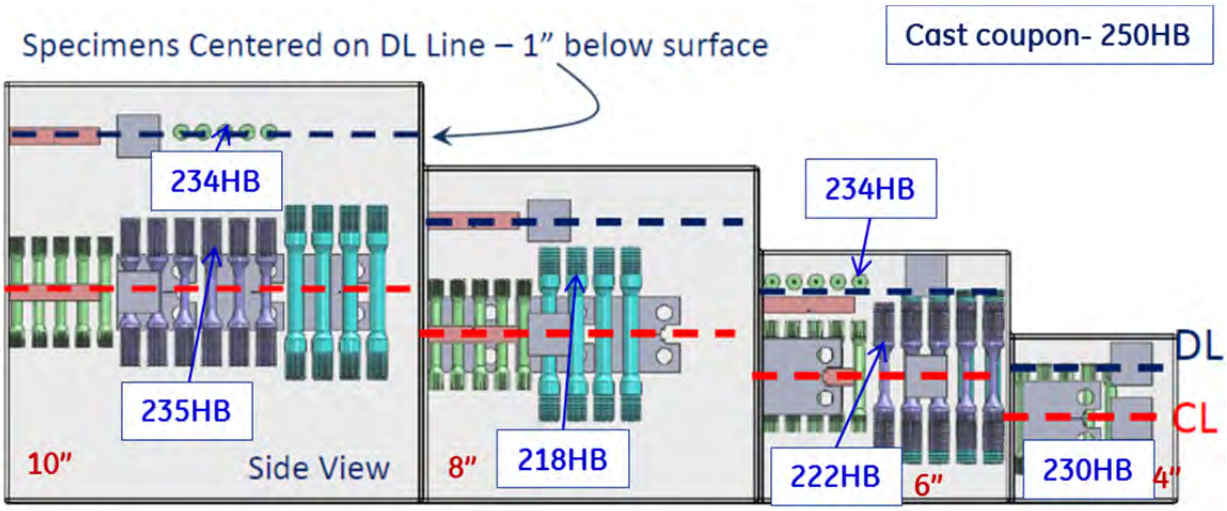

Figure 65: N263 Cast hardness values are not section thickness dependent

Table 11: N263 Casting section hardness values raw data

Sample ID	Hardness (HRBW/HRC)	Conversion (HBW)
10-TN-CL-RT-H	98.98 HRBW *	235 HBW
8-TN-CL-RT-H	96.58 HRBW *	218 HBW
6-TN-CL-RT-H	97.21 HRBW *	222 HBW
4-TN-CL-RT-H	98.36 HRBW *	230 HBW
10-TN-DL-RT-H	99.27 HRBW *	234 HBW
6-TN-DL-RT-H	20.82 HRC *	234 HBW
GJOJ-263-TB-RT-H	23.91 HRC *	250 HBW

Appendix 1-D [Centrifugal Castings of Haynes 282]

CENTRIFUGAL CASTING OF HAYNES 282

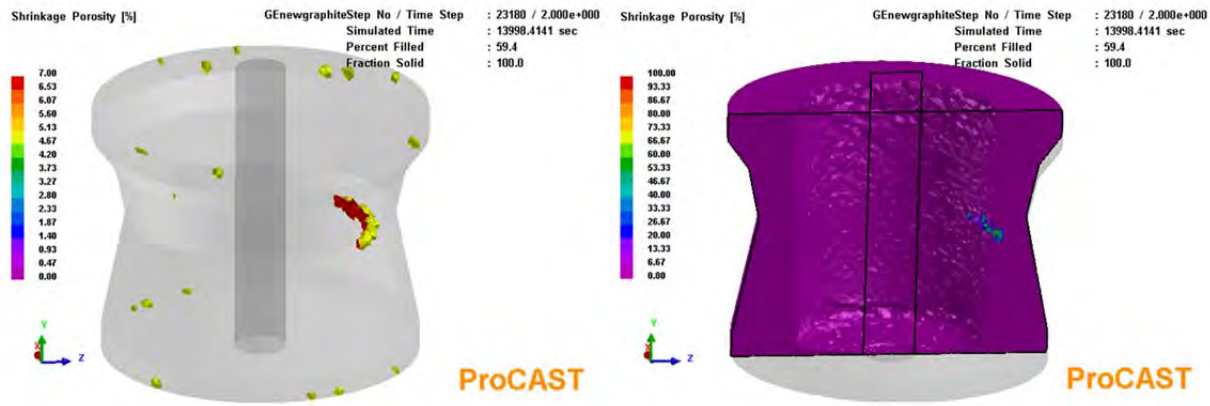

Figure 1: Chromite sand mold section mid height on ID surface visual shrinkage was detected as per simulation test findings.

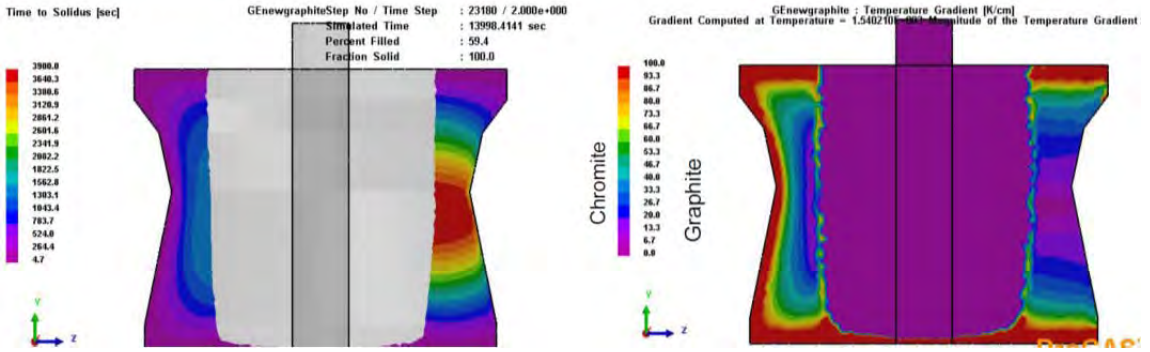

Figure 2: Solidification simulation analysis indicates Chromite mold takes longer time for solidification [Left] and temperature gradient, late in mushy zone provides potential microstructural features.

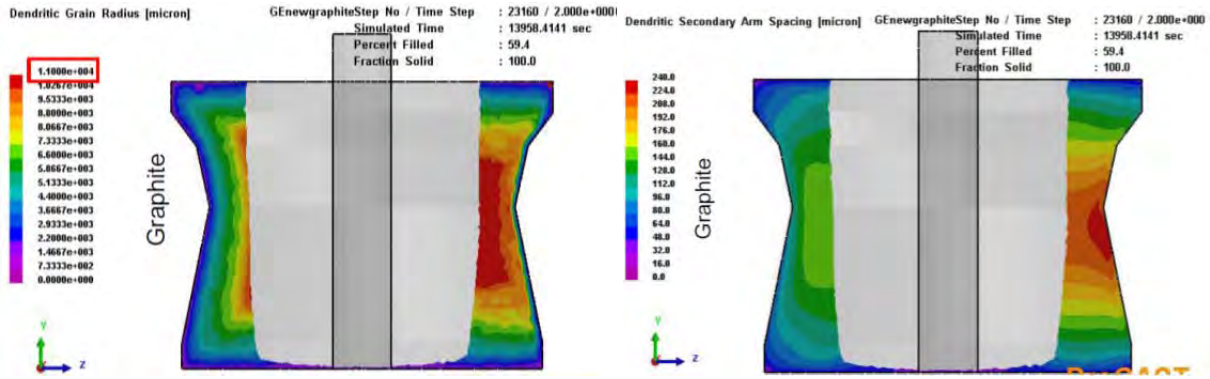

Figure 3: Faster cooling rateson graphite results in smaller dendritic grain radius, spread more uniformly [Left], Graphite mold interface has smaller SDAS due to faster cooling over Chromite sand mold.

GENERAL ELECTRIC COMPANY
1 RIVER RD BLDG ~~55-315H~~ 55-115H, MPE
SCHENECTADY, NY 12345

Attention: ~~PURCHASING DEPT~~ MANI THANGIRALA

Page 1 of 1

MetalTek INTERNATIONAL
Wisconsin Centrifugal Division
905 E. St Paul Avenue Waukesha, WI 53188 USA
Phone: 262-544-7820 Fax: 262-544-7837
E-Mail: kathy.gapinski@metaltek.com

Job No.: M711270 (CO103084)
P.O. No.: 900374389
Part No.: 4013522-309 P01 HYBRID
Part No. Rev.:
Spec.: Ni Alloy Centrifugal Cast
Quantity: 1
Shipping Date: 02/06/2013

CERTIFICATION TEST REPORT

Heat No.	Final Chem	PC	AL	C	CO	CR	CU	FE	MN	MO	NB	P	S	SI
			wt %	wt %	wt %	wt %	wt %	wt %	wt %	wt %	wt %	wt %	wt %	wt %
P8001		1	1.57	0.06	9.76	19.35	0.00	0.11	0.15	8.44	0.00	0.00	0.00	0.10

Heat No.	Final Chem	PC	TI	W	ZR
			wt %	wt %	wt %
P8001		1	2.08	0.05	0.01

Test Methods used: Chemical Analysis – XRF Carbon / Sulfur, Oxygen / Nitrogen Analysis – Combustion. Standard Industry Spec's used for testing, unless otherwise stated: Tensile ASTM E 8, Brinell ASTM E 10, Elevated Temperature Tensile ASTM E 21, Rockwell Hardness ASTM E 18, Impact ASTM E 23, Stress Rupture ASTM E 139.

We hereby certify that the material represented by this document has been tested and is in conformance with the Purchase Order, Drawing and Specification Requirements. This report should not be reproduced except in full, without prior written approval. The recording of false, fictitious or fraudulent statements or entries on this report may be punishable as a felony under federal statues.

Quality Assurance Representative
KATHY GAPINSKI, LAB SERVICES COORDINATOR

02/07/2013 Cert #: 42292, Master # :6, Master Rev: 33

Figure 4: Certificate of chemistry from centrifugal casting at Metaltek. All chemistry met the requirements

Cycle	Heating Media / Rate	Temperature (F)	Time (Hours)	Cooling Media / Rate
Homogenize	Vacuum, 5°F/min.	2057	1.0	Ramp 5°F/min. to 2120 F
Homogenize	Vacuum	2120	3.0	Ramp 5°F/min. to 2174 F
Homogenize	Vacuum	2174	6.0	Ramp 5°F/min. to 2192 F
Homogenize	Vacuum	2192	10.0	Argon Quench
Age	Vacuum, 5°F/min.	1850	2.0	Air Cool
Age	Vacuum, 5°F/min.	1450	8.0	Air Cool

Figure 4: Final heat treatment cycle on the centrifugal casting.

Table 1: Raw tensile data of Haynes 282 casting at the thick location [5S = 5 inch wall thickness] and thin location [2S=2 inch wall thickness]. Data is from the side of the casting that solidified in a sand mold

Specimen ID	Temp	UTS	0.02 YS	0.2YS	% Elong	% RA	Mold	Thickness	Orientation
5S-TNSL-A-01	75	91.1	84.1		1.0	3.9	Sand	Thick	Axial
5S-TNSL-A-02	500	86.2	76.3	83	3.0	5.0	Sand	Thick	Axial
5S-TNSL-A-03	1000	86.5	69.7	80.6	5	10.5	Sand	Thick	Axial
5S-TNSL-A-04	1250	102.6	74.7	82.6	8.0	16.0	Sand	Thick	Axial
5S-TNSL-R-01	75	98.9	80.9	85.7	5.0	10.0	Sand	Thick	Radial
5S-TNSL-R-02	500	93.5	78.6	85.1	6.0	7.0	Sand	Thick	Radial
5S-TNSL-R-03	1000	109	74.1	80.4	16.0	27.0	Sand	Thick	Radial
5S-TNSL-R-04	1250	89.2	71.6	80.1	5.0	12.0	Sand	Thick	Radial
5S-TNSL-R-05	1500	96.8	65.7	76.5	15.0	17.5	Sand	Thick	Radial
5S-TNSL-T-01	75	98.8	79.3	86.7	6.0	10.0	Sand	Thick	Tangential
5S-TNSL-T-02	500	96.9	72.9	76.5	10.0	19.0	Sand	Thick	Tangential
5S-TNSL-T-03	1000	97.5	70.3	72.9	24.0	28.0	Sand	Thick	Tangential
5S-TNSL-T-04	1250	114.5	72.2	76.3	23.0	34.0	Sand	Thick	Tangential
5S-TNSL-T-05	1500	92.7	76.5	78.7	30.0	35.5	Sand	Thick	Tangential
2S-TNSL-A-01	75	87.9	85.2	83.5	6.0	10.0	Sand	Thin	Axial
2S-TNSL-A-04	1250	108.6	77	83.9	11.0	18.0	Sand	Thin	Axial
2S-TNSL-A-05	1500	100.2	70.8	75.5	17.0	14.5	Sand	Thin	Axial
2S-TNSL-R-01	75	104.7	82.8	90.9	4.7	8.5	Sand	Thin	Radial
2S-TNSL-R-02	1000	96.7	72.3	77.9	11.0	15.5	Sand	Thin	Radial
2S-TNSL-R-03	1500	89.2	64.1	71.7	6.0	10.5	Sand	Thin	Radial
2S-TNSL-T-01	75	96.7	83.5	87.4	8.0	7.5	Sand	Thin	Tangential
2S-TNSL-T-02	500	96.2	85.8	94.6	9.5	8.5	Sand	Thin	Tangential
2S-TNSL-T-03	1000	99.7	79.1	86.9	6	15.5	Sand	Thin	Tangential
2S-TNSL-T-04	1250	90.1	74.5	82.8	3	10	Sand	Thin	Tangential
2S-TNSL-T-05	1500	90.4	55.2	66.8	25	51.5	Sand	Thin	Tangential

Table 2: Raw Tensile data of H282 Casting at the thick location [5S = 5 inch wall thickness] and thin section [2S = 2 inch wall thickness]. Data is from the side of the casting that solidified in Graphite mold.

Specimen ID	Temp	UTS	0.02 YS	0.2YS	% Elong	% RA	Mold	Thickness	Orientation
5G-TNSL-A-01	75	96.9	82.7	87.7	3.0	10.0	Graphite	Thick	Axial
5G-TNSL-A-02	500	100.5	75.9	85.1	5.0	8.5	Graphite	Thick	Axial
5G-TNSL-A-03	1000	103	87.4	88.9	10.0	18.5	Graphite	Thick	Axial
5G-TNSL-A-04	1250	100.3	72.8	76	13.0	13.5	Graphite	Thick	Axial
5G-TNSL-A-05	1500	95	72.6	74.5	9.0	13.5	Graphite	Thick	Axial
5G-TNSL-R-01	75	117.7	81.6	85.5	14.0	17.0	Graphite	Thick	Radial
5G-TNSL-R-02	500	117.1	77.3	83.6	13.0	17.5	Graphite	Thick	Radial
5G-TNSL-R-03	1000	109.8	71	76.6	23.0	25.0	Graphite	Thick	Radial
5G-TNSL-R-04	1250	109.1	70.2	76.2	13.0	18.5	Graphite	Thick	Radial
5G-TNSL-R-05	1500	96	66	71.9	19.0	30.0	Graphite	Thick	Radial
5G-TNSL-T-01	75	121.1	79.7	82.1	13.0	14.0	Graphite	Thick	Tangential
5G-TNSL-T-02	500	96.9	74.7	82.8	6.0	11.5	Graphite	Thick	Tangential
5G-TNSL-T-03	1000	100.9	72.6	75.6	20.0	27.5	Graphite	Thick	Tangential
5G-TNSL-T-04	1250	105.4	71.5	74.1	16.0	25.0	Graphite	Thick	Tangential
5G-TNSL-T-05	1500	89.1	67.1	69.4	20.0	40.0	Graphite	Thick	Tangential
2G-TNSL-A-01	75	97.6	86.7	91.6	6.0	6.5	Graphite	Thin	Axial
2G-TNSL-A-02	500	101.5	71.6	72.8	17.0	18.0	Graphite	Thin	Axial
2G-TNSL-A-03	1000	82.3	69	74	11.0	21.5	Graphite	Thin	Axial
2G-TNSL-A-04	1250	99.8	70.9	75.7	22.0	26.5	Graphite	Thin	Axial
2G-TNSL-A-05	1500	85.4	65.3	69.5	14.0	34.5	Graphite	Thin	Axial
2G-TNSL-R-01	75	137.4	80	82.6	34.0	29.0	Graphite	Thin	Radial
2G-TNSL-R-02	1000	107	64	72.5	34.5	37.0	Graphite	Thin	Radial
2G-TNSL-R-03	1500	95.9	64	70.2	37.5	51.0	Graphite	Thin	Radial
2G-TNSL-T-01	75	119.5	84.1	88.5	14.0	14.0	Graphite	Thin	Tangential
2G-TNSL-T-02	500	119.3	71	77.8	17.0	17.5	Graphite	Thin	Tangential
2G-TNSL-T-03	1000	96.6	69.9	74.3	17.0	21.0	Graphite	Thin	Tangential
2G-TNSL-T-04	1250	117.1	72	79.6	22.0	20.5	Graphite	Thin	Tangential
2G-TNSL-T-05	1500	92.3	63.5	70.5	22.0	31.5	Graphite	Thin	Tangential

Table 3: LCF results of specimens extracted from the Sand (S) and Graphite (G) side of the centrifugal cast H282 alloy. IX = Inside Extensometer, OX = Outside Extensometer, S = Surface

Specimen ID	Temp (F)	TSR (%)	Astrain	Midlife		Total Strain Range (%)	Elastic (%)	Plastic Calc. (%)	Plastic Measured (%)	Ni	Nf	Location	Initiation
				Max Stress	Min. Stress								
5G-LCF-R-07	75	1.000	1.0	94.7	-96.5	1.00	0.69	0.30	0.30	3,185	3,250	IX	S
5G-LCF-R-08	75	0.900	1.0	97.3	-96.3	0.90	0.68	0.23	0.22	4,710	5,130	IX	S
5G-LCF-R-10	75	0.700	1.0	92.0	-88.9	0.70	0.63	0.06	0.07	7,994	10,228	IX	S
5G-LCF-R-11	75	0.600	1.0	84.2	-75.6	0.60	0.59	0.00	0.01	22,421	23,340	IX	S
5G-LCF-R-03	1400	0.800	1.0	84.2	-89.9	0.78	0.65	0.10	0.14	464	482	IX	S
5G-LCF-R-04	1400	0.700	1.0	92.7	-61.1	0.69	0.66	0.02	0.03	491	560	IX	S
5G-LCF-R-05	1400	0.600	1.0	66.4	-47.4	0.60	0.59	0.01	0.01	4,555	5,942	IX	S
5G-LCF-R-06	1400	0.500	1.0	72.9	-34.1	0.50	0.48	0.00	0.01	3,325	4,142	IX	S
5G-LCF-R-01	1400	1.000	1.0	90.5	-91.1	1.00	0.88	0.11	0.11	719	741	OX	S
5G-LCF-R-02	1400	0.900	1.0	75.4	-79.4	0.89	0.82	0.05	0.07	2,607	2,675	OX	S
5S-LCF-R-07	75	1.000	1.0	100.7	-101.4	1.00	0.64	0.36	0.36	581	589	IX	S
5S-LCF-R-09	75	0.800	1.0	102.6	-100.7	0.80	0.63	0.16	0.17	1,642	1,865	IX	S
5S-LCF-R-10	75	0.700	1.0	87.8	-77.1	0.70	0.67	0.02	0.03	8,519	15,669	IX	S
5S-LCF-R-12	75	0.500	1.0	94.6	-61.3	0.50	0.49	0.00	0.00	22,512	24,496	IX	S
5S-LCF-R-02	1400	0.900	1.0	80.5	-88.6	0.90	0.77	0.20	0.13	1,170	1,216	IX	S
5S-LCF-R-03	1400	0.800	1.0	74.3	-76.3	0.79	0.74	0.02	0.05	1,795	1,885	IX	S
5S-LCF-R-04	1400	0.700	1.0	70.8	-83.7	0.69	0.67	0.01	0.02	1,594	1,998	IX	S
5S-LCF-R-05	1400	0.600	1.0	72.8	-58.9	0.60	0.59	0.01	0.01	2,876	2,892	IX	S
5S-LCF-R-06	1400	0.500	1.0	70.3	-31.2	0.50	0.49	0.01	0.00	1,400	2,313	IX	S
5S-LCF-R-08	75	0.900	1.0	101.3	-96.9	0.90	0.65	0.24	0.24	233	234	OX	S
5S-LCF-R-01	1400	1.000	1.0	95.8	-100.6	1.00	0.75	0.25	0.25	112	125	OX	S

Table4: Table showing the short term rupture tests from Centrifugal Cast H282.

Location	Specimen ID	Status	Temp	Stress	Tf	% Elong	% RA
Sand	5G-RUP-R-01	Failed	1472	40	285.9	14.4	32.9
	5G-RUP-R-02	Failed	1472	35	893.1	15.6	45.2
	5G-RUP-R-03	Failed	1472	30	1591.0	23.4	15.3
	5G-RUP-R-05	Failed	1400	45	539.4	7.4	29.6
	5G-RUP-R-06	Failed	1400	40	1714.5	11.4	35.6
	5G-RUP-R-04	Stopped	1472	25	2983.7		
	5G-RUP-R-07	Stopped	1400	35	2980.0		
	5G-RUP-R-08	Stopped	1400	30	2984.2		
Graphite	5S-RUP-R-01	Failed	1472	40	283.9	7.9	14.5
	5S-RUP-R-02	Failed	1472	35	654.5	11.0	23.1
	5S-RUP-R-03	Failed	1472	30	1474.8	11.3	23.2
	5S-RUP-R-05	Failed	1400	45	789.8	8.0	13.3
	5S-RUP-R-06	Failed	1400	40	1218.7	9.0	23.3
	5S-RUP-R-08	Failed	1400	30	2292.4	8.6	43.0
	5S-RUP-R-04	Stopped	1472	25	2983.6		
	5S-RUP-R-07	Stopped	1400	35	2984.7		

Appendix 1-E [FUNDAMENTAL STUDIES ON COOLING RATES AND SDAS]

FUNDAMENTAL STUDIES ON COOLING RATES AND SDAS

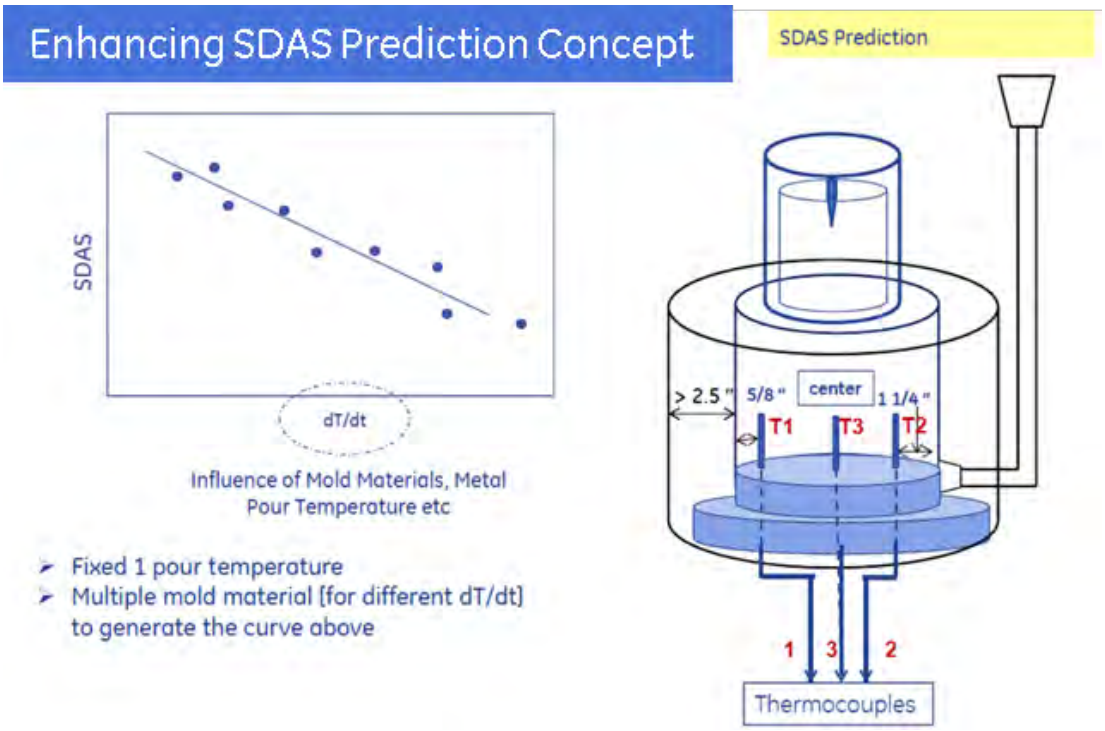

Figure 1: Enhancing SDAS prediction with casting solidification mold cooling rate studies. Six molds with different mold materials [to simulate different cooling rates] were poured with thermocouples located as shown to measure casting cooling rates

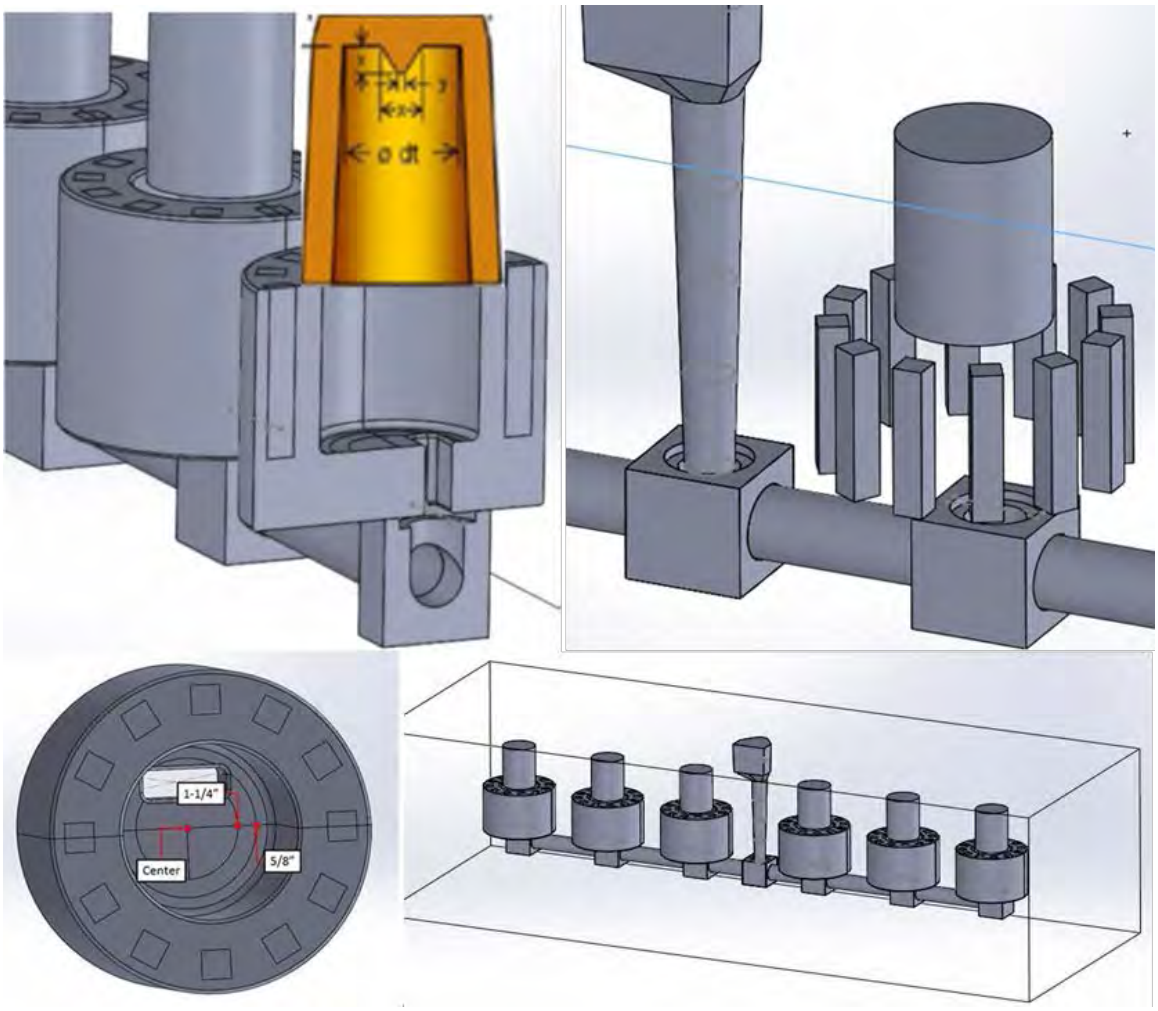

Figure 2: Detailed plan of casting solidification cooling rates measurement mold layout assembly

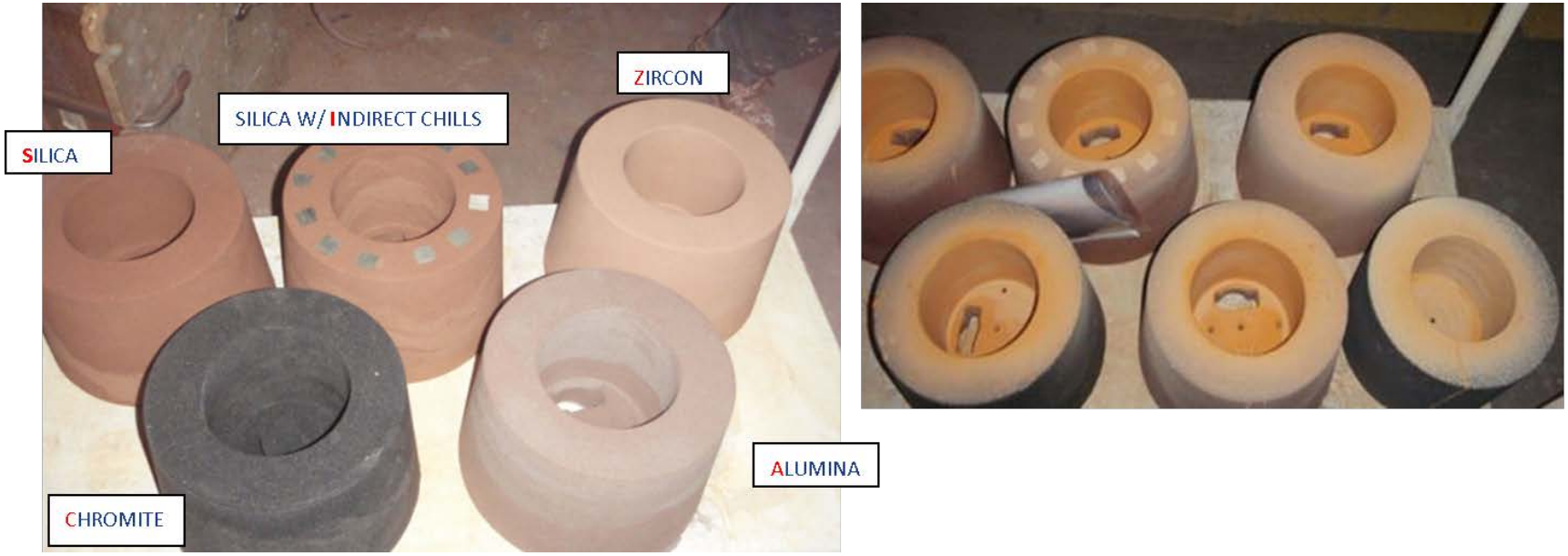

Figure 3: Sand molds from 5 different mold materials [left] coated with refractory paint and dried [right]. Six mold materials were evaluated: 1. Silica, 2. Chromite, 3. Graphite, 4. Alumina, 5. Zircon, 6. Silica with indirect chills placement.

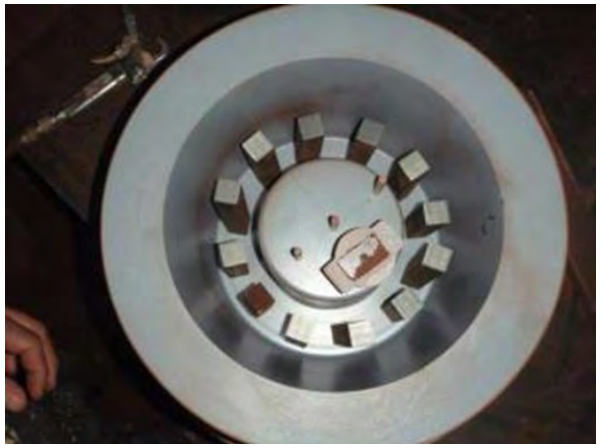

Figure 4: Photograph of chills location in mold pattern prior to molding

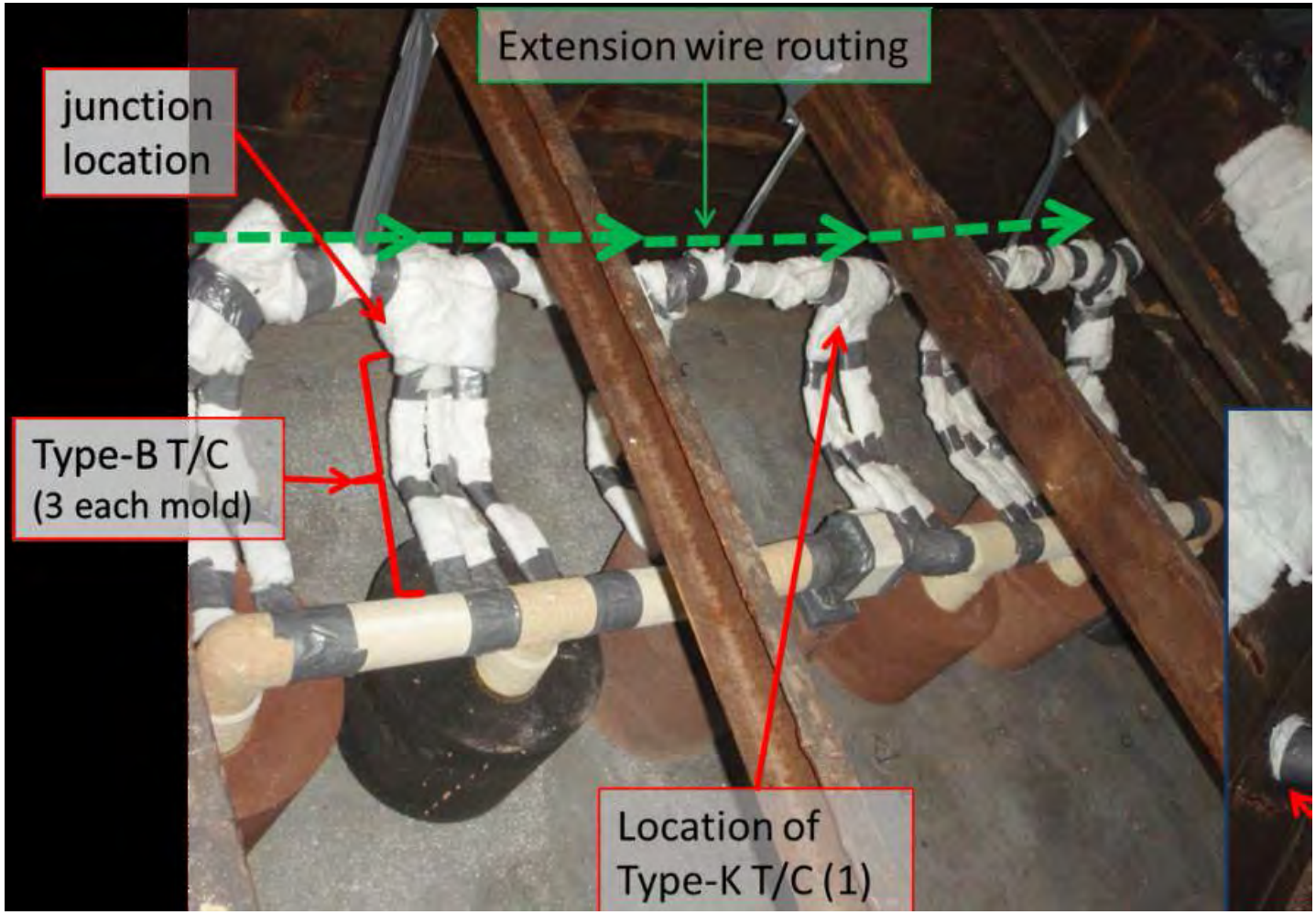

Figure 5: Thermocouples and extension wire were wrapped with Kaowool thermal insulation.

Figure 6: Photograph of thermocouple compensating cables routing within the drag mold

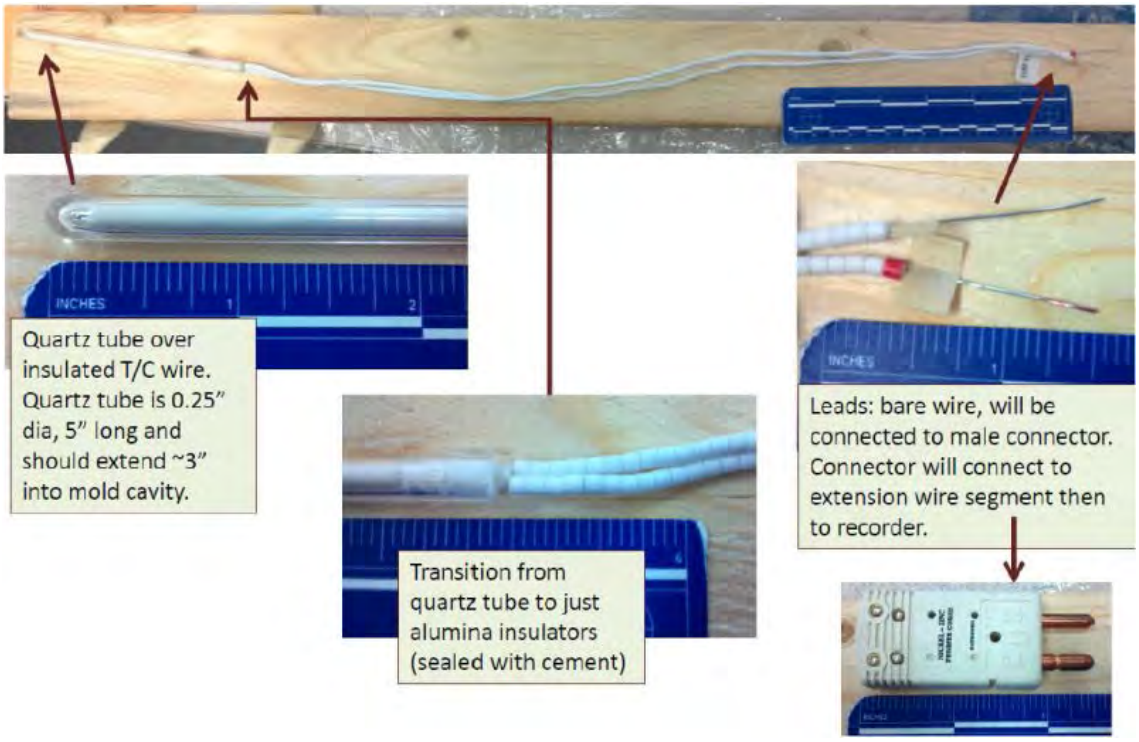

Figure 7: Type B Thermocouples, insulators and connectors assembly components

Figure 8: Drag mold with the six mold material inserts were attached; tile gating was used to connect the downsprue with each mold in-gates [Left]. Photograph of the Cope mold with 5 inch OD x 7.5 inch riser thermal sleeves shown [Right]

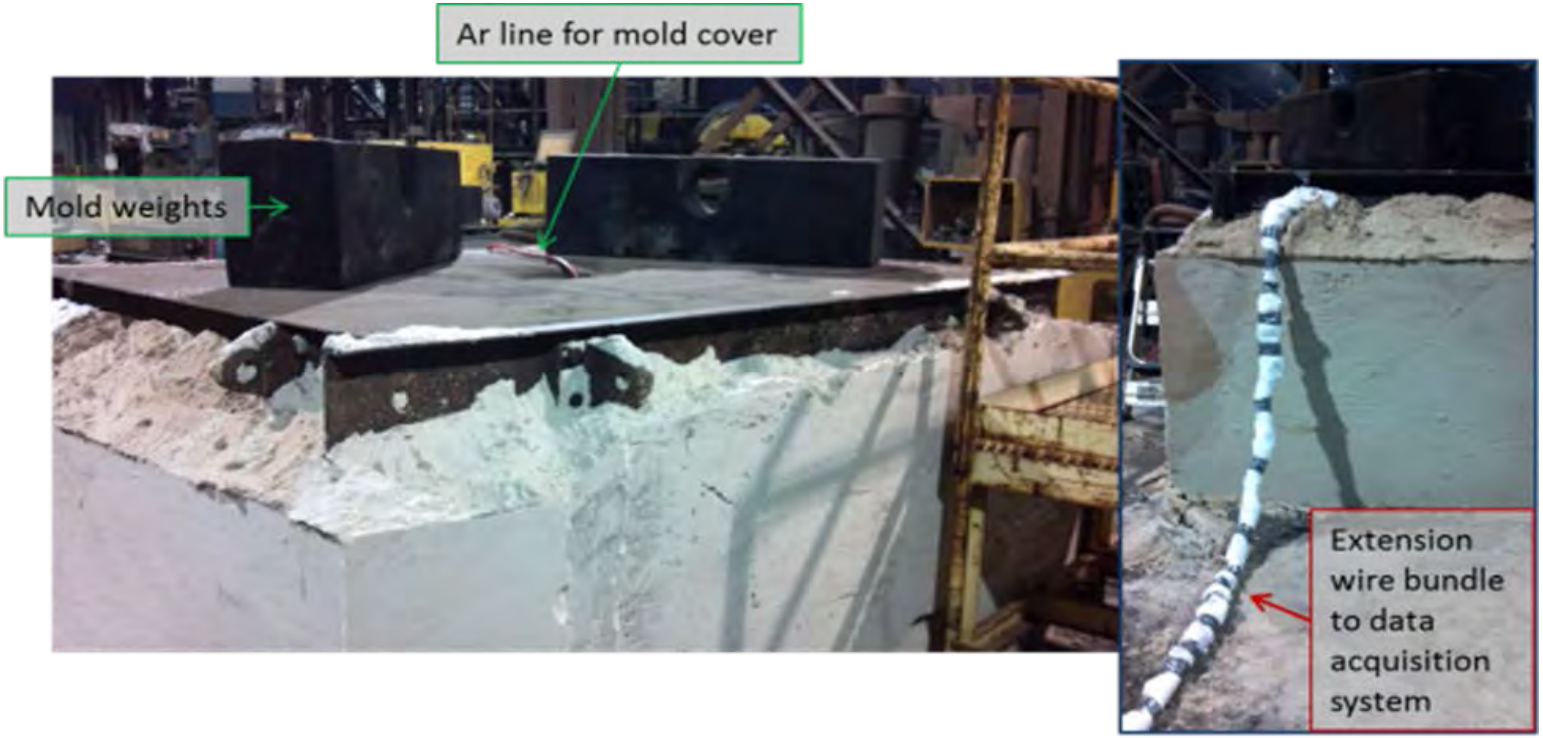

Figure 9: Photograph of completed mold ready for pour

Figure 10: Photograph of castings immediately after molds shakeout

Figure 11: Photograph showing castings after mold shake out, gating and feeders removal

Table 1: Mold and thermocouple location ID tabulation

Channel	Thermocouple ID	Mold	Location	Type
0	Type K	Backing sand	near junction between center type B thermocouple and extension wire	Type K, SS sheath
1	S1	silica	5/8 inch from edge	Type B: 26 gauge wire, alumina insulation. 24 inch long with 5" long quartz sheath
2	S2	silica	1.25 inch from edge	
3	S3	silica	center	
4	C1	chromite	5/8 inch from edge	
5	C2	chromite	1.25 inch from edge	
6	C3	chromite	center	
7	Z1	zircon	5/8 inch from edge	
8	Z2	zircon	1.25 inch from edge	
9	Z3	zircon	center	
10	A1	alumina	5/8 inch from edge	
11	A2	alumina	1.25 inch from edge	
12	A3	alumina	center	
13	G1	graphite	5/8 inch from edge	
14	G2	graphite	1.25 inch from edge	
15	G3	graphite	center	
16	I1	Indirect chill	5/8 inch from edge	
17	I2	Indirect chill	1.25 inch from edge	
18	I3	Indirect chill	center	

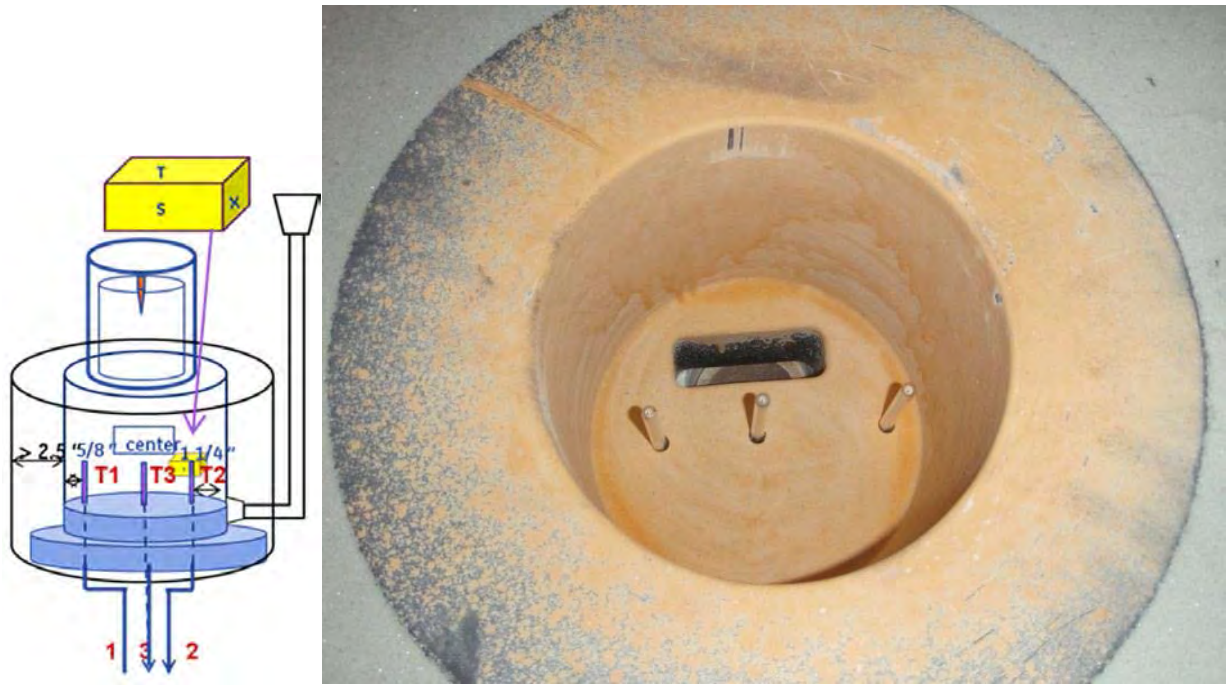

Figure 12: Haynes 282 cylinder castings thermocouple arrangements schematic view. Photograph showing Quartz sheathed Type–B thermocouples located within the molds

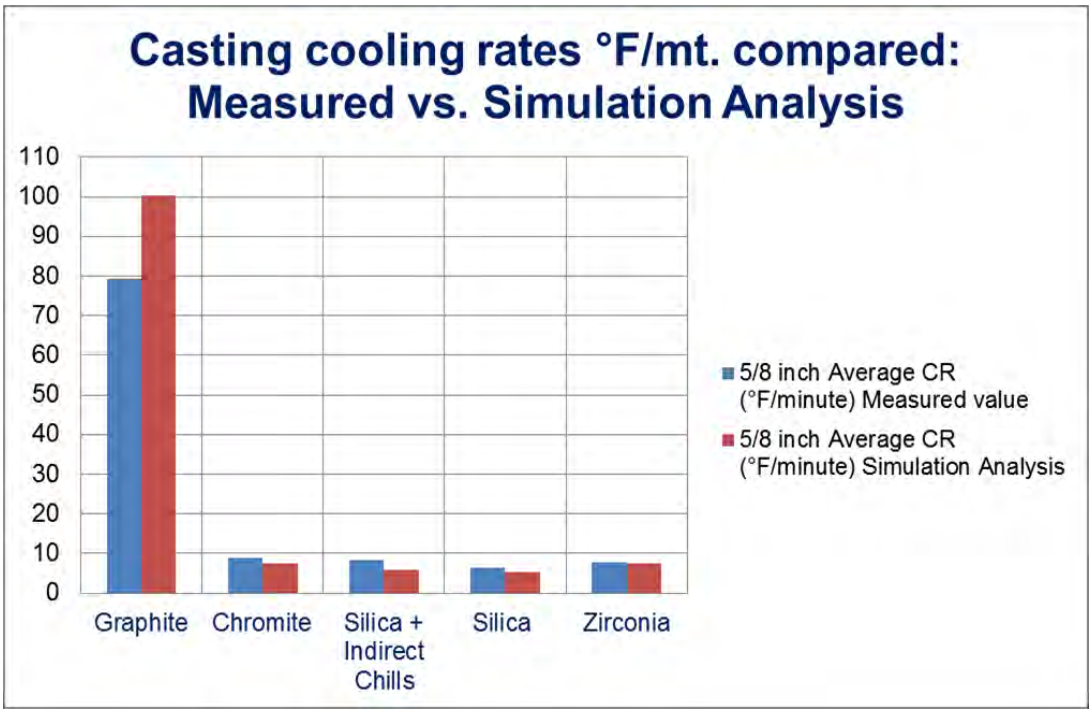

Figure 13: Casting cooling rates measured and simulated compared for different mold materials during liquidus to solidus transition temperature range

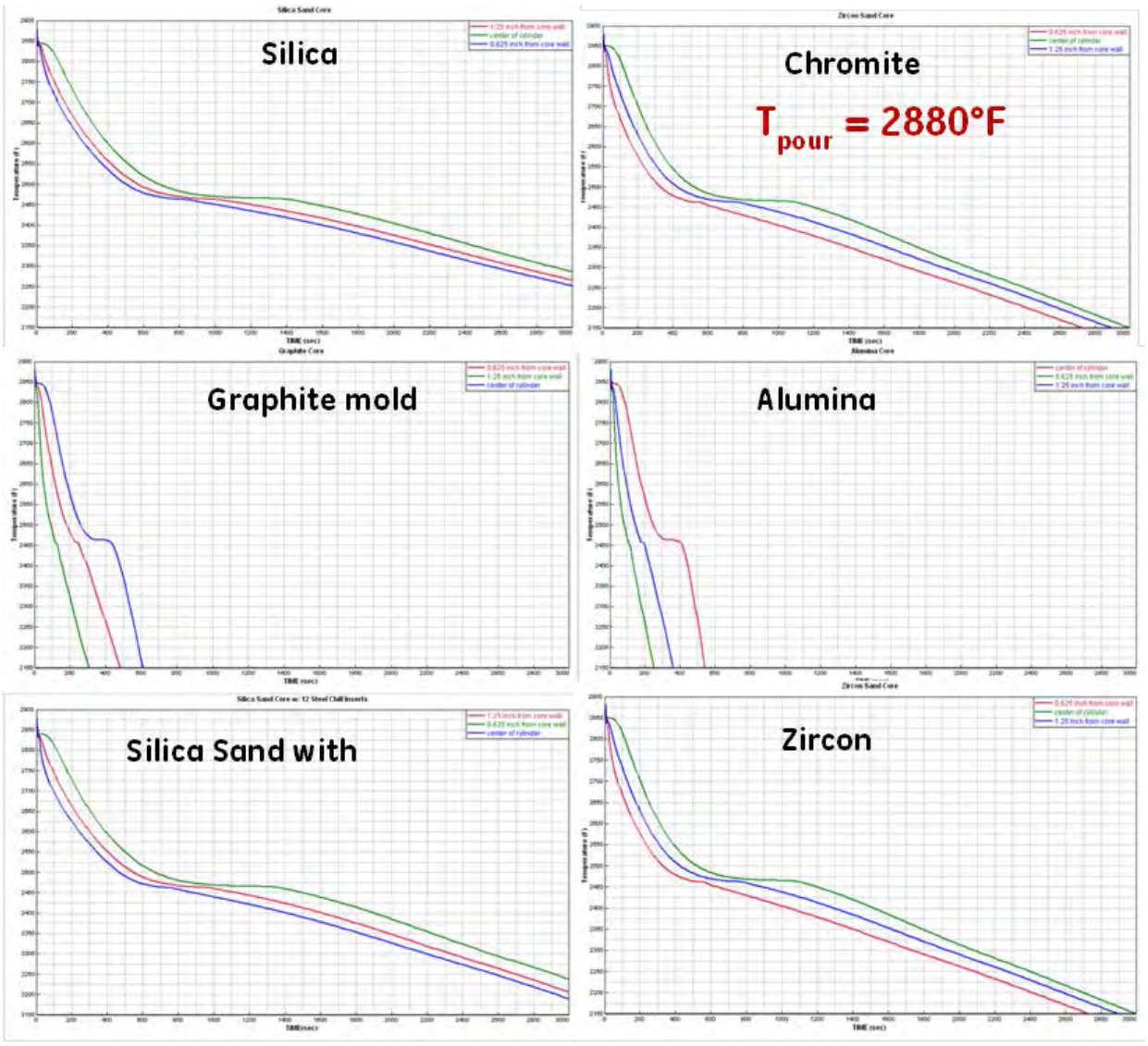

Figure 14: Casting Solidification Simulation Analysis cooling rates plot from pour to post solidification elevated temperature range for all the mold materials. Data from the 3 thermocouples T1, T2 and T3 vs. casting cooling time are plotted for different molds.

Table 2: Haynes 282 Cast Cylinders Chemical Analysis

Element by weight (%)	Haynes 282 Virgin stock	Heat chemical analysis
Heat #	Z4820	59507
C	0.06	0.048
Mn	0.01	0.019
Si	0.02	0.074
Cr	19.4	18.880
Ni	Bal.	58.948
Mo	8.3	8.110
Cu	0.01	0.005
W	0.01	0.184
Nb	0.02	0.028
N (ppm)	28	3.1
Fe	0.04	0.183
Ti	2.1	2.128
Zr	0.001	0.0064
Al	1.48	1.387
Co	9.9	9.94
P	0.001	0.0028
S	0.0005	0.0005
O (ppm)	5	8

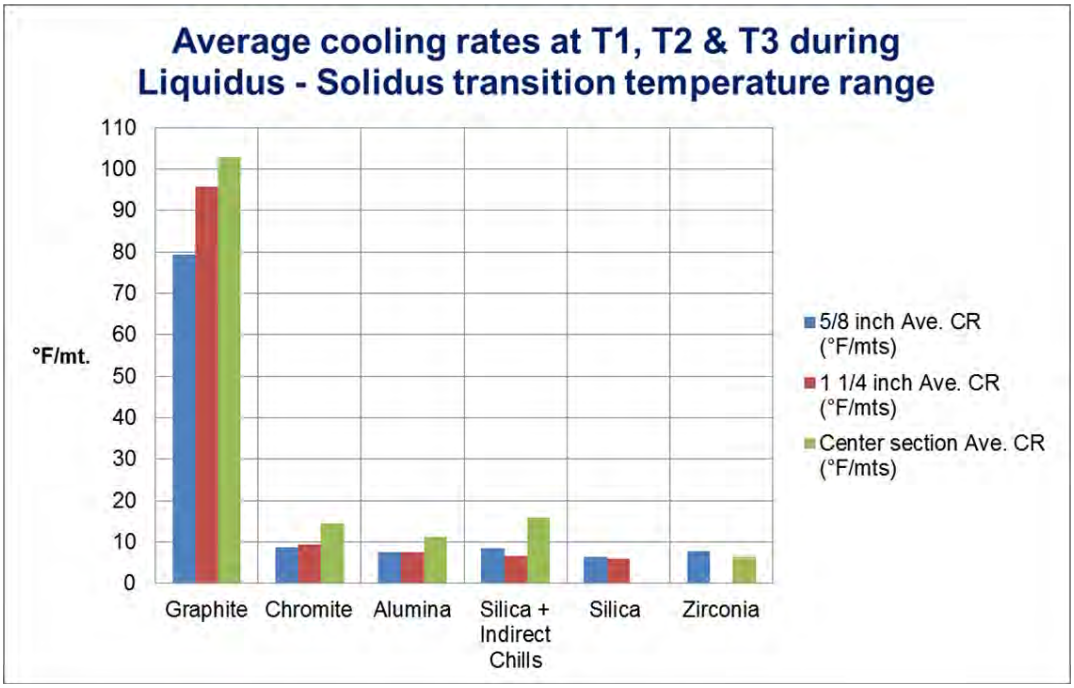

Figure 15: Haynes 282 Casting cooling rates during Liquidus to Solidus temperature range for different mold materials

Table 3: Casting cooling rates, both measured and simulated compared for different mold materials at 3 different locations within each mold

Mold material	5/8 inch Average CR (°F/minute)		1 1/4 inch Average CR (°F/minute)		Center Average CR (°F/minute)	
	Measured	Simulation	Measured	Simulation	Measured	Simulation
Graphite	79.3	100.16	95.74	62.82	102.86	41.44
Chromite	8.85	7.592	9.42	7.61	14.44	6.8
Silica + Indirect Chills	8.41	5.97	6.67	5.82	15.91	5.82
Silica	6.34	5.23	5.98	5.12	NA	5.09
Zirconia	7.73	7.46	NA	7.01	6.43	6.91

Table 4: Mold materials influence on microstructure SDAS values for Graphite, Zircon and Silica sand with indirect chills

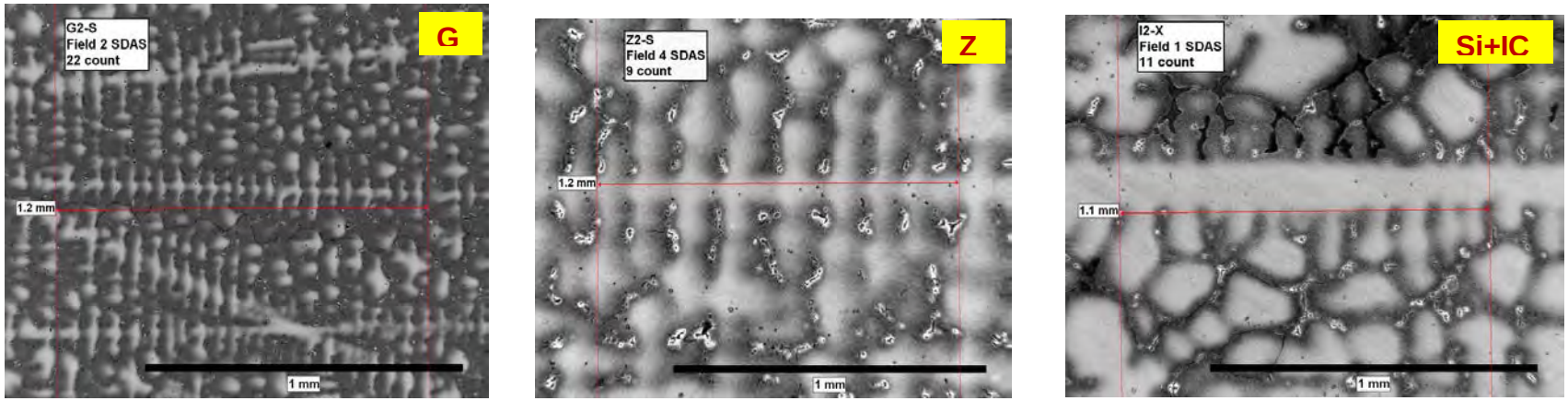

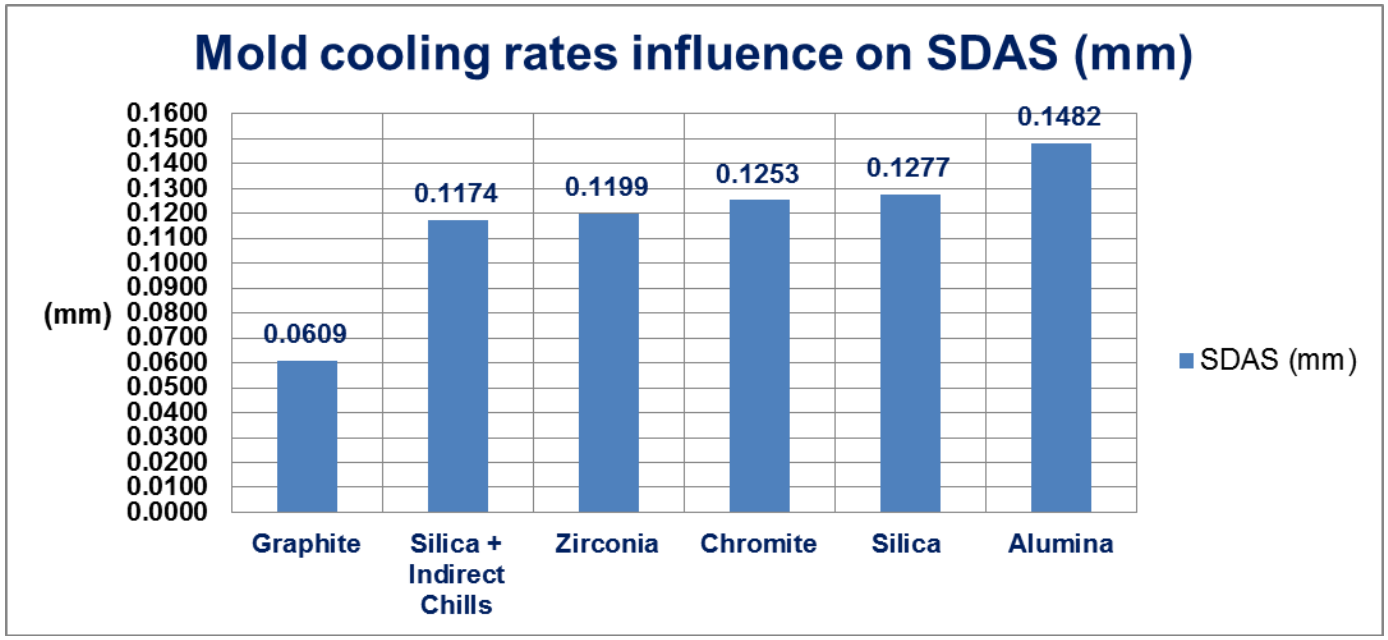

Figure 16: Mold cooling rates influence on SDAS values

Table 5: Mold materials influence on SDAS values through casting liquidus to solidus range cooling rates variation

Mold material	SDAS (mm)	SDAS Count #
Graphite	**0.0609**	**274**
Silica + Indirect Chills	0.1174	138
Zirconia	0.1199	146
Chromite	0.1253	128
Silica	0.1277	137
Alumina	0.1482	106

Appendix 1-F [LARGE CASTING OF HAYNES 282]

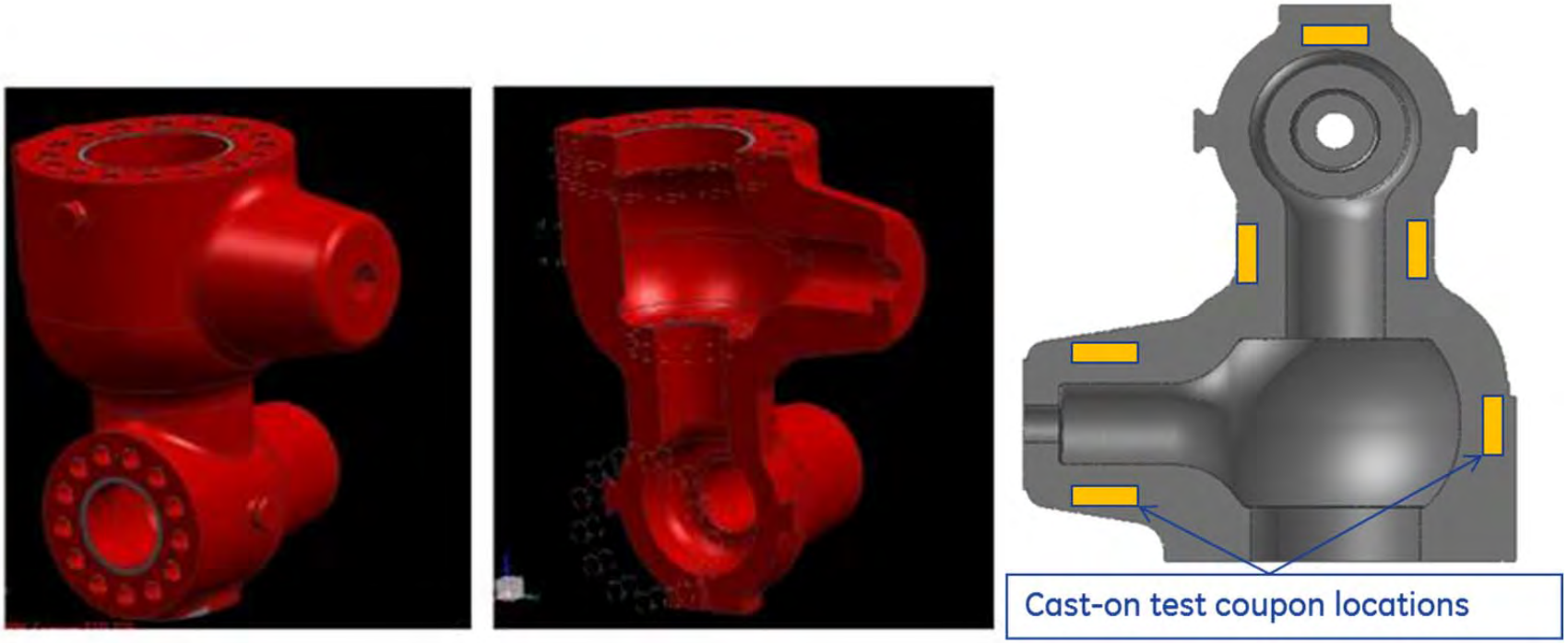

Figure 1: Steam turbine half valve casing solid model for the selected large casting trial. Also showing cast on coupon locations for material testing.

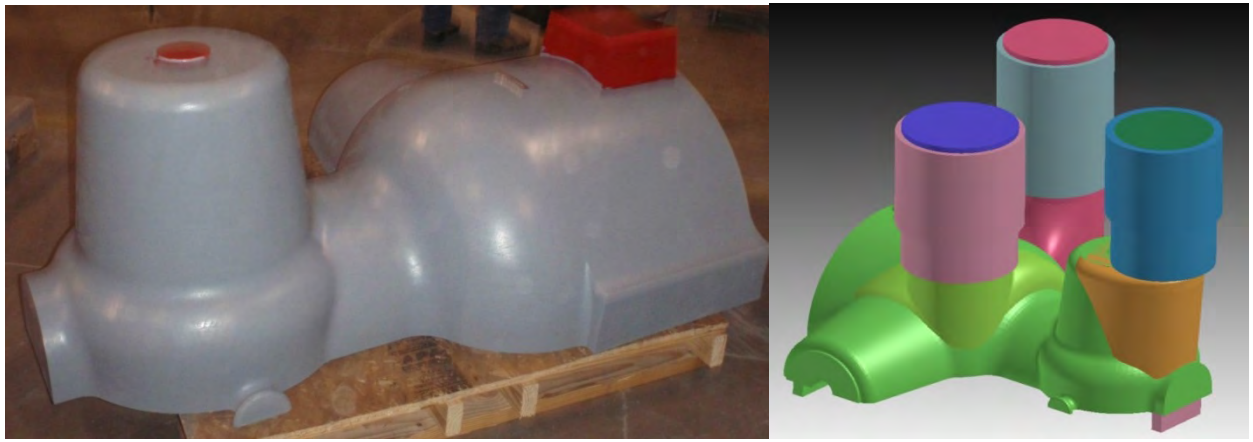

Figure 2: Foundry Casting Pattern and feeder design

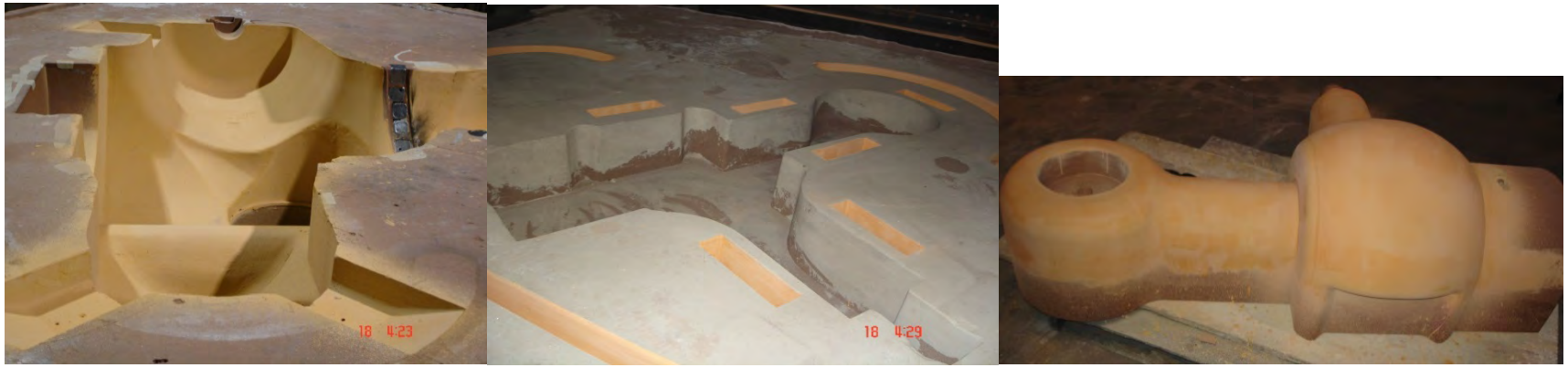

Figure 3: Picture showing Cope, drag molds and the valve body core after refractory coating and drying.

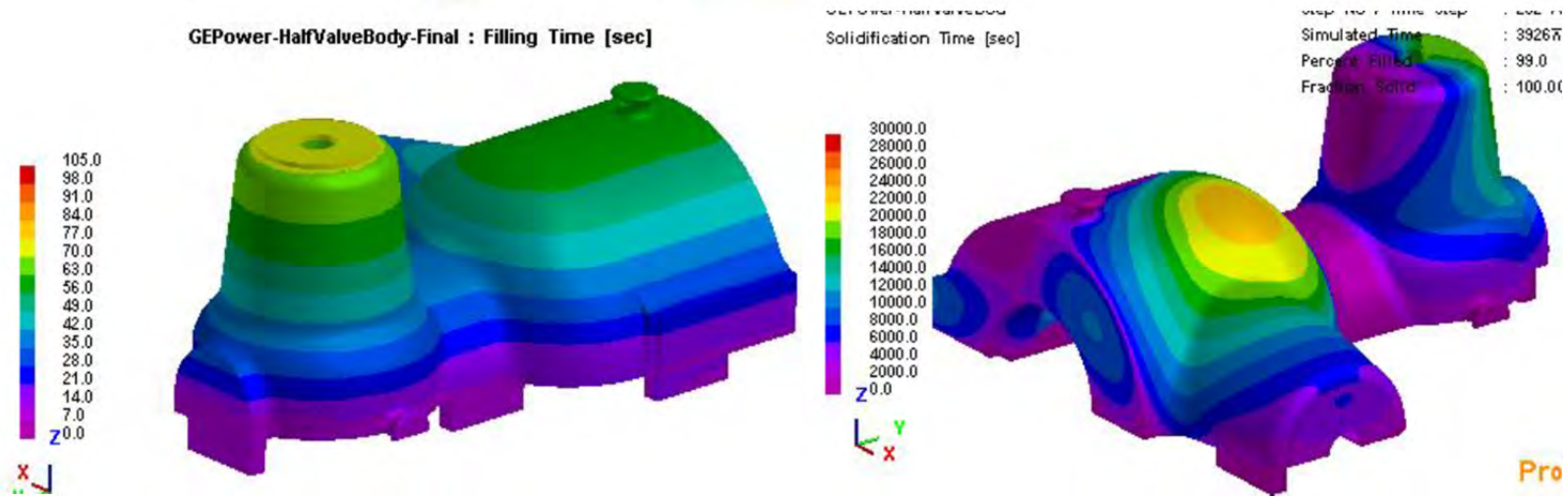

Figure 4: Solidification simulation indicates bottom to top filling (left) and temperature variation during liquidus to solidus transition temperature range (right)

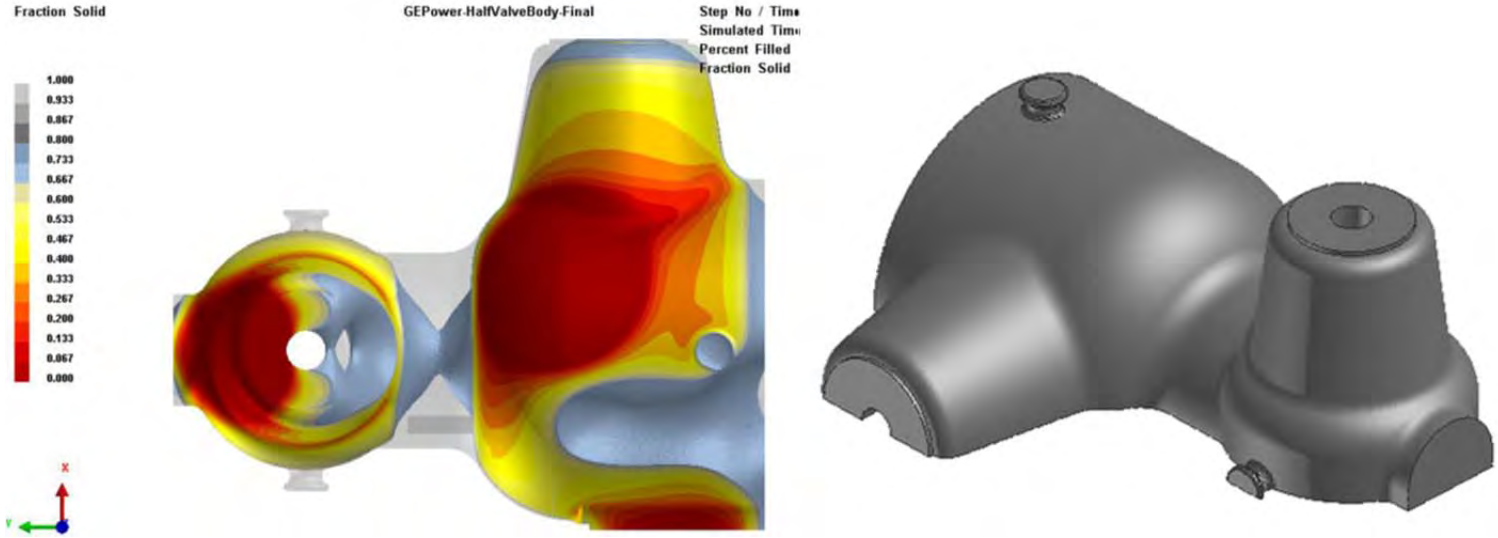

Figure 5: Solidification fraction solid cut off indicates no trail of shrinkage

Figure 6: Assembled mold, hot air dried and purged with Argon prior to pouring [Courtesy-MetalTek MO]

Figure 7: Induction melted, composition controlled with argon cover during melting and tapping melt quality controlled [Courtesy-MetalTek MO]

Figure 8: Pouring the mold after deslagging with covered ladles ensuring targeted pouring temperature and pour times [Courtesy-MetalTek MO]

Figure 9: Casting after in mold cooling and shake out [Courtesy-MetalTek MO]

A. Homogenizing Heat Treatment Steps

- **Casting Preparation**: Coat all casting surfaces, including the cast on coupons with AO Smith CG-11 Ceram-Guard Coating or similar HT coat application.
- Part should be loaded into a room temperature furnace with **Contact thermocouples attached** for recording stepped Homogenization HT cycle. Along with Furnace thermocouples - HT cycle record required.

1. **Ramp furnace at a rate not exceeding 350^{0}F/Hour**
    - **Hold at 2040^{0}F ± 25^{0}F for 3 hours**
2. **Ramp furnace to 2130^{0}F**
    - **Hold at 2130^{0}F ± 10^{0}F for 3 hours**
3. **Ramp furnace to 2147^{0}F.**
    - **Hold at 2147^{0}F ± 10^{0}F for 3 hours**
4. **Ramp furnace to 2174°F**
    - **Hold at 2174^{0}F ± 10^{0}F for 8 hours**
5. **Ramp to 2205°F**
    - **Hold at 2205^{0}F ± 10^{0}F for 12 hours**
6. **Ramp to 2228°F**
    - **Hold at 2228^{0}F ± 10^{0}F for 24 hours**
7. **Ramp to 2237°F**
    - **Hold at 2237^{0}F ± 10^{0}F for 24 hours**

- **Forced Air Cool** to RT with fans, keeping contact thermocouples attached for measuring cooling rate

B. Double Age Heat Treatment Steps

1. **Ramp furnace to 1850°F at a rate not exceeding 350^{0}F/hour**
    - **Hold at 1850°F ± 10°F for 2 Hours**
2. **Forced air cool** with fans measuring cooling rate with contact thermocouples attached
3. **Ramp furnace to 1450°F**
    - **Hold at 1450°F ± 10°F for 8 Hours (plus add ½ hour for through heating)**

Still Air Cool to Room Temperature upon completion of the heat treatment measuring cooing rate with contact thermocouples attached

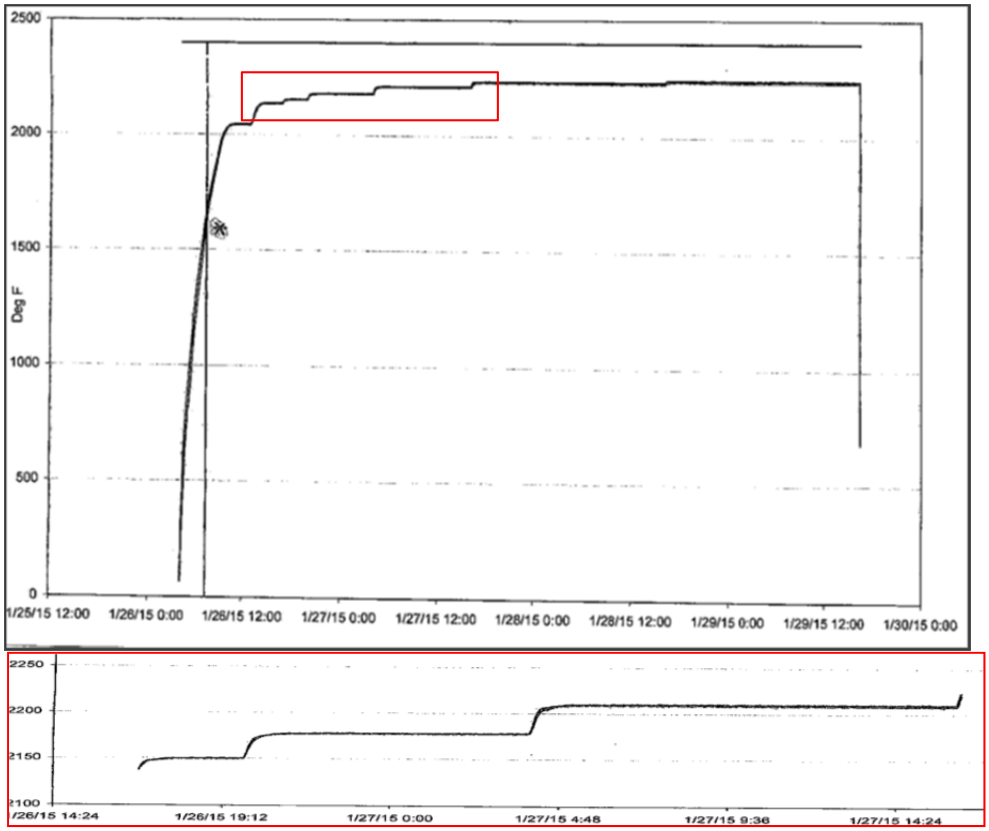

Figure 10: Homogenization HT cycle with insert HT step detailed view

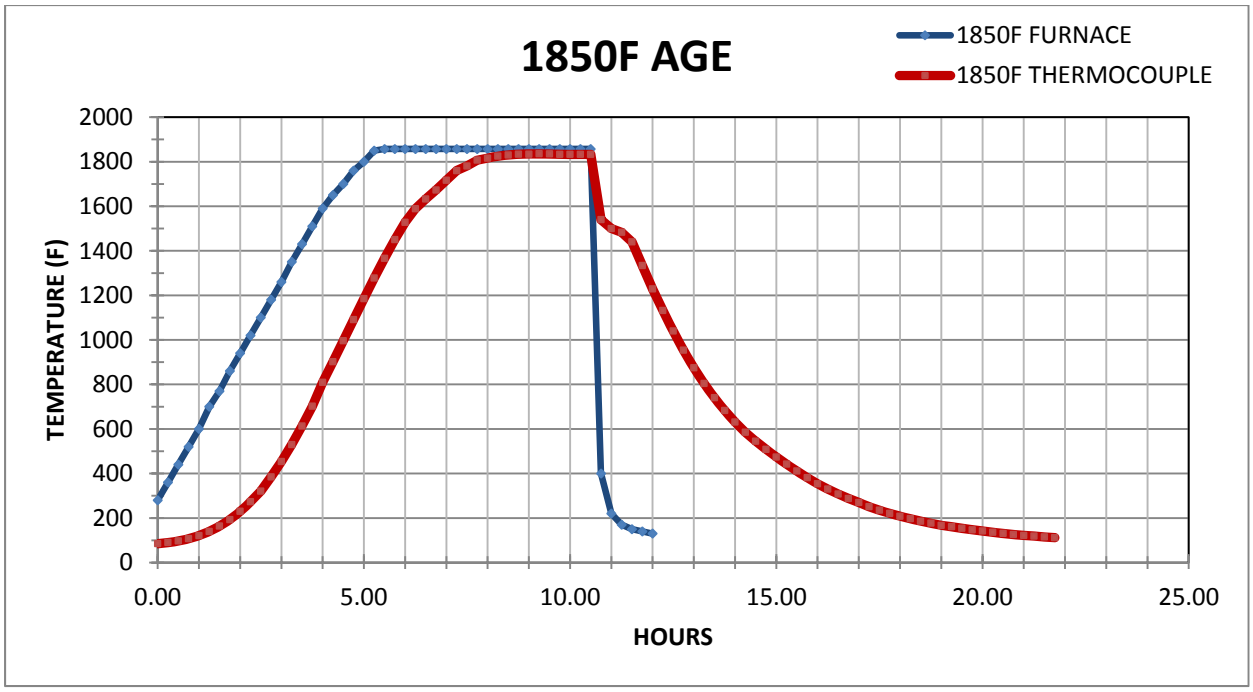

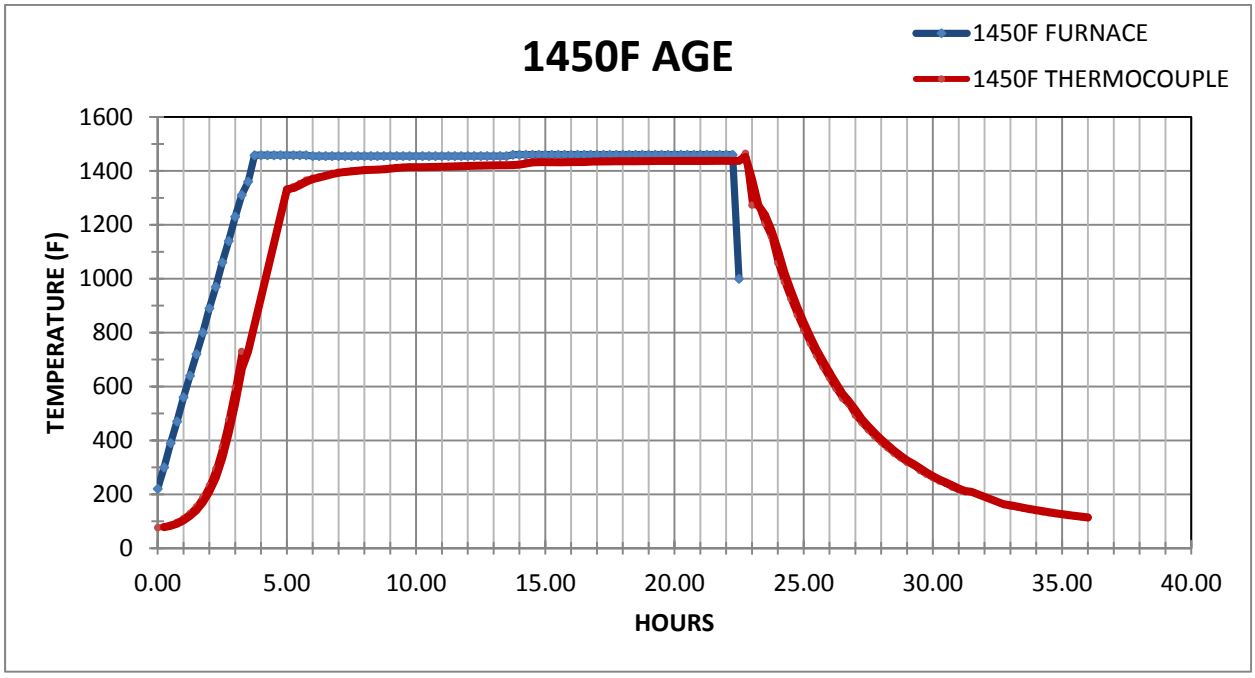

Figure 11: Two step Aging heat treat cycles thermocouple plot

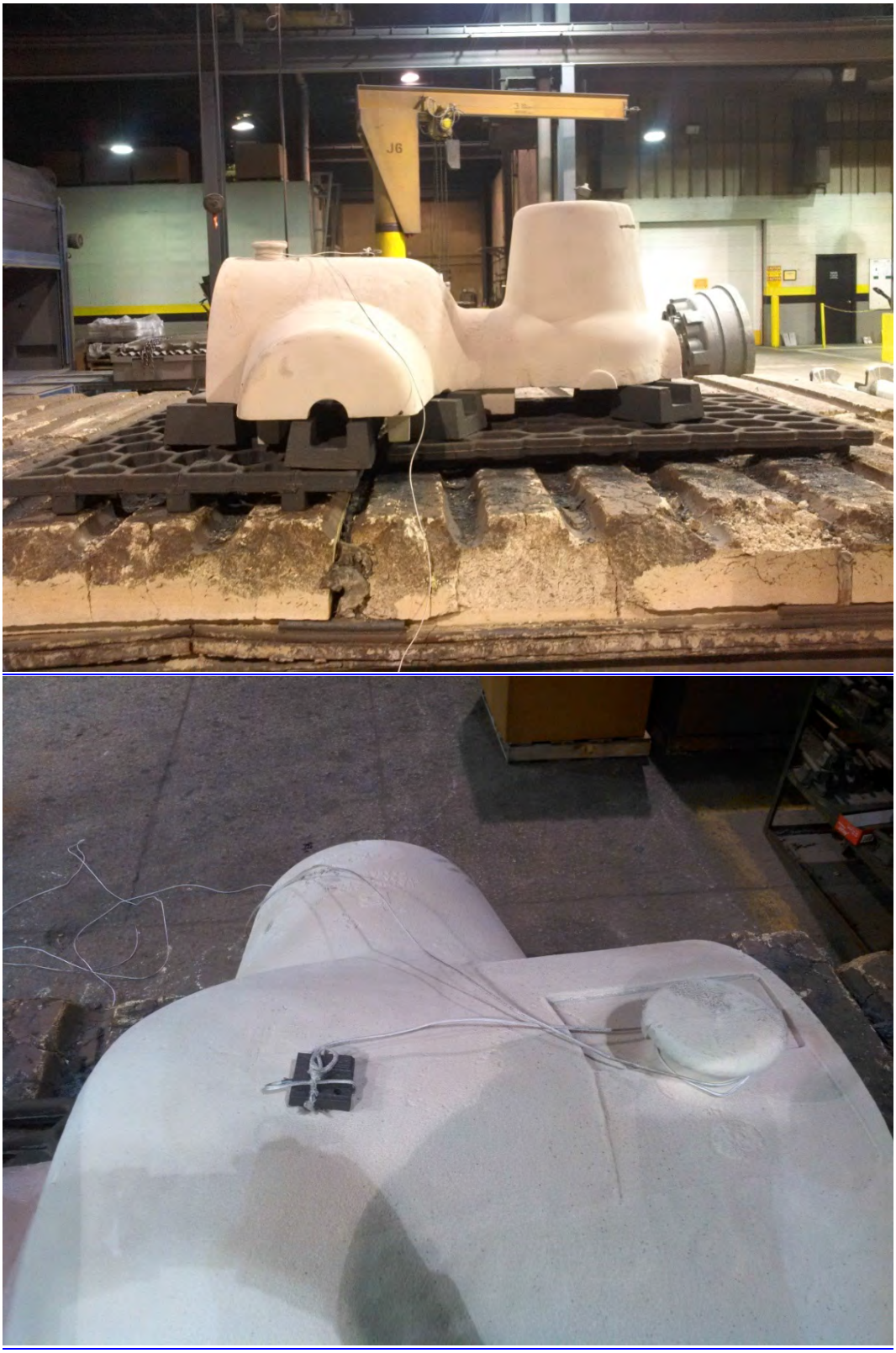

Figure 12: Thermocouples attached, coated for double Age heat treat cycle

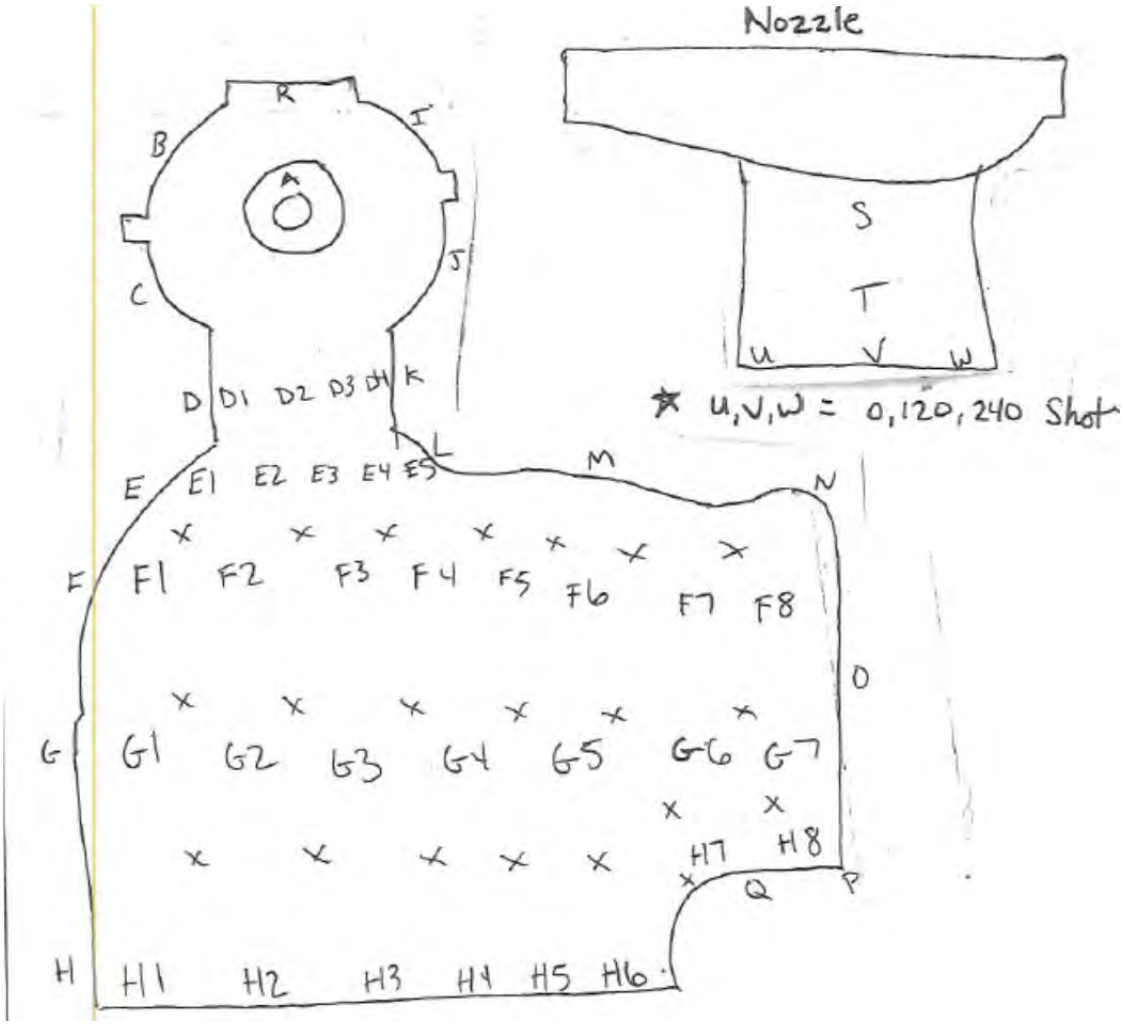

Figure 13: RT Scan sheet for the partial valve casing

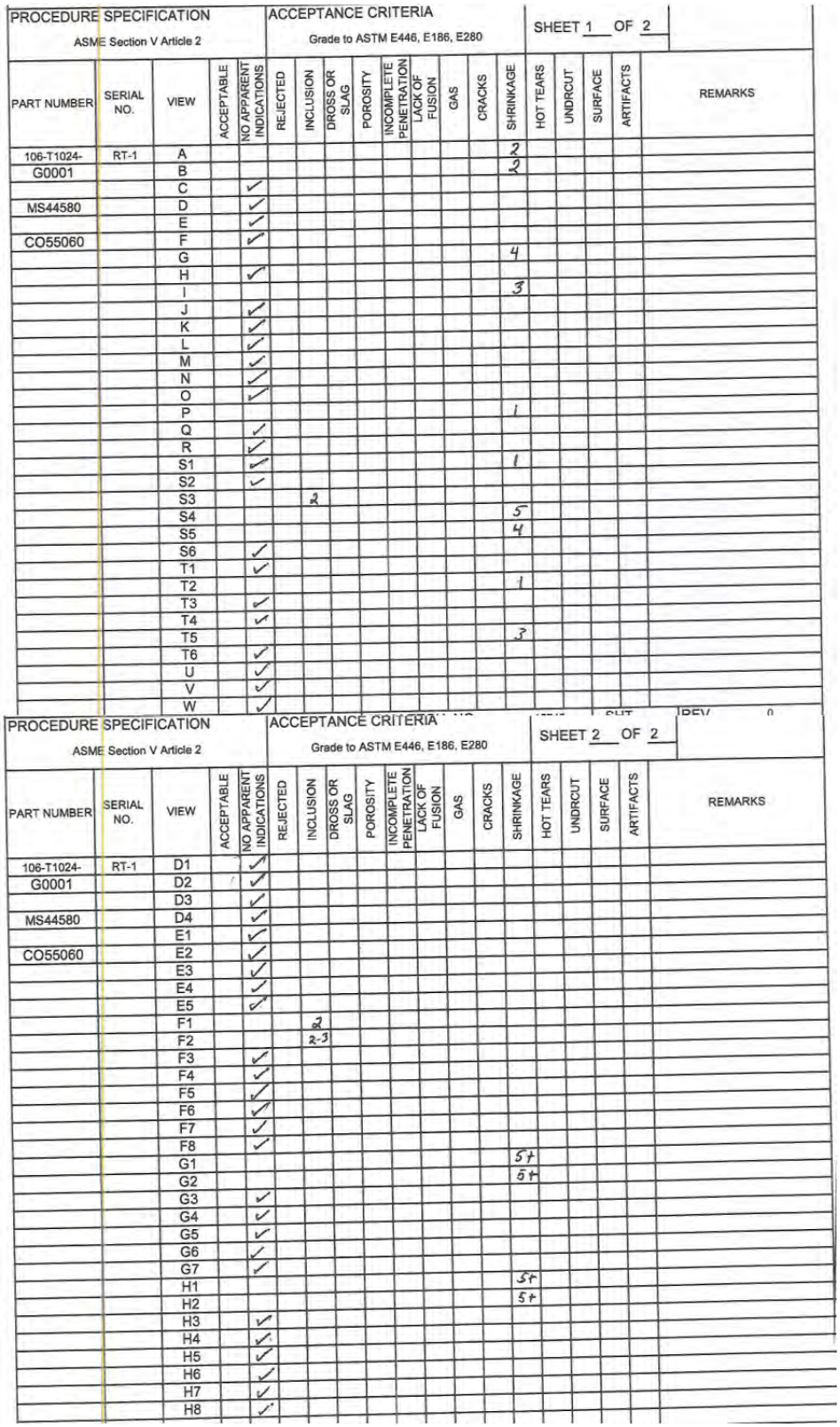

PROCEDURE SPECIFICATION
ASME Section V Article 2

ACCEPTANCE CRITERIA
Grade to ASTM E446, E186, E280

SHEET 1 OF 2

PART NUMBER	SERIAL NO.	VIEW	ACCEPTABLE	NO APPARENT INDICATIONS	REJECTED	INCLUSION	DROSS OR SLAG	POROSITY	INCOMPLETE PENETRATION	LACK OF FUSION	GAS	CRACKS	SHRINKAGE	HOT TEARS	UNDRCUT	SURFACE	ARTIFACTS	REMARKS
106-T1024-	RT-1	A											2					
G0001		B											2					
		C		✓														
MS44580		D		✓														
		E		✓														
CO55060		F		✓														
		G											4					
		H		✓														
		I											3					
		J		✓														
		K		✓														
		L		✓														
		M		✓														
		N		✓														
		O		✓														
		P											1					
		Q		✓														
		R		✓														
		S1		✓									1					
		S2		✓														
		S3				2												
		S4											5					
		S5											4					
		S6		✓														
		T1		✓														
		T2											1					
		T3		✓														
		T4		✓														
		T5											3					
		T6		✓														
		U		✓														
		V		✓														
		W		✓														

PROCEDURE SPECIFICATION
ASME Section V Article 2

ACCEPTANCE CRITERIA
Grade to ASTM E446, E186, E280

SHEET 2 OF 2

PART NUMBER	SERIAL NO.	VIEW	ACCEPTABLE	NO APPARENT INDICATIONS	REJECTED	INCLUSION	DROSS OR SLAG	POROSITY	INCOMPLETE PENETRATION	LACK OF FUSION	GAS	CRACKS	SHRINKAGE	HOT TEARS	UNDRCUT	SURFACE	ARTIFACTS	REMARKS
106-T1024-	RT-1	D1		✓														
G0001		D2		✓														
		D3		✓														
MS44580		D4		✓														
		E1		✓														
CO55060		E2		✓														
		E3		✓														
		E4		✓														
		E5		✓														
		F1				2												
		F2				2-3												
		F3		✓														
		F4		✓														
		F5		✓														
		F6		✓														
		F7		✓														
		F8		✓														
		G1											5+					
		G2											5+					
		G3		✓														
		G4		✓														
		G5		✓														
		G6		✓														
		G7		✓														
		H1											5+					
		H2											5+					
		H3		✓														
		H4		✓														
		H5		✓														
		H6		✓														
		H7		✓														
		H8		✓														

Figure 14: RT Inspection report for the H282 valve casing

Figure 15: Haynes 282 Valve casing Liquid penetrant testing 100% surface area

Figure 16: LPT inspection pictures on 100 % Cast surface areas

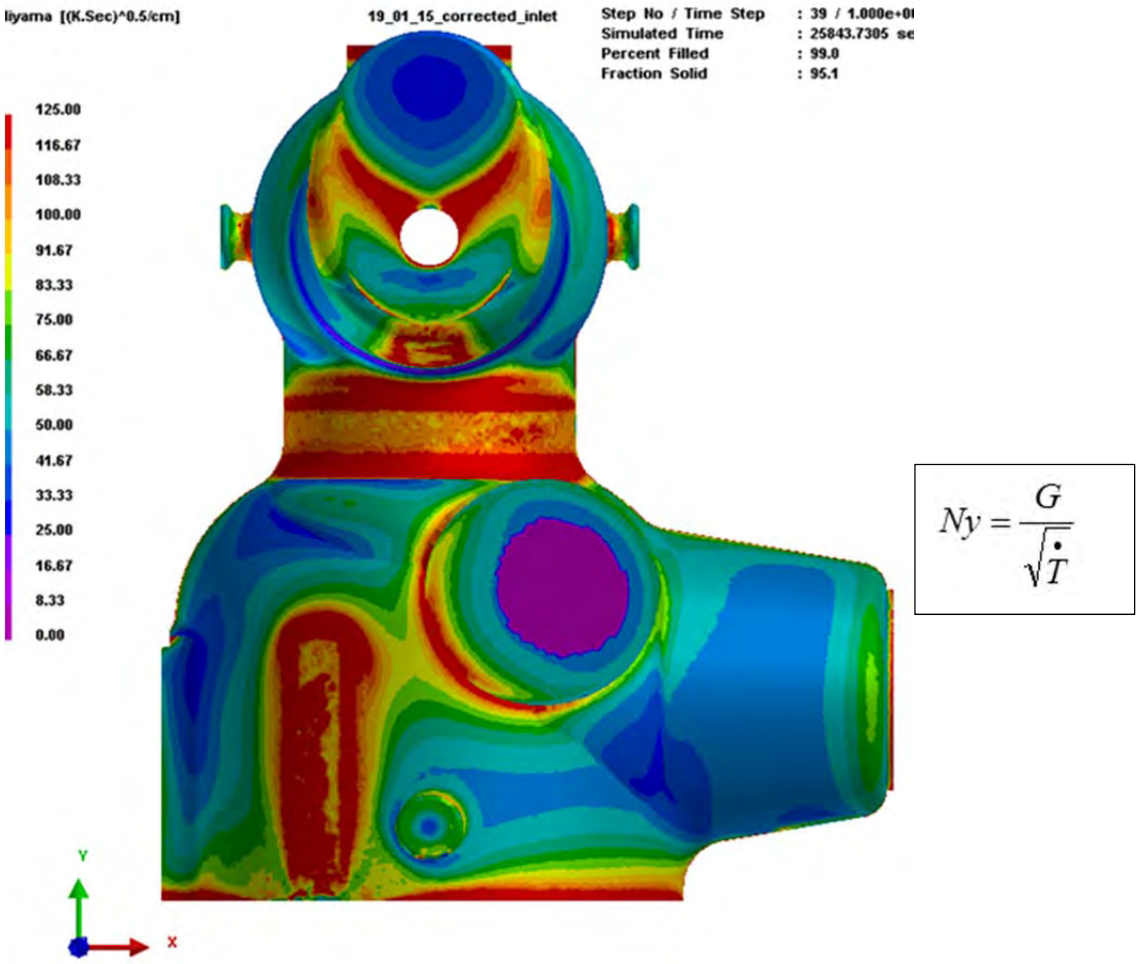

Figure 17: Niyama criteria per solidification simulation analysis. Niyama indicates potential feeding difficulty zones in the casting with lower (Nẏ) values. This plot is primarily used to avoid sectioning through potential zones for micro shrinkage

Table 1: H282 casting sections and cast on coupons test matrix and specimens identification

Haynes 282 casting test matrix:					Specimens Identification (ID)							
Test #	Test Type	Test condition	Step sections	Total Tests	Cast-on coupon ID (*1)		Cast Sections ID (*2)					
		Temperature deg.F			CA	CC	H	D	B	C	E	K
1	Tensile Test (UTS, 0.2% & 0.02% YS, % EL, %RA) Tensile Specimen: MPE-TNSL-001 P4 36 specimens	RT/ 75 deg. F	1 Test/section in CL plane	6	CA-T-75	CC-T-75	HT-75	DT-75	BT-75	CT-75		
		500 deg. F		6	CA-T-500	CC-T-500	HT-500	DT-500	BT-500	CT-500		
		1000 deg.F		6	CA-T-1000	CC-T-1000	HT-1000	DT-1000	BT-1000	CT-1000		
		1250 deg.F		6	CA-T-1250	CC-T-1250	HT-1250	DT-1250	BT-1250	CT-1250		
		1400 deg.F		6	CA-T-1400	CC-T-1400	HT-1400	DT-1400	BT-1400	CT-1400		
		1500 deg F		6	CA-T-1500	CC-T-1500	HT-1500	DT-1500	BT-1500	CT-1500		
2	Charpy V Notch Impact Impact Energy (J); % Shear, Lateral Expansion 12 Specimens	RT/ 75 deg F	2 Tests per section	6	CB-CV-1	CD-CV-1	H-CV-01	D-CV-01	B-CV-01			K-CV-01
				6	CB-CV-2	CD-CV-2	H-CV-02	D-CV-02	B-CV-02			K-CV-02
3	LCF Data Frequency: 20 cpm Waveform: Triangular A Strain 1, TSR% (1.0; 0.90; 0.80; 0.70; 0.60; 0.50) 2 temperatures: RT & 1400 deg. F. Specimen Drg. # 4013195-741 48 specimens		A strain / TSR (%)		CB	CD	H	D	B	C	E	J
		RT/ 75 deg F	1 / 1.00	4	CB-LCF-01	CD-LCF-01		D-LCF-01			E-LCF-01	
			1 / 0.90	4	CB-LCF-02	CD-LCF-02		D-LCF-02			E-LCF-02	
			1 / 0.80	4	CB-LCF-03	CD-LCF-03		D-LCF-03			E-LCF-03	
			1 / 0.70	4	CB-LCF-04	CD-LCF-04		D-LCF-04			E-LCF-04	
			1 / 0.60	4	CB-LCF-05	CD-LCF-05		D-LCF-05			E-LCF-05	
			1 / 0.50	4	CB-LCF-06	CD-LCF-06		D-LCF-06			E-LCF-06	
		1400 deg F	1 / 1.00	4		CD-LCF-07		D-LCF-07	B-LCF-07	C-LCF-07		
			1 / 0.90	4		CD-LCF-08		D-LCF-08	B-LCF-08	C-LCF-08		
			1 / 0.80	4		CD-LCF-09		D-LCF-09	B-LCF-09	C-LCF-09		
			1 / 0.70	4		CD-LCF-10		D-LCF-10	B-LCF-10	C-LCF-10		
			1 / 0.60	4		CD-LCF-11		D-LCF-11	B-LCF-11	C-LCF-11		
			1 / 0.50	4		CD-LCF-12		D-LCF-12	B-LCF-12	C-LCF-12		
4	Stress rupture Specimen per MPE-RUP 003-P3 12 specimens Creep data required	Temperature deg.F	Stress (ksi)			CC	H		B		E	
		1450	37.5	1			H-SR-01					
		1400	45.0	1			H-SR-02					
		1300	67.5	1			H-SR-03					
		1450	35.0	1					B-SR-01			
		1400	42.5	1					B-SR-02			
		1300	62.5	1					B-SR-03			
		1450	40.0	1		CC-SR-01						
		1400	47.5	1		CC-SR-02						
		1300	70.0	1		CC-SR-03						
		1450	33.5	1							E-SR-01	
		1400	40.0	1							E-SR-02	
		1300	58.0	1							E-SR-03	
5	Fracture Toughness Specimen per # 8024 ASTM E1820-11 Kq; J1C -16 specimens	RT/ 75 deg. F		4		CD-Kq-01		D-KQ-01	B-Kq-01			J-Kq-01
		1000 deg.F		4		CD-Kq-02		D-KQ-02	B-Kq-02			J-Kq-02
		1300 deg.F		4		CD-Kq-03		D-KQ-03	B-Kq-03			J-Kq-03
		1400 deg F		4		CD-Kq-04		D-KQ-04	B-Kq-04			J-Kq-04
6	Chemical Analysis 8 Specimens	Ni,Cr,Co,Mo,Ti,Al,Fe, Mn,Si,C,B,P,S, Cu, Co,Nb, W, Zr, N(ppm), O (ppm)	Thermal Center	1 test section	CA	CD	H	D	B			K

Table 2 : Valve casing cast on coupons and casting trepan sections chemical analysis tabulation

Valve Casing Casting-Trepan Sample Chemical Analysis							
By Weight [%]	Appended Cast on Coupons		Chilled Section	Cast Section Trepan Samples Chemical Analysis			
Element (%)	CA	CD	D	H	B	K	E
Carbon	0.08	0.09	0.07	0.06	0.06	0.12	0.06
Manganese	0.04	0.04	0.04	0.04	0.04	0.04	0.03
Iron	0.25	0.56	0.3	0.28	0.26	0.28	0.21
Sulfur	0.002	0.002	0.002	0.002	0.002	0.003	0.001
Silicon	0.25	0.19	0.25	0.25	0.25	0.27	0.32
Copper	0.01	0.01	0.01	0.01	0.01	0.01	0.01
Nickel	REM	REM	REM	REM	REM	REM	REM
Chromium	19.17	19.49	19.47	19.54	19.38	19.3	18.48
Aluminum	1.51	1.51	1.5	1.53	1.53	1.53	1.52
Titanium	2.39	2.36	2.49	2.38	2.41	2.43	2.33
Cobalt	10.02	10.08	9.92	10	9.91	9.94	10.03
Molybdenum	8.37	8.22	8.43	8.12	8.31	8.41	8.43
Niobium	0.05	0.06	0.05	0.05	0.05	0.05	0.05
Phosphorus	<0.01	<0.01	<0.01	<0.01	<0.01	<0.01	<0.01
Tungsten	<0.06	<0.06	<0.06	<0.06	<0.06	<0.06	<0.10
Zirconium	0.02	0.02	0.02	0.02	0.02	0.02	0.02
Boron	0.005	0.005	0.005	0.005	0.005	0.005	0.006
Nitrogen	87 ppm	116 ppm	127 ppm	53 ppm	116 ppm	75 ppm	118 ppm
Oxygen	21 ppm	19 ppm	22 ppm	18 ppm	24 ppm	24 ppm	30 ppm

Table 3 Tensile properties across cast section trepans within RT to 1500°F temperature range

UTS (ksi) vs. Temperature data

Temperature deg.F	CA [Cast on Coupon]	CC [Cast on Coupon]	H [Cast Section Trepan]	B [Cast Section Trepan]	C [Cast Section Trepan]	D [Chilled Cast Section Trepan]
75	109.1	115.3	92.5	103.7	92.3	82.4
500	109.2	121	86.5	98.2	81.9	77.1
1000	109.7	104.7	93.7	92.2	86	78
1250	112.1	114.1	82.4	86.4	92.3	76.7
1400	113.1	111.9	76.4	111.6	101.2	78.2
1500	91.5	94.3	90.6	91.1	91.4	72.9

0.2% Yield strength (ksi) vs. Temperature data

75°F	83.7	88.9	83.6	88.4	79	77.6
500°F	77.8	81.6	77.3	78.8	70.5	73.2
1000°F	76.1	73.2	75.6	74	72.8	70.6
1250°F	74.3	77.2	70.4	80.4	73.6	71.3
1400°F	77.6	73.1	NA	75.3	75.9	69.9
1500°F	74.9	72.2	72.8	75.2	74	64.1

0.02% Yield strength (ksi) vs. Temperature data

75°F	76.7	79.1	78	83.5	77.2	68.8
500°F	70.5	75.1	72.2	72.4	64.1	64.7
1000°F	68.8	67	66.1	65.5	68.7	65.8
1250°F	67.7	69	65.3	72.8	70.2	65.2
1400°F	70.4	65.9	NA	68.5	67.9	63.3
1500°F	65.7	64	64.5	69.4	62.6	56.3

Table 3: Tensile properties continued.

% Elongation (%) vs. Temperature data

Temperature deg.F	CA	CC	H	B	C	D
75°F	10	8	5	6	11	2
500°F	11	15	3.5	7.5	10	1.5
1000°F	16.5	17.5	10.5	9	12.5	6
1250°F	15.5	15	2.5	3	10	2.5
1400°F	14	17.5	2.5	9	7.5	3
1500°F	18	18.5	15	16.5	12.5	3

% RA (%) vs. Temperature data

75°F	11	7	6.5	11	9	1.8
500°F	17.5	16	12.5	14	12	1.5
1000°F	21.5	17.5	12	17.5	17	7.5
1250°F	20.5	18	14.5	8.5	13	2.5
1400°F	15.5	20	3	8.5	9.5	4.5
1500°F	26	29.5	33	36.5	22.5	4

Modulus [Msi]

75°F	25.4	25.6	29.7	28.1	29.4	25.1
500°F	23.2	29.1	27.6	33.1	29.8	25.4
1000°F	23.9	23.5	23.5	26.4	29.6	26.9
1250°F	21.5	21.6	25.9	21.8	26.1	19.7
1400°F	19.1	22.3	22.2	21.6	25.9	22.9
1500°F	18.5	20.1	20.3	22.6	24.1	19.1

Table 4: H282 Casting trepanned sections Stress rupture test data

Location	Sample ID	Status	Temp. °F	Stress ksi	Time hrs.	LMP [C=20]	% Elongation	% RA
CC Cast on Coupon	CC-SR-01	Stopped	1450	30	932.11	43.86		
	CC-SR-02	Stopped	1400	35	936.96	42.72		
	CC-SR-03	Stopped	1300	50	911.02	40.40		
H Cast section trepan	H-SR-01	Test Completed	1450	35	799.9	43.74	17.5	37.3
	H-SR-02	Test Completed	1400	42.5	469.63	42.16	22.7	24.1
	H-SR-03	Test Completed	1300	62.5	627.78	40.12	16.6	42.9
B Cast section trepan	B-SR-01	Stopped	1450	27.5	937.62	43.87		
	B-SR-02	Stopped	1400	40	936.08	42.72		
	B-SR-03	Test Completed	1300	57.5	344.4	39.66	7.8	6
E Cast section trepan	E-SR-01	Stopped	1450	32.5	938.28	43.87		
	E-SR-02	Stopped	1400	37.5	936.39	42.72		
	E-SR-03	Stopped	1300	55	910.91	40.40		

Table 5: Fracture toughness of Haynes 282 casting trepan sections at RT and 1400°F

Temperature deg.F	CD-Cast On Coupon		B-Trepan Cast section		J-Trepan Cast section		D- Chilled Cast Section	
	K jq (ksi√in)	CD-Kq (ksi√in)	K jq (ksi√in)	B-Kq (ksi√in)	K jq (ksi√in)	J-Kq (ksi√in)	K jq (ksi√in)	D-Kq (ksi√in)
75	111.25	67.8	111.13	64.2	95.69	63.2	89.66	58
1300	120.45	76.7						
1400	93.61	66.7	47.88	46.7			142.56	62.9

Table 6: Low Cycle Fatigue data at RT from cast on coupons [CB, CD], Trepan sections [E, D].
All tests were performed at 20 cpm with a triangular wave form, A Strain 1

		E		Em						PLASTIC	PLASTIC		
		AT		AT	ALT.				ELASTIC	STRAIN	STRAIN		
SPECIMEN I.D.		R.T.		TEMP.	PSEUDO	MAX.	MIN.	STRAIN	STRAIN	RANGE	RANGE		
	TARGET STRAIN				STRESS	STRESS	STRESS	RANGE	RANGE	CALC.	MEAS.	Ni	Nf
TEST ID.	RANGE (%)	MSI	CYCLE	MSI	KSI	KSI	KSI	%	%	%	%	CYCLES	CYCLES
					#REF!								
CB-LCF-01	1.000	24.1	2,000	23.28	114.92	97.0	-92.7	0.990	0.833	0.175	0.157	3,837	5,826
CB-LCF-02	0.900	24.8	2,000	24.02	112.60	93.9	-89.6	0.897	0.767	0.133	0.130	3,116	4,228
CB-LCF-03	0.800	23.3	4,000	22.44	91.85	90.8	-83.9	0.799	0.773	0.020	0.026	7,007	8,938
CB-LCF-04	0.700	24.5	6,000	23.18	83.43	91.2	-66.9	0.701	0.683	0.019	0.018	11,208	12,405
CB-LCF-05	0.600	24.8	10,000	25.45	74.08	66.2	-80.6	0.595	0.593	0.018	0.002	22,711	26,262
CD-LCF-01	1.000	27.8	1,000	26.73	132.48	92.0	-90.8	0.985	0.692	0.301	0.293	2,070	2,488
CD-LCF-02	0.900	25.1	3,000	24.21	116.31	91.4	-91.0	0.895	0.753	0.141	0.142	3,636	6,516
CD-LCF-03	0.800	24.1	2,000	23.53	99.44	91.4	-86.0	0.796	0.747	0.042	0.049	4,309	5,349
CD-LCF-04	0.700	31.1	900	30.00	106.52	91.9	-89.7	0.696	0.612	0.091	0.084	1,652	1,960
CD-LCF-05	0.600	29.4	6,000	28.00	85.16	79.3	-81.4	0.596	0.591	0.022	0.005	12,390	13,568
CD-LCF-06	0.500	25.9	20,000	25.92	63.06	80.4	-47.7	0.498	0.498	0.004	0.000	38,692	42,500
E-LCF-01	1.000	28.2	600	27.20	139.76	84.8	-82.9	0.991	0.632	0.375	0.359	995	1,371
E-LCF-02	0.900	34.6	100	33.92	158.56	93.9	-97.5	0.893	0.595	0.329	0.298	293	303
E-LCF-03	0.800	30.5	1,000	28.30	119.21	87.7	-88.2	0.792	0.615	0.170	0.177	1,945	2,025
E-LCF-04	0.700	27.7	1,000	26.35	94.28	90.0	-79.3	0.696	0.642	0.053	0.054	2,760	3,517

Table 6 LCF Data continued

E-LCF-05	0.600	31.0	3,000	30.50	91.50	88.5	-79.9	0.596	0.555	0.044	0.041	3,300	6,908
E-LCF-06	0.500	34.0	3,000	33.27	81.79	92.1	-71.2	0.496	0.490	0.005	0.006	6,076	6,222
D-LCF-01	1.000	37.1	20	33.45	170.86	90.1	-90.0	0.991	0.532	0.452	0.459	43	46
D-LCF-02	0.900	29.1	400	27.60	125.51	87.4	-86.3	0.878	0.665	0.248	0.213	591	883
D-LCF-03	0.800	34.1	1,000	32.72	132.47	87.8	-91.2	0.789	0.589	0.242	0.200	1,318	2,514
D-LCF-04	0.700	27.7	200	25.93	89.56	81.6	-76.4	0.681	0.623	0.072	0.058	399	494
D-LCF-05	0.600	23.7	2,000	22.88	70.99	74.5	-60.3	0.592	0.585	0.002	0.007	4,511	5,274
D-LCF-06	0.500	28.6	8,000	28.21	69.28	81.0	-55.2	0.493	0.493	0.010	0.000	13,847	17,244

Table 7: Low Cycle Fatigue Data at 1400°F for Cast on coupon [CD], trepan cast sections [B, C, D].
All tests were performed at 20 cpm with a triangular wave form, A Strain 1

SPECIMEN I.D.		E AT R.T.		Em AT TEMP.	ALT. PSEUDO	MAX.	MIN.	STRAIN	ELASTIC STRAIN	PLASTIC STRAIN RANGE	PLASTIC STRAIN RANGE		
	TARGET STRAIN				STRESS	STRESS	STRESS	RANGE	RANGE	CALC.	MEAS.	Ni	Nf
TEST ID.	RANGE (%)	MSI	CYCLE	MSI	KSI	KSI	KSI	%	%	%	%	CYCLES	CYCLES
#REF!													
CD-LCF-07	1.000	24.0	600	17.92	89.47	75.6	-74.7	1.000	0.850	0.161	0.150	1,171	1,260
CD-LCF-08	0.900	23.5	1,000	16.85	72.41	75.5	-65.6	0.889	0.830	0.052	0.059	2,189	2,380
CD-LCF-09	0.800	25.5	800	19.14	79.97	74.0	-73.5	0.797	0.765	0.027	0.032	1,292	1,683
CD-LCF-10	0.700	27.8	1,000	23.40	84.14	79.4	-72.3	0.693	0.643	0.044	0.050	1,858	2,477
CD-LCF-11	0.600	26.4	1,000	22.04	64.65	76.4	-53.9	0.590	0.585	0.000	0.005	2,639	2,874
CD-LCF-12	0.500	25.5	4,000	19.21	46.22	70.8	-22.1	0.489	0.485	0.006	0.004	6,152	8,045
C-LCF-08	0.900	33.8	90	26.00	109.09	86.2	-94.8	0.873	0.658	0.176	0.215	151	190
C-LCF-09	0.800	30.2	10	22.81	77.05	71.8	-71.3	0.676	0.638	0.048	0.038	25	31
C-LCF-10	0.700	30.7	700	21.72	82.43	74.7	-75.0	0.691	0.672	0.002	0.019	799	1,581
C-LCF-11	0.600	33.5	900	25.13	76.73	68.1	-77.7	0.600	0.578	0.020	0.022	811	1,857
C-LCF-12	0.500	32.8	2,000	24.02	60.20	63.0	-55.3	0.498	0.490	0.005	0.008	2,884	4,616
D-LCF-07	1.000	30.9	10	22.38	115.47	77.4	-78.2	1.004	0.697	0.309	0.307	19	22
D-LCF-08	0.900	27.7	100	20.18	92.36	70.1	-74.4	0.894	0.730	0.178	0.164	139	238
D-LCF-10	0.700	27.1	100	18.43	69.90	55.4	-62.5	0.699	0.647	0.059	0.052	314	320
D-LCF-11	0.600	29.9	800	21.50	71.16	43.8	-65.1	0.611	0.591	0.105	0.020	1,704	1,730
B-LCF-07	1.000	25.7	200	19.19	94.17	88.0	-82.8	0.946	0.881	0.056	0.065	382	509
B-LCF-08	0.900	28.3	500	20.41	93.62	82.2	-87.2	0.887	0.789	0.057	0.098	1,019	1,128
B-LCF-09	0.800	26.1	300	19.98	79.24	78.6	-74.9	0.792	0.763	0.024	0.029	568	754
B-LCF-10	0.700	32.0	500	24.23	82.78	76.7	-82.4	0.690	0.611	0.033	0.079	873	1,052
B-LCF-11	0.600	27.8	2,000	20.02	62.90	63.5	-53.7	0.593	0.577	0.008	0.016	4,615	4,899
B-LCF-12	0.500	30.0	900	22.50	58.93	81.7	-29.2	0.495	0.476	0.002	0.019	1,878	1,939

Table 8: Charpy V-Notch Impact Energies for various cast sections

Charpy V-notch impact energy (ft.lbs)						
	Cast on Coupons		Chilled Section	Cast Trepans		
Specimen	CB	CD	D	H	B	K
1	35	35	4	17	17	18
2	16	43	12	24	22	16
% Shear Fracture						
	Cast on Coupons		Chilled Section	Cast Trepans		
Specimen	CB	CD	D	H	B	K
1	5	10	5	5	5	5
2	5	5	5	5	10	5
Mils. Lateral expansion						
	Cast on Coupons		Chilled Section	Cast Trepans		
Specimen	CB	CD	D	H	B	K
1	29	28	0	11	3	11
2	10	20	7	12	13	3

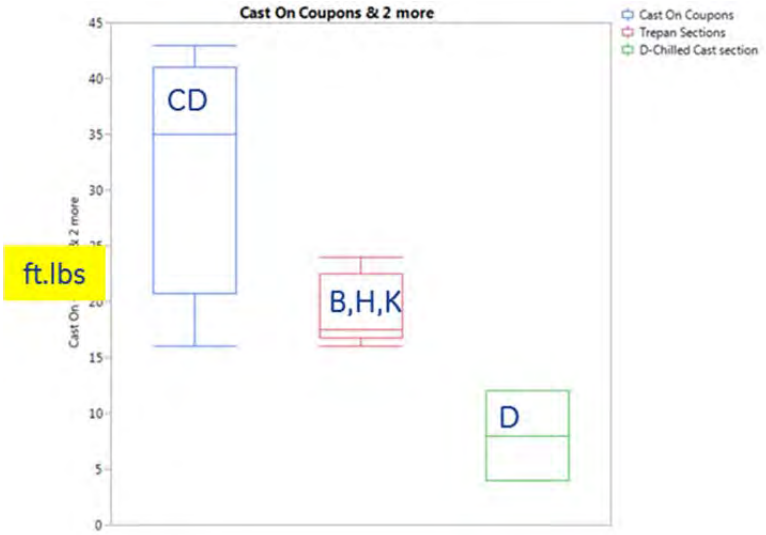

Figure 18: Box plot showing Charpy V-Notch Impact energy for cast section trepans

Typical Haynes 282 large size steam turbine Casting Order to Delivery Activity Schedule

#	Description	# Weeks	1	2	3	4	5	6	7	8	9	10	12	13	14	15	16	17	18	19	20	21	22	23	24	25	26
1	Sales and commercial review	3	X	X	X																						
2	Engineering Drawings_models review	4			X	X	X	X																			
3	Pattern and core box manufacturing	6							X	X	X	X	X	X													
4	Casting process engineering review	4							X	X	X	X															
5	FEM and solidifcation simualtion analysis	4										X	X	X	X												
6	Gating & Feeder Attachments, Ceramic tiling	2													X	X											
7	Molding and coremaking production scheduling	6															X	X	X	X	X	X					
8	Melting planning and schedule	3																					X	X	X		
9	Pouring, cooling and shake out	2																								X	X

Figure 19: Schedule from Purchase Order Placement to Casting Pouring ~ 26 weeks

		Weeks	27	28	29	30	31	32	33	34	35	36	37	38	39	40	41	42	43	44	45	46	47	48	49	50	51	52	53	54	55
10	Shot blast and riser cutting, gates removal	3	X	X	X																										
11	Homogenizing , solutionizing HT furnace prep	4				X	X	X	X																						
12	Grinding, Fettling	2								X	X																				
13	Aging HT Cycle, cooling	2										X	X																		
14	VT and LPT NDT inspections	2												X	X																
15	Radiographic inspection	4														X	X	X	X												
16	Mechanical testing, Chemical anlysis test certs	4												X	X	X	X														
17	Casting weld repair upgrdaes and Aging PWHT	4																		X	X	X	X								
18	NDT after weld repairs and casting upgrades	3																						X	X	X					
19	Casting Final Inspection and testcerts	3																									X	X	X		
20	Package and delivery	2																												X	X
		#REF!																													
Total 55-56 Weeks lead time from Order to Delivery																															

Figure 20: Schedule from Pouring to Delivery 30 weeks~

5. Task 5 – Superalloy Weld Repair Technology Development

Note: this section contains its own numbering

5.0 Task 5 – Superalloy Weld Repair Technology Development

Objective

The objective of this task is to produce and characterize repair welds in a casting alloy suitable for the casing using a weld filler material similar to the casing alloy.

Initial development of casing repair weld procedures will be performed on small (~20-50 lb) castings of the casing alloy, which likely will be one of the nickel-base alloys 617, 625, 263, or 282. Casing weld repairs will be made using a filler metal similar to the casing alloy. If the casing alloy is precipitation-hardened, development tests will be performed to determine the maximum width and depth of defect that can be weld-repaired without cracking of the weld metal or in the HAZ.

After development of weld repair procedures, larger casing castings [From Task 4.0] will be made with simulated repair welds. The completed welds will be extensively characterized to develop materials property data needed for design. Testing will include non-destructive evaluation, metallography, and a variety of mechanical tests (tensile, creep-rupture, impact, and low-cycle fatigue). Sections of the completed welds will be subject to long-term isothermal aging at anticipated service temperatures. Additional characterization of the aged welds will be performed, particularly with respect to potential loss of ductility and toughness.

Material and Test Data

The six plates of H282 and five plates of H263 each approximately 2x4x5 inches poured by NETL-Albany. Figure 1 and Figure 2 show the radiograph images from the six plates. Some casting defects were identified and marked on the castings. The pieces were shipped to Arc Applications (York, PA) for machining and welding. The machining was performed to avoid the defect areas of the casting.

Arc Applications was selected because of their experience working with superalloys and explicit work with H282 via B&W as part of the A-USC Boiler materials project. The groove design, weld process and parameters are documented in Appendix 5.A.

Plates were sent to ORNL for detailed microstructural and long term creep testing of the specimens. Figure 5 to Figure 12 show the tensile, low cycle fatigue and short term rupture properties obtained from the plates tested at GE.

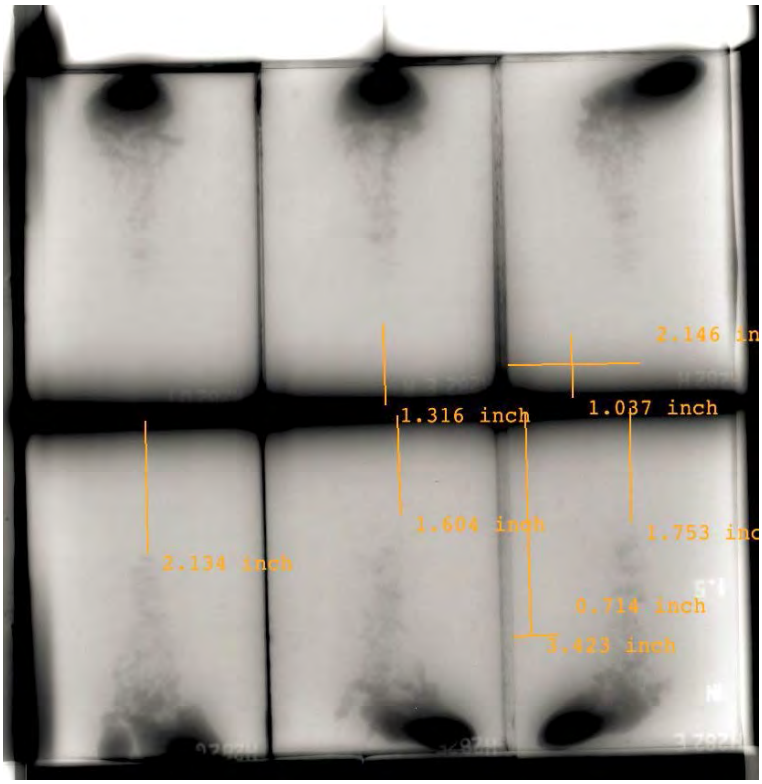

Figure 1: Radiographs from cast plates of H282

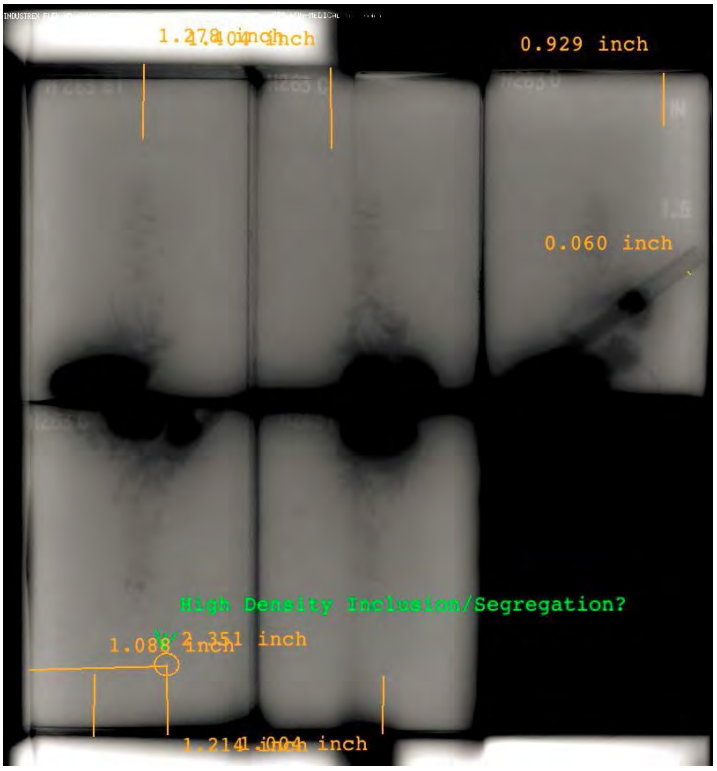

Figure 2: Radiographs from the cast plates of N263

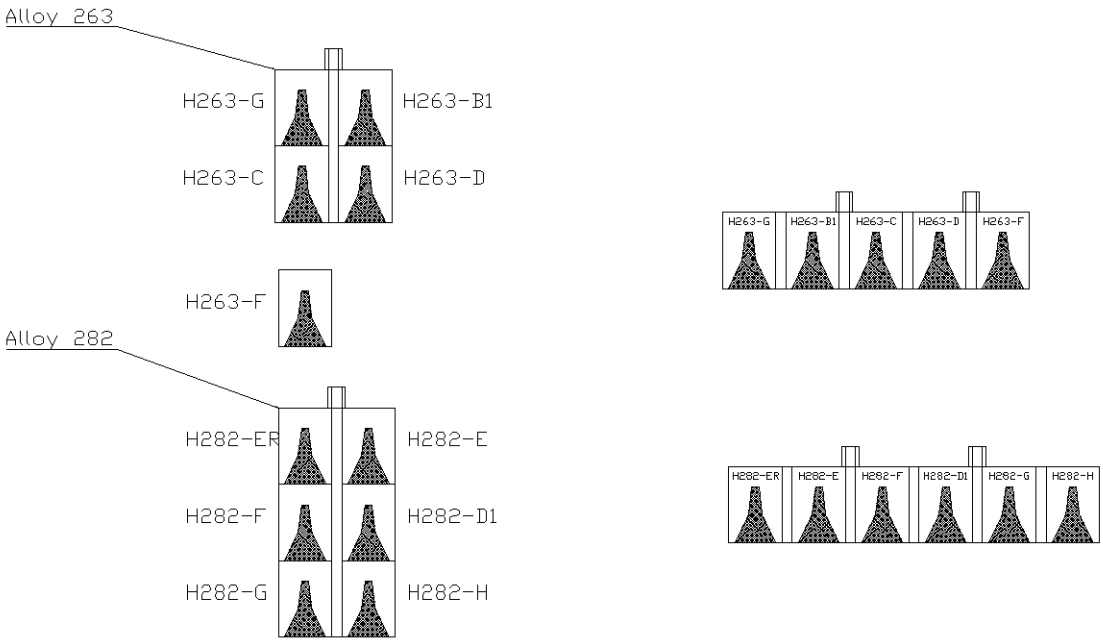

Figure 3: Weld layout of the various plates for welding

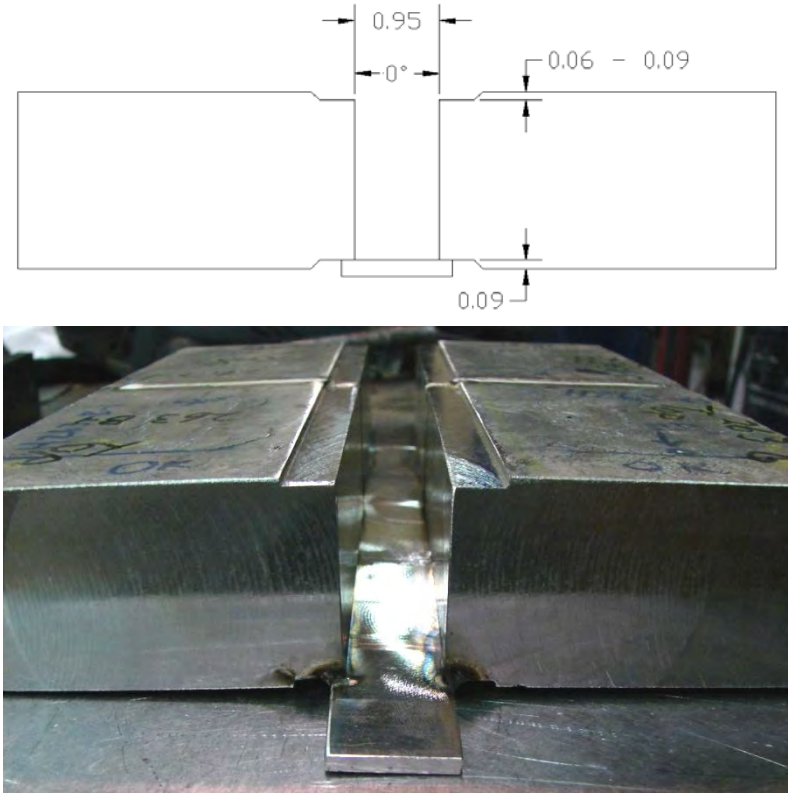

Figure 4: Weld layout dimensions and an example [263 plates]

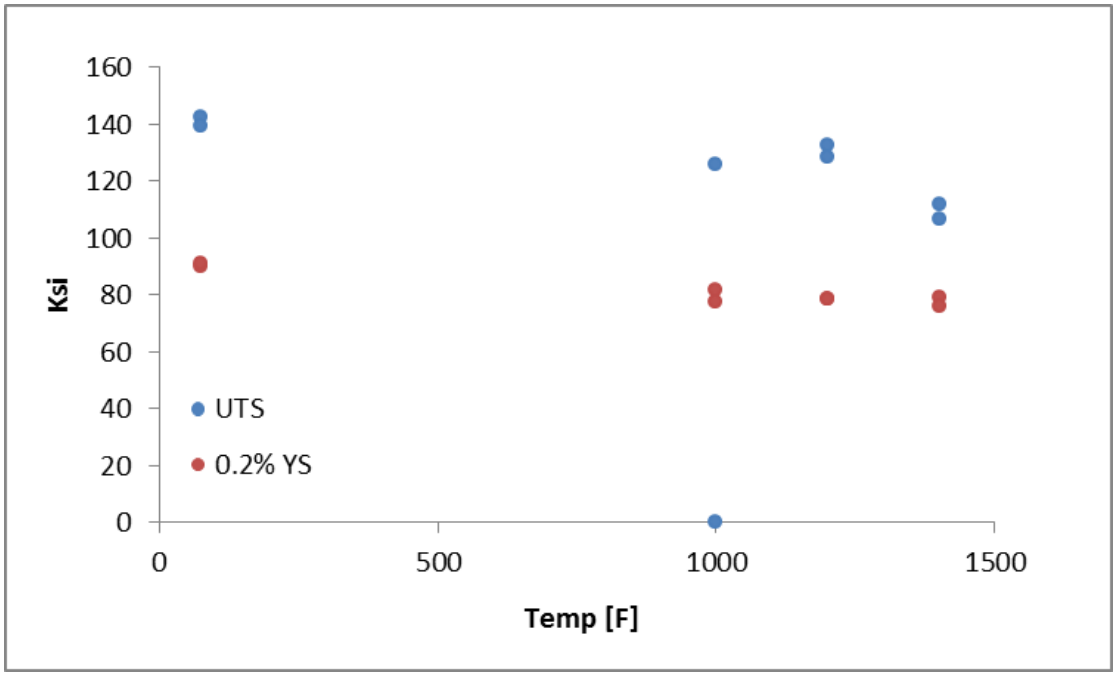

Figure 5: UTS and 0.2% YS obtained from H282 cross-weld

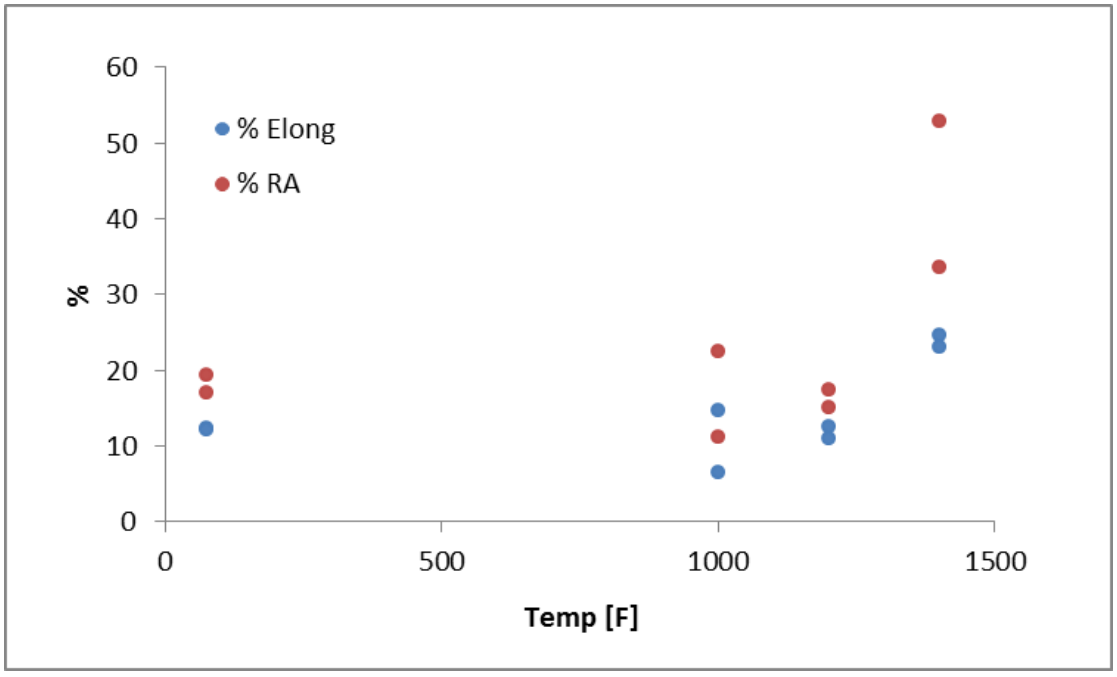

Figure 6: % Elongation and % RA obtained from H282 Cross-weld

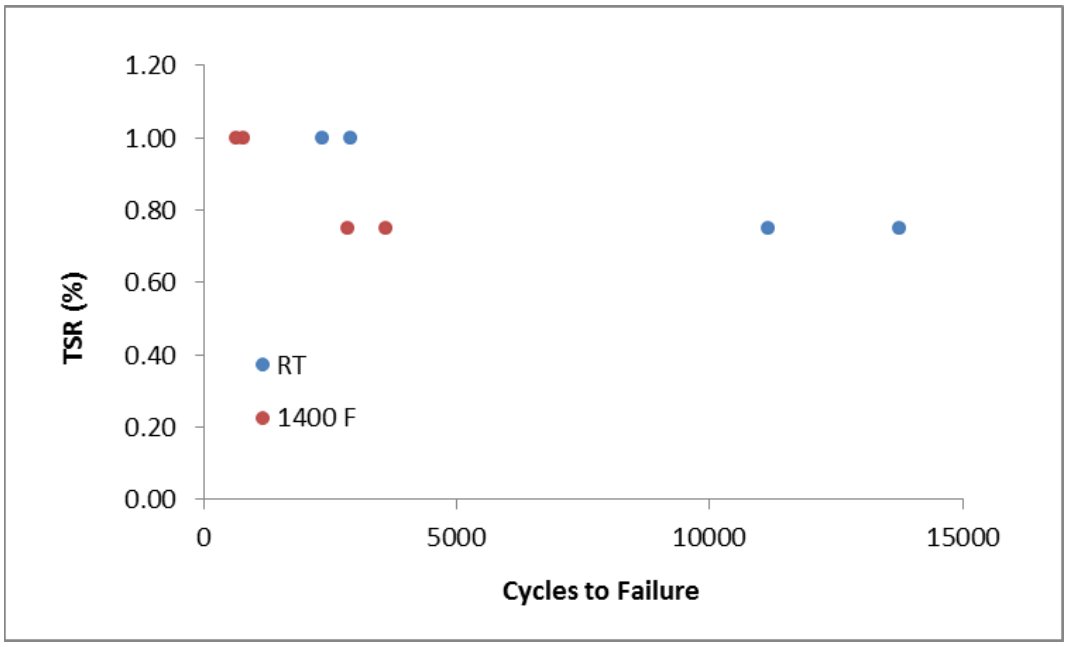

Figure 7: Low cycle fatigue data obtained from H282 cross weld data

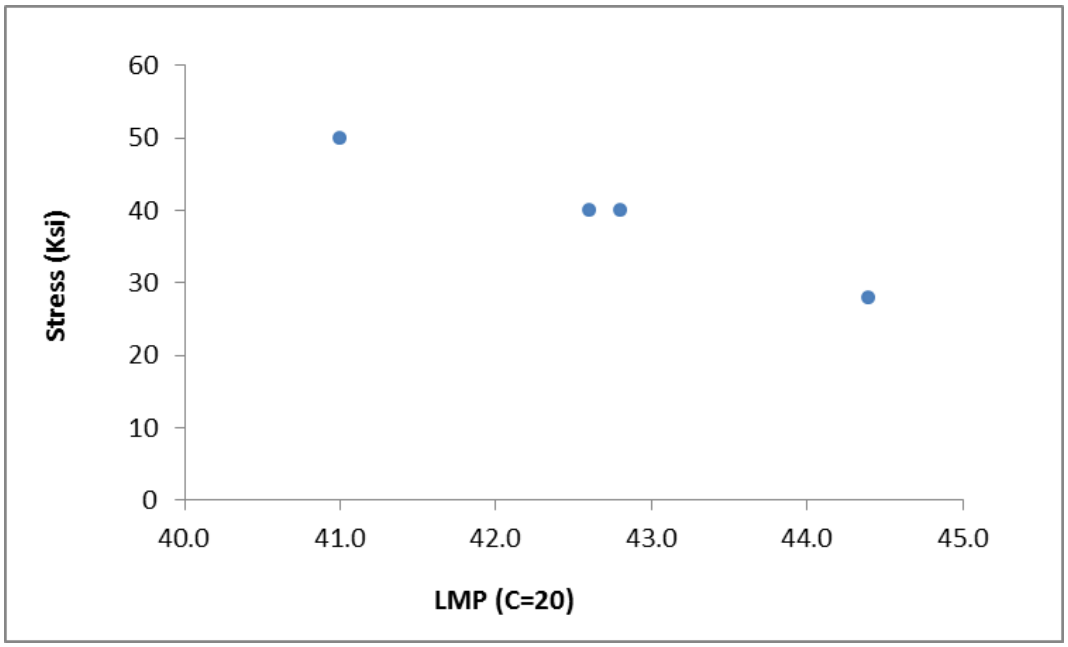

Figure 8: LMP-Stress plots obtained from H282 cross weld data

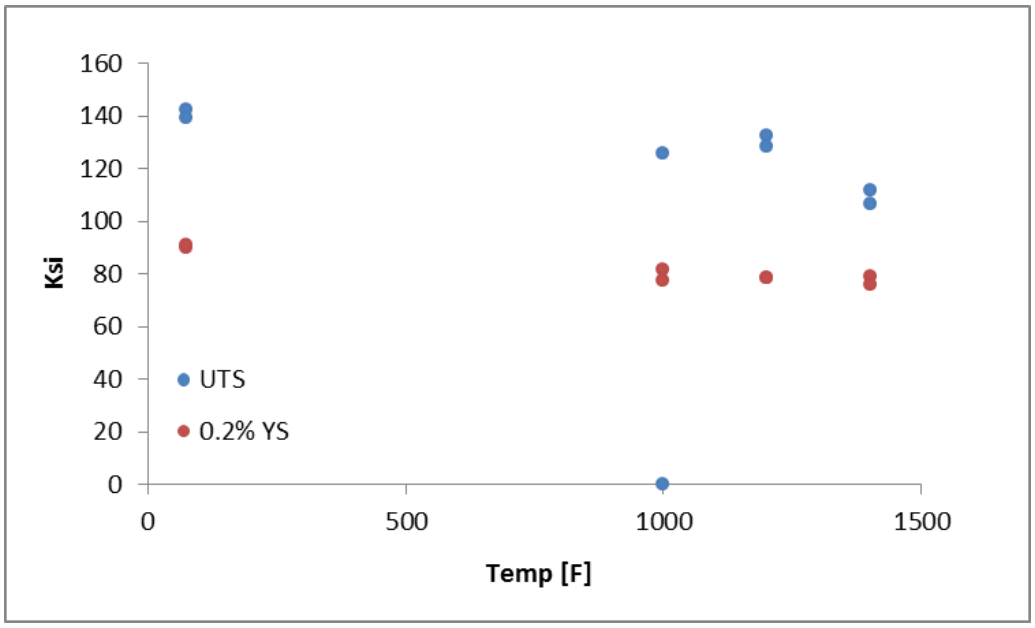

Figure 9: UTS and 0.2% YS obtained from N263 cross-weld

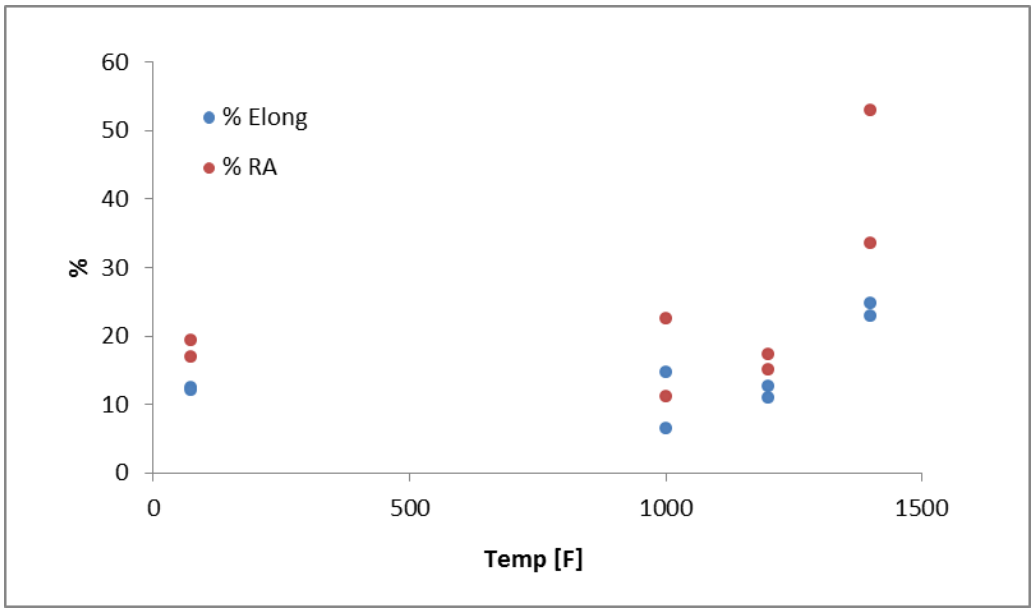

Figure 10: % Elongation and % RA obtained from N263 Cross-weld

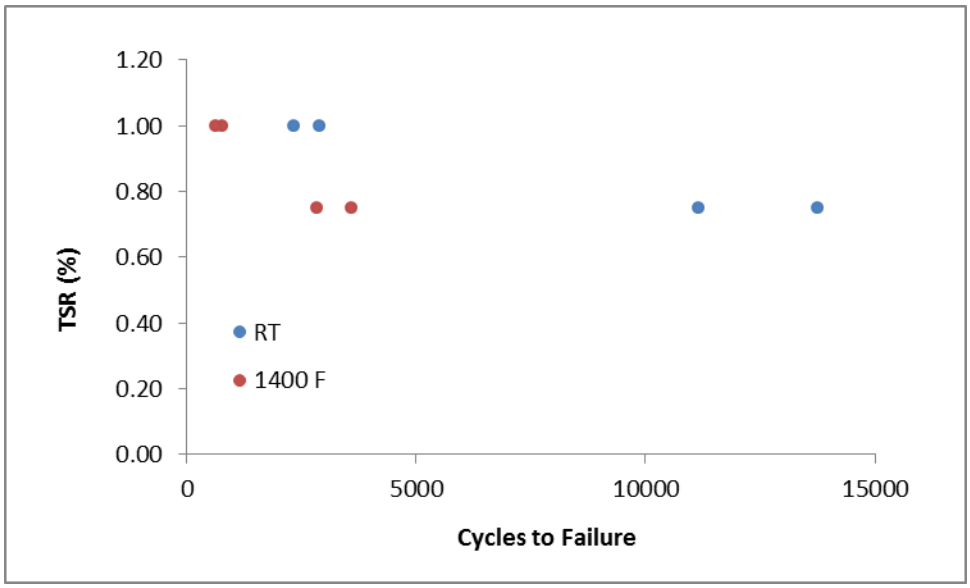

Figure 11: Low cycle fatigue data obtained from N263 cross weld data

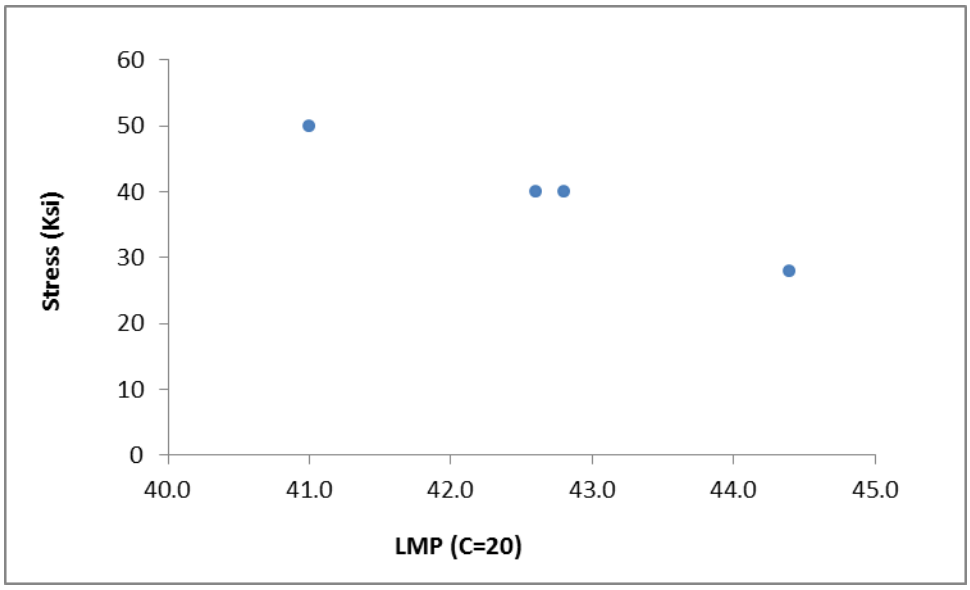

Figure 12: LMP-Stress plots obtained from H282 cross weld data

Conclusions

The welds tests at GE from small plates behaved as expected without any detrimental results. Figure 13 shows some areas along the fusion and line showing small cracks [100-300 micrometers]. The large casting [Task 4.0] was poured during CY Q4/2014, Inspected and Heat Treated in CY Q1/2015, machined in CY Q2/2015. The project ended on 9/30/2015 and no attempts were made to perform weld repair procedure on the larger casting. However, sufficient material exists to perform weld repair procedure in the future.

Figure 13: Example of cracks in welded H282 adjacent to the fusion line

Appendix 5.A: Arc Applications, Inc. Test Plate Welding of Cast Nickel Alloys 282 and 263

Machining and Setup

Customer provided cast Nickel Alloy 282 and 263 blocks were machined to produce the desired 0° included angle joint geometry, Figure 5A- 1 and Figure 5A- 2. The groove width was adjusted to the indicated 0.95” width to accommodate for stock removed from the as-cast surface during machining. The machined blocks were cleaned and assembled with the provided backing material to produce the first test assemblies, Figure 5A- 3 and Figure 5A- 4. As proposed, these longer test assemblies were used with the customer specified block matching scheme to simplify the welding efforts and minimize the number of setups (Setup 1). After welding, these longer test assemblies will be sectioned and re-machined to produce material for the final weld setup (Setup 2).

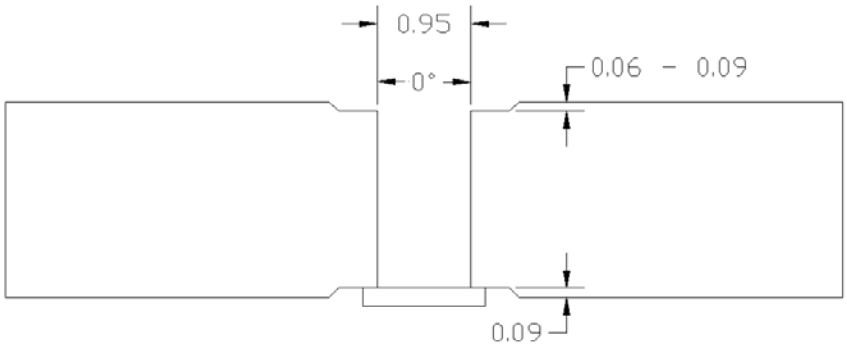

Figure 5A- 1

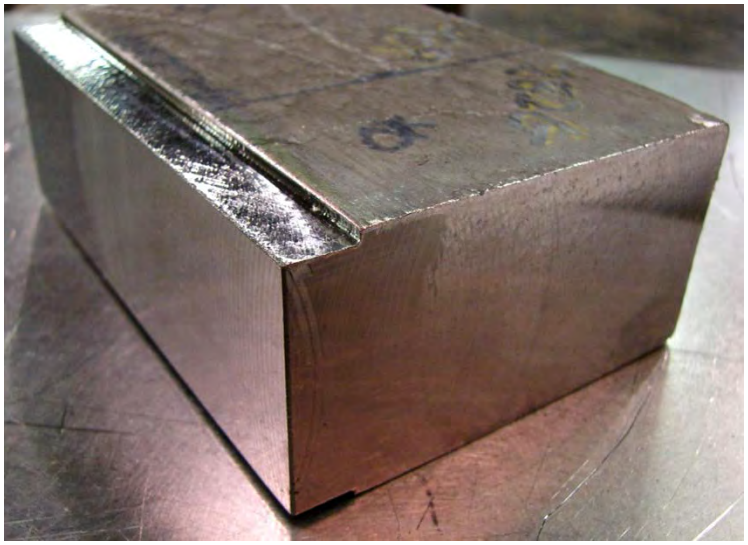

Figure 5A- 2

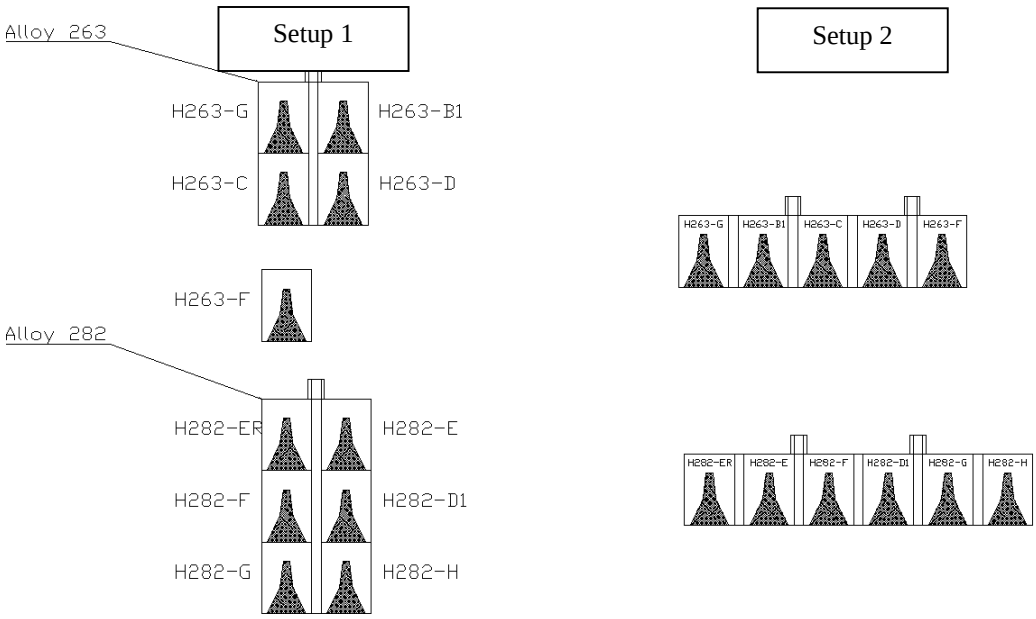

Figure 5A- 3

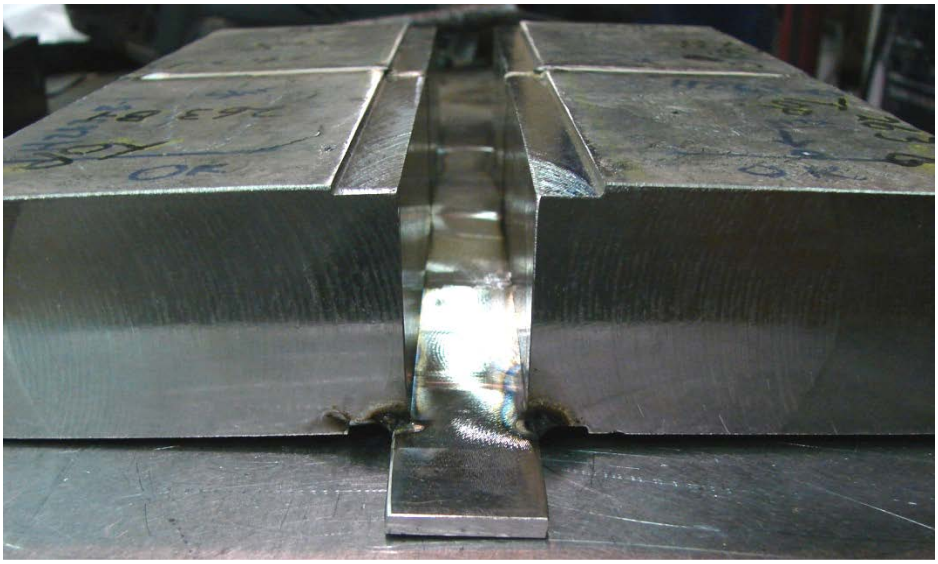

Figure 5A- 4

Station Setup and Starting Welding Parameters

A station was setup with the following automated GTA welding equipment to provide the required cold wire and hot wire Alloy 282 and 263 deposits. Electrode current and weld head control was provided by the Arc Machines, Inc. (AMI) M415 power supply. Linear and cross seam motion will be provided by the AMI M15 weld head. This weld head was equipped with an AMI NGT-B narrow gap rotating tungsten torch to provide synchronized movement of the rotating tungsten and wire positioning. A Linde VAC-250 hot wire power supply was used to provide current during hot wire welding.

Nominal starting parameters will establish the baseline welding parameters for the cold and hot wire deposits. The parameters were adjusted as needed based on the wetting and joint fill characteristics of the test deposit; updated parameters were provided to GE as required. The anticipated adjustment ranges are provided for informational purposes. The pre-heat and inter-pass temperature range will be 60°F to 250°F, respectively.

The cold wire deposit required four passes per layer and two layers to establish a favorable contour for the subsequent hot wire deposit. The hot wire deposit required three passes per layer. Parameters for the hot wire deposit were provided to GE as “sidewall” and “center” for clarity. Capping passes were run using hot wire welding. Typically capping passes use decreased current due to the lower amount of energy required to perform the welds.

Appendix 5.B: Cross-weld properties

Table 5B- 1: Alloy 282 Cross-weld Tensile Data

Specimen ID	Temp. (F)	UTS (ksi)	0.2% YS (ksi)	0.02% YS (ksi)	%EL	%RA
Cross Weld 1	75	142.4	90.2	82.1	12.4	19.3
Cross Weld 2	75	139.3	91.2	82.3	12.1	17
Cross Weld 3	1000	95.7*	77.8	65.9	6.5	11.1
Cross Weld 4	1000	126	81.8	66.2	14.7	22.5
Cross Weld 5	1200	132.9	78.6	66.4	12.6	15
Cross Weld 6	1200	128.7	78.6	67.8	10.9	17.4
Cross Weld 7	1400	111.9	79.4	65.1	23	33.6
Cross Weld 8	1400	106.6	75.8	63	24.7	52.9

Table 5B- 2: Alloy 282 Impact Properties at RT

Impact	ft-lbs	ave
Base Metal	14	13.75
	14	
	15	
	12	
Fusion Line	19	20.25
	21	
	23	
	18	
Weld Metal	17	18.5
	19	
	20	
	18	

Table 5B- 3: Cross-Weld Low-Cycle Fatigue Data for H282

ID	TEMP (F)	FREQUENCY		A-RATIO	RANGE	MAX	MIN	NFCYCLE
282-LCF-1	75	20	CPM	INF	1	0.5	-0.5	2902
282-LCF-2	75	20	CPM	INF	1	0.5	-0.5	2329
282-LCF-3	75	20	CPM	INF	0.75	0.375	-0.375	11147
282-LCF-4	75	20	CPM	INF	0.75	0.375	-0.375	13757
282-LCF-5	1400	20	CPM	INF	1	0.5	-0.5	764
282-LCF-6	1400	20	CPM	INF	1	0.5	-0.5	638
282-LCF-7	1400	20	CPM	INF	0.75	0.375	-0.375	3598
282-LCF-8	1400	20	CPM	INF	0.75	0.375	-0.375	2839

Table 5B- 4: Cross-Weld Rupture Data for H282

Specimen	Temp	Stress	Time	% Elong	%RA	LMP (C=20)
282W-1	1400	50	106	21.3	75.0	41.0
282W-2	1400	40	1036	19.9	54.9	42.8
282W-3	1472	40	106	23.8	76.2	42.6
282W-4	1472	28	1002	7.0	13.6	44.4

282W-4 failed in the weld; 282W-1 and 282W-3 failed in the base metal. None showed HAZ cracks like in the bulk cross section.

Table 5B- 5: Alloy 263 Cross-weld Tensile Data

Specimen ID	Temp. (F)	UTS (ksi)	0.2% YS (ksi)	0.02% YS (ksi)	%EL	%RA
Cross Weld 1	75	122.2	94	86.4	13.5	21.3
Cross Weld 2	75	128.1	87.2	82.4	25.1	37.5
Cross Weld 3	1000	97.4	74.8	62.9	21.4	46.9
Cross Weld 4	1000	99.8	71.8	51.1	19.7	36.1
Cross Weld 5	1200	102.4	73.7	56.3	20.2	35.1
Cross Weld 6	1200	93.9	71.8	65.4	21.8	42.7
Cross Weld 7	1400	88.6	71.1	59.2	16.5	30.8
Cross Weld 8	1400	91.1	68.2	55.2	22.5	38.4

Table 5B- 6: Cross-Weld Impact Data at RT

Impact	ft-lbs	ave
Base Metal	11	15
	14	
	23	
	12	
Fusion Line	28	29.5
	36	
	29	
	25	
Weld Metal	61	45.5
	39	
	39	
	43	

Table 5B- 7: Cross-Weld Low-Cycle Fatigue Data for N263

ID	TEMP (F)	FREQUENCY		A-RATIO	RANGE	MAX	MIN	NFCYCLE
263-LCF-1	75	3	CPM	INF	1	0.5	-0.5	2089
263-LCF-2	75	3	CPM	INF	1	0.5	-0.5	2834
263-LCF-3	75	10	CPM	INF	0.75	0.375	-0.375	8510
263-LCF-4	75	5	CPM	INF	0.75	0.375	-0.375	3115
263-LCF-5	1400	20	CPM	INF	1	0.5	-0.5	348
263-LCF-6	1400	20	CPM	INF	1	0.5	-0.5	511
263-LCF-7	1400	20	CPM	INF	0.75	0.375	-0.375	2589
263-LCF-8	1400	20	CPM	INF	0.75	0.375	-0.375	1216

Table 5B- 8: Cross-Weld Rupture Data for N263

Specimen	Temp	Stress	Time	% Elong	%RA	LMP (C=20)
263W-1	1400	40	76.2	3.20	4.80	40.7
263W-2	1400	25	1726.1	3.20	4.70	43.2
263W-3	1472	25	204.6	2.00	4.40	43.1
263W-4	1472	15	2550.5	4.50	4.00	45.2

263W-2, 263W-3, 263W-4 failed in the weld. None showed HAZ cracks like in the bulk cross section.

6. Task 6 – Process development and characterization of Casting-Pipe Welds

Note: this section contains its own numbering

Task 6 – Process development and characterization of Casting-Pipe Welds

Objective

Butt welds of prototypical main steam line pipe to cast casing alloy will be made. Short lengths of pipe, approximately 10-12 inches in diameter, with a wall thickness 2-3 inches, will be procured commercially. If necessary, round bar of appropriate diameter will be procured and machined to pipe dimensions. A cylindrical casting of the casing alloy will be produced with dimensions similar to the pipe, and the two will be joined using appropriate weld filler metal. The completed welds will be extensively characterized to develop materials property data needed for design. Testing will include non-destructive evaluation, metallography, and a variety of mechanical tests (tensile, creep-rupture, and impact). Sections of the completed welds will be subject to long-term isothermal aging at anticipated service temperatures. Additional characterization of the aged welds will be performed, particularly with respect to potential loss of ductility and toughness

Material

A successful valve body was cast in CY Q4/2014 and was subsequently homogenized and heat treated to full Haynes 282 properties in CY Q1/Q2 2015. A section of the pipe was cut from the main casting for a pipe-cast welding. Figure 6- 1shows the casting pipe extracted from the large casting for the cast – pipe weld trial. The pieces were sent to Arc Applications to machine and develop the welding process for the pipe-cast welding. Appendix 6A includes the report from Arc Application.

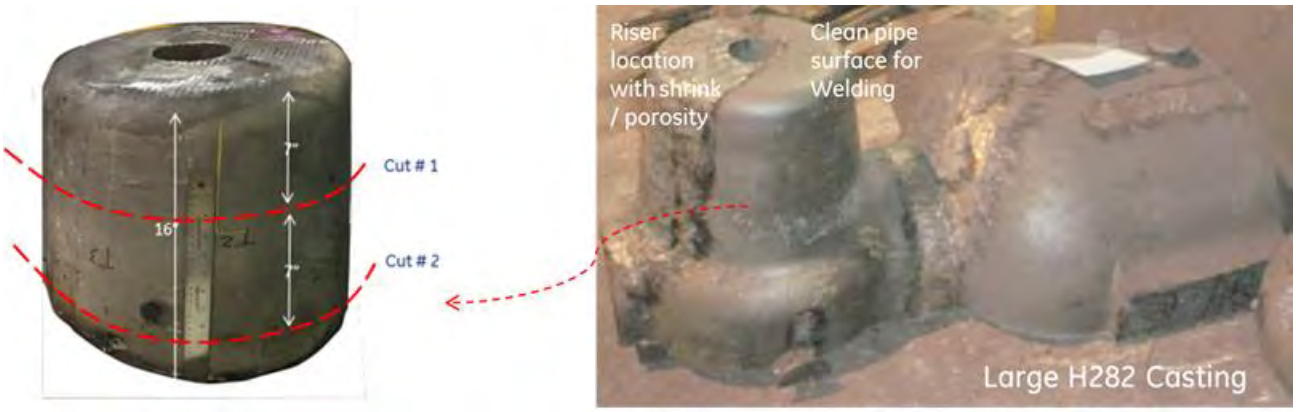

Figure 6- 1: Picture showing the extraction of the pipe from the large H282 casting.

The dimension of the Inconel 740H pipe and the Cast H282 pipe are show in Figure 6- 2. Figure 6- 3 shows the dimensions of the weld groove for the pipe-cast welding.

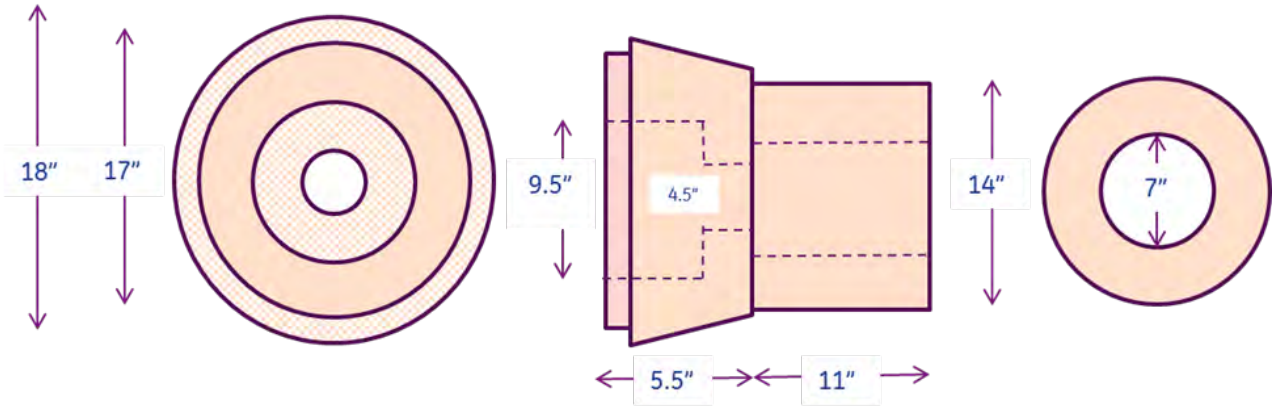

Figure 6- 2: Dimensions of the Inconel 740 Pipe [14" OD] to be welded to the cast H282 pipe

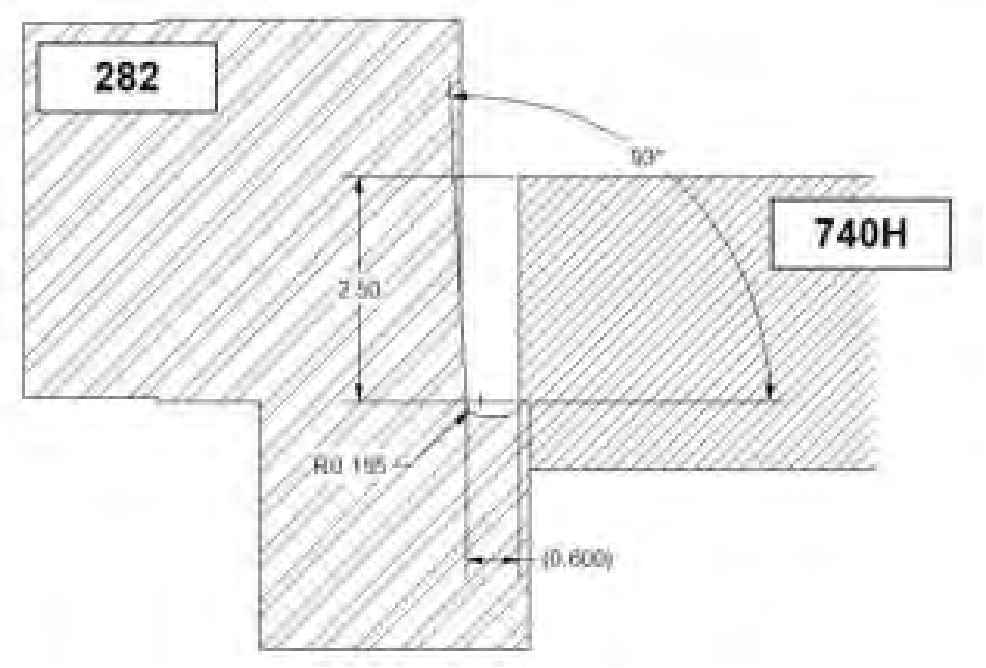

Figure 6- 3: Dimensions of the weld groove for the pipe-cast weld

During the machining of the casting it was discovered that the section of the pipe closest to the riser, exhibited large casting porosity [refer to Figure 6- 4]. The 0° axis was located in the center of the large voided area to concentrate any possible welding complications experienced during start up/shut down in this defective region. The as welded structures were cut into 4 pieces [cuts along the 0-180^0 and 90-270 ^{0} planes].

Figure 6- 5 is an example of a weld cross-section at a location that had no casting defects. The weld fusion lines were clean and exhibited no defects. Figure 6- 6 is a close image of the Figure 6-5.

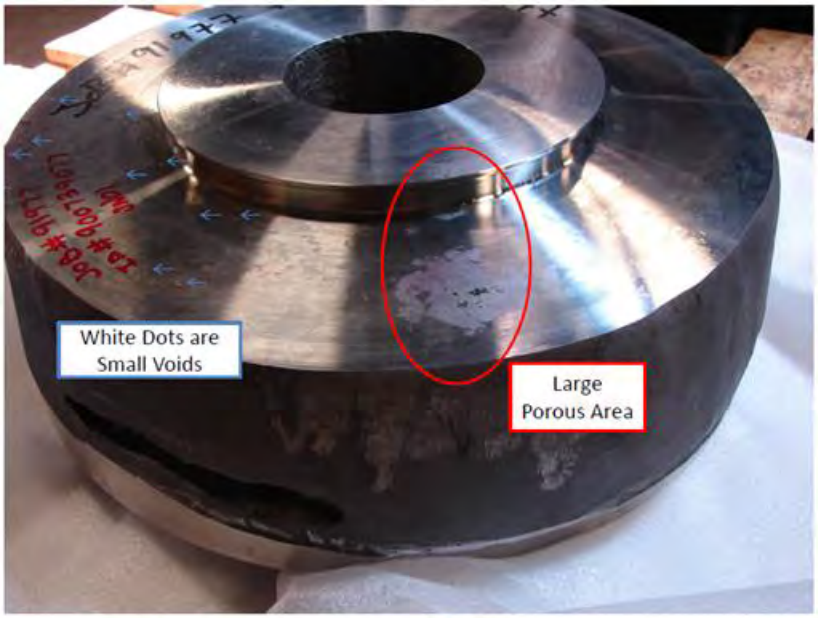

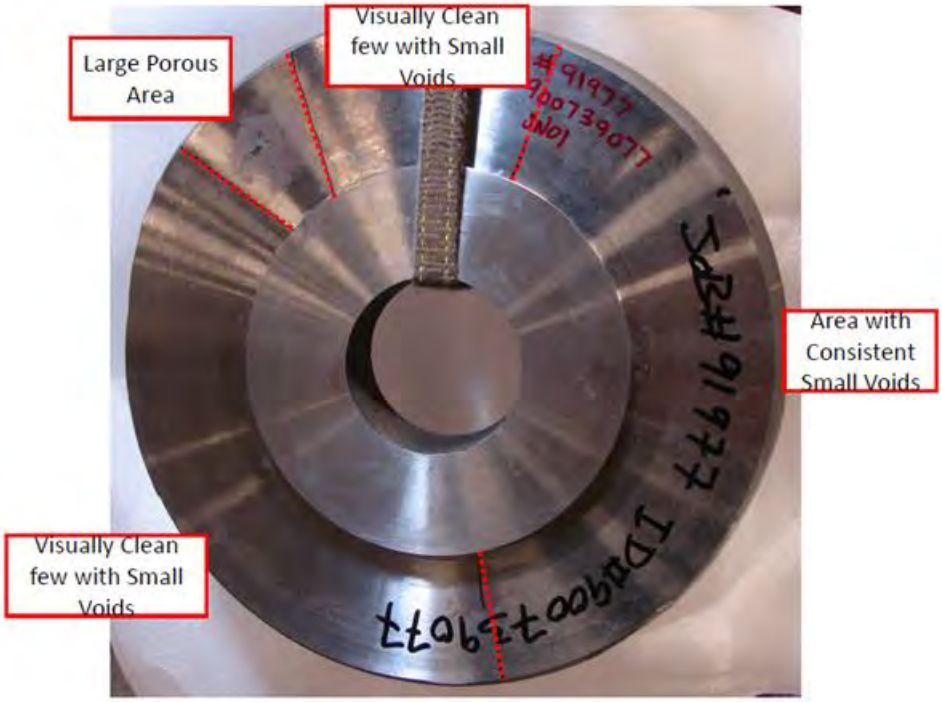

Figure 6- 4: Surface of the casting exhibited small casting pores with some areas exhibiting large casting porosity.

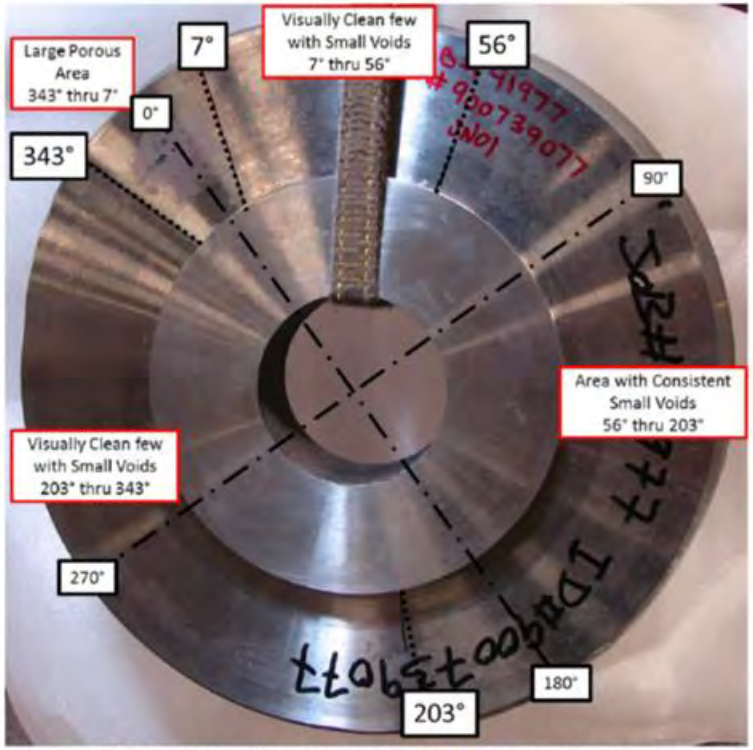

Casting Condition Layout of 282 Machined Surface

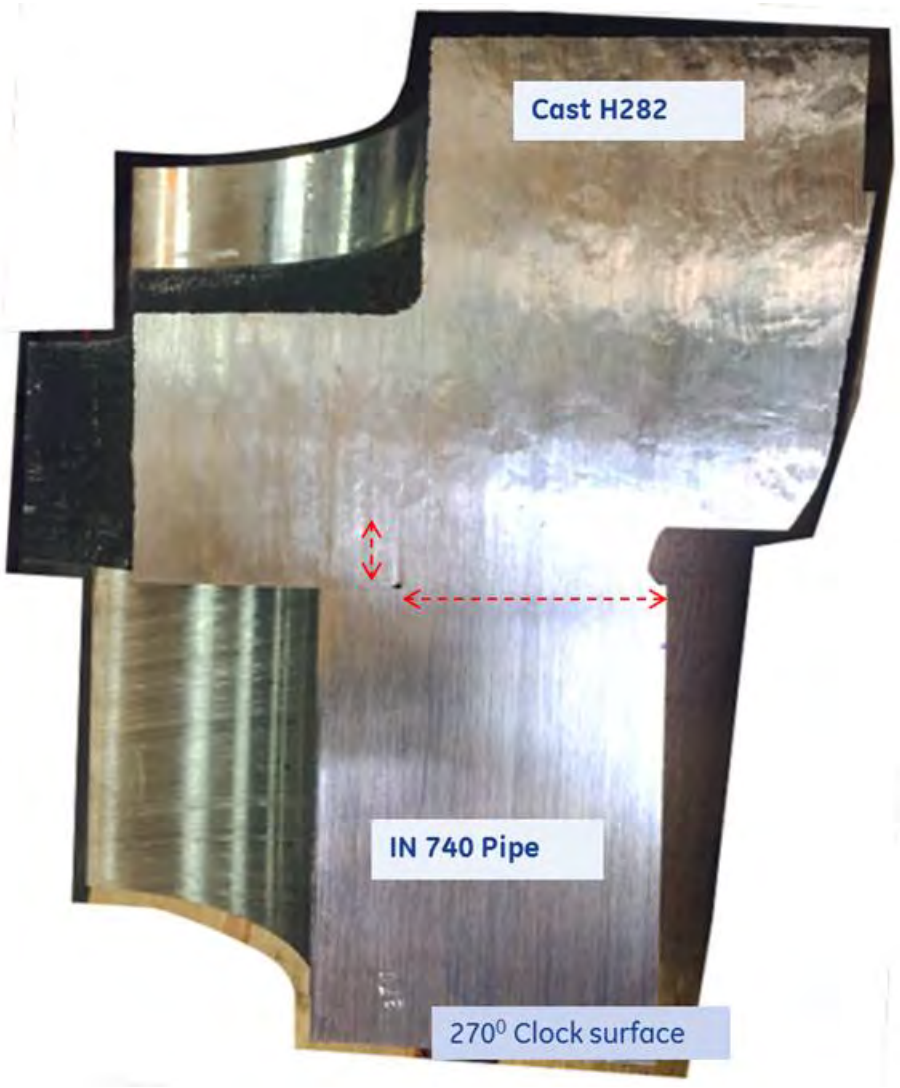

Figure 6- 5: Image showing the successful weld in areas without cast defects [Clock Position 270^0]

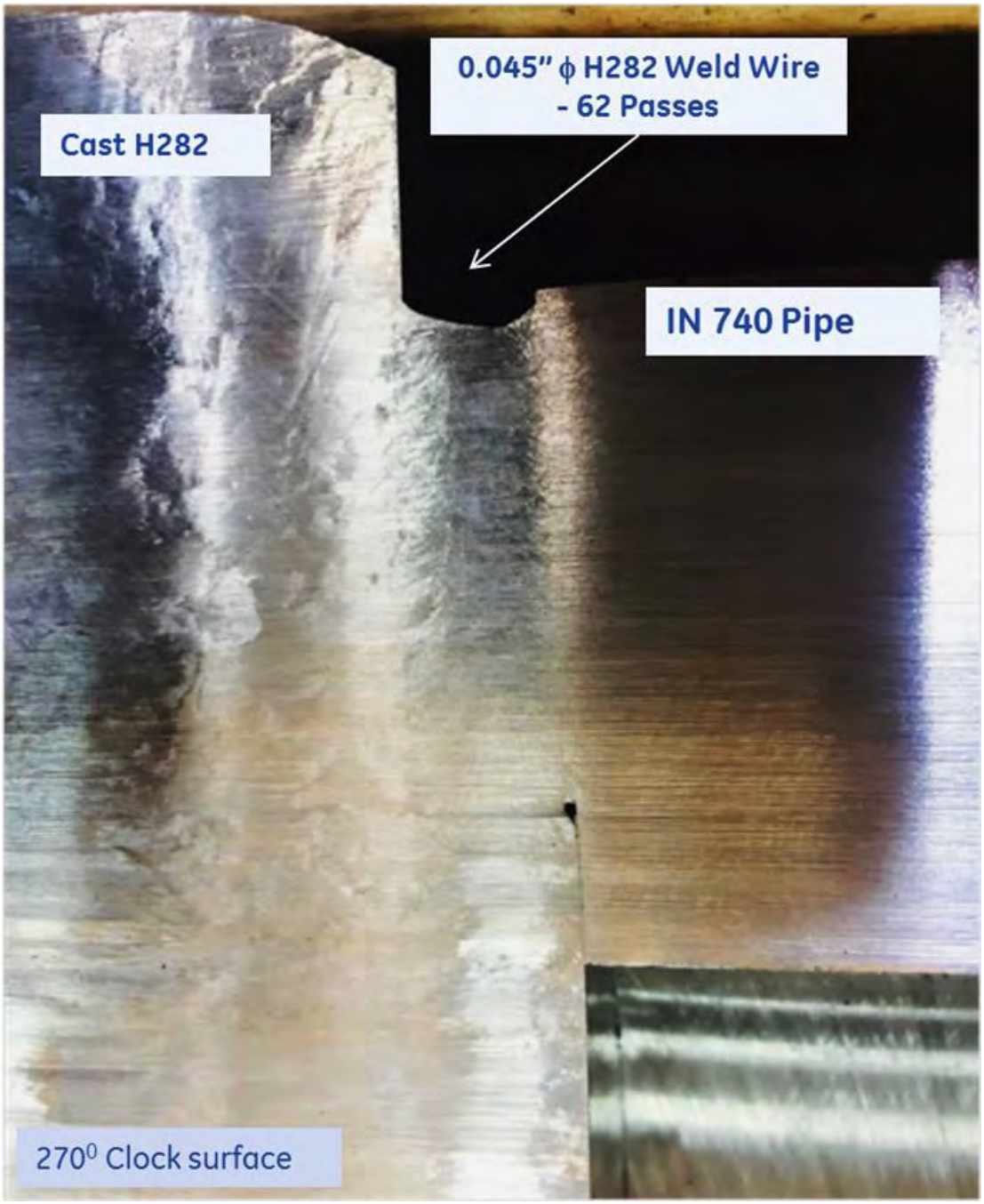

Figure 6- 6: Close up image of the IN 740 – Cast H282 weld [270^0 Clock Position]

Pieces from various locations were EDM cut and polished for microstructural analysis. Figure 6- 7 and Figure 6- 8, show the macro and microstructures at two separate locations and weld faces. No issues were observed in the IN 740H pipe weld wall while the area with casting defect exhibited cracks and the cleaner casting exhibited no cracks.

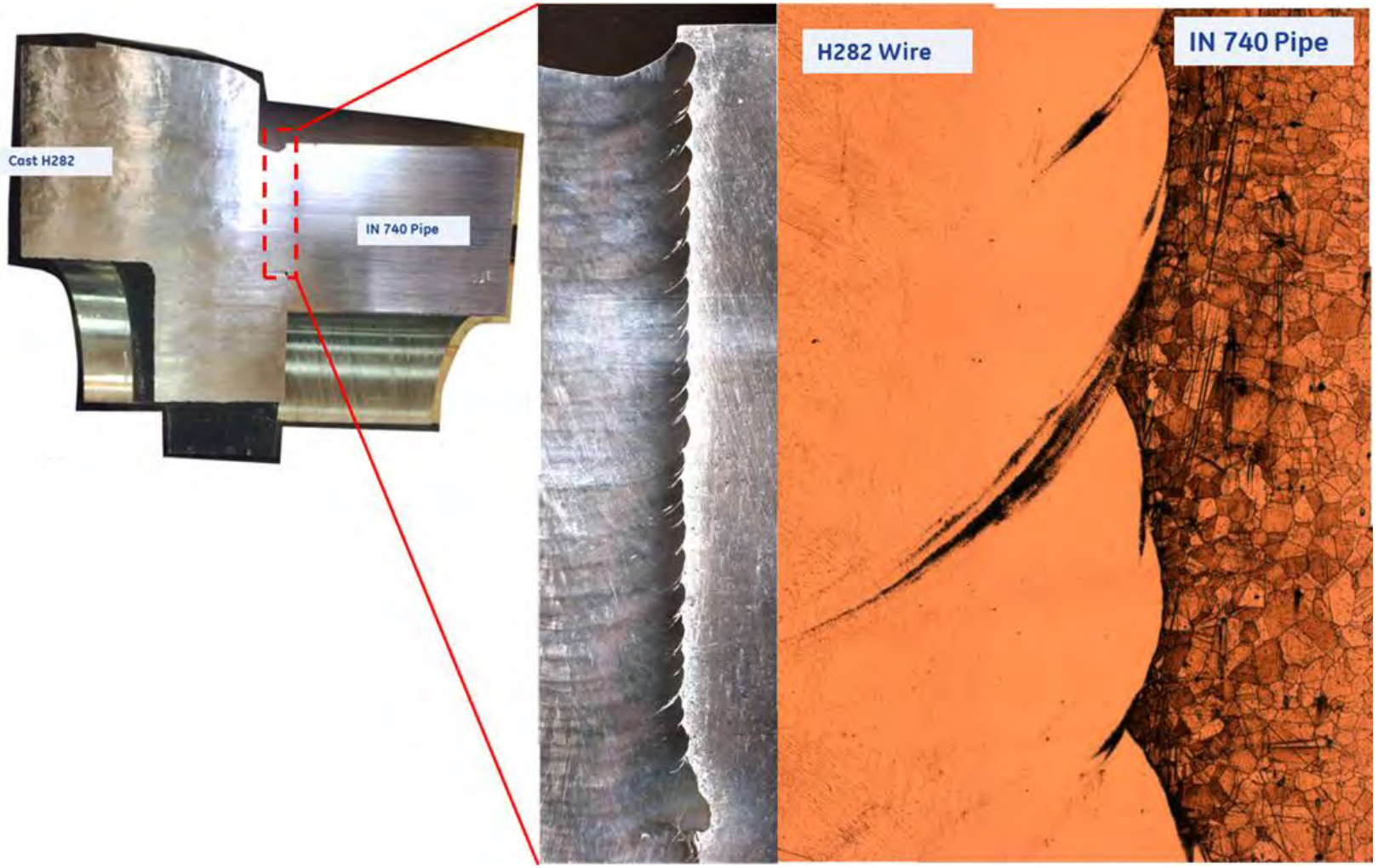

Figure 6- 7: Figure showing the overall weld quality [Marco and Micro] between IN 740H Pipe and Haynes 282 wire

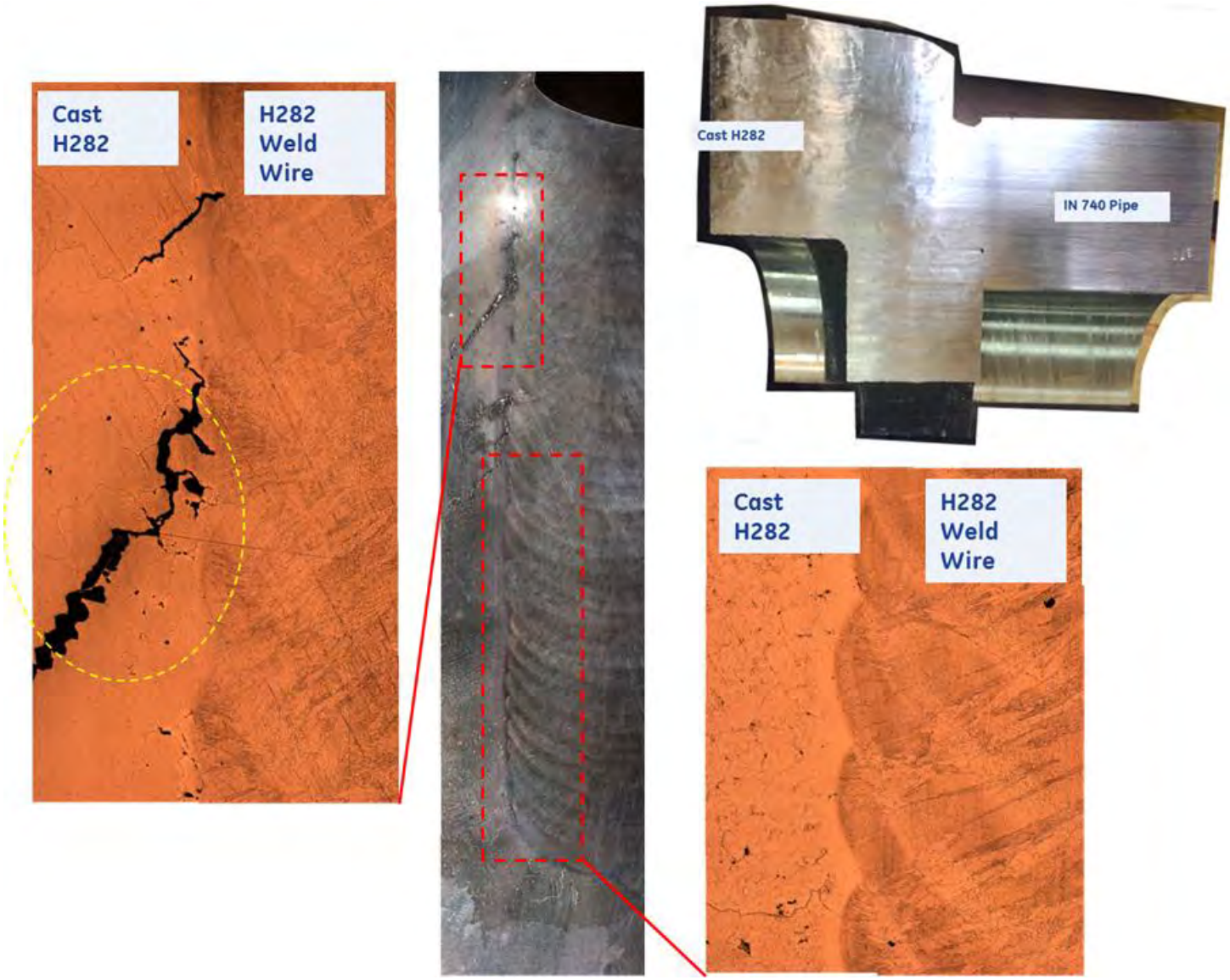

Figure 6- 8: Figure showing the cutup across the weld showing a good weld in location without defect and a location [top] with a casting defect

CONCLUSION

Successful welds were completed between H282 cast and IN 740 Pipe. The casting was fully heated and machined during CY Q1/Q2 2015, with the project officially ending in CY Q3/2015. The pieces will be shipped to ORNL for weld property evaluation.

APPENDIX 6.A

Arc Applications, Inc.

AAI 21519 Alloy 740H/Cast 282 Welding Evaluation 07-31-2015

GE #900739627

COLD WIRE NARROW GROOVE GAS TUNGSTEN ARC WELDING EVALUATIONS ALLOY 740H PIPE AND CAST 282 MATERIALS JOINED WITH 282 FILLER

740H/282 Welding Support (Parameters Appendix I)

This work is a continuation of previously completed 740H/282 welding completed during 2013 as part of AAI 21220/GE 900449348. To support for these evaluations, a test was designed to provide a narrow groove deposit with a cold wire gas tungsten arc welding (CW-GTAW) split bead deposit technique. A single bevel groove was designed to produce a deposit approximately 2.5 inches in depth suitable for testing, Figure 1. Customer supplied 740H pipe, fully heat treated 282 casting and 0.045 inch diameter Haynes 282 filler material, HT# 2082-8-8361, were used for these tests. Heat numbers for the base materials were not provided. The base materials were machined to provide the desired groove dimensions, Figure 2 and Figure 3. Due to complications in machining the fully heat treated 282 casting, the insertion of the 282 into the 740H pipe was reduced to 0.1 inches. This created complications during welding which will be covered later in this report.

Figure 1

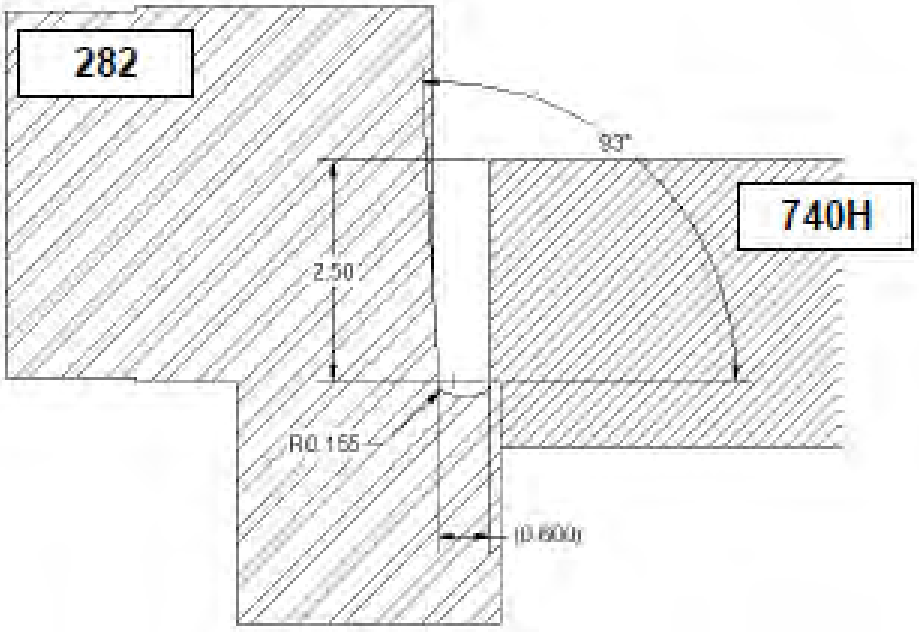

Sketch of Weld Groove

Figure 2

Final Machined 740H Pipe

Figure 3

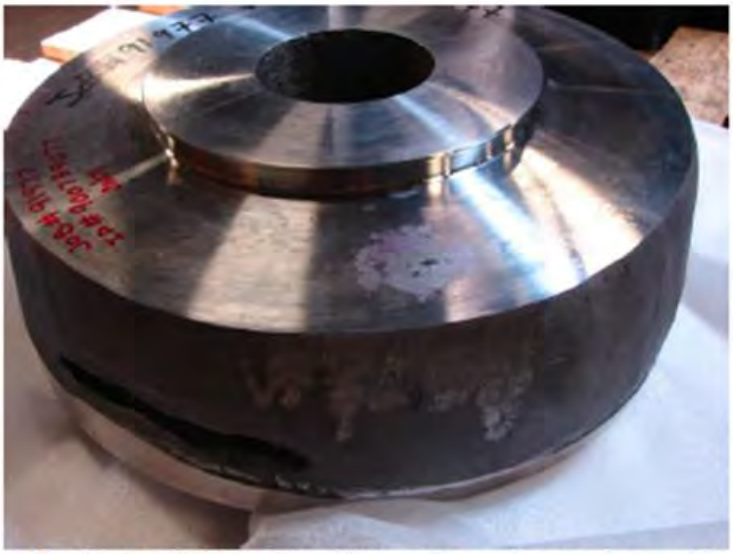

Final Machined 282 Casting Presenting a Large Area of Voids

Upon receipt of the 282 casting, the machined surface was inspected and several surface void discontinuities were noted. These voids appeared to be mainly present in certain regions of the surface and largely absent in others. A survey of the surface was made and the different regions marked to allow examination during cross sectioning, Figure 4. The 0° axis was located in the center of the large voided area to concentrate any possible welding complications experienced during start up/shut down in this defective region.

Figure 4

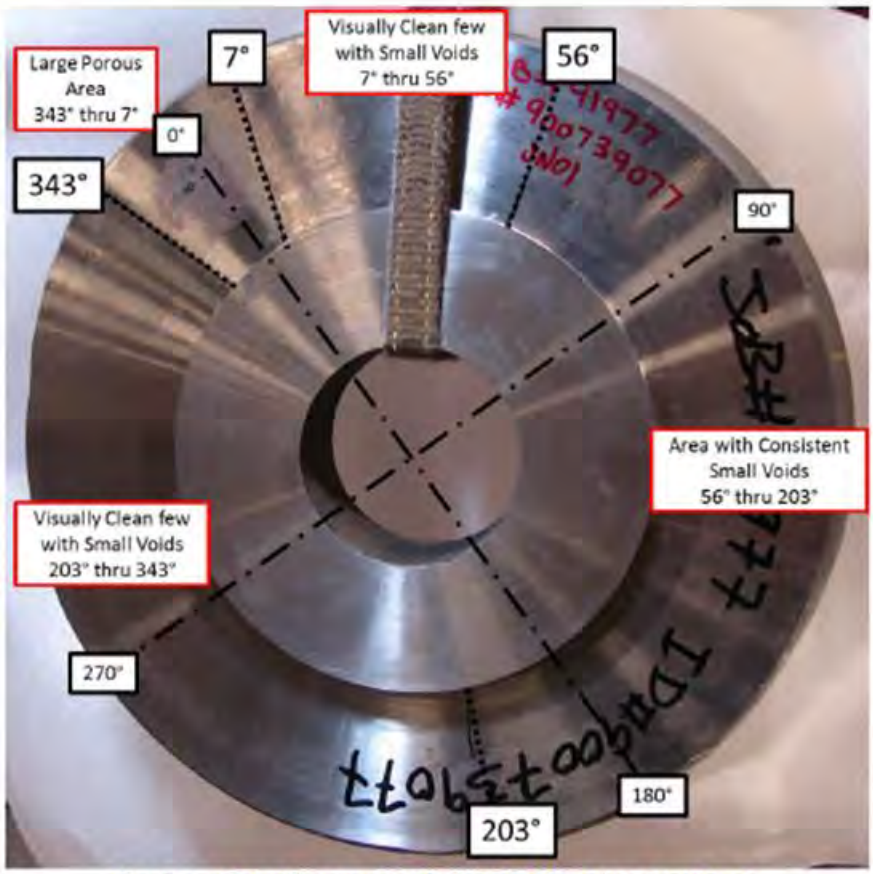

Casting Condition Layout of 282 Machined Surface

A station was setup to provide mechanized welding with an Arc Machines, Inc. (AMI) Model 415 (M415) power supply/weld head controller. An AMI Model 15 weld head with a NGT-B rotating tungsten electrode torch, Figure 5, was used to provide the required arc control in the prescribed weld groove, Figure 6. The test assembly was fixtured to a Pandjiris Model 30-6 welding positioner and aligned to the welding torch, Figure 7. For this test, 50% Ar – 50% He shielding gas was used with a supplemental trailing shield with 100% Ar gas to provide additional coverage of the weld and the trailing deposit as it cooled.

Figure 5

Model 15 Weld Head and NGT-B Torch

Figure 6

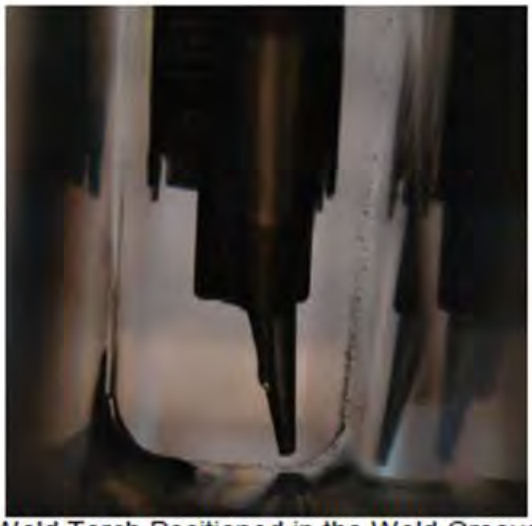

Weld Torch Positioned in the Weld Groove

Figure 7

Welding Setup with Pandjiris 30-6 Positioner and AMI Weld Head/Torch

After the station was setup to support welding activities, auxiliary audio equipment was configured to provide audio recordings of the welding operations. Recordings were planned to allow post weld analysis of the audio which would capture "pings" heard during welding. With this data, a map of likely crack locations could be generated.

To support these activities, a Focusrite Safire 6i6 USB interface, a laptop with multi-channel recording software, and two microphones were setup, Figure 8 and Figure 9. A condenser microphone was secured to a section of stainless steel tubing which was inserted into the thru hole in the positioner table. This allowed recording in the ID of the 282 which was anticipated to provide greater pickup of any "pings" heard during welding which could indicate cracking. The dynamic microphone was positioned under the mockup in line with the welding groove. This area was chosen to minimize pickup of noise from the shielding gas, positioner motor, and welding power supply cooling system. Audio recordings were started at the beginning of each weld pass and audible indications of the details of the weld were given to facilitate post weld customer analysis of the audio data.

Figure 8

Laptop with Multi-Channel Recording Software and Focusrite 6i6 USB interface

Figure 9

Pickup Tube of Condenser Microphone and Setup Position of Dynamic Microphone

Upon receipt of the machined sections, the pieces were cleaned with acetone and alcohol to remove cutting fluids from the machining operations. The mockup was then assembled, Figure 10, and small manual GTA tack welds were applied to the 740H/282 seam in the weld groove to restrain the sections during initial welding operations, Figure 11. After completion of the tack welds, the mockup was set in the horizontal position for welding.

Figure 10

Cast 282 and 740H Groove Prior to Tacking

Figure 11

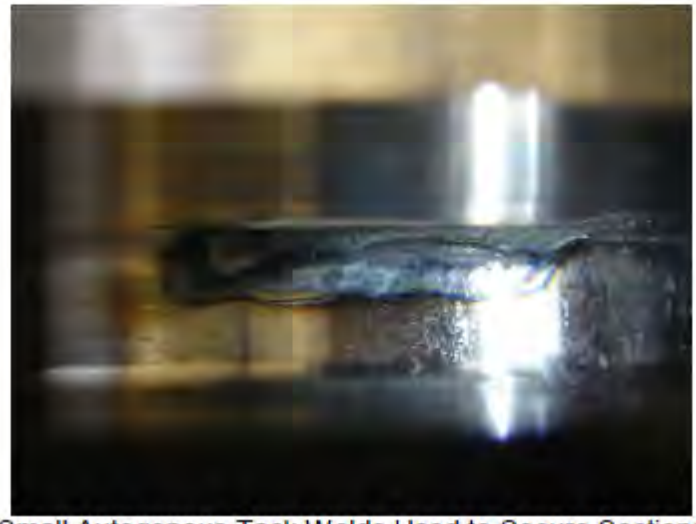

Small Autogenous Tack Welds Used to Secure Sections

After positioning the mockup, arc current, voltage, wire feed and rotational speed calibrations were performed. For current and voltage this was achieved by striking a constant current arc in the weld groove and monitoring voltage and current. Adjustments were made to achieve a voltage tolerance of ±0.1v and current tolerance of ±2.5 amps. After completion of this test it was noted that the localized weld zone had cracked, Figure 12. A repair for the tack was not attempted due to the location of the calibration tack in the region of the 282 casting which presented a large voided area from which samples would not be removed.

Figure 12

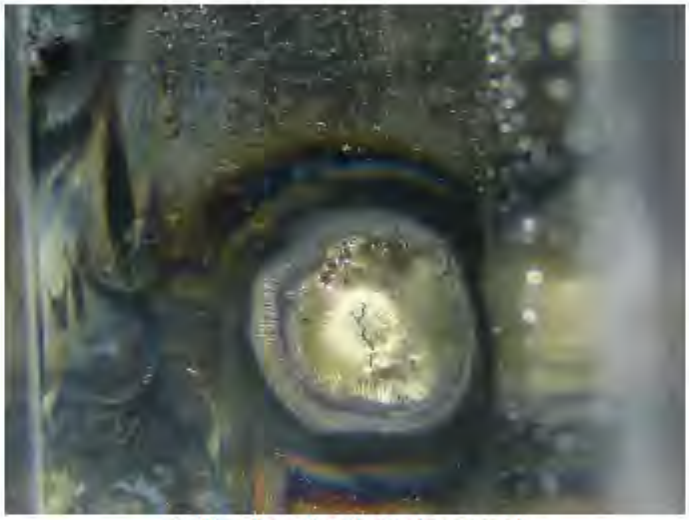

Calibration Spot Crater Crack

The first root pass was deposited against the 282 side of the groove. During and immediately after welding, an audible "pinging" sound was heard which prompted a detailed visual inspection of the weld surface. Small crack like indications were noted in areas of the 282 base material adjacent to the root pass, Figure 13. As these cracks were anticipated, welding resumed without repair attempts.

Figure 13

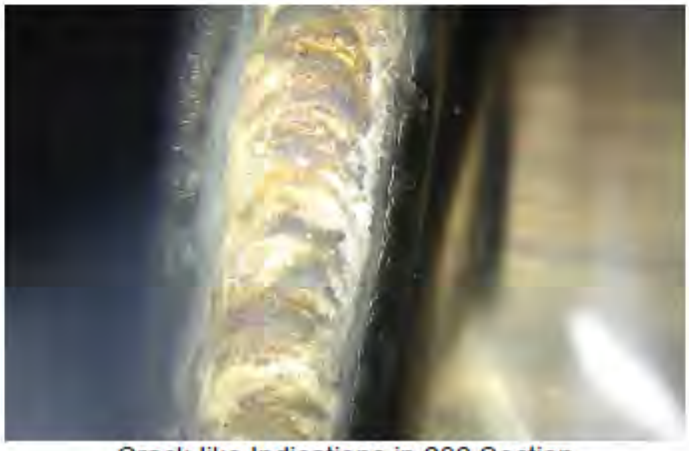

Crack-like Indications in 282 Section

Subsequent passes were performed in a continuous fashion, first initiating on the 282 side then automatically switching to the 740H side upon reaching the 0 deg. axis. These passes experienced complications due to increased oxide formation from the 282 casting and localized melting of the 0.100 inch 282 insert into the 740H pipe, Figure 14. Autogenous repair welds were used to fuse the 0.100 inch 282 insert to the 740H pipe, after which no further repair welds were required for the remainder of the test, Figure 15. Many audible pings were heard during these repair welds, often corresponding to the cracking of the autogenous tack welds. Generally, all material within the first 8 passes of the deposit should be considered suspect as grind-out repairs were not attempted due to the nature of the complications.

Figure 14

Localized Melting of the 740H pipe (left) with complete melting of the 0.100 inch 282 insert (left weld) without producing the desired fillet condition (right weld)

Figure 15

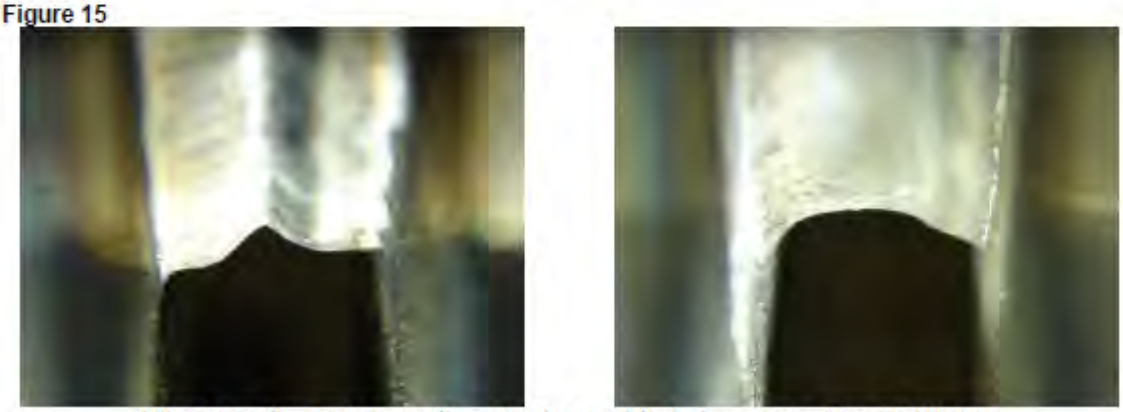

Weld Profile Before (left) and after (right) Autogenous Repair Welds
Note: The Jagged White Line on the Right Sidewall of the Right Image is a Region Where the 282 Sidewall Separated from the Casting

During the initial welds, parameters from the previously completed 740H/282 test were evaluated. These parameters produced unfavorable welding conditions due to increased surface oxides from the 282 casting/filler material. To compensate for the oxides which inhibited wetting of the weld pool, increased welding current and decreased travel speed were required. After these changes were applied, the welding operation was stable and consistent to operate. Periodically during welding, a carbide burr was used to remove the oxides from the weld surface in order to promote deposit quality and welding operability, Figure 16.

Figure 16

Weld Surface after Light Burring to Remove Surface Oxides

Between each layer a visual inspection of the weld surface was performed. Observations indicated that areas of increased oxidation were consistent with the regions of the 282 casting that presented voids on the machined surface. Similarly, these regions often presented cracks at the weld to where the 282 sidewall had separated from the bulk of the casting Figure 17, or open voids into the 282 casting, Figure 18. These were often accompanied by cracks in the deposit proximal to the separations or voids. Conditions were most notably seen in the area between 56° and 203° and visible on the surface of the finished weld. Repairs were not attempted in these areas as the root cause of the indications was believed to be the quality of the casting, not a result of the welding operation. These areas of increased oxidation often presented a novel "red" oxide that appeared to be similar to the red oxide that was present in a large gouge on the surface of the 282 casting, Figure 19.

Figure 17

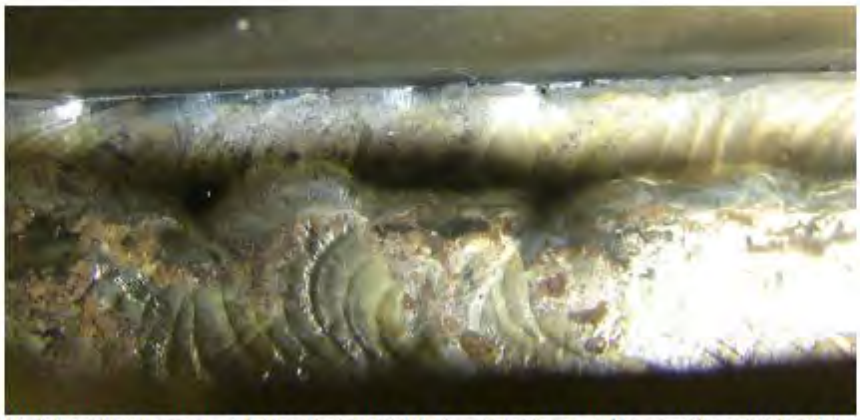

Region of Weld with Increased Surface Oxides and Separation of the 282 Sidewall (upper sidewall in image) from the Bulk of the 282 Casting

Figure 18

Voids that Opened on the 282 Sidewall (upper sidewall in image)

Figure 19

Red Oxide in Gouge on Side of 282 Casting

In the areas that did not present voids on the 282 machined surface, welds presented limited surface oxides and were free of cracks or other indication of significant quality concerns, Figure 20. As compared to the previously completed weld with 740H filler material, the 282 filler material was more sluggish and tended to produce increased surface oxides which can complicate welding operation due to decreased wetting and increased propensity for lack of fusion to the sidewall. The modified parameters produced a favorable sidewall fillet profile, Figure 21.

Figure 20

Characteristic Oxide Condition Created by 282 Filler Material in Areas

Figure 21

Characteristic Surface Profile of Weld Deposit

Welding activities continued until a groove depth of approximately 0.15 inches from the surface. At this time, the limited supply of filler material was consumed and welding activities stopped. Select images of the finished mockup and surface conditions are presented in Figure 22 thru Figure 26.

Figure 22

Completed Mockup

Figure 23

Final Weld Contour

Figure 24

Final Weld Surface Condition in Region with Sound 282 Casting

Figure 25

Final Weld Surface Condition in Region with Voided 282 Casting

Figure 26

Voids in the 282 Sidewall at the Location of the Large Voided Area Located at the 0° Axis

7. Engineering and Economic Analysis of an Advanced Ultra-Supercritical Pulverized Coal Power Plant with and without Post-Combustion Carbon Capture

Note: this section contains its own numbering and table of contents

Abstract

As the U.S. Environmental Protection Agency (EPA) and permitting agencies in countries around the world set limits on greenhouse gas emissions from power plants, it becomes more challenging for coal-based technologies to remain competitive. Adding carbon dioxide (CO_2) capture to a pulverized coal (PC) generating unit to meet these emission requirements decreases the plant's net power output and increases its capital and operating cost. One of the key strategies to mitigate this "penalty" for carbon capture is to increase the efficiency of the generating unit. Raising efficiency decreases coal consumption per megawatt-hour (MWh) of electricity produced, so less CO_2 is emitted. Increasing unit efficiency also decreases the operating costs associated with purchasing and handling coal, disposing of ash, and purchasing and preparing limestone for flue gas desulfurization and ammonia for selective catalytic nitrogen oxides (NO_X) reduction. The plant's water consumption is also decreased.

Although power plant designers can employ several approaches to increase the efficiency of a PC unit, the most significant gain is obtained by increasing the high-pressure and intermediate-pressure turbine inlet steam temperatures. Increasing the temperature above today's "state of the art" ultra-supercritical (USC) steam conditions requires the substitution of high nickel content alloys in place of ferritic steel alloys in the highest temperature and pressure sections of the boiler, steam turbine, and interconnecting piping. Such use of nickel alloys allows main and reheat steam temperatures in the range of 705–760°C (1300–1400°F). Plants operating at these steam conditions are referred to as advanced ultra-supercritical (A-USC) units.

In 2001, the U.S. Department of Energy (DOE) and the Ohio Coal Development Office (OCDO) launched a research program to develop and certify the nickel alloys required to operate a PC plant at A-USC steam conditions. Initial work focused on boiler components and was conducted by a consortium of U.S. companies and research organizations, including DOE's National Energy Technology Laboratory (NETL), OCDO, Energy Industries of Ohio (EIO), EPRI, ALSTOM Power, Babcock and Wilcox, Foster Wheeler, Oak Ridge National Laboratory, and Riley Power. A subsequent steam turbine consortium was formed, including many of the same organizations and General Electric. The consortia conducted tasks covering conceptual design, material properties, steamside oxidation, fireside corrosion, welding, fabricability, design data and rules, coatings, rotor/disc testing, blade/airfoil alloy testing, valve casting and testing, rotor alloy welding and characterizing, and casing welding and repair.

This report evaluates the economics and performance of two A-USC PC power plants:

- Case 1 is a conventionally configured A-USC PC power plant with superior emission controls, but without CO_2 removal.
- Case 2 adds a post-combustion carbon capture (PCC) system to the plant of Case 1, using the design and heat integration strategies from EPRI's 2015

report, “Best Integrated Coal Plant.” The capture design basis for this case is “partial,” to meet EPA’s proposed New Source Performance Standard, which was initially proposed as 500 kg-CO_2/MWh (gross) or 1100 lb-CO_2/MWh (gross), but modified in August 2015 to 636 kg-CO_2/MWh (gross) or 1400 lb-CO_2/MWh (gross). Both standards are examined.

This report draws upon the collective experience of consortium members, with EPRI and General Electric leading the study. General Electric provided the steam cycle analysis as well as the steam turbine design and cost estimating. EPRI performed integrated plant performance analysis using EPRI’s PC Cost model.

Burning Powder River Basin (PRB) coal, the Case 1 configuration has an estimated efficiency of 41.4% on a higher heating value (HHV) basis. The arrangement of the boiler in PC Cost for this case is based on a “traditional” boiler configuration. Using on these assumptions, the plant in Case 1 has a capital cost of $2,933/kW and a levelized cost of electricity (LCOE) of $84.70/MWh.

Case 2 added a near term “advanced” solvent for CO_2 removal. The plant also included a high degree of heat integration to maximize the net power output while meeting CO_2 emissions regulations. With this design approach, for a proposed emission standard of 500 kg-CO_2/MWh (1100 lb-CO_2/MWh), plant efficiency dropped by only 2.5 percentage points to 38.9% (HHV basis). The capital cost of the A-USC plant increased by only 8%, but on a $/kW (net) basis, the cost increased to $3,370/kW (a 15% increase) due to the decrease in net power. The LCOE with CO_2 removal increased to $100.20/MWh.

Two weeks prior to the release of the initial draft of this report, President Obama and the EPA released the Clean Power Plan. Under this plan, the CO_2 emission rate for a new coal fired power plant was increased from 500 kg-CO_2/MWh (1100 lb-CO_2/MWh) to 636 kg-CO_2/MWh (1400 lb-CO_2/MWh). This improved the Case 2 plant efficiency to 40.3% (HHV) or 1.1 percentage points below the “base” AUSC plant with no carbon capture. The capital cost was estimated to be $3,190/kW, and the LCOE was estimated to be $93.30/MWh – an increase of approximately 10% above the Case 1 AUSC power plant.

For the economic analysis, the assumed price per pound for the nickel-based alloys for boiler tubing and piping was based on mid-2015 prices and estimated to be $40/lb. The turbine cost, which was effectively double the cost of a comparable USC turbine, assumed a finished nickel-based forging and casting cost approximately 8 times the cost of an advanced ferritic steel forging or casting. The high price of nickel piping, which for the A-USC cases was found to be 9.6 to 9.8% of the total plant Direct Field Costs (DFC), has led engineering organizations to develop boiler and turbine configurations that minimize the amount of nickel piping required in the design. Two initial alternative designs are discussed in this report. Preliminary economic analyses suggest such designs could reduce the cost of an A-USC boiler by more than 10% relative to a conventional configuration, making A-USC technology competitive with the current “state of the art” USC PC units.

ACRONYMS AND SYMBOLS

AQCS	air quality control system
ASME	American Society of Mechanical Engineers
A-USC	advanced ultra-supercritical
DCS	distributed control system
DOE	U.S. Department of Energy
ESP	electrostatic precipitator
FD	forced draft
FGD	flue gas desulfurization
FSH	final superheater
FWH	feedwater heater
h_o	heat transfer coefficient at tube OD
h_{io}	heat transfer coefficient at tube ID referred to tube OD
HHV	higher heating value
HMB	heat and material balance
HP	high pressure
IP	intermediate pressure
LCOE	Levelized cost of electricity
LHV	lower heating value
LP	low pressure
MCR	maximum continuous rating
MEA	monoethanolamine
NETL	National Energy Technology Laboratory
OCDO	Ohio Coal Development Office
OD	outside diameter
PA	primary air
PC	pulverized coal
PCC	post-combustion CO_2 capture

PRB	Powder River Basin
SA	secondary air
SCR	selective catalytic reduction
TPC	total plant cost
USC	ultra-supercritical

CONTENTS

***1* INTRODUCTION 417**

A-USC Drivers 418

RD&D Programs and Progress 419

Europe 419

Test Loop 1: Development of pipe repair concept 420

Test Loop 2: Test of Hot Isostatic Pressing (HIP) parts and weldments as well as life-time monitoring 420

Test Loop 3: Test of different Ni-based alloys and elements 420

Test Loop 4: Test of turbine cast material and weldments 421

United States 421

Japan 424

China 425

India 425

***2* DESIGN BASIS SPECIFICATIONS 427**

Site Location 427

Ambient Conditions 427

Environmental Requirements 427

Design Data 428

Coal Specification 428

Limestone and Reagents 430

Water Source and Wastewater 430

Plant Operating Criteria 431

Duty 431

Capacity Factor 431

Plant Design Life 431

Mechanical Design Criteria 431

Boiler Description 431

Air Heater 437

Coal Mills (Pulverizers) 437

Condenser and Cooling System 437

Air Quality Control System 438

SCR System 438

Mercury Control 439

Electrostatic Precipitators 439

FGD System 439

Limestone Handling 440

Limestone Preparation 440

Gypsum Dewatering 441

Balance of Plant 441

Raw Coal Receiving, Storage, and Handling....441
Solid Waste Handling Systems....441
Fly Ash Handling....441
Other Ash Handling....442
Control Systems....442
Electrical System....442
Project Transportation Size Limitations....442
Overland Transportation Size....442
Barge Transportation Size....442
***3* MODELING METHODOLOGY....443**
Boiler – PC Cost Model....443
Modifications to PC Cost....444
AspenPlus™ HMB Model....444
Heat Transfer Calculations....446
Selection of Boiler Materials....446
Steam Tubing and Piping....447
Auxiliary Loads....447
Steam Cycle Modeling....448
***4* CASE 1: PERFORMANCE RESULTS WITHOUT CO_2 CAPTURE....449**
Steam Turbine....449
High-Pressure Turbine....449
Intermediate-Pressure Turbine....450
Low-Pressure Turbine....451
Cycle Performance Determination....451
Steam Cycle Main Inlet Pressure....451
Condensate System....455
Feedwater Heaters....456
Circulating Water System....457
Plant Performance....457
***5* CASE 2: PERFORMANCE WITH CO_2 CAPTURE....461**
Process Description....462
Design of the PCC System....468
Heat Integration....468
CO_2 Regeneration and CO_2 Compression Heat Recovery....469
Combustion Air Preheater....469
Plant Performance....475
Out of Service Operation....478
***6* ECONOMIC EVALUATION....481**
Case 1 – A-USC PC without Carbon Capture....481
Total Plant Cost....481

Steam Turbine Costs....481
Levelized Cost of Electricity....484
Case 2 – A-USC PC with Post-Combustion CO_2 Capture....486
Total Plant Cost....486
Levelized Cost of Electricity....487
A-USC Boiler Configurations to Reduce Capital Cost....489
***7* CONCLUSIONS AND FUTURE WORK....495**
Summary of Findings....495
The Next Step....499
***8* REFERENCES....507**
***A* PROCESS FLOW DIAGRAM/HEAT AND MATERIAL BALANCE....509**

LIST OF FIGURES

Figure 2-1 Flows, Temperatures, and Pressures through the Boiler (U.S. Customary Units)...434
Figure 2-2 Flows, Temperatures, and Pressures through the Boiler (SI Units) 435
Figure 2-3 Boiler Island Process Flow Diagram.....436
Figure 3-1 Original PC Cost Boiler Configuration.....445
Figure 4-1 Layout of HP, IP, and LP Steam Turbines.....449
Figure 4-2 Impact of Main Steam Pressure on A-USC Cycle Efficiency 453
Figure 4-3 A-USC Plant Cost Increase vs. Heat Rate Improvement.....454
Figure 4-4 Levelized Cost of Electricity, Cost Component Distribution 455
Figure 4-5 3500 psig Steam Cycle Diagram for Case 1.....458
Figure 5-1 CO_2 Capture System.....464
Figure 5-2 CO_2 Compression System 467
Figure 5-3 PCC Heat Integration Scheme.....471
Figure 5-4 Combustion Air Preheater (from EPRI Report 3002003740) 472
Figure 5-5 PCC Heat Integration Scheme.....473
Figure 5-6 Heat Exchanger Network Diagram.....474
Figure 5-7 Low Pressure Condensate Heat Balance with PCC System Out of Service.....479
Figure 6-1 Steam Generator Cost Study Results 484
Figure 6-2 Layout of a High and Low Position Steam Turbine Arrangement 490
Figure 6-3 Turbine Train Schematic Showing Components 491
Figure 6-4 Babcock and Wilcox Downdraft Inverted Tower Design 492
Figure 7-1 Overall A-USC ComTest Program Concept 501
Figure 7-2 General Electric A-USC Steam Turbine Concept (Dimensions in inches) 502
Figure 7-3 Proposed Youngstown Thermal Flowsheet.....503
Figure 7-4 Babcock and Wilcox A-USC ComTest Superheater TowerReferences 505
Figure A-1 Boiler Island.....510
Figure A-2 Post-Combustion CO_2 Removal System.....513
Figure A-3 CO_2 Compression System.....514
Figure A-4 4250 psig Inlet Pressure Steam Cycle Diagram, No PCC.....517
Figure A-5 3500 psig Inlet Pressure Steam Cycle Diagram, PCC System.....518
Figure A-6 3500 psig Inlet Pressure Steam Cycle Diagram, PCC System Off.....519
Figure A-7 4250 psig Inlet Pressure Steam Cycle Diagram, PCC 520

LIST OF TABLES

Table 1-1 Comparison of Topics Pursued by International A-USC RD&D Programs 419
Table 1-2 Nickel-Based Alloys under Evaluation 421
Table 2-1 Annual Average Ambient Conditions 427
Table 2-2 Stack Gas Emissions Limits 427
Table 2-3 Wastewater Discharge Permit 428
Table 2-4 Coal and Ash Analysis for Wyoming Subbituminous Coal 429
Table 2-5 Limestone Design Composition 430
Table 2-6 Raw Water Quality for Cooling Tower Makeup 430
Table 2-7 Steam Piping Pressure Drop and Attemperation Assumptions 432
Table 2-8Table 2-8 Summary of Boiler Performance 432
Table 2-9 Cooling Tower Design Conditions 438
Table 4-1 Summary of Cycle Parameter Assumptions 451
Table 4-2 Feedwater Heater Design Parameters 456
Table 4-3 Summary Performance of the Advanced Ultra-Supercritical Plants without PCC 459
Table 4-4 Auxiliary Loads for the Advanced Ultra-Supercritical Plants without PCC 460
Table 5-1 Summary Performance of the Advanced Ultra-Supercritical Plant with a 1100 lb CO_2/MWh PCC System 475
Table 5-2 Auxiliary Loads for the Advanced Ultra-Supercritical Plant with a 1100 lb CO_2/MWh PCC System 476
Table 6-1 Total Plant Cost and Cost of Electricity – without Post-Combustion CO_2 Capture 486
Table 6-2 Total Plant Cost and Cost of Electricity – with an 1100 lb CO_2/MWh Post-Combustion CO_2 Capture 488
Table 6-3 Performance Comparison of a 242 bara (3500 psig) steam cycle compared to a 294 bara (4250 psig) steam cycle with Carbon Capture to meet 1100 lb CO_2/MWh standard 493
Table 7-1 Case Comparison (SI Units) 497
Table 7-2 Case Comparison (U.S. Customary Units) 498
Table A-1 Boiler Island Material Balance for Case 1 & 2 511
Table A-2 Boiler Island Material Balance for Case 1 & 2 (Continued) 512
Table A-3 Post-Combustion CO_2 Removal System Material Balance for Case 2 515
Table A-4 Post-Combustion CO_2 Removal System Material Balance for Case 2 (Continued) 516
Table A-5 PC-Cost Output Datafile 521

1
INTRODUCTION

This report describes the performance and cost of pulverized coal (PC) power plants with ultra-supercritical (USC) and advanced ultra-supercritical (A-USC) steam conditions, both without and with post-combustion capture (PCC) of CO_2. It draws upon past and current work by EPRI, General Electric, and members of the Advanced Materials for Ultra-Supercritical Boiler and Steam Turbine Consortia funded by the U.S. Department of Energy and the Ohio Coal Development Office. Results are presented for two design cases:

- Case 1 is a "conventionally configured" A-USC PC power plant (i.e., without CO_2 removal or novel equipment arrangements). New for 2015 is engineering and costing of the steam cycle and steam turbine by General Electric. Integrated plant performance analyses were conducted by EPRI; boiler performance and costing drew upon EPRI's PC Cost model.
- Case 2 adds a PCC system to the A-USC power plant from Case 1, using PCC design and heat integration strategies from EPRI's 2015 "Best Integrated Coal Plant" report.[1] GE also provided input on how to best integrate the steam cycle with the PCC system to optimize overall unit performance. The CO_2 capture rate is "partial," meaning to the extent necessary to comply with the U.S. Environmental Protection Agency's proposed New Source Performance Standard, which was initially proposed as 500 kg-CO_2/MWh (gross) or 1100 lb-CO_2/MWh (gross), but modified in August 2015 to 635 kg-CO_2/MWh (gross) or 1400 lb-CO_2/MWh (gross). The impact of both standards are examined in this report.

Design, performance, and cost information in this report also draws from other recent engineering-economic analyses by EPRI and members of the Advanced Materials for Ultra-Supercritical Boiler and Steam Turbine Consortia:

- A 2008 EPRI report[2] described the design, performance, and economics of a 750 MW (net) 1300°F (~700°C) series USC PC burning Powder River Basin (PRB) subbituminous coal. This design did not include CO_2 capture.
- A 2011 EPRI report[3] estimated the energy penalty associated with adding 90% CO_2 capture to the A-USC design from the 2008 report. The PCC system design employed a 30% (wt) monoethanolamine (MEA) solvent; design details are

[1] *EPRI's Best Integrated Coal Plant with Post-Combustion Capture Case Study.* EPRI, Palo Alto, CA: 2015. 3002003740.

[2] *Engineering and Economic Evaluation of 1300°F Series Ultra-Supercritical Pulverized Coal Power Plants: Phase 1.* EPRI, Palo Alto, CA: 2008. 1015699.

[3] *Engineering and Economic Analysis of 1300°F Series USC Plant with Post-Combustion Capture.* EPRI, Palo Alto, CA: 2011. 1026645.

described in a 2010 EPRI report examining PCC for 1100°F (~600°C) USC PC units.[4]

- A 2013 EPRI report[5] estimated the performance and cost of a "demonstration size" A-USC unit with a net output of 350–400 MW after CO_2 capture using a 30% (wt) MEA PCC system. The CO_2 capture design basis was not 90%, but rather targeted a stack emissions rate of 363 kg-CO_2/MW (net) or 800 lb-CO_2/MW (net), which is roughly equivalent to the emissions rate of a modern natural gas combined cycle unit without CO_2 capture.
- In 2013, EPRI evaluated a series of A-USC steam cycle temperatures and pressures for plants with and without PCC to identify "optimum" cycle conditions. This resulting report[6] was published in early 2014.
- In past evaluations of A-USC units with CO_2 capture, a PCC system using a 30% (wt) MEA solvent served as the design basis, primarily due to the large amount of information in the public domain. With reports of numerous advanced amine solvents having lower regeneration energy requirements, EPRI chose for its 2015 "Best Integrated Coal Plant" report[7] a "near term" advanced CO_2 removal solvent based on the research results from the National Carbon Capture Center in Wilsonville, AL. The overall plant performance with this PCC solvent was significantly better than that for the same plant using the previous MEA-based PCC design and, as noted above, serves as the basis for the Case 2 in this report.

A-USC Drivers

A significant component of the global drive to decrease emissions from pulverized coal plants focuses on increasing the efficiency of the generating unit. This reduces both the amount of coal required per megawatt-hour (MWh) of energy output and the plant's emissions, including CO_2. Where CO_2 capture is required to meet a regulatory emissions limit, the higher efficiency reduces the size and capital costs of the capture equipment. Additional benefits of higher efficiency include the decreased operating costs associated with purchasing coal, ash disposal, limestone for the flue gas desulfurization (FGD) unit, ammonia for the selective catalytic reduction (SCR) unit, reduced water consumption, and, where applicable, decreased costs for transport and storage of the CO_2.

State-of-the-art PC plants employ ultra-supercritical steam conditions, traditionally defined by EPRI as temperatures in excess of 593°C (1100°F). The maximum steam temperature typically used with the currently available ferritic steels is 610°C (1130°F) for the main steam and 621°C (1150°F) for the reheat steam. A-USC steam conditions

---

[4] *An Engineering and Economic Assessment of Post-Combustion CO_2 Capture for 1100°F Ultra-Supercritical Pulverized Coal Power Plant Applications: Phase II Task 3 Final Report.* EPRI, Palo Alto, CA: 2010. 1017515.

[5] *Engineering and Economic Analysis of a 1300°F Series USC Demonstration Plant with Natural Gas Equivalency Post-Combustion Capture.* EPRI, Palo Alto, CA: 2013. 1026644.

[6] *Advanced Ultra-Supercritical Steam Cycle Optimization.* EPRI, Palo Alto, CA: 2014. 3002001788.

[7] *EPRI's Best Integrated Coal Plant with Post-Combustion Capture Case Study.* EPRI, Palo Alto, CA: 2015. 3002003740.

are at temperatures above those of USC, typically in the range of 705–760°C (1300–1400°F). Realizing these higher steam temperatures requires a transition to high-nickel alloys in the boiler, steam piping, and steam turbine.

To date, significant progress has been made in identifying, evaluating, and qualifying the alloys needed for the construction of the critical components of coal-fired boilers and steam turbines capable of operating at higher efficiencies than ultra-supercritical plants. As discussed below, the scope of RD&D efforts encompasses the world's major coal-burning regions, and the materials and fabrication technologies to build a first-of-a-kind demonstration A-USC plant have now become available.

RD&D Programs and Progress

The materials development programs discussed below are united by their aim to pursue higher steam conditions for coal-fired power plants. However, as Table 1-1 shows,[8] the focus of these diverse research efforts reflect variances in fuels and operating conditions, as well as the objectives of coal fleets and jurisdictions they serve.

Table 1-1
Comparison of Topics Pursued by International A-USC RD&D Programs

Research Topic	EU	US	Japan	China
Retrofit to older units	No	Yes	Yes	No
Cyclic operation	Yes	Yes	No	No
Oxy-combustion	Yes	Yes	No	No
High-sulfur coal firing on fireside corrosion	No	Yes	No	No
Biomass co-firing on fireside corrosion	Yes	No	Yes	No
Waste co-firing on fireside corrosion	Yes	No	No	No
Coatings	Yes	Yes	Yes	No
New 1200ºF (650ºC) steels	Yes	No	Yes	Yes
New nickel/iron alloys	No	No	Yes	Yes
New nickel alloys	No	Yes	Yes	No
Welded rotors	Yes	No	Yes	Yes

Europe

In the late 1990s, a consortium of major European power generators, equipment suppliers, and materials makers spurred the formation of the Components Test (ComTes) program. A component test facility, COMTES700, installed at E.ON's Scholven Power Plant in Gelsenkirchen, Germany, provided materials exposure information at temperatures up to 700°C (1290°F) for large-scale boiler components and

[8] Adapted from: Nicol, Kyle. "Status of Advanced Ultrasupercritical Pulverised Coal Technology in 2013," presented at the IEA Second AUSC Workshop, Rome, Italy, October 2014.

valves. The current ENCIO (European Network for Component Integration and Optimization) project is aimed at qualifying materials, components, and manufacturing processes, as well as erection and repair concepts, as a follow-up of COMTES700 activities with the objective of erecting and operating a new Test Facility.

Unit 4 of ENEL's Andrea Palladio Power Station in Fusina, Italy, has been selected for installation of the Test Facility. Four test loops are planned for 20,000 hours of operation at 700°C (1290°F).[9]

Test Loop 1: Development of pipe repair concept

Complementary to COMTES700, different heat treatments (pre-/post-) will be applied and a trial weld of each material combination and/or welding method will be tested destructively. Trial welds will be carried out, and those without any crack indication will then be selected to produce components to be installed in the test loop.

Different nondestructive test (NDT) methods will be applied and tested to assure high standards of quality.

Nondestructive surface tests will be performed frequently during operation for all test welds. A final repair with orbital tungsten inert gas (TIG) narrow gap and electrode welding will be executed on additionally aged pieces of A617B (having been in operation in COMTES700).

Test Loop 2: Test of Hot Isostatic Pressing (HIP) parts and weldments as well as life-time monitoring

HIP technology holds promise for fabrication of T-pieces, valve bodies, and turbine parts. Although this technology is commercially applied in other fields, it has not yet been adopted for boiler and turbine pressure parts in power plants (alloy 617B or alloy 625). HIP fabrication may substitute for expensive castings, yielding savings for applications at 700°C (1290°F) steam conditions.

NDT will be performed frequently during operation for all test welds. After the end of operation, final repair welds will be executed on all dismantled pipes of Test Loop 2.

The creep behavior of alloy 617B will be monitored by running tests under respective load and temperature, as well as by using a thin-wall piece designed for ~30,000 hours (measuring and monitoring of the creep online).

Test Loop 3: Test of different Ni-based alloys and elements

The optimized chemical composition of A617B, known as A617OCC, will be used to explore possible improvements in weldability through decreased formation of chromium carbides. Additionally, an optimized melting process will be implemented to reduce the amount of impurities in the ingot. Such an optimization has the potential to make welds more reliable. This is also expected to be an option to reduce relaxation-cracking and

[9] Di Gianfrancesco, A. et al. "Encio Project: An European Approach to 700°C Power Plant." presented at the Seventh International Conference on Advances in Materials Technology for Fossil Power Plants, Waikoloa, Hawaii, October 2013.

hot-cracking occurrences. Due to the new melting process, the improved weldability may lead to fewer and simpler pre- and post-weld heat treatment requirements, providing a possible cost reduction for 700°C (1290°F) steam cycle applications.

Other Ni-based alloys such as A263, HR6W, and A625 will be tested and the weldments of the material combinations A617B OCC–HR6W and A263–A625 cast will be tested and compared. This is necessary as the combinations A263–A625 cast (neither with nor without heat treatment) and A617B OCC–HR6W have not yet been tested and investigated with the required heat treatment.

NDT will be performed frequently during operation for test welds. After the end of operation, final repair welds will be executed on dismantled pipes of Test Loop 3, which are long enough for this purpose, followed by microstructural investigations and mechanical and creep testing.

Test Loop 4: Test of turbine cast material and weldments

This will provide a platform to test thick-wall welds in the range of the real pipe dimensions of a demonstration plant with material combination alloy 617 OCC–alloy 625 cast. This combination was not tested at real dimensions in COMTES700.

Although there was no negative indication about the behavior of the welded material in the combination alloy A617B forged–A625 cast material, the dimensions of the test weld in COMTES700 had been at relatively thin wall thickness (80 mm or 3.15 in). Thus, thick-walled welds in the range of the real cast dimensions of a demonstration plant with material combinations A617B OCC–A625 cast need to be tested. The weldments A625 cast–A625 cast with wall thickness in the range of 150 mm (5.9 in) was not foreseen in earlier designs for this component, but with the post-weld heat treatment needed for A617B OCC–A625 cast, this design also needs to be tested.

United States

In 2001, U.S. DOE/NETL—in conjunction with the Ohio Coal Development Office (OCDO), major boiler- and turbine-equipment manufacturers, and other key groups[10] including EPRI—launched a research program to develop and certify nickel alloys to achieve boiler and turbine steam conditions up to 760°C/35 MPa (1400°F/5000 psi). Table 1-2 lists the alloys selected for evaluation.[11]

Table 1-2
Nickel-Based Alloys under Evaluation

Alloy	Component	Comments
Alloy 263	Castings, Rotor	Back-up cast alloy to Haynes 282, good castability and weldability, lower strength but good ductility

[10] ALSTOM Power, Babcock and Wilcox, Foster Wheeler, General Electric, Oak Ridge National Laboratory, and Riley Power, Inc.

[11] *Combustion Technology Status 2014.* EPRI, Palo Alto, CA: 2014. 3002003618.

Alloy	Component	Comments
CCA617	Superheater/Reheater, Pipe	Higher strength than Inconel 740, but not enough data to change American Society of Mechanical Engineers (ASME) code stress values, not suitable for high-sulfur coals, only certain welds are successful, strain-age cracking concerns, low-strength limits applicability for turbine rotor
Haynes 230	Superheater/Reheater, Pipe	Successful welding trials, maximum-size limitations for pipe may limit applicability
Haynes 282	Castings, Rotor	Higher creep strength than Inconel 740, relatively insensitive to starting microstructural condition, good forging 'window' for rotor, can be cast for valves and casings
Inconel 740/740H	Superheater/Reheater, Pipe	Highest strength alloy in ASME code to achieve up to 760°C (1400°F), excellent fireside corrosion resistance, successful fabrication and welding, prime candidate for boiler components, cannot be air cast for valves and shells
Nimonic 105	Bolts, Blades	Highest creep-strength alloy, only considered for bolting and blading (non-welded components)
Waspalloy	Rotor, Bolts, Blades	Back-up alloy with good turbine history, cannot be welded reliably, poor ductility

A significant milestone for the consortium was achieved in 2011 with the successful approval of Inconel Alloy 740 by the American Society of Mechanical Engineers Boiler & Pressure Valve Vessel Code Committee (Code Case 2702). This material is rated for continuous operation at steam conditions of 760°C (1400°F).

The consortium's boiler project has operated a steam test loop manufactured with materials of interest at Southern Company's Plant Barry in Alabama for more than 17,000 hours at temperatures exceeding 760°C (1400°F). The loop contained a combination of 94 specimens with eight different superalloys and three different surface coatings. Upon removal at the end of testing, the components appeared to be in good condition and to have retained their mechanical integrity. The components are undergoing an extensive corrosion, oxidation, and material properties examination at Alstom's Material Technology Center in Chattanooga, Tennessee.[12]

With the successful test of the steam loop at Plant Barry, the next logical step is to move toward a commercial demonstration of the technology. The consortium is now developing a Component Test (ComTest) Program to remove the identified risk barriers to full-scale implementation of advanced materials. The five major areas of development cover:[13]

[12] http://www.alstom.com/press-centre/2014/12/major-milestone-achieved-in-the-development-of-advanced-ultra-supercritical-steam-power-plants/

[13] *Combustion Technology Status 2014,* EPRI, Palo Alto, CA: 2014. 3002003618.

- **Membrane Wall**—This component will be to use optimized manufacturing routes for T91/92 and other alternative materials to prove manufacturability and operation of an A-USC membrane wall and reduce the risk of early life issues. Main steam from the host utility will be cooled before flowing through the membrane wall section, which will operate at temperatures expected in an A-USC boiler.
- **Superheater**—The ComTest superheater will be installed inside the boiler and used to heat the main steam temperature up to 760°C (1400°F). As a result, the material will be exposed to the high temperatures and gas/ash constituents found in a utility boiler. Because the boiler may cycle during daily load changes, a gas-fired auxiliary superheater will be installed at the outlet of the superheater to accommodate swings in load and provide a constant temperature for downstream equipment.
- **High-Temperature, High-Pressure Steam Valve Testing**—The ComTest steam turbine will operate at a reduced pressure to increase steam volumetric flow. However, it is important to be able to design and operate the steam stop and control valves at the temperature and pressures expected during commercial A-USC operation. It is anticipated that two valve systems will be installed in parallel and cycle continuously during the test. Producing these valves, as well as the other valves needed for ComTest, will allow for the qualification of the vendors to produce high-quality valves from nickel alloys and determine the performance of the valves at these operating conditions.
- **Desuperheater and Thick-Wall Section**—Steam temperature control will be required for A-USC boilers. Injection of water in the desuperheater will produce a temperature gradient at the nozzle connection as well as along the length of the device. The A-USC desuperheater will be based on a conventional design, but with advanced materials to determine their reliability in this service. The thick-wall test section will be a component similar to a header with tube penetrations. By building the thick-walled component, the supply chain of these header sections will be developed and shop manufacturing processes and procedures will be proven. The desuperheater will be used to thermally cycle a thick-wall test section to evaluate its durability.
- **Steam Turbine**—The steam turbine for ComTest will operate with an inlet temperature of 760°C (1400°F). ComTest objectives include the selection of materials and manufacturing technologies required for reliable steam turbine operation, evaluation of component life, inspection of any oxidation and/or deposits that develop over the testing period, and the evaluation of steam path, sealing, and bearing design.
- As originally conceived, all of these components would be installed in, and adjacent to, a utility USC power plant. However, as the consortium searched for hosts for the ComTest, Youngstown Thermal in Youngstown, Ohio, expressed interest in hosting the lower-pressure components, primarily the A-USC steam turbine. Youngstown Thermal is currently a district heating facility that provides saturated steam to its customers in the downtown area. The envisioned modification would accommodate the ComTest high-temperature (i.e., A-USC) turbine employing a turbine inlet valve pressure of 585 psig and an exhaust pressure of 170 psig. Proposals for this project have been submitted to DOE and are under review as of mid-2015. Discussions

continue between the consortium and potential utility hosts about testing the steam generator components of the ComTest program that require high-pressure steam.

Japan

Since 2008, major Japanese equipment and materials manufacturers, utility companies, and two research institutes have been cooperating to develop 700°C (1290°F) class A-USC technology with the support from the Japanese government.

Boiler Technology Development. HR6W, HR35, Alloy 617, Alloy 263, Alloy 740, and Alloy141 are candidate Ni-based alloys developed under the Japanese program for use at temperatures higher than 650°C (1200°F).

High-boron 9Cr steel, low-carbon 9Cr steel, and SAVE 12AD are ferritic steels for use at temperatures below 650°C (1200°F). These materials are being tested to verify their characteristics regarding creep rupture, fatigue, oxidation, and corrosion. Welding and bending tests have been conducted to ascertain the manufacturability of the materials.

HR6W is being developed by Nippon Steel and Sumitomo Metal for pipes and tubes in A-USC applications, with an emphasis on good corrosion resistance to combustion gas in the boiler and good creep strength for pressurized pipes and tubes at 700°C (1290°F). The 100,000-hr creep rupture stress at 700°C (1290°F) is expected to be about 90 MPa, meeting the program target for large steam piping materials.

In 2015 and 2016, boiler components such as superheaters, pipes, valves, and turbine casing will be tested using an actual boiler.

Turbine Technology Development. Three Ni-based alloys are being developed for use at temperatures higher than 700°C (1290°F), namely FENIX-700, LTES, and TOS1X. Each is expected to meet a target 100,000-hour creep rupture stress at 700°C (1290°F) of about 90 MPa (13,000 psi). Development of FENIX-700 aims to allow building of a rotor heavier than 10 tons without segregation in the material. Both LTES and TOS1X are targeted for weights of about 10 tons, which will be welded to steel parts to make a 30- to 40-ton rotor.

FENIX-700, which has superior long-term stability at 700°C (1290°F), was developed from Alloy 706 by reducing Nb content and increasing Ti and Al content. The 100,000-hour creep rupture strength at 700°C (1290°F) is expected to be higher than 100 MPa (14,500 psi).

LTES700R is a Ni-based alloy developed by MHI. This alloy was developed to have a thermal expansion coefficient similar to 12Cr steel, so it conforms well to conventional steels. In addition, the creep rupture strength of LTES700R is higher than the target for 700°C (1290°F) class rotor material. Originally, LTES700 was developed for small parts, such as casing bolts. LTES700R was developed from LTES700 for large steam turbine rotors. Welding technology is crucial for this material, and numerous tests have been conducted, including the welding of dissimilar materials.

TOS1X was developed from Alloy617. The earlier version of TOS1X, which is now called TOS1X-I, is expected to have approximately 200 MPa (29,000 psi) of 100,000

hour creep rupture strength at 700°C (1290°F). A piece of forged material, 1000 mm (39 in) in diameter and weighing 7 tons, has been made successfully using TOS1X-I. TOS1X-II was developed from TOS1X-I by increasing the Al and Ti content. TOS1X-II is also expected to have about 200 MPa (29,000 psi) of 100,000 hour creep rupture strength at 700°C (1290°F). A 13-ton piece of forged material of TOS1X-II has been made successfully.

Three rotors made of the three candidate rotor materials will be tested in 700°C (1290°F) atmosphere and at actual speed from 2014 to 2016. The rotors will be heated by electric heaters in a vacuum chamber and driven by an electric motor.

China

In 2010, China launched the National 700°C USC Coal-Fired Power Generation Technology Innovation Consortium, an 18-member body consisting of material research institutes, power plant equipment manufacturers, and power companies. The Consortium's R&D plan calls for a ten-year program culminating in a demonstration project.

Target steam parameters are 35 MPa/700°C/720°C (5075 psia/1290°F/1330°F) for a 600 MW unit. The program includes developing indigenous materials as well as modifying imported materials for further enhancement, including optimization of G115 and Inconel 740H.[14]

The Chinese test facility (CTH 700) will be similar to the European ComTes700 but with a two-pass 320 MW boiler. The pressure of the existing boiler will be raised to 25 MPa (3625 psia) and the temperature to 725°C (1340°F). The steam flow rate will be limited to 3 kg/s (6.6 lb/s). The construction of the test loop was scheduled to start in 2014. Test data will be collected for 100,000 hours.

India

A joint A-USC Project consortium between the Indira Gandhi Center for Atomic Research (IGCAR), Bharat Heavy Electrical Limited (BHEL, an equipment manufacturer), and the National Thermal Power Corporation (NTPC, India's largest power generation utility) entails a materials testing program specific to the combustion of Indian coals.

The consortium is working to select materials and develop welding and fabrication technologies, as well as collaborating with national/international institutions to support the A-USC project. They have designed and fabricated a steam loop, similar to the Plant Barry loop, with plans to install it into a boiler in 2014 and operate for two years. The preliminary conceptual design of the boiler is complete. Materials selected for use in the high-temperature zone of the boiler are SS 304HCu and Alloy 617M.[15]

---

[14] Zhang, Dongke, Ed. *Ultra-Supercritical Coal Power Plants: Materials, Technologies, and Optimization,* Elsevier, August 2013.

[15] Gandy, D. and J. Shingledecker, eds. *Advances in Materials Technology for Fossil Power Plants: Proceedings from the Seventh International Conference,* October 2013, Waikoloa, Hawaii.

The consortium envisions building an 800 MW plant with 300 bar/700°C/700°C (4350 psi/1290°F/1290°F) steam conditions with an efficiency target of 46% (HHV basis),[16] over a seven-year timeframe following government approval of funding.

[16] http://www.projectsmonitor.com/daily-wire/india-may-have-advanced-ultra-super-critical-power-unit-by-2021/

2
DESIGN BASIS SPECIFICATIONS

Site Location

The plant is of indoor construction and is located in Kenosha, Wisconsin. The site is clear and level in a Seismic Zero Zone and 30-meters (100-feet) deep pile foundations are required. Available at the site boundary are rail and transmission access, raw water supplied from Lake Michigan, and natural gas is available.

Ambient Conditions

Annual average ambient air conditions shown in Table 2-1 are required to calculate material balances and thermal efficiencies, to develop system designs, and to size equipment.

Table 2-1
Annual Average Ambient Conditions

Site Elevation Above Mean Sea Level	183 m	600 ft
Atmospheric Pressure	1 bar	14.4 psia
Annual Average Ambient Air Dry Bulb Temperature	15.6°C	60°F
Maximum Ambient Dry Bulb Temperature	35°C	95°F
Maximum Ambient Wet Bulb Temperature	23.9°C	75°F
Seismic Zone	0	0

Environmental Requirements

The stack gas emission limits for the unit are listed in Table 2-2:

Table 2-2
Stack Gas Emissions Limits

Pollutants		**Emission Limits (HHV Basis)**
PM_{10}	~10 mg/m^3	0.01 lb/MBtu
$PM_{2.5}$	~13 mg/m^3	0.013 lb/MBtu
SO_2	~30 mg/m^3	0.03 lb/MBtu
NO_X	~30 mg/m^3	0.03 lb/MBtu
VOC	~10 mg/m^3	0.0025 lb/MBtu
Mercury	90% capture	

The permitted levels for wastewater disposal or discharge are shown in Table 2-3. Following treatment, the wastewater complies with the U.S. Environmental Protection Agency (U.S. EPA) Effluent Guidelines and Standards. (Interim Detailed Study Report for the Steam Electric Power Generating Point Source Category, November 2006).

Table 2-3
Wastewater Discharge Permit

Makeup Water	Makeup for potable, process, and de-ionized water are drawn from municipal sources.
Process Wastewater	Water associated with combustion activity and storm water that contacts equipment surfaces is collected and treated for disposal through a permitted discharge.
Sanitary Waste Disposal	Design includes a packaged domestic sewage treatment plant with effluent discharged to the industrial wastewater treatment system. Sludge is hauled off site. Package plant is sized for 1,500 gallons per day.
Water Discharge	Blow-down is treated for pH, chloride and metals. Evaluation of other constituents is needed to determine if additional treatment is required before discharge.

In-plant noise levels must not exceed 90 dBA for an 8-hour exposure. Plant perimeter noise levels must not exceed 65 dBA during the day and 55 dBA at night.

Design Data

Coal Specification

The fuel delivered by rail is Wyoming PRB subbituminous coal, with characteristics detailed in Table 2-4.

Table 2-4
Coal and Ash Analysis for Wyoming Subbituminous Coal

Proximate Analysis Weight, % As Received	
Moisture	30.24
Ash	5.32
Volatile	31.39
Fixed Carbon	33.05
Ultimate Analysis Weight, % As Received	
Carbon	48.18
Hydrogen	3.31
Nitrogen	0.70
Chlorine	0.01
Sulfur	0.37
Oxygen	11.87
Ash	5.32
Moisture	30.24
Heating Value, As Received	
HHV, kJ/kg (Btu/lb)	19,400 (8340)
LHV, kJ/kg (Btu/lb)	17,900 (7710)
Ash Softening Temperature for Reducing Conditions	
°C (°F)	1190 (2170)
Ash Mineral Analysis Weight %	
SiO	31.38
Al_2O_3	15.12
TiO_2	1.11
Fe_2O_3	5.36
CaO	23.56
MgO	4.68
Na_2O	1.48
K_2O	0.31
P_2O_5	0.86
SO_3	14.67
Undetermined	1.46

Limestone and Reagents

The nominal design composition of the limestone to be used in the FGD is shown in Table 2-5.

Table 2-5
Limestone Design Composition

Design Limestone Analysis, wt. % (as received)	
$CaCO_3$	94.1
$MgCO_3$	3.3
SiO_2	0.6
Water	2.0
Balance	0.0
Total	100

Water Source and Wastewater

The raw water for the cooling tower makeup is from Lake Michigan with a typical quality shown in Table 2-6. The distance from the plant to the raw water source is assumed to be 0.8 km (0.5 mile.

Table 2-6
Raw Water Quality for Cooling Tower Makeup

	mg/l	mg/l $CaCO_3$
Silica (SiO_2)	6.8	—
Calcium (Ca)	76.0	189.0
Magnesium (Mg)	16.0	66.0
Sodium (Na)	20.0	44.0
Potassium (K)	2.9	3.7
Bicarbonate (HCO_3)	246.0	202.0
Sulfate (SO_4)	56.0	58
Chloride (Cl)	26.0	37.0
Nitrate (NO_3)	6.9	5.6
Total dissolved solids	457.0	—
Total hardness	—	255.0
pH	8.0	
Ionic strength (meg/l)	9.2×10^{-3}	
Temperature range, °C (°F)	5–27 (40–80)	

Potable water and makeup water for process and de-ionized water for the plant facility is drawn from municipal sources. The distance from the plant to the tie-in point is assumed less than 1.5 km (1.0 mile). The municipal water quality is assumed to be the same as the raw water presented above.

Plant Operating Criteria

Duty

The plant operates primarily as a base-load unit, with infrequent stop-start cycles. It is designed with reliability features to minimize forced outages and achieve high availability.

Capacity Factor

The PC plants have an annual capacity factor of 80%. Annual capacity factor is defined as the actual annual production divided by the plant rated capacity times 8760 hours.

Plant Design Life

The plant design is based on using components suitable for a 30-year life, with provision for periodic maintenance and replacement of critical parts.

Mechanical Design Criteria

This section establishes the criteria for the mechanical design of the PC power plant components and systems.

Boiler Description

The Boiler Island scope and general design basis are summarized below.

- Greenfield, balanced-draft unit fired with subbituminous coal, and designed for base-loaded operation with 30-year life.
- The gross power of the steam turbine is 825 MW without CCS.
- Low-NO_X axial-swirl burners with over-fired air and SCR are used to achieve emission limits of 30 mg/m^3 (0.03 lb/MBtu).
- The steam conditions entering the HP turbine are 242.3 bar (3515 psia) and 732°C (1350°F). The reheat temperature is 760°C (1400°F).
- The steam piping pressure drop and attemperation assumptions are shown in Table 2-7.

Table 2-7
Steam Piping Pressure Drop and Attemperation Assumptions

Feedwater heater outlet to the boiler inlet	0.5%
Through the economizer, boiler and superheater	8%
Main steam from the boiler outlet to the turbine inlet	6%
Cold reheat, exiting the turbine to the boiler inlet	2%
Reheat steam through the boiler	4%
Hot reheat steam from the boiler outlet to the turbine	2%
Loss from the IP turbine to the LP turbine	<1%
Superheater uses two-stage attemperation, % of BFW used for attemperation	4%

- There is a separator, recirculation pump and start-up system, and economizer.
- A bottom-ash system (submerged chain conveyor) to remove ash from the hopper throat feeding it into a water-filled trough.
- Soot-blowing system and mechanical draft cooling tower.
- Single fans for FD and PA.
- Seven operating coal mills are installed at the side of the furnace.
- The main design performance data of the A-USC boiler are summarized in Table 2-8. Selection of main and reheat steam pressure and temperature are described in Section 6.

Table 2-8Table 2-8
Summary of Boiler Performance

	Main Steam
Flow, kg/h x 10^3 (lb/h x 10^3)	1818 (4008)
Temperature leaving boiler °C (°F)	733 (1352)
Pressure leaving boiler, bar (psia)	347 (3585)
	Reheat Steam
Flow, kg/h x 10^3 (lb/h x 10^3)	1563 (3375)
Temperature leaving boiler °C (°F)	760 (1400)
Pressure leaving boiler, bar (psia)	51 (740)
	Feedwater
Temperature entering boiler °C (°F)	305 (580)
Pressure entering boiler, bar (psia)	273 (3865)
	Heat Duties
Heat to Main Steam, MW, (MBtu/hr)	1293 (4412)
Heat to Reheat Steam, MW (MBtu/hr)	285 (972)
Total Heat to Steam, MW (MBtu/hr)	1567 (5348)

Boiler Efficiency, %	86.6
Heat In Fuel, HHV, MW (MBtu/hr)	1822 (6218)
Fuel Fired, kg/hr (lb/hr)	338,000 (746,000)
CO_2 Emission without PCC, kg/hr (lb/hr)	596,000 (1,313,000)

Figure 2-1 and Figure 2-2 are diagrams depicting the hot flue gas and steam/water flows, temperatures, and pressures calculated by the AspenPlus™ model of the steam generator in U.S. Customary and SI units, respectively. Figure 2-3 presents the general process flow diagram of the boiler island. Appendix A contains the heat and mass balance information for Case 1 and Case 2.

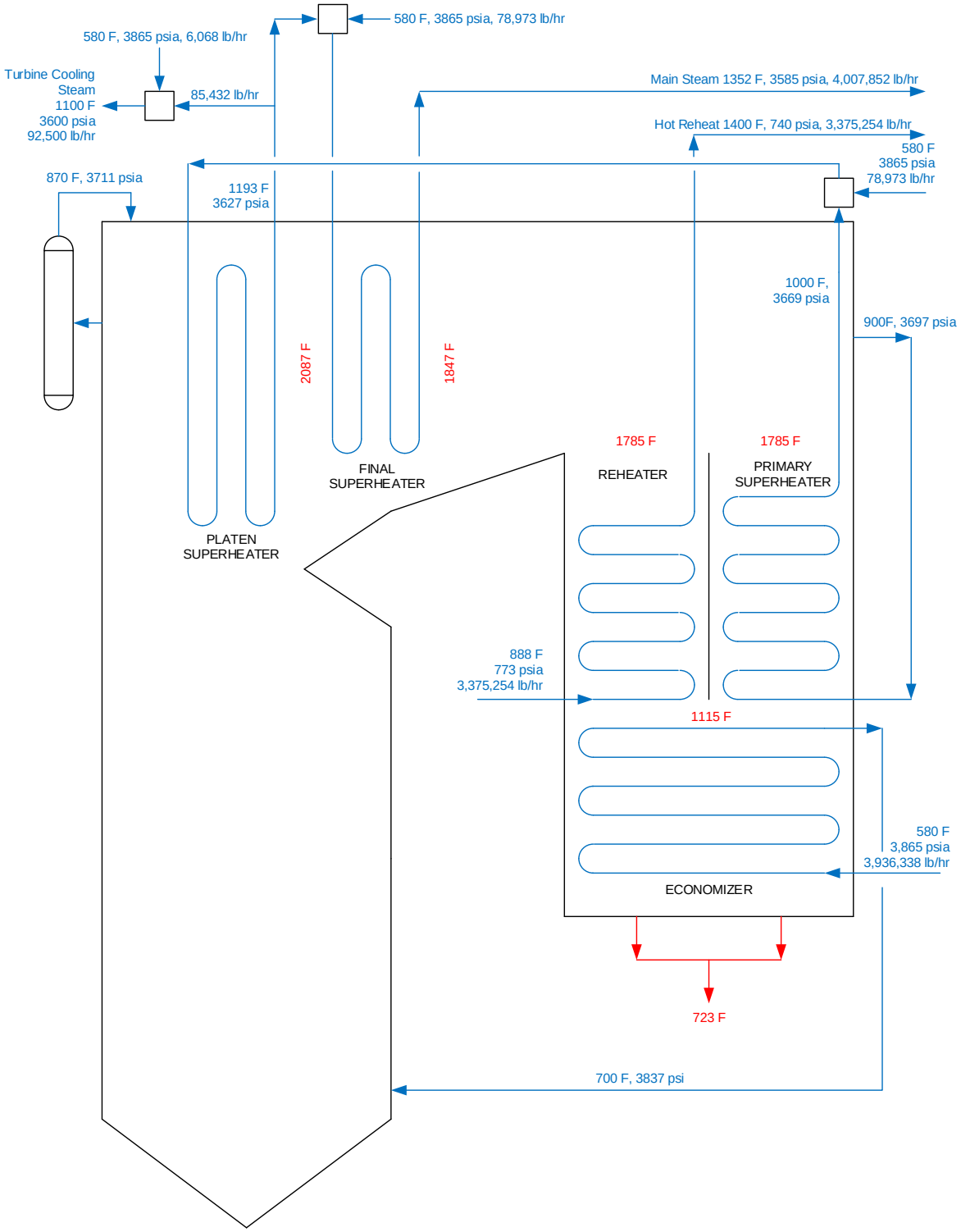

Figure 2-1
Flows, Temperatures, and Pressures through the Boiler (U.S. Customary Units)

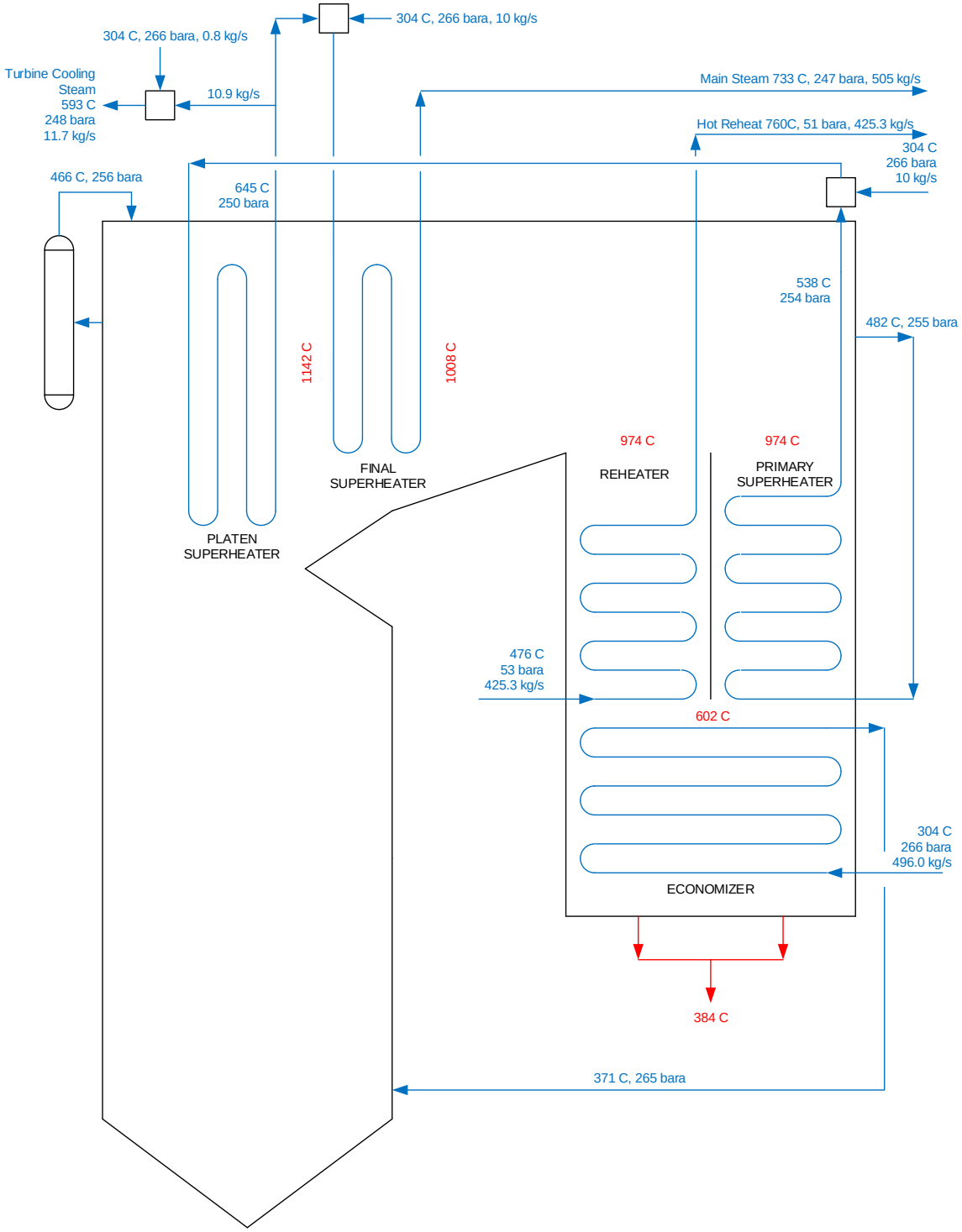

Figure 2-2
Flows, Temperatures, and Pressures through the Boiler (SI Units)

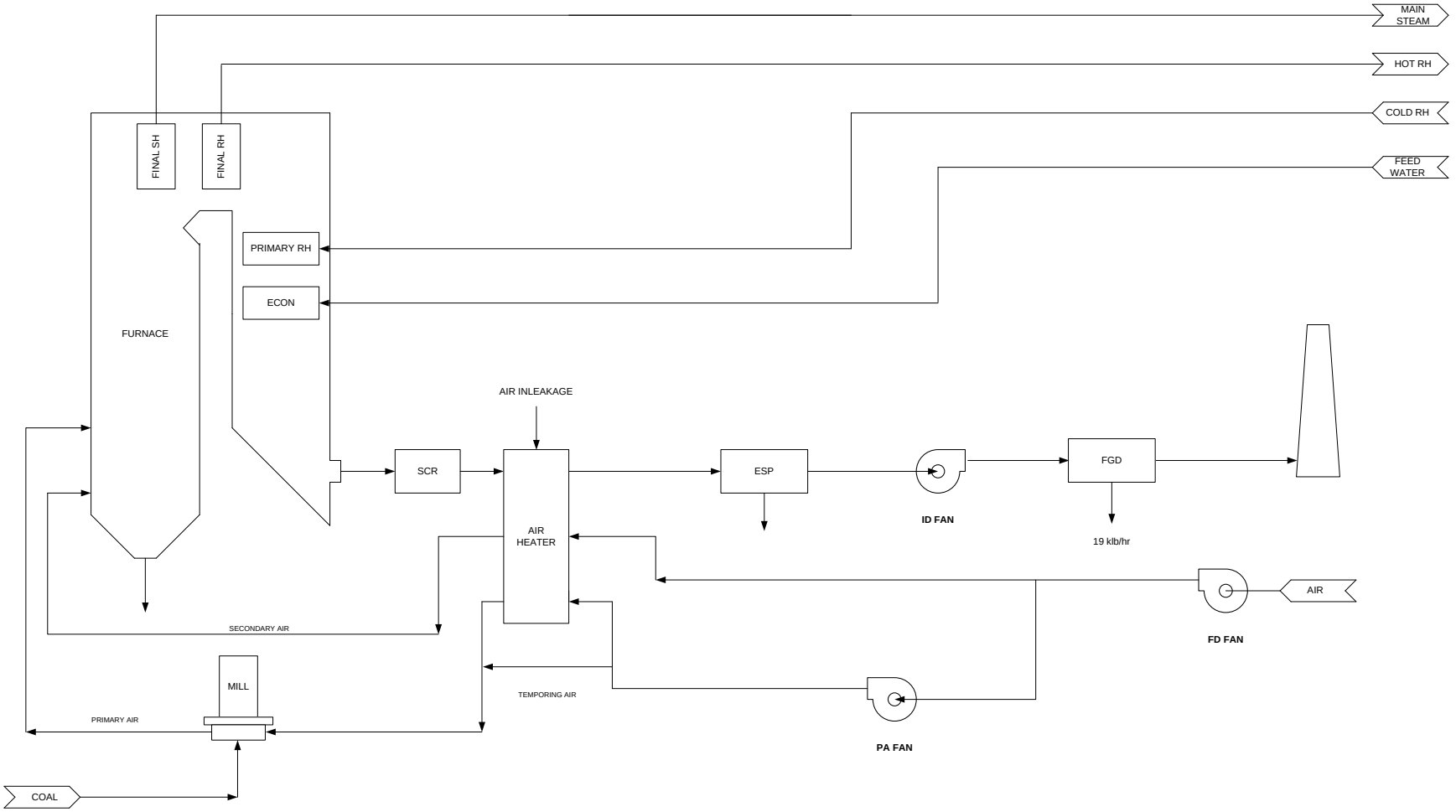

Figure 2-3
Boiler Island Process Flow Diagram

FD and PA Fans

One axial-flow FD fan with variable-pitch blade control provides the combustion air. The air is drawn from within the boiler house to make use of the heat lost from the boiler surfaces and to assist with ventilation and cooling. The fan is selected with sufficient margins on volume and pressure to meet all specified modes of operation.

Likewise, one axial-flow PA fan with variable-pitch, blade control draws air from the FD fan discharge to dry the coal in the mills and convey it to the burners. The fan is selected with sufficient margins on volume and static head to meet all specified modes of operation.

Air from the FD fan is split into the primary and secondary air streams, both of which are preheated in the regenerative air heater before passing to the furnace. A booster fan passes the PA to the milling plant to dry the coal before it is pulverized and conveyed to the burners for combustion.

Heat released in the furnace is transferred to the steam-water circuits providing evaporative, superheat, and reheat duty. Exhaust gases from the economizer pass through the SCR unit and enter the regenerative air heater, where the final extraction of heat from the flue gas takes place to preheat the primary and secondary air streams. The ESP downstream of the air heater removes fly ash entrained in the flue gas, followed by an FGD plant that removes the majority of the SO_2. The scrubbed flue gas in the non-PCC design (Case 1) is discharged to the atmosphere via the stack.

Air Heater

The design for PRB coal targets an outlet flue gas temperature of approximately 130°C (265°F). It is assumed in this model that air in-leakage of 10% occurs in the air heater.

Coal Mills (Pulverizers)

The “milling plant” comprises the vertical mills together with associated bunkers, coal feeders, outlet chutes, PC pipe work, and seal air fans. Part load is achieved by turning down the mills and shutting off burners. One mill supplies all the burners at a single elevation (front and rear wall), with each burner supplied by its own PC pipe from the mill outlet. The mill inlet air temperature is controlled by air bypassing the regenerative air-heater as shown in Figure 2-3.

Condenser and Cooling System

Wet mechanical draft cooling towers are used to provide cooling water for the condenser and other heat loads. The cooling water design conditions are shown in Table 2-9:

Table 2-9
Cooling Tower Design Conditions

	Max Summer 35°C (95°F)	Avg. Ambient 16°C (60°F)
Maximum Supply Temperature, °C (°F)	29.4 (85)	22.2 (72)
Maximum Return Temperature, °C (°F)	38.8 (100)	As calculated
Minimum Supply Pressure, bara (psia)	3.8 (55)	3.8 (55)
Return Pressure Drop, bara (psi)	2.75 (40)*	2.75 (40)*

(*) Minimum return pressure at grade at the cooling tower is 1.5 bar, a (30 psia). Value shown represents minimum at PCC battery limit which included 0.7 bar (10 psi) return header pressure drop allowance.

Air Quality Control System

The AQCS design is developed to achieve the emission levels tabulated below.

Pollutant	Emission Levels mg/m^3 (lb/MBtu)	Emission Intensity kg/MWh (lb/MWh)
PM_{10}	10 (0.010)	0.038 (0.08)
$PM_{2.5}$	13 (0.013)	0.045 (0.10)
SO_2	30 (0.03)	0.11 (0.24)
NO_X	30 (0.03)	0.11 (0.24)

The AQCS technologies used are summarized below.

NO_X control	SCR (included in boiler island)
Particulate removal, PM_{10}	ESP
SO_2 removal	Wet FGD
Mercury capture	Halogen injection into boiler promoting mercury oxidation over SCR catalyst with co-capture in FGD. Possible supplemental capture using activated carbon injection ahead of ESP.

Condensable particulate emissions, $PM_{2.5}$, are primarily SO_3, and are calculated based on the system chemistry. For the PRB coal, the uncontrolled $PM_{2.5}$ emissions are estimated to be 18 mg/m^3 (0.018 lb/MBtu), and a wet FGD typically achieves 30% removal, reducing $PM_{2.5}$ emissions to 13 mg/m^3 (0.013 lb/MBtu).

SCR System

The SCR is designed to reduce NO_X to 30 mg/m^3 (0.03 lb/MBtu) at full load, and 25% Benson load operating conditions. A single SCR reactor is mounted between the economizer outlet and the regenerative air heater gas inlet. The reactor is orientated for

downward flue gas flow and incorporates two catalyst layers for initial loading, with space for the addition of a further layer to facilitate catalyst management.

The reagent is liquid anhydrous ammonia pumped from storage tanks to 2 x 100% vaporizers, and then injected into dilution air from dedicated fans.

Mercury Control

Because oxidized mercury (Hg^{2+}) is soluble, a large percentage of it is absorbed in the wet FGD. Conversely, because elemental mercury (Hg^{0}) is insoluble, the wet FGD does not capture it effectively. The oxidation state of the mercury entering the FGD has been found to be strongly dependent on the coal chemistry and system configuration.

SCR catalysts are designed to reduce NO_X but also have the dual function of oxidizing mercury. This can be a significant co-benefit because SCR installed upstream of an FGD can result in a higher overall mercury capture. Halogens promote the oxidation reaction and capture of mercury in the FGD.

To compensate for the low halogens in subbituminous coal, bromine can be introduced directly into the furnace or into the flue gas stream to promote oxidation and enhance mercury removal in the FGD.

Re-emission of up to 15% of the mercury captured in the FGD has been observed, but this can be nearly eliminated by the use of suitable additives, as included in the current design.

If 90% mercury capture cannot be achieved by the above steps, sorbent injection ahead of the ESP can be utilized as a polishing stage. Only small quantities of sorbent are required for this purpose. However, the fly ash collected by the ESP now contains captured mercury, and EPA rulings state that this material can no longer be used in cement kilns due to the re-emission of the captured mercury.

Electrostatic Precipitators

The ESP components included in the design are:

- Gas distribution devices
- Collecting system
- Collecting plate rappers
- High-voltage system
- Discharge electrodes
- Insulator compartments
- Discharge electrodes rappers
- Control system

FGD System

The limestone slurry contacts the flue gas in the FGD absorber to remove the SO_2. A generic spray tower design is used, although several alternative designs are available. Gypsum generated in the process can easily be disposed of on site.

The flue gas exits the ID fans and is ducted to the vertical up-flow spray tower absorber. The hot flue gas enters the lower portion of the tower through the inlet nozzle, turns upward, and flows counter-currently through multiple levels of spray headers and associated nozzles. The scrubbing slurry cools the flue gas to the adiabatic saturation temperature at which the SO_2 is absorbed.

The cleaned flue gas enters the vertical flow, two-stage mist eliminator section located in the absorber flue gas exit, which removes carryover mist by inertial contact. The mist eliminator consists of a primary stage for capturing large particles and a secondary stage for capturing wash water droplets and finer particles. Both stages are kept free of slurry deposits by a water-wash spray system directed to the upstream and downstream faces of the first stage and the upstream face of the second stage. The cleaned flue gas then exits the absorber and enters the chimney designed for wet operation.

The slurry falls into the reaction tank located at the base of the tower, where injected air completes the scrubbing reaction by oxidizing the calcium sulfite into calcium sulfate (gypsum). Agitators in the tank ensure the air and slurry are well mixed and that the solids remain in suspension.

Recycle pumps taking suction from the reaction tank pump the slurry to the headers and nozzles in the spray tower for further reaction with the flue gas. The absorber has a spare recycle pump and associated header. This can be brought into service to increase SO_2 capture if so required.

Limestone slurry from the Limestone Preparation System is added to the reaction tank to neutralize and regenerate the scrubbing slurry. A bleed system removes the appropriate amount of slurry from the reaction tank to maintain process equilibrium. The absorber has two bleed pumps (one operating and one spare) to transfer slurry to the gypsum dewatering and storage facility.

Limestone Handling

Limestone for the FGD system is received by trucks that unload directly onto the uncovered storage pile. The limestone is moved by dozer to the platform reclaim conveyor that transports the limestone to the crusher. A series of conveyors delivers the crushed limestone to one of two storage silos. Dust collection devices are installed in the vicinity of the crusher, transfer locations, and on the limestone silos.

Limestone Preparation

Belt feeders deliver the crushed limestone from the storage silos to 2 x 100% capacity horizontal wet, ball-mill grinding systems, one in operation and on standby. Before entering the mills the limestone is mixed with process recycle water. The ground limestone passes into the mill slurry tank and exits at the opposite end of the mill to be pumped to hydrocyclones that remove the coarse limestone. The underflow, containing the larger particles enters a distributor box and flows by gravity to the ball mill to be reground. The overflow containing the fine slurry with 30% solids passes to a distributor box and flows by gravity into the reagent storage tank. Slurry pumps transport the limestone slurry to the absorber reaction tank based on a demand signal from the absorber.

Gypsum Dewatering

The solid waste handling system is designed to accommodate the collection of FGD byproduct gypsum from the boiler and transport it off-site for disposal. It is assumed that there is no resale value for the FGD byproduct. The system receives slurry containing approximately 15% solids from the FGD system absorber bleed pump and produces a gypsum product containing 85% solids.

The bleed slurry is pumped in a continuous loop to the hydrocyclones located adjacent to the absorber. An on/off valve, controlled by density, admits slurry to the hydrocyclones for initial separation of the gypsum from the water. The underflow containing 50% solids flows by gravity to a tank located adjacent to the absorber and is then pumped to a surge tank located in the gypsum dewatering area. To prevent solids settling, all tanks are furnished with an agitator. The partially dewatered slurry is pumped to the vacuum belt filters to dewater the gypsum, which is discharged onto a transport conveyor and sent to either of two uncovered storage piles near the dewatering building. The filtrate is pumped to the filtrate tank and returned to the absorber and reagent preparation systems for process use.

Balance of Plant

Raw Coal Receiving, Storage, and Handling

This system unloads, conveys, prepares, and stores the coal delivered to the plant. The scope of the system is from the rotary car dumper and coal receiving hoppers to the pulverizer fuel inlets.

The PRB coal is delivered to the site by unit trains of 100-ton rail cars. Each unit train consists of 100, 100-ton rail cars. The unloading is by a rotary dumper, which unloads the coal to two receiving hoppers. Coal from each hopper is fed directly into a vibratory feeder. The 150 x 0 mm (6 x 0 inch) coal from the feeder is discharged onto a belt conveyor. The coal is then transferred to a second conveyor that transfers the coal to the reclaim area. The conveyor passes under a magnetic plate separator to remove tramp iron, and then to the reclaim pile.

Coal from the reclaim pile is fed by two vibratory feeders, located under the pile, onto a belt conveyor that transfers the coal to the coal surge bin located in the crusher tower. The coal is reduced in size to 75 x 0 mm (3 x 0 inch) by the first of two coal crushers. The coal then enters a second crusher that reduces the coal size to 25 x 0 mm (1 x 0 inch). The coal is transferred by conveyor to the transfer tower. In the transfer tower the coal is routed to the tripper, which loads the coal into one of the coal silos.

Solid Waste Handling Systems

Fly Ash Handling

This system is designed to collect fly ash from the ESP and transport it for disposal. On-site emergency ash storage is sized for 90 days. The final disposal is off site.

Other Ash Handling

The bottom ash handling system is designed to collect ash from the boiler and transport it for disposal.

The economizer ash handling system is designed to collect the ash from the economizer and transport it for disposal.

On-site emergency ash storage is sized for 90 days. The final disposal is off site.

Control Systems

Each of the systems comprising the A-USC PC power plant contains the instrumentation necessary to monitor the critical operating parameters. Each of the systems is controlled by a digital control system (DCS) that is integrated with an overall plant DCS to result in efficient and safe operation of the plant processes.

Electrical System

This system consists of the equipment necessary to receive and distribute power to the electrically driven components and building support systems in the PC power plant. It includes station service equipment, switchgear and motor control centers, conduit and cable trays, wire and cables, protective equipment (grounding, cathodic protection, etc.), and standby equipment.

Project Transportation Size Limitations

Overland Transportation Size

The maximum overland transportable dimension is 35 m (100 ft) long by 4.5 m (15 ft) wide by 4.5 m (15 ft) height (including carriage height). Maximum equipment height is 4.1 m (13.5 ft) assuming using 0.45 m (1.5 ft) height low-boy carriage. Maximum overland transportable weight is 109 tonnes (120 tons).

Barge Transportation Size

Although there is no maximum barge transportation size limitation, the project site is 10 km (6 miles) inland from Lake Michigan and thus overland transportation from the dock to job site is required. Maximum permissible barge transportation size may be restricted and will need to be reviewed on a case-by-case basis.

3
MODELING METHODOLOGY

The modeling for this project utilizes several resources:

- EPRI's PC Cost is used to size and cost the PC boiler system.
- AspenTech's AspenPlus™ is used to perform the heat and material balance for the PC boiler system.
- General Electric's in-house software is used for the steam turbine cycle and design.
- The design of the CO_2 capture system in Case 2 is based on EPRI report 3002003740.[17]

Boiler – PC Cost Model

PC Cost is an Excel based spreadsheet costing tool developed by EPRI and its subcontractors that "evolved" for ~25 years. Its purpose is to allow engineers and planners to estimate the conceptual and preliminary costs of subcritical and supercritical PC power plants.[18] It performs heat and material balance calculations and performance calculations for the PC unit based on the fuel specification. It then estimates the cost of the major equipment subsystems by scaling from reference costs. These reference costs are based on budgetary quotes and/or in-house developed quotations for the boiler, turbine, air quality control systems (AQCS), and material handling equipment. These reference costs have been updated periodically over the life of the costing tool. The goal is to provide a ±30% cost estimate for the equipment and materials within the plant boundary, including all the direct and indirect costs for site preparation, earthwork, concrete and structural steel, building construction, major equipment, auxiliary equipment, piping, electrical/instrumentation/control equipment, construction labor, bulk materials, and subcontractors.

Sizing of the PC furnace is performed using proprietary methods. PC Cost then sizes the backpass of the boiler using conventional heat transfer methods to determine the surface area. The temperature and pressure of the steam/water is used to determine the wall thickness of the tubes and tube weights. The cost is determined from unit costs for the boiler components.

For the other plant equipment, the costs are scaled from reference plant costs using industry-accepted algorithms.

---

[17] *EPRI's Best Integrated Coal Plant with Post-Combustion Capture Case Study*. EPRI, Palo Alto, CA: 2015. 3002003740.

[18] Hoskins, Bill (URS) and Booras, George (EPRI), "Assessing the Cost of New Coal-Fired Power Plants," *Power Magazine*, October 2005, pp 24-28.

Modifications to PC Cost

In 2011, EPRI began developing a version of PC Cost to allow for the evaluation of A-USC PC units. Several modifications were implemented during this transition:

- It was decided to create a version of PC Cost that used AspenTech's AspenPlus™ to perform the majority of the heat and material balance calculations.
- To determine the cost of the boiler, PC Cost has to first calculate the weight of the individual boiler components (superheater, reheater, etc.). Using the operating conditions, PC Cost calculates a tube metal temperature and then based on an assumed tubing material calculates a wall thickness. To accommodate A-USC boilers, a wider range of alloys were included including nickel based alloys.
- In the original PC Cost, the individual sections of the boiler are made from only one material. A modification was made to allow materials to be chosen based on the estimated metal temperature of an individual row of tubes (perpendicular to the flue gas flow). This approach is described in more detail below.

AspenPlus™ HMB Model

PC Cost assumes a boiler configuration to perform its heat transfer calculations. This configuration and the corresponding AspenPlus™ model are shown in Figure 3-1. For both cases, the steam turbine heat balance was developed by GE and the steam/water flows were used as inputs to the PC Cost model. A temperature profile for the steam/water is assumed through the boiler backpass, and the enthalpy rise across each section is calculated and summed to estimate the coal and air flows. AspenPlus™ then calculates the heat and material balance and the flow rates, temperatures, pressures.

One key parameter for sizing the heat transfer surface in the backpass of the boiler is the temperature exiting the furnace. PC Cost uses proprietary algorithms for determining this temperature based on coal ash analysis and correlations for estimating the slagging properties of the coal as well as its corrosion and erosion potential.

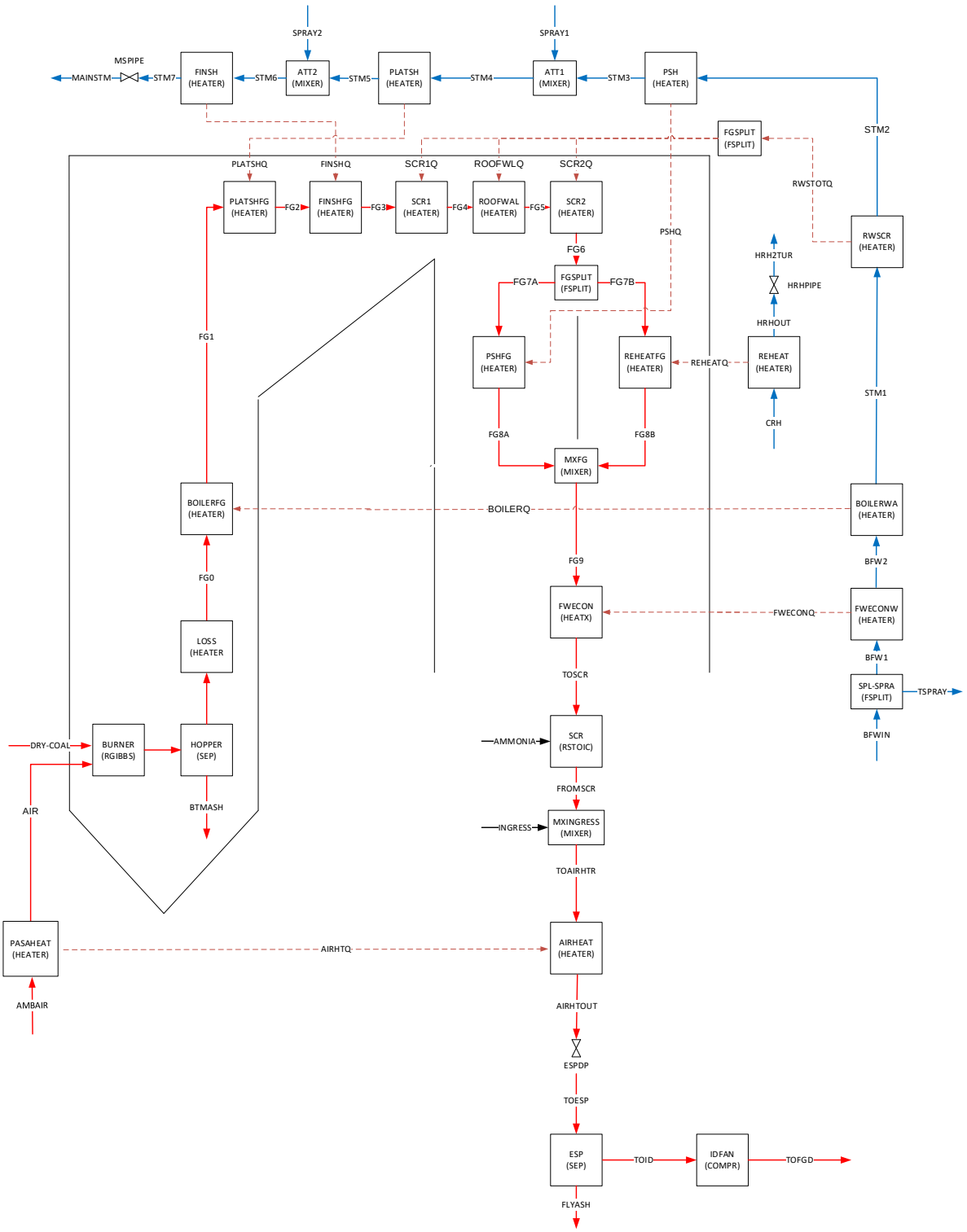

Figure 3-1
Original PC Cost Boiler Configuration

Heat Transfer Calculations

The assumed temperature profile of the steam/water circuit through the boiler set the enthalpy of the fluid at the inlet and outlet of each boiler section. Combined with the flow rate of the fluid, this determined the overall duty for each section of the boiler, and is used to determine the temperature of the flue gas.

AspenPlus™ provided values for the physical properties at the inlet and outlet of each section for the steam and the flue gas, and these values are averaged to calculate the inside and outside heat transfer coefficients. Once the individual heat transfer coefficients are calculated, the overall heat transfer coefficient and the log-mean temperature difference are calculated using standard heat transfer methods. Using this information, the area of each boiler section can be calculated.

PC Cost uses proprietary calculations based on the coal ash properties and the heat input to the furnace to determine the furnace dimensions (depth, width and height). This set the width of the convective pass. The height of the convective pass is set by the flue gas conditions and ash properties entering the finishing superheater (FSH).

Selection of Boiler Materials

In the original version of PC Cost only two materials are used for the boiler sections—carbon steel and T91. In the A-USC version of PC Cost, the following materials were added to the program to accommodate the higher steam temperatures:

- Austenitic stainless steels: Super 304H, HR3C, and HR6W
- Nickel alloys: IN617, HR230, and IN740

For A-USC cases, PC Cost was modified so that material selection within a boiler section is based on local design conditions, hence allowing the most appropriate material to be selected and minimize costs. The following approach is used for each section of the boiler:

- From the heat transfer calculations for a section, the total surface area, the tube OD, the tube spacing, and the convective section height and width are determined.
- Based on the total surface area and the tube OD, the total required length of tubing can be calculated.
- Using the height of the convective section as the length of a single tube, the number of tubes in a section can be calculated.
- The tube center-to-center spacing of the convective section is based on the design flue gas velocity. Using this spacing, the number of tubes in a row perpendicular to the flue gas flow was calculated. Each of these rows represents a “platen.”
- From the total number of tubes calculated and the number of platens, the number of tubes in each platen parallel to the flue gas flow was calculated.
- To simplify the calculations, it was assumed that the steam temperature increase and flue gas temperature decrease are linear as they pass through the convective section. It was also assumed that the temperature distribution was uniform across the width of the convective section (perpendicular to the gas flow). For each row, the inlet and outlet flue gas temperatures were used to calculate an average flue gas

temperature. Likewise, the inlet and outlet steam temperatures were used to calculate an average steam temperature for each row. These values as well as the heat transfer coefficients were used to calculate a tube wall metal temperature.

- A temperature margin of 28°C (50°F) was added to this metal temperature to set the design metal temperature for the row being evaluated. For the design pressure, the pressure of the steam entering this section of the boiler is multiplied by 1.25.
- For each of the alloys being evaluated the program calculated the allowable stress at the design temperature based on the values in the ASME Boiler and Pressure Vessel code. If the design temperature is greater than the temperature allowed by Code for a given material, that material is removed from consideration for that row of tubes.
- A tube OD is assumed for each section of the backpass, and a tube wall thickness calculated based on the allowable stress. If the calculated tube wall thickness exceeded 20% of the OD, this material was allowed for this row of tubes. This criterion was set to maintain a reasonable pressure drop.
- From the tube length, diameter, and wall thickness, the weight of a single tube can be calculated. This is multiplied by the material costs utilized for this study.

The unit weight cost of the materials meeting the code design criteria was multiplied by the tube weight for a single tube, and the lowest cost material was chosen. It is assumed that this material was used for all of the tubes in a row perpendicular to the flue gas flow.

Steam Tubing and Piping

The material selection method for the steam piping was similar to that of the tubing. First, PC Cost assumed a velocity of 61 m/s (200 ft/sec) for the steam in the piping. Based on the volumetric flow rate of the steam and this assumed velocity, the inside cross-sectional area and the pipe ID are calculated.

The pipe wall thickness is calculated using an approach similar to the tubing approach discussed above. If the wall thickness for a selected material is greater than 20% of the tube OD, then the material is not allowed for the pipe. The same material unit weight costs are used to calculate the cost per meter of pipe. The material with the lowest cost is used for the design.

Auxiliary Loads

For the fans and pumps, the motor power is calculated from AspenPlus™ based on the flow rate calculated in the Heat and Material Balance (HMB). Values in the Boiler Island not calculated by AspenPlus™ (mill power, for example) are ratioed from values reported in EPRI report 1015699[19] based on the calculated flow rates.

[19] *Engineering and Economic Evaluation of 1300°F Series Ultra-Supercritical Pulverized Coal Power Plants: Phase 1*. EPRI, Palo Alto, CA: 2008. 1015699.

Pump load and condenser duties for the steam turbine and feedwater system are calculated by AspenPlus™.

Steam Cycle Modeling

The steam cycle design and corresponding steam turbine configuration were modeled entirely through the use of General Electric's internally developed turbine design and thermodynamic heat balance modeling tools. GE steam turbine efficiencies are determined using precision field test results, laboratory analysis, and comprehensive aerodynamic modeling. Turbine efficiencies presented in this report are consistent with GE's current quoting practices and are representative of a cycle-specific turbine design. Development of the preliminary steam turbine thermodynamic design adhered to all GE design practices.

4
CASE 1: PERFORMANCE RESULTS WITHOUT CO_2 CAPTURE

Steam Turbine

One of the largest barriers to the potential market penetration of A-USC steam turbine technology is the expense associated with the nickel alloy materials necessary for such high temperature service. GE has therefore focused on developing a steam turbine design which reduces the need for high temperature material application and, subsequently, unit cost. This study assumes a tandem-compound four casing machine with a single flow high-pressure (HP) turbine section, a single flow intermediate-pressure (IP) turbine section, and a four flow two casing low-pressure (LP) turbine design. A representation of this turbine layout is shown in

Figure 4-1.

Figure 4-1
Layout of HP, IP, and LP Steam Turbines

High-Pressure Turbine

The HP turbine of the evaluated A-USC steam cycle is a full arc admission single flow steam path contained within a double shell bolted horizontal joint configuration. Based on GE's coal-fired plant steam turbine design experience, the HP section steam path design is an impulse wheel and diaphragm turbine. Over half of the HP stages will require nickel alloy materials to satisfactorily operate at 732°C (1350°F) inlet temperature conditions. An extraction for a feedwater heater above reheater pressure is taken in the second half of the HP steam expansion.

To reduce the cost and manufacturing cycle of this steam turbine section, GE has applied a bolted rotor architecture of individual bucketed disks derived from GE's F-Class gas turbine, in lieu of a single rotor forging design common to most modern steam turbines. This bolted structure allows for smaller nickel alloy material rotor forgings than

either a monoblock or welded rotor design. The material selected for these steam path components is Haynes 282.

The double shell architecture utilizes two HP inner shells. The inlet inner shell is made of the nickel alloy H282. The exhaust inner shell is made of a current state-of-the-art shell alloy. The use of two inner shells of different material localizes and limits the use of the expensive nickel alloy material.

High temperature steam is contained within the HP steam path through the use of an external cooling line which routes high pressure boiler steam, at a temperature lower than 593°C (1100°F) from the steam boiler to the HP inlet steam endpacking through a flow control valve configuration. At sufficient flow rates, cooling steam supplies the entirety of HP inlet seal steam. Cooling flows are expected to be less than two percent of the total boiler flow, eliminate the leakage of high temperature steam, and generate power through the entire HP section, minimizing the associated performance impact. This ensures the majority of the HP inlet endpacking remains below 593°C (1100°F), limiting high temperature alloy material to the HP steam path and initial packing rings adjacent the steam path. Endpacking rotor material with lower temperature capabilities is welded or bolted to the rest of the HP steam path.

Intermediate-Pressure Turbine

Similar in concept to the HP section, the IP turbine of the evaluated A-USC steam cycle is a single flow steam path contained within a double shell bolted horizontal joint configuration. The IP section steam path design is also an impulse wheel and diaphragm bolted rotor construction. Over half of these stages require high temperature-capable materials (H282) to satisfactorily operate at 760°C (1400°F) inlet temperature conditions. An extraction for a feedwater heater is taken halfway through the IP steam expansion.

Similar to the HP section, the double shell architecture employs two inner shells. The inlet inner shell is made of the nickel alloy H282. The exhaust inner shell is made of a current state-of-the-art alloy. The use of two inner shells of different material localizes and limits the use of the expensive nickel alloy material.

The IP exhaust pressure was selected considering steam cycle as well as turbine architecture implications. The IP exhaust pressure is 8.3 bara (120 psia). This pressure is chosen to allow for a single-flow IP steam path. At pressures lower than approximately 8.3 bara, the required active length of the last IP stage presents challenges that require a two-flow IP section design with shorter stage active lengths. This design suffers IP efficiency penalties due to the increased secondary and leakage losses of smaller stage designs and requires roughly twice the expensive high-temperature rotor material to operate at A-USC conditions. Plant value is diminished through both higher costs and poorer performance.

The IP inlet endpacking cooling strategy resembles that used in the HP inlet. High temperature steam is contained within the IP steam path through the use of a cooling line taken off the HP inlet endpacking by a flow control valve configuration. An attemperation line from the HP section exhaust is available, if necessary, to maintain

temperatures below 593°C (1100°F). At sufficiently high flow rates, cooling steam supplies the entirety of IP inlet seal steam. The majority of the IP inlet endpacking remains below 593°C (1100°F), limiting nickel alloy material to the IP steam path and initial packing rings adjacent the steam path.

Low-Pressure Turbine

The four flow, two casing LP turbine applies a 1016 mm (40 inch) high efficiency last-stage bucket that leverages the latest designs used in GE combined cycle products. LP non-margin steam path stages are of traditional wheel and diaphragm impulse construction. As noted in the previous IP turbine description, steam is admitted into the LP section at higher pressures than seen in other A-USC conceptual designs. When considered alongside a 760°C IP section inlet temperature, high LP bowl temperatures require application of a welded rotor, two-casing design to avoid material temperature concerns in the first LP stage. Although costs of this design will increase over a monoblock rotor LP design, the savings in superalloy material reduction from limiting the IP section design to a single flow configuration more than offsets any increased LP section costs.

The LP section contains four or five extractions, depending on cycle inlet pressure, and exhaust conditions evaluated are chosen to reduce the exhaust losses of the applied last-stage bucket configuration.

Cycle Performance Determination

Steam cycle conditions, including reheat pressure, LP inlet pressure, and extraction pressures, were adjusted to increase performance for each cycle within the set of defined design constraints. GE steam turbine section efficiencies were determined using precision field test results, laboratory analysis, and comprehensive aerodynamic modeling. Turbine efficiencies presented in this report are consistent with GE's current quoting practices and are representative of a cycle-specific turbine design.

Table 4-1 summarizes additional steam cycle assumptions that affect modeled plant performance.

Table 4-1
Summary of Cycle Parameter Assumptions

Parameter Description	Value
Main Stop and Control Valves (MSCV) Pressure Drop	2.0%
Combined Reheat Valves (CRV) Pressure Drop	2.0%
Reheater Pressure Drop, Cold Reheat to CRV Inlet	8.0%
Flange Pressure Drop of Feedwater Heater Extractions	3.0%

Steam Cycle Main Inlet Pressure

The length of the steam turbine expansion from HP section inlet to LP section exhaust is a fundamental cycle performance parameter. It is well known that the two big drivers

of Rankine cycle efficiency are main steam pressure and temperature. The current assumption for this study was the establishment of main steam temperature at 732°C (1350°F), with reheat temperature at 760°C (1400°F). Therefore, for a fixed LP exhaust condition and established main steam temperature, raising the main steam pressure was a key consideration for achieving desired objectives related to cycle efficiency and value.

Several steam turbine cycle balance of plant characteristics work against any gains achieved with higher main steam pressure. The increase in boiler feedpump power requirements associated with increased throttle pressure will substantially reduce steam cycle benefits associated with the increase in main steam pressure. An increase in inlet pressure will also reduce the HP steam path efficiency due to the lower inlet volumetric flow and resultant smaller steam path annulus. Selecting an appropriate steam turbine inlet pressure for an A-USC plant first requires balancing these factors to determine the net cycle performance impact.

To determine if increasing inlet pressure adds plant value, performance gains must be considered alongside an evaluation of the additional plant costs required to reach higher inlet pressures. Increasing steam pressure will increase the wall thickness of the boiler tubing and piping materials. At the high temperatures of A-USC conditions, the highest temperature material is Inconel 740, which cost about $100/kg ($45/lb) in mid-2015. Its use increases capital cost significantly as the pressure increases.

As part of this study, GE and EPRI evaluated three steam cycles by varying the main steam inlet pressures: 242 bar (3515 psia), 294 bar (4265 psia), and 346 bar (5015 psia). This assessment concluded that increasing the main inlet pressure above 242 bar (3515 psia) provides a diminishing return in cycle performance, as shown in Figure 4-2. The benefit to net steam turbine thermal efficiency from increasing inlet pressure from 242 bara to 294 bara is over twice that of increasing inlet pressure from 294 bara to 346 bara. Cycle efficiency values in Figure 4-2 are representative, and do not necessarily reflect final heat balance values.

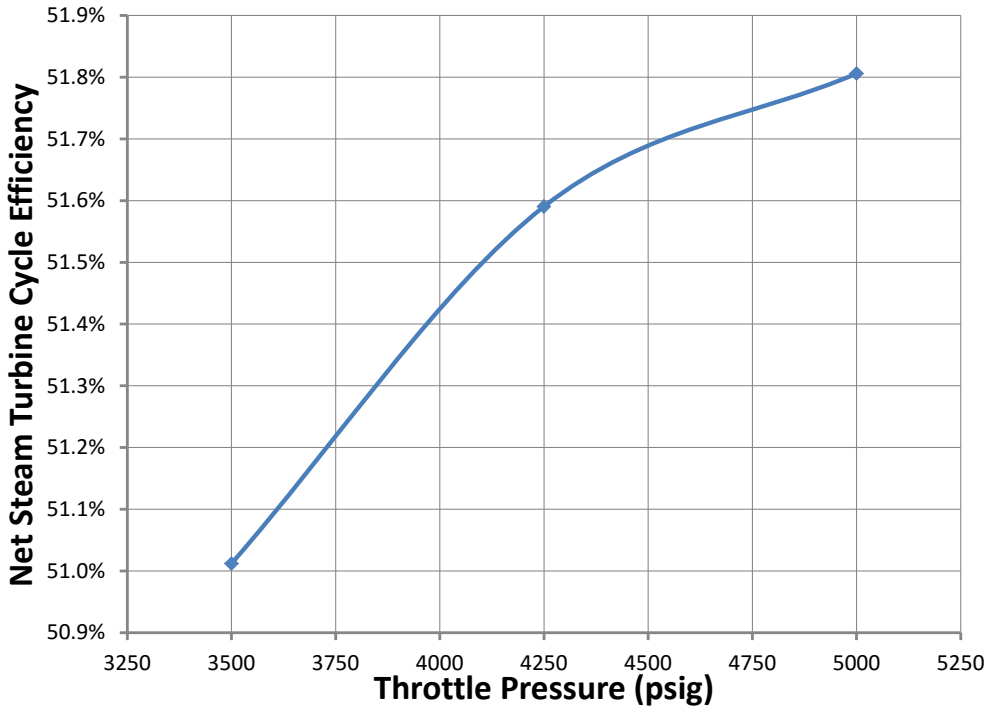

Figure 4-2
Impact of Main Steam Pressure on A-USC Cycle Efficiency

A capital cost increase for each operating pressure above 242 bar (3515 psia) was estimated, and compared to the efficiency improvement. The results are shown in Figure 4-3 and indicate that relative to a 242 bar (3515 psia) unit, the cost increase of the 294 bar (4265 psia) unit was approximately $350,000 per Btu/kWh. The cost increase of the 346 bar (5015 psia) unit was approximately $650,000 per Btu/kWh more than the 242 bar (3515 psia) case. Previous studies and recent commercial experience have shown that a 1 Btu/kWh of heat rate improvement is valued by U.S. utilities in the range of $50,000 to $150,000. As a result, these cost increases are higher than what the U.S. utility industry would traditionally pay for improvements in heat rate. Therefore, it was decided to use the 242 bar (3515 psia) steam cycle as the basis for Case 1.

The analysis showed that the main driver of the cost increases depicted in Figure 4-3 are the boiler, at 45–47%, and the main steam piping, at 17–21% of the cost increase for increased steam pressure.

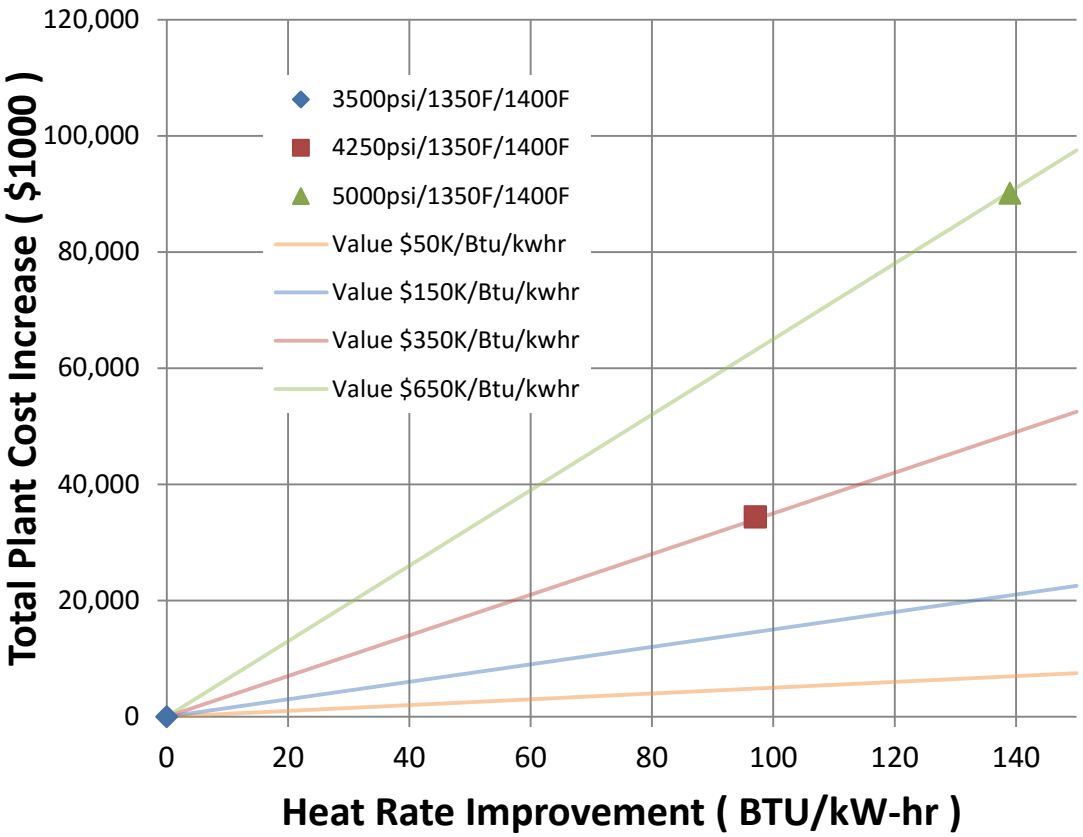

Figure 4-3
A-USC Plant Cost Increase vs. Heat Rate Improvement

This analysis is primarily based on a U.S. utility market for an A-USC PC unit with no carbon capture. In this scenario, the largest component of the LCOE is the capital cost, as shown in Figure 4-4, because a coal price of $1.80/MBtu was used for this study and there is no cost associated with CO_2 removal. For international utilities with high fuel prices, or for U.S. utilities building A-USC units with carbon capture facilities, it may be economic to increase the steam cycle pressure to increase the overall plant efficiency. Case 2 in Section 5 of this report evaluates a higher pressure cycle to determine if the higher cost is offset by the efficiency improvement.

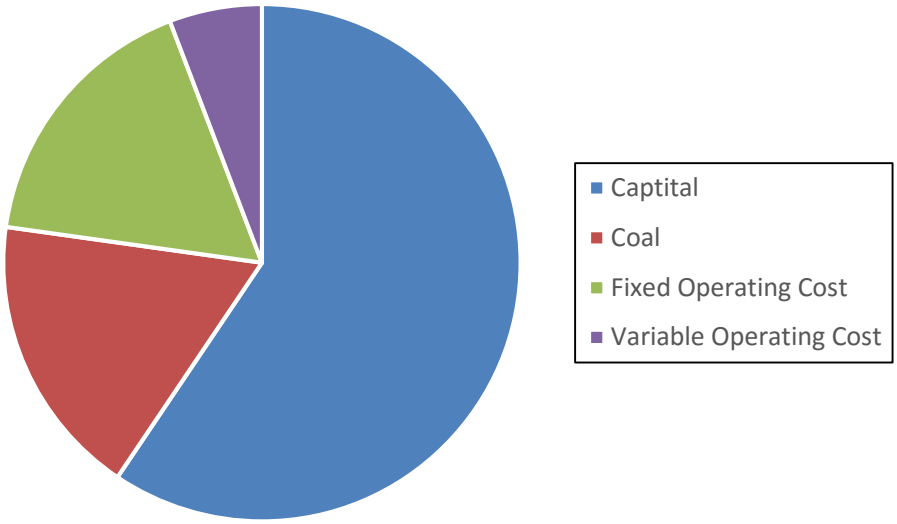

Figure 4-4
Levelized Cost of Electricity, Cost Component Distribution

Condensate System

The function of the condensate system is to pump condensate from the condenser hot well to the deaerator, through the gland steam condenser and low-pressure feedwater heaters. The system consists of the following major components:

- Water cooled condenser
- Three 50% capacity motor-driven condensate pumps
- One 100% capacity condensate polishing system
- One gland steam condenser

The steam from the LP turbine section exhausts into parallel-string condensers. The steam is condensed with cooling water at a maximum temperature of 29.4°C (85°F), and the condenser is designed to operate at 6.7 kPa (2 in-Hg).

The main condensate pumps are correspondingly divided into two sets. The first-stage set overcomes the pressure drop of the condensate polishing plant and the gland steam condenser. The second-stage set includes a booster pump set to overcome the relatively high pressure of the deaerator. A minimum flow recirculation line, discharging to the condenser, is provided to maintain the minimum flow requirement for the gland steam condenser and condensate pumps. A 100% in-line condensate polisher is used at all times to maintain the condensate quality required by the boiler.

Feedwater Heaters

The boiler feedwater heaters consist of LP and HP heater trains. Selected design parameters are presented in Table 4-2, and the steam cycle diagram is shown in Figure 4-5. The main condensate LP heater train is equipped with four heaters, FWH 1 through FWH 4. The deaerator is equipped with a storage tank that provides buffering storage capacity for the boiler feedwater system. The heating steam for the deaerator is from the IP turbine exhaust extraction.

Table 4-2
Feedwater Heater Design Parameters

Name	Type	Terminal Temperature Difference	Drain Temperature Difference
LP Heater 1 - FWH 1	Shell & tube	2.2°C (4°F)	5°C (9°F)
LP Heater 2 - FWH 2	Shell & tube	2.2°C (4°F)	5°C (9°F)
LP Heater 3 - FWH 3	Shell & tube	2.2°C (4°F)	5°C (9°F)
LP Heater 4 - FWH 4	Shell & tube	2.2°C (4°F)	5°C (9°F)
Deaerator	Direct Contact	-	-
HP Heater 1 - FWH 6	Shell & tube	-1.7°C (-3°F)	5.6°C (10°F)
HP Heater 2 - FWH 7	Shell & tube	-1.7°C (-3°F)	5.6°C (10°F)
HP Heater 3 - FWH 8	Shell & tube	-1.7°C (-3°F)	5.6°C (10°F)
Topping Desuperheater	Shell & tube	-	-

The HP heater train consists of three HP feedwater heaters, FWH 6 through FWH 8, and an additional topping desuperheater using extraction from the IP turbine. Due to the relative high degree of superheating, FWH 6, FWH 7, and FWH 8 are equipped with desuperheaters to utilize the extracted steam before condensing. All three HP heaters are equipped with extraction condensate subcoolers. The first extraction on the IP turbine, shortly downstream of the hot reheat, contains a very high degree of superheat. The temperature of this steam is in excess of 611°C (1132°F), but its saturation temperature is only about 215°C (419°F). An additional desuperheater located above the top HP heater can remove most of this superheat before the steam flows to the normal feedwater heater. This configuration will increase the final feedwater temperature with a corresponding decrease in turbine cycle heat rate. This additional heater is simply a shell-and-tube heat exchanger, no different than the desuperheating zone of any other feedwater heater, but it does not contain the condensing and subcooling sections.

The overall unit heat rate decreases with increased final feedwater temperature. The selection of final feedwater temperature was based on steam cycle studies for the selected main steam conditions with consideration of boiler implications. Boiler (economizer) limits on final feedwater temperature were based on requirements on flue gas outlet temperature and the impacts on boiler efficiency.

Boiler Feedwater Pump

Two 50% capacity motor-driven boiler feedwater pumps with booster pumps and hydraulic couplings are selected for the project. Although turbine driven feedwater pumps are more conventional for large supercritical units in the United States, motor-driven feedwater pumps offer several advantages compared to turbine-driven pumps:

- No additional start-up pump required.
- Simplification of plant layout because of less scope and complexity of equipment.
- Smaller impact on the LP turbine design when a large quantity of low-pressure steam is extracted for future use in post-combustion CO_2 capture plants.
- Lower capital cost. This assumes the same size of electrical generators for both configurations. The turbine driven pump configuration may have a relatively smaller electrical generator and main transformer, which will offset the higher capital cost of the turbine.
- Lower operating and maintenance costs.

Because Case 2 incorporates a CO_2 capture plant into the design, it was decided to use a motor-driven pump.

Circulating Water System

The circulating water system consists of two 50% capacity vertical circulating water pumps, a multi-cell mechanical draft cooling tower, and carbon-steel cement-lined interconnecting piping.

Plant Performance

Based on the configuration described in this report, the performance of the power plant without CO_2 removal is presented in Table 4-3. The estimated auxiliary power loads of the plant without PCC are presented in Table 4-4.

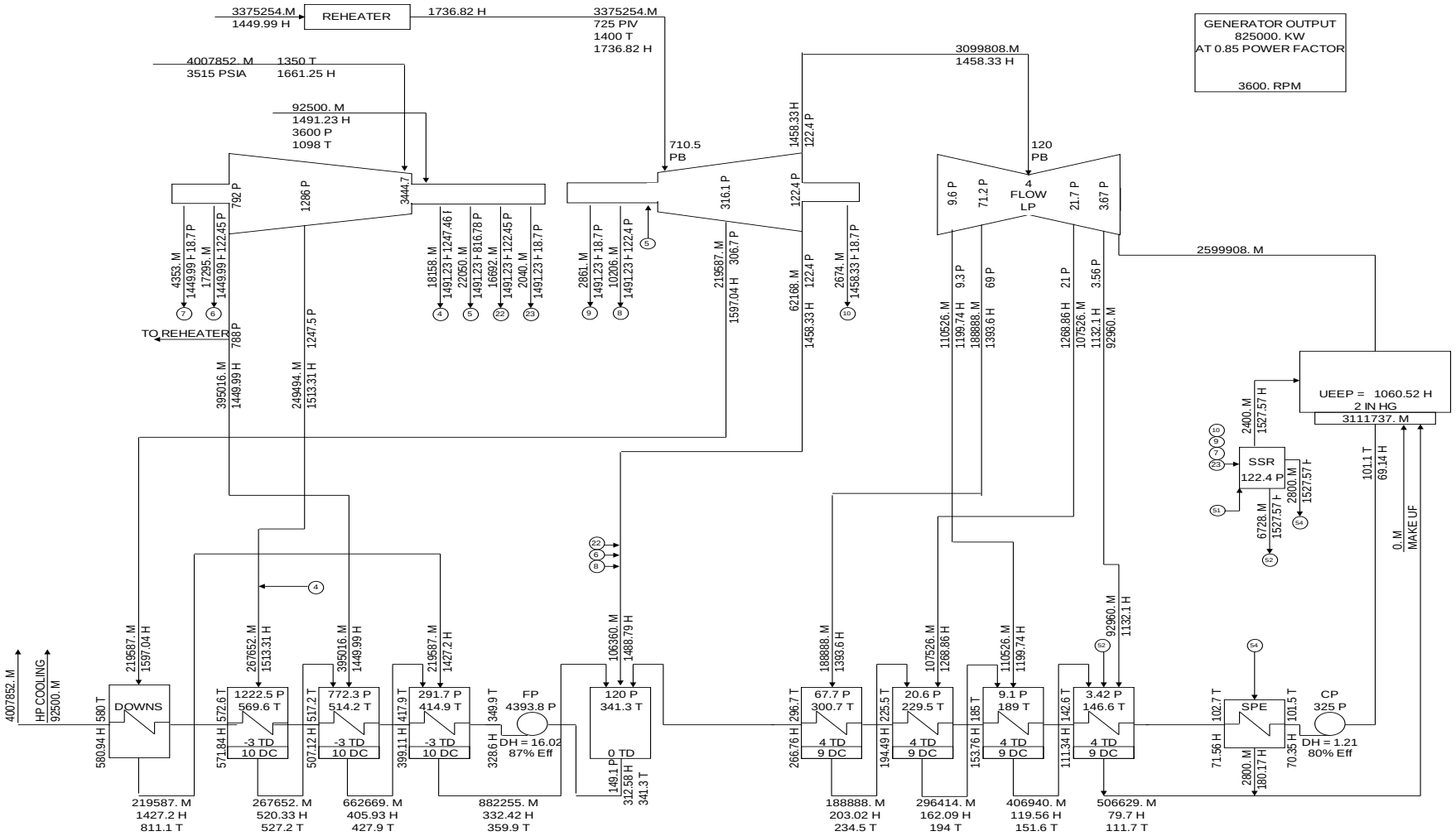

Figure 4-5
3500 psig Steam Cycle Diagram for Case 1

Table 4-3
Summary Performance of the Advanced Ultra-Supercritical Plants without PCC

Description	SI Units	U.S. Customary Units
Feedwater heaters	Five LP, deaerator, three HP, topping desuperheater	
Feed pump drive	Motor	
Cooling system	Mechanical draft cooling tower	
Emission controls	SCR, ESP, Wet FGD, and $CaBr_2$ injection into the furnace for NO_x, particulate, sulfur, and mercury control	
Throttle conditions	242 bar/732°C/760°C	3515 psia/1350°F/1400°F
Main steam flow	1,818,000 kg/h	4,008,000 lb/hr
Hot reheat flow	1,563,000 kg/h	3,375,000 lb/hr
Condenser flow	1,412,000 kg/h	3,112,000 lb/hr
Condenser pressure	6.7 kPa	2 inches mercury
Final feedwater temp	304°C	580°F
Gross plant output, kW	825,000	825,000
Auxiliary load, kW	70,801	70,801
Net plant output, kW	754,199	754,199
Net plant heat rate	8698 kJ/kWh	8244 Btu/kWh
Net plant efficiency, % (HHV)	41.4	41.4
Plant fuel consumption	338,000 kg/hr	746,000 lb/hr
CO_2 emission without PCC	596,000 kg/hr	1,313,000 lb/hr
CO_2 emission without PCC	722 kg/MWh, gross basis	1592 lb/MWh, gross basis

Table 4-4
Auxiliary Loads for the Advanced Ultra-Supercritical Plants without PCC

Equipment	kW
Condensate Pump	1188
Circulating Water Pumps	5262
Motor-Driven Feedwater Pumps	21,263
Pulverizers	3105
PA Fans	1740
SA/FD Fans	2587
Induced Draft Fans	10,783
Ash Handling System	1352
Coal Handling	436
Cooling Tower Fans	6364
Steam Turbine Auxiliaries	695
Electric Static Precipitator	639
Wet FGD System	7906
SCR	208
Water Treatment	496
Miscellaneous Loads (Controls, Lighting, etc.)	2980
Transfer and Cable Losses	2772
Allowance for unknowns	1024
Total Auxiliary Power Consumption	70,801

5
CASE 2: PERFORMANCE WITH CO_2 CAPTURE

Case 2 estimates the performance of the same A-USC plant described in Case 1 but incorporates the CO_2 removal necessary to meet EPA's proposed standard for CO_2 emissions of new coal-fired power plants (section 111(b) of the Clean Air Act). This standard of performance was proposed at 500 kg-CO_2/MWh (1100 lb-CO_2/MWh) on a gross power basis, and was subsequently modified in August 2015 to 636 kg-CO_2/MWh (1400 lb-CO_2/MWh) on a gross power basis. For a PC plant, EPA defines gross power as the steam turbine gross output minus the boiler feedwater pump power. Analyses were conducted using the Case 1 base plant performance values from Section 4 showing the gross steam turbine power is 825,000 kW and the boiler feedwater pump power is 21,263 kW. Thus, for Case 2, the gross power as defined by EPA would be 803,737 kW. To meet the EPA 111(b) limit as originally proposed, the unit would be allowed to emit no more than 401,000 kg/hr (884,000 lb/hr) of CO_2. The CO_2 emitted from the plant in Case 1 was 596,000 kg/hr (1,313,000 lb/hr), so approximately one-third of the CO_2 would have to be removed from the flue gas. Under the modified EPA 111(b) limit, approximately 510,000 kg/hr (1,125,000 lb/hr) of CO_2 would be allowed, and preliminary analyses suggest only about 15% of the CO_2 would have to be removed from the flue gas.

The steam required to regenerate the CO_2 removal solvent is extracted from the LP turbine steam path. Extracting this steam at constant heat input decreases steam turbine gross output. By using significant thermal energy in the PCC system to heat the condensate instead of rejecting it to the cooling tower, less steam needs to be extracted for low pressure feedwater heating and more steam is available to generate power, tempering the output impact of solvent regeneration steam extraction. Both the steam used to regenerate the solvent and the "CO_2 removal waste heat" available are dependent on the amount of CO_2 removed and the CO_2 removed is dependent on the steam turbine gross power, resulting in an. iterative calculation. When heat integration was included, the amount of flue gas required to be treated was 34% for the 500 kg/MWh standard.

The HMB for the PCC system was based on the system presented in EPRI report 1017515[20] with the exception being that the solvent used for this study was a "near-term" solvent that has been evaluated at the National Carbon Capture Center (NCCC). Due to proprietary agreements in place, the name and manufacturer of this solvent cannot be disclosed, and only minimal information about the solvent is available. Using this information, as well as some assumptions based on the performance of typical amine solvent systems, an approximate heat and material balance was developed.

[20] *An Engineering and Economic Assessment of Post-Combustion CO_2 Capture for 1100°F Ultra-Supercritical Pulverized Coal Power Plant Applications: Phase II Task 3 Final Report.* EPRI, Palo Alto, CA: 2010. 1017515.

Process Description

The PCC technology for this case was assumed to be a conventional two column absorber/regenerator scheme as shown in Figure 5-1. To meet the EPA's requirement, only a portion of the CO_2 had to be removed from the flue gas. For this study, this removal is accomplished by flowing a portion of the flue gas through the PCC system, while the remaining flue gas bypasses the system. For the flue gas entering the PCC system it was assumed that 90% of the CO_2 was removed. The CO_2 depleted flue gas exiting the absorber mixed with the bypassed flue gas before entering the stack. The bypass flow rate is adjusted so that the rate of CO_2 exiting the stack is 500 kg/MWh (1100 lb/MWh) on a gross output basis. In the design of an actual plant, it may be necessary to treat more of the flue gas to account for start-up, shut-down, part-load operation, etc., as the EPA emission regulation is based on an annual average.

Before entering the absorber, the flue gas stream from the boiler entered a flue gas scrubber where it was contacted with circulating, cooled water. This scrubber served several purposes:

- By cooling the flue gas, the volumetric flow of the flue gas decreased, which reduced the power requirement of the flue gas blower.
- Water was condensed from the flue gas. This minimized condensation of water in the absorber, which would dilute the solvent. The excess water would have to be removed during regeneration, which would increase the reboiler duty and decrease the steam turbine power.
- By adding a dilute caustic solution to the circulating water, sulfur and other contaminants that remain in the flue gas after the FGD could be removed.
- Any residual solids carried over from the FGD were reduced, minimizing the potential for foaming in the absorber.

The flue gas scrubber is a packed column. The flue gas enters the bottom of the column, where it is contacted with recirculated, cooled water. This water cools the flue gas to below the dew point, simultaneously condensing water from the flue gas and reducing the volumetric flow rate. As the water was condensed from the flue gas, the level in the column was controlled by purging the excess water back to the FGD or the cooling towers as makeup. The circulating water and the condensed water were warmed by the latent heat from the water condensation. This water was then cooled by the flue gas scrubber cooler before being recycled back to the top of the flue gas scrubber.

From the flue gas scrubber, the cooled gas entered the flue gas blower where the pressure of the flue gas was increased to overcome the pressure drop of the absorber and piping. The scrubbed flue gas was compressed to about 0.1 barg (1.5 psig) before it entered the bottom of the CO_2 absorber.

The flue gas was brought into contact with the advanced solvent in the absorber. The flue gas flowed upward through the column and the "lean" solvent flowed downward, removing 90% of the CO_2 from the flue gas. Good mass transfer occurred as the flue gas and solvent were brought into intimate contact in the column as they flowed through

structured packing. The capture of CO_2 from the flue gas was assumed to be an exothermic process similar to amine solvents, so it was assumed that the temperature of the solvent increased as it flowed through the column. The flue gas exited the “lower” section of the column, before entering the upper “wash” section of the column, where it was brought into contact with circulating water. As the flue gas flowed through the bubble cap trays in this section of the column, the water cooled the flue gas and scrubbed it of any solvent that had escaped the lower section of the absorber. The flue gas then flowed to the stack and was combined with the bypassed flue gas flow before discharging to the atmosphere. The wash-water stream was heated by the flue gas and was cooled by the absorber wash cooler before being pumped back to the top of the CO_2 absorber. A small purge stream removed the recovered solvent and condensed water from the wash section and returned them to the absorber section of the column as makeup.

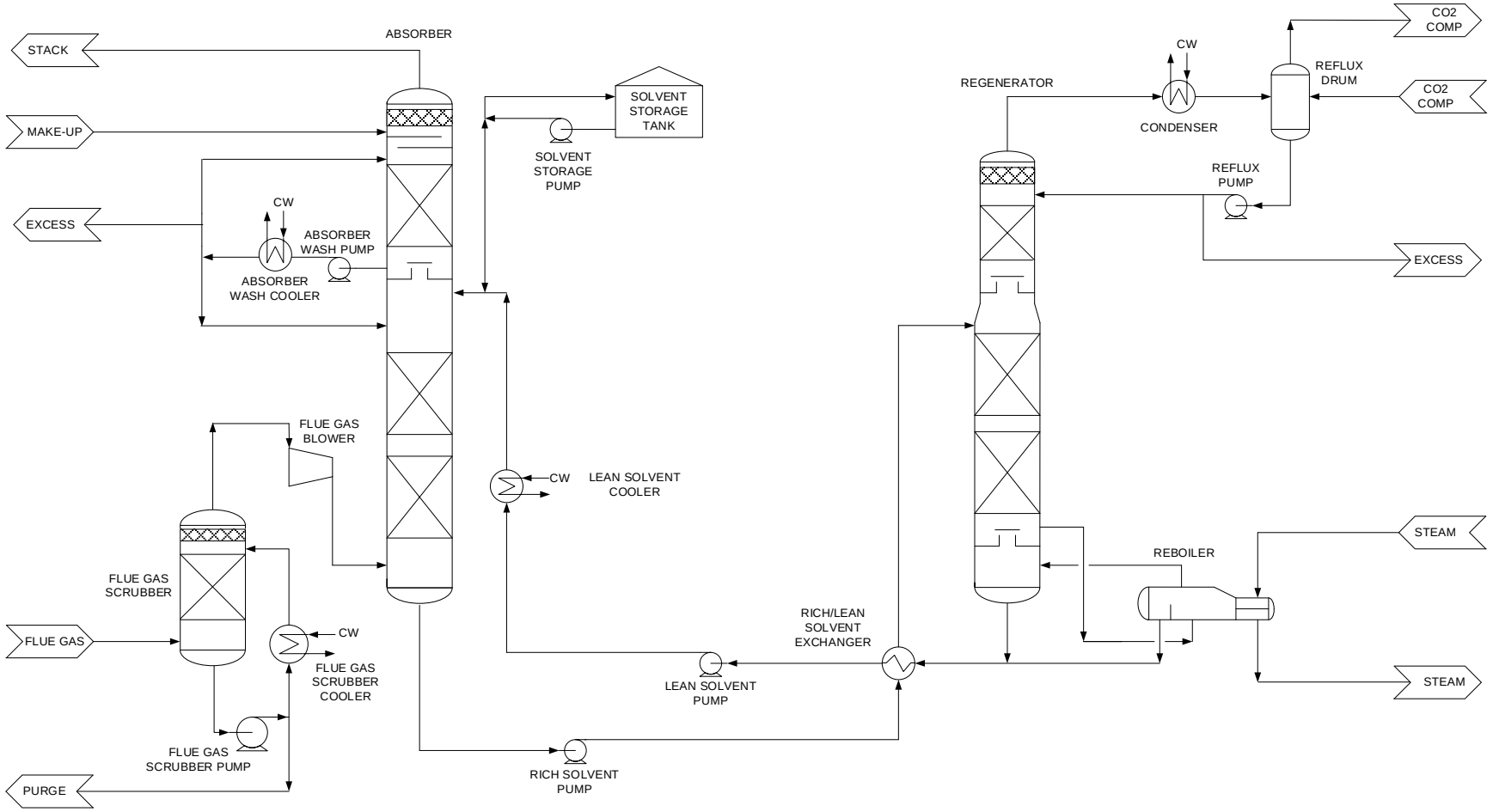

Figure 5-1
CO_2 Capture System

The CO_2 “rich” solvent exited the bottom of the absorber where it was pumped using the rich solvent pump through the plate and frame rich/lean solvent exchanger and into the regenerator. The rich solvent leaving the absorber was assumed to be 63°C (145°F), and the CO_2 “lean” solvent was assumed to exit the bottom of the regenerator at about 124°C (255°F). It was desirable to heat the rich solvent before it entered the regenerator to decrease the steam required for regeneration, and to cool the “lean” solvent as much as practical before it entered the absorber. Therefore, heat was transferred between the two streams in the rich/lean solvent exchanger.

The rich solvent entered the top of packed column regenerator where the CO_2 was removed from the solvent by the addition of heat. This heat breaks the chemical bonds, liberating the CO_2 and regenerating the solvent so that it can be returned to the absorber for further CO_2 capture. The heat was provided by the condensation of low pressure steam at approximately 2.5 bar (36 psia) in the regenerator’s kettle-type reboilers. This source of this steam was the first extraction port in the low pressure steam turbine.

The vapor leaving the regenerator was cooled to 38°C (100°F) before entering the reflux drum. The vapor exiting the reflux drum is the product CO_2, which is sent to the CO_2 compressor system, shown in Figure 5-2. Part of the condensed liquid was returned to the regenerator as reflux, and the remaining water was used as makeup for the absorber.

The “lean” solvent exited the bottom of the regenerator and flowed through the previously mentioned rich/lean solvent plate and frame exchanger where it was cooled. The cooled lean solvent was pumped using the lean solvent pumps, and then flowed through the lean solvent plate and frame cooler before returning to the absorber. The lean solvent cooler reduced the temperature of the lean solvent as much as practical to maximize the capture of CO_2 from the flue gas, minimizing the circulation rate of the solvent and decreasing the regeneration duty.

The cooled CO_2 flowed from the regenerator into the first stage CO_2 compressor knockout drum to remove any entrained water droplets before it entered the first stage of the centrifugal compressor. The CO_2 was then compressed, cooled in the intercooler, and entered another knockout drum to separate condensed water. The CO_2 then flowed through a second stage of compression, cooling, and water separation before entering the dehydration unit, where water was removed to meet CO_2 pipeline requirements. The water from the second and third stage CO_2 knockout drums flowed back to the first stage knockout drum where it was collected in a single stream and returned to the regenerator.

The dehydration unit was assumed to be a parallel-bed, molecular-sieve system. The CO_2 flowed through one bed until the molecular sieve was almost saturated with water, at which point, the beds were swapped. The saturated bed was regenerated with heated CO_2 to remove the adsorbed water. The hot CO_2/vapor stream was cooled (internal to the dehydration package) and flowed back to the first stage CO_2 compressor knockout drum where the water was separated.

The dried CO_2 leaving the dehydration unit entered the third stage of the centrifugal compressor where it was compressed and cooled to 91 bar (1315 psia). The supercritical fluid was collected in a drum and pumped and cooled to the final pipeline pressure of 153 bar (2215 psia). At this pressure, the supercritical CO_2 can enter an enhanced oil recovery (EOR) pipeline and be utilized for increased petroleum production, or be injected underground for geologic storage.

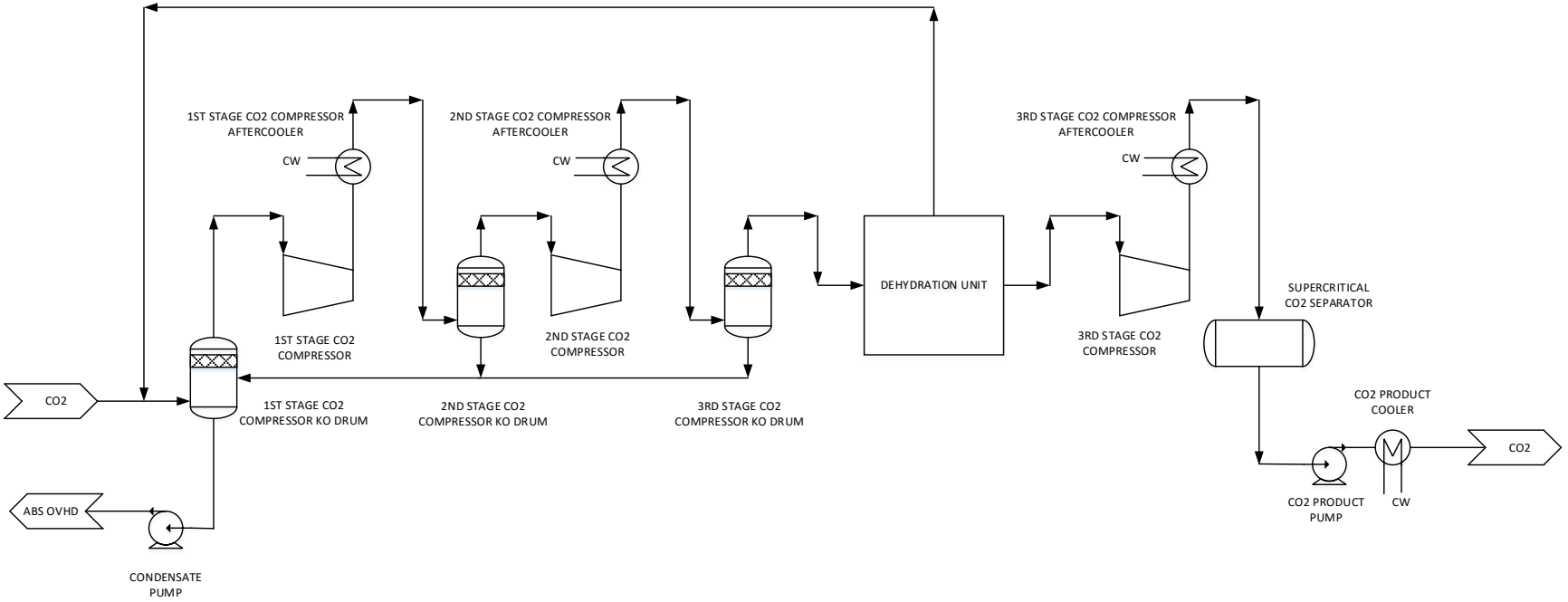

Figure 5-2
CO_2 Compression System

Design of the PCC System

Because of the proprietary nature of this solvent, a minimum amount of information about it was provided by the NCCC. Therefore, to produce a heat and material balance and to estimate the performance, the following information and assumptions were used:

- The steam to the solvent regenerator reboiler was 2080 kJ/kg (895 Btu/lb) of CO_2 removed.
- The CO_2 concentration in the lean solvent was 2.55 wt%.
- The CO_2 concentration in the rich solvent was 11.3 wt%.
- The flue gas scrubber and flue gas blower parameters were the same as in EPRI report 1017515. (These are shown in Appendix A).
- The lean solvent entered the absorber at 38°C (100°F).
- It was assumed that the reaction between the solvent and CO_2 is exothermic. Therefore, the temperature of the rich solvent leaving the absorber was assumed to be 63°C (145°F), and the flue gas exiting the absorber to the cooling portion of the column was 57°C (135°F).
- It was assumed that the lean solvent exiting the regenerator is at 124°C (255°F).
- Thermal properties are based on water.
- As in EPRI report 3002003740, the temperature of the CO_2/water stream leaving the regenerator overhead was 105°C (221°F.)
- The parameters for the CO_2 compression system were the same as EPRI report 1017515. These are also shown in Appendix A.

The steam for the regenerator reboiler was supplied from the first extraction of the low-pressure steam turbine section. At this point, the superheated steam was at 4.8 bar (69 psia), but at a temperature of 385°C (725°F). Desuperheating water from the condensate pump outlet was used to cool the steam to approximately 150°C (300°F) before entering the regenerator reboiler.

Heat Integration

In a typical utility Rankine cycle, once the steam flows through the turbine to produce electricity, it is condensed in the steam turbine condenser. For this case, it was assumed that the condenser operated at 6.7 kPa (2 in-Hg), and the condensate exited at 38°C (101°F). A conventional PC unit, has few opportunities to heat this water with process streams utilizing heat integration, outside of steam extracted from the steam turbine into a series of LP and HP feedwater heaters. The presence of a PCC thus presents a unique heat integration opportunity.

This study assumed that process streams for heating the condensate were available from two primary sources:

- Because the steam for regenerating the solvent was supplied from the LP turbine, the steam turbine gross output decreases. However, a significant portion of this heat could be recovered from the PCC system to heat the condensate. This reduced the

extraction steam used for boiler feedwater heating and allowed the steam turbine to generate more power.

- The addition of a “combustion air preheater” to transfer heat between the flue gas and the secondary air stream was proposed in EPRI report 3002003740 and was included in this study.

CO_2 Regeneration and CO_2 Compression Heat Recovery

Within the CO_2 capture system, there are several sources of high temperature heat. For this study, it was assumed that the PCC system was located at a significant distance from the condensate system. Therefore a “tempered water” loop was added to transfer the heat between these two systems. The tempered water acted as cooling water for the exchangers in the PCC system; this hot water was then sent to the condensate system. The maximum temperature of the tempered water was approximately 104°C (220°F); therefore, the pressure of the tempered water loop could be lower than the condensate system. Even though the tempered water would be demineralized, this would act to protect the condensate in the event of a tube leak—condensate would flow into the tempered water system instead of vice versa.

The sources of heat in the PCC system, described below, are shown in Figure 5-3:

- The hot CO_2/water stream leaving the top of the regenerator was cooled before flowing to the CO_2 compressor. There was a significant quantity of water in the overhead stream that condensed as the stream was cooled. Thus the bulk of the energy transferred was latent heat. Because of the significant latent heat, the cooling curve was non-linear and AspenPlus™ was used to determine the amount of heat available for heat integration.
- The CO_2 compressor intercoolers cool the hot gas from each CO_2 compressor stage to increase the compressor efficiency and to control the gas temperature entering the next compression stage. Like the regenerator overhead stream, this stream contained water vapor, so the cooling curve was non-linear and AspenPlus™ was used to determine the amount of heat available for heat integration.
- The individual tempered water streams were combined into a single stream that flowed from the PCC system to the feedwater heater system and was used to heat a portion of the condensate.

Combustion Air Preheater

The combustion air preheater concept presented in EPRI report 3002003740 noted that the flue gas leaving the primary air heater was at a significantly higher temperature (approximately 127°C or 260°F) than that of the combustion air. Typically, the flue gas stream leaving the ID Fan would be quenched before entering the FGD, and this heat would not be recovered.

In the report, it was proposed that a heat exchanger between the ID Fan and the FGD would be added, as shown in Figure 5-4, to transfer the heat from the flue gas to the combustion air. Because the combustion air would now enter the “primary” air heater at a higher temperature, a portion of the hot flue gas exiting the SCR could be bypassed

around the air heater. This high temperature (>370°C or >700°F) could then be used as heat source for a second tempered water loop and used to heat the condensate.

For this study, it was decided that because low-sulfur PRB coal was used as the fuel, the flue gas could be cooled to a minimum temperature of 82°C (180°F) in these heat exchangers to maximize heat recovery.

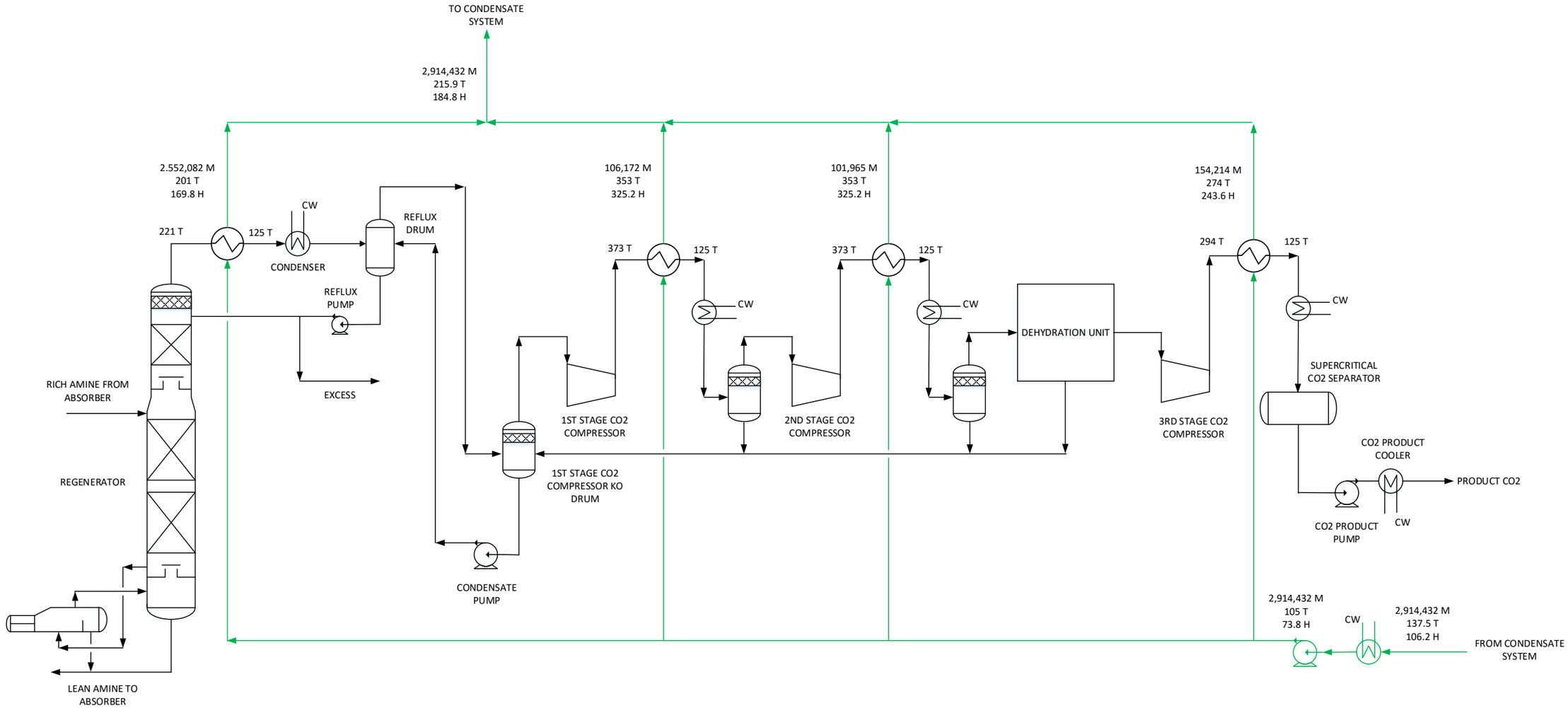

Figure 5-3
PCC Heat Integration Scheme

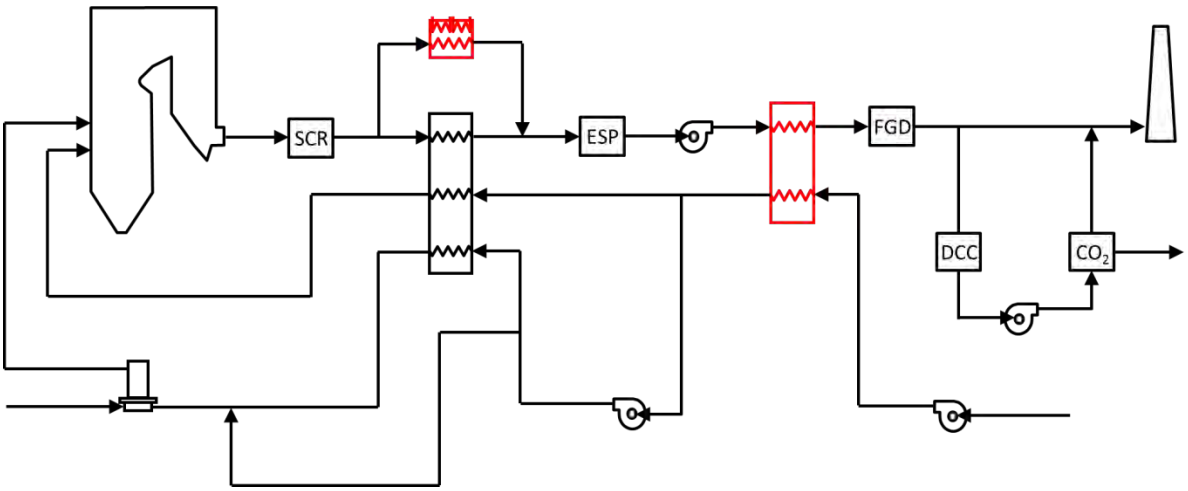

Figure 5-4
Combustion Air Preheater (from EPRI Report 3002003740)

The overall heat integration scheme for the plant is shown in the heat exchanger network diagram of Figure 5-5. The cold streams are indicated by the blue lines at the top, flowing from right to left, and the hot streams are at the bottom in red flowing from left to right. The two tempered water streams are indicated by the green lines at the bottom of the diagram. Each heat exchanger is identified by a “dumb-bell” shape that matches the hot and cold streams with each end a vertical line. Arrows have been added to the vertical “exchanger” line to indicate the direction of heat flow. The number below the lower circle in the “dumb-bell” shape is the duty for the heat exchanger in million Btu per hour.

The overall heat balance diagram for the plant, incorporating the heat integration, is shown in Figure 5-6.This diagram focuses only on the low pressure section of feedwater heating between the condenser and the deaerator. Using the heat integration scheme described eliminated feedwater heaters 1-3. The steam that would be been used by these exchangers flowed through the LP turbine and generated power, which partially offset the power lost by extracting steam to operate the PCC regenerator reboiler.

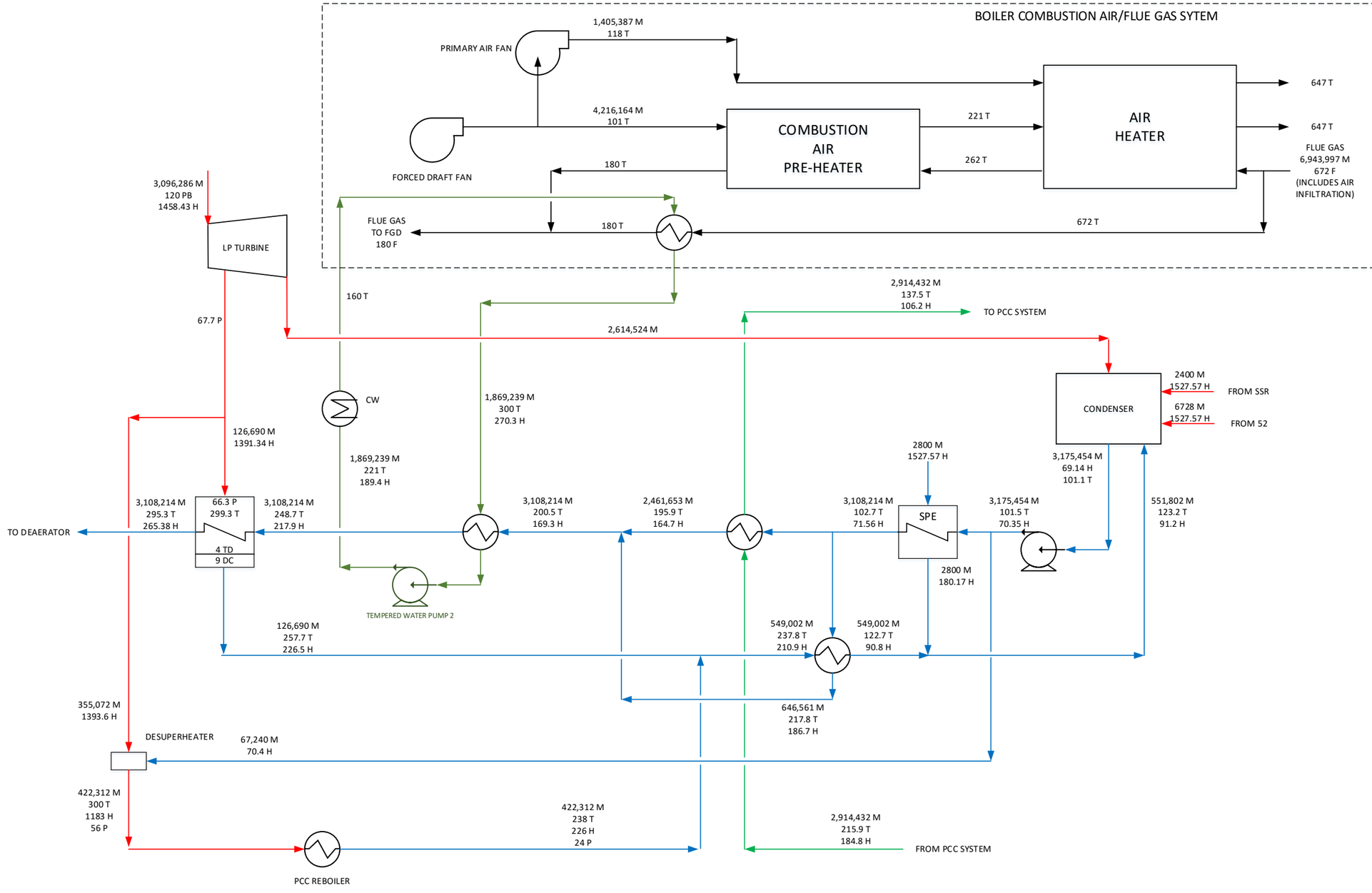

Figure 5-5
PCC Heat Integration Scheme

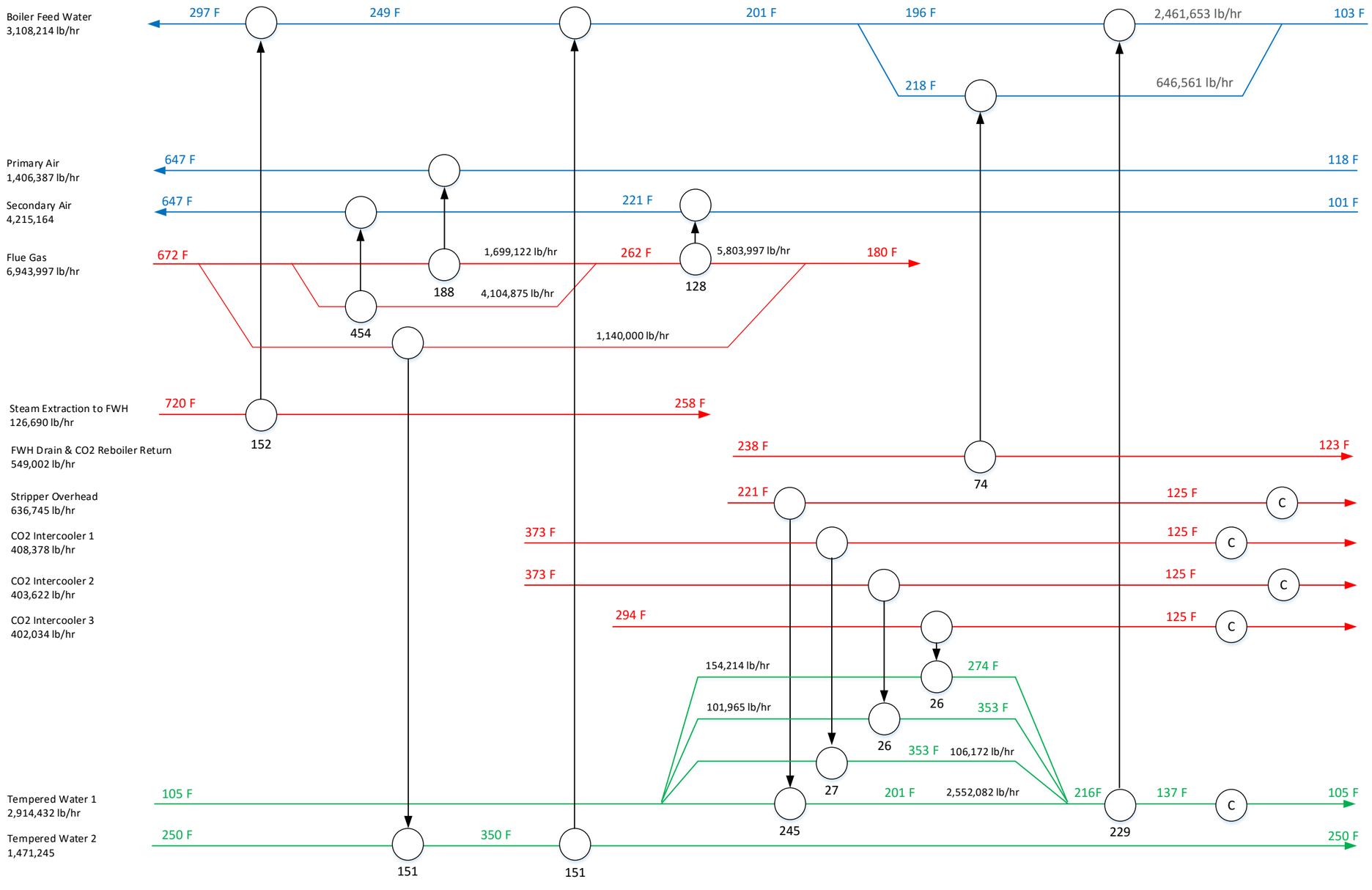

Figure 5-6
Heat Exchanger Network Diagram

Plant Performance

Based on the configuration described, the performance of the A-USC power plant utilizing the advanced solvent for CO_2 capture to meet EPA's 111(b) requirement for new coal plants is shown in Table 5-1. The auxiliary load associated with the PCC system is shown in Table 5-2.

Table 5-1
Summary Performance of the Advanced Ultra-Supercritical Plant with a 1100 lb CO_2/MWh PCC System

Description	SI Units	U.S. Customary Units
Throttle conditions	242 bar/732°C/760°C	3515 psia/1350°F/1400°F
Main steam flow	1,818,000 kg/h	4,008,000 lb/h
Hot reheat flow	1,563,000 kg/h	3,375,000 lb/h
Condenser flow	1,440,000 kg/h	3,175,000 lb/h
Condenser pressure	6.7 kPa	2 inches mercury
Final feedwater temp	304°C	580°F
Steam to PCC System	161,000 kg/h	355,000 lb/h
Gross plant output, kW	809,071	809,071
Auxiliary load, kW	100,742	100,742
Net plant output, kW	708,329	708,329
Net plant heat rate	9,261 kJ/kWh	8,778 Btu/kWh
Net plant efficiency, % (HHV)	38.9	38.9
Plant fuel consumption	338,000 kg/hr	746,000 lb/hr
CO_2 emission with PCC	393,000 kg/hr	867,000 lb/hr
CO_2 emission with PCC	500 kg/MWh, EPA gross basis	1100 lb/MWh, EPA gross basis

Table 5-2
Auxiliary Loads for the Advanced Ultra-Supercritical Plant with a 1100 lb CO_2/MWh PCC System

Equipment	kW
Original "Base" Plant Load (From Table 4-3)	70,801
PCC Plant Loads	
Wash Water Pump	496
Flue Gas Blower	5,261
Absorber Wash Cooler	163
Rich Solvent Pump	507
Lean Solvent Pump	331
Reflux Pump	15
CO_2 Compressor	21,106
Circulating Water Pump (PCC)	933
Cooling Tower Fan (PCC)	1,129
Total Auxiliary Power Consumption	100,742

Final 111(b) Rule

On August 3, 2015, President Obama and the EPA announced the Clean Power Plan. The Clean Power Plan changed the CO_2 emission basis for new coal fired power plants from 500 kg CO_2/MWh (1100 lb CO_2/MWh) to 635 kg CO_2/MWh (1400 lb CO_2/MWh). At DOE's request, EPRI evaluated the performance of the same unit under the same criteria, but with the revised emission limit. The results of this study are shown in Tables 5-3 and 5-4.

With the higher CO_2 emission rate, only about 15% of the flue gas is required for treatment. This significantly reduces the steam extraction from the steam turbine to regenerate the steam from 161,000 kg/hr (355,000 lb/hr) to 71,700 kg/hr (158,000 lb/hr) allowing the steam turbine to generate more gross power. Also, since less CO_2 is being processed in the PCC system and compressed for EOR or sequestration, the total auxiliary power consumption improves over 16 MW. The combination of the increased gross power and the decreased auxiliary load increased the net power by 26 MW and improved the net efficiency by 1.4 percentage points. Compared to the performance of the "base plant" with no PCC as shown in Table 4.3, there is a performance penalty of 1.1 percentage points for this A-USC unit to meet the EPA's Clean Power Plan.

Table 5-3
Summary Performance of the Advanced Ultra-Supercritical Plant with a 1400 lb CO_2/MWh PCC System

Description	SI Units	U.S. Customary Units
Throttle conditions	242 bar/732°C/760°C	3515 psia/1350°F/1400°F
Main steam flow	1,818,000 kg/h	4,008,000 lb/h
Hot reheat flow	1,563,000 kg/h	3,375,000 lb/h
Condenser flow	1,186,000 kg/h	2,615,000 lb/h
Condenser pressure	6.7 kPa	2 inches mercury
Final feedwater temp	304°C	580°F
Steam to PCC System	71,700 kg/h	158,000 lb/h
Gross plant output, kW	818,438	818,438
Auxiliary load, kW	84,060	84,050
Net plant output, kW	734,338	734,338
Net plant heat rate	8,933 kJ/kWh	8,467 Btu/kWh
Net plant efficiency, % (HHV)	40.3	40.3
Plant fuel consumption	338,000 kg/hr	746,000 lb/hr
CO_2 emission with PCC	506,200 kg/hr	1,116,000 lb/hr
CO_2 emission with PCC	635 kg/MWh, EPA gross basis	1400 lb/MWh, EPA gross basis

Table 5-4
Auxiliary Loads for the Advanced Ultra-Supercritical Plant with a 1400 lb CO_2/MWh PCC System

Equipment	kW
Original “Base” Plant Load (From Table 4-3)	70,801
PCC Plant Loads	
Wash Water Pump	219
Flue Gas Blower	2,320
Absorber Wash Cooler	72
Rich Solvent Pump	224
Lean Solvent Pump	146
Reflux Pump	7
CO_2 Compressor	9,307
Circulating Water Pump (PCC)	433
Cooling Tower Fan (PCC)	523
Total Auxiliary Power Consumption	84,050

Out of Service Operation

For a power plant that has a PCC system installed, there are several scenarios that could lead to the PCC system being taken out of service:

- A failure in any of the equipment in the PCC system.
- If the product CO_2 is supplied to an EOR pipeline, there could be a trip in the EOR system that prevents the “off-taker” of the CO_2 from taking delivery.
- The EPA regulations are written on an annual CO_2 emission basis. Therefore, it might be possible to oversize the PCC system to capture more CO_2 during non-peak hours and trip the PCC system during the utility’s peak demand hours. As shown in Table 5-2, for Case 2 this would provide the utility with an additional 30 MW of electricity.

With the elimination of the first three LP feedwater heaters, the power plant in Case 2 must evaluate operation with the PCC system out of service, compare this operating case to the performance of Case 1, and determine how much steam extraction would be required from this first LP turbine nozzle to heat the condensate to the same temperature. For this analysis, the following assumptions were made regarding the heat integration:

- Heat from the LP feedwater heater drain would be recovered by heating condensate before the LP feedwater heater drain flow entered the condenser.
- There would be no steam extraction to the PCC system, and likewise, there would be no hot tempered water from the PCC system.
- The combustion air pre-heater system would be still be operational and would transfer heat from the flue gas to the condensate.

The low pressure condensate heat balance is shown in Figure 5-7. Notice that the steam extraction flow is approximately 158,000 kg/hr (349,000 lb/hr), almost three times as much as the extraction steam flow to the LP feedwater heater during normal operation with the PCC in service. But with the PCC reboiler out of service, the steam extracted from the LP turbine is about 60,000 kg/hr (133,000 lb/hr) less than the combined PCC reboiler steam plus the steam for the LP feedwater heater. A practical solution may be to have 2 or 3 LP feedwater heaters installed in parallel, and if the PCC system trips, split the condensate and extraction steam to multiple heaters to accommodate the increased duty. With the heat balance arrangement shown in Figure 5-7, the gross power of the steam turbine was estimated to be 821,131 kW, approximately 3.8 MW less than in Case 1.

Performance analyses for an A-USC plant with PCC designed to meet the modified EPA’s 111(b) CO_2 emission standard of 635 kg/MWh (1400 lb/MWh), on a gross output basis, are under way. Preliminary findings suggest that the efficiency and heat rate would improve, respectively to 40.3% (HHV) and 8930 kJ/kWh (8470 BTU/kWh). Auxiliary loads are reduced to about 84,000 kW; gross power is about 818,000 kW and net power is about 734,000 kW.

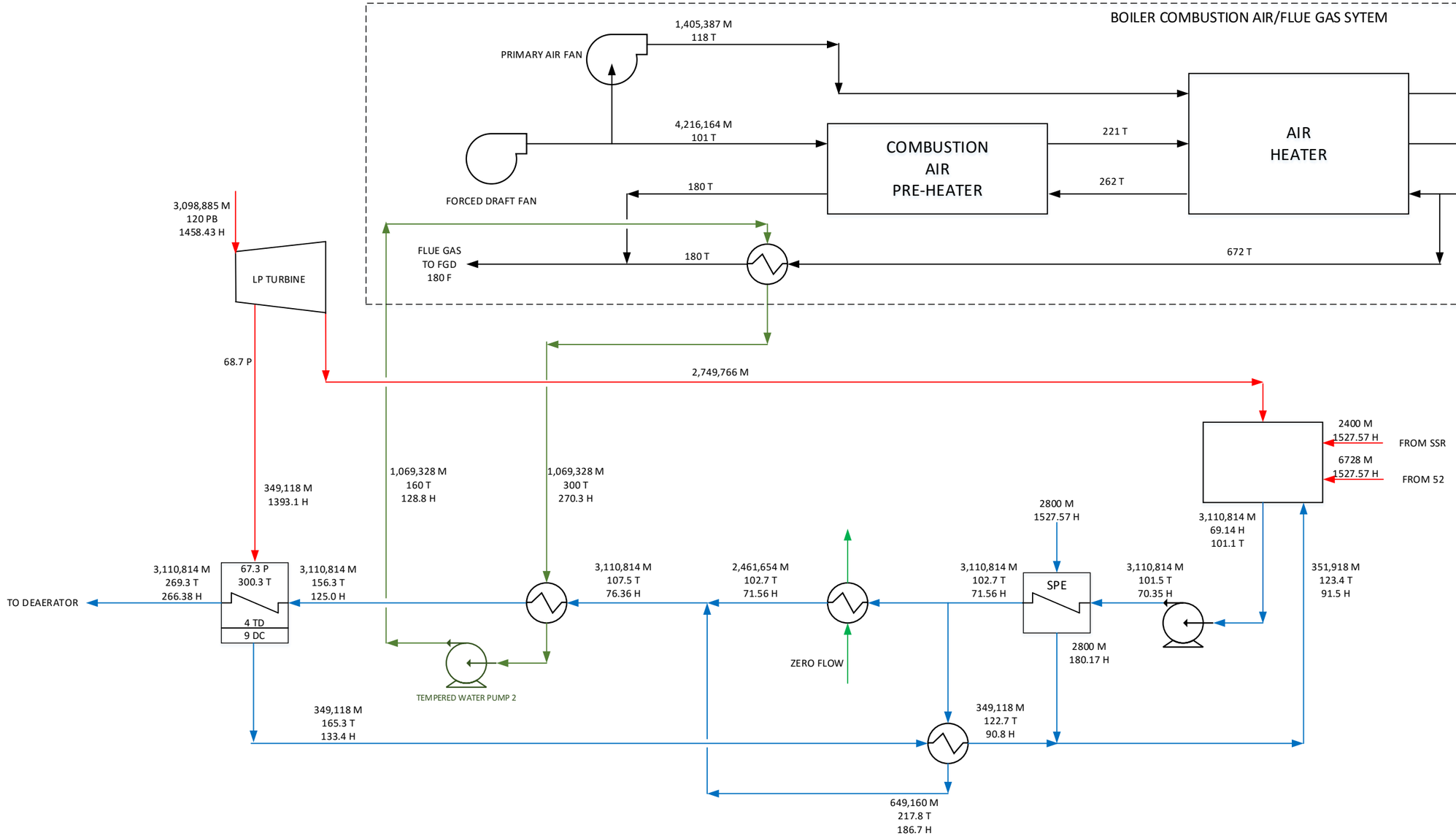

Figure 5-7
Low Pressure Condensate Heat Balance with PCC System Out of Service

6
ECONOMIC EVALUATION

Case 1 – A-USC PC without Carbon Capture

Total Plant Cost

The Total Plant Cost (TPC) for the A-USC without the PCC system is estimated using EPRI's PC Cost program. The program was developed primarily to accommodate subcritical and supercritical designs up to 593°C (1100°F) and therefore had to be modified for this study, as discussed in Section 3, to accommodate the higher cycle temperatures of an A-USC power plant.

PC Cost is not intended to be a design program and is used to provide a conceptual (±30%) cost estimate. The costs are presented on an n^{th}-of-a-kind basis; therefore, no process contingencies are applied. A contingency of 10% is applied to the project cost, and all costs are escalated to December 2014.

Steam Turbine Costs

The primary thermodynamic factors that influence the cost of a large steam turbine cycle are the steam inlet and exhaust pressure, inlet temperature and mass flow rate. Inlet pressure and temperature determine the specific volume of the steam entering the turbine. Combining this with the steam mass flow rate yields the volumetric flow rate. This determines the flow area. As the steam expands through the turbine, the pressure drops and the specific volume increases. The flow area and overall size of each turbine section increases. At the LP exhaust, the condenser pressure determines the specific volume of the steam. LP last stage buckets are designed for optimum efficiency at a fixed axial velocity. To maintain highest LP efficiency, the last stage bucket flow area should be matched to the condenser pressure and specific volume that yields the optimum axial velocity. In order to accomplish this across a range of possible condenser designs and pressures, a turbine supplier must have several last stage bucket sizes to choose from.

Once turbine section flow area and size is determined, the next major influence is steam temperature. For highest reliability, turbine materials are selected that provide adequate creep rupture and fatigue life, wear resistance, oxidation characteristics and resistance to erosion for 30 year life. As temperatures increase, the strength of turbine materials decreases. Turbine suppliers must find materials with higher and higher strength as steam temperatures increase. Higher strength alloys cost more and these costs must be exceeded by the value for the increased efficiency and output provided by the higher temperature thermodynamic cycle.

The bulk of the existing U.S. supercritical fleet operates at turbine inlet conditions of 230–242 bar (3320–3500 psig) and 538°C (1000°F). The materials applied at this temperature have generally been low alloy CrMoV steels in the HP and Reheat sections. In the LP sections, where inlet temperatures are below about 370°C (700°F),

the LP casings are generally low carbon steel and the rotors are a NiCrMoV alloy. Many of these turbines have been in operation since the 1970s and are still operating today.

The advent of USC steam cycles have taken HP inlet temperatures as high as 610°C (1130°F) and reheat temperatures up to 621°C (1150°F). To achieve these temperatures, turbine suppliers have applied advanced 9–12Cr alloys in the HP and reheat sections. In some cases, steam cooling is used to lower the local temperature where stresses are highest. Inlet temperatures to the LP section have generally remained below 370°C (700°F), allowing the continued use of conventional supercritical plant materials in the LP section.

During the early years of USC technology, the advanced 9–12Cr materials commanded large cost premiums, as much 200–300% compared to the more common low-alloy steels. As of mid-2015, the cost difference between a low-alloy steel casting and a 10Cr casting is less than 100%.

The materials down-selected for steam turbine applications at A-USC temperatures are Haynes 282 and Nimonic 105. These nickel alloys are expensive to produce, process and machine. Based on the Haynes 282 castings and forgings procured during this program, the material cost of steam turbine castings and forgings, ready for machining, was estimated. The cost for machining Haynes 282 was based on experience machining other nickel alloys.

This A-USC cost estimate used an 800 MW USC reference design of the same tandem compound architecture described in Section 4. Steam conditions for the reference design are 242 bar (3514.7 psia), 600°C (1112°F) main steam, and 621°C (1150°F) reheat steam. The reference HP section is a single flow steam path with double shell construction. There are two inner shells contained within the outer shell. The inlet valves are mounted close by the HP section on each side. There are two bearings supporting the HP rotor. The HP rotor is a welded construction. The reference Reheat section is similar in all aspects to the HP section. The Reheat steam path flow direction is opposite the HP section. There are two double flow LP casings, each LP flow containing a 1016 mm (40 inch) last-stage bucket. Each LP rotor is supported by two bearings. The LP sections exhaust downward into two condensers.

This reference steam turbine design provided HP and Reheat components of similar size, quantity and weight to the A-USC design described by the heat balance. For the estimate of the stationary components, it was only necessary to adjust the material and labor costs for those components exposed to steam temperatures above the capability of advanced 9-12 Cr steels. For the HP and Reheat turbine rotating components, the total rotor weights are similar to the A-USC design. Cost adjustments were made to factor in the bolted rotor architecture with associated material changes. For the buckets and nozzles, once again, the critical sizes were similar to the reference design. Cost adjustments were made to account for material, method of attachment to the rotor and labor.

For the A-USC design, the LP inlet steam temperature is 460°C (860°F), which meant that the standard LP inner casing and the LP rotor, both designed for 370°C (700°F) inlet steam, had to be adjusted to account for the increased temperature. For the inner

casing, it was assumed that the component would be made from a CrMo alloy typically used at that temperature. For the LP rotor, a three piece welded rotor was designed and the associated cost was applied to the estimate.

The main stop and control valves for the reference turbine were of the same type and size needed for the A-USC design. Material and labor cost adjustments were made to account for the required nickel alloy material needed for the higher temperature. The combined reheat valves for the reference design were larger than those required for the A-USC design and the next smaller valve design was applied to A-USC and material and labor cost adjustments were made to this valve.

The reference design uses piping to conduct the steam from the main stop and control valves to the HP turbine inlet. For A-USC this piping will be Inconel 740 and the reference piping cost has been adjusted to reflect the material change.

The A-USC Steam Turbine and Generator cost includes the flange-to-flange steam turbine-generator with electrical, controls and accessories as listed:

1. Main Stop & Control valves
2. Main steam piping
3. HP Section
4. Reheat Stop & Intercept Valve
5. IP Section
6. Crossover between IP Exhaust & LP Section
7. Two (2) Double Flow LP sections
8. Bearings, Bearing enclosures
9. Generator
10. Electrical System, Instruments & Control System
11. Accessories (to include):
    a. Lube Oil System
    b. Hydraulic Power Unit
    c. Steam Seal System
    d. Turbine Drain Valves

A-USC Steam Turbine & Generator cost does not include:

1. Installation Cost
2. Extraction Piping
3. Hot & Cold Reheat Piping

The results of the A-USC Steam Turbine-Generator cost study are summarized in Figure 6-1.

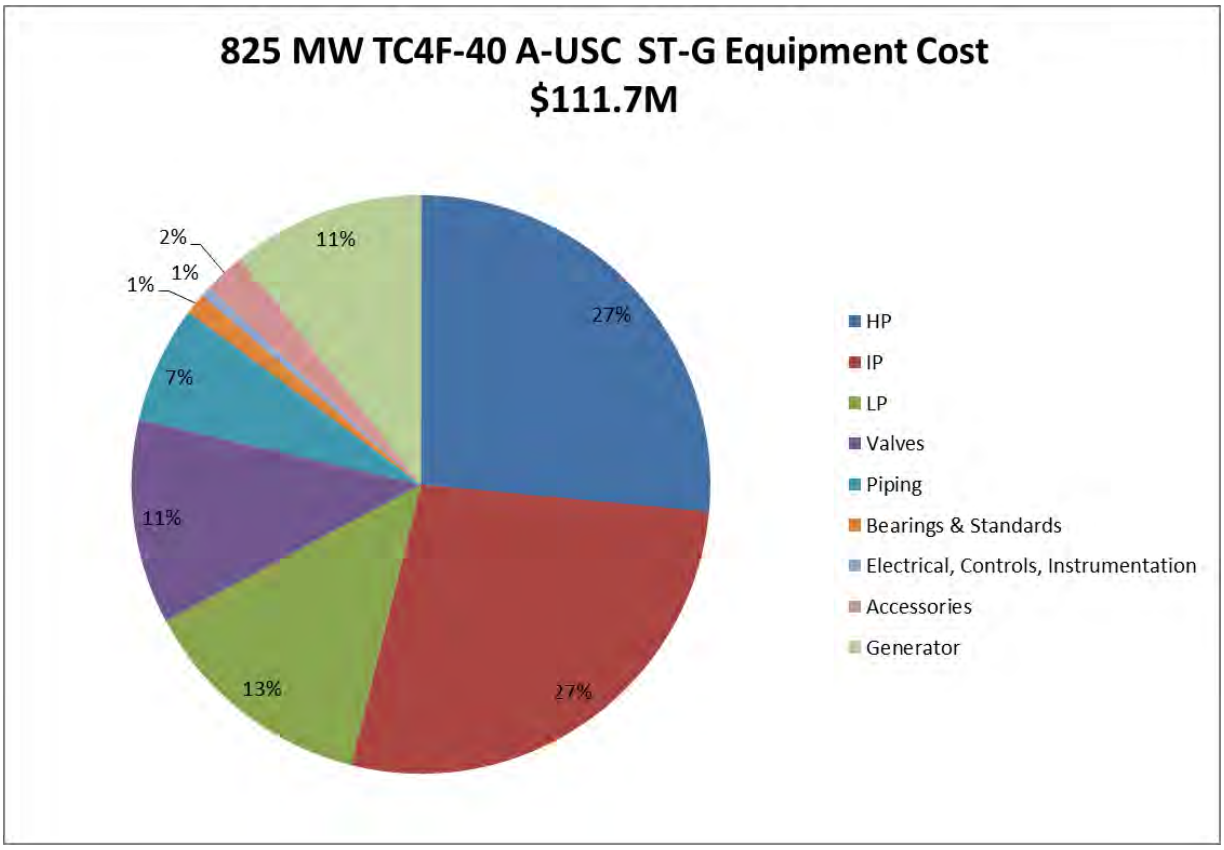

Figure 6-1
Steam Generator Cost Study Results

Compared to the USC reference design, the A-USC steam turbine-generator cost is nearly double the comparable USC cost. This is due mainly to cost increases of 3-4 times in the HP and IP sections, with the increase higher in the IP section due to its larger size. Valve and piping increases contribute significantly to the remaining cost increases.

These large increases are mainly the result of the high cost of the nickel alloys, which currently represent an increase in cost for a delivered casting or forging of close to 8 times compared to advanced 9–12Cr ferritic steels. Add to this the difficulty for machining super-alloys and the nickel alloy multiplier reaches 10 times.

Regarding the ST-G cost for Case 1 and Case 2 at 3500 psi inlet pressure, it is assumed to be the same. The ST-G cost increase for the 4250 psi case was estimated to be $1.8 million. This was based on calculations of wall thickness changes and the influence on component weight.

It remains to be seen how the cost for these nickel alloys changes in the future. This study made no attempt to predict the "n^{th} unit" cost for these materials.

Levelized Cost of Electricity

The LCOE includes the fuel costs, variable and fixed operating costs, as well as the capital cost "carrying charge."

The costs are based on the following assumptions:

- Annual capacity factor: 80%
- Coal cost: $1.71/GJ ($1.80/MBtu)
- Annual Capital Carrying Charge: 12.1% of Total Plant Cost (TPC)
- Operator Cost: 18 operators per shift
- Administration/Overhead Cost: 22 personnel
- Maintenance labor: 2% of TPC/yr
- Maintenance materials: 1% of TPC/yr
- Ammonia for SCR: $573/tonne ($520/ton)
- FGD reagent cost: $19/tonne ($17/ton)
- FGD solids disposal costs: $13/tonne ($12/ton)
- Ash disposal costs: $19/tonne ($17/ton)
- Other miscellaneous variable costs: 1% of TPC/yr
- Select material costs ($/lb):[21]
    - Carbon steel – $1.18
    - T91 – $2.63
    - S304H – $7.03
    - HR3C – $8.11
    - HR6W – $16.23
    - HR230 – $21.64
    - IN617/IN740 – $40

Based on this information, the TPC and the LCOE for Case 1 is shown in Table 6-1.

[21] EPRI market analysis based on material purchases from 2012-2014, informal discussions with vendors, and raw alloy costs.

Table 6-1
Total Plant Cost and Cost of Electricity – without Post-Combustion CO_2 Capture

Total Plant Cost – 754,199 kW Net Power		
Cost Category	**Capital Cost, $(000)**	**$/kW**
Earthwork	$25,400	$34
Boiler Room Structure	$54,800	$73
Turbine/BOP/Yard Structures	$94,900	$126
Boiler Plant Equipment & Systems	$471,500	$625
Turbine & BOP	$548,300	$727
Flue Gas Desulfurization	$241,400	$320
Miscellaneous Directs	$152,800	$203
Indirect Costs	$421,700	$559
Contingency	$201,100	$267
Total	$2,212,000	$2,933
Levelized Cost of Electricity – 80% Capacity Factor		
Cost Category	**Annual Operating Cost, $(000)/yr**	**$/MWh**
Capital Cost	$267,652	$50.60
Fuel Costs	$78,433	$14.80
Fixed Operating Costs	$76,287	$14.40
Variable Operating Costs	$26,038	$4.90
Total	$448,410	$84.70

Case 2 – A-USC PC with Post-Combustion CO_2 Capture

Total Plant Cost

For Case 2, the design and cost of the PCC system is based on the system described in Appendix D of EPRI report 1017515.[22] Because only 34% of the flue gas is treated in the PCC system, only one CO_2 removal/compression "train" would be necessary for the plant to meet EPA's 111(b) requirement. For scaling purposes the following assumptions were made:

- The columns and fan cost was scaled based the flue gas flow rate
- The pump and vessel/storage costs were scaled based on the solvent flow rate
- The heat exchangers were scaled based on the calculated heat duties
- The CO_2 compressor was scaled based on the CO_2 product flow rate

[22] *An Engineering and Economic Assessment of Post-Combustion CO_2 Capture for 1100°F Ultra-Supercritical Pulverized Coal Power Plant Applications: Phase II Task 3 Final Report.* EPRI, Palo Alto, CA: 2010, 1017515.

The cost basis for the original report is October 2009, and Chemical Engineering's Plant Cost Index was used to escalate the costs to a December 2014 basis.

The estimate produced by PC Cost for the boiler island does not include the modifications to the ductwork that are required to incorporate the PCC system. Therefore a "retrofit" cost is added to incorporate the modifications made to accommodate the PCC system to the existing plant design ductwork, steam system, controls, etc. The costs necessary to incorporate the heat integration scheme from Section 5 were included as well.

Levelized Cost of Electricity

To adjust the LCOE to incorporate CO_2 capture, the following changes to the previously mentioned assumptions are made:

- The number of plant operators is increased from 18 to 22 per shift.
- The number of administration personnel is increased from 22 to 25 to accommodate additional lab personnel.
- A variable cost of $4.08/yr*(hr/lb) or $1.85/yr*(hr/kg) multiplied by the solvent circulation rate was added to account for the annual costs associated with the MEA solvent (replacement and disposal).
- A CO_2 transportation and storage cost of $10/tonne ($9.07/ton) is added.

The TPC and the LCOE for Case 2 are shown in Table 6-2.

Table 6-2
Total Plant Cost and Cost of Electricity – with an 1100 lb CO_2/MWh Post-Combustion CO_2 Capture

Total Plant Cost – 708,362 kW Net Power		
Cost Category	**Capital Cost, $(000)**	**$/kW**
Base Plant	$2,212,000	$3,120
Modifications for PCC System	$178,000	$250
Total	$2,390,000	$3,370
Levelized Cost of Electricity – 80% Capacity Factor		
Cost Category	**Annual Operating Cost, $(000)/yr**	**$/MWh**
Capital Cost	$287,859	$58.00
Fuel Costs	$78,433	$15.80
Fixed Operating Costs	$83,632	$16.90
Variable Operating Costs	$34,032	$6.90
CO_2 Transportation & Storage	$12,800	$2.60
Total	$498,067	$100.20
Cost of CO_2 Avoided, $/tonne	$70	
Cost of CO_2 Captured, $/tonne	$45	

The capital savings associated with the alternative A-USC boiler arrangements to reduce the nickel piping length and the reduction in materials would also apply to the capital cost of the system with a PCC system installed, lowering the overall plant capital cost and the cost of electricity.

Cost Under the Final 111b Rule

As described in Section 5, because of the higher CO_2 emission rate under the final version of the 111b regulation issued in August 2015, the plant is required to treat approximately 15% of the flue gas in the PCC system. This slightly decreases the cost of the PCC system. On a $/kW basis, the more significant contribution is the increase in net power by 26 MW. The net effect of these two changes decreased the capital cost from $3,370 $/kW to $3,190 $/kW. Note that the "base" A-USC power plant with no carbon capture had an estimated capital cost of $2933 $/kW. So meeting the Clean Power Plan for this plant incurred a capital penalty of less than 10%.

Also, due to the increased net power, the LCOE under the Clean Power Plan was $93.30/MWh, an increase of approximately 10% more than that of the base plant with no carbon capture. However, the relatively smaller amount of CO_2 being captured results in dis-economies of scale, and the cost of CO_2 avoided, at $104/tonne, is greater

than it is for the 1100 lb CO_2/MWh case. Table 6-3 summarizes the economics of the 1400 lb CO_2/MWh case.

Table 6-3
Total Plant Cost and Cost of Electricity – with a 1400 lb CO2/MWh Post-Combustion CO_2 Capture

Total Plant Cost – 734,388 kW Net Power		
Cost Category	**Capital Cost, $(000)**	**$/kW**
Base Plant	$2,212,000	$3,010
Modifications for PCC System	$132,000	$180
Total	$2,344,000	$3,190
Levelized Cost of Electricity – 80% Capacity Factor		
Cost Category	**Annual Operating Cost, $(000)/yr**	**$/MWh**
Capital Cost	$283,660	$55.10
Fuel Costs	$78,430	$15.20
Fixed Operating Costs	$82,260	$16.00
Variable Operating Costs	$30,240	$5.90
CO_2 Transportation & Storage	$5,640	$1.10
Total	$480,231	$93.30
Cost of CO_2 Avoided, $/tonne	$104	
Cost of CO_2 Captured, $/tonne	$62	

A-USC Boiler Configurations to Reduce Capital Cost

Past EPRI studies (Reports 1015699, 1026644, 3002001788) estimate the capital cost of an A-USC PC unit at approximately 10% more than the cost of a “state-of-the-art” USC PC unit based on U.S. market prices and labor rates. A significant portion of this increase is due to the high cost of the main steam and reheat steam lines in a conventionally arranged boiler. These lines are approximately 140 m (450 ft) long, and would be constructed from IN740. IN740 is a new material for this application, and the price is very high—approximately $75–90/kg ($35–40/lb) at the time of the studies. Due to the long length of these piping runs and the thickness of the main steam line, the cost of these two piping runs can approach the cost of the boiler!

Two design approaches have emerged to address the cost of these piping leads. One approach, being pursued in China is to split the HP and IP steam turbine into two components. The HP turbine and a “high temperature” IP (HTIP) turbine section would be located at the top of the boiler near the main and reheat steam outlets, with a conventional IP/LP turbine located on the turbine floor several hundred feet away (i.e.,

short connecting piping runs where nickel alloy is required and longer runs where ferritic alloys are sufficient). The exhaust of the HTIP turbine would be reheated, but to a more "typical" reheat temperature before flowing to a conventional IP/LP turbine. This arrangement is illustrated in Figure 6-2 and Figure 6-3.

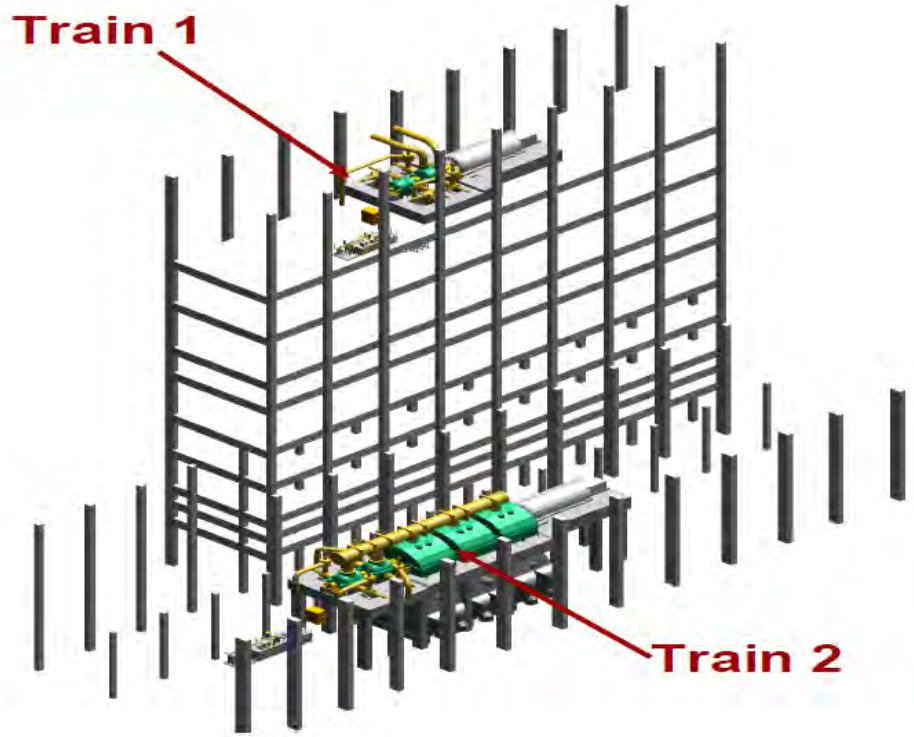

Figure 6-2
Layout of a High and Low Position Steam Turbine Arrangement

(Source: Shanghai Waigaoqiao)

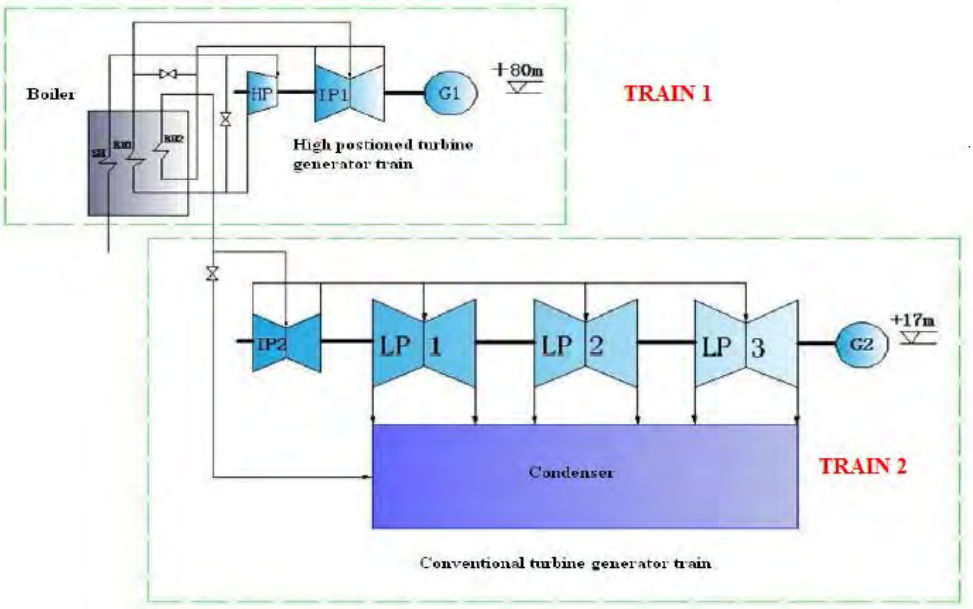

Figure 6-3
Turbine Train Schematic Showing Components

(Source: Shanghai Waigaoqiao)

A second approach is the “Inverted Tower” arrangement proposed by Babcock and Wilcox, shown in Figure 6-4.[23]

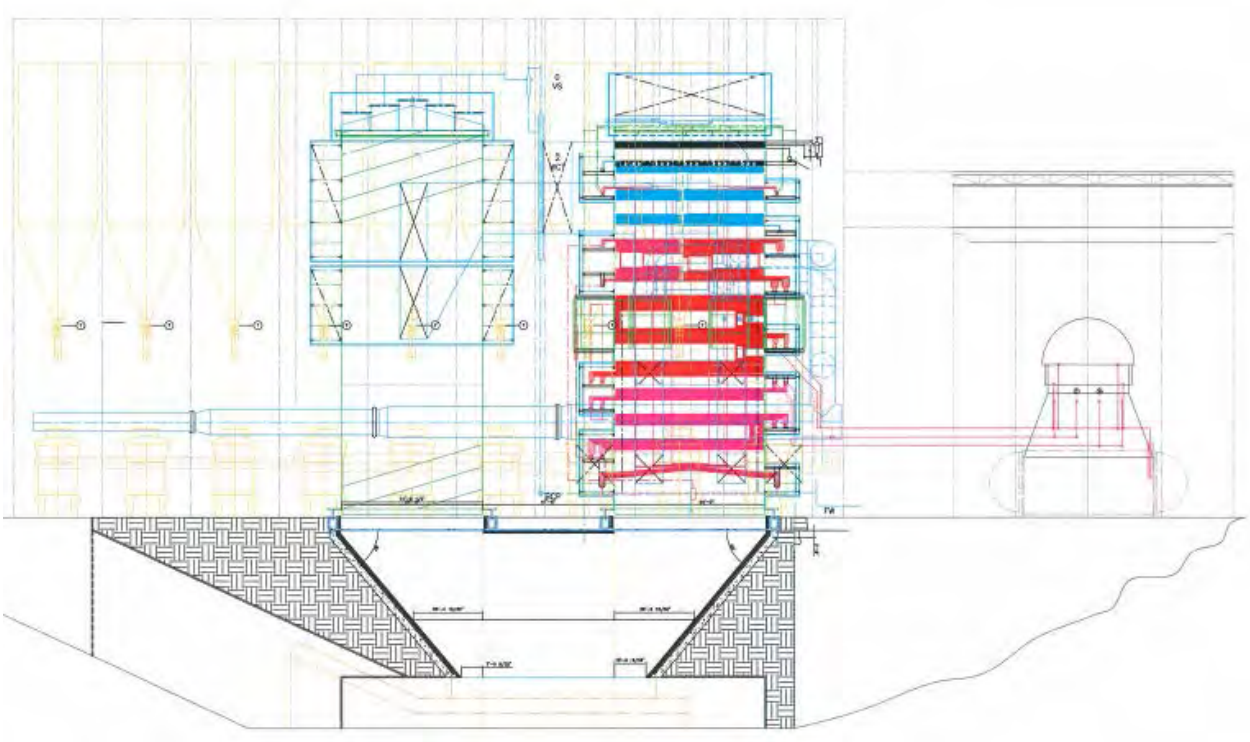

Figure 6-4
Babcock and Wilcox Downdraft Inverted Tower Design

In this design, coal is fed into the furnace enclosure (shown on the left in the drawing) and the hot gas exhausts vertically down into a refractory lined “adiabatic tunnel,” where the flue gas turns 180 degrees and flows upward through the backpass. In this configuration, the finishing superheater and reheater are located at the turbine elevation, minimizing the length of the nickel alloy piping. According to a DOE study[24], the capital cost of an A-USC PC boiler with this configuration could be comparable to that of a USC PC boiler.

There was insufficient information to estimate the design and cost of these two arrangements. However, a “sensitivity” was performed assuming that main steam/reheat steam piping was one-half of the original length. This would decrease the capital cost by about $95 million or 4.3%.

Another likely decrease in capital cost would be due to a drop in the cost of the IN740 piping. IN740 is a relatively new material, and to date the supply for the material in boiler applications has been very limited. As A-USC boiler technology becomes more widespread, the demand for the material will create a greater supply base and the price

[23] Courtesy of Babcock and Wilcox.

[24] “Estimated Costs of the AUSC Boiler, Steam Turbine, and Steam Piping”, U.S. Department of Energy/NETL Office of Fossil Energy, under DOE Contract Number DE-FE0004001, ESPA Task 341.03.01, September 5, 2014.

may fall. A second sensitivity analysis was performed, which indicated that a 20% decrease in IN740 cost would decrease the capital cost by approximately $41 million or 1.9%. The combination of the lower IN740 cost with the shorter main steam/reheat steam piping would decrease the cost by over $110 million or 5.1%.

Higher Pressure Steam Cycle

Increasing efficiency is the motivation behind increasing the temperature for A-USC steam conditions and, as discussed in Section 4, increasing the steam cycle pressure further increases the cycle efficiency. One of the sensitivities studied for this report included evaluating the performance and economics of a 242 bara (3500 psig) steam cycle compared with a 294 bara (4250 psig) steam cycle for Case 2 CO_2 removal. Section 4 concluded that higher inlet pressure was not economical for an A-USC PC unit without carbon capture. Following the same methodology laid out for the PCC system with heat integration as described in Section 5, a comparison of the two steam cycles is shown in Table 6-3 to determine if higher inlet pressures are economical for an A-USC PC unit with carbon capture.

Table 6-3
Performance Comparison of a 242 bara (3500 psig) steam cycle compared to a 294 bara (4250 psig) steam cycle with Carbon Capture to meet 1100 lb CO_2/MWh standard

Description	241 bara (3500 psia)	293 bara (4250 psia)
Gross Power, kW	809,071	809,628
Auxiliary load, kW	100,742	101,918
Net Power, kW	708,329	707,710
Heat Rate, Btu/kWh	8,778	8,640
Net Efficiency, %	38.9	39.5
Portion of flue gas treated, %	34.0	33.1
TIC, $(000)	$2,390,000	$2,430,000
TIC, $/kW	$3,370	$3,430
Annual Operating Cost, $/yr,	$498,067,000	$503,382,000
LCOE, $/MWh	$100.20	$101.50
Heat Rate Improvement, Btu/kWh	138	
Delta Plant Cost, $(000)	$40,000	
Delta cost per Btu/kWh	$290,000	

Based on the assumptions made in the analysis, interesting observations include:

- The increased efficiency of the steam cycle decreased the coal being burned in the boiler by about 2.7%. This decreased the amount of flue gas required to be treated

in the PCC system and reduced the auxiliary load of the PCC system approximately 1 MW.

- However, the increased discharge pressure of the boiler feedwater pump for the 4250 psi case was approximately 2 MW, so the 4250 psig cycle had a higher auxiliary load.
- Even though the cost of the 4250 psig system PCC system was marginally lower in cost, the difference was relatively small. What was more significant was the increased capital cost due to the thicker boiler components, especially the high-cost nickel alloys.

From this analysis, it appears that the addition of a PCC system decreases the cost per unit of heat rate improvement associated with moving from 3500 psig to 4250 psig when compared to the value presented in Section 4. However, a value of roughly $290,000 per Btu/kWh of heat rate is still higher than the U.S. utility market is likely to accept.

7
CONCLUSIONS AND FUTURE WORK

Summary of Findings

A-USC development over the past 15+ years has significantly advanced the technology to the point where it is on the cusp of commercial deployment. The increased efficiency of the technology has two significant business "drivers:"

1) In power markets where CO_2 regulations require the use of carbon capture on coal plants, increasing the efficiency of the power cycle decreases the CO_2 emitted per MW of electricity produced. In scenarios that require partial CO_2 capture, such as that proposed by the U.S. EPA 111(b) regulation, the higher efficiency decreases the penalty associated with adding carbon capture to the power plant.

2) In the U.S. power industry market, coal fired plants typically have low fuel prices and high capital/labor costs. The largest component of the LCOE is associated with the capital for building the plant. However, this is not the case in other parts of the world where fuel prices are much higher and labor is less expensive. In these cases the fuel cost savings associated with the improved efficiency offsets the higher capital cost.

Past EPRI studies have shown that when compared to USC, the cost of A-USC is approximately 10% higher in capital cost. For this study, the estimated capital cost was $2,933/kW, and the LCOE was $84.70 (Table 7-1 and Table 7-2). A significant contributor to the higher cost has been the long main and reheat steam piping lines, which would be fabricated from Inconel 740. This impact on capital cost has led the power industry to respond with several innovative boiler concepts, as discussed in Section 6. Capital cost estimates on some of these concepts indicate that they may result in reductions that would bring the cost of an A-USC plant into parity with an equivalently sized USC plant. As these concepts are further developed, A-USC technology will likely become more cost competitive. The A-USC programs in countries such as China and India have announced plans to build plants within the next decade. As experience is gained with the technology, the risks and cost associated with a new technology will diminish.

In addition to the research on A-USC, research continues around the world on CO_2 capture technologies for PC plants. Facilities like the DOE's National Carbon Capture Center are evaluating the performance of new solvents and CO_2 technologies that will dramatically decrease the cost of post-combustion carbon capture. Coupling the high efficiency of A-USC technology with these advanced solvents and other removal technologies should minimize the cost of carbon capture from pulverized coal plants.

In this study, an advanced solvent system was used to remove CO_2 down to a level of 500 kg CO_2/MWh (1100 lb CO_2/MWh). To meet this requirement, only 34% of the flue gas had to be treated. Steam from the turbine was required to regenerate the solvent,

but due to the high efficiency and the advanced solvent the steam flow was dramatically reduced compared to past studies on USC power plants using MEA as the solvent for carbon capture. In Case 2 the gross power from the steam turbine decreased only 16 MW (about 2%) when this regeneration steam was extracted from the turbine. The auxiliary load increased nearly 30 MW, with 21 of the 30 MW associated with CO_2 compression.

The capital cost of the CO_2 removal equipment was estimated to be approximately $178 million, approximately 8% more than the base plant cost. But when divided by the net power the cost increased $440/kW (about 15%) due to a combination of the increased capital and lost generation. The LCOE increased about 19% due to the increased capital, lost generation, and increased operating labor and materials associated with the carbon capture system.

Shortly before the initial draft of this report, President Obama and the EPA announced the Clean Power Plan. At DOE's request, EPRI evaluated a case using the same basis as the 500 kg CO_2/MWh (1100 lb CO_2/MWh), but using the new emission limit of 636 kg CO_2/MWh (1400 lb CO_2/MWh). Because of the higher emission limit, only 15% of the flue gas had to be treated. This combination of the decreased PCC solvent regeneration requirement and the decreased auxiliary load of the PCC system, the net power for this case improved 26 MW compared to the 500 kg CO_2/MWh (1100 lb CO_2/MWh) case and improved the economic performance. The economic "penalty" associated with the carbon capture system under the Clean Power Plan for this AUSC unit is approximately 10% when compared to the "base" AUSC power plant with no PCC system as shown in Tables 7-1 and 7-2.

Table 7-1
Case Comparison (SI Units)

Description	No Carbon Capture	500 kg CO_2/MWh	635 kg CO_2/MWh
Feedwater heaters	Five LP, deaerator, three HP, topping desuperheater		
Feed pump drive	Motor		
Cooling system	Mechanical draft cooling tower		
Emission controls	SCR, ESP, Wet FGD, and $CaBr_2$ injection into the furnace for NO_x, particulate, sulfur, and mercury control		
Throttle conditions	242 bar/732°C/760°C	242 bar/732°C/760°C	242 bar/732°C/760°C
Main steam flow	1,818,000 kg/h	1,818,000 kg/h	1,818,000 kg/h
Hot reheat flow	1,563,000 kg/h	1,563,000 kg/h	1,563,000 kg/h
Condenser flow	1,412,000 kg/h	1,440,000 kg/h	1,186,000 kg/h
Condenser pressure	6.7 kPa	6.7 kPa	6.7 kPa
Final feedwater temp	304°C	304°C	304°C
Steam to PCC System	N/A	161,000 kg/h	71,700 kg/h
Gross plant output, kW	825,000	809,071	818,438
Auxiliary load, kW	70,801	100,742	84,060
Net plant output, kW	754,199	708,329	734,338
Net plant heat rate	8,698 kJ/kWh	9,261 kJ/kWh	8,933 kJ/kWh
Net plant efficiency, % (HHV)	41.4	38.9	40.3
Plant fuel consumption	338,000 kg/hr	338,000 kg/hr	338,000 kg/hr
CO_2 emission without PCC	596,000 kg/hr	393,000 kg/hr	506,200 kg/hr
CO_2 emission without PCC	722 kg/MWh, gross basis	500 kg/MWh, EPA gross basis	635 kg/MWh, EPA gross basis
Total Capital Cost, $(000)	$2,212,000	$2,379,000	$2,344,000
Total Capital Cost, $/kW	$2,933	$3,370	$3,190
Total Operating Costs, $(000)/yr	$448,410	$498,067	$480,231
LCOE, $/MWh	$84.70	$100.20	$93.30

Table 7-2
Case Comparison (U.S. Customary Units)

Description	No Carbon Capture	1100 lb CO_2/MWh	1400 lb CO_2/MWh
Feedwater heaters	Five LP, deaerator, three HP, topping desuperheater		
Feed pump drive	Motor		
Cooling system	Mechanical draft cooling tower		
Emission controls	SCR, ESP, Wet FGD, and $CaBr_2$ injection into the furnace for NO_x, particulate, sulfur, and mercury control		
Throttle conditions	3515 psia/1350°F/1400°F	3515 psia/1350°F/1400°F	3515 psia/1350°F/1400°F
Main steam flow	4,008,000 lb/hr	4,008,000 lb/hr	4,008,000 lb/h
Hot reheat flow	3,375,000 lb/hr	3,375,000 lb/hr	3,375,000 lb/h
Condenser flow	3,112,000 lb/hr	3,175,000 lb/h	2,615,000 lb/h
Condenser pressure	2 inches mercury	2 inches mercury	2 inches mercury
Final feedwater temp	580°F	580°F	580°F
Steam to PCC System	N/A	355,000 lb/h	158,000 lb/h
Gross plant output, kW	825,000	809,071	818,438
Auxiliary load, kW	70,801	100,742	84,050
Net plant output, kW	754,199	708,329	734,338
Net plant heat rate	8,244 Btu/kWh	8,778 Btu/kWh	8,467 Btu/kWh
Net plant efficiency, % (HHV)	41.4	38.9	40.3
Plant fuel consumption	746,000 lb/hr	746,000 lb/hr	746,000 lb/hr
CO_2 emissions (Case 2 with PCC)	1,313,000 lb/hr	867,000 lb/hr	1,116,000 lb/hr
CO_2 emissions (Case 2 with PCC)	1592 lb/MWh, gross basis	1100 lb/MWh, EPA gross	1400 lb/MWh, EPA gross
Total Capital Cost, $(000)	$2,212,000	$2,379,000	$2,344,000
Total Capital Cost, $/kW	$2,933	$3,370	$3,190
Total Operating Costs, $(000)/yr	$448,410	$498,067	$480,231
LCOE, $/MWh	$84.70	$100.20	$93.30

The Next Step

As discussed in Section 1, many of the international programs, including the DOE/EIO lead program in the United States have tested or are planning to test steam loops at A-USC conditions. The next logical step is to move toward a commercial demonstration of the technology. With guidance from the U.S. Utility Industry, the Advanced Materials for Ultra-Supercritical Boiler and Steam Turbine Consortia developed the “Component Test (ComTest) Program Concept” as illustrated in Figure 7-1. The utility members working with the consortium identified these components, previously described in Section 1, as needing further development and demonstration: the Membrane Wall, Superheater, High-Pressure, High-Temperature Valve Test, Desuperheater/Thick-Wall Section and the Steam Turbine.

As originally conceived all of these components would be installed in and adjacent to a utility host’s USC power plant. Steam would be withdrawn from the power plant’s main steam line. A portion of the steam would be desuperheated and flow through the membrane wall, which would be installed inside the furnace. The second portion of the steam would flow through the in-furnace superheater where it would be heated to approximately 760°C (1400°F). From the exit of this superheater, the steam would flow through a gas-fired auxiliary superheater which would be used to control the temperature of the steam as the host unit changes load throughout the day. The high pressure, 760°C (1400°F) steam would next flow through the High Pressure, High Temperature valve test apparatus. Two steam turbine stop and control valves would be installed in parallel and cycle continuously throughout the test. Desuperheating the steam will be a requirement for temperature control in any utility boiler, so the steam leaving the valve test will next enter the desuperheating section. This component proved problematic in the European COMTES700 facility, so validation of this technology is crucial. A downstream thick wall section will simulate a superheater header, complete with flowing pipe penetrations. The desuperheater will be used thermally cycle this component to determine its susceptibility to cracking during boiler cycling. After the thick wall section, the steam from the membrane wall will combine with the steam flowing through the thick wall section and be depressurized to approximately 48 bar (700 psia) before flowing through the steam turbine. Depressurizing the steam will decrease its temperature, so the steam will flow through a gas-fired auxiliary reheater to increase the temperature back to 760°C (1400°F) before expanding through the steam turbine. The exhaust steam will then be desuperheated and depressurized (if necessary) before returning to the host’s steam/condensate system.

As the consortium searched for hosts for the ComTest, Youngstown Thermal in Youngstown, Ohio, expressed interest early in hosting the lower pressure components—primarily the A-USC steam turbine (Figure 7-2). Youngstown Thermal is a district heating facility that provides saturated steam at approximately 10 bar (150 psi) to its customers in the downtown area. To test the steam turbine, natural gas-fired package boilers would be rented and brought to the site (Figure 7-3). These boilers would provide steam at nominally 48 bar (700 psia) and 400°C (750°F). The steam from the package boilers would flow through a gas-fired superheater developed by Babcock and Wilcox with DOE funding (see Figure 7-4). The superheater is designed to heat the steam to 760°C (1400°F). The steam would then flow through the steam turbine and

would be exhausted at approximately 12 bar (170 psia) and desuperheated to saturated temperature before flowing into the header system supplying Youngstown Thermal's customers. This project would evaluate membrane walls (in the superheater), superheater coil, steam turbine, and high temperature (but lower pressure) steam control and stop valves at A-USC temperatures. Proposals for this project have been submitted to the DOE and these proposals are under review as of mid-2015. At the same time, conversations continue between the Consortium and potential utility hosts about testing the components of the ComTest Program that require high-pressure steam.

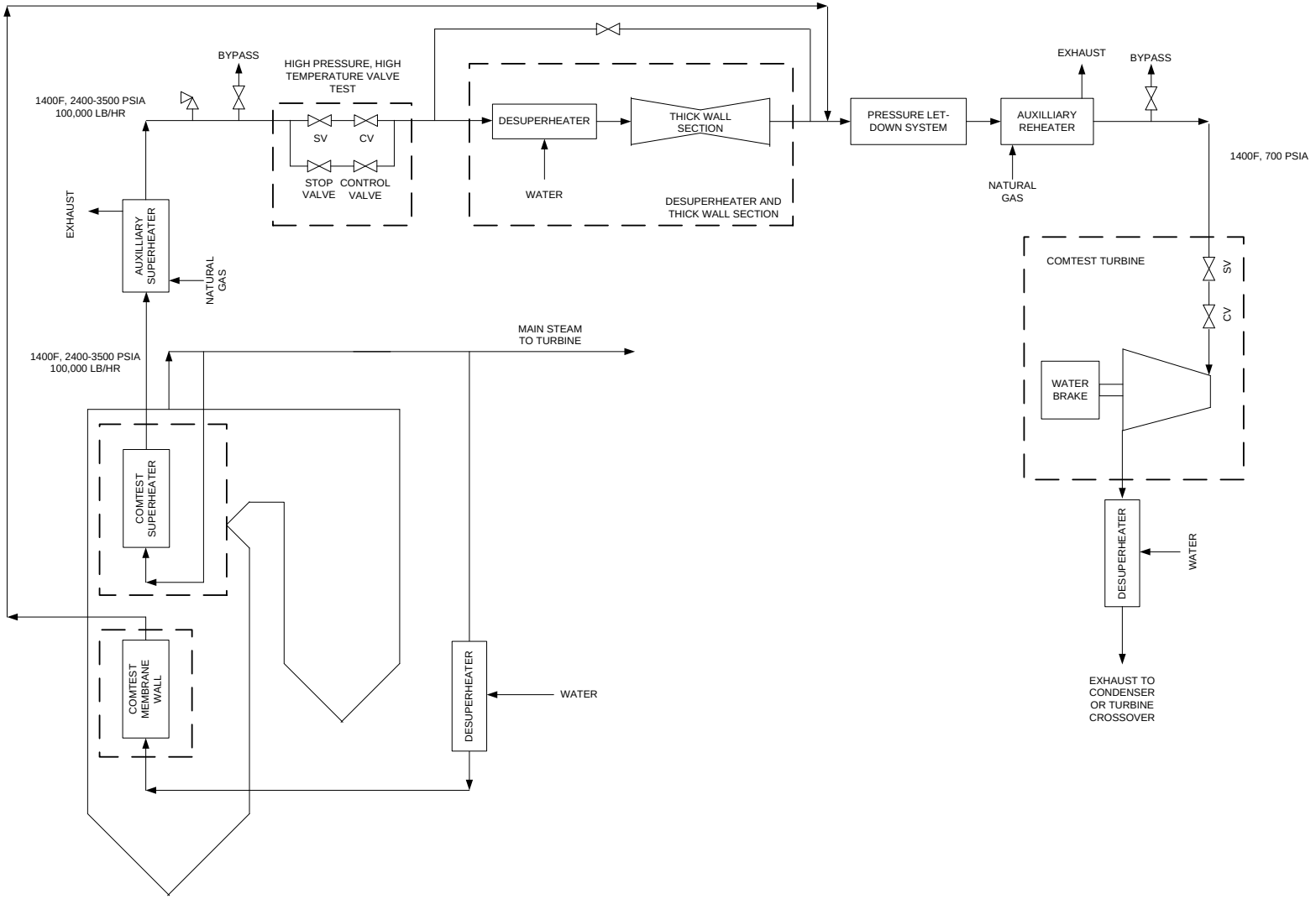

Figure 7-1
Overall A-USC ComTest Program Concept

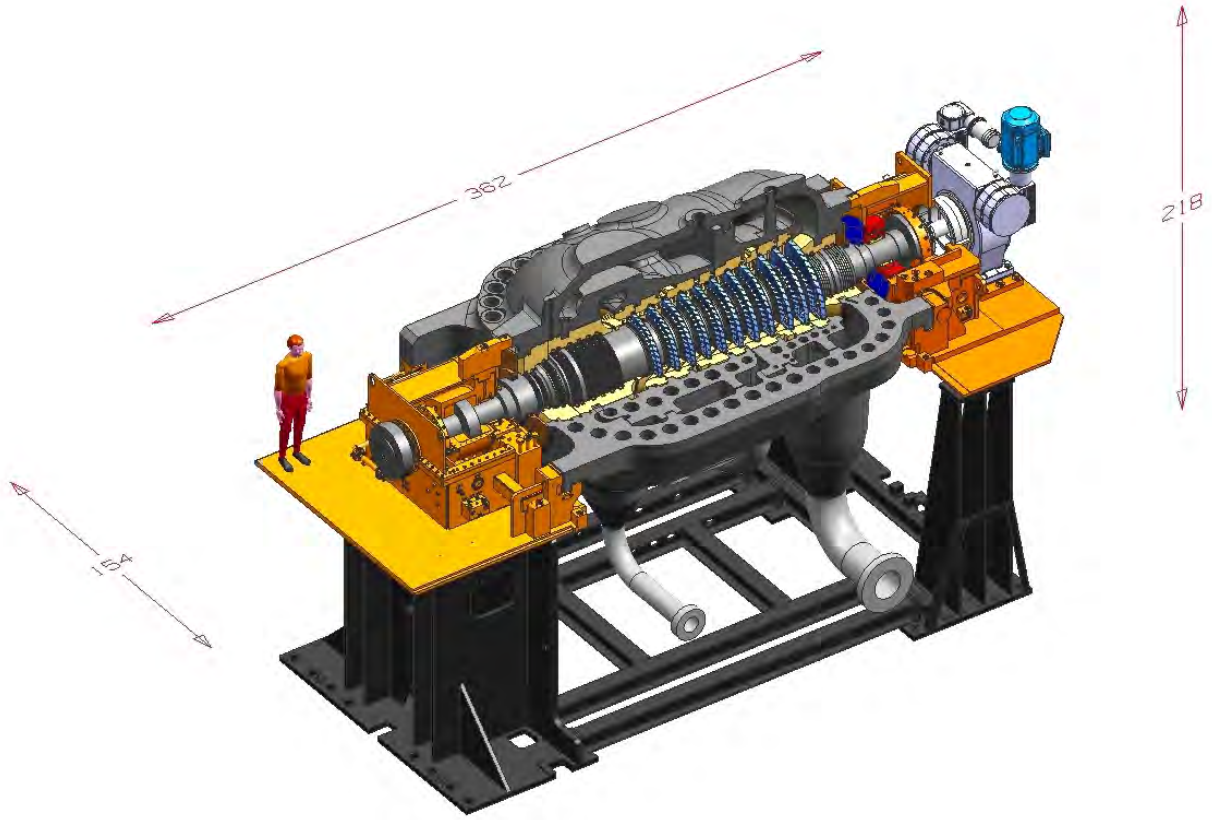

Figure 7-2
General Electric A-USC Steam Turbine Concept (Dimensions in inches)[25]

[25] Courtesy of General Electric

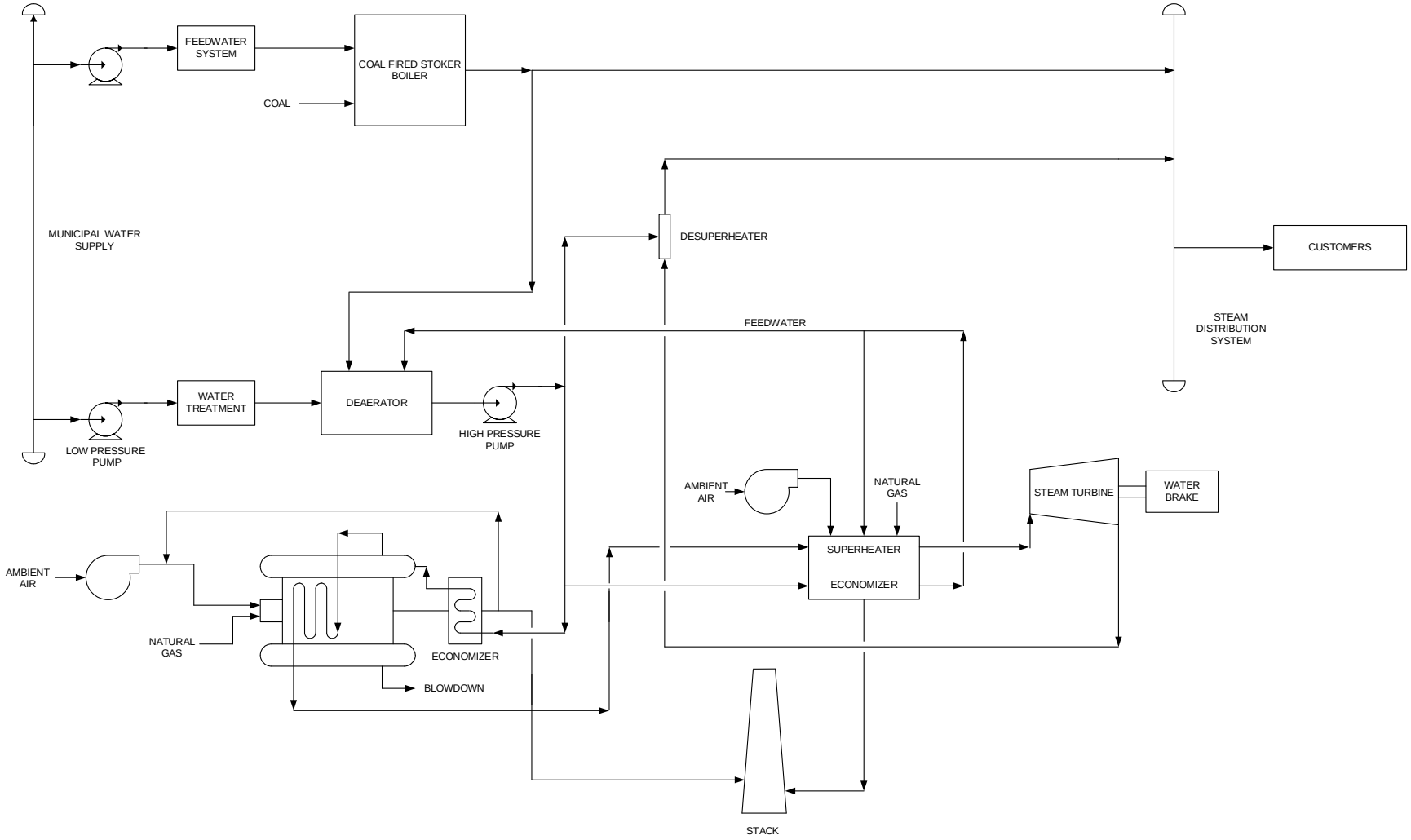

Figure 7-3
Proposed Youngstown Thermal Flowsheet

Figure 7-4
Babcock and Wilcox A-USC ComTest Superheater Tower[26]References

[26] Courtesy of Babcock and Wilcox

8
REFERENCES

1. Engineering and Economic Evaluation of 1300°F Series Ultra-Supercritical Pulverized Coal Power Plants: Phase 1. EPRI, Palo Alto, CA: 2008. 1015699.
2. Engineering and Economic Analysis of 1300°F Series USC Plant with Post-Combustion Capture. EPRI, Palo Alto, CA, 2011. 1026645.
3. An Engineering and Economic Assessment of Post-Combustion CO_2 Capture for 1100°F Ultra-Supercritical Pulverized Coal Power Plant Applications: Phase II Task 3 Final Report. EPRI, Palo Alto, CA: 2010, 1017515.
4. Engineering and Economic Analysis of a 1300°F Series USC Demonstration Plant with Natural Gas Equivalency Post-Combustion Capture. EPRI, Palo Alto, CA, 2013. 1026644.

A
PROCESS FLOW DIAGRAM/HEAT AND MATERIAL BALANCE

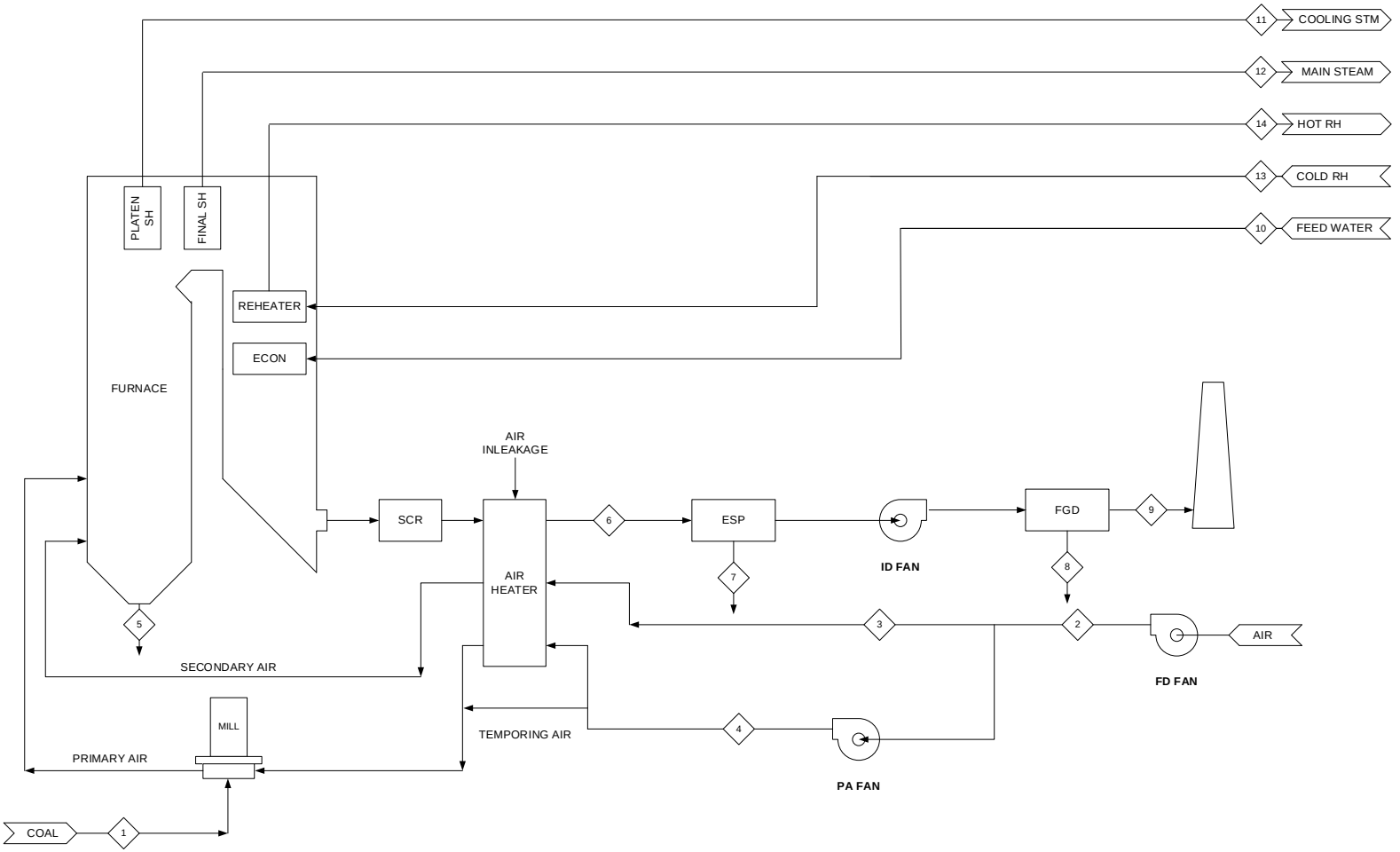

Figure A-1
Boiler Island

Table A-1
Boiler Island Material Balance for Case 1 & 2

Boiler/AQCS Heat and Material Balance											
PFD Stream		1	2	3	4	5	6	7	8	9	10
Aspen Stream		WET-COAL	TOTAIR	SATOAIRH	PATOAIRH	BTMASH	AIRHTOUT	FLYASH		0	BFW1
Description		As Received Coal	Air From FD Fan	Secondary Air to Air Heater	Primary Air To Air Heater	Bottom Ash	Flue Gas to ESP	Fly Ash	Gypsum	To Stack	Boiler Feed Water
Temperature	F	95	101	101	118	95	264	95	95	138	581
Pressure	psia	14.7	15.2	15.2	16.6	14.7	13.7	13.5	14.7	14.8	3865.3
Component											
N2	lb/hr	-	4,202,215	3,151,661	1,050,554	-	4,674,018	-	-	4,680,608	-
O2	lb/hr	-	1,275,960	956,970	318,990	-	354,011	-	-	354,679	-
CO2	lb/hr	-	-	-	-	-	1,309,556	-	-	1,313,228	-
CO	lb/hr	-	-	-	-	-	-	-	-	-	-
H2O	lb/hr	-	143,379	107,534	35,845	-	606,406	-	-	859,264	4,100,352
NO2	lb/hr	-	-	-	-	-	251	-	-	251	-
SO2	lb/hr	-	-	-	-	-	5,508	-	-	161	-
SO3	lb/hr	-	-	-	-	-	4	-	-	4	-
HCL	lb/hr	-	-	-	-	-	77	-	-	-	-
NO	lb/hr	-	-	-	-	-	-	-	-	-	-
S	lb/hr	-	-	-	-	-	-	-	-	-	-
H2	lb/hr	-	-	-	-	-	-	-	-	-	-
CL2	lb/hr	-	-	-	-	-	0	-	-	-	-
C	lb/hr	-	-	-	-	0	-	-	-	-	-
NH3	lb/hr	-	-	-	-	199	1,597	1,594	-	-	-
COAL	lb/hr	745,528	-	-	-	-	-	-	-	-	-
ASH	lb/hr	-	-	-	-	4,405	35,257	35,201	-	-	-
LIMESTONE	lb/hr	-	-	-	-	-	-	-	-	-	-
GYPSUM	lb/hr	-	-	-	-	-	-	-	18,645	-	-
Total Mass Flow	lb/hr	745,528	5,621,554	4,216,165	1,405,388	4,604	6,986,684	36,795	18,645	7,208,195	4,100,352

Table A-2
Boiler Island Material Balance for Case 1 & 2 (Continued)

Boiler/AQCS Heat and Material Balance											
PFD Stream		**11**	**12**	**13**	**14**						
Aspen Stream			STM7	CRH	HRHOUT						
Description		Cooling Steam	Main Steam	Cold Reheat	Hot Reheat						
Temperature	F	1100	1352	888	1400						
Pressure	psia	3600.0	3585.3	772.5	739.5						
Component											
Component	lb/hr	-	-	-	-						
N2	lb/hr	-	-	-	-						
O2	lb/hr	-	-	-	-						
CO2	lb/hr	-	-	-	-						
CO	lb/hr	-	4,007,852	3,375,254	3,375,254						
H2O	lb/hr	92,500	-	-	-						
NO2	lb/hr	-	-	-	-						
SO2	lb/hr	-	-	-	-						
SO3	lb/hr	-	-	-	-						
HCL	lb/hr	-	-	-	-						
NO	lb/hr	-	-	-	-						
S	lb/hr	-	-	-	-						
H2	lb/hr	-	-	-	-						
CL2	lb/hr	-	-	-	-						
C	lb/hr	-	-	-	-						
NH3	lb/hr	-	-	-	-						
COAL	lb/hr	-	-	-	-						
ASH	lb/hr	-	-	-	-						
LIMESTONE	lb/hr	-	-	-	-						
Total Mass Flow	lb/hr	92,500	4,007,852	3,375,254	3,375,254	-	-	-	-	-	-

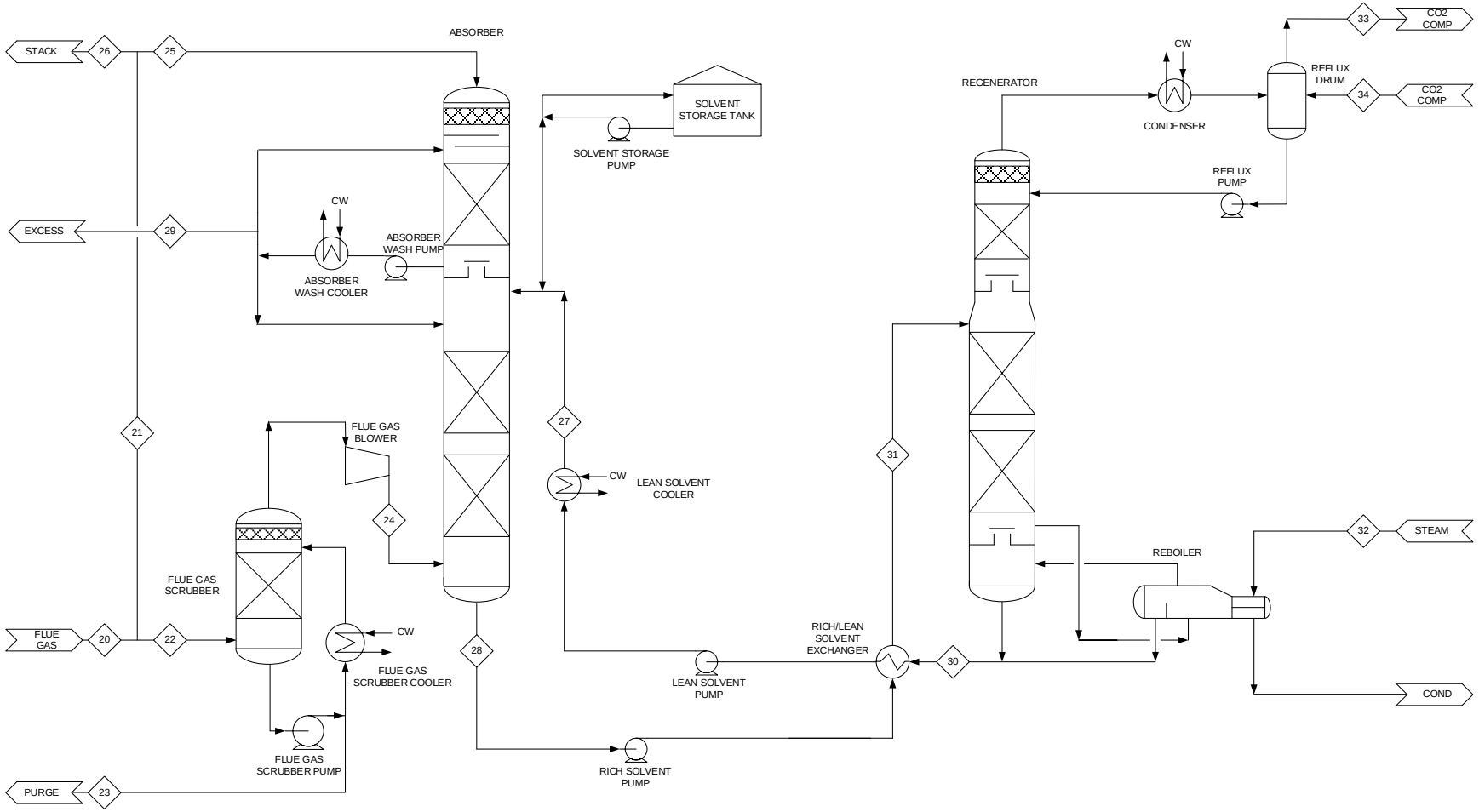

Figure A-2
Post-Combustion CO_2 Removal System

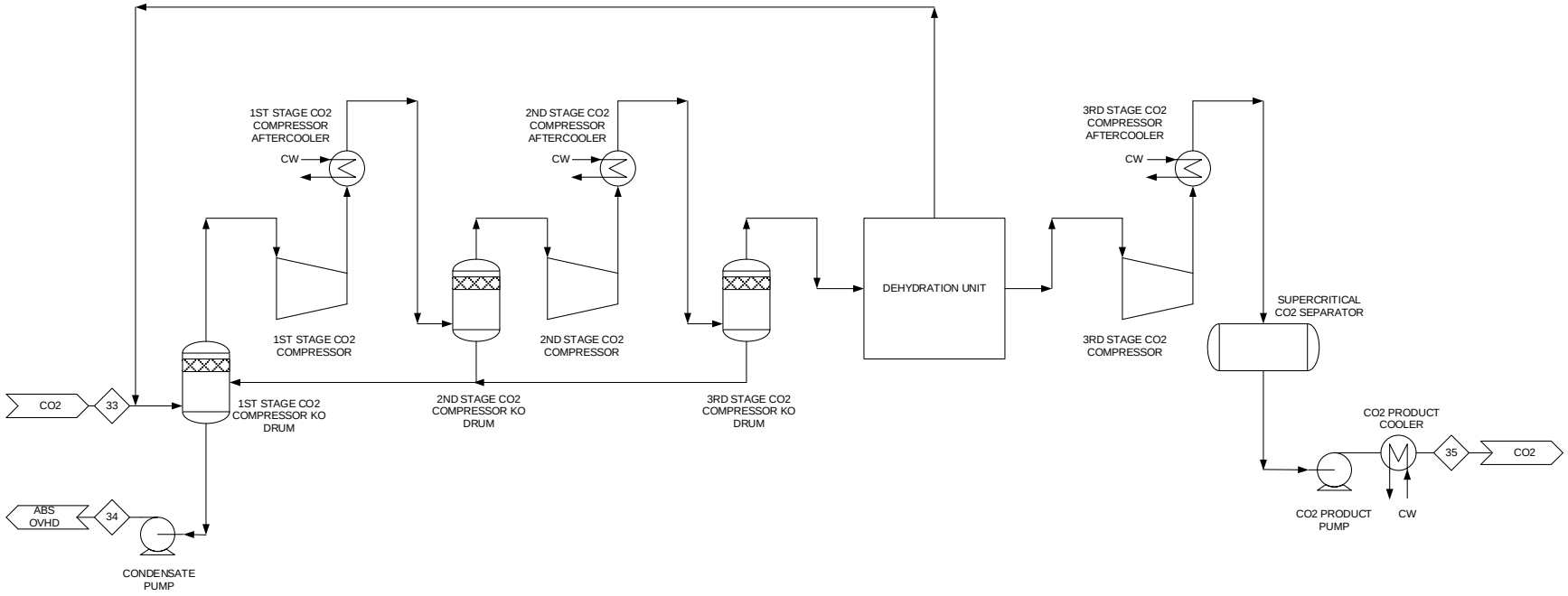

Figure A-3
CO_2 Compression System

Table A-3
Post-Combustion CO_2 Removal System Material Balance for Case 2

Stream Number	20	21	22	23	24	25	26	27	28	29	30
Stream Description	Flue Gas Downstream of ID Fan	Bypass Flow	Flue Gas to PCC System	Feed Gas Water Condensate	Flue Gas Entering Absorber	Flue Gas Exiting Absorber	Flue Gas Exiting Stack	Lean Solvent Entering Absorber	Rich Amine Exiting Absorber	Purge water from Absorber Cooler	Lean Amine Leaving Stripper Bottoms
Temperature (F)	138	138	138	123	136	130	136	100	145	130	255
Pressure (psia)	14.8	14.8	14.8	60.0	15.6	14.7	14.7	60.0	15.6	14.7	28.2
Mass Flow, lb/hr											
N2	4,680,608	3,088,465	1,592,144	-	1,592,144	1,592,144	4,680,608	-	-	-	-
O2	354,679	234,032	120,647	-	120,647	120,647	354,679	-	-	-	-
CO2	1,313,228	866,524	446,704	-	446,704	44,670	911,194	82,941	484,975	-	82,941
CO	-	-	-	-	-	-	-	-	-	-	-
H2O	859,447	567,100	292,347	161,416	130,931	198,012	765,112	-	-	28,284	-
NO2	251	165	85	-	85	85	251	-	-	-	-
SO2	161	106	55	-	55	55	161	-	-	-	-
SO3	4	3	1	-	1	1	4	-	-	-	-
HCL	-	-	-	-	-	-	-	-	-	-	-
NO	-	-	-	-	-	-	-	-	-	-	-
S	-	-	-	-	-	-	-	-	-	-	-
H2	-	-	-	-	-	-	-	-	-	-	-
CL2	-	-	-	-	-	-	-	-	-	-	-
NH3	-	-	-	-	-	-	-	-	-	-	-
C	-	-	-	-	-	-	-	-	-	-	-
COAL	-	-	-	-	-	-	-	-	-	-	-
ASH	-	-	-	-	-	-	-	-	-	-	-
SOLVENT FLOW	-	-	-	-	-	-	-	3,169,664	3,169,664	-	3,169,664
TOTAL, LB/HR	7,208,378	4,756,395	2,451,983	161,416	2,290,567	1,955,614	6,712,009	3,252,605	3,654,639	28,284	3,252,605

Table A-4
Post-Combustion CO_2 Removal System Material Balance for Case 2 (Continued)

Stream Number	31	32	33	34	35						
Stream Description	Rich Amine Entering Stripper	Steam Entering Reboiler	CO2 to Compressor	Water from CO2 Compressor	Product CO2						
Temperature (F)	235	271	100	100	100						
Pressure (psia)	60.0	36.0	21.3	30.0	2215.0						
Mass Flow, lb/hr											
N2	-	-	-	-	-						
O2	-	-	-	-	-						
CO2	484,975	-	402,034	-	402,034						
CO	-	-	-	-	-						
H2O	-	422,312	7,682	7,682	-						
NO2	-	-	-	-	-						
SO2	-	-	-	-	-						
SO3	-	-	-	-	-						
HCL	-	-	-	-	-						
NO	-	-	-	-	-						
S	-	-	-	-	-						
H2	-	-	-	-	-						
CL2	-	-	-	-	-						
NH3	-	-	-	-	-						
C	-	-	-	-	-						
COAL	-	-	-	-	-						
ASH	-	-	-	-	-						
SOLVENT FLOW	3,169,664	-	-	-	-						
TOTAL, LB/HR	3,654,639	422,312	409,715	7,682	402,034						

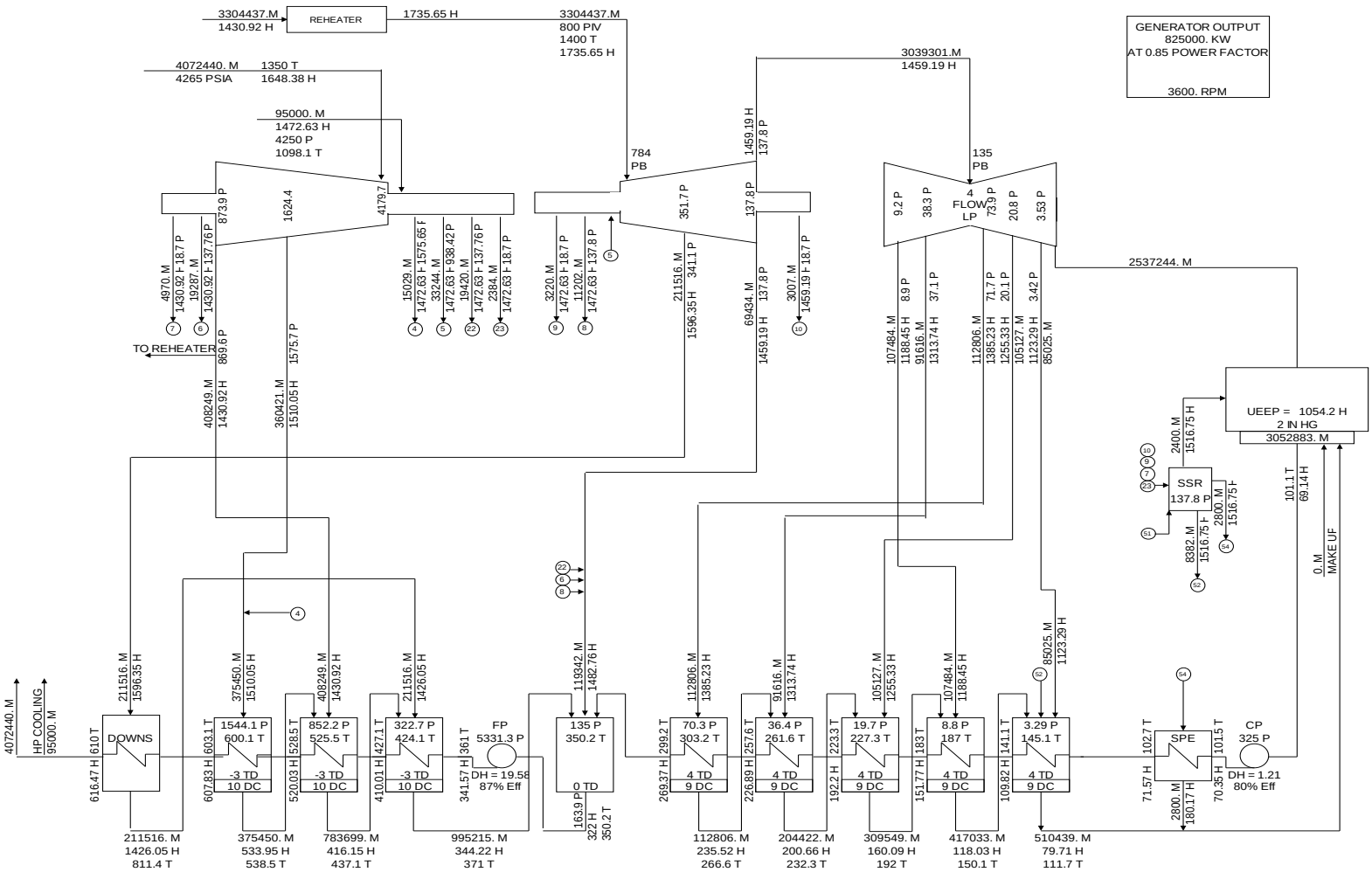

Figure A-4
4250 psig Inlet Pressure Steam Cycle Diagram, No PCC

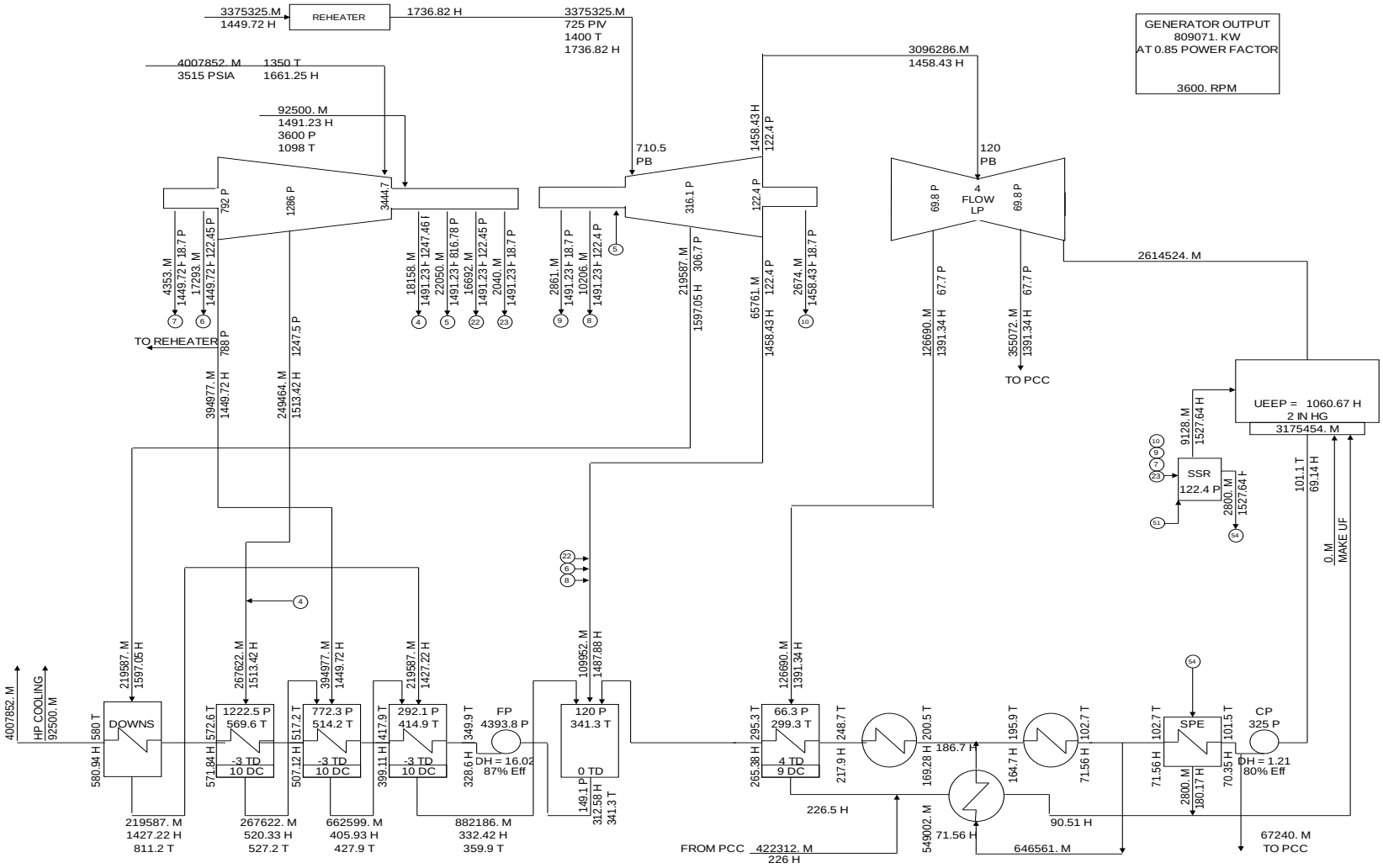

Figure A-5
3500 psig Inlet Pressure Steam Cycle Diagram, PCC System

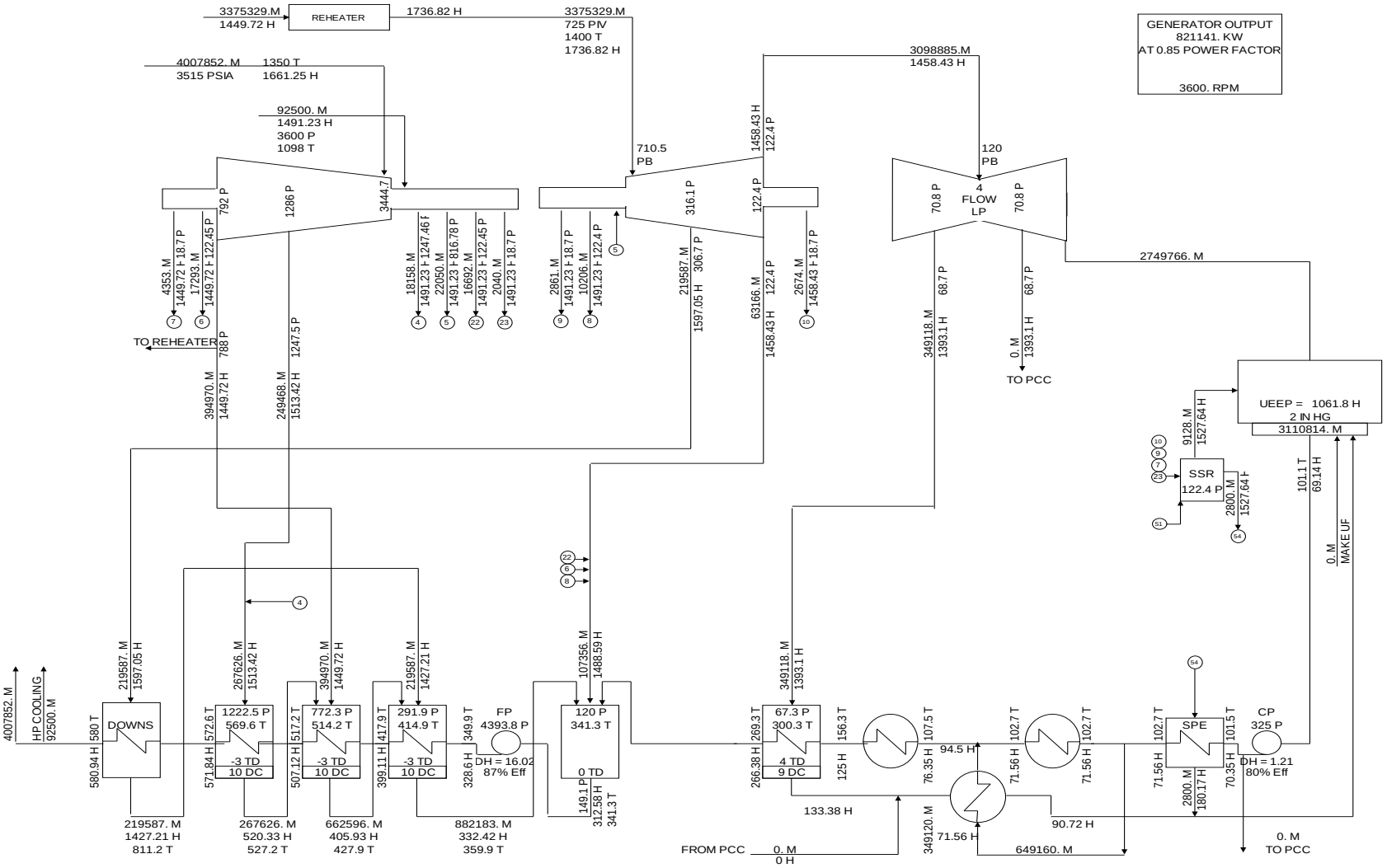

Figure A-6
3500 psig Inlet Pressure Steam Cycle Diagram, PCC System Off

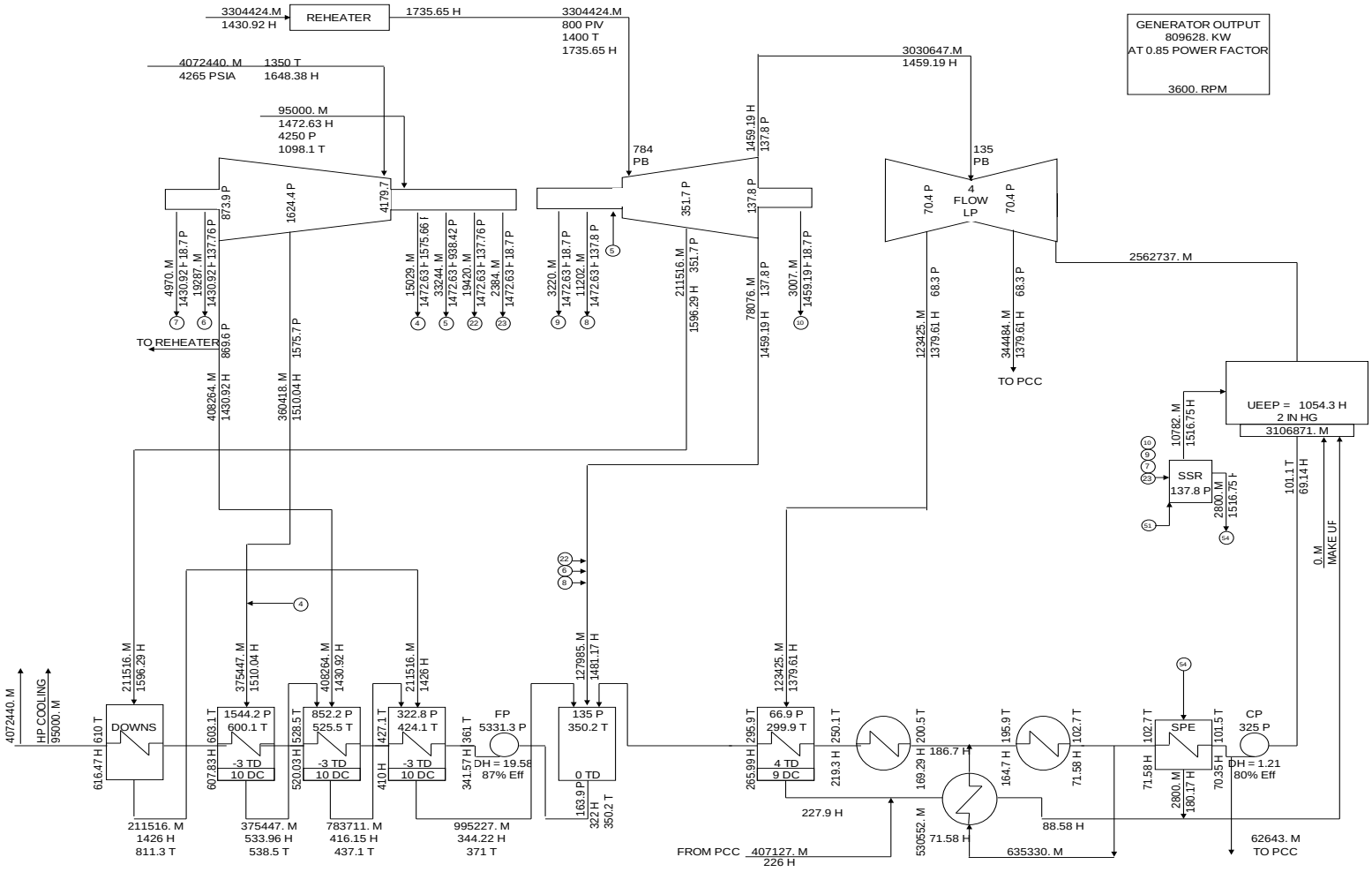

Figure A-7
4250 psig Inlet Pressure Steam Cycle Diagram, PCC

Table A-5
PC-Cost Output Datafile

Account		3500 psig $1000s of Dollars	4250 psig $1000s of Dollars
1.0 EarthWork			
Labor	Acct1.0_L	$ 9,904	$ 9,855
Materials	Acct1.0_M	$ 4,936	$ 4,921
Subcontractors	Acct1.0_S	$ 10,610	$ 10,552
Subtotal		$ 25,450	$ 25,327
1.1 Landscaping Earthwork			
Labor	Acct1.1_L	$ -	$ -
Materials	Acct1.1_M	$ -	$ -
Subcontractors	Acct1.1_S	$ 1,452	$ 1,433
Subtotal		$ 1,452	$ 1,433
1.2 Gravel Earthwork			
Labor	Acct1.2_L	$ 3,260	$ 3,260
Materials	Acct1.2_M	$ 1,304	$ 1,304
Subcontractors	Acct1.2_S	$ -	$ -
Subtotal		$ 4,563	$ 4,563
1.3 Offshore and Waterfront Additions - Dock			
Labor	Acct1.3_L	$ -	$ -
Materials	Acct1.3_M	$ -	$ -
Subcontractors	Acct1.3_S	$ -	$ -
Subtotal		$ -	$ -
1.4 Plant Roads			
Labor	Acct1.4_L	$ 1,022	$ 1,022
Materials	Acct1.4_M	$ 2,392	$ 2,392
Subcontractors	Acct1.4_S	$ 2,799	$ 2,799
Subtotal		$ 6,213	$ 6,213
1.4.1 Road Earthwork and Subbase			
Labor	Acct1.4.1_L	$ 950	$ 950
Materials	Acct1.4.1_M	$ 2,392	$ 2,392
Subcontractors	Acct1.4.1_S	$ -	$ -
Subtotal		$ 3,341	$ 3,341
1.4.2 Road Paving			
Labor	Acct1.4.2_L	$ 72	$ 72
Materials	Acct1.4.2_M	$ -	$ -
Subcontractors	Acct1.4.2_S	$ 2,799	$ 2,799
Subtotal		$ 2,871	$ 2,871
1.5 Railroad			
Labor	Acct1.5_L	$ 389	$ 389
Materials	Acct1.5_M	$ -	$ -
Subcontractors	Acct1.5_S	$ 1,993	$ 1,993
Subtotal		$ 2,382	$ 2,382
1.6 Surface Drainage			
Labor	Acct1.6_L	$ 193	$ 190
Materials	Acct1.6_M	$ 206	$ 203
Subcontractors	Acct1.6_S	$ 41	$ 41
Subtotal		$ 440	$ 434
1.7 Fences & Gates			
Labor	Acct1.7_L	$ -	$ -
Materials	Acct1.7_M	$ -	$ -
Subcontractors	Acct1.7_S	$ 343	$ 338
Subtotal		$ 343	$ 338
1.8 Site Preparation and Piles			
Labor	Acct1.8_L	$ 5,041	$ 4,994
Materials	Acct1.8_M	$ 1,035	$ 1,022
Subcontractors	Acct1.8_S	$ 3,982	$ 3,947
Subtotal		$ 10,058	$ 9,964
1.8.1 Cut/Fill			
Labor	Acct1.8.1_L	$ -	$ -
Materials	Acct1.8.1_M	$ -	$ -
Subcontractors	Acct1.8.1_S	$ 2,271	$ 2,242
Subtotal		$ 2,271	$ 2,242
1.8.2 Mobilization/Demobilization (Entire Plant)			
Labor	Acct1.8.2_L	$ 1,379	$ 1,379
Materials	Acct1.8.2_M	$ 35	$ 35
Subcontractors	Acct1.8.2_S	$ 1,242	$ 1,242

Subtotal		$	2,657	$	2,657
1.8.3 Piles, concrete					
Labor	Acct1.8.3_L	$	-	$	-
Materials	Acct1.8.3_M	$	-	$	-
Subcontractors	Acct1.8.3_S	$	-	$	-
Subtotal		$	-	$	-
1.8.4 All Other Site Preparation					
Labor	Acct1.8.4_L	$	3,661	$	3,615
Materials	Acct1.8.4_M	$	1,000	$	987
Subcontractors	Acct1.8.4_S	$	469	$	463
Subtotal		$	5,130	$	5,065
1.8.5 Intake Shaft & Tunnel Earthwork (Once-Through Cooling)					
Labor	Acct1.8.5_L	$	-	$	-
Materials	Acct1.8.5_M	$	-	$	-
Subcontractors	Acct1.8.5_S	$	-	$	-
Subtotal		$	-	$	-
1.8.6 Construction Dewatering					
Labor	Acct1.8.6_L	$	-	$	-
Materials	Acct1.8.6_M	$	-	$	-
Subcontractors	Acct1.8.6_S	$	-	$	-
Subtotal		$	-	$	-
2 Boiler Room Structure					
Labor	Acct2.0_L	$	23,519	$	24,610
Materials	Acct2.0_M	$	31,199	$	32,608
Subcontractors	Acct2.0_S	$	44	$	46
Subtotal		$	54,763	$	57,264
2.1 Boiler Substructure Foundation					
Labor	Acct2.1_L	$	7,409	$	7,803
Materials	Acct2.1_M	$	5,900	$	6,214
Subcontractors	Acct2.1_S	$	-	$	-
Subtotal		$	13,309	$	14,017
2.2 Boiler Building Superstructure					
Labor	Acct2.2_L	$	16,110	$	16,807
Materials	Acct2.2_M	$	25,300	$	26,394
Subcontractors	Acct2.2_S	$	44	$	46
Subtotal		$	41,454	$	43,247
2.2.1 Structural Steel					
Labor	Acct2.2.1_L	$	15,831	$	16,516
Materials	Acct2.2.1_M	$	25,007	$	26,089
Subcontractors	Acct2.2.1_S	$	44	$	46
Subtotal		$	40,881	$	42,650
2.2.2 Other					
Labor	Acct2.2.2_L	$	279	$	292
Materials	Acct2.2.2_M	$	293	$	306
Subcontractors	Acct2.2.2_S	$	-	$	-
Subtotal		$	572	$	597
3 Turbine/BOP/Yard Structures					
Labor	Acct3.0_L	$	53,226	$	52,679
Materials	Acct3.0_M	$	40,925	$	40,563
Subcontractors	Acct3.0_S	$	792	$	792
Subtotal		$	94,943	$	94,034
3.1 Misc Building Substructure (Foundations - Fdns)					
Labor	Acct3.1_L	$	25,674	$	25,412
Materials	Acct3.1_M	$	15,005	$	14,848
Subcontractors	Acct3.1_S	$	-	$	-
Subtotal		$	40,679	$	40,260
3.1.1 Particulate Control Foundation					
Labor	Acct3.1.1_L	$	623	$	615
Materials	Acct3.1.1_M	$	405	$	399
Subcontractors	Acct3.1.1_S	$	-	$	-
Subtotal		$	1,027	$	1,014
3.1.2 Administration Building Foundation					
Labor	Acct3.1.2_L	$	540	$	540
Materials	Acct3.1.2_M	$	250	$	250

Subcontractors	Acct3.1.2_S	$ -	$ -
Subtotal		$ 790	$ 790
3.1.3 Coal Handling Foundation (In-Plant and Yard)			
Labor	Acct3.1.3_L	$ 7,614	$ 7,511
Materials	Acct3.1.3_M	$ 5,648	$ 5,571
Subcontractors	Acct3.1.3_S	$ -	$ -
Subtotal		$ 13,262	$ 13,082
3.1.4 Cooling Tower and ACC Fdns			
Labor	Acct3.1.4_L	$ 791	$ 791
Materials	Acct3.1.4_M	$ 601	$ 601
Subcontractors	Acct3.1.4_S	$ -	$ -
Subtotal		$ 1,392	$ 1,392
3.1.5 Electrical Foundations			
Labor	Acct3.1.5_L	$ 908	$ 908
Materials	Acct3.1.5_M	$ 387	$ 387
Subcontractors	Acct3.1.5_S	$ -	$ -
Subtotal		$ 1,294	$ 1,294
3.1.6 Miscellaneous, General Foundations			
Labor	Acct3.1.6_L	$ 11,052	$ 10,901
Materials	Acct3.1.6_M	$ 5,491	$ 5,416
Subcontractors	Acct3.1.6_S	$ -	$ -
Subtotal		$ 16,542	$ 16,317
3.1.7 Turbine Area Foundations			
Labor	Acct3.1.7_L	$ 4,147	$ 4,147
Materials	Acct3.1.7_M	$ 2,224	$ 2,224
Subcontractors	Acct3.1.7_S	$ -	$ -
Subtotal		$ 6,371	$ 6,371
3.2 Stack Foundation			
Labor	Acct3.2_L	$ 330	$ 326
Materials	Acct3.2_M	$ 1,441	$ 1,421
Subcontractors	Acct3.2_S	$ -	$ -
Subtotal		$ 1,771	$ 1,747
3.3 Turbine/Boiler Building (Bldg)			
Labor	Acct3.3_L	$ 8,156	$ 8,065
Materials	Acct3.3_M	$ 8,661	$ 8,565
Subcontractors	Acct3.3_S	$ -	$ -
Subtotal		$ 16,817	$ 16,630
3.3.1 Turbine/Boiler Building Structural Steel			
Labor	Acct3.3.1_L	$ 2,952	$ 2,919
Materials	Acct3.3.1_M	$ 4,295	$ 4,247
Subcontractors	Acct3.3.1_S	$ -	$ -
Subtotal		$ 7,247	$ 7,166
3.3.2 Building Siding			
Labor	Acct3.3.2_L	$ 1,618	$ 1,600
Materials	Acct3.3.2_M	$ 1,068	$ 1,056
Subcontractors	Acct3.3.2_S	$ -	$ -
Subtotal		$ 2,687	$ 2,657
3.3.3 Architectural Features and Finishes			
Labor	Acct3.3.3_L	$ 1,954	$ 1,933
Materials	Acct3.3.3_M	$ 1,923	$ 1,901
Subcontractors	Acct3.3.3_S	$ -	$ -
Subtotal		$ 3,877	$ 3,834
3.3.4 Building Roofing			
Labor	Acct3.3.4_L	$ 1,172	$ 1,159
Materials	Acct3.3.4_M	$ 734	$ 726
Subcontractors	Acct3.3.4_S	$ -	$ -
Subtotal		$ 1,906	$ 1,885
3.3.5 Misc Building and Architectural			
Labor	Acct3.3.5_L	$ 459	$ 454
Materials	Acct3.3.5_M	$ 641	$ 634
Subcontractors	Acct3.3.5_S	$ -	$ -
Subtotal		$ 1,101	$ 1,088
3.4 Coal Handling Structures			
Labor	Acct3.4_L	$ 11,001	$ 10,878
Materials	Acct3.4_M	$ 8,059	$ 7,969
Subcontractors	Acct3.4_S	$ -	$ -

Subtotal		$	19,060	$	18,848
3.5 Plant Coal Conveyors Bldg/Bunkers					
Labor	Acct3.5_L	$	6,037	$	5,969
Materials	Acct3.5_M	$	5,806	$	5,806
Subcontractors	Acct3.5_S	$	-	$	-
Subtotal		$	11,843	$	11,775
3.6 All Other Buildings/Structures					
Labor	Acct3.6_L	$	2,029	$	2,029
Materials	Acct3.6_M	$	1,953	$	1,953
Subcontractors	Acct3.6_S	$	792	$	792
Subtotal		$	4,774	$	4,774
3.7 Offshore & Waterfront Structures - Dock					
Labor	Acct3.7_L	$	-	$	-
Materials	Acct3.7_M	$	-	$	-
Subcontractors	Acct3.7_S	$	-	$	-
Subtotal		$	-	$	-
3.8 Intake Piping, Shaft and Tunnel Structure (once-through cooling)					
Labor	Acct3.8_L	$	-	$	-
Materials	Acct3.8_M	$	-	$	-
Subcontractors	Acct3.8_S	$	-	$	-
Subtotal		$	-	$	-
4 Boiler Plant Equipment & Systems					
Labor	Acct4.0_L	$	192,446	$	193,672
Materials	Acct4.0_M	$	267,830	$	287,779
Subcontractors	Acct4.0_S	$	11,268	$	12,207
Subtotal		$	471,544	$	493,658
4.1 Steam Generator Steel					
Labor	Acct4.1_L	$	931	$	1,026
Materials	Acct4.1_M	$	15,148	$	16,389
Subcontractors	Acct4.1_S	$	-	$	-
Subtotal		$	16,080	$	17,415
4.1.1 Support Steel					
Labor	Acct4.1.1_L	$	687	$	732
Materials	Acct4.1.1_M	$	13,341	$	14,212
Subcontractors	Acct4.1.1_S	$	-	$	-
Subtotal		$	14,028	$	14,944
4.1.2 Platforms & Stairs					
Labor	Acct4.1.2_L	$	244	$	294
Materials	Acct4.1.2_M	$	1,807	$	2,177
Subcontractors	Acct4.1.2_S	$	-	$	-
Subtotal		$	2,051	$	2,471
4.2 Steam Generator and Pressure Parts					
Labor	Acct4.2_L	$	2,887	$	3,692
Materials	Acct4.2_M	$	59,552	$	77,890
Subcontractors	Acct4.2_S	$	-	$	-
Subtotal		$	62,440	$	81,582
4.2.1 Boiler Feed Pump					
Labor	Acct4.2.1_L	$	504	$	529
Materials	Acct4.2.1_M	$	4,651	$	4,880
Subcontractors	Acct4.2.1_S	$	-	$	-
Subtotal		$	5,155	$	5,409
4.2.2 Heat Transfer Surface, Carbon Steel					
Labor	Acct4.2.2_L	$	266	$	270
Materials	Acct4.2.2_M	$	5,667	$	5,738
Subcontractors	Acct4.2.2_S	$	-	$	-
Subtotal		$	5,934	$	6,008
4.2.2.1 Pressure Parts					
Labor	Acct4.2.2.1_L	$	228	$	231
Materials	Acct4.2.2.1_M	$	4,432	$	4,488
Subcontractors	Acct4.2.2.1_S	$	-	$	-
Subtotal		$	4,661	$	4,719
4.2.2.2 Headers & Legs					
Labor	Acct4.2.2.2_L	$	21	$	21
Materials	Acct4.2.2.2_M	$	665	$	673
Subcontractors	Acct4.2.2.2_S	$	-	$	-

Subtotal		$ 685	$ 694
4.2.2.3 Risers, Feeders, Misc Tubes			
Labor	Acct4.2.2.3_L	$ 18	$ 18
Materials	Acct4.2.2.3_M	$ 570	$ 577
Subcontractors	Acct4.2.2.3_S	$ -	$ -
Subtotal		$ 587	$ 595
4.2.3 Heat Transfer Surface, Alloy			
Labor	Acct4.2.3_L	$ 2,117	$ 2,894
Materials	Acct4.2.3_M	$ 49,234	$ 67,272
Subcontractors	Acct4.2.3_S	$ -	$ -
Subtotal		$ 51,352	$ 70,165
4.2.3.1 Pressure Parts			
Labor	Acct4.2.3.1_L	$ 1,600	$ 2,189
Materials	Acct4.2.3.1_M	$ 32,009	$ 43,782
Subcontractors	Acct4.2.3.1_S	$ -	$ -
Subtotal		$ 33,609	$ 45,971
4.2.3.2 Headers & Legs			
Labor	Acct4.2.3.2_L	$ 278	$ 379
Materials	Acct4.2.3.2_M	$ 9,275	$ 12,648
Subcontractors	Acct4.2.3.2_S	$ -	$ -
Subtotal		$ 9,554	$ 13,028
4.2.3.3 Risers, Feeders, Misc Tubes			
Labor	Acct4.2.3.3_L	$ 239	$ 325
Materials	Acct4.2.3.3_M	$ 7,950	$ 10,841
Subcontractors	Acct4.2.3.3_S	$ -	$ -
Subtotal		$ 8,189	$ 11,167
4.3 Boiler Coal Feed System			
Labor	Acct4.3_L	$ 507	$ 501
Materials	Acct4.3_M	$ 5,273	$ 5,215
Subcontractors	Acct4.3_S	$ 3,651	$ 3,606
Subtotal		$ 9,431	$ 9,321
4.4 Ash Removal			
Labor	Acct4.4_L	$ 119	$ 118
Materials	Acct4.4_M	$ 936	$ 929
Subcontractors	Acct4.4_S	$ -	$ -
Subtotal		$ 1,055	$ 1,047
4.5 Air & Gas System			
Labor	Acct4.5_L	$ 6,636	$ 6,600
Materials	Acct4.5_M	$ 21,586	$ 21,834
Subcontractors	Acct4.5_S	$ -	$ -
Subtotal		$ 28,222	$ 28,434
4.5.1 Air Heater and Steam Coil Preheater			
Labor	Acct4.5.1_L	$ 4,174	$ 4,116
Materials	Acct4.5.1_M	$ 12,821	$ 12,689
Subcontractors	Acct4.5.1_S	$ -	$ -
Subtotal		$ 16,996	$ 16,805
4.5.1.1 Air Heater			
Labor	Acct4.5.1.1_L	$ 3,414	$ 3,366
Materials	Acct4.5.1.1_M	$ 11,877	$ 11,759
Subcontractors	Acct4.5.1.1_S	$ -	$ -
Subtotal		$ 15,291	$ 15,126
4.5.1.2 Steam Coil Preheater			
Labor	Acct4.5.1.2_L	$ 761	$ 749
Materials	Acct4.5.1.2_M	$ 944	$ 930
Subcontractors	Acct4.5.1.2_S	$ -	$ -
Subtotal		$ 1,705	$ 1,679
4.5.2 Secondary Air (SA) Fans (2 X 60%)			
Labor	Acct4.5.2_L	$ 820	$ 814
Materials	Acct4.5.2_M	$ 2,063	$ 2,047
Subcontractors	Acct4.5.2_S	$ -	$ -
Subtotal		$ 2,884	$ 2,861
4.5.3 Primary Air (PS) Fans (2 X 60%)			
Labor	Acct4.5.3_L	$ 352	$ 349
Materials	Acct4.5.3_M	$ 867	$ 860
Subcontractors	Acct4.5.3_S	$ -	$ -
Subtotal		$ 1,219	$ 1,209

4.5.4 Induced Draft Fans				
Labor	Acct4.5.4_L	$ 1,030	$ 1,023	
Materials	Acct4.5.4_M	$ 3,064	$ 3,041	
Subcontractors	Acct4.5.4_S	$ -	$ -	
Subtotal		$ 4,094	$ 4,064	
4.5.5 Flue Gas Ducts				
Labor	Acct4.5.5_L	$ 259	$ 299	
Materials	Acct4.5.5_M	$ 2,771	$ 3,196	
Subcontractors	Acct4.5.5_S	$ -	$ -	
Subtotal		$ 3,030	$ 3,495	
4.6 Pulverizers				
Labor	Acct4.6_L	$ 3,811	$ 3,776	
Materials	Acct4.6_M	$ 11,424	$ 11,320	
Subcontractors	Acct4.6_S	$ -	$ -	
Subtotal		$ 15,236	$ 15,096	
4.7 Subtotal of Boiler Items				
Labor	Acct4.7_L	$ 2,713	$ 2,855	
Materials	Acct4.7_M	$ 19,710	$ 21,715	
Subcontractors	Acct4.7_S	$ 7,388	$ 8,374	
Subtotal		$ 29,811	$ 32,944	
4.7.1 Other Boiler Items				
Labor	Acct4.7.1_L	$ 1,123	$ 1,109	
Materials	Acct4.7.1_M	$ 954	$ 942	
Subcontractors	Acct4.7.1_S	$ -	$ -	
Subtotal		$ 2,076	$ 2,050	
4.7.2 Insulation/Lagging				
Labor	Acct4.7.2_L	$ 622	$ 614	
Materials	Acct4.7.2_M	$ 6,412	$ 6,322	
Subcontractors	Acct4.7.2_S	$ -	$ -	
Subtotal		$ 7,034	$ 6,936	
4.7.3 Hangers, Springs & Buckstays				
Labor	Acct4.7.3_L	$ 127	$ 153	
Materials	Acct4.7.3_M	$ 2,040	$ 2,457	
Subcontractors	Acct4.7.3_S	$ -	$ -	
Subtotal		$ 2,167	$ 2,610	
4.7.4 Windbox and Burners				
Labor	Acct4.7.4_L	$ 394	$ 455	
Materials	Acct4.7.4_M	$ 5,417	$ 6,248	
Subcontractors	Acct4.7.4_S	$ -	$ -	
Subtotal		$ 5,811	$ 6,703	
4.7.5 Miscellaneous Supports/Seals/Sheathing				
Labor	Acct4.7.5_L	$ 188	$ 226	
Materials	Acct4.7.5_M	$ 2,128	$ 2,563	
Subcontractors	Acct4.7.5_S	$ -	$ -	
Subtotal		$ 2,316	$ 2,789	
4.7.6 Casing/Enclosure				
Labor	Acct4.7.6_L	$ 258	$ 298	
Materials	Acct4.7.6_M	$ 2,760	$ 3,183	
Subcontractors	Acct4.7.6_S	$ -	$ -	
Subtotal		$ 3,018	$ 3,481	
4.7.7 Freight for All Boiler Items				
Labor	Acct4.7.7_L	$ -	$ -	
Materials	Acct4.7.7_M	$ -	$ -	
Subcontractors	Acct4.7.7_S	$ 7,388	$ 8,374	
Subtotal		$ 7,388	$ 8,374	
4.8 Solids Handling System				
Labor	Acct4.8_L	$ 39,217	$ 38,782	
Materials	Acct4.8_M	$ 42,634	$ 42,140	
Subcontractors	Acct4.8_S	$ 228	$ 227	
Subtotal		$ 82,079	$ 81,148	
4.8.1 Coal Handling (Entire Plant)				
Labor	Acct4.8.1_L	$ 28,824	$ 28,465	
Materials	Acct4.8.1_M	$ 35,320	$ 34,880	
Subcontractors	Acct4.8.1_S	$ -	$ -	
Subtotal		$ 64,144	$ 63,344	
4.8.2 Ash Handling (Entire Plant)				

Labor	Acct4.8.2_L	$	10,393	$	10,317
Materials	Acct4.8.2_M	$	7,314	$	7,260
Subcontractors	Acct4.8.2_S	$	228	$	227
Subtotal		$	17,935	$	17,804
4.9 Boiler OEM Labor					
Labor	Acct4.9_L	$	18,808	$	19,102
Materials	Acct4.9_M	$	-	$	-
Subcontractors	Acct4.9_S	$	-	$	-
Subtotal		$	18,808	$	19,102
4.10 Particulate Control (ESP)					
Labor	Acct4.10_L	$	39,603	$	39,084
Materials	Acct4.10_M	$	44,440	$	43,858
Subcontractors	Acct4.10_S	$	-	$	-
Subtotal		$	84,043	$	82,942
4.11 Stack (Concrete Shell)					
Labor	Acct4.11_L	$	9,230	$	9,131
Materials	Acct4.11_M	$	4,706	$	4,656
Subcontractors	Acct4.11_S	$	-	$	-
Subtotal		$	13,937	$	13,786
4.12 Erection Labor (Boiler Only)					
Labor	Acct4.12_L	$	60,709	$	61,659
Materials	Acct4.12_M	$	-	$	-
Subcontractors	Acct4.12_S	$	-	$	-
Subtotal		$	60,709	$	61,659
4.13 Boiler OEM Indirects & Fees					
Labor	Acct4.13_L	$	4,064	$	4,179
Materials	Acct4.13_M	$	-	$	-
Subcontractors	Acct4.13_S	$	-	$	-
Subtotal		$	4,064	$	4,179
4.14 Selective Catalytic Reduction					
Labor	Acct4.14_L	$	3,212	$	3,167
Materials	Acct4.14_M	$	42,419	$	41,834
Subcontractors	Acct4.14_S	$	-	$	-
Subtotal		$	45,630	$	45,002
5 Turbine & BOP					
Labor	Acct5.0_L	$	109,703	$	110,160
Materials	Acct5.0_M	$	437,817	$	445,627
Subcontractors	Acct5.0_S	$	802	$	790
Subtotal		$	548,322	$	556,578
5.1 Turbine Generator					
Labor	Acct5.1_L	$	7,352	$	7,423
Materials	Acct5.1_M	$	112,104	$	113,904
Subcontractors	Acct5.1_S	$	-	$	-
Subtotal		$	119,456	$	121,327
5.1.1 Turbine Generator					
Labor	Acct5.1.1_L	$	7,277	$	7,348
Materials	Acct5.1.1_M	$	111,700	$	113,500
Subcontractors	Acct5.1.1_S	$	-	$	-
Subtotal		$	118,977	$	120,848
5.1.2 Lube Oil					
Labor	Acct5.1.2_L	$	75	$	75
Materials	Acct5.1.2_M	$	404	$	404
Subcontractors	Acct5.1.2_S	$	-	$	-
Subtotal		$	479	$	479
5.2 Surface Condenser & Auxiliaries					
Labor	Acct5.2_L	$	2,081	$	2,025
Materials	Acct5.2_M	$	11,321	$	11,015
Subcontractors	Acct5.2_S	$	-	$	-
Subtotal		$	13,402	$	13,040
5.3 Proces & Process Piping					
Labor	Acct5.3_L	$	42,167	$	42,915
Materials	Acct5.3_M	$	187,308	$	193,923
Subcontractors	Acct5.3_S	$	-	$	-
Subtotal		$	229,475	$	236,838
5.3.1 Main Steam Piping					

Labor	Acct5.3.1_L	$ 7,576	$ 7,894	
Materials	Acct5.3.1_M	$ 145,108	$ 151,198	
Subcontractors	Acct5.3.1_S	$ -	$ -	
Subtotal		$ 152,683	$ 159,092	
5.3.2 Aux/Extraction Steam Piping				
Labor	Acct5.3.2_L	$ 1,040	$ 1,053	
Materials	Acct5.3.2_M	$ 1,394	$ 1,411	
Subcontractors	Acct5.3.2_S	$ -	$ -	
Subtotal		$ 2,434	$ 2,464	
5.3.3. Low Pressure FW System				
Labor	Acct5.3.3_L	$ 1,070	$ 1,083	
Materials	Acct5.3.3_M	$ 2,058	$ 2,083	
Subcontractors	Acct5.3.3_S	$ -	$ -	
Subtotal		$ 3,128	$ 3,166	
5.3.4 High Pressure FW System				
Labor	Acct5.3.4_L	$ 1,063	$ 1,076	
Materials	Acct5.3.4_M	$ 7,127	$ 7,215	
Subcontractors	Acct5.3.4_S	$ -	$ -	
Subtotal		$ 8,190	$ 8,291	
5.3.5 All Other Steam and Process Piping & Valves				
Labor	Acct5.3.5_L	$ 31,419	$ 31,809	
Materials	Acct5.3.5_M	$ 31,622	$ 32,015	
Subcontractors	Acct5.3.5_S	$ -	$ -	
Subtotal		$ 63,041	$ 63,824	
5.3.5.1 All Other Steam and Process Piping				
Labor	Acct5.3.5.1_L	$ 27,007	$ 27,342	
Materials	Acct5.3.5.1_M	$ 26,896	$ 27,231	
Subcontractors	Acct5.3.5.1_S	$ -	$ -	
Subtotal		$ 53,903	$ 54,573	
5.3.5.2 All Other Steam and Process Valves				
Labor	Acct5.3.5.2_L	$ 4,412	$ 4,467	
Materials	Acct5.3.5.2_M	$ 4,726	$ 4,784	
Subcontractors	Acct5.3.5.2_S	$ -	$ -	
Subtotal		$ 9,138	$ 9,251	
5.4 Plant Water Systems				
Labor	Acct5.4_L	$ 1,912	$ 1,895	
Materials	Acct5.4_M	$ 3,356	$ 3,355	
Subcontractors	Acct5.4_S	$ 591	$ 580	
Subtotal		$ 5,859	$ 5,829	
5.4.1 Raw/Service Water				
Labor	Acct5.4.1_L	$ 976	$ 957	
Materials	Acct5.4.1_M	$ 536	$ 525	
Subcontractors	Acct5.4.1_S	$ 591	$ 580	
Subtotal		$ 2,102	$ 2,061	
5.4.2 Closed Cooling Water				
Labor	Acct5.4.2_L	$ 118	$ 120	
Materials	Acct5.4.2_M	$ 1,031	$ 1,044	
Subcontractors	Acct5.4.2_S	$ -	$ -	
Subtotal		$ 1,150	$ 1,164	
5.4.3 Waste Water Treatment System				
Labor	Acct5.4.3_L	$ 196	$ 192	
Materials	Acct5.4.3_M	$ 622	$ 610	
Subcontractors	Acct5.4.3_S	$ -	$ -	
Subtotal		$ 818	$ 803	
5.4.4 Condensate Storage & Transfer				
Labor	Acct5.4.4_L	$ 493	$ 497	
Materials	Acct5.4.4_M	$ 885	$ 893	
Subcontractors	Acct5.4.4_S	$ -	$ -	
Subtotal		$ 1,378	$ 1,391	
5.4.5 Potable Water				
Labor	Acct5.4.5_L	$ 57	$ 57	
Materials	Acct5.4.5_M	$ 105	$ 105	
Subcontractors	Acct5.4.5_S	$ -	$ -	
Subtotal		$ 162	$ 162	
5.4.6 Plant Water - Miscellaneous				
Labor	Acct5.4.6_L	$ 72	$ 72	

Materials	Acct5.4.6_M	$	177	$	177
Subcontractors	Acct5.4.6_S	$	-	$	-
Subtotal		$	248	$	248
5.5 Auxiliary Steam System					
Labor	Acct5.5_L	$	1,586	$	1,607
Materials	Acct5.5_M	$	1,463	$	1,482
Subcontractors	Acct5.5_S	$	-	$	-
Subtotal		$	3,048	$	3,089
5.6 Chemical Feed System					
Labor	Acct5.6_L	$	2,268	$	2,279
Materials	Acct5.6_M	$	7,482	$	7,526
Subcontractors	Acct5.6_S	$	-	$	-
Subtotal		$	9,750	$	9,806
5.6.1 Water Sampling/Treatment					
Labor	Acct5.6.1_L	$	392	$	384
Materials	Acct5.6.1_M	$	1,080	$	1,059
Subcontractors	Acct5.6.1_S	$	-	$	-
Subtotal		$	1,472	$	1,443
5.6.2 Boiler/Feedwater Treatment					
Labor	Acct5.6.2_L	$	1,876	$	1,895
Materials	Acct5.6.2_M	$	6,402	$	6,468
Subcontractors	Acct5.6.2_S	$	-	$	-
Subtotal		$	8,278	$	8,363
5.7 Misc Mechanical Equipment					
Labor	Acct5.7_L	$	4,520	$	4,467
Materials	Acct5.7_M	$	8,132	$	8,035
Subcontractors	Acct5.7_S	$	-	$	-
Subtotal		$	12,652	$	12,502
5.7.1 HVAC (All Plant)					
Labor	Acct5.7.1_L	$	2,347	$	2,321
Materials	Acct5.7.1_M	$	3,106	$	3,073
Subcontractors	Acct5.7.1_S	$	-	$	-
Subtotal		$	5,453	$	5,394
5.7.2 Compressed Air					
Labor	Acct5.7.2_L	$	198	$	195
Materials	Acct5.7.2_M	$	1,253	$	1,237
Subcontractors	Acct5.7.2_S	$	-	$	-
Subtotal		$	1,451	$	1,432
5.7.3 Cranes, Hoists & Elevators (Entire Plant)					
Labor	Acct5.7.3_L	$	1,192	$	1,176
Materials	Acct5.7.3_M	$	2,148	$	2,119
Subcontractors	Acct5.7.3_S	$	-	$	-
Subtotal		$	3,340	$	3,295
5.7.4 Fire Protection (Entire Plant)					
Labor	Acct5.7.4_L	$	713	$	706
Materials	Acct5.7.4_M	$	1,372	$	1,358
Subcontractors	Acct5.7.4_S	$	-	$	-
Subtotal		$	2,086	$	2,063
5.7.5 Diesel Generator					
Labor	Acct5.7.5_L	$	70	$	69
Materials	Acct5.7.5_M	$	252	$	249
Subcontractors	Acct5.7.5_S	$	-	$	-
Subtotal		$	323	$	318
5.8 Electrical Equipment					
Labor	Acct5.8_L	$	2,384	$	2,384
Materials	Acct5.8_M	$	45,942	$	45,942
Subcontractors	Acct5.8_S	$	-	$	-
Subtotal		$	48,325	$	48,325
5.8.1 Main Power Equipment					
Labor	Acct5.8.1_L	$	1,999	$	1,999
Materials	Acct5.8.1_M	$	32,742	$	32,742
Subcontractors	Acct5.8.1_S	$	-	$	-
Subtotal		$	34,742	$	34,742
5.8.2 Auxiliary Power Equipment					
Labor	Acct5.8.2_L	$	275	$	275
Materials	Acct5.8.2_M	$	12,340	$	12,340

Subcontractors	Acct5.8.2_S	$ -	$	-
Subtotal		$ 12,614	$	12,614
5.8.3 Uninterruptible & DC Power System				
Labor	Acct5.8.3_L	$ 110	$	110
Materials	Acct5.8.3_M	$ 860	$	860
Subcontractors	Acct5.8.3_S	$ -	$	-
Subtotal		$ 969	$	969
5.9 Electrical Bulk Material				
Labor	Acct5.9_L	$ 33,543	$	33,543
Materials	Acct5.9_M	$ 33,429	$	33,429
Subcontractors	Acct5.9_S	$ 211	$	211
Subtotal		$ 67,183	$	67,183
5.9.1 Cable Trays				
Labor	Acct5.9.1_L	$ 7,543	$	7,543
Materials	Acct5.9.1_M	$ 7,807	$	7,807
Subcontractors	Acct5.9.1_S	$ -	$	-
Subtotal		$ 15,349	$	15,349
5.9.2 Conduit				
Labor	Acct5.9.2_L	$ 8,335	$	8,335
Materials	Acct5.9.2_M	$ 4,506	$	4,506
Subcontractors	Acct5.9.2_S	$ -	$	-
Subtotal		$ 12,841	$	12,841
5.9.3 Wiring (High Voltage)				
Labor	Acct5.9.3_L	$ 1,282	$	1,282
Materials	Acct5.9.3_M	$ 7,104	$	7,104
Subcontractors	Acct5.9.3_S	$ -	$	-
Subtotal		$ 8,386	$	8,386
5.9.4 Wiring (Low Voltage)				
Labor	Acct5.9.4_L	$ 851	$	851
Materials	Acct5.9.4_M	$ 1,744	$	1,744
Subcontractors	Acct5.9.4_S	$ -	$	-
Subtotal		$ 2,595	$	2,595
5.9.5 Terminators				
Labor	Acct5.9.5_L	$ 3,667	$	3,667
Materials	Acct5.9.5_M	$ 1,400	$	1,400
Subcontractors	Acct5.9.5_S	$ -	$	-
Subtotal		$ 5,066	$	5,066
5.9.6 Lighting				
Labor	Acct5.9.6_L	$ 3,672	$	3,672
Materials	Acct5.9.6_M	$ 4,938	$	4,938
Subcontractors	Acct5.9.6_S	$ -	$	-
Subtotal		$ 8,611	$	8,611
5.9.7 Communications System				
Labor	Acct5.9.7_L	$ 1,020	$	1,020
Materials	Acct5.9.7_M	$ 414	$	414
Subcontractors	Acct5.9.7_S	$ 211	$	211
Subtotal		$ 1,645	$	1,645
5.9.8 Freeze protection				
Labor	Acct5.9.8_L	$ 260	$	260
Materials	Acct5.9.8_M	$ 433	$	433
Subcontractors	Acct5.9.8_S	$ -	$	-
Subtotal		$ 693	$	693
5.9.9 Cathodic Protection				
Labor	Acct5.9.9_L	$ 379	$	379
Materials	Acct5.9.9_M	$ 391	$	391
Subcontractors	Acct5.9.9_S	$ -	$	-
Subtotal		$ 770	$	770
5.9.10 Grounding				
Labor	Acct5.9.10_L	$ 1,615	$	1,615
Materials	Acct5.9.10_M	$ 1,306	$	1,306
Subcontractors	Acct5.9.10_S	$ -	$	-
Subtotal		$ 2,921	$	2,921
5.9.11 Misc Electrical Bulk Material				
Labor	Acct5.9.11_L	$ 4,919	$	4,919
Materials	Acct5.9.11_M	$ 3,387	$	3,387
Subcontractors	Acct5.9.11_S	$ -	$	-

	Subtotal		$	8,306	$ 8,306
5.10	Turbine/BOP Instruments and Controls				
	Labor	Acct5.10_L	$	2,873	$ 2,872
	Materials	Acct5.10_M	$	16,279	$ 16,272
	Subcontractors	Acct5.10_S	$	-	$ -
	Subtotal		$	19,152	$ 19,144
5.10.1	Plant Distributed Control System (DCS)				
	Labor	Acct5.10.1_L	$	912	$ 912
	Materials	Acct5.10.1_M	$	9,975	$ 9,975
	Subcontractors	Acct5.10.1_S	$	-	$ -
	Subtotal		$	10,886	$ 10,886
5.10.2	Controls and Valves				
	Labor	Acct5.10.2_L	$	1,491	$ 1,491
	Materials	Acct5.10.2_M	$	4,470	$ 4,470
	Subcontractors	Acct5.10.2_S	$	-	$ -
	Subtotal		$	5,962	$ 5,962
5.10.3	Bulks, Instrumentation & Controls				
	Labor	Acct5.10.3_L	$	365	$ 365
	Materials	Acct5.10.3_M	$	943	$ 943
	Subcontractors	Acct5.10.3_S	$	-	$ -
	Subtotal		$	1,308	$ 1,308
5.10.4	Continuous Emission Monitoring				
	Labor	Acct5.10.4_L	$	105	$ 104
	Materials	Acct5.10.4_M	$	770	$ 762
	Subcontractors	Acct5.10.4_S	$	-	$ -
	Subtotal		$	875	$ 866
5.10.5	Misc Instrument and Controls				
	Labor	Acct5.10.5_L	$	-	$ -
	Materials	Acct5.10.5_M	$	122	$ 122
	Subcontractors	Acct5.10.5_S	$	-	$ -
	Subtotal		$	122	$ 122
5.11	Circ Water & Cooling Tower				
	Labor	Acct5.11_L	$	9,019	$ 8,751
	Materials	Acct5.11_M	$	11,000	$ 10,743
	Subcontractors	Acct5.11_S	$	-	$ -
	Subtotal		$	20,019	$ 19,494
5.11.1	Cooling Tower				
	Labor	Acct5.11.1_L	$	8,608	$ 8,344
	Materials	Acct5.11.1_M	$	7,068	$ 6,851
	Subcontractors	Acct5.11.1_S	$	-	$ -
	Subtotal		$	15,676	$ 15,195
5.11.2	Cooling Tower Pumps				
	Labor	Acct5.11.2_L	$	411	$ 407
	Materials	Acct5.11.2_M	$	3,932	$ 3,892
	Subcontractors	Acct5.11.2_S	$	-	$ -
	Subtotal		$	4,343	$ 4,299
6	Flue Gas Desulfurization				
	Labor	Acct6.0_L	$	48,554	$ 48,207
	Materials	Acct6.0_M	$	191,448	$ 189,983
	Subcontractors	Acct6.0_S	$	1,354	$ 1,341
	Subtotal		$	241,355	$ 239,531
6.1	Reagent Feed System				
	Labor	Acct6.1_L	$	9,814	$ 9,786
	Materials	Acct6.1_M	$	25,761	$ 25,688
	Subcontractors	Acct6.1_S	$	-	$ -
	Subtotal		$	35,575	$ 35,474
6.1.1	Foundation for Reagent Feed System				
	Labor	Acct6.1.1_L	$	6,508	$ 6,490
	Materials	Acct6.1.1_M	$	6,301	$ 6,283
	Subcontractors	Acct6.1.1_S	$	-	$ -
	Subtotal		$	12,809	$ 12,773
6.1.2	Structural Steel for Reagent Feed System				
	Labor	Acct6.1.2_L	$	243	$ 242
	Materials	Acct6.1.2_M	$	545	$ 544
	Subcontractors	Acct6.1.2_S	$	-	$ -

Subtotal		$ 788	$ 786
6.1.3 Equipment & Other for Reagent Feed System			
Labor	Acct6.1.3_L	$ 3,063	$ 3,055
Materials	Acct6.1.3_M	$ 18,915	$ 18,861
Subcontractors	Acct6.1.3_S	$ -	$ -
Subtotal		$ 21,978	$ 21,916
6.2 SO2 Removal System			
Labor	Acct6.2_L	$ 33,656	$ 33,361
Materials	Acct6.2_M	$ 143,416	$ 142,160
Subcontractors	Acct6.2_S	$ -	$ -
Subtotal		$ 177,072	$ 175,521
6.2.1 SO2 Removal System Foundation			
Labor	Acct6.2.1_L	$ 4,057	$ 4,022
Materials	Acct6.2.1_M	$ 4,323	$ 4,285
Subcontractors	Acct6.2.1_S	$ -	$ -
Subtotal		$ 8,380	$ 8,307
6.2.2 Structural Steel for SO2 Removal System			
Labor	Acct6.2.2_L	$ 8,987	$ 8,908
Materials	Acct6.2.2_M	$ 25,376	$ 25,154
Subcontractors	Acct6.2.2_S	$ -	$ -
Subtotal		$ 34,363	$ 34,062
6.2.3 Equipment & Other for SO2 Removal System			
Labor	Acct6.2.3_L	$ 20,612	$ 20,432
Materials	Acct6.2.3_M	$ 113,717	$ 112,721
Subcontractors	Acct6.2.3_S	$ -	$ -
Subtotal		$ 134,329	$ 133,153
6.3 Flue Gas System			
Labor	Acct6.3_L	$ 2,118	$ 2,097
Materials	Acct6.3_M	$ 13,183	$ 13,057
Subcontractors	Acct6.3_S	$ 1,323	$ 1,310
Subtotal		$ 16,624	$ 16,465
6.3.1 Flue Gas System Foundation			
Labor	Acct6.3.1_L	$ 228	$ 226
Materials	Acct6.3.1_M	$ 183	$ 181
Subcontractors	Acct6.3.1_S	$ -	$ -
Subtotal		$ 411	$ 407
6.3.2 Flue Gas System Structural Steel			
Labor	Acct6.3.2_L	$ 82	$ 81
Materials	Acct6.3.2_M	$ 441	$ 437
Subcontractors	Acct6.3.2_S	$ -	$ -
Subtotal		$ 523	$ 518
6.3.3 Equipment and Other for Flue Gas System			
Labor	Acct6.3.3_L	$ 1,807	$ 1,790
Materials	Acct6.3.3_M	$ 12,559	$ 12,439
Subcontractors	Acct6.3.3_S	$ 1,323	$ 1,310
Subtotal		$ 15,689	$ 15,540
6.4 Solids Handling System			
Labor	Acct6.4_L	$ 1,731	$ 1,729
Materials	Acct6.4_M	$ 4,198	$ 4,192
Subcontractors	Acct6.4_S	$ -	$ -
Subtotal		$ 5,929	$ 5,920
6.4.1 Solids Handling System Foundation			
Labor	Acct6.4.1_L	$ 285	$ 285
Materials	Acct6.4.1_M	$ 163	$ 163
Subcontractors	Acct6.4.1_S	$ -	$ -
Subtotal		$ 449	$ 448
6.4.2 Solids Handling System Structural Steel			
Labor	Acct6.4.2_L	$ -	$ -
Materials	Acct6.4.2_M	$ -	$ -
Subcontractors	Acct6.4.2_S	$ -	$ -
Subtotal		$ -	$ -
6.4.3 Equipment and Other for Solids Handling System			
Labor	Acct6.4.3_L	$ 1,446	$ 1,444
Materials	Acct6.4.3_M	$ 4,035	$ 4,028
Subcontractors	Acct6.4.3_S	$ -	$ -
Subtotal		$ 5,480	$ 5,472

6.5 General FGD Support Equipment					
Labor	Acct6.5_L	$	1,235	$	1,234
Materials	Acct6.5_M	$	4,889	$	4,886
Subcontractors	Acct6.5_S	$	31	$	31
Subtotal		$	6,155	$	6,150
6.5.1 General FGD Support Equipment Foundations					
Labor	Acct6.5.1_L	$	135	$	135
Materials	Acct6.5.1_M	$	77	$	76
Subcontractors	Acct6.5.1_S	$	-	$	-
Subtotal		$	212	$	211
6.5.2 General FGD Support Equipment Structural Steel					
Labor	Acct6.5.2_L	$	20	$	20
Materials	Acct6.5.2_M	$	29	$	29
Subcontractors	Acct6.5.2_S	$	-	$	-
Subtotal		$	49	$	49
6.5.3 Equipment and Other for General FGD Support Equipment					
Labor	Acct6.5.3_L	$	1,080	$	1,079
Materials	Acct6.5.3_M	$	4,784	$	4,780
Subcontractors	Acct6.5.3_S	$	31	$	31
Subtotal		$	5,895	$	5,890
7 Miscellaneous Directs					
Labor	Acct7.0_L	$	3,192	$	3,149
Materials	Acct7.0_M	$	93,036	$	93,052
Subcontractors	Acct7.0_S	$	56,601	$	56,713
Subtotal		$	152,829	$	152,914
7.1 Freight & Unloading For All Equipment Other Than Boiler					
Labor	Acct7.1_L	$	-	$	-
Materials	Acct7.1_M	$	-	$	-
Subcontractors	Acct7.1_S	$	38,306	$	38,615
Subtotal		$	38,306	$	38,615
7.2 Painting					
Labor	Acct7.2_L	$	-	$	-
Materials	Acct7.2_M	$	-	$	-
Subcontractors	Acct7.2_S	$	2,478	$	2,452
Subtotal		$	2,478	$	2,452
7.3 Scaffolding (Entire Plant)					
Labor	Acct7.3_L	$	3,192	$	3,149
Materials	Acct7.3_M	$	7,463	$	7,364
Subcontractors	Acct7.3_S	$	-	$	-
Subtotal		$	10,654	$	10,513
7.4 Insulation					
Labor	Acct7.4_L	$	-	$	-
Materials	Acct7.4_M	$	-	$	-
Subcontractors	Acct7.4_S	$	15,817	$	15,647
Subtotal		$	15,817	$	15,647
7.5 Construction Equipment					
Labor	Acct7.5_L				
Materials	Acct7.5_M	$	62,535	$	62,618
Subcontractors	Acct7.5_S				
Subtotal		$	62,535	$	62,618
7.6 Small Tools and Consumables					
Labor	Acct7.6_L				
Materials	Acct7.6_M	$	23,039	$	23,070
Subcontractors	Acct7.6_S				
Subtotal		$	23,039	$	23,070
Total Direct Field Costs (DFC)					
All Labor Costs (Includes Boiler OEM Labor)		$	440,545	$	442,334
Material Costs		$	1,067,192	$	1,094,531
Subcontractor Costs (Labor & Materials)		$	81,470	$	82,440
Direct Field Cost (DCF)		$	1,589,206	$	1,619,305
Indirect Costs					
Field Office Nonmanual (Construction Management)		$	47,676	$	48,579
Support Labor		$	28,423	$	28,461

Temporary Site Improvements		$	17,647	$	17,709
Subcontracts & Insurance		$	28,606	$	29,147
Miscellaneous Construction Expenses		$	6,977	$	7,001
Sales Tax		$	64,032	$	65,672
Indirect Field Costs (IFC)		$	193,360	$	196,569
Total Plant Cost (TPC)					
Process Facilities Capital, "PFC" (Directs + Indirects)		$	1,782,567	$	1,815,875
Engineering		$	95,352	$	97,158
General & Administrative		$	53,477	$	54,476
Fee		$	71,303	$	72,635
Craft Premium Pay		$	8,208	$	8,237
Process Contingency (Need to add for Steam Generator and Turbine?)					
Steam Generator		$	-	$	-
Turbine Island		$	-	$	-
FGD/SO2 Removal		$	-	$	-
Particulate Control		$	-	$	-
Coal Handling		$	-	$	-
Ash Handling		$	-	$	-
Water Treatment		$	-	$	-
Auxiliaries		$	-	$	-
Selective Catalytic Reduction		$	-	$	-
Total Process Contigency		$	-	$	-
Project Contingency		$	201,091	$	204,838
Total Plant Cost (TPC) with EPC Fee	TPC	$	2,211,998	$	2,253,219
Capital Cost Summary in $/KW (Rounded)					
Total Plant Cost (TPC) with EPC Fee		$	2,930	$	3,000